Ocean Acidification and Marine Biogenic Trace Gas Production

A thesis submitted to the School of Environmental Sciences of the University of East Anglia in candidature for the degree of

Doctor of Philosophy

By

Frances Elizabeth Hopkins

March 2010

Abstract

The oceanic uptake of anthropogenic CO_2 emissions is leading to an alteration of seawater carbonate chemistry, manifested as increasing $[H^+]$, falling $[CO_3^{2-}]$ and a drop in seawater pH. Over the coming centuries this process, termed "ocean acidification", is expected to negatively impact marine biota, with implications for marine biological and biogeochemical processes. In this thesis, the impact that such changes may have on the net production of a range of climatically- and atmospherically-important marine biogenic trace gases, including halocarbons and dimethyl sulphide (DMS), is assessed through a mesocosm phytoplankton bloom CO_2 perturbation experiment, two laboratory CO_2 incubation experiments on natural seawater samples, and at a volcanically-acidified shallow marine fieldsite in Italy. Large and significant reductions in DMS and DMSP concentrations under future high CO_2 conditions were observed during the mesocosm experiment (mean decreases of 57 percent and 24 percent, respectively), a finding in strong support of a previous study (Avgoustidi 2007). Furthermore, concentrations of iodocarbons showed large decreases, with mean decreases under high CO_2 ranging from 59 to 93 percent. Results for the laboratory incubation experiments also showed a reduction in iodocarbon concentrations (when normalised to chlorophyll *a*) under high CO_2. These changes may be the result of shifts in plankton community composition in response to the high CO_2 conditions, and/or impacts on dissolved organic matter and the bacterial communities involved in the formation of these compounds. The response of bromocarbons was less clear cut during the experimental studies. Following investigations at a naturally-acidified fieldsite in Italy, it was concluded that this site was a poor natural analogue to the impact of future ocean acidification on marine trace gas production. Taking the results of the mesocosm and laboratory incubations into consideration, a combined decrease in both DMS and iodocarbons in response to ocean acidification may have considerable impacts on future atmospheric chemistry and global climate.

Acknowledgements

Many people have contributed to making my PhD experience both enjoyable and rewarding. Firstly, my supervisory team: Professor Peter Liss and Dr. Sue Turner at the University of East Anglia, Dr. Phil Nightingale at Plymouth Marine Laboratory (PML), and Dr. Michael Steinke at the University of Essex, all of whom have consistently provided invaluable guidance, advice, expertise and support. I am extremely grateful to Claire Hughes and Manuela Martino for providing training and advice on halocarbon analysis, and to Tom Bell and Dan Franklin for help and training in DMS/DMSP analysis. This work would not have been possible without the amazing technical assistance of Gareth Lee, both in the lab at UEA and during the mesocosm experiment in Norway. I also thank Gareth, as well as Andy Macdonald and Rob Utting of the UEA technical department, for organising the often tricky logistics involved in the transportation of equipment, analytical instruments, chemicals and gases to far-flung locations, including Norwegian fjords and Italian islands. I am indebted to all those involved in the mesocosm experiment in Bergen, Norway for making the experiment both a great experience and a success, in particular Ian Joint for his leadership of the experiment, Dorothee Bakker for the pCO_2 measurements, Isabelle Mary for phytoplankton flow cytometry data and Claire Widdicombe for phytoplankton biomass data. I am also extremely grateful to Claire for taking the time to analyse plankton samples for my Plymouth incubation experiments. I gratefully acknowledge all those at PML who offered help, assistance, advice and friendship during the summer of 2007, in particular Rachael Beale, Laura Goldson, Susan Kimmance, Malcolm Woodward, Glen Tarran, Steve Archer and Malcolm Liddicoat, and made me feel part of the PML "family" during those months spent working at the lab. There were many people involved in the Ischia fieldwork that deserve lots of thanks: Matt Jones, Phil Kerrison, Jason Hall-Spencer, Riccardo Rodolfo-Metalpa, the staff at Institute Laboratorio di Ecologia del Benthos, (Stazione Zoologica Anton Dohrn, Ischia), Roger and Josie Phillips, Tony Dolphin and of course, Sue Turner. A special thank you goes to the ENV PhD gang, all of whom made the last 4 years some of the best of my life, especially my second family Helen Band and Simon Busby, and Nem Vaughan, Laura Bristow and Gemma Bates. Lots of love and thanks goes to my family (Hopkins and Pask!) for all their love and support, and for encouraging me to pursue a career in my love of all things marine. And finally, all my love to Edward Pask, for being more than I could ever have wished for.

Table of Contents

Chapter 2: Methods of Marine Trace Gas Analysis

Chapter 3: Marine biogenic trace gas production during a mesocosm CO_2 perturbation experiment

Chapter 4: High-CO_2 Laboratory Seawater Incubation Experiments

List of Figures Page

Chapter 1: Introduction and Literature Review

Chapter 2: Methods of Marine Trace Gas Analysis

Chapter 3: Marine biogenic trace gas production during a mesocosm CO_2 perturbation experiment

Chapter 4: High-CO_2 Laboratory Seawater Incubation Experiments

Chapter 5: A Natural Analogue to Ocean Acidification: Marine CO_2 Vents, Ischia, Italy.

List of Tables Page

Chapter 1: Introduction and Literature Review

Chapter 2: Methods of Marine Trace Gas Analysis

Chapter 3: Marine biogenic trace gas production during a mesocosm CO_2 perturbation experiment

Chapter 4: High-CO_2 Laboratory Seawater Incubation Experiments

CHAPTER 1
Introduction and Literature Review

1 Introduction

The oceanic uptake of anthropogenic CO_2 emissions is leading to an alteration of seawater carbonate chemistry, manifested as increasing $[H^+]$, falling $[CO_3^{2-}]$ and a drop in surface seawater pH. Over the coming centuries this process, termed "ocean acidification", is expected to negatively impact marine biota, with implications for both ecological processes and biogeochemical cycles. Through both experimental and *in situ* studies, this thesis attempts to assess the potential impacts ocean acidification (OA) may have on the production of climatically- and atmospherically-important pelagic marine biogenic trace gases, including iodine- and bromine-containing halocarbons and dimethyl sulphide (DMS). The local and global climatic and atmospheric impacts that a future change in the production of these gases may have will be discussed.

1.1 The Global Carbon Cycle

Carbon is the single most fundamental element to life on Earth. As a result, the biogeochemical cycling of carbon in the Earth system is an immensely complex process, not only encompassing all living organisms, but all inorganic carbon reservoirs, as well as the fluxes between them. In the atmosphere, the majority of carbon is present as carbon dioxide (CO_2), with only minor contributions from methane (CH_4), carbon monoxide (CO) and other gases (Holmen 2000). CO_2 constitutes one of the most important atmospheric gases, strongly influencing the Earth's radiative heat budget and controlling the oceanic carbonate equilibrium system.

Throughout Earth's history, atmospheric CO_2 concentrations have naturally fluctuated (Pearson and Palmer 2000). On Millennial timescales, these include changes to geological and volcanic processes (Pearson and Palmer 2000), as well as variations in ocean temperatures associated with climatic shifts which affect the

solubility of CO_2 in seawater (Barker *et al.* 2003). Biological processes, including the formation of biogenic carbonate and burial of organic carbon in deep ocean sediments are significant sinks (Pearson and Palmer 2000; Barker *et al.* 2003). In addition, changes in ocean primary productivity associated with temperature-induced stratification and shifts in availability of nutrients can affect the amount of CO_2 drawdown from the atmosphere by marine organisms (Barker *et al.* 2003).

1.1.1 Atmospheric CO_2 in Earth's Past

Trace gas concentrations obtained from Antarctic Vostok and Dome C ice core data have allowed reconstructions of past atmospheric CO_2 concentrations to extend back to 650,000 year before present (B.P.) (Siegenthaler *et al.* 2005; Spahni *et al.* 2005). Figure 1.1 shows concentrations of CH_4, CO_2, and δD (D = deuterium – Antarctic temperature proxy), and illustrates that this period of Earth's history is characterised by ~100,000 year cyclical periods of cold glacials punctuated by warmer interglacials (Augustin *et al.* 2004). These fluctuations between cooler and warmer periods correlate closely with atmospheric concentrations of CO_2 and CH_4, suggesting these atmospheric gases exert a strong influence on the Earth's climate (Augustin *et al.* 2004; Siegenthaler *et al.* 2005).

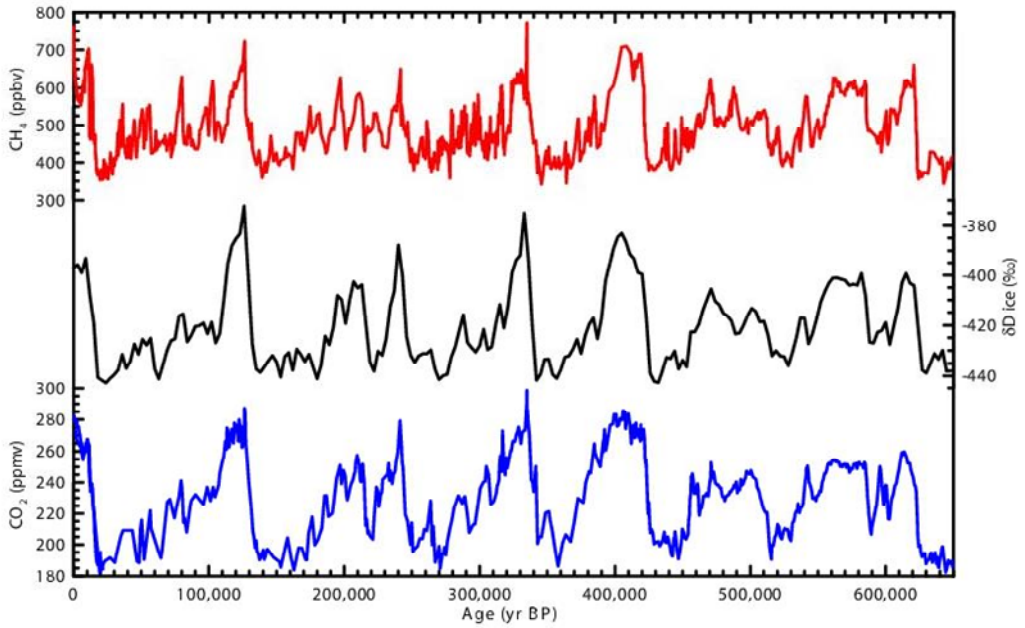

Figure 1.1. Antarctic Vostok and Dome C ice core records for CO_2 (blue), CH_4 (red) and δD (deuterium – Antarctic temperature proxy, black) extending back from present day to 650,000 years BP. After: Siegenthaler *et al.* (2005), and Spahni *et al.*, (2005).

Over the course of the past 650,000 years, CO_2 concentrations have oscillated between ~180 ppmv (parts per million by volume) during glacial periods, up to 280-300 ppmv during interglacial periods (Figure 1.1) (Petit *et al.* 1999; Siegenthaler *et al.* 2005). The use of boron isotopes ($\delta^{11}B$) in ancient planktonic formainifera shells has enabled the reconstruction of atmospheric CO_2 concentrations (derived from surface ocean pH) extending back to around 60 million years (Pearson and Palmer 2000). For the period from 60 M – 52 M year B.P. atmospheric CO_2 concentrations were exceptionally high at around 2000 ppmv, creating 'super greenhouse' climatic conditions. However, from this point CO_2 concentrations gradually became lower, and since about 24 M year B.P. atmospheric CO_2 has not exceeded 500 ppmv (Pearson and Palmer 2000).

1.1.2 Anthropogenic CO_2 emissions

Over Earth's more recent history, atmospheric CO_2 concentrations have reached levels typical of interglacial periods for at least the last 400,000 years – around 280 ppmv (see Figure 1.1). However, since the start of the Industrial Revolution, atmospheric CO_2 concentrations have steadily risen as a result of cement production, changing land-use patterns and our unwavering reliance on the combustion of fossil fuels as our primary energy source. In just the last 200 years atmospheric CO_2 concentrations have increased at an unprecedented rate to ~380 ppm, its highest level for at least 650,000 years, a rate of increase that is around one hundred times more rapid than any other time during the last hundreds of thousands of years of the Earth's history (Raven *et al.* 2005; Kleypas *et al.* 2006).

1.1.3 Atmospheric C flux to the oceans

So far, approximately half of all anthropogenic CO_2 emissions have remained in the atmosphere, with twenty per cent having been taken up by the terrestrial biosphere. The oceans constitute a critical sink for atmospheric CO_2, and have so far absorbed around thirty per cent of all anthropogenic CO_2 (Sabine *et al.* 2004; Raven *et al.* 2005). This uptake is expected to continue, resulting in a doubling of surface ocean CO_2 partial pressure from pre-industrial levels within the next 50 years (Kleypas *et al.* 2006). In the long term, model projections show that the oceans are expected to absorb around ninety per cent of anthropogenic CO_2 over the next millenium (Archer *et al.* 1998; Kleypas *et al.* 2006).

1.1.4 Seawater dissolved organic carbon (DIC), Total Alkalinity (TA) and carbonate equilibrium

CO_2 obeys Henry's Law, in that the mean partial pressure of CO_2 in the surface ocean is virtually equal to that of the atmosphere (Caldeira and Berner 1999). Consequently, an increase in atmospheric CO_2 (pCO_2) leads to a concomitant increase of CO_2 concentration in the surface oceans (PCO_2). The chemical behaviour of DIC is critical in controlling the carbonate chemistry and pH of seawater. Dissolution of CO_2 into seawater results in the production of carbonic acid (H_2CO_3 (aq.)) which rapidly dissociates to produce bicarbonate (HCO_3-) and carbonate (CO_3^{2-}) ions.

$$CO_2\,(aq) + H_2O\,(l) \leftrightarrow H_2CO_3\,(aq) \leftrightarrow H^+\,(aq) + HCO_3^-\,(aq) \leftrightarrow 2H^+\,(aq) + CO_3^{2-}\,(aq) \quad (1)$$

This process also results in an increase in the concentration of H^+. As shown by Figure 1.2, at an average surface seawater pH of 8.2 units, the three forms of DIC are present in seawater in proportions that are characteristic of that pH. HCO_3^- dominates at around 91 per cent of total DIC, with ~8 per cent CO_3^{2-} and ~1 per cent CO_2 (Raven *et al.* 2005).

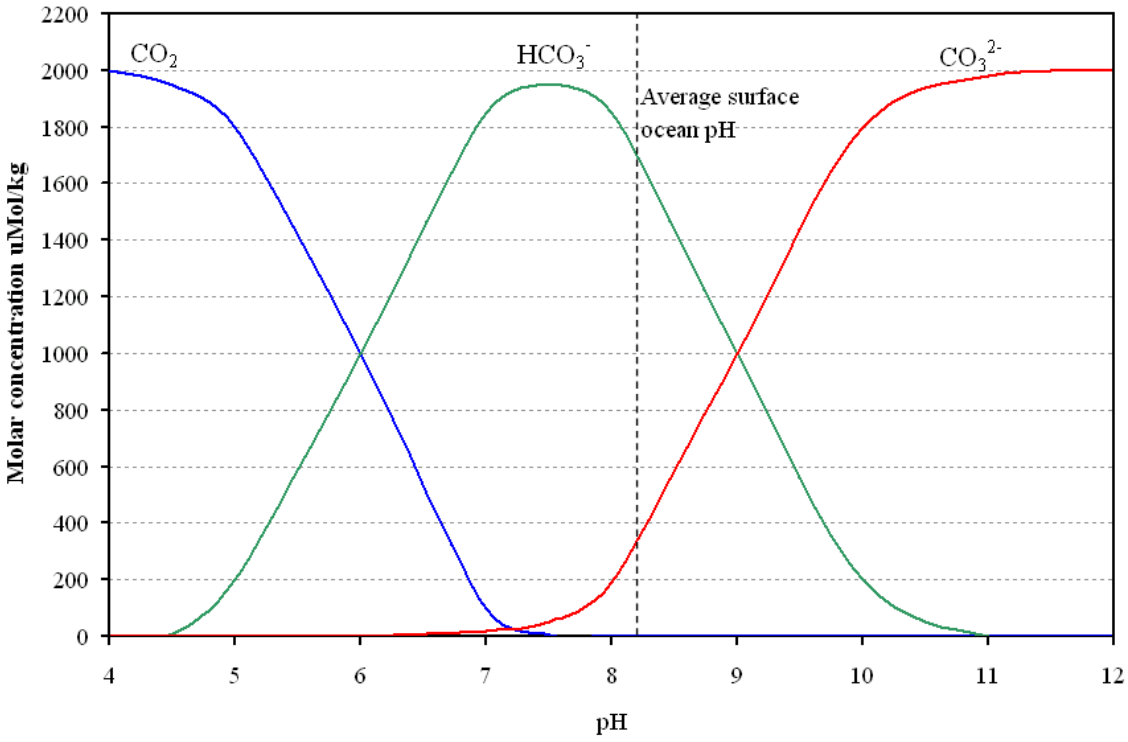

Figure 1.2. Relationship between pH and dominant DIC species in seawater.

Total Alkalinty (TA) is also crucial to an understanding of the seawater carbonate chemistry. A precise definition of the TA of a water sample is the "number of moles of H^+ equivalent to the excess of proton acceptors (bases formed from weak acids) over proton donors (acids) in one kg of sample" (DOE 1994), or:

$$TA = [HCO_3^-] + 2[CO_3^{2-}] + [B(OH)_4^-] + [OH^-] + [HPO_4^{2-}] + 2[PO_4^{3-}] + [H_3SiO_4^-] + [NH_3] + [HS^-] - [H^+]_F - [HSO_4^-] - [HF] - [H_3PO_4] \quad (2)$$

$[H^+]_F$ = free concentration of H^+

However, in natural seawater with a pH greater than 8, TA can be approximated by:

$$TA \approx [HCO_3^-] + 2[CO_3^{2-}] + [B(OH_4)^-] + [OH^-] - [H^+] = \text{Practical Alkalinity (PA)}. \quad (3)$$

When the TA and [DIC] of a water sample are known, along with temperature and salinity, all the other parameters of the seawater carbonate system ($[CO_2]$, $[HCO_3^-]$, $[CO_3^{2-}]$ and pH) can be calculated (Zeebe and Wolf-Gladrow 2001).

1.1.5 Seawater pH Buffering Capacity

The pH of seawater is maintained at a stable level as a result of its ability to buffer itself against changes in pH, by counteracting changes in concentration of H^+ ions. Following the addition of CO_2 to seawater, the resulting excess of H^+ reacts with CO_3^{2-} to produce HCO_3^-, as shown by Equation 1. This results in a reduction of H^+ concentration, thereby lessening the expected fall in pH.

The ability of seawater to buffer the input of CO_2 can be quantified using the Revelle Factor (ß), an expression which relates the fractional change in seawater pCO_2 to the fractional change in total DIC at constant temperature, alkalinity and salinity (Revelle and Suess 1957; Zeebe and Wolf-Gladrow 2001):

$$ß = (\Delta[CO_2] / [CO_2]) / (\Delta[DIC] / [DIC]) \quad (4)$$

The ability of seawater to buffer itself against increases, or decreases, in CO_2 ensures that TA remains constant, as the net reaction produces the same number of equivalents of proton donors (H^+) as proton acceptors (HCO_3^-, CO_3^{2-}) (see equation 1). Therefore variations in the Revelle Factor are mainly due to changes in pCO_2 and the ratio of DIC to TA (Zeebe and Wolf-Gladrow 2001). At current atmospheric pCO_2, the

Revelle factor varies between 8 and 13 (Sabine *et al.* 2004), with the lower values found at the tropics, and higher values in colder high latitude waters where CO_2 solubility is greatest (Archer 2005).

1.1.6 Biological Pump

The oceans' large capacity for CO_2 absorption can be attributed to a number of processes, an important one of which is referred to as the "biological pump". This process involves the removal of CO_2 from the surface oceans by phytoplankton, the conversion of this CO_2 to living matter, and its subsequent export to deeper waters, where it is out of contact with the atmosphere (Longhurst and Harrison 1989).

Phytoplankton and autotrophic foraminifera exploit carbon as a resource during photosynthesis and calcification, resulting in depletions of CO_2 in surface waters. This leads to diminished pCO_2 in surface oceans, and an imbalance between the oceans and the atmosphere. As a result, the influx of C in the form of CO_2 from the atmosphere is promoted. The vast majority of phytoplankton in the surface oceans may be grazed by zooplankton and bacteria, or undergo viral lysis, resulting in the process of regenerative production. In fact, 70 to 90 per cent of C is regenerated in surface waters. The remainder, comprising dead and decaying phytoplankton and other detritus, referred to as particulate organic matter (POM), sinks to the ocean floor. It is this process of "pumping" and regeneration of some of that organic C that augments the absorptive capacity of the oceans. As a result of this process, bottom waters are supersaturated with CO_2 relative to the atmosphere by ~30 percent with respect to the surface waters (Libes 1992). Further description of this process, in the context of ocean acidification, is found in section 1.6.2.3.

1.2 Seawater $CaCO_3$ Saturation and the Carbonate Compensation Depth

1.2.1 Forms of Carbonate

The surface waters of the oceans are currently supersaturated with respect to calcium carbonate ($CaCO_3$). This means that $CaCO_3$ is able to precipitate out of solution and remain in solid form provided the concentration of carbonate ions [CO_3^{2-}] is sufficiently high (Milliman 1974). The two most common forms of $CaCO_3$ in the marine environment, aragonite and calcite, are precipitated by marine organisms. The

principle difference between the two forms is their crystalline structures; aragonite has a orthorhomobic structure with a 9-fold coordination, favouring the incorporation of large cations such as strontium (Sr), lead (Pb) and barium (Ba), whilst calcite has a rhombohedral structure with a 6-fold coordination which favours smaller cations including Mg, Fe and Mn (Milliman 1974). These structural disparities lead to differences in their physical and chemical properties, with aragonite displaying at least 50 per cent greater solubility in seawater (Zeebe and Wolf-Gladrow 2001; Feely *et al.* 2004).

1.2.2 Factors controlling saturation states

The principal controlling factor in the precipitation and dissolution of aragonite and calcite is their saturation state in seawater (Ω_{arag} and Ω_{calc}). This is defined as the ion product of Ca^{2+} and CO_3^{2-} at the *in situ* temperature, salinity and pressure, divided by the stoichiometric solubility product (k*sp) for those conditions (Feely *et al.* 2004):

$$\Omega_{arag} = [Ca^{2+}][CO_3^{2-}] / k^*arag \quad (5)$$

$$\Omega_{calc} = [Ca^{2+}][CO_3^{2-}] / k^*calc \quad (6)$$

$[Ca^{2+}]$ in seawater is governed by salinity; in fact the ratio of $[Ca^{2+}]$ to salinity does not vary by more than 1.5 per cent. Therefore the degree of saturation of seawater with respect to calcite and aragonite is determined by variations in the ratio of $[CO_3^{2-}]$ to k*sp (Feely *et al.* 2004). When Ω is greater than 1, the seawater is supersaturated and $CaCO_3$ can exist in solid form. Conversely, Ω less than 1 indicates undersaturation and increased solubility of $CaCO_3$ (Zeebe and Wolf-Gladrow 2001).

The solubility of $CaCO_3$ is also dependent on temperature and pressure. Although seeming counterintuitive, the solubility increases with decreasing temperature and increasing pressure. As a consequence, the solubility of $CaCO_3$ increases with depth in the ocean (Zeebe and Wolf-Gladrow 2001) as illustrated by Figure 1.3. The point at which the *in situ* $[CO_3^{2-}]$ crosses the calcite or aragonite saturation concentration is referred to as the *saturation horizon*, and it signifies the boundary between saturated seawater above and undersaturated seawater below. As a result, carbonate in the solid form should exist above the saturation horizon in seawater. Due to the differences in solubility between aragonite and calcite, the

aragonite saturation horizon is shallower than that for calcite (Broecker and Peng, 1987).

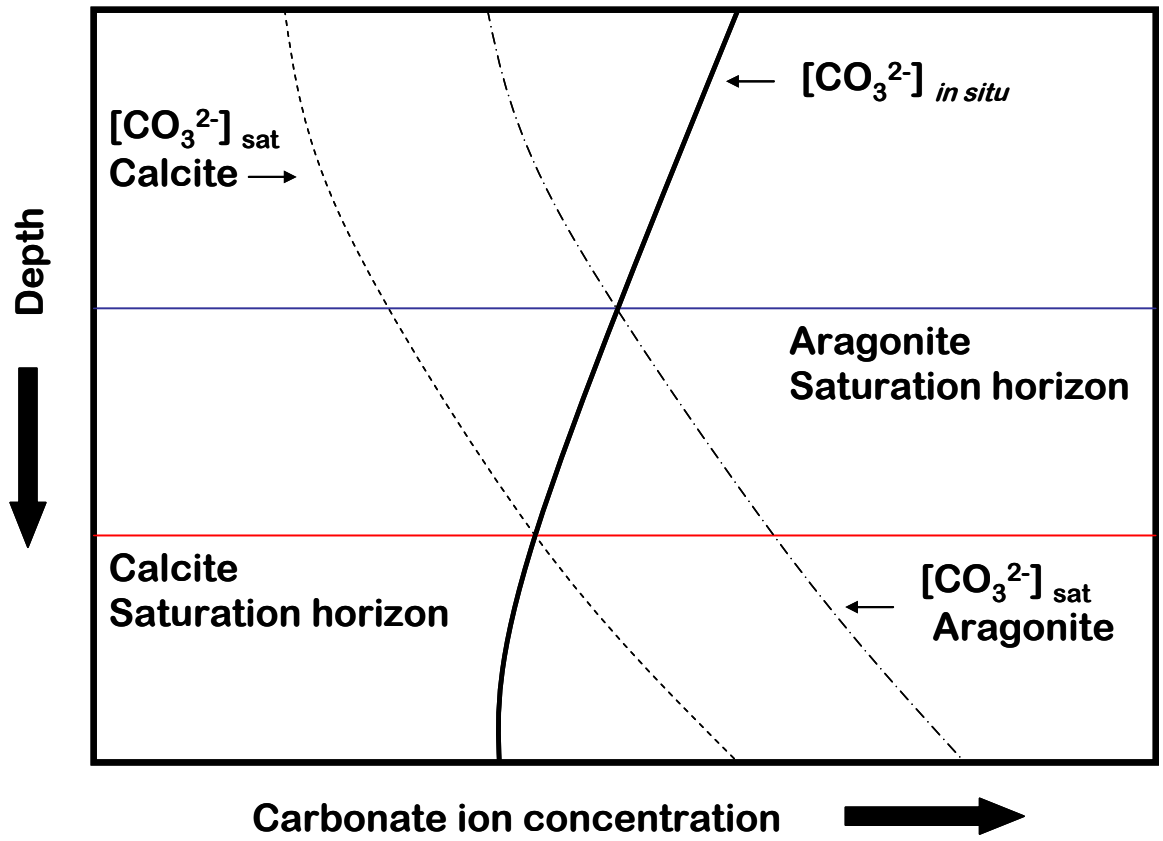

Figure 1.3. A diagrammatic representation of the calcite and aragonite saturation horizons in the ocean. After (Hinga, 2002; Millero and Sohn, 1992; Raven*, et al.*, 2005). With increasing depth and pressure, calcite and aragonite solubility ($[CO_3^{2-}]_{sat}$) also increases. The saturation horizon is indicated by the point at which $[CO_3^{2-}]_{in\ situ}$ (solid curve) crosses over the dashed curve of calcite saturation concentration and the dot-dashed curve of aragonite saturation concentration.

1.3 Natural Variability of seawater pH

1.3.1 Average surface ocean pH

The surface waters of the oceans are in CO_2 equilibrium with the atmosphere, resulting in an average natural surface ocean pH of approximately 8.2 (Millero and Sohn 1992; Hinga 2002; Raven *et al.* 2005). This average value can vary spatially, locally and seasonally by up to ± 0.3 units (Millero and Sohn 1992; Hinga 2002; Raven *et al.* 2005; Blackford and Gilbert 2007). The spatial variability of pH is influenced by large- and small-scale oceanographic and biological processes.

1.3.2 Natural variations in pH

Firstly, temperature is a key factor influencing the spatial variation of seawater pH. The solubility of CO_2 in seawater displays an inverse relationship with temperature, as shown by Figure 1.4. At higher temperatures, the solubility of CO_2 in seawater is lowered, driving the pH up, and vice versa in cold waters (Zeebe and Wolf-Gladrow 2001; Blackford and Gilbert 2007). Therefore cold regions of the oceans act as a sink for CO_2, resulting in lowered pH values, whereas warmer oceans act as a net CO_2 source. The upwelling of CO_2 –rich waters from the deep to the surface oceans, which occurs in Equatorial regions of the Atlantic and Pacific (Raven *et al.* 2005) is another process by which spatial variation in pH is produced. These regions therefore have characteristically lowered surface water pH. Eutrophic, highly productive coastal and shelf waters tend to have pH values that range by as much as 1 pH unit. This is a result of a combination of the effects of biological uptake of dissolved CO_2 and the chemical activity of riverine inputs, particularly total dissolved inorganic C and total alkalinity (Hinga 2002). Additionally, salinity can control the magnitude of pH change due to the presence of weak acids and bases (Skirrow 1975; Hinga 2002).

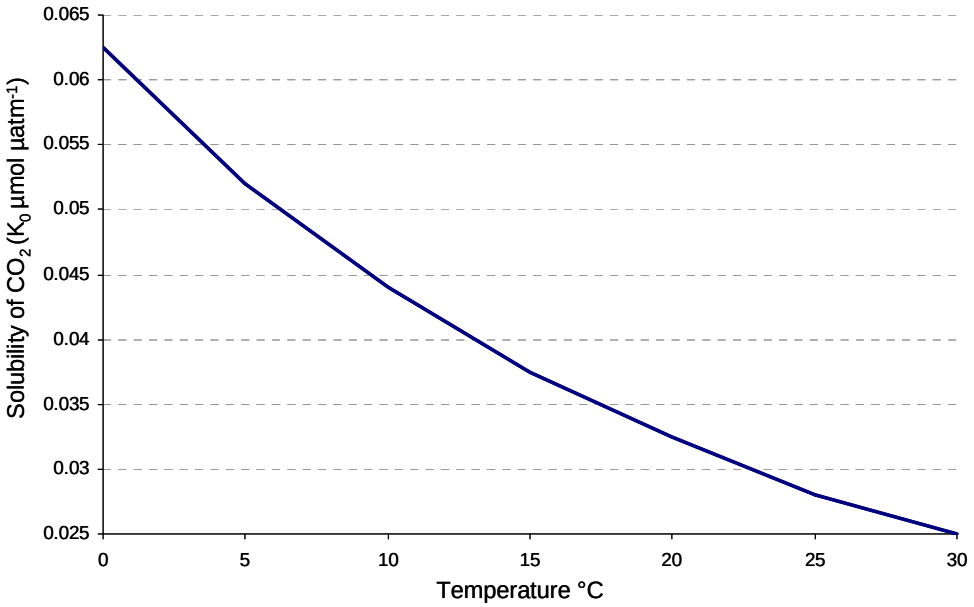

Figure 1.4. The solubility of CO_2 (K_0) as a function of temperature at S = 35. Adapted from: Zeebe & Wolf-Gladrow, 2001.

1.3.3 Spatial pH variations

pH can vary locally as a result of smaller scale processes. Considerable diurnal variations in pH between 8.2 and 8.9 can arise in closed or small bodies of water where exchange with fresh water is limited; a decrease in the evening is the result of

increased production of CO_2 by respiration, with an increase in pH in the afternoon due to depletion of CO_2 as a result of photosynthesis (Millero and Sohn 1992). In the oceans, pH can display variation with depth. A maximum is observed in surface waters again as a result of the loss of CO_2 through photosynthesis. A pH minimum as low as ~7.5 is reached at around 1000m depth owing to the oxidation of decaying plant material, manifested as an O_2 minimum and a pCO_2 maximum. As the deepest waters are approached, the pH rises again due to the dissolution of $CaCO_3$ at depth (Millero and Sohn 1992).

1.3.4 Seasonal variability

Seasonal variability of surface ocean pH is controlled by temperature changes which impact on CO_2 solubility, and biological processes. Where productivity is high, DIC is rapidly converted to organic matter by phytoplankton and a proportion is exported to the deep ocean through the biological pump (Raven *et al.* 2005). This process results in depletion of CO_2 thus driving the pH higher. Therefore during the most productive times of the year, such as during the Spring bloom, surface ocean pCO_2 will be diminished while pH will be relatively high in such regions (Libes 1992). The opposite conditions will be experienced in the unproductive winter months with decreased surface ocean pH as a result of excess CO_2. The metabolic uptake and release of nutrients, predominantly the N nutrients, can also result in seasonal variability in alkalinity and consequently pH. Biological uptake of NH_4^+ leads to a drop in both alkalinity and pH, whereas the uptake of NO_3^- elevates the alkalinity, producing a concomitant increase in pH (Hinga 2002).

1.4 The Future of Atmospheric CO_2

1.4.1 Emissions scenarios

As the possible implications of anthropogenic emissions of CO_2 and other greenhouse gases were realised in the early 1990s, the Intergovernmental Panel on Climate Change (IPCC) devised a set of emissions scenarios of future greenhouse gas and aerosol precursor emissions (Houghton 1992). The scenarios were based on assumptions concerning population growth and economic growth, land use, technological changes, energy availability and fuel mix for the period 1990 to 2100. Initially six IS92 scenarios were published in the 1992 Supplementary Report to the IPCC Assessment, encompassing a broad range of assumptions concerning the

progression of future greenhouse gas emissions in the absence of climate policies beyond those already developed (IPCC 1994). The IS92a scenario was extensively adopted as a standard scenario for use in impact assessments. It was intended to be the best estimation of what would happen if environmental concerns had no major influence on policy, and as a consequence is often referred to as the "Business as Usual" scenario. Using this scenario, it is predicted that by the year 2100, anthropogenic emissions of CO_2 and consequently CO_2 will attain 20.3 Gt year^{-1} (compared to 7.4 Gt year^{-1} in 1990) and ~ 750 ppm respectively (See Figure 1.5). Subsequently, IPCC developed a new set of emissions scenarios, with improved baselines and the inclusion of economic and technological changes (IPCC, 2007). These emissions, known as the SRES (Special Report on Emissions Scenarios), comprise a set of four main scenarios (A1, A2, B1, B2) with three additional groups within the A1 scenario (A1FI, A1B, A1T). In the A1 scenario, the world of the future is one of very rapid economic growth, with a global population that peaks in the middle of the century and declines thereafter. It also sees the swift introduction of new and more efficient technologies. The three A1 groups are distinguished by their technological emphasis: fossil intensive (A1FI), non-fossil energy sources (A1T), or a balance (not relying too heavily on a particular energy source) across all sources (A1B). The A2 scenario depicts a very diverse world with a continuously increasing population. Economic development is principally regionally oriented and economic growth and technological change is slower than other storylines. The B1 scenario shows a convergent world with the same global population as A1, but with fast alteration of economic structures toward a service and information economy, with reductions in material intensity and the introduction of clean and resource-efficient technologies. In the B2 scenario, the prominence is on local solutions to economic, social and environmental sustainability. The population continues to steadily increase but at a lower rate than A2, with intermediate levels of economic development, and less rapid and more diverse technological change than in the A1 and B1. Uniquely to this scenario, there is some focus on environmental protection and social justice. The predicted increases in atmospheric CO_2 concentrations associated with all the above scenarios are shown in Figure 1.5, with concentrations for 2100 ranging from 500 ppm for the conservative B1 scenario to 1000 ppm for A1FI.The intermediate estimate of 750 ppm for the IS92a scenario is still often favoured in studies of future impacts of rising CO_2 levels.

In 2007, the IPCC released their most up-to-date report (I.P.C.C. 2007), stating that warming of the climate system as a result of man-made CO_2 emissions is now unequivocal, with evidence from increased sea surface and air temperatures, widespread melting of snow and ice, and rising global average sea level. The report concluded that it is "very likely" that the observed global temperature increase since the mid-twentieth century is due to the increase in anthropogenic emissions of greenhouse gases (GHGs). It was also recognised that the uptake of excess CO_2 by the oceans is likely to have a negative impact on marine organisms and processes, and this will be discussed in greater detail in the following section.

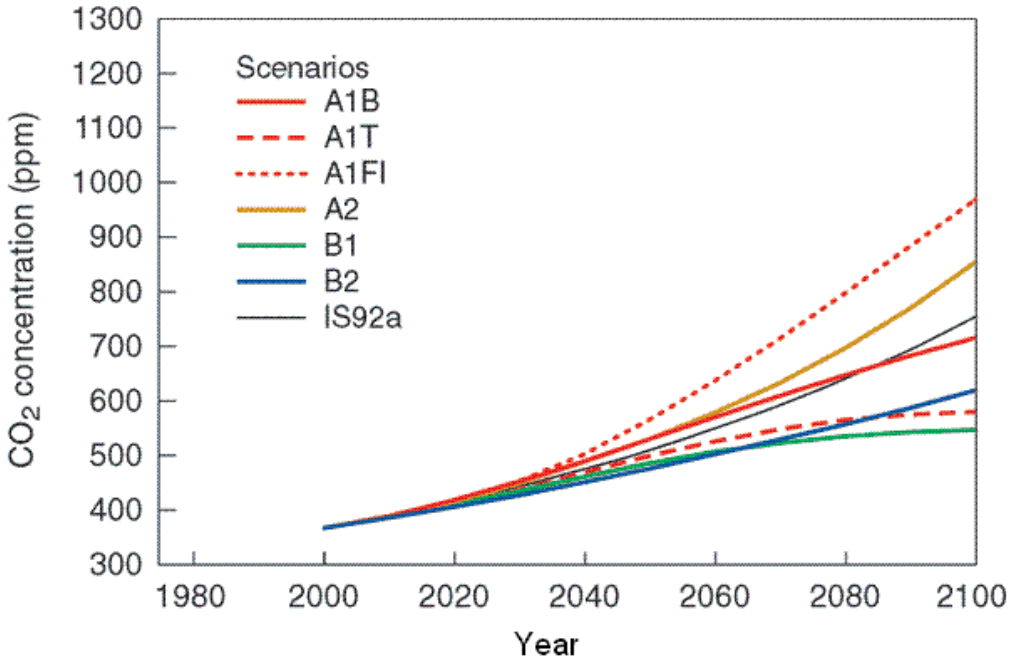

Figure 1.5. Predicted increases in atmospheric concentrations of CO_2, resulting from the six SRES scenarios and from the IS92a scenario.

1.4.2 Impacts on ocean chemistry and pH

The dramatic anthropogenic perturbation to the global carbon cycle that has occurred in the last two hundred years is now resulting in measurable changes to the carbonate chemistry of the surface oceans. The results of the World Ocean Circulation Experiment/ Joint Global Ocean Flux Study showed that between 1800 and 1994 the total oceanic uptake of anthropogenic CO_2 was ~ 118 ± 19 Pg C which corresponds to around half (~48 per cent) of all anthropogenic CO_2 emissions (Feely *et al.* 2004; Raven *et al.* 2005). It is this process of oceanic uptake of excess CO_2 which is having a significant impact on the buffering capacity of the waters of the oceans. As CO_2 absorption by seawater increases, more H^+ ions are available to react with CO_3^{2-}.

Consequently, the [CO_3^{2-}] is reduced and the buffering capacity of the oceans lessens as more CO_2 is absorbed. It is now possible to accurately calculate these changes, taking into account the rate of CO_2 absorption and retention in surface waters and the use of *in situ* measurements of pH, as well as ice core analysis of past pCO_2 concentrations and a knowledge of the carbonate buffer system. Caldeira & Wickett (2003) forced the Lawrence Livermore National Laboratory ocean general-circulation model with pCO_2 for the period 1975 to 2000, and future CO_2 emissions from the IS92a scenario.

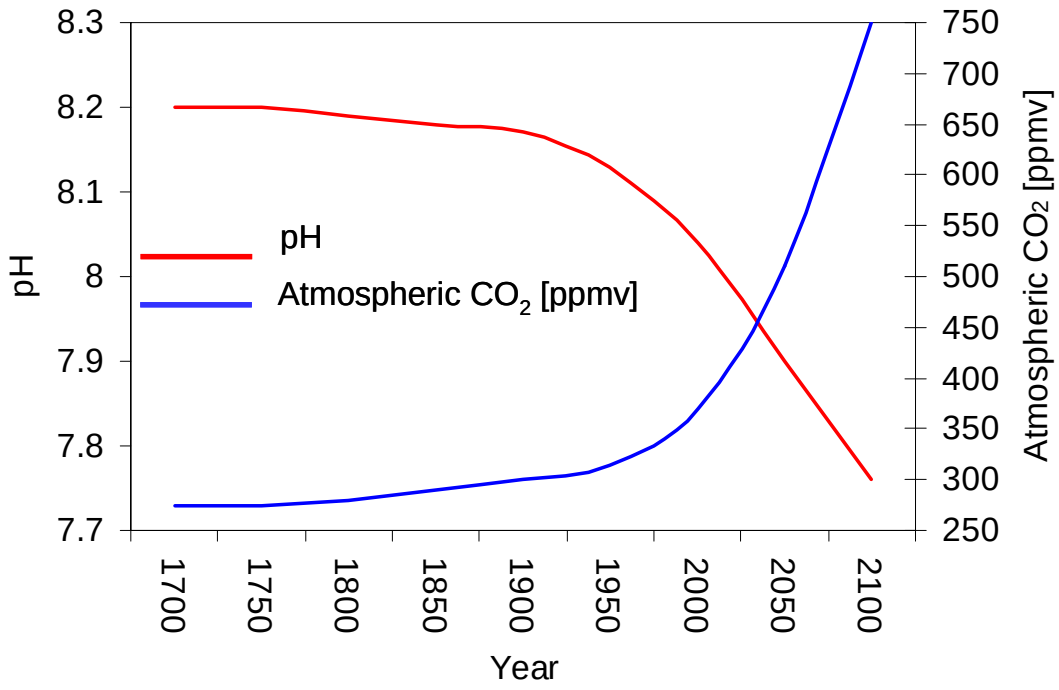

Figure 1.6. The relationship between the concentration of atmospheric CO_2 and surface ocean pH. After Cicerone *et al.* (2004).

Figure 1.6 gives a simple representation of the relationship between pCO_2 and surface ocean pH, which shows that by the year 2100 the pH is expected to drop by ~0.3 units. It is important to note that the present average surface ocean pH is already 0.1 pH units lower than pre-industrial times, due to equilibration of surface waters with the increased amount of CO_2 in the atmosphere (Caldeira and Wickett 2003; Barry *et al.* 2005). Owing to the logarithmic nature of the pH scale, this represents a thirty per cent increase in the concentration of H^+. Looking into the more distant future, Caldeira & Wickett (2003) found that ahead of 2100, if emissions continue to increase following a logistic function, atmospheric pCO_2 will exceed 1900

ppm by the year 2300. This would lead to a reduction in average surface ocean pH of up to 0.77 units. Such pH changes would be greater than seen at anytime within the last 300 million years of Earth's history (Caldeira and Wickett 2003).

1.5 Impacts of Anthropogenic CO_2 Emissions on the Oceanic Carbonate System

1.5.1 Impacts on seawater DIC

The current and predicted increase in atmospheric CO_2 as a result of human activities is expected to produce significant changes to the oceanic carbonate system, with stark implications for organisms that precipitate calcium carbonate. As atmospheric [CO_2] rises, the surface layers of the ocean absorb excess gaseous CO_2, leading to an increase in dissolved organic carbon (DIC) concentrations in seawater (Zeebe and Wolf-Gladrow, 2001). However, when CO_2 dissolves in seawater, less than 1 per cent remains as aqueous CO_2 (Zeebe and Wolf-Gladrow 2001). The remainder forms carbonic acid (H_2CO_3):

$$[CO_2] + [H_20] \rightarrow [H_2CO_3]\ (aq) \qquad (7)$$

As it is an acid, H_2CO_3 immediately dissociates into it constituents:

$$[H_2CO_3] \rightarrow [H^+] + [HCO_3^-] \qquad (8)$$

This release of excess H^+ combines with some CO_3^{2-} and drives down the pH:

$$[H^+] + [CO_3^{2-}] \rightarrow [HCO_3^-] \qquad (9)$$

The outcome is a rise in [CO_2] (aq) and [HCO_3^-], accompanied by a decrease in [CO_3^{2-}], and hence a concomitant fall in $CaCO_3$ saturation state (Ω_{CaCO3}) (Gattuso and Buddemeier 2000; Andersson *et al.* 2003; Langdon and Atkinson 2005; Orr *et al.* 2005; Raven *et al.* 2005)(Hinga, 2002; Zeebe and Wolf-Gladrow, 2001).

Using estimates of future atmospheric and oceanic CO_2 concentrations based on IPCC scenarios and general circulation models, it is predicted that by the end of the twenty-first century atmospheric [CO_2] could exceed 800 ppm, leading to an increase in surface water DIC of more than 12 per cent, and a decrease of [CO_3^{2-}] of

approximately 60 per cent (Feely *et al.* 2004). Therefore it is apparent that the persistent release of anthropogenic CO_2 to the atmosphere will result in a decrease in saturation of the surface ocean with respect to $CaCO_3$ which would have severe consequences for $CaCO_3$-precipitating organisms, such as coral, molluscs, and $CaCO_3$-secreting plankton (Caldeira and Wickett 2005; Raven *et al.* 2005).

The formation and dissolution of carbonate minerals can be summarised as follows, with the forward reaction representing dissolution and the reverse reaction representing mineral formation:

$$CaCO_3\,(s) \leftrightarrow Ca^{2+}(aq) + CO_3^{2-}\,(aq) \qquad (10)$$

As the dissolution of CO_2 in seawater drives $[CO_3^{2-}]$ lower, the conditions will favour the forward reaction, therefore hindering the precipitation of carbonate minerals, and encouraging their dissolution (Raven *et al.* 2005). Ultimately, the extent of this dissolution will depend on the decrease in Ω_{CaCO3} (Feely *et al.* 2004).

Another important aspect of the oceanic carbonate system considers the distribution of DIC and total alkalinity (TA). TA is controlled by several processes, the most relevant of which is the precipitation of $CaCO_3$ by marine organisms. TA is not affected by CO_2 exchange with the atmosphere, or CO_2 uptake by algae, but is coupled to the precipitation and dissolution of $CaCO_3$, and uptake of NO_3^- (Zeebe and Wolf-Gladrow 2001; Hinga 2002). The dissolution of $CaCO_3$ both increases TA and assists in the uptake of anthropogenic CO_2 from the atmosphere (Gattuso and Buddemeier 2000; Feely *et al.* 2004):

$$CO_2 + CaCO_3 + H_2O \leftrightarrow 2HCO_3^- + Ca^{2+} \qquad (11)$$

The calcifying phytoplankton, such as the coccolithophores, contribute to this porcess. As earlier explained, such organisms are involved in the "biological pump" which acts to transport biologically produced $CaCO_3$ down through the water column, where it either re-dissolves in deep waters, or reaches the deep ocean sediments where it may be stored for geological periods of time.

Such changes in TA have the potential to affect the global role that $CaCO_3$ plays in carbon sequestration by the oceans. Firstly, TA is currently ~50 – 150 μmol kg^{-1} less in surface waters compared to the deep oceans (Feely *et al.* 2004). This is a result of the removal of alkalinity by $CaCO_3$ precipitation in the upper ocean, and an

increase in alkalinity due to dissolution at depth. As $CaCO_3$ dissolution in surface waters increases, the TA profile will become more homogeneous with depth, thus potentially increasing the capacity of the surface oceans to absorb atmospheric CO_2, and producing a negative feedback (Feely *et al.* 2004). Unfortunately, there is evidence to suggest that this may not be the case. Andersson *et al.* (2003) used a box model representation of the global shallow-water ocean environment in order to investigate whether the dissolution of carbonates would act as a buffer to increasing atmospheric CO_2. The results of their numerical simulations revealed that by the end of the twenty-first century biological $CaCO_3$ production could diminish by 7 – 44 per cent as a result of depressed saturation state of surface waters, whilst although alkalinity would accumulate as a result of dissolution of carbonate minerals, it would not be enough to produce a significantly increased buffering effect. Therefore the evidence suggests that the future high CO_2-world may be one where calcifying marine organisms are significantly negatively impacted, without beneficial negative CO_2 feedback effects from the reduction in calcification. As aragonite is nearly 50 per cent more soluble in seawater than calcite, it is the aragonite-precipitating organisms such as coral-reefs, planktonic pteropods and heteropod molluscs that will be particularly affected (Feely *et al.* 2004). However, there is also evidence for negative impacts on calcite-producing organisms such as the coccolithophores and foraminiferans (Riebesell 2000; Zondervan *et al.* 2001). The potential and observed effects on these organisms will be discussed in more detail.

1.5.2 Future projections

Attempts have been made to predict when certain regions of the oceans may start to become undersaturated with respect to aragonite or calcite, and there have been some conflicting results. Feely *et al.* (2004) quite optimistically calculated that even the most susceptible areas of the oceans would only face undersaturation when atmospheric CO_2 reaches 1200 ppmv (aragonite) and 1900 ppmv (calcite) for the subarctic North Pacific and 1700 ppmv (aragonite) and 2800 ppmv (calcite) for the warm subtropical and tropical seas. As these values are unlikely to be experienced for several hundred years, it may seem unnecessary to start worrying about the impacts. However, using 13 models of the ocean-carbon cycle to assess Ω_{CaCO3} under the IS92a scenario, Orr *et al.* (2005) found the some Polar and sub-Polar waters may become undersaturated with respect to aragonite when CO_2 concentrations double from the pre-industrial level of ~280 ppm to around 500-600 ppm. Worryingly, this is expected

to occur within the next 50 years. Blackford and Gilbert (2007) used a coupled carbonate system-marine ecosystem-hydrodynamic model to simulate temporal and spatial pH variability across the southern North Sea. The results suggest a >0.1 pH unit drop over the next 50 years, and total acidification of 0.5 units relative to pre-industrial levels at atmospheric CO_2 concentrations of 1000 ppmv. Another study has shown that the uptake of CO_2 by the North Sea has increased in recent years, rising by 22 ppmv between 2001 and 2005 – double the rate for the atmosphere for the same period (Thomas *et al.* 2007).

Some areas of the oceans are naturally undersaturated with respect to aragonite, particularly upwelling systems where CO_2-rich water is brought up from the deep-ocean. Recent observations have shown that anthropogenic ocean acidification is already impacting on one such upwelling region situated off the west coast of North America (Feely *et al.* 2008). An increase in areal extent of the upwelling has been observed, with undersaturated seawater reaching 40-120m depth in large parts of the upwelling, and even reaching the surface off the coast of north California.

1.6 Biological Impacts of Ocean Acidification (OA)

1.6.1 Introduction

The rapid changes to ocean chemistry that are predicted to occur in the next few hundred years as a result of oceanic uptake of anthropogenic CO_2 are expected to have a detrimental impact on the large proportion of the biota of the world's oceans. Marine organisms are far more vulnerable than their terrestrial counterparts to rising CO_2 levels due to small differences in $[CO_2]$ between internal body fluids and the external medium for water-breathing organisms (Ishimatsu *et al.* 2005). In all organisms studied so far, increasing $[CO_2]$ has resulted in lowered internal pH and elevated $[HCO_3^-]$, with concurrent impacts on reproductive success, growth and survival (Portner *et al.* 2005).The most obvious and damaging impact of hypercapnia (high seawater $[CO_2]$) will be on calcifying marine organisms, caused by the decline in aragonite- and eventually the calcite-saturation states of seawater. The organisms that have been identified as at risk from this are the aragonitic reef-building corals of the shallow tropical and sub-tropical seas (Kleypas *et al.* 1999; Hoegh-Guldberg 2005), planktonic pteropods (Orr *et al.* 2005), foraminifera (Barker and Elderfield 2002) and calcifying phytoplankton such as coccolithophores (Riebesell *et al.* 2000a). Other organisms, including a number of fish species (Ishimatsu *et al.* 2004; Ishimatsu *et al.* 2005), molluscs including the mussels *Mytilus galloprovincialis* and *M. edulis*

(Michaelidis *et al.* 2005; Berge *et al.* 2006), the sipunculid worm *Sipunculus nudus* (Laugenbuch and Portner 2004), a marine planktonic copepod *Acartia steuri* (Kurihara *et al.* 2005), several sea urchin species (Kurihara *et al.* 2005; Shirayama and Thornton 2005) and a range of benthic meiofauna species (Barry *et al.* 2005) have been found to react negatively to hypercapnia, displaying a range of symptoms that include acidosis of tissues and body fluids, reductions in growth, reproduction and metabolism, and death.

1.6.2 Marine Phytoplankton

1.6.2.1 Introduction

As the oceans cover around 71 per cent of Earth's surface, primary production by marine photosynthetic organisms is a globally-important process (Hays *et al.* 2005). In fact, marine primary production accounts for around half of the total production on Earth, annually fixing around 50 Gt C (Raven *et al.* 2005). A total of around 5000 species of phytoplankton are responsible for the majority of this marine production (Graham and Wilcox 2000; Millero 2006). Populations of phytoplankton can become so large that the blooms are visible from space using satellite remote sensing technology (Graham and Wilcox 2000). For over 2.7 million years, these key organisms have been modifying the Earth's atmosphere, and to the present day continue to maintain a strong influence on atmospheric chemistry and the biogeochemical cycling of carbon, sulphur, nitrogen and phosphorus (Graham and Wilcox 2000). Phytoplankton are critical to the marine ecosystem. They form the base of the food web and support both microbial and zooplankton communities upon which ecologically significant marine mammal and bird populations and commercially-important marine fisheries depend (Graham and Wilcox 2000). Future changes to ocean chemistry, combined with the effects of human-induced climate change, could have a severe negative impact on marine phytoplankton populations. It has been proposed that an increase in CO_2 in surface seawater could lead to changes in the activity of individual species, favouring some species over others, resulting in shifts in phytoplankton community structure. In turn this could have significant ecological and economic repercussions.

1.6.2.2 Photosynthesis and growth rates

Terrestrial plants are known to be CO_2 limited (Drake *et al.* 1997). As a consequence, an increase in atmospheric CO_2 concentrations is expected to "fertilise"

terrestrial plants, increasing the rate of photosynthesis and overall growth. Conversely, the majority of marine phytoplankton are not CO_2 limited, instead actively taking up HCO_3^-. As a result they are not expected to benefit from increasing CO_2 (Schippers *et al.* 2004). During the dark reaction of photosynthesis, CO_2 is fixed by RUBISCO (Ribulose – 1,5 – bisphosphate carboxylase/oxygenase), using CO_2 as a C substrate. However the half-saturation concentration of RUBISCO is 20-70 μmol kg^{-1} CO_2, whilst the seawater concentration is only around 10-25 μmol kg^{-1} CO_2, insufficient to guarantee efficient operation of RUBISCO (Riebesell 2004). As a consequence, algae have developed a means of actively raising the CO_2 concentrations at the site of carboxylation by the active uptake of HCO_3^-, known as Carbon Concentrating Mechanism (CCM). This process requires further energy in the form of light, but ensures the organism never experiences C limitation (Wolf-Gladrow *et al.* 1999; Riebesell 2004). Diatoms are known to possess CCM, along with the haptophyte *Phaeocystis globosa* (Riebesell 2004), dinoflagellates (Dason and Colman 2004) and the chlorophyte *Chlamydomona* (Collins and Bell 2004). However, it has been suggested that an increase in CO_2 may lessen the need for CCM. This would be of benefit to phytoplankton cells through reduced metabolic cost for inorganic C assimilation (Engel *et al.* 2005). Nevertheless, a number of phytoplankton species lack CCM and may therefore be expected to experience enhanced photosynthesis and growth rate at higher CO_2 concentrations (Riebesell 2004; Leonardos and Geider 2005). The coccolithophores *Emiliania huxleyi* and *Gephyrocapsa oceanica* experience CO_2 limitation, as they perform photosynthesis at present day CO_2 concentrations well below CO_2 saturation levels (Riebesell 2004; Leonardos and Geider 2005). Consequently, the growth and productivity of such species are expected to directly benefit from increasing CO_2.

Other than directly affecting the rate of photosynthesis, increased CO_2 has the potential to indirectly influence the growth and productivity of phytoplankton. Most species are adapted to a narrow range of seawater pH, with the fastest growth at the most commonly occurring pH (Hinga 2002). *E. huxleyi,* the most widespread and abundant species of coccolithophore, has been shown to be relatively sensitive to changes in pH. A decrease in growth rate to only 10 per cent of the maximum growth rate has been observed with a drop in pH from 8.1 to 7.6 (Johnston 1996), a similar pH change to that projected to occur over the next century.

1.6.2.3 Calcification and C cycling

The coccolithophores comprise a globally-important group of calcifying phytoplankton, dominated by the ubiquitous bloom-forming *E. huxleyi* (Graham and Wilcox 2000). They represent the most productive calcifying organisms on Earth and play a critical role in the global carbon cycle (Rost and Riebesell 2004). Along with foraminifera, coccolithophores have a huge impact on marine biogeochemical cycling with significant effects on the climate (Rost and Riebesell 2004). Coccolithophores produced calcite tests, or liths, the function of which is not clear, but is thought to include: Protection from grazing and/or viral lysis; enhancement of light interception through aggregation of coccoliths; and/or a mechanism by which the use of HCO_3^- in photosynthesis is assisted by $CaCO_3$ precipitation (Riebesell 2004). Calcifying phytoplankton play key roles in two processes: the Organic C Pump and the Carbonate Counter pump (see Figure 1.7). Through the fixation of organic C in surface waters by photosynthesis, and the subsequent vertical export of some of this organic matter to depth, the Organic Carbon Pump draws down CO_2 from surface waters. Following remineralisation at depth, this organically-bound CO_2 accumulates, creating an oceanic CO_2 sink (Rost and Riebesell 2004). Conversely, the production of $CaCO_3$ results in a net release of CO_2 to the atmosphere (Riebesell 2004; Hays *et al.* 2005). The relative strength of the two processes determines the sea-air flux of CO_2 (Rost and Riebesell 2004).

As the increasing emissions of anthropogenic CO_2 alter the carbonate chemistry of the surface oceans and lower $CaCO_3$ saturation states, the ability of coccolithophores to produce $CaCO_3$ is likely to be affected. Laboratory and mesocosm experiments have revealed conflicting impacts on calcification. A number of studies have identified a decrease in calcification rate accompanied by an increase in the proportion of misshapen liths and incomplete coccospheres at CO_2 of around 780-850 ppm (Riebesell *et al.* 2000a; Engel *et al.* 2005). In addition, during a mesocosm experiment in 2001 CO_2 experiment, coccolithophores subjected to low 'glacial' CO_2 concentrations (180 µatm) produced larger and heavier coccoliths compared with higher CO_2 treatments (Engel *et al.* 2005). Under a 'Year 2100' high CO_2 treatment, the observed reduction in calcification rates, in combination with direct pH effects on cell physiology affected cell division rates, and result in lowered population growth rates (Engel *et al.* 2005). In addition, calcification was delayed under these conditions, leading to a reduction in the overall amount of $CaCO_3$ production. Decreased calcification is likely to affect the competitive advantage of coccolithophores, through

impacts on resource utilisation and cellular protection, along with diminished protection against grazing and viral attack (Riebesell 2004). This in turn may impact on the abundance and distribution of coccolithophores and in the most extreme case may lead to shifts in the relative abundance of calcifying phytoplankton to siliceous diatoms (Riebesell 2004).

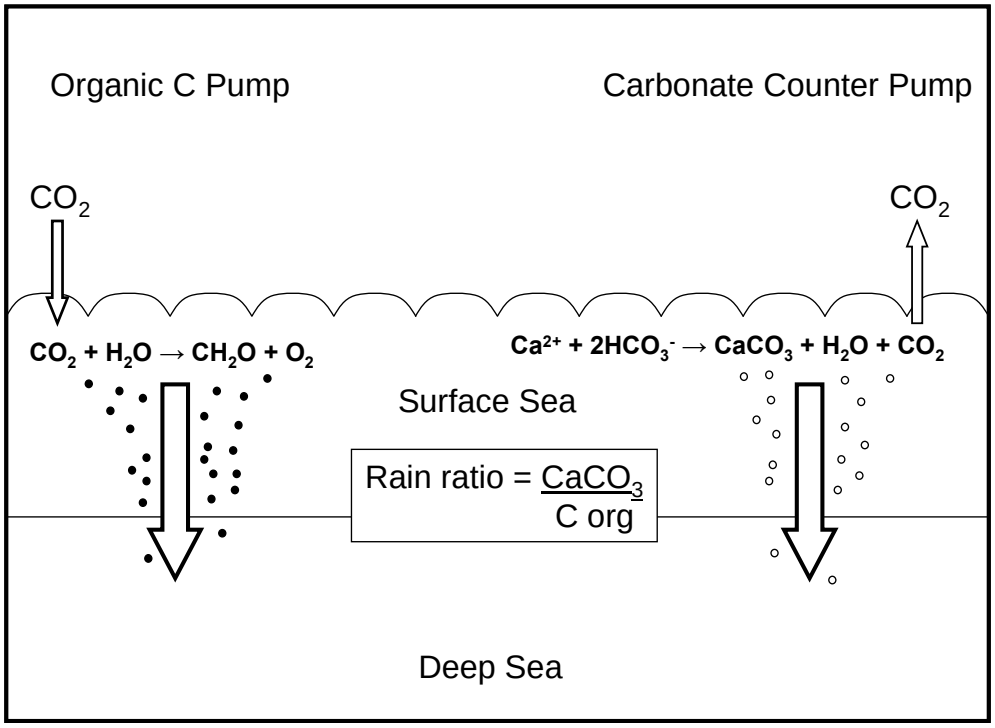

Figure 1.7. The biological carbon pumps. The Organic Carbon Pump generates a CO_2 sink in the oceans through the export of organic matter from the surface ocean, whilst the Carbonate Counter Pump acts as a net source of CO_2 to the atmosphere through the biogenic production of $CaCO_3$ in the surface ocean. From Rost and Riebesell 2004.

Coccolithophores exert a major influence on marine biogeochemical cycling, and in concert with foraminifera, are responsible for producing and sustaining the ocean's vertical alkalinity gradient (Rost and Riebesell 2004). Therefore reduced calcification by coccolithophores as a result of OA has the potential to have significant global impacts. As calcification acts as a net source of CO_2 to the atmosphere, a reduction in calcification by such an important group of organisms has the potential to increase the CO_2 storage capacity of the oceans (Riebesell 2004). So although this would negatively impact on coccolithophore populations, it may produce a slight negative feedback with respect to anthropogenic CO_2 emissions (Wolf-Gladrow *et al.* 1999; Riebesell 2004; Delille *et al.* 2005).

In contrast, a recent study has produced evidence to suggest *E. huxleyi* may in fact experience an increase in calcification with increasing CO_2 concentrations (Iglesias-Rodriguez *et al.* 2008). Batch incubations of this coccolithophore at CO_2 levels ranging from 280 – 750 ppmv revealed a doubling of particulate inorganic and organic carbon (PIC and POC) at 750 ppmv. Although growth rates were reduced as CO_2 increased, coccosphere volume and coccoliths increased, in line with the increase in PIC and POC. To accompany the laboratory studies, Iglesias-Rodriguez *et al.*, assessed the response of natural coccolithophore assemblages to anthropogenic OA since the Industrial Revolution. The average mass of calcite per coccolith was calculated for samples from box core RAPID 21-12-B from the sub-polar North Atlantic, covering the period 1780 – 2004. An increase in average mass from 1.08×10^{-11} to 1.55×10^{-11} g was observed, with an accelerated increase over recent decades. These conflicting results clearly show that further work is needed in order for us to fully understand the response of this important calcifying group of organisms to OA.

1.6.2.4 Organic C Export

Phytoplanktonic CO_2 fixation and the subsequent export of organically-bound C represents an important mechanism in the regulation of atmospheric CO_2 (Organic C Pump – Fig. 1.7) (Engel *et al.* 2005). The degree of C sequestration as a result of this process should depend on nutrient availability in the surface oceans, estimated from nitrate uptake using the Redfield C:N ratio of 106:16 (Redfield *et al.* 1963). However the drawdown of DIC can exceed this expected amount as a result of several process, in particular the formation of C-rich extracellular particles known as Transparent Exopolymer Particles (TEP) (Engel *et al.* 2005). TEP formation occurs as a result of C overproduction, leading to the exudation of polysaccharides by algal cells (Delille *et al.* 2005). So, although originating from dissolved precursors, TEP are known to favour particle aggregation (Engel *et al.* 2005). The results of a 2001 mesocosm CO_2 experiment revealed increased TEP production at high CO_2 concentrations, resulting in enhanced aggregation of detrital particles. Consequently, under high CO_2 conditions particles sediment out at a greater rate and are characterised by increased C:N ratio and depletions of P (Engel *et al.* 2005). A similar phenomenon has been observed with increased CO_2 concentrations in a study in the Baltic Sea (Engel 2002). Therefore, a shift in organic C export as a result of OA could potentially have important consequences. As TEP formation enhances C export and hence the Organic C Pump (Fig. 1.7), the overall response of *E. huxleyi* represents a

negative feedback with respect to rising CO_2 concentrations. If this enhancement of C export is as significant for other phytoplankton groups, and works synergistically with the effects of decreasing biogenic calcification, it could correspond to a major negative feedback to anthropogenic CO_2 (Delille *et al.* 2005).

1.6.2.5 Trace gas production

Marine phytoplankton produce a range of climatically- and atmospherically-important trace gases, which enter the atmosphere via sea-air exchange. Little is know about how the production of these gases may be affected by OA, although data has now been obtained from two mesocosm CO_2 experiments, performed in 2003 and 2005 at a large-scale mesocosm facility in Norway. During the 2003 experiment Avgoustidi revealed a significant reduction in the production of dimethyl sulphide (DMS) (Avgoustidi 2007). DMS is a breakdown-product of the algal compound dimethyl sulphoniopropionate (DMSP), and undergoes rapid oxidation in the atmosphere to produce an array of stratospheric sulphate aerosols. Through direct and indirect interactions with incoming solar radiation and planetary albedo, such aerosols have the potential to lead to climate feedbacks. Furthermore, they contribute to the acidity of atmospheric particles, a natural phenomenon that is being enhanced by man-made sulphur emissions from the combustion of fossil fuels (Liss 1983; Malin *et al.* 1992; Millero 2006). Therefore a reduction in oceanic emissions of DMS has the potential to produce a feedback of the same sign as global-warming, with a reduction in the natural ability of the Earth to regulate its climate (Gunson *et al.* 2006). Conversely, the 2005 experiment produced opposite results. At 2 x CO_2 (750 ppm) there was 22 per cent more DMS produced relative to present CO_2 (375 ppm), whilst at 3 x CO_2 14 per cent greater DMS production was observed (Wingenter *et al.* 2007; Vogt *et al.* 2008). If this effect was produced as a result of future OA, a negative feedback to global warming could be produced. Therefore it is clear that further experiments are required in order for more definitive conclusion to be drawn as to the future of the global S cycle and its climate interactions with increasing ocean acidity.

Biologically-produced iodocarbon compounds comprise a major vector of halogens to the atmosphere, and in turn, to the biosphere (Manley 2002). Halocarbon compounds are known to be produced copiously by both marine macroalgae and phytoplankton, with a further large contribution hypothesised to be attributable to marine bacteria (Manley and Cuesta 1997; Amachi *et al.* 2001). During the 2005 mesocosm CO_2 experiment, concentrations of chloroiodomethane (CH_2ClI) were

quantified (Wingenter *et al.* 2007). An increase of ~50 per cent was observed in mesocosms exposed to 2 x CO_2 (750 ppm) relative to present CO_2 (375 ppm), whilst under the 3 x CO_2 conditions, a 300 per cent increase was observed. The authors concluded that production by viruses may be more important than that by coccolithophores as such dramatic differences were not observed in coccolithophore numbers between treatments. Once in the atmosphere, I species promote the destruction of tropospheric ozone, a compound which is not only a potent greenhouse gas, but is also a major contributor to poor air quality with implications for human health (Manley 2002). Similarly to DMS, the photolysis and oxidation products of iodocarbons, are known to contribute to new particle formation and cloud condensation nuclei (CCN) production in the marine boundary layer. This suggests that marine iodocarbon emissions, perhaps synergistically with DMS, have the potential to significantly affect the global climate through changes in planetary albedo (O'Dowd *et al.* 2002). So an increase in oceanic emissions of the magnitude observed in this experiment could significantly impact on the global I budget, with implication for both air quality and climate feedbacks. Nevertheless, the results of one experiment are insufficient to draw any definitive conclusions, and the impacts of OA on marine biogenic trace gas production require much further investigation.

1.7 Marine Biogenic Trace Gases

1.7.1 DMS

Marine emissions of the trace gas dimethyl sulphide (DMS: $(CH_3)_2S$) comprise a critical component of the global biogeochemical sulphur cycle. Since the first field measurements of DMS were made (Lovelock *et al.* 1972) it has become apparent that the surface oceans are supersaturated with DMS relative to the atmosphere, resulting in a constant flux from sea to air (Watson and Liss 1998). DMS represents over 90 per cent of the total flux of volatile S compounds from the natural marine environment to the atmosphere, with the remainder of the flux made up by COS and CS_2 (Liss *et al.* 1997). This natural source, which amounts to around 12 to 58 x 10^{12} g S per year (Malin *et al.* 1994; Liss *et al.* 1997; Simo 2001), was dominant for the last several hundreds of millions of years of Earth's history until anthropogenic emissions of S in the form of SO_2 from the combustion of fossil fuels began to take over (Liss *et al.* 1997). Although this human flux now dominates by mass of S (70 to 100 x 10^{12} g S per year, Liss *et al.* 1997), such emissions are localised to the industrialised Northern Hemisphere. In addition, S in the form of SO_2 has a short residence time in the

atmosphere due to rapid oxidation and removal via precipitation and fallout (Liss *et al.* 1997; Watson and Liss 1998). As a consequence, marine biogenic emissions can be considered to be slightly dominant over the anthropogenic in the clean, marine-dominated air of the Southern Hemisphere.

1.7.1.1 Sources

DMS is a breakdown product of the biogenically produced dimethylsulphoniopropionate (DMSP $(CH_3)_2S^+CH_2CH_2COO^-$):

$$\mathbf{(CH_3)_2S^+CH_2CH_2COO^- \rightarrow (CH_3)_2S + CH_2CHCOOH\ (acrylic\ acid)} \quad (12)$$

This reaction is catalysed intra- and extra-cellularly by the enzyme DMSP-lyase in particular species of phytoplankton and bacteria (Liss *et al.* 1997). Single-celled marine phytoplankton are the chief producers of DMSP, although macroalgae are also strong producers (Challenger and Simpson 1948; Malin *et al.* 1992). The capacity of phytoplankton to produce DMSP varies between species; phytoplankton of the class Haptophyte are the most prolific producers, with the coccolithophores leading the way, followed by *Phaeocystis*. At the other end of the scale, dinoflagellates and diatoms are considered poor producers (Malin *et al.* 1992; Malin *et al.* 1994; Liss *et al.* 1997; Watson and Liss 1998; Stefels 2000; Burkhill *et al.* 2002). There are thought to be several biological reasons for the production of DMSP by phytoplankton. An increase in DMS production has been observed with increasing salinity, suggesting that this compound plays a key role in osmoregulation and protection against salinity stress (Vairavamurthy *et al.* 1985). Additionally, observations of increases in DMS with decreasing temperature have implicated it as a cryoprotectant in phytoplankton that inhabit Polar waters and ice (Malin *et al.* 1992; Malin *et al.* 1994; Liss *et al.* 1997). Stefels *et al.* (2000) suggested that the synthesis and release of DMSP and DMS by phytoplankton cells may constitute a mechanism by which excess reduced S can be lost. A grazing deterrent role has been identified in the coccolithophore *Emiliania huxleyi;* grazing of this species causes the degradation of DMSP to DMS through mixing with DMSP-lyase. The resulting concentrated acrylate that is produced is thought to deter protozoan grazers (Wolfe *et al.* 1997). A final role that has been suggested is that of anti-oxidant protection, also in part controlled by the enzymatic breakdown of DMSP. Sunda *et al.* (2002) proposed that the breakdown products of DMSP, which include DMS and acrylate, and also dimethyl sulphoxide

(DMSO – $(CH_3)_2O$), act to scavenge reactive oxygen species thereby protecting the cell from oxidation by free radicals. Nevertheless, it seems that as a general rule, healthy phytoplankton cells and populations experiencing exponential growth produce little DMS (Malin *et al.* 1992; Burkhill *et al.* 2002). Production is often associated with the stationary and senescing stages of phytoplankton growth, when cells begin to breakdown, enabling DMSP to come into contact with DMSP-lyase (Burkhill *et al.* 2002). This same process occurs when cells are subject to grazing by zooplankton (Malin *et al.* 1992; Malin *et al.* 1994) or lysis by viral infection (Malin *et al.* 1998). Therefore peaks in DMS production often coincide with the degradation of a phytoplankton bloom.

1.7.1.2 Oceanic distribution

Due to the biogenic nature of DMS production, the highest sea surface DMS concentrations are associated with areas of high biological activity, particularly upwelling and frontal regions (Malin *et al.* 1993; Shenoy and Patil 2003) and coastal and nearshore regions (Bates *et al.* 1987; Erikson *et al.* 1990; Nguyen *et al.* 1990; Bates *et al.* 1992; Turner *et al.* 1996; Simo *et al.* 1997). Large seasonal variations in DMS occurrence are seen in temperate and boreal regions where productivity is at a maximum in the summer months, and very low in the winter.

Table 1.1 is a summary of DMS emission fluxes (μmol m^{-2} day^{-1}), either given as a mean value or a range, for a number of studies carried out over the last 20 years. The differences in DMS emission between open oceans and coastal or shelf oceans are apparent (Andreae 1990; Simo *et al.* 1997; Simo and Grimalt 1998), as are the seasonal differences between winter and summer.

Table 1.1. Regional DMS fluxes to the atmosphere.

Region	Season	DMS flux mean or range μmol m^{-2} day^{-1}	Ref.
Global temperate seas Global shelf and coastal seas		3.3-9.9 5.6-11.2	Andreae, 1990
Pacific Ocean 20°-50°N	Winter Summer	2.1-2.2 5.0-5.1	Bates *et al.*, 1987, 1992
North Atlantic/North Sea	Summer	32	Turner *et al.*, 1989
Southern Indian Ocean	Winter Summer	1.3 3.0	Nguyen *et al.*, 1990
Mediterranean	Winter Summer	2 5	Erickson *et al.*, 1990
North Sea	Summer	10.9	Leck & Rodhe, 1991
Baltic Sea	Summer	4.1	Leck & Rodhe, 1991
North Sea	Winter Summer	0.2 16.4	Turner *et al.*, 1996
North Atlantic	Winter Summer - Autumn	1.3 5.0-10.0	Berresheim *et al.*, 1997
Western Mediterranean *Shelf/Coastal* *Open Sea*	Spring/Summer	5.4 10.3 2.7	Simo *et al.*, 1997
Northern Hemisphere temperate Northern Hemisphere coastal		7.9-16.7 6.2-13.6	Uher *et al.*, 2000
NW Mediterranean *Shelf/Coastal* *Open Sea*		11.2 2.5	Simo & Grimmalt, 2001
Black Sea Open water Shelf water	Summer	1.6 2.1	(Bell, *et al.*, 2006)
Atlantic Provinces: NAST(E)[1] NATR[2] WTRA[3] SATL[4]		0.2-6.8 0.4-13.1 0.4-9.5 0.1-13.0	(Archer, *et al.*, 2002)

[1] = North Atlantic Subtropical Gyre (East), [2] = North Atlantic Tropical Gyre, [3] = Western Tropical Atlantic, [4] = South Atlantic Subtropical Gyre.

1.7.1.3 Sinks

Greater than 99 per cent of the marine pool of DMSP and DMS remains in the water column, with the remaining 1 per cent fluxing to the atmosphere. The seawater pool undergoes transformation or metabolism by a number of chemical and biological processes (Archer *et al.* 2002). Firstly, there is evidence that around 35 per cent of seawater DMS is subject to rapid photochemical oxidation to DMSO by exposure to ultraviolet radiation (UVR) (Brimblecombe and Shooter 1986; Malin *et al.* 1992; Larsen 2005). The most effective wavelengths for this process have been identified as UVA (Toole *et al.* 2003), UVA/visible (Hatton 2002) and UVA/blue (Kieber *et al.* 1996). These are wavelengths that undergo least attenuation in seawater. As a result DMS photolysis can occur at depths of up to ~60 m in oligotrophic seas, such as the equatorial Pacific (Kieber *et al.* 1996). A significant proportion of seawater DMS (~64 per cent) is metabolised by marine bacterial populations. DMSP and DMS are highly labile in seawater, and therefore easily assimilated by marine bacteria, resulting in a short residence time of one to several days (Simo 2001). These compounds represent a valuable carbon and energy source to such bacteria, and are thus rapidly consumed at approximately ten times the rate that DMS is lost through emission to the atmosphere (Kiene and Bates 1990). Some DMSP is also taken up opportunistically by bacteria and used as an osmoprotectant in the same way as phytoplankton; when osmotic conditions are unfavourable, bacterial growth may be enhanced by the uptake of DMSP (Kiene and Bates 1990). In addition, DMSP represents a significant source of reduced sulphur in the surface oceans, one role of which is its incorporation into proteins by bacterioplankton (Kiene and Bates 1990). There are two main pathways by which DMSP is degraded in seawater, the first of which is the DMSP-lyase pathway, as previously described, and which contributes only a very small fraction to DMSP metabolism in seawater. The favoured and dominant process is the dimethylation/demethiolation pathway, which diverts S away from DMS production. In fact, this pathway can be considered a major control on DMS production. This is because if all DMSP was transformed to DMS via the DMSP-lyase pathway, the total production of DMS would be 2 to 20 fold greater (Kiene and Bates 1990).

1.7.1.4 Atmospheric consequences

Following production by phytoplankton, the remaining ~1 per cent of the seawater DMS that was not photolyzed or metabolised is transported to the atmosphere via sea–air exchange. Before a direct method of determining this flux of DMS was developed, emission rates were calculated from the product of the concentration difference across the air-sea interface and the transfer velocity (Malin *et al.* 1992; Malin *et al.* 1994):

$$\text{Flux} = A.k.\Delta c \qquad (13)$$

where A = total ocean surface area available for gas exchange, k = transfer velocity (a function of turbulence in the sea-air interface) and Δc = concentration gradient across the air-sea interface ($\Delta C = C_{water} - C_{air} / H$, H = Henry's Law coefficient) (Liss and Merlivat 1986; Charlson *et al.* 1987).The concentration of DMS in the surface water ultimately determines the driving force of this flux; the atmosphere is inherently undersaturated in DMS with respect to the water as a result of its rapid oxidation in the atmosphere. A number of physical processes act as a further control on the transfer velocity, and these include wind speed, the temperature of the water and the incidence of bubbles, waves and surface slicks (Liss and Merlivat 1986; Malin *et al.* 1992). It is now possible to measure DMS fluxes and transfer velocity directly using eddy correlation from ship platforms (Huebert *et al.* 2004). These direct measurements have allowed modelling approaches to be developed, which account for wind-speed and the effect of bubbles, in order to more accurately parameterise the sea-to-air exchange of DMS and reproduce the observations (Blomquist *et al.* 2006).

The residence time of DMS in the atmosphere is relatively short, lasting only 8 to 49 hours, as it undergoes rapid oxidation by free radicals (Watson and Liss 1998; Millero 2006). DMS is photochemically oxidised by OH during daytime and at night, particularly in polluted air, NO_3 is the primary oxidising agent (Malin *et al.* 1992; Millero 2006). Figure 1.8 is a schematic representation of the reaction pathways for these oxidisation processes. DMS is able to react with OH either through (i) addition of OH to the DMS molecule or (ii) removal of H from the DMS molecule. $CH_3S(OH)CH_3$ formed through step (i) either reacts with O_2 to produce DMSO during step (iii), or loses a CH_3 radical and reacts with O_2 to produce methane sulphonic acid (MSA) during step (iv). The CH_3SCH_2· radical formed in (ii) goes on to react with O_2 and NO, eventually leading to the formation of SO_2 and SO_4^{2-} aerosol. Finally, DMS also reacts with NO_3 either through (v) removal of an H atom, again leading to the eventual formation of SO_2/SO_4^{2-} aerosol, or through (vi) O_2 addition to produce DMSO.

The oxidation products of DMS mentioned above play a number of important roles in the atmosphere. Firstly, they comprise a significant flux of S from the oceans, which is sufficient to balance the global S budget (Liss 1983; Malin *et al.* 1992). SO_2, SO_4^{2-} and MSA are all acidic, and as a result these compounds influence the pH of atmospheric aerosols and marine precipitation (Liss 1983). Therefore, in remote marine areas away from the influence of anthropogenic S pollutants, the oxidation products of DMS comprise the primary source of acidity (Malin *et al.* 1992).

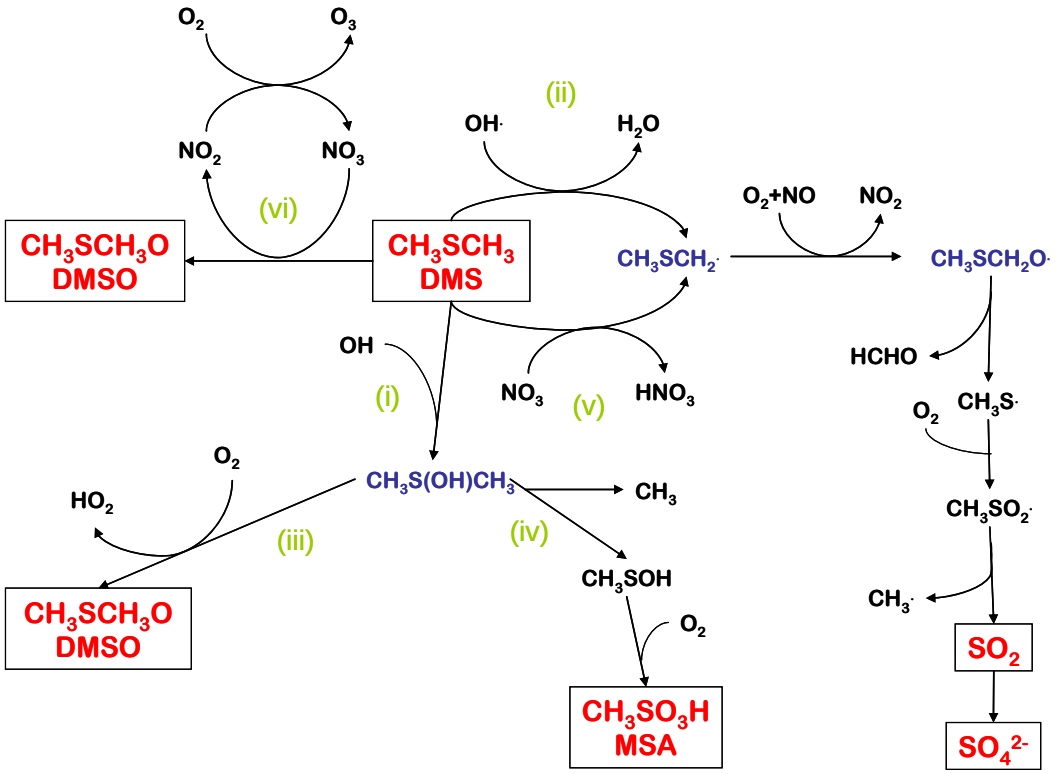

Figure 1.8. The reaction pathways for the oxidation of DMS in the marine atmosphere by OH and NO_3 radicals, leading to the production of DMSO, MSA and SO_4^{2-} aerosols. After (Ayers, *et al.*, 1991; Hegg, *et al.*, 1991).

Finally, SO_2/SO_4^{2-} and MSA can have atmospheric effects through the formation of tropospheric aerosols which (i) have the ability to scatter and absorb incoming solar radiation, thereby modifying the planetary radiation budget (Liss 1983; Malin *et al.* 1992) and (ii) act as cloud condensation nuclei in remote marine regions, with the ability to influence cloud formation and thus the albedo of the atmosphere, with the potential to lead to climate feedbacks (Malin *et al.* 1992; Millero 2006).

1.7.1.5 DMS-CCN-Climate system

The potential role that DMS-derived atmospheric sulphate aerosols play in climate regulation is a topic that has generated a great amount of interest and debate in the last 23 years since the hypothesis was first proposed by Charlson *et al.* (1987), and made famous by James Lovelock through his Gaia theory. The CLAW hypothesis, as it became known from the initials of the authors (Charlson, Lovelock, Andreae, Warren), suggested that the production of DMS by phytoplankton may represent a method by which the Earth is able to regulate its climate. As described above, DMS is rapidly oxidised in the atmosphere resulting in the formation of sulphate aerosols (SO_4^{2-}). These forms of non-sea-salt sulphate (NSS-sulphate) are ubiquitous to the marine boundary layer, and make up the majority of cloud condensation nuclei (CCN) in unpolluted marine air. Charlson *et al.* (1987) proposed that the biological regulation of climate may be possible through the effects of changes in temperature and sunlight on marine phytoplankton DMS production. Ayers *et al.* (1991) and Hegg *et al.* (1991) both found significant correlations between CCN and DMS in the marine boundary layer and marine air. This helps to support the theory that an increase in production of DMS may lead to an increase in NSS-SO_4^{2-} and CCN, thereby producing longer-lived clouds and a greater droplet density. Consequently, this has the potential to produce a cooling effect on the global climate through increased albedo of the troposphere. So, in theory, if DMS production were to increase as a result of rising temperature or solar irradiance, a negative feedback is possible, whereby the increase in CCN would offset the changing climatic conditions. These ideas are a component of the Gaia theory, in which the Earth is considered a self-regulating "organism", capable of maintaining homeostasis through biological regulation of climatic processes. Charlson *et al.* (1987) produced some evidence that the greatest DMS flux is from the warmest seas in the tropics and equatorial regions. This would suggest that the most important climatic role of DMS is to produce a cooling effect over the warmest oceans, leading to a consequent reduction in DMS flux, thereby producing a stabilising negative feedback. However, as more data has become available, it has become clear that the situation in the global oceans is far more complex than originally suggested. High-latitude waters and upwelling regions have also been identified as strong source regions of DMS (Kettle *et al.* 1999).

Figure 1.9 is a schematic representation of the interactions involved, spanning the oceans, atmosphere, the climate and the biota. It must be noted that although Charlson *et al.* (1987) considered the effects of DMS to be negative feedback, there is

still no general agreement whether this is the case. The actual sign of the feedback loop (positive or negative) is still in need of further investigation because there is a degree of uncertainty concerning the reaction of biological DMS production to warming of surface seawaters, shifts in nutrient availability, changes in phytoplankton speciation, variations in solar radiation (Watson and Liss 1998) and the effects of OA.

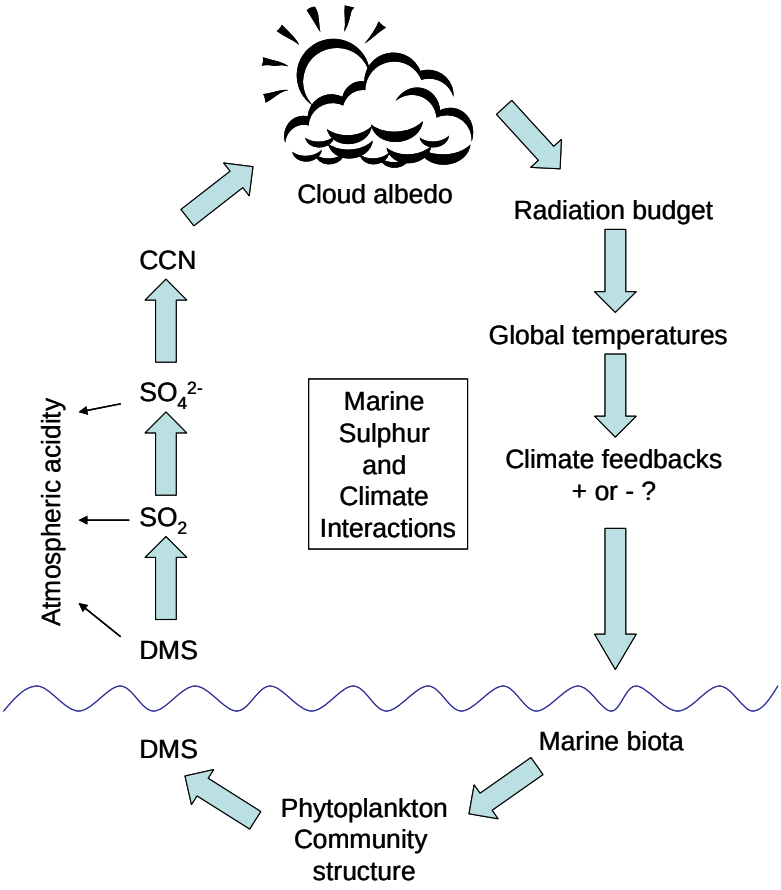

Figure 1.9. Marine S-CCN-Climate interactions. From: Watson & Liss 1998.

1.7.1.6 DMS-CCN-Climate interactions in a high CO_2 world

Model studies have provided some clues as to the behaviour of the DMS-CCN-climate system in a warmer, high-CO_2 world, and how they may impact on the future oceanic production of DMS. The availability of nutrients is a key control on the production of DMS by marine phytoplankton (Watson and Liss 1998). This is demonstrated by the ability of phytoplankton to produce DMSP and/or its nitrogen analogue glycine betaine (GBT). As sulphate is never limiting in seawater, phytoplankton are able to switch between production of the two depending on the

availability of nitrate in the seawater (Andreae 1986; Watson and Liss 1998). In addition, the role of iron in phytoplankton productivity has been demonstrated by the addition of soluble iron to patch of seawater in the equatorial Pacific through the IRONEX I and II experiments (Martin *et al.* 1994). Over the course of the experiments, an order of magnitude increase in chlorophyll *a* levels was recorded, along with simultaneous increases in DMS and DMSP. Climate change is likely to affect the availability of nutrients for utilisation by phytoplankton in a number of ways, thus affecting the productivity and level of DMS production by phytoplankton communities (Watson and Liss 1998). For example, strengthened winds may enhance the nutrient supply from deep waters due to stronger vertical mixing, resulting in increased primary productivity in surface waters. Furthermore, increasing aridity of land surfaces as result of bad agricultural practices and climatic shifts may result in increased deposition of iron-rich dust to the oceans (Watson and Liss 1998; Gunson *et al.* 2006). Both processes would lead to increased DMS production and potentially produce a negative feedback to anthropogenic global warming.

Bopp *et al.* (2003) performed simulations of the climate response to increased greenhouse gases using an atmosphere-ocean general circulation model (GCM), in order to project changes in oceanic DMS production. Although a global mean annual reduction in primary production of 9 per cent at 2 x CO_2 was observed, large variation between the low and high latitudes was apparent. At the low latitudes, a 20 per cent reduction in primary production was observed, whilst at the high latitudes, primary production increased by 30 per cent. The authors attributed this discrepancy to the impacts of two opposing mechanisms. At the low latitudes, productivity is dependent on the availability of nutrients. At 2 x CO_2, warmer sea surface temperatures create enhanced vertical stratification of the water column, resulting in a reduction in the upwelling of nutrients from deeper water (Gunson *et al.* 2006). The result is lowered productivity and a concomitant decrease in DMS emissions. Conversely, productivity at the high latitudes is limited by the length of the growing season. With a warmer world under 2 x CO_2 conditions, the growing season is lengthened, increasing the light efficiency and productivity. The result is increased DMS emissions. In addition, the Southern Ocean and eastern Equatorial Pacific also experience higher DMS emissions under 2 x CO_2. This can be attributed to shifts in phytoplankton speciation. Siliceous, predominantly diatom, communities retreat and are replaced by non-siliceous, prolific-DMSP producing communities.

In addition to the influence of nutrient availability, the degree of DMS production by a phytoplankton community can also be affected by solar forcing (Larsen 2005). Changes in solar forcing are a natural component of climate variability, although anthropogenic damage to the ozone layer has created an artificial enhancement of solar ultraviolet radiation (UVR) reaching the earth's surface (Larsen 2005). The complex interactions and feedbacks involved in the UVR-DMS-CCN system are shown in Fig. 1.10.

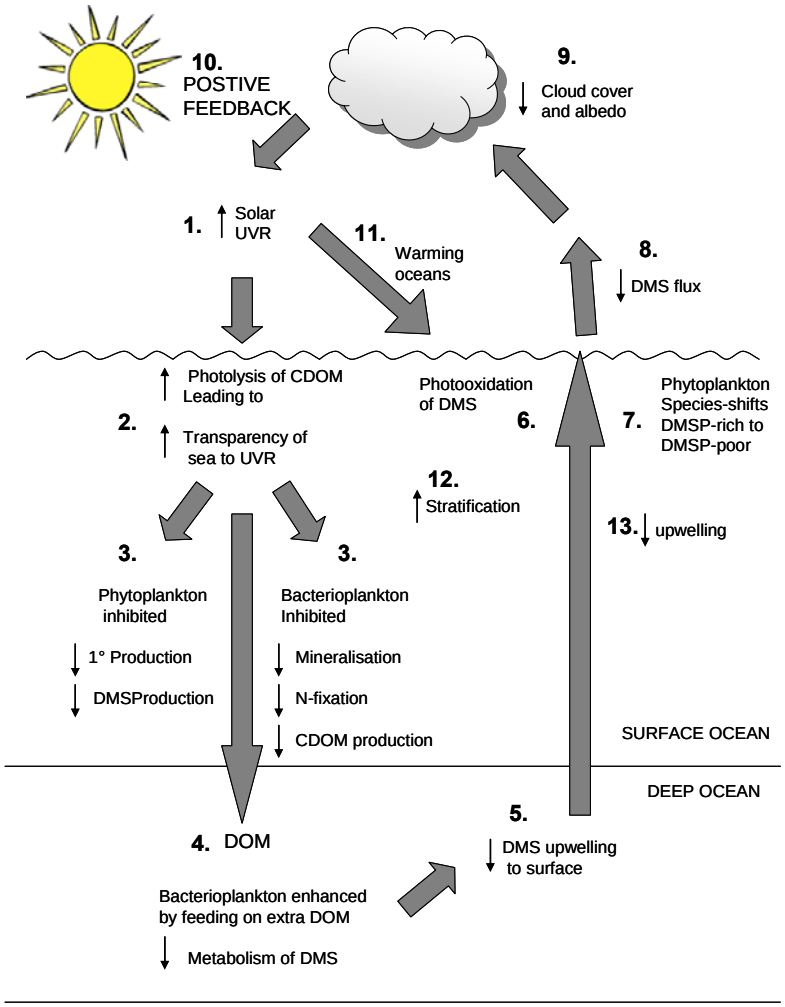

Figure 1.10. The effect of increasing solar ultraviolet radiation (UVR) on the DMS-CCN-albedo system. Alternatively, if a decrease in solar UVR was forced, all the impacts would be opposite in sign, and the system as a whole would display a negative feedback (Gribble, 2003).

↓ = decrease ↑ = increase

Although the interactions are very complex, an overall increase in UVR would result in an eventual decrease in DMS (and *vice versa*). Both UVA and UVB have an inhibitory effect on marine primary productivity, and marine bacterial activity. Marine bacterial populations play a key role in DMS and DMSP metabolism, and are

responsible for removal of around 64 per cent of seawater DMS (Simo 2001). They also play a key role in nutrient cycling, so a reduction in their activity would lead to reduced export and mineralisation of nutrients in deeper waters (Larsen 2005). Phytoplankton speciation is an additional important component of the system. Haptophytes, the major DMS producers including *E. huxleyi,* are much more sensitive to UVR than diatoms (Larsen 2005). As a result enhanced UVR may produce species shifts that result in reductions in numbers of DMS-producing species. A drop in DMS flux to the atmosphere would result, potentially creating a positive feedback to global warming. Changes in UVR intensity also has the potential to impact on other DMS-related water column processes, with further repercussions for the sea-air flux. Increased warming would lead to warmer sea surface temperatures and enhanced vertical stratification, further limiting DMS production due to phytoplankton nutrient-limitation. Synergies between any of these effects in response to UVR forcing may further enhance the forcing with respect to atmospheric DMS concentrations (Larsen 2005). Not all oceanic regions will be prone to such a UVR-DMS mechanism, as factors such as cloud cover, atmospheric optical path length, and aerosol concentration increase the attenuation of UVR in the atmosphere. Therefore, it is most likely to exert an influence in the subtropical oceans, with low cloud cover, shallow mixing depths, nutrient-limitation and where DMS-derived sulphate is the major component of CCN (Larsen 2005).

The response of Earth's climate to anthropogenic CO_2 emissions is still uncertain, and even more so is the response of the DMS-CCN-climate system. Many complex feedbacks are involved, in combination with the natural variability of climatic and oceanic processes, creating large uncertainties that make it impossible at this stage to quantify either the magnitude or sign of any feedbacks. Model studies have attempted to quantify the sensitivity of the climate to variations in the ocean source of DMS. Gunson *et al.* (2006) used coupled ocean-atmosphere GCM to reveal large climate responses to perturbations in the ocean DMS flux. Again large spatial heterogeneity of the global response was observed. A halving of DMS emissions caused net cloud radiative forcing to increase enough to raise the surface air temperature by 1.6 °C. This elevation of surface temperatures and light then promoted phytoplankton growth at high latitudes. This increased the flux of DMS from these regions, thus counteracting the initial warming. This model study supports the ideas of the CLAW hypothesis and demonstrates that perturbations to ocean DMS production may significantly impact on global climate. The role that OA may play in

this complex system is an area which now needs further attention so that it can be considered in future modelling studies.

1.7.2 Halocarbon Compounds

It has been estimated that there are in excess of 3800 known naturally-produced volatile halocarbon compounds, containing chlorine (Cl), bromine (Br), iodine (I) and few containing fluorine (F) (Gribble 2003). Such compounds are produced both directly and indirectly by living organisms, and *via* natural abiotic process including volcanic eruptions, forest fires and other geothermal processes (Gribble 2003).

The oceans are the main global reservoir of the halogens; in the case of iodine, the majority is present as iodate (IO_3^-) (Moore and Tokarczyk 1993). A very small percentage of the marine halogens exist as organic compounds, with the more volatile of these acting as vectors of gaseous halogens to the atmosphere (Moore and Tokarczyk 1993). The oceans constitute the greatest source of biologically-produced volatile halocarbon compounds, a reflection of the limitless supply of halogens in seawater (Manley 2002; Gribble 2003). Production of halocarbons has been confirmed in a wide range of marine species, including phytoplankton (Tokarczyk and Moore 1994; Abrahamsson *et al.* 1995; Tait and Moore 1995; Moore *et al.* 1996; Manley and Cuesta 1997; Saemundsdottir and Matrai 1998; Scarratt and Moore 1998; Murphy *et al.* 2000; Hughes 2004), seaweeds (Manley and Dastoor 1988; Nightingale *et al.* 1995), corals, tunicates (Gribble 2003) and bacteria (Amachi *et al.* 2001).

In the marine environment, Br-containing compounds tend to dominate over those containing Cl, even though concentrations of Br in seawater are much lower than those of Cl. The main sources of these compounds can be found in upwelling regions in nearshore and offshore areas, and both cold water and tropical regions of high primary productivity. (Abrahamsson *et al.* 1995; Ballschmiter 2003).

Biologically-produced halocarbon compounds are considered to be 'secondary compounds', produced via 'secondary metabolism'. 'Primary compounds' are deemed to be those associated with basic metabolism, including the products of photosynthesis and respiration, and compounds such as proteins and lipids. 'Primary compounds' act as the starting material for the more unusual and complex 'secondary compounds' (Manley 2002). The function of many of these compounds is still not known, and in fact, the evolutionary advantage of producing such compounds may not yet exist (Manley 2002).

As the oceanic flux is still an uncertain factor in atmospheric budgets of halogens, an understanding of the production, degradation and transformation pathways is fundamental in order to predict the sea-to-air fluxes of these compounds. The following section will describe the main marine biological sources and production processes of halocarbon trace gases, as well as the main marine abiotic source – photochemistry. The air-sea exchange and atmospheric consequences of these trace gases will also be discussed.

1.7.2.1 Sources

1.7.2.1.1. Macroalgae

Since James Lovelock and colleagues first reported evidence for a marine biological source of halocarbons (Lovelock *et al.* 1973), there has been sustained interest in the large biological oceanic source of these compounds. In 1975, Lovelock revealed the potentially large contribution from marine macroalgae, particularly by kelp, with measurements of CH_3I over beds of *Laminaria digitata* that were 1000-fold greater than over the open North Atlantic (Lovelock 1975). Following this, numerous studies have reported the production of a range of halocarbons, both by macroalgae, and also by associated microbes and epiphytes (Gschwend *et al.* 1985; Manley and Dastoor 1988; Reifenhauser and Heumann 1992; Nightingale *et al.* 1995; Sundstrom *et al.* 1996; Manley and Cuesta 1997).

Macroalgae can indirectly produce both mono- (methyl halides CH_3X) and polyhalogenated halocarbons (e.g. CH_2I_2, $CHBr_3$, CH_2Br_2, $CHBr_2Cl$, CH_2BrCl). The monohalogenated compounds are formed through common haloform reactions, resulting in the methylation of inorganic I (Urhahn and Ballschmiter 1998), and the polyhalogenated through the halogenation of organic precursors, catalysed by haloperoxidases (BrPO and IPO) produced in algal cells (Manley and Dastoor 1987; Nightingale *et al.* 1995; Butler and Walker 2002).

The production of halocarbons by macroalgae appears to be a response to, or by-product of, photo-oxidative or mechanical stress (Nightingale *et al.* 1995; Sundstrom *et al.* 1996; Goodwin *et al.* 1997b; Manley 2002). Haloperoxidases present in macroalgal cells scavenge harmful intracellular H_2O_2, an inhibitor of photosynthesis and respiration. When the production of H_2O_2 is restricted, production of polybrominated compounds has been shown to be reduced (Nightingale *et al.* 1995; Goodwin *et al.* 1997b). Haloperoxidases present on the outer cellular surface of seaweeds protect the tissue from H_2O_2 in the surrounding seawater (Manley and

Barbero 2001). Release rates of halocarbons have also been shown to be related to air exposure and dessication during low tide, light availability, tissue age, tissue wounding and grazing (Nightingale *et al.* 1995; Carpenter *et al.* 1999), and thus can be considered to be indicative of the activity of biological defence mechanisms.

Although macroalgae are considered to be prolific producers of halocarbons, their contribution to the total global oceanic source of these compounds is minor due to their limited distribution in terms of the surface area of the oceans. As an example, Manley and Dastoor (1988) estimated that kelp directly contribute around <0.1 percent to the global CH_3X pool.

1.7.2.1.2. Phytoplankton

A phytoplanktonic source of halocarbons was first postulated nearly 30 years ago (Chameides and Davis 1980), with an unverified report of CH_3I production by phytoplankton incubations as a function of phytoplankton number density and growth time. This led other workers to investigate this potentially globally-important source of halocarbons. Table 1.2 gives a summary of the experiments that have been performed on a range of phytoplankton species, showing the phytoplankton species and class, and the compounds that were detected. The available information suggests that diatoms can be considered to be the most prolific producers of halocarbons. Although phytoplankton production rates are 10s to 100s of times lower than those of macroalgae, this is considered to be a much more important source as the area occupied by phytoplankton is ~200 times greater than that inhabited by macroalgae (Moore 2003).

In order to gain a better understanding of the relationships between the size and composition of phytoplankton communities and the production of halocarbons, numerous open ocean measurements of halocarbons, away from the influence of strong coastal macroalgal production, have been reported (Klick 1992; Krysell and Nightingale 1994; Baker *et al.* 1999; Yamamoto *et al.* 2001; Yvon-Lewis *et al.* 2002; Sturrock *et al.* 2003; Abrahamsson *et al.* 2004a; Chuck *et al.* 2005; Smythe-Wright *et al.* 2005; Smythe-Wright *et al.* 2006; Archer *et al.* 2007; Quack *et al.* 2007b; Wang *et al.* 2009). Many of the above studies were able to detect significant correlations between seawater halocarbons and various indicators of phytoplankton activity, including abundance and photosynthetic pigments. In addition, seasonal cycles in concentrations of some halocarbons have been reported, further linking their presence to phytoplankton activity (Archer *et al.* 2007; Wang *et al.* 2009). The studies cover a

range of oceanic regions, from highly productive upwelling systems (Quack *et al.* 2007a), to oligotrophic tropical waters (Smythe-Wright *et al.* 2005), to temperate shelf seas (Archer *et al.* 2007), thus giving a representative overview of global biogenic halocarbon production.

Table 1.2. Phytoplankton species and associated halocarbon compounds measured in laboratory cultures.

Species	Class	Compounds	Reference
Alexandrium tamarense	Dinoflagellate	C_2H_5Br CH_2Br_2	Hughes 2004
Amphidinium carterae	Dinoflagellate	CH_3Br	Manley & de la Cuesta 1997
Aureococcus anophagefferens	Chrysophytes	C_2H_5Br CH_2Br_2	Hughes 2004
Aureoumbra lagunensis	Chrysophytes	C_2H_5Br CH_2Br_2	Hughes 2004
Chaetoceros atlanticus	Diatom	CH_3Br	Saemundsdottir & Matrai 1998
Chaetocerus calcitrans	Diatom	CH_3Cl CH_3Br	Scarrat & Moore 1998
Chaetoceros diversum	Diatom	CH_3Br	Scarrat & Moore 1999
Crypthecodinium cohnii	Dinoflagellate	CH_3Br	Saemundsdottir & Matrai 1998
Emiliania huxleyi	Prymnesiophyte	CH_3Cl CH_3Br C_2H_5Br	Hughes 2004 Scarratt & Moore 1998
Guillardia theta	Cryptophyte	CH_3Br	Saemundsdottir & Matrai 1998
Hemiselmis rufescens	Cryptophyte	CH_3Br	Saemundsdottir & Matrai 1998
Isochrysis sp.	Prymnesiophyte	CH_3Cl	Scarrat & Moore 1998
Navicula sp.	Diatom	CH_3I CH_2ClI CH_2I_2	Manley & de la Cuesta 1997 Moore et al 1996
Nitzschia sp.	Diatom	CH_3Cl CH_3Br $CHBr_3$ C_2H_5Br CH_2Br_2 $CHBr_2Cl$ CH_2ClI CH_2BrI C_2H_2I $CHBr_2I$ CH_2I_2	Hughes 2004 Manley & de la Cuesta 1997 Moore et al 1996 Tait & Moore 1995 Tokarczck & Moore 1994
Nitzschia arctica	Diatom	CH_3Br CH_2Br_2 CH_2ClI CH_2I_2	Moore et al 1996

Pavlova sp.	Prymnesiophyte	CH_3Br	Saemundsdottir & Matrai 1998
Pavlova gyrans	Prymnesiophyte	CH_3Br	Saemundsdottir & Matrai 1998
Pavlova lutheri	Prymnesiophyte	CH_3Br	Saemundsdottir & Matrai 1998
Phaeocystis sp.	Prymnesiophyte	CH_3Cl CH_3Br CH_3I $CHBr_3$ C_2H_5Br CH_2Br_2 $CHBr_2Cl$ CH_2ClI C_2H_5I CH_2I_2	Hughes 2004, Manley & de la Cuesta 1997 Scarratt & Moore 1996
Phaeodactylum tricornutum	Diatom	CH_3Cl CH_3Br CH_2Br_2 CH_2BrCl	Hughes 2004 Scarratt & Moore 1996
Pleurochrysis carterae	Prymnesiophyte	CH_3Br	Saemundsdottir & Matrai 1998
Porphyridium purpureum	Rhodophyte	CH_3Cl CH_3Br $CHCl_3$ CH_3I C_2H_5Br $ClCHCCl_2$ C_2Cl_4 CH_2Cl_2	Hughes 2004 Scarratt & Moore 1999 Abrahamsson et al 1995 Murphy et al 2000
Porosira glacialis	Diatom	CH_3Cl CH_3Br	Hughes 2004 Manley & de la Cuesta 1997 Moore et al 1996 Tokarczck & Moore 1994
Porphyridium sp.	Rhodophyte	CH_3Br CH_3I $CHBr_3$ CH_2Br_2 $CHBr_2Cl$ CH_2ClI $CHBr_2I$ C_2H_5I CH_2I_2	Scarrat & Moore 1998
Prorocentrum sp.	Diatom	CH_3Br CH_3Cl	Scarrat & Moore 1998
Prorocentrum micans	Diatom	CH_3Br	Saemundsdottir & Matrai 1998
Pycnococcus provasolii	Prymnesiophyte	CH_3Br	Saemundsdottir & Matrai 1998
Synechococcus sp.	Prymnesiophyte	CH_3Cl CH_3Br	Scarrat & Moore 1998
Tetraselmis sp.	Flagellate	CH_3Br	Scarrat & Moore 1998
Thalassiosira pseudonana	Diatom	CH_3Br CH_3I C_2H_5Br CH_2Br_2	Hughes 2004 Manley & de la Cuesta 1997
Thalassiosira weisflogii	Diatom	CH_3Cl CH_3Br	Scarratt & Moore 1996

The purpose of the biosynthesis of halocarbons by marine phytoplankton is not fully understood. Methyl halides (CH_3X) are produced when halides (I-, Br-, Cl-) are enzymatically methylated by methyl transferase-utilising S-adenosyl-L-methionine (SAM) (Wuosmaa and Hager 1990; Manley 2002). Thus it has been suggested that

such compounds may be produced as a means of halide excretion. However, there is no firm evidence that halomethane production serves any function in phytoplankton, and rather it simply appears to be a by-product of normal metabolism (Manley 2002). Polyhalomethanes are indirectly produced through haloperoxidases activity – in algae vanadium-containing peroxidises (V-BrPO, V-IPO) are most common, and function to oxidise halides (Manley 2002). Similarly to macroalgae, the production of these compounds may be connected to cellular defence mechanisms (Kladi *et al.* 2004), with an important role in scavenging harmful H_2O_2. In addition, drawing on evidence from other marine organisms (macroalgae, corals, sponges), polyhalogenated compounds may function as chemical deterrents to grazing and other competition (Manley 2002; Kladi *et al.* 2004). Despite a number of studies investigating the impact of environmental and physical stressors on macroalgal halocarbon production, similar information on phytoplankton is sparse. One study (Hughes *et al.* 2006) has investigated the impact of light stress on halocarbon production in three species of marine phytoplankton (the prymnesiophyte *E. huxleyi*, the prasinophyte *Tetraselmis* sp., and the diatom *T. pseudonana*) and concluded that light stress does not induce iodocarbon production. Further work is required to gain a better understanding of the function these compounds in marine phytoplankton.

The oceans constitute the greatest source of halogens to the atmosphere, and the ubiquitous distribution of phytoplankton throughout the oceans means that production by these organisms is highly significant in terms of the global cycling of halogens. Estimates of the flux of Br and I from the ocean to the atmosphere have been made by several workers, by extrapolating measurements of seawater concentrations obtained during scientific cruises and surveys. Oceanic CH_3I emissions to the atmosphere comprise around 4.3 x 10^9 mol I yr^{-1} (Smythe-Wright *et al.* 2006; Butler *et al.* 2007), whilst the global oceanic flux of $CHBr_3$ and CH_2Br_2 accounts for ~2.5 – 10 x 10^9 mol Br yr^{-1} and 3~3.5 x 10^9 mol Br yr^{-1}, respectively (Butler *et al.* 2007; Carpenter *et al.* 2009).

1.7.2.1.3. Bacteria

In recent years, it has become clear that production of halocarbons by marine bacteria must be taken into consideration when estimating the flux of these compounds to the atmosphere. In comparison to production by phytoplankton and macroalgae, the bacterial source is potentially some orders of magnitude greater. For example, of the estimated global flux of CH_3I of 1 – 4 x 10^{11} g yr^{-1}, annual production

by algae can only account for around 0.1 percent of this total (Nightingale *et al.* 1995; Manley and Cuesta 1997; Giese *et al.* 1999), suggesting a large contribution from another source. Manley and Dastoor (1988) suggested the involvement of bacteria may account for this discrepancy. Subsequently, Amachi *et al.* (2001) reported methylating capabilities in a wide-range of marine bacteria at environmental levels of iodide, and specifically found that cell extract of *Rhizobium* sp. strain MRCD 19 catalysed the methylation of iodide with SAM as the methyl donor. However, this work revealed production of only CH_3I, and not of any other monoiodinated compounds. More recently, Hughes *et al.* (2008) observed production of a range of monoiodinated compounds (CH_3I, C_2H_5I, 2-C_3H_7I, 1-C_3H_7I) from incubations of plankton aggregates and diatom mucilages. As such aggregates are also likely to display high levels of bacterial heterotrophic production (Smith *et al.* 1992), and therefore also provide the necessary precursors for iodocarbon formations, this implicates bacteria in the production of these compounds in such situations (Hughes *et al.* 2008).

1.7.2.1.4. Photochemistry

The photochemical production of volatile iodocarbons in seawater is considered to be an important source of these compounds (Moore and Zafiriou 1994; Happell and Wallace 1996; Richter and Wallace 2004). Moore and Zafiriou (1994) observed the production of CH_3I in irradiated and filtered seawater, and noted that production was enhanced when the water was deoxygenated or received addition of iodide. The presence of CH_3I in open oceanic water was attributed predominantly to photochemical production by Happell and Wallace (1996), citing a relationship between CH_3I saturation anomalies and light intensity in the Greenland and Norwegian Seas as evidence for this process. The mechanism is assumed to involve a reaction between photochemically-produced methyl radicals and iodine atoms (Richter and Wallace, 2004). So although an essentially abiotic process, the methyl radicals are likely to be derived from a biological source, and hence an indirect biogenic control on the process exists (Richter and Wallace 2004).

The photochemical production of a number of dihalogenated compounds has also been investigated. Martino *et al.* (2005) observed the formation of CH_2ClI following the photolysis of CH_2I_2 (photolytic lifetime of ~12 minutes), with a yield of 25 – 30 percent. Natural and artificial seawater samples were irradiated using a 1-kW Xe lamp, with optical filters to simulate the solar spectrum at the Earth's surface. The

photolysis of CH_2I_2 occurs via homolytic scission of a C-I bond to form CH_2I and a significant amount of I radicals (Martino *et al.* 2005). The subsequent formation of CH_2ClI is the result of nucleophilic attack of Cl^- or Cl_2^- on the CH_2I radical:

$$CH_2I + Cl^- \rightarrow CH_2ClI + e^-(H_2O) \quad (16)$$

or

$$CH_2I + Cl_2^- \rightarrow CH_2ClI + Cl^- \quad (17)$$

Martino *et al.* (2005) reported that the photolysis of CH_2I_2 to give CH_2ClI has a yield of ~25 – 30 percent, and therefore constitutes an important source of CH_2ClI in surface seawater. This information supports field observations of CH_2I_2 depletions in surface seawater and the marine boundary layer, where this compound is likely to be photolysed before escaping to the atmosphere, whilst CH_2ClI is detectable (Martino *et al.* 2005). Similarly to Martino *et al.*, Jones and Carpenter (2005) revealed that when seawater is exposed to UV radiation, the photolysis of CH_2I_2, CH_2BrI and CH_2ClI leads to the production of CH_2ClI, CH_2BrCl and CH_2Cl_2, respectively.

1.7.2.1.5. Reactions with ozone and organic matter

Recent work has revealed an additional and previously un-described source of iodocarbons in surface seawater (Martino *et al.* 2009). Experiments on North Sea water, involving exposure to ambient levels of ozone led to the production of CH_2I_2, $CHClI_2$ and CHI_3. The production of these compounds is the result of reaction between DOM and hypoiodous acid/molecular iodine, formed in surface waters when ozone reacts with dissolved iodine.

1.7.2.2 Sinks

1.7.2.2.1 Air-sea exchange

The sea-to-air flux of volatile halogenated compounds from the marine environment represents the main source of halogens to the atmosphere (Class and Ballschmiter 1988; Klick and Abrahamsson 1992; Nightingale and Liss 2003; Richter and Wallace 2004). Figure 1.11 shows a box model of the global cycle of I and highlights the dominance of the ocean flux in the natural cycling of this element. The

main factors that affect the transfer velocity of gases from the oceans to the atmosphere (k, see Equation 11), and hence the overall rate of transfer to the atmosphere are principally wind speed and sea surface temperature, with smaller contributions from wave type, the effect of bubbles, temperature gradients and the presence of surfactants (Liss and Merlivat 1986; Nightingale and Liss 2003).

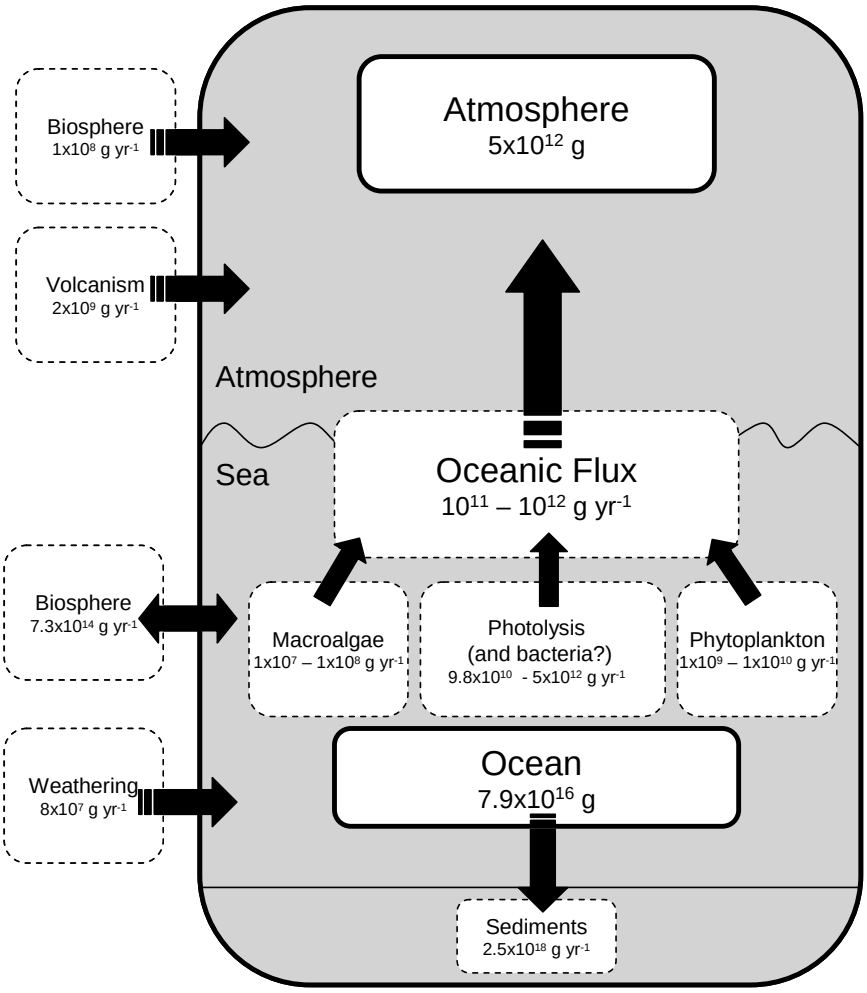

Figure 1.11. Box model of the annual global Iodine cycle.
(Miyake and Tsunogai 1963; Johnson 1980; 2003).

A number of attempts have been made to estimate the magnitude of the flux of volatile halocarbons from the oceans to the atmosphere, deriving information from the reasonably large database of seawater and air measurements (Klick and Abrahamsson 1992; Moore and Groszko 1999; Vogt *et al.* 1999; Carpenter *et al.* 2003; Quack and Wallace 2004; Butler *et al.* 2007). Of the iodocarbons, estimates of the flux of CH_3I show some consistency: (0.9 – 2.5) x 10^9 mol yr^{-1} (Moore and Groszko 1999), 2.1 x 10^9 mol yr^{-1} (Butler *et al.* 2007), and <3.3 x 10^9 mol yr^{-1} (Nightingale 1991). Only

two studies have estimated the flux of marine CH_2I_2 to the atmosphere, one estimating it to be of a similar order of magnitude to CH_3I (Klick and Abrahamsson 1992), while the other gave a figure of 5.7 x 10^7 mol yr^{-1}, somewhat lower than previous estimates for CH_3I (Vogt *et al.* 1999). Vogt *et al.* (1999) also gave estimates for the emissions of the following iodocarbons: 1-C_3H_7I 1.9 x 10^7 mol yr^{-1}, CH_2ClI 3.8 x 10^7 mol yr^{-1}.

Of the bromocarbons, $CHBr_3$ is considered to be the major carrier of organic Br to the atmosphere (Quack and Wallace 2004). Using data from numerous previous studies Quack and Wallace (2004) estimated a flux of 3 – 22 x 10^9 mol yr^{-1}. Butler *et al.* (2007) used data obtained from seven cruises over a ten-year period from a range of oceanic locations to give an estimate of 1.9 x 10^9 mol yr^{-1} from the open oceans, and a overall global flux of 10 x 10^9 mol yr^{-1}. The ten-fold difference between the open ocean and global flux estimates reflects the strength of the source of this compound from macroalgae in coastal regions. Butler *et al.* also estimated a flux of CH_2Br_2 of 0.6 x 10^9 mol yr^{-1} from the open oceans, and highlights the dominant role of $CHBr_3$ in the flux of Br to the atmosphere.

1.7.2.2.2 Hydrolysis and nucleophilic substitution

In seawater, methyl halides undergo attack by both nucleophiles and H_2O, resulting in their degradation *via* abiotic chemical processes (Moelwyn-Hughes 1938; Bathgate and Moelwyn-Hughes 1959; Zafiriou 1975; Elliott and Rowland 1993):

Nucleophilic substitution: $CH_3X + Y^- \rightarrow CH_3Y + X^-$ (14)

Hydrolysis: $CH_3X + H_2O \rightarrow CH_3OH + H^+ + X^-$ (15)

where X = I, Br, Cl, and Y = I, Br, Cl or other ion.

The significance of these removal pathways varies between methyl halides, and is dependent on seawater temperature (Elliott and Rowland 1993; Jeffers and Wolfe 1996; Jones and Carpenter 2007). For example, at 15°C CH_3Br has a half-life in seawater of 16 days, which falls to <2 days at 30°C (Jeffers and Wolfe 1996). For CH_3I, seawater concentrations have been reported to be negatively correlated with SST (Moore and Groszko 1999), a reflection of the temperature-dependence of removal processes. The removal of CH_3I from seawater is considered to be almost exclusively

by reactions with Cl^- and H_2O, at a rate similar to its typical sea-to-air flux, and there are so far no reports of its biological consumption (Jones and Carpenter 2007).

One study has assessed the chemical destruction of other mono-iodinated compounds in seawater (Jones and Carpenter 2007) and found that the rate of destruction varies considerably. Lifetimes in seawater with respect to chemical removal increased in the order: 2-C_3H_7I < CH_3I < C_2H_5I < 1-C_3H_7I.

Dark incubations of CH_2I_2 of > 1 week in duration revealed no nucleophilic substitution of this compound, with photochemical removal pathways occurring over much more significant timescales (Martino *et al.* 2005) (described in the following section).

1.7.2.2.3 Photochemistry

In situ observations of iodocarbons have produced evidence for their photochemical decay in surface seawater, in particular observations that the CH_2I_2 maximum occurred deeper in the water column than the CH_2ClI maximum, as well as difficulty in detecting CH_2I_2 in the marine boundary layer (MBL) (Yamamoto *et al.* 2001; Carpenter *et al.* 2003). Laboratory studies have now produced evidence for, and quantification of, these photochemical removal processes, demonstrating that the solar photolysis of CH_2I_2, CH_2BrI and CH_2ClI yields CH_2ClI, CH_2BrCl and CH_2Cl_2, respectively (Jones and Carpenter 2005; Martino *et al.* 2005) (See section 1.7.2.1.4 for further description).

1.7.2.2.4. Bacteria

Studies on the bacterial uptake of halocarbons have generally focussed on CH_3Br (Connell *et al.* 1997; Goodwin *et al.* 1997a; King and Saltzman 1997; Goodwin *et al.* 1998) with only one study that also considered $CHBr_3$ and CH_2Br_2 (Goodwin *et al.* 1998), and no reports of the bacterial removal of iodocarbons. These studies involved the addition of stable and radio-isotopes ($^{13}CH_3Br$, $^{14}CH_3Br$) to incubated seawater samples, with assessments made of the loss rates of these tracer compounds. By comparing whole seawater to filter-sterilised seawater, biological and chemical loss rates can be differentiated. Additionally, filter fractionating seawater samples allowed bacteria to be implicated in the removal of these compounds. The above studies have been performed on water from various oceanic regions, suggesting that the bacterial uptake of halocarbons may be a ubiquitous process. Additionally, these

studies suggest that biological loss processes may be significant even in warm oceanic waters where chemical losses are likely to be high.

1.7.2.3 Atmospheric consequences

Following exchange from the oceans to the atmosphere, volatile marine halocarbons undergo photolysis and oxidation to produce highly reactive halogen radicals. Such radicals are involved in a number of important atmospheric and climatic processes that are described in more detail in the following sections.

1.7.2.3.1 Sea-to-land transfer

The oceans represent the greatest source of iodine to the atmosphere, and the transfer of some of iodine to the land represents a crucial step in the geochemical cycling of iodine (Miyake and Tsunogai 1963; Fuge and Johnson 1986). This sea-to-land transfer of iodine, through both wet and dry deposition, is important in terms of human health – any human lacking adequate iodine in the diet is susceptible to a range of medical conditions, grouped under the general heading of Iodine Deficiency Disorders (IDD) which include cretinism, goitre, decreased fertility, increased perinatal death and infant mortality (Johnson 2003). Therefore it is important to understand the factors that control the availability of iodine in the environment.

1.7.2.3.2 New particle formation

In recent years, the potential climate influence of the atmospheric oxidation products of marine iodocarbons has received increasing attention. In 2001, it was demonstrated that iodocarbons such as CH_2I_2 and CH_2BrI can act as photolytic precursors to IO/OIO radicals in the marine boundary layer (Carpenter *et al.* 2001). Following this O'Dowd *et al.* (2002) used smog chamber experiments to show that, in the presence of ozone and UV radiation, new particles can form from realistic atmospheric concentrations of marine biogenic-derived IO/OIO radicals. This phenomenon is particularly pronounced in coastal zones with dense beds of macroalgae, and this particular study focused on activity over kelp beds at Mace Head, Eire. Similarly to DMS-derived aerosols, IO radical aerosols can indirectly influence climate through involvement with CCN and cloud formation, and thereby impact on the reflection of solar radiation (Andreae and Crutzen 1997). O'Dowd *et al.*

(2002) extended their experimental observations with aerosol formation model simulations, and concluded that even at open ocean concentrations the production of new particles is feasible, suggesting that marine iodocarbon emissions may exert a significant impact on global radiative forcing. Further modelling work has shown that IO radicals are most important for the growth for existing particles, rather than for the formation of new nuclei (Pechtl *et al.* 2005), with marine sulphate-derived aerosols being most important for the latter process. However, in the clean marine atmosphere, IO radicals can significantly contribute to both initial nuclei formation and to subsequent growth of particles to CCN sizes (Pechtl *et al.* 2005). The extent of the climate-regulating ability of marine I-derived aerosols is still not fully understood, but future changes to the production rate of iodocarbons in response to changing environmental and climatic conditions could potentially impact on local, and more speculatively, global radiative budgets.

1.7.2.3.3 Interactions with ozone

Ozone (O_3) is a highly oxidising atmospheric gas that performs a number of important roles: in the stratosphere (~25km above the surface of the Earth) it absorbs harmful solar ultraviolet-B (UV-B) radiation (Solomon 1999), and in the troposphere acts as a potent greenhouse gas and air pollutant (Ramaswamy *et al.* 2001; Buse *et al.* 2003; West *et al.* 2006). In polluted atmosphere of the Northern Hemisphere, the photo-oxidation of pollutants such as CH_4, NO_x and volatile organic compounds (VOCs) results in an increase in tropospheric O_3 (Crutzen 1974; Tang *et al.* 1998). This process leads to the formation of photochemical smog, and is responsible for causing a range of severe respiratory diseases and premature deaths in humans (Buse *et al.* 2003). However, the production of photochemical smog leads to an increase in hydroxyl (OH) radicals which are effective atmospheric cleansers, promoting the removal of greenhouse gases and other pollutants, such as CO, CH_4, NMHCs, SO_2, NO_x and CFCs (Tang *et al.* 1998). In clean, remote air, an increase in UV-B simply results in a decrease in tropospheric O_3 through photolysis in the presence of water vapour. This leads to an increase in OH radicals and an enhancement of the atmosphere's oxidative capacity (Tang *et al.* 1998).

The photolysis products of volatile marine halocarbons participate in a number of interactions with ozone. Halocarbon-derived free radicals (I, IO, Br, BrO) act as

effective catalytic ozone depleting species (Chameides and Davis 1980; Solomon *et al.* 1994; Davis *et al.* 1996). As iodocarbons are very photochemically active and thus have an atmospheric lifetime of only a few days to weeks (Solomon *et al.* 1994), their ozone depleting capacity is generally limited to the troposphere, where a significant impact on ozone levels is possible under certain conditions (Davis *et al.* 1996). Where strong atmospheric convection is experienced, iodocarbons can be rapidly transported to the upper troposphere and lower stratosphere, and can contribute to ozone depletion at these levels (Solomon *et al.* 1994). The ozone-depleting capacity of the more photolytically-stable and thus longer-lived bromocarbons exert a greater influence in the stratosphere (Wofsy *et al.* 1975).

Research into the extent of the impact of marine-derived I on ozone has received attention in recent years. Several modelling studies postulated tropospheric ozone loss through interactions with both Br and I emitted from the open ocean (Vogt *et al.* 1999; Glasow and Sander 2002; Yang *et al.* 2005) but these have not so far been verified by observations. *In situ* observations, supported by modelling studies, of ozone destruction pathways by halogen oxides over the open oceans have now been reported (Read *et al.* 2008), with the possibility that this data is typical of prevailing open ocean conditions. The authors reported 8 months of spectroscopic measurements, at the Cape Verde Observatory in the eastern Atlantic, which indicated the presence of ubiquitous daytime BrO and IO radicals in the tropical MBL. The mean daily observed ozone loss was ~50 percent higher than that simulated by global chemistry models that utilise photochemistry schemes that exclude halogen chemistry. Therefore, the work of Read *et al.* demonstrates that halogen chemistry exerts a significant and widespread influence on photochemical ozone loss in the tropical Atlantic MBL, and such processes may be common over the global oceans.

1.8 Research Aims and Objectives

Over the coming decades to centuries, OA is expected to have serious consequences for a range of marine biological and biogeochemical processes. The net production of trace gases in the open oceans, by phytoplankton, bacteria and abiotic chemistry, is considered to exert a significant effect on global climatic and atmospheric processes. Therefore the overarching aim of this work is to investigate how seawater concentrations of a range of climatically- and atmospherically-

important pelagic marine biogenic trace gases may respond to future OA, by testing the following hypothesis:

Future ocean acidification will significantly impact on the production of a range of pelagic marine biogenic trace gases, including halocarbons and DMS.

During this thesis, the hypothesis is tested through the following experimental approaches:

1. *Mesocosm CO_2-perturbation experiment.*

   The production of halocarbons and DMS is assessed during a mesocosm experiment, through the growth and decline of nutrient-stimulated blooms of phytoplankton, under two triplicated CO_2 treatments (Present day 380 ppmv, Future ~750 ppmv).

   Specific aims:

   - To obtain the first measurements of the response of a suite of halocarbons to CO_2-perturbation during phytoplankton blooms.
   - To gain further information on the response of DMS/DMSP to future high CO_2 conditions, following two previous studies (Avgoustidi 2007; Vogt *et al.* 2008).
   - To assess the response of trace gas concentrations to high-CO_2 conditions in relation to the response of the phytoplankton community.

2. *Laboratory CO_2 incubation experiments using natural community assemblages*

   The response of the production of halocarbons is assessed during two 3-week laboratory incubations of natural seawater assemblages from UK coastal waters, under two quadruplicated CO_2 treatments (Present day 380 ppmv, Future ~750 ppmv).

   Specific aims:

   - To assess the response of a suite of halocarbons to CO_2-perturbation during small-scale laboratory incubations of phytoplankton.
   - To assess the response of trace gas concentrations to high-CO_2 conditions in relation to the response of two compositionally-diverse phytoplankton communities.

The above approaches allow assessments of the impacts of OA to be made in carefully controlled conditions, and represent state-of-the-art tools in OA research. Nevertheless, there is a need to find existing sites that may function as "natural-analogues" to future OA (Orr *et al.* 2009), allowing assessments to be made to whole-communities that have potentially shown long-term adaptation to high CO_2 and low seawater pH, and thus are more representative of the communities of the future oceans. Therefore the final approach in this research involved:

3. Assessment of a naturally-acidified shallow marine site in Italy.

A volcanically-acidified shallow marine site in Ischia, Italy is investigated to infer its potential in studies of the impacts of OA on pelagic communities, and specifically, the net production of trace gases.

Specific aims:

- To assess the response of seawater trace gas concentrations to a natural pH gradient.
- To determine whether the pelagic community are adapted to the low seawater pH though prolonged exposure, and are therefore representative of the communities of the future oceans.

Following the description and discussion of each of the above experimental and *in situ* approaches, the final chapter of this thesis will draw comparisons with previous studies, explore the implications that changes to future trace gas production may have for atmospheric and climatic processes and recommend a number of areas that require further research.

Blank Page

CHAPTER 2
Methods of Marine Trace Gas Analysis

2.1 Introduction

The analysis of trace gas concentrations in seawater involves a number of steps. As seawater concentrations of the compounds of interest are low (DMS nanomolar (10^{-9}) and halocarbons picomolar (10^{-12})), they must firstly undergo extraction and concentration from seawater in order to reduce the volume of gas required for analysis. Following this, the compounds are separated with the use of gas chromatography. Finally, the compounds are detected and quantified. In the following chapter the full range of extraction, concentration, separation and detection methods by which seawater concentrations of both halocarbons and DMS were determined during this study will be described.

2.2 Analytical Procedures, Materials and Methods

2.2.1 Gas extraction and pre-concentration techniques

During this study, halocarbons were extracted from seawater, and concentrated prior to analysis using purge and trap. Purge and trap is a technique commonly used to extract volatile organic compounds (VOCs) from water samples for subsequent analysis by gas chromatography (GC) and various detectors. This technique involves passing a known volume of an inert gas, such as nitrogen, through a water sample. As the bubbles pass through the water, VOCs partition between the water phase and gas bubbles and are subsequently carried out of solution into the stream of gas. The efficiency of extraction of VOCs by purge and trap is dependent on the Henry's Law coefficient (H) (the concentration in air divided by the concentration in water at equilibrium) (Liss and Slater 1974) of the compounds of interest. VOCs with lower H values will be extracted more efficiently relative to compounds with higher values of H.

Following extraction from the water sample, the compounds are pre-concentrated before analysis by either being cryogenically-trapped or accumulated on an absorptive material. When the required volume of gas has passed through the

sample, the accumulation of VOCs is thermally desorbed in a stream of inert gas in order to carry it into the GC oven for separation and subsequent detection.

2.3 Halocarbon Analysis

2.3.1 Analytical techniques

2.3.1.1 Sample collection and preparation

Seawater samples were analysed for halocarbon concentrations according to the previously described methods of Hughes (2004; 2006; 2008), Chuck *et al.* (2005) and Martino *et al.*, (2005; 2009). Seawater samples were collected in 100ml glass syringes. Initially, approximately 50 ml of seawater was drawn up to thoroughly rinse the tubing and syringe, and then rejected. Next a small quantity was drawn into the syringe, which was then inverted and tapped so that any air bubbles could be expelled. Thus when the sample was drawn up into the syringe, there was minimal addition of air. Samples were injected with 2µl of an internal standard mixture (see section 2.3.2) and then injected into the glass purge tower for extraction of trace gases. If immediate processing of samples was not possible, the glass syringes were placed in a refrigerator or cool box in the dark. Samples were always processed within two hours of collection. Each sample was filtered before analysis, through a 0.7µm filter (GF/F Whatman) between two syringes, with an inline Swinnex filtration unit. Again it was ensured that introduction of air was minimised during the process.

2.3.1.2 Purge and cryogenic trap

The purge and trap system for halocarbons was constructed of stainless steel and glass (See Figure 2.1). Consistent with the methods of Hughes (2004; 2006; 2008) and Chuck *et al.* (2005), 40ml of seawater was purged for 20 minutes at a flow rate of 40 ml min^{-1}. With these volumes and flow rates, purge efficiencies range from 90 percent for lower molecular weight halocarbons (e.g. CH_3I) to 75 percent for higher molecular weights compounds (e.g. $CHCl_2Br$) (Chuck*, et al.*, 2005). Organic contaminants were eliminated from the purge gas using a hydrocarbon trap (Alltech Co. Ltd.). The purge gas was passed through glass wool (Supelco Co. Ltd.) to remove any aerosols, and dried using a static Nafion drier (Nafion tubing (International Science Consultants Co. Ltd.) surrounded by molecular sieve (10X) and two Nafion counterflow driers in succession (183 and 122 cm, Permapure C. Ltd.), with a counterflow rate of 100 ml min^{-1}. The target analytes were pre-concentrated in a non-

packed stainless steel sample loop, which was cooled in the headspace of a liquid nitrogen-filled dewar, thermostatically held at -150°C. Analytes were injected onto the GC column by heating the sample loop to ~100°C using boiling water. This method was used during the mesocosm experiment (Chapter 3).

2.3.1.3 Purge and trap on sorbent tubes

The use of commercial sorbent tubes in the analysis of seawater halocarbons has been developed by Claire Hughes (UEA), eliminating the need for liquid nitrogen, and reducing sample analysis time. However, initial attempts at the method were unsatisfactory for lower molecular weight halocarbons, so progressive modifications have been made to the method by Claire Hughes, and will be described in the following the section.

A purge system, consisting of stainless steel and glass was employed, as shown in Figure 2.2 and 2.3. Similarly to the cryogenic purge and trap method, 40 ml of seawater was purged, this time for 10 minutes, at a flow rate of 95 ml min^{-1}, according to the method developed by Claire Hughes. Target analytes were pre-concentrated onto Markes sorbent tubes (See Section 2.3.1.4.). In the early stages of the use of this method, sorbent tubes were held at ambient temperature (Used in Chapter 5). Due to lack of detection of the more volatile halocarbons (particularly CH_3I and C_2H_5I) it was recognised that lower temperatures would be required to trap such compounds, so the first modification to the method involved holding the tubes at ~10°C inside a small chiller (Used in Chapter 4). Although this method improved the detection of CH_3I and C_2H_5I, large temperature fluctuations inside the chiller during opening and closing to place and remove tubes resulted in variations in sensitivity. The method was improved by placing the sorbent tube in an electronically-cooled block held at 1°C during sample extraction (Chapter 5 – Ischia) (Figure 2.3). These methods will be described in further detail in the following sections.

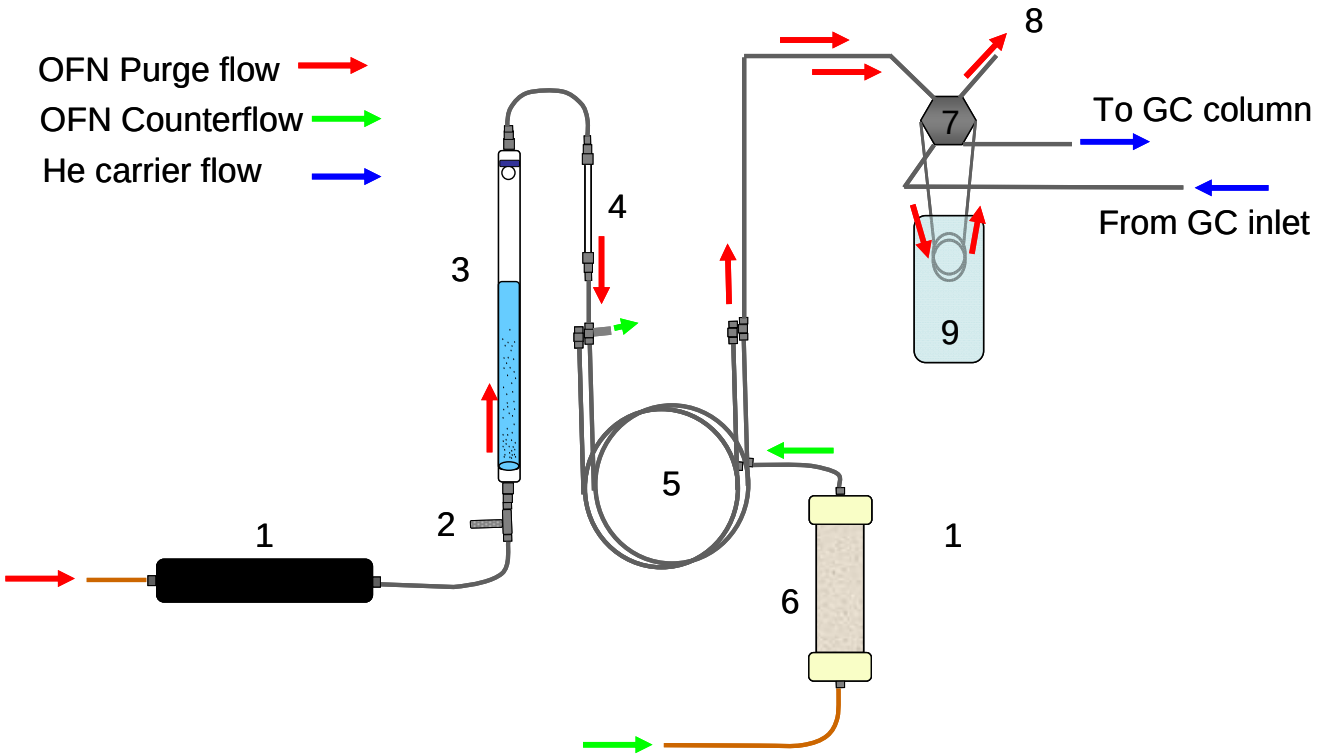

Figure 2.1. Schematic diagram of purge and cryogenic trap system. 1. Hydrocarbon trap (Restech), 2. Swagelok stainless steel metering valve, 3. Glass purge tower, 4. Glass wool in ¼" glass tubing, 5. 2 x Counterflow Nafion drier, 6. Static nafion drier for counterflow gas, 7. 2-way 6-port stainless steel valve, 8. Vent, 9. Stainless steel sampling loop suspended in cooled headspace of liquid-nitrogen dewar at -150°C. OFN = Oxygen-free nitrogen.

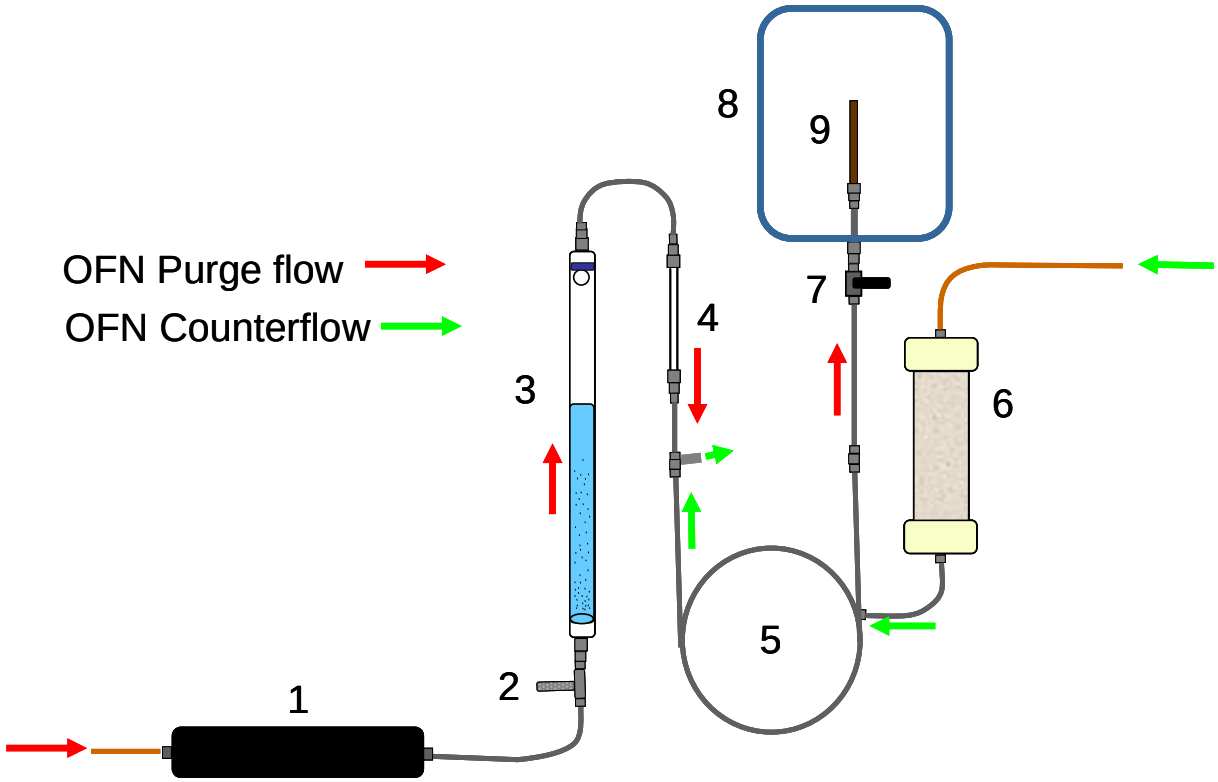

Figure 2.2. Schematic diagram of the purge systems using Markes tubes held in a chiller
1. Hydrocarbon trap (Restech), 2. Swagelok stainless steel metering valve, 3. Glass purge tower, 4. Glass wool in ¼" glass tubing, 5. Counterflow Nafion drier (183cm, Permapure), 6. Static nafion drier, 7. 2-way stainless steel valve, 8. Chiller, 9. Cajon stainless steel fitting and Markes tube. OFN = Oxygen-free nitrogen.

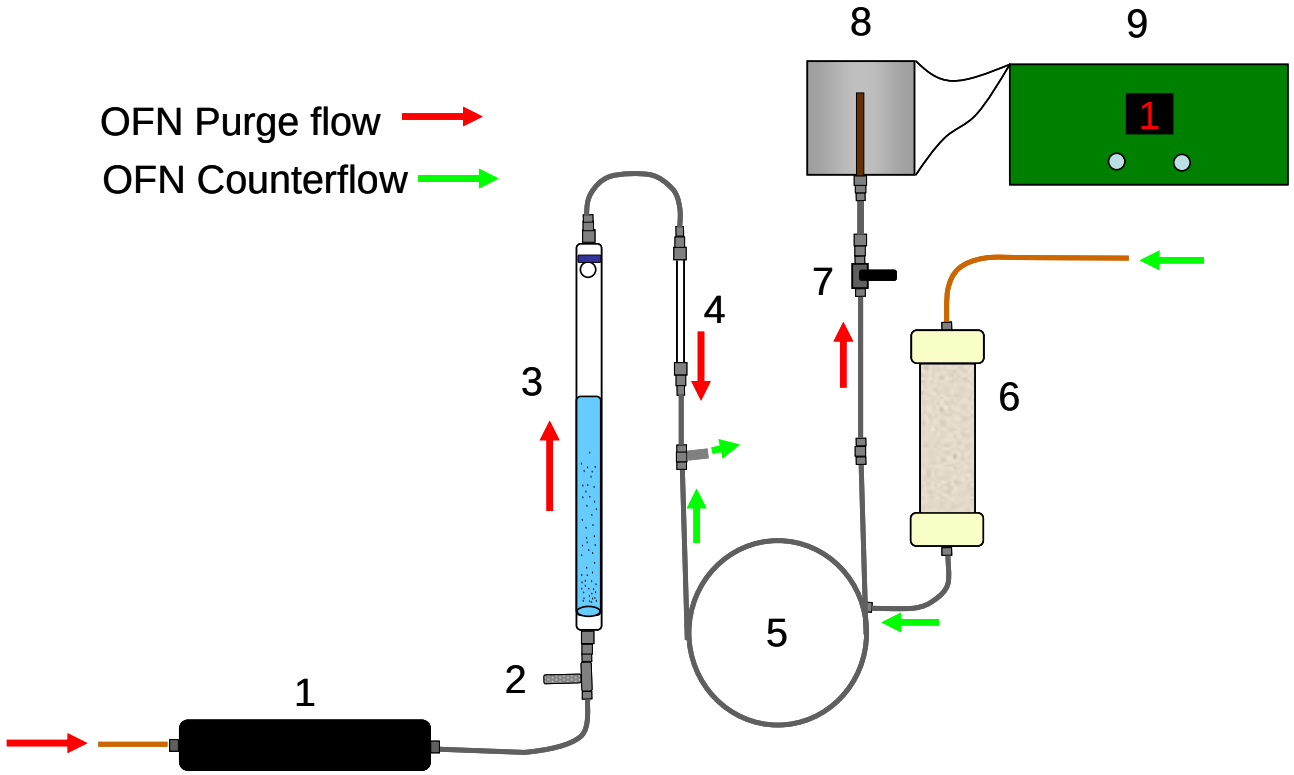

Figure 2.3. Schematic diagram of the purge systems using Markes tubes held in an electronically-cooled block.
1. Hydrocarbon trap (Restech), 2. Swagelok stainless steel metering valve, 3. Glass purge tower, 4. Glass wool in ¼" glass tubing, 5. Counterflow Nafion drier (183cm, Permapure), 6. Static nafion drier, 7. 2-way stainless steel valve, 8. Peltier-cooled tube block, 9. Temperature control unit. OFN = Oxygen-free nitrogen.

2.3.1.4 Markes UltrA autosampler and Unity TD platform

Following purge and trap, the quantification of halocarbon concentrations using Markes sorbent tubes begins in the Markes International UltrA multi-tube autosampler and Unity thermal desorption (TD) platform. This system is a combined autosampler/thermal desorption system, with the capacity to process up to 100 Markes sorbent tubes at a time. In preparation for TD, the tubes are sealed with Difflok caps, which are pushed onto each end in order to both prevent loss of analyte and introduction of artefacts, whilst allowing thermal desorption to be performed. The tubes are then placed into a tray in UltrA. A PC-controlled software programme controls the process. A two-stage desorption process was used, comprising of a secondary refocusing mechanism to concentrate analytes from the sorbent tube before discharging them into the analytical system. This method minimises the vapour volume as much as possible. The following section will describe the principles and application of the UltrA/Unity system in more detail.

Thermal desorption (TD) is a method by which samples are heated in a stream of inert gas allowing target analytes to be extracted into the vapour stream. For this study, volatile halogenated compounds were retained on a triple-sorbent bed inside a stainless steel sorbent tube (Markes International Ltd.). The tubes are industry standard for TD and measure 3 ½" long x ¼" OD. They are packed with the sorbent material by Markes International Ltd. before shipment and have a lifetime of around 200 thermal cycles, after which time the sorbent material needs to be replaced. Samples were collected by passing a stream of inert gas carrying the target analytes through the tube, at a maximum flow rate of ~100 ml $minute^{-1}$. The volatile halogenated compounds were adsorbed onto a triple-sorbent bed of increasing strength, comprising Tenax TA, Carbograph 1TD, Carboxen 1000 (See Figure 2.4 and Table 2.1).

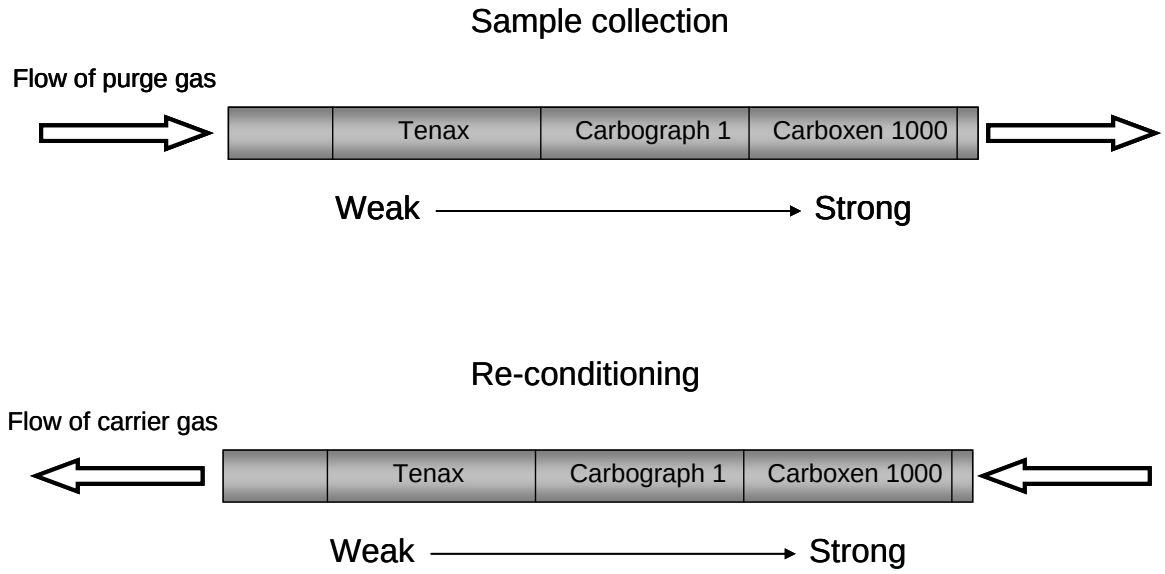

Figure 2.4. Markes sorbent tubes with a triple-sorbent bed.
Direction of gas flow during sample collection (top) and tube re-conditioning (bottom). Sorbents increase in strength with sample carrier flow direction. Flow is reversed during re-conditioning.

Table 2.1. Markes tube sorbents – properties and characteristics.
The Markes tubes used for halocarbon analyses contain a triple sorbent bed comprising of three sorbents: Tenax TA, Carbograph 1 TD and Carboxen 1000. Details of sorbent strength, analyte volatility range and maximum operating temperature are shown.

Sorbent	**Absorbance Strength**	**Approximate analyte volatility range (B.P. = boiling point)**	**Sorbent max. temp (°C)**
Tenax TA	Weak porous polymer	n-C_7 to n-C_{30} B.P 100 to 450°C	350
Carbograph 1 TD	Medium carbon black	n-$C_{5/6}$ to n-C_{14}	>400
Carboxen 1000	Very strong carbon molecular sieve	Permanent gases and light hydrocarbons C_2 to C_3 B.P. -60 to -80°C	>400

Once a sample had been collected, the tube could be sealed using Swagelok ¼" brass caps and plugs with nylon ferrules. By storing the tubes at -20°C in this fashion, they could be kept for up to 9 months before analysis. All compounds except CH_3I and C_2H_5I can be stored for this length of time with no significant loss of analyte (Claire Hughes, *pers. comm.*).

The following analytical steps took place in UltrA:

1. Leak Test.

One tube at a time was loaded into the analytical position and sealed into the carrier gas flow path. Firstly, an automated ambient temperature-no flow leak test was performed to ensure there are no leaks. If a leak was detected, the tube was unloaded, then re-loaded and a second leak test performed. If the tube again failed the leak test, the sample run was aborted. If the sample was to be processed in the presence of a leak, some of the sample could be lost and the result would not be accurate.

2. Carrier gas purge ("Pre-purge").

Each tube was thoroughly purged in order to remove all air before heating. If oxygen was present during the heating process, there was the risk of oxidation of both sorbent and analyte, with the production of interfering artefacts. For this study, the pre-purge was 1 minute in duration.

3. Primary (tube) desorb.

During this process, the sample tube was heated to 200°C for 5 minutes, desorbing the sample which was swept through a short heated transfer line in a flow of carrier gas into the cold trap in Unity where the sample is trapped and re-concentrated at -10°C.

The final step was performed in Unity:

4. Cold trap desorption

After 5 minutes of primary tube desorption, the cold trap underwent rapid heating up to 290°C at a rate of ~100°C min^{-1}. This triggered the GC run to start. The cold trap was held at 290°C for 4 minutes and during this process the sample flow path was directed through the heated transfer line into the GC column (Figure 2.5). The cold-trap consisted of an electronically-cooled Unity "Water Management Trap" (Markes International Ltd.) held at -10°C, comprised of a 60 mm glass tube packed with a quadruple-sorbent bed (Quartz wool, Tenax TA, Carbograph 1TD, Carboxen 1000) and suitable for volatile organic compounds from ethane to n-C_{20}. Following refocusing at -10°C, the cold trap undergoes rapid heating up to 290°C (100°C sec^{-1}) in a reverse flow of carrier gas and a 100-200 µl of vapour was carried

to the analytical system for detection. Such small sample volumes have minimal band spreading and therefore optimise detector response.

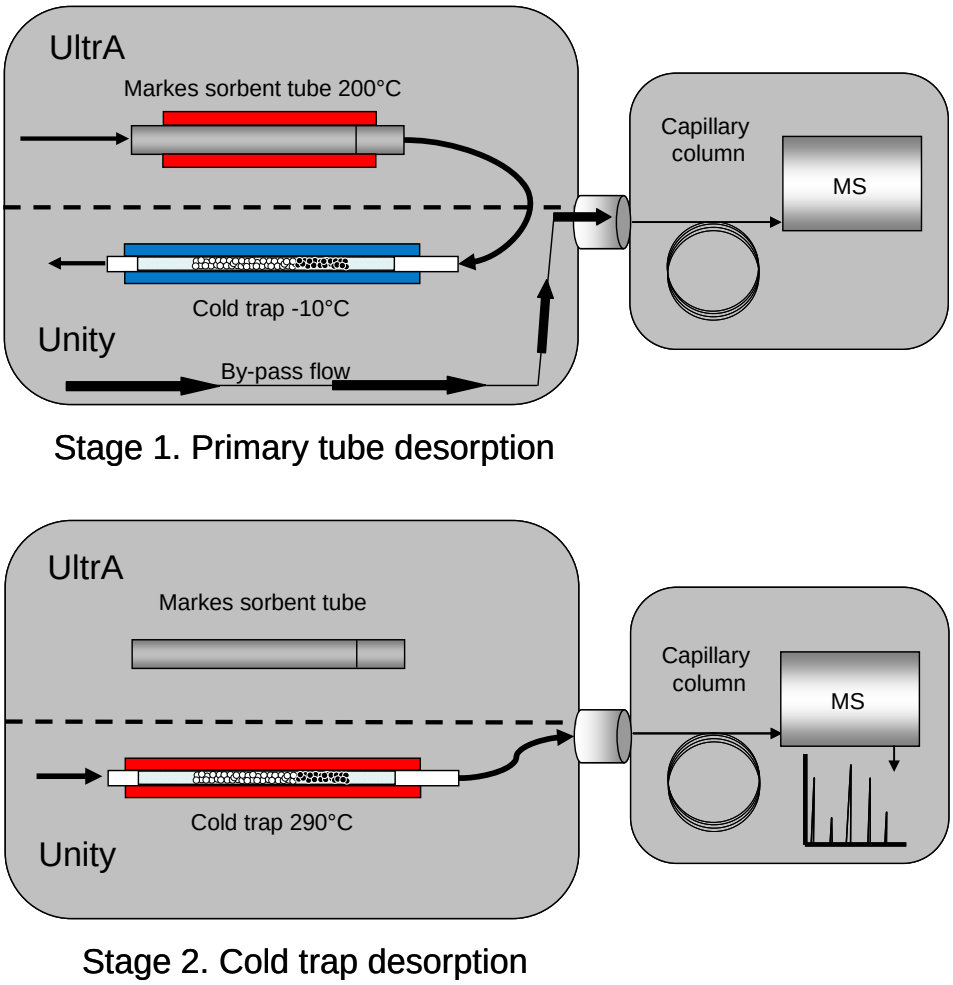

Figure 2.5. 2-stage thermal desorption in UltrA/Unity.
Modified from a diagram on www.markesinternational.com

Following use, the sorbent tubes were re-conditioned to prepare them for the next sample collection (Figure 2.4). A Markes TC-20 tube conditioning oven was used to re-condition 20 tubes at a time on a manifold. A flow of inert gas (oxygen-free nitrogen, OFN)) was passed through the tubes in the opposite direction to that during sample collection, in addition to being heated at four temperatures in order to remove all VOCs, according to the following programme:

1. 20 minutes at 100°C
2. 20 minutes at 200°C

3. 20 minutes at 300°C
4. 20 minutes at 320°C (Close to upper thermal limit of Tenax)

Following re-conditioning, the tubes were allowed to cool whilst OFN was still flowing through them, then capped and sealed with Swagelok ¼" brass caps and plugs with nylon ferrules until next use. The extraction of volatile halogenated compounds from seawater using purge and trap on Markes sorbent tubes was used for the majority of the work presented. However, due to on-going development of this technique by Claire Hughes over the duration of this research, the methods were used in three different ways:

1. Trapping at ambient temperature

During the early stages of development of the method, the sorbent tubes were held at ambient temperature whilst trapping. The most volatile of the halocarbons of interest - CH_3I - requires low temperatures to enable it to be trapped onto the sorbents, and in addition, has the shortest storage time on the tubes. Therefore, this method was used where long-term storage of the tubes before analysis was anticipated. During the first field campaign to Ischia, the analytical system for halocarbons was not transported to the field location, so all halocarbon samples were to be stored on sorbent tubes, and analysed on return to the UK. Therefore CH_3I could not be quantified during this fieldwork campaign and there was no need for cooling during trapping onto sorbent tubes.

2. Trapping on Markes tubes in a chiller

During the development of this technique, it became apparent that the ability to trap and analyse CH_3I was affected by the temperature. When the tube was cooled down, trapping efficiency of CH_3I was improved, and the response of all other compounds also increased. Therefore, small commercially-produced chillers (WAECO "My Fridge" mini chiller, serial number 05012079, 19cm x 31cm x 28cm) were modified so the sorbent tube could be positioned inside whilst trapping samples at a temperature of approximately 10-13°C (Figure 2.2A). This method was used during the seawater incubation experiments (Chapter 4). There were some limitations - the temperature inside the chillers fluctuated whenever the door was opened and closed to place and remove sample tubes, causing variations in trapping efficiency of CH_3I and C_2H_5I. However, it showed the method could be improved and led to the development of a more reliable technique described below.

3. Trapping on Markes tubes with Peltier-cooling

A Peltier-cooled tube block was designed by Claire Hughes and Sue Turner and constructed in-house at UEA. The sorbent tube could be placed securely inside an electronically-cooled metal block. A temperature control box held the temperature at 1°C (Figure 2.2B). This system greatly improved the sensitivity of all compounds, allowed reliable detection of CH_3I and C_2H_5I, and provided a very stable temperature for consistency of samples. This method was used during the Spring field campaign to Ischia.

2.3.1.5 Gas Chromatograph – Mass Spectrometer (GC-MS) system and methods

Gas chromatography (GC) is a method by which complex mixtures of volatile compounds within a sample can be separated and individually quantified. The sample to be analysed is vaporised on injection into the GC or injected in a gaseous form, then carried on a flow of inert gas into a column. Depending on the requirements, the temperature of the oven may be held isothermally, or subjected to a program of gradually increasing temperature. Differences in the volatility between the components of the mixture and the coating/sorbent of the column leads to a differential separation of the components that then exit the column at different times. The time a compound leaves the column and is detected is referred to as the retention time (RT), and is a function of the absorptive characteristics of individual compounds. The most soluble compounds are retained for the longest time on the column, so leave the column after the less soluble compounds (McMaster and McMaster 1998; Watson and Sparkman 2008). A range of detectors are used in conjunction with GC in order to identify the components of a sample.

GC does have a number of disadvantages – the main one being that there is a lack of certainty as to the true identity of detected compounds. Identification of compounds by most GC detectors is based on the retention time of compounds on the column. A peak is produced by the detector, giving a measure of the intensity of the response. As a number of compounds may elute from the column at the same time, definitive identification of the compounds in a separated peak is difficult (McMaster and McMaster 1998).

Mass spectrometry is an analytical technique that enables identification of compounds based on the mass-to-charge (m/z) ratio of composite ions, where mass is

in Daltons (Da). The ions are separated according to their m/z and a mass spectrum is produced, giving a representation of the abundance of ions in the gas phase as a function of their m/z ratios (Budde 2001; De Hoffmann and Stroobant 2007). Consequently, a major advantage of MS is that the only information needed to interpret most spectra is the masses of the major isotopes of the elements. Furthermore, MS possesses high sensitivity to minute quantities (10^{-9} – 10^{-15} g) of analyte, allowing the use of smaller, less expensive and more convenient samples (Budde 2001). MS is an exceptional tool for clearly identifying the structure of a single compound. Nevertheless, this proves to be less useful when analysing a mixture of compounds, as is often the case with environmental samples. Therefore, combining GC and MS into one analytical system allows efficient separation of individual components of a mixture through GC, followed by identification and quantification of each compound by MS (McMaster and McMaster 1998; Watson and Sparkman 2008).

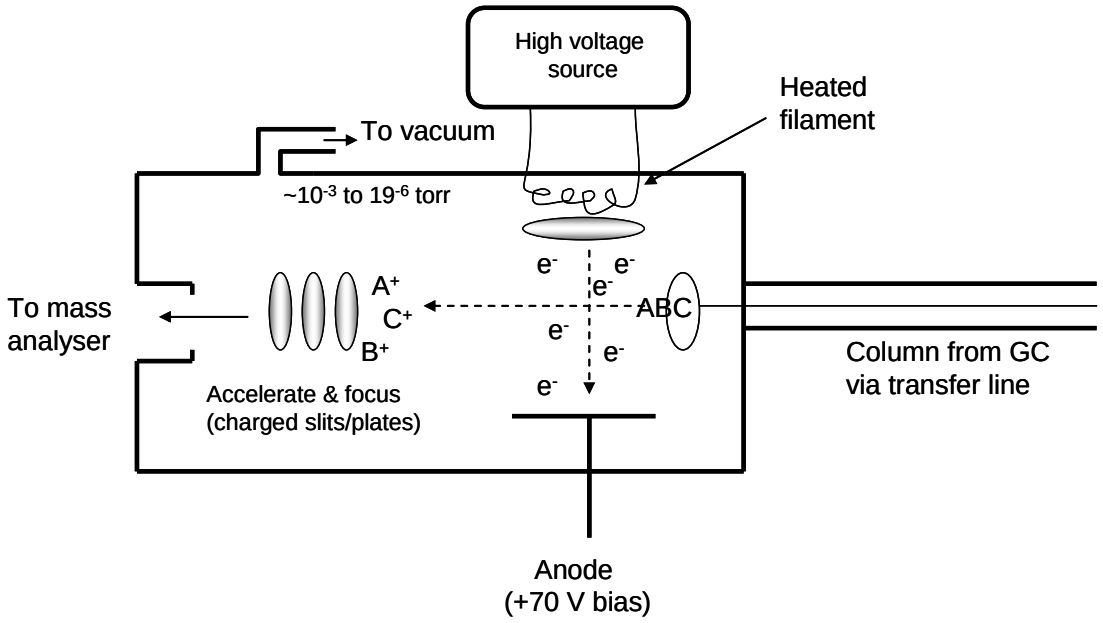

Figure 2.6. Schematic of the process of Electron Ionization (EI) within a mass spectrometer.

A mass spectrometer is made up of three key components, each of which plays an important role in the process of MS. As sample vapour leaves the GC, it immediately enters the MS where it undergoes electron ionization within the ion source. During this stage, energetic electrons are emitted from an electronically-heated filament under vacuum, and focused into the sample path (Figure 2.6) (Budde 2001). The molecules within the sample path are transformed into gas-phase ionized fragments (De Hoffmann and Stroobant 2007):

$M + e^- \rightarrow M^{-+} + 2e^-$ (1)

The energy of the energising electrons is 70eV, a value far greater than the ionization potential of all compounds and elements (Budde 2001). Next, the ions enter the highly evacuated analyser chamber where a scannable magnetic field is used to separate them according to their m/z. Only specific fragments are allowed to exit into the detector where the abundance of ions is measured. The scanning magnetic field continues throughout the sample run, starting as soon as the samples enters from the GC, and ending when the GC has completed its temperature program. Finally, a signal, which varies according to the amount of analyte eluting from the GC column, is sent to the processing software of a computer. A chromatogram is produced, plotting time vs. total ion chromatogram (TIC). All the intensities yielded during each scan of the magnetic field for each m/z fragment are added together to give this TIC detector signal. In addition, the abundance of ions is calculated to produce a mass spectrum. The most intense peak of a mass spectrum is called the base peak, and is given a relative abundance of 100 percent. The abundances of all other peaks are calculated relative to the base peak.

As MS operates under very low pressures (~10^{-5} Torrs), GC-MS requires the use of a capillary column, comprising a fused silica tube with polyimide coating, and a chemically-bonded stationary phase. The low pressures are maintained with the use of constant pumping with a vacuum pump. The capillary column is plumbed directly into the ionisation source, and compounds are kept in the gas phase once leaving the GC oven by travelling through a heated transfer line across the GC-MS interface.

During this study, halocarbon samples were determined using an Agilent Gas Chromatograph (GC 6890N) and Mass Selective Detector (5975 Series MSD), with a 60m DB-VRX capillary column installed (0.32 μm film thickness, J & W Ltd.). Following cryogenic purge and trap and subsequent introduction of the samples into the GC, the oven was held at 40°C for 2 minutes, heated up to 130°C at 8°C min^{-1}, then 200°C at 60°C min^{-1} and held for 2 minutes, and finally heated up to 240°C at 60°C min^{-1} and held for a 2 minutes. The total runtime was 19.08 minutes, and the data was collected between 3 and 13 minutes of the run. The set up of the total analytical system using Markes UltrA and Unity is shown in Figure 2.7. The GC program for samples introduced via the Markes Unity was as follows: the oven was held at 40°C for 5 minutes, then heated to 200°C at a rate of 20°C min^{-1} and held for 2

minutes. Finally the oven was heated to 240°C at a rate of 20°C min^{-1} and held for 4 minutes. The total runtime was 21 minutes, and data was collected between 6 and 14 minutes of the run. Data was collected and integrated using ChemStation chromatography data handling software.

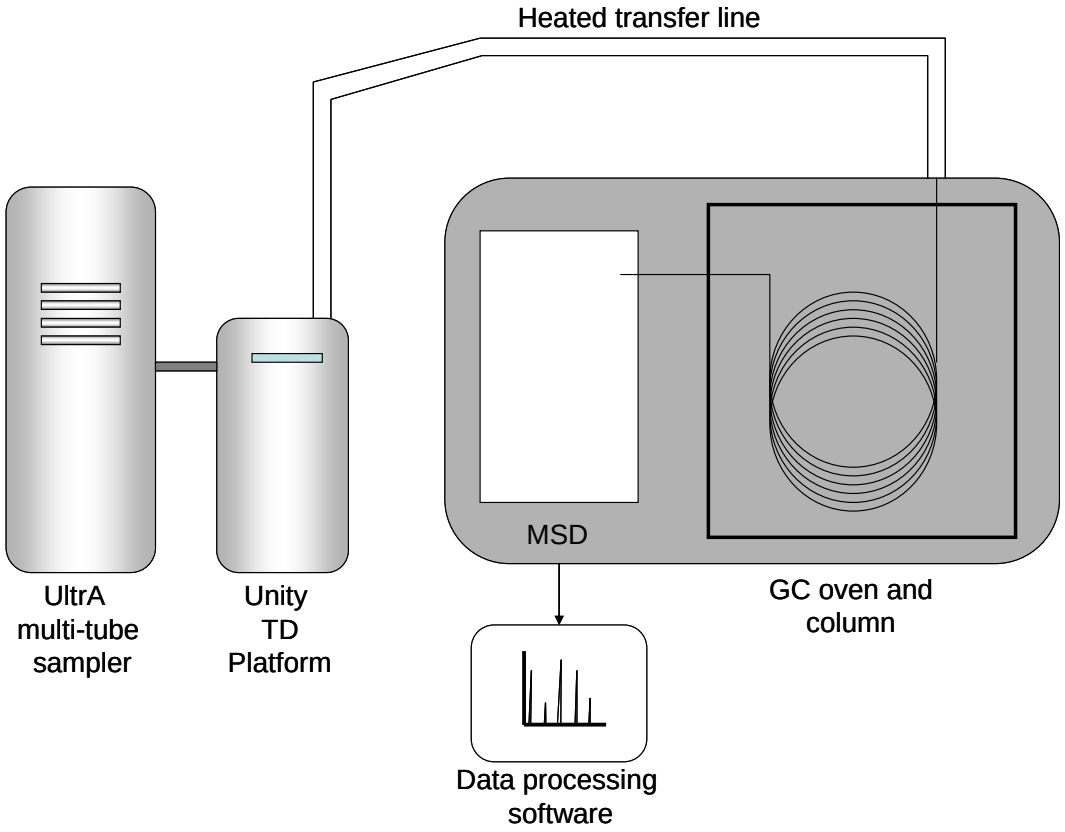

Figure 2.7. Set-up of the analytical system for halocarbon analyses using the UltrA multi-tube autosampler and Unity TD platform.

The MSD was operated in electron ionization (EI)/ selective ion monitoring mode (SIM) throughout the analyses. SIM mode is a means of detecting and recording only certain ions at selected m/z values (Watson and Sparkman, 2008). This method ensures more time is available to be spent measuring the ion current of ions of interest rather then using up measurement time at m/z vales where there may be no ion current, and provides a lower limit of detection and higher quantitative precision (Watson and Sparkman 2008). A SIM programme can be created whereby detection of specific ions can be changed as a function of time, permitting the best possible detection of the components of a sample. In this way, the detector can monitor for a small number of ion currents (2 – 6) during a specified time period when the analogous compounds are expected to be emerging from the GC (Watson and

Sparkman 2008). An example of a SIM programme used during this study is shown in Table 2.2.

Table 2.2. SIM programme was used during halocarbon analysis with UltrA/Unity-GC-MS.

Target compounds	Target ions	Start time (mins)
1. CH_3I CD_3I	142, 145, 127	6.30
2. C_2H_5Br	108, 110	7.15
3. C_2H_5I	156, 127	8.20
4. 2-IP, 2-IP(D)	170, 177, 127	9.00
5. CH_2Br2	174	10.10
6. CH_2ClI, 1-IP	176, 170, 127	10.40
7. CH_2BrI	222, 141	12.00
8. $CHBr_3$	173, 175	12.80
9. CH_2I_2	268, 141	13.20
10. $CHBr_2I$, $CHClI_2$	300, 302	14.00

The performance of the GC-MS was validated by tuning against an internal calibration compound, perfluorotributylamine (PFTBA). This process, known as autotuning and controlled by the ChemStation software, was performed when deemed necessary, i.e. following a period of instrument down-time, or when a change in sensitivity had been observed.

2.3.2 System sensitivity drift and surrogate analytes

Instrument sensitivity drift is a problem inherent to the use of analytical instruments such as GC-MS. Sensitivity drift is defined as progressive change in sensitivity over time, and can result in poor repeatability relative to that which would be achievable under drift-free conditions (Winchester and Miller 2000; Morris 2001). If no correction is made, sensitivity drift can have negative effects on data quality and may create a large source of bias (Winchester and Miller 2000). Potential causes of sensitivity drift during analysis of halocarbons by purge and trap/GC-MS have previously been discussed by Hughes (2004), and could potentially occur at any stage in the analysis of halocarbons, from sample preparation, to separation, to detection, to quantification.

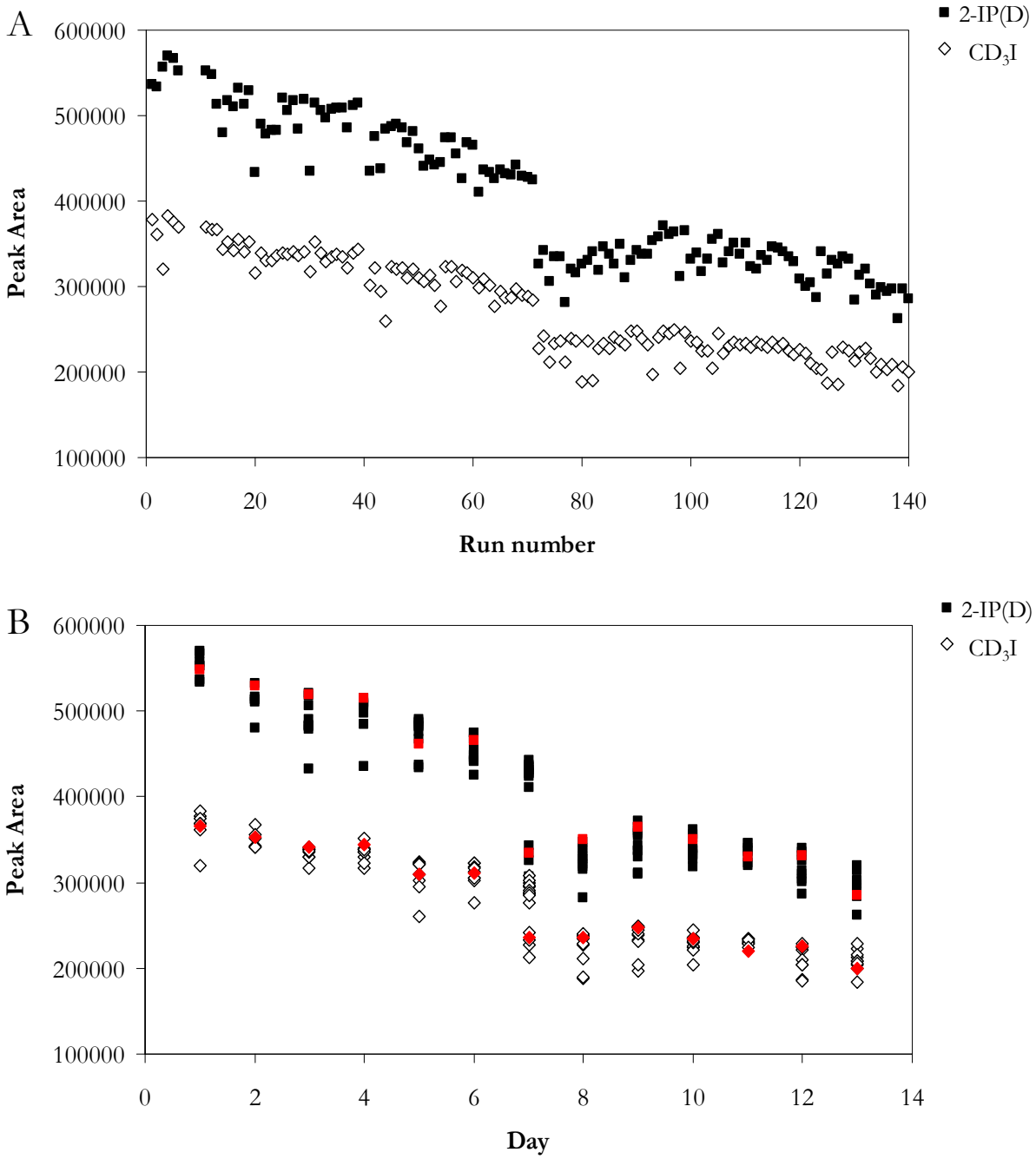

Figure 2.8. System drift during the mesocosm experiment using cryogenic purge and trap. Plotted against A. Run number and B. Day. Closed squares = 2-IP(D) and Open diamonds = CD_3I. The drop in sensitivity at run ~75, day 7, occurred immediately following an MS tune. The red data points show the last measurement taken every day.

Figure 2.8 shows an example of typical CD_3I and 2-IP(D) peak areas, measured during the mesocosm experiment (Chapter 3). In general, there is a pattern of decrease in sensitivity with increasing run number. This can be attributed to a

recognized phenomenon, resulting from the build-up of deposition products on ion source walls, repeller and lens, inside the MSD. As deposits increase on the ion source surface, ionization efficiency, and consequently, sensitivity of the detector decrease (Hughes 2004). Ion source deposition products can be removed by periodic abrasive cleaning of the affected parts, and detector sensitivity is increased as a result. This intrinsic instrument bias can be overcome by including surrogate analytes in the analysis of target compounds, allowing stringent quality control and consistency of data.

The purpose of surrogate analytes is to monitor both the method, instrument and analyst performance, and allow for the correction of instrumental performance and drift for sample consistency. Surrogate analytes have a defined set of characteristics; ideally they should be pure and chemically and thermally stable, and very unlikely to occur in samples (Budde 2001). With these requirements in mind, deuterated iodocarbons have been employed for use in the analysis of seawater concentrations of halocarbons (Hughes 2004; Martino *et al.* 2005; Hughes *et al.* 2006). These compounds are considered to reliably replicate system sensitivity drift of target analytes and would almost certainly not occur in natural samples (Hughes 2004). As it is unfeasible to have separate surrogate analytes for each compound in a study such as this where numerous compounds are under consideration, just two compounds are used: deuterated methyl iodide (CD_3I) (Sigma Aldrich, 99.5 atom % D) and deuterated 2-iodopropane (CD_3CDICD_3 or 2-IP(D)) (Sigma Aldrich, 98 % atom D). For the compounds with the highest sensitivities (CH_3I and C_2H_5I) changes in CD_3I peak were used to correct instrument drift, and 2-IP(D) was used for the compounds with lower sensitivities (CH_2ClI, CH_2I_2, $CHBr_3$, CH_2Br_2, $CHBr_2Cl$). The primary standards were prepared gravimetrically, and the secondary and working standard by serial dilution of microlitre volumes into HPLC-grade methanol (Fisher Scientific). Working standards of both surrogate analytes were aliquoted into one 4ml amber vial and stored in the freezer at -20°C. Immediately before analysis, 2µl of the surrogate analyte mixture was directly injected into a syringe containing 40ml seawater samples using a Hamilton repeating dispenser syringe.

A daily reduction in sensitivity, attributed to a build-up of humidity and non-target analytes in the system has previously been discussed (Hughes 2004). However, in this study, a reduction in sensitivity over the course of a day was generally not seen. Figure 2.8B shows peak areas of the surrogate analytes on consecutive days during the mesocosm experiment. The red data points show the last measurement

taken every day. It is clear that these do not represent the lowest peak areas measured on each particular day.

2.3.3 Halocarbon system calibrations

Calibration and quantification of all halocarbons shown in Table 2.2 was performed using liquid standards prepared in our laboratory. Standards were made up by dilution of the pure halocarbon compounds (see Table 2.3) into HPLC-grade methanol (Fisher Scientific), and each compound was calibrated individually.

Table 2.3. Purity, molecular weight and density (g/ml at 25°C) of pure halocarbon standards (Sigma Aldrich and Co.).

Compound	Purity %	Molecular weight	Density g/ml at 25°C
CH_3I	99.0	142	2.28
C_2H_5I	98.0	156	1.95
CH_2ClI	98.0	176	2.422
CH_2I_2	98.0	268	3.32
1-C_3H_7I	99.0	170	1.743
2-C_3H_7I	99.0	170	1.703
$CHBr_3$	99.0	253	2.89
CH_2Br_2	99.0	174	2.477
$CHBr_2Cl$	98.0	208	2.451
CH_2BrCl	99.5	129	1.991

The primary standard was prepared gravimetrically, and the secondary and working standard by serial dilution of microlitre volumes. Microlitre volumes of the working standard and 2 µl of surrogate analyte mixture (see section 4) were injected into 40 ml of pre-purged seawater. In order to prepare this seawater, it was pre-filtered then placed in a 2 litre custom-made glass purge vessel, and purged with oxygen-free nitrogen at a flow rate of 100-200 ml min^{-1}. Volatile organic contaminants, including all halocarbons, were stripped from the purge gas using a hydrocarbon trap (Alltech Co. Ltd.). Seawater was purged for up to 24 hours in order to produce halocarbon-free seawater. The pre-purged seawater was then processed as a sample, starting with purge and trap, followed by analysis by GC-MS. Surrogate analyte peak areas collected during each calibration were used to correct standard peak areas for

system sensitivity drift (ratio of analyte and surrogate analyte peak area) and produce a response factor. Halocarbon concentrations were determined from plots of this response factor vs. known concentration of standard. Calibration curves were produced at approximately two week intervals, or following tuning of the GC-MS, and up to three calibration checks were carried out daily. Figures 2.9 and 2.10 show typical calibration curves for two selected halocarbons (CH_3I and CH_2ClI). The figure shows both raw peak area data (a) and data that has been drift-corrected relative to their respective surrogate analytes (CD_3I and 2-IP(D). As is clearly shown, the drift-correction greatly improves the precision of the calibration, with an increase in the least squares correlation coefficient R^2 value relative to the uncorrected data. This is particularly clear for CH_2ClI, which experienced an increase in R^2 from 0.9353 to 0.9998 following drift-correction. This demonstrates that the use of surrogate analytes in purge and trap/GC-MSD analyses of halocarbons is an effective means of system sensitivity drift correction.

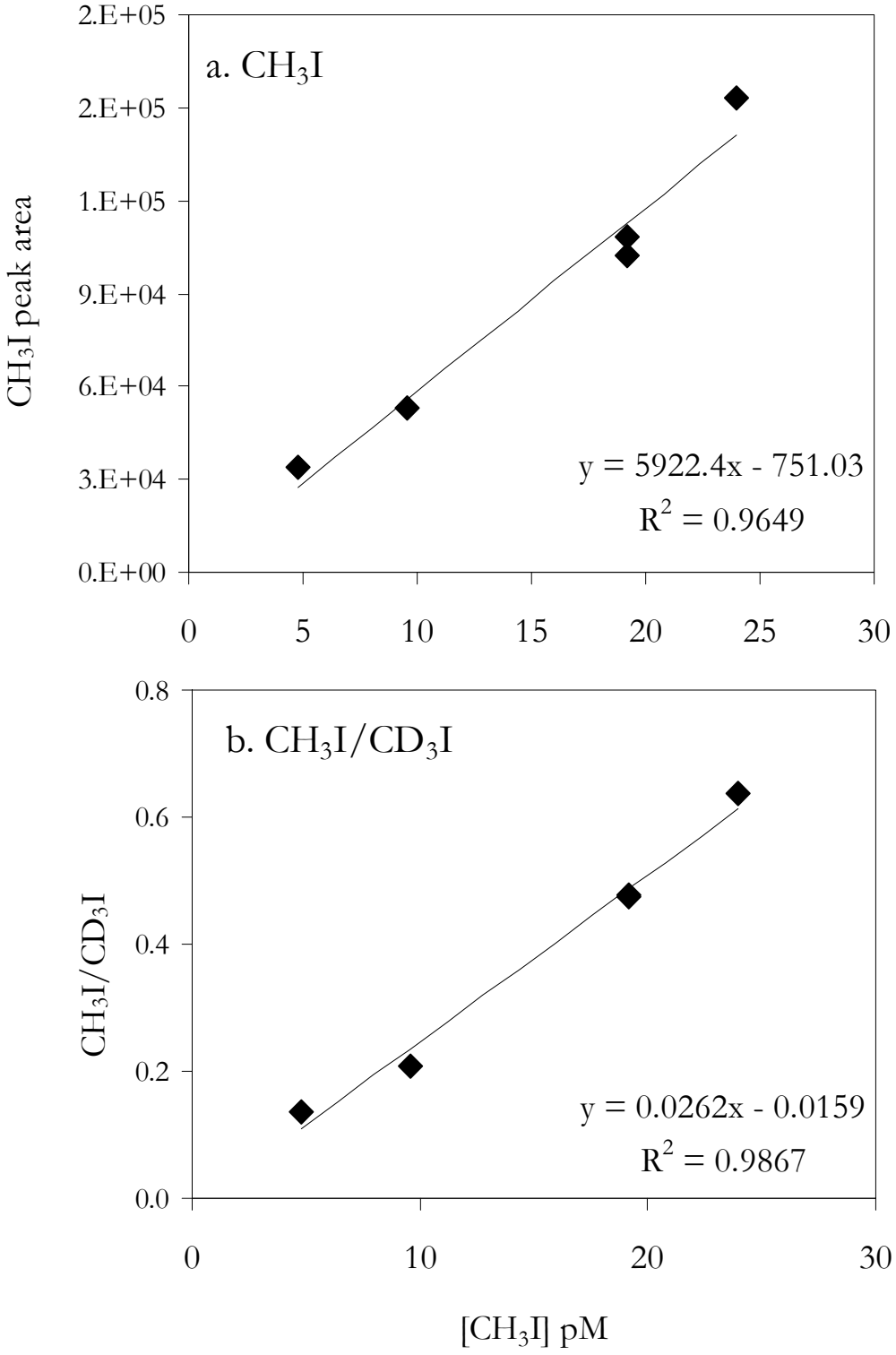

Figure 2.9. Typical calibration curve for CH_3I, showing a. CH_3I peak area only, and b. Drift-corrected CH_3I, using ratio of CH_3I/CD_3I.

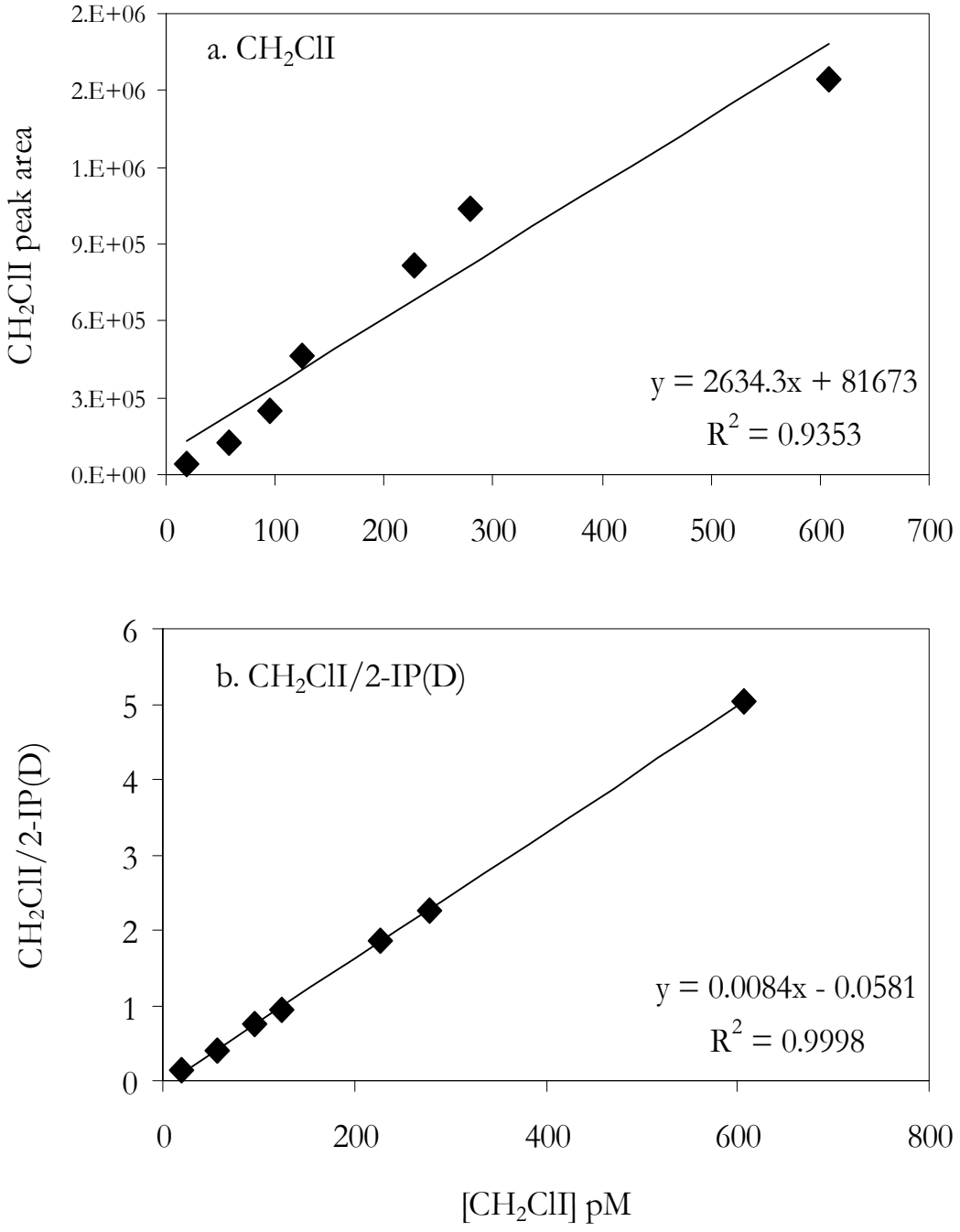

Figure 2.10. Typical calibration curves for CH_2ClI, showing a. CH_2ClI peak area only, and b. drift-corrected CH_2ClI, using ratio of CH_2ClI/2-IP(D).

Detection limits of the target analytes for the methods used during this study are shown in Table 2.4, and were calculated based on the minimum peak size that could be adequately resolved. The analytical error of halocarbon analysis during this study is shown in Table 2.5, and ranged from 3 to 14 percent.

Table 2.4. Halocarbon detection limits of the analytical methods used during this study. Detection limits are based on minimum peak size that could be adequately resolved.

Compound	Identifying ions	Mesocosm Cryogenic purge and trap	L4 Purge and trap, Markes tubes 10°C	Ischia Purge and trap, Markes tubes 2°C
CH_3I	142, 127	0.3 pM	0.6 pM	N/A
C_2H_5I	156, 127	0.3 pM	0.09 pM	N/A
CH_2ClI	176, 127	0.1 pM	1 pM	0.3 pM
CH_2I_2	268, 141	0.3 pM	N/A	0.3 pM
1-C_3H_7I	170, 127	N/A	N/A	0.1 pM
2-C_3H_7I	170, 127	N/A	0.2 pM	0.06 pM
$CHBr_3$	173, 175	4 fM	0.2 pM	0.8 pM
CH_2Br_2	174, 93	0.1 pM	0.9 pM	0.3 pM
$CHBr_2Cl$	129, 127	10 fM	N/A	0.2 pM
CH_2BrCl	130, 93	N/A	1.3 pM	0.2 pM

Table 2.5. Analytical error (Coefficient of variation %) of replicate samples (CoV = StDev/Mean X 100) of halocarbon calibrations of the analytical methods used in this study.

Compound	Identifying ions	Cryogenic purge and trap	Purge and trap, sorbent tubes
CH_3I	142, 127	9%	N/A
C_2H_5I	156, 127	5%	12%
CH_2ClI	176, 127	3%	13%
CH_2I_2	268, 141	9%	3%
1-C_3H_7I	170, 127	N/A	4%
2-C_3H_7I	170, 127	N/A	4%
$CHBr_3$	173, 175	14%	6%
CH_2Br_2	174, 93	4%	3%
$CHBr_2Cl$	129, 127	5%	N/A
CH_2BrCl	130, 93	N/A	7%

2.4 Dimethylsulphide (DMS) and Dimethylsulphoniopropionate (DMSP) Analysis

2.4.1 Analytical techniques

2.4.1.1 Sample collection and preparation

Water samples for DMS and DMSP analysis were taken with 5 litre polycarbonate aspirators. The aspirators were inverted, and then slowly pushed into the water with taps open so that they gently filled up with least addition of bubbles. A 200 μm mesh was used to cover the opening of the aspirator in order to exclude large zooplankton and other detritus from entering. 500 ml sub-samples were immediately taken from the aspirators. Tygon tubing was attached to the tap of the aspirators. The tube was then placed to the bottom of a glass-stoppered bottle, and a large aliquot taken which was shaken around the bottle to rinse it, and then rejected. Water was then allowed to fill from the bottom of the bottle and to overflow for an estimated 3 times the volume of the bottle. The glass-stopper was firmly placed onto the bottle, ensuring the absence of headspace and bubbles. The bottles were placed in the dark until return to the laboratory, where they were kept in the dark in a constant temperature room (9-11°C).

2.4.1.2 Purge and cryogenic trap

A 20 ml seawater sample was drawn from the glass-stoppered bottle into a glass gas-tight syringe (20 ml), then slow-filtered through a 25 mm GF/F filter in a Swinnex filtration unit directly into the glass purge vessel for purge and trap analysis. The purge system for DMS was constructed of PTFE and glass, and the system was very similar in construction to that shown in Figure 2.1, except all stainless steel parts shown in the diagram were replaced with PTFE, and the system was built in triplicate, essentially consisting of three concurrent purge systems, allowing the purging of three samples simultaneously. Samples were purged for 15 minutes at a flow rate of 60 ml min^{-1}, and DMS was pre-concentrated in a non-packed PTFE sample loop, which was cooled in the headspace of a liquid nitrogen-filled dewar, thermostatically held at -150°C. Analytes were injected onto the GC column by heating the trap to ~100°C using boiling water.

2.4.1.3 Headspace analysis

For particulate DMSP (DMSP*p*), the filter paper used to filter the sample for DMS analysis was placed into a glass vial containing 15 ml of 500 nM NaOH and immediately capped with a crimp seal, cleaving all DMSP to DMS via alkaline hydrolysis. Dissolved DMSP samples were taken from the purge vessel following purging for DMS. 13 ml of samples was taken, and 1ml of distilled water and 1ml 500mM NAOH was added to a 20ml crimp vial, and sealed. Samples of the headspace, ranging from 50ul-250µl were taken using a 250 µl Hamilton gas-tight syringe and manually injected into a GC.

2.4.1.4 Gas chromatograph – Flame Photometric Detector (GC-FPD) system and methods

Flame photometric detectors work on the basis of the information that is derived from chemiluminescent reactions of atoms in a H_2/air flame. Figure 2.11 is a schematic diagram of an FPD. Using chemiluminescence, analyte concentrations are quantified based on the optical emission from excited chemical species. For the analysis of DMS, the optical response of the S species is used to determine analyte concentration. The end of a GC column is fed directly into the reaction chamber in front of the FPD, and the FPD itself is contained within a combustion chamber and it fuelled by a continuous flow of H_2 and air at flow rates of 50 ml min^{-1} and 60 ml min^{-1}, respectively. The FPD has a thermal filter which separates the visible and UV radiation emitted by the flame and an optical filter isolates the S wavelength emission band.

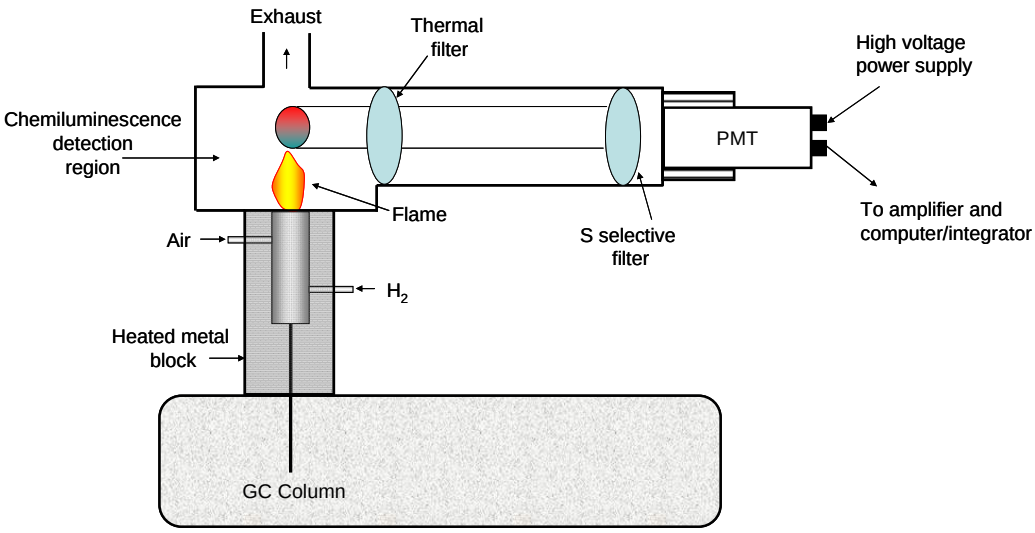

Figure 2.11. Schematic diagram of a flame photometric detector.

DMS samples were analyzed using a Shimadzu GC-14B with FPD, with a Shimadzu C-5A Chromatopac integrator. The GC was equipped with a Chromosil 330 (Supelco) packed column, with the oven set at 60°C, the injector set at 150°C and the detector at 175°C. The retention time for DMS was around 1.2 – 1.3 minutes. Headspace samples for DMSPp/DMSPd were directly injected into a Shimadzu GC-2010 with FPD, with the oven set at 120°C, the injector at 200°C and the detector at 25°C. The retention time of DMS was around 1 minute. The GC-FPD was programmed and controlled by the GCSolution Realtime Anlaysis software and data processing was carried out using the GC Postrun Analysis software.

2.4.2 GC-FPD system calibrations

Calibration of DMS by purge and trap was performed on each vessel of the triple purge system every 3-5 days by cold alkaline hydrolysis of DMSP (0.17 to 87.6 nM L^{-1}) with 10M NaOH (Turner *et al.* 1988; Turner *et al.* 1990). DMSP working standard was prepared by dissolving 1ml of 812.19 ng S in 250-500ml of distilled water, to give a working standard of 3.25 ng S l^{-1}. 1ml of 1M NaOH was placed in the purge vessel, the lid was replaced, and the system leak checked. When it was ensured the system was leak-free, a known volume of the working standard was drawn up into a 20 ml glass syringe, and injected into the purge vessel through the luer valve. Purge flow was switched on and the standard was purged for 15 minutes at a flow rate of 60ml min^{-1}. DMS was trapped in the PTFE sample loop held at -15°C in the cooled headspace of a dewar containing liquid N_2. After 15 minutes, DMS was injected onto the GC column by submerging the sample loop in boiling water. This was repeated for a range of volumes (1 ml – 20 ml), and hence concentrations (1.6 – 32.5 ng S ml^{-1}), to produce calibration curves for each purge vessel, as shown in Figure 2.12. The equations derived from the calibration were used to calculated seawater concentrations of DMS. The analytical error of the system was 6%, as based on triplicate samples.

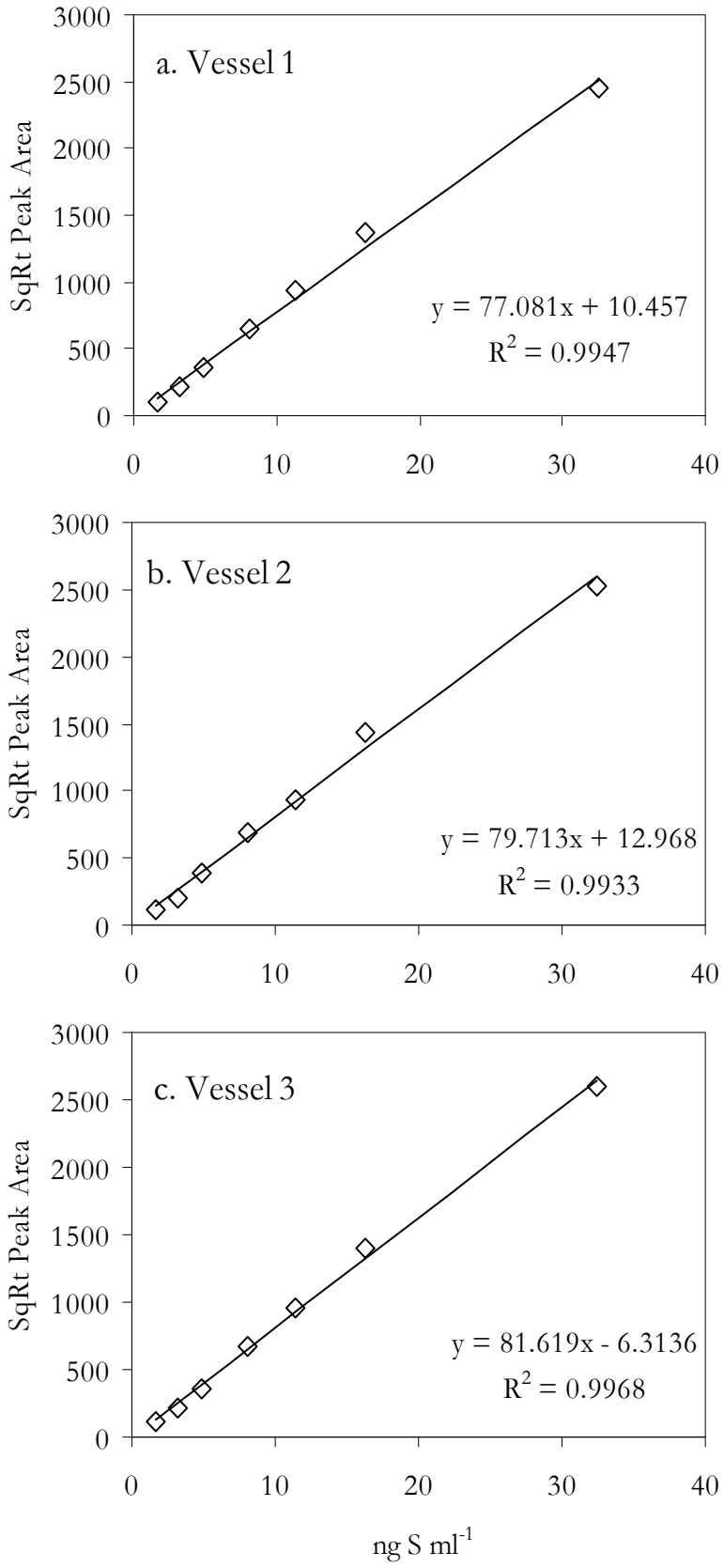

Figure 2.12. Typical calibrations curves produced on the triplicate purge system (a. Vessel 1, b. Vessel 2, c. Vessel 3) used for DMS analysis used during the mesocosm experiment.

Calibration of the system for DMSP (particulate and dissolved) was performed using DMSP standard diluted in 500 mM NaOH. 15ml was aliquoted into 20 ml glass vials with crimp seal caps identical to those used for the samples, retaining a 5ml headspace. Standards were equilibrated in a 30°C waterbath for 24 hours. Gas tight microlitre syringes were used to penetrate the septum and draw up samples of the headspace. Samples were directly injected into the injection port of the GC-2010, using volumes ranging from 100µl to 250µl and over a concentration range of 0.5 – 300 nmol L^{-1}. The analytical error of the system was 11 % based on replicate samples.

2.5 Other measurements

2.5.1 Chlorophyll a and phaeopigments

Chlorophyll *a* and phaeopigment determinations were performed as accompanying measurements for all work described in this study. Seawater samples, ranging from 100ml (L4 experiments and Ischia fieldwork, Chapters 4 and 5) to 500ml (Mesocosm experiment, Chapter 3) were filtered through either 47 mm GF/F (Whatman) (L4 experiments and Ischia fieldwork) or 0.2 µm cellulose acetate membrane filters (Mesocosm experiment). The filters were then folded in half twice using forceps, and wrapped in aluminium foil envelopes, followed by storage at either -20°C or -80°C until chlorophyll *a* extraction (1 week to 3 months)..

In order to extract the chlorophyll *a*, the frozen filters were soaked in 10-20ml 90% acetone for 24 hours, and stored in the dark at -20°C. After 24 hours, the samples were centrifuged for 3 minutes at 4000 rpm in order to separate out any particles from the acetone/chlorophyll *a* solution, and then immediately analysed on a Turner 10-AU-005 fluorometer, using a wide excitation band of 450 nm – 670 nm. Once a fluorescence reading for chlorophyll *a* had been attained, 3 drops of 10% hydrochloric acid (HCl) were added to the cuvette, and after 1 – 3 minutes, a second fluorescence reading for phaeopigments was taken. Calibration was performed using serial dilutions of 1mg l^{-1} chlorophyll *a* standard, again followed by acidification with 10% HCl to derive a phaeopigment correction value. A typical calibration curve for chlorophyll *a* and phaeopigments is shown in Figure 2.13, with the derived equations used to calculate concentrations in seawater samples.

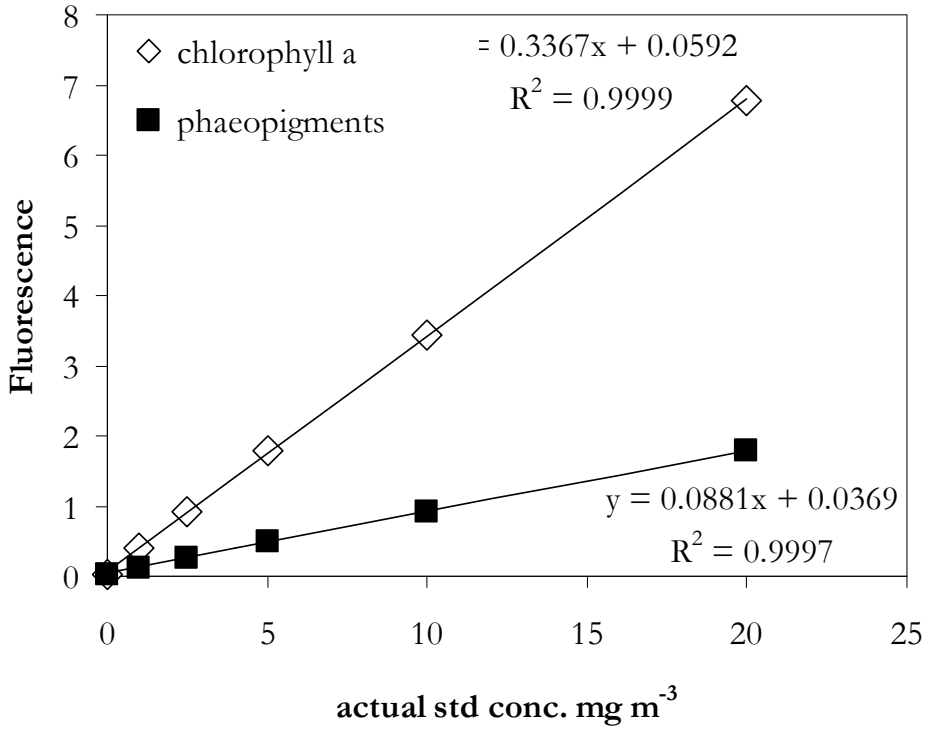

Figure 2.13 Calibration curve for chlorophyll a (diamonds) and phaeopigments (squares) (µg l^{-1}).

2.5.2 Phytoplankton counts (Flow cytometry)

Flow cytometry was used during the mesocosm experiment (Chapter 3) and the L4 incubation experiments (Chapter 4) to make daily counts of phytoplankton. The phytoplankton counts on live samples were performed by F.H during the L4 experiments and by Isabelle Mary (NOCS) during the mesocosm experiment. The analyses were performed on a Becton Dickinson FACSort™ flow cytometer which was set up to measure chlorophyll fluorescence (>650 nm), phycoerythrin fluorescence (585 ± 21 nm) and side scatter. 1 – 2 ml live samples were analyses for 3 – 4 minutes at a flow rate of 50 µl min^{-1}. Measurements of side scatter and fluorescence were made using the software package Cell Quest™ . Bivariate scatter plots of phycoerythrin (orange) and chlorophyll fluorescence (red) were used to discriminate *Synechococcus* sp. The other phytoplankton were resolved using bivariate plots of side scatter against chlorophyll fluorescence (red). Yellow-green beads of 0.5 µm diameter (Fluoesbrite Microparticles; Polysciences, USA) were used in all analyses as an internal standard for both fluorescence and flow rates (Zubkov *et al.* 2002).

2.5.3 Phytoplankton enumeration (Microscopy)

Phytoplankton enumeration was carried out by Claire Widdecombe (PML). 100ml samples were preserved with acid Lugol's iodine solution (2% final concentration) or formalin, and stored in cool, dark conditions until analysis in the laboratory by inverted settlement microscopy (Utermohl 1958). Fifty millilitre sub-samples were concentrated by sedimentation for > 24 hours and all cells between 2 and 200 µm were enumerated at x200 or x400 magnification. Cells were identified, where possible, to species level and their linear dimensions were measured using an ocular micrometer. Cell volumes were calculated using simple geometric shapes and converted to carbon according to the equations of Menden-Deuer and Lessard (2000). During the mesocosm experiment, samples were taken from mesocosm 1 and 6 on selected days (see Chapter 3), and samples were taken every 3 days during the L4 incubation experiments from all incubation vessels (see Chapter 4).

2.5.4 Seawater pH measurements

The determination of pH in seawater is complicated by the chemical composition of seawater, and the existence of a number of pH scales: the NBS scale, the free scale, the total scale and the seawater scale. pH may simply be defined as the negative logarithm of the activity of hydrogen ions [H^+] in a solution, or:

$$pH_a = -\log a_{H+} \qquad (2)$$

However, it is not possible to measure pH according to this equation as the individual seawater ion activities cannot be determined experimentally (Zeebe and Wolf-Gladrow 2001). Therefore an operational definition of pH can be given by the NBS scale:

$$pH_{NBS} \approx pH_a \qquad (3)$$

The NBS scale is defined by a series of standard buffer solutions with assigned pH values. However, the buffer solutions have very low ionic strengths of ~0.1, compared to the very high ionic strength of seawater of ~0.7. Therefore use of such buffers is not recommended for measurements in seawater (Zeebe and Wolf-Gladrow 2001).

Following recognition of the problem with NBS standards, a new set of standards was developed, based on artificial seawater and therefore taking into account the ionic strength of seawater (Hansson 1973). Known as the total scale, it can be described with:

$$pH_T = -\log ([H^+]_F + [HSO_4^-]) = -\log [H^+]_T \quad (4)$$

where $[H^+]_F$ = "free" $[H^+]$, and it includes the effect that $[HSO_4^-]$ has on $[H^+]$.

The free scale is the simplest to describe:

$$pH_F = -\log [H^+]_F \quad (5)$$

However, as this scale does not take into account $[HSO_4^-]$, errors are introduced into accurate determinations of seawater pH.

Finally the seawater scale takes into account both $[HSO_4^-]$ and $[F^-]$:

$$pH_{SWS} = -\log ([H^+]_F + [HSO_4^-] + [HF] = -\log [H^+]_{SWS} \quad (6)$$

to give accurate determinations of seawater pH (Zeebe and Wolf-Gladrow 2001). However, as the effect of $[HSO_4^-]$ is much greater than [HF], the difference between the total scale and the seawater scale is minimal.

During this study, direct seawater pH[1] values were determined in two ways. During the L4 incubation experiments and the autumn 2007 Ischia field campaign, NBS standards were used to calibrate the pH electrode, and while this is not ideal for accurate measurements of pH in seawater, it enables relative changes in pH to be assessed.

During the spring Ischia fieldwork, pH electrodes were calibrated against NIST certified freescale standards, followed by conversion of values to the total scale.

[1] pH values reported for the mesocosm study (Chapter 3) were calculated from total alkalinity and pCO_2 with CO2SYS (Lewis and Wallace 1988) with the equations of Mehrbach *et al.* (1973) and Dickson and Millero (1987), and data was supplied by Dorothee Bakker, University of East Anglia. See Chapter 3, section 3.2.3.

To estimate numerical differences between Freescale (pH_F) and Total scale (pH_T) in seawater, it is necessary to use values for K_S (SO_4 dissociation constant) and S_T (Total SO_4) in the following term:

Total Scale = Log $(1 + S_T / Ks)$ ≈ 0.11 (Zeebe and Wolf-Gladrow 2001) (7)

At S = 35, T = 25°C
$K_S \approx 0.10$ mol kg^{-1}
S_T, = 28.24 mmol $(kg.soln)^{-1}$ (DOE, 1994)

So if e.g. $pH_F = 8.22$
$pH_T = 8.11$

pH data collected during the spring field campaign in Ischia (Chapter 5, 5.2.1) underwent numerical conversion to total scale, taking account of the salinity of Mediterranean seawater. Mean salinities were calculated for the field campaign:

Spring 2008: $S_{mean} = 37.8$ (8)

As salinity affects total $[SO_4^{2-}]$, S_T is re-calculated at the relevant salinity:

$S_T = (0.1400/ 96.062) * (S / 1.80655)$ (DOE, 1994) (9)

0.1400 = $[SO_4^{2-}]$ g/Cl
96.062 = molecular weight of SO_4^{2-}
1.80655 = relates salinity to chlorinity via the Kundsen relationship S = 1.80655 Cl

Spring 2008: At S = 37.8, S_T = 30.49 $mmol(kg.soln)^{-1}$
Therefore numerical differences between freescale field measurements and total scale values, using S_T relevant to mean salinity:

Spring 2008: log (1 + 30.49/0.1) = **0.12** (10)

This demonstrates that the higher salinity experienced in the Mediterranean made little difference to the conversion calculations. Nevertheless, 0.12 was subtracted from Spring pH readings to give pH measurements on the total scale.

2.6 Summary

Trace gases are extracted from seawater by being forced from the water phase into the gas phase by purging seawater samples with inert gas such as OFN, and trapping the target compounds either cryogenically, or in specially-selected sorbent materials. Both halocarbons and DMS/DMSP have been quantified during this study, requiring the use of suitable purge systems (stainless steel for halocarbons, PTFE for DMS), and analytical systems (GC-MS for halocarbons, GC-FPD for DMS). During the following chapters, a range of experimental work (Chapter 3 Mesocosm Experiment, Chapter 4 L4 Incubations) and fieldwork (Chapter 5 Ischia, Italy) that has been used to investigate the impact of high-CO_2 and lowered seawater pH on the seawater concentrations of a range of marine trace gases will be described in detail.

Blank Page

CHAPTER 3
Marine biogenic trace gas production during a mesocosm CO_2 perturbation experiment

3.1. Introduction

3.1.1. Mesocosm experiments in marine science research

The simulation of future scenarios of OA in a real ocean setting is logistically and experimentally challenging, as large-scale manipulation of atmospheric pCO_2 and ocean pH would be required. For example, it has been calculated that in order to acidify a patch of seawater 10 km x 10 km in size and 50 m deep from pH 8.1 to 7.8, around 30,000 t of CO_2 or 54,000 t of concentrated HCl would be required, and this is currently outside the realms of conventional research capabilities (Riebesell *et al.* 2008). Therefore it is necessary to construct experiments that can replicate these conditions on a smaller-scale, in as close to a natural environmental situation as is possible. Furthermore, there is a growing body of evidence suggesting that single-species tests and laboratory experiments are less sufficient at assessing the response of marine pelagic ecosystems to environmental changes such as OA, and make extrapolation to the oceans difficult (Kuiper and Gamble 1988; Kwint and Kramer 1995). In recent years, mesocosm experiments have been at the forefront of OA research. They are considered to be a powerful tool in this fast growing field, as they offer an ideal way of exploring the impact of changes to oceanic carbonate chemistry on complex pelagic communities, in relatively large volumes of water (compared to laboratory studies), under quasi-natural meteorological and oceanic conditions.

Numerous past studies have proven that mesocosms can play a crucial role in developing our understanding of the biological, physical and geochemical aspects of marine planktonic ecosystems (Barlow *et al.* 1998; Williams and Egge 1998; Wilson *et al.* 1998). In practical terms, mesocosm experiments display a number of benefits. Intensive sampling over a number of days or weeks is possible, generally with good laboratory facilities available nearby. The data obtained through mesocosm experiments is of great use in modelling studies. When coupled with data

assimilation, mesocosm experiments can be an influential tool in the development and testing of aquatic ecosystem models, covering a range of oceanographic conditions in order to address a variety of modelling needs (Vallino 2000). Field data is intrinsically unpredictable but some of this variation is lost in mesocosm experiments, without loss of the possibility for extrapolation to the natural system (Kuiper and Gamble 1988).

During the late 1930s the first land-based mesocosms were built in which to study plankton ecology. By the 1960s the availability of flexible plastic materials meant that transparent enclosures could be made, to house natural seawater communities in near-natural conditions (Banse 1982). Since these early developments, mesocosms studies have been used to examine numerous aspects of plankton ecosystems, including photosynthesis, the effects of light, nutrients, and turbulence, and impacts on the production of extracellular material (Kuiper and Gamble 1988; Barlow *et al.* 1998; Williams and Egge 1998; Wilson *et al.* 1998). They represent an experimental tool that creates linkage between artificial laboratory culture and incubation experiments, and inherently variable oceanic measurements. This kind of tool is required until our knowledge of planktonic ecosystems is sufficient to produce confident, predictive mathematical models. Furthermore, information on perturbed and unperturbed ecosystems from mathematical models can be validated by mesocosm studies much better than by field studies in terms of cost and data variability (Kuiper and Gamble 1988).

3.1.2. Mesocosm experiments in ocean acidification research

Mesocosm experiments provide the ideal setting for research into the impacts of OA on pelagic communities, as they present the opportunity to manipulate environmental factors, such as pCO_2 and pH in thousands of litres of seawater during a controlled bloom situation. Mesocosms are now considered to be a vital tool in OA research; Raven *et al.* (2005) stressed that a major internationally coordinated research effort into OA must be launched to include "…global monitoring, experimental, mesocosm and field studies.", whilst Ridgwell *et al.* (2007) stated that further mesocosm experiments are necessary in order for scientists to make "….more reliable assessments of the future impact of ocean acidification…".

3.1.3. Results of past ocean acidification mesocosm studies

In the last 5 years, three such mesocosm CO_2 perturbation experiments have been performed at the Marine Biological Field Station, Raunefjorden, Norway

(60.3°N, 5.2°E). This facility represents an internationally-important site for OA research, with only one other such facility in operation in South Korea (Kim *et al.* 2006). For each of the experiments, polyethylene enclosures were suspended in the fjord from a moored floating raft. Each enclosure was filled with 11 m^3 of nutrient-poor unfiltered fjord water, and the tops of the mesocosms were covered with tetrafluoroethylene films in order to form a tent covering >90 per cent of the mesocosm surface area. The atmospheric CO_2 was controlled inside the mesocosms by injecting a constant stream of gases with a known CO_2 content. Nutrients were added in order to stimulate phytoplankton blooms, and the bloom was monitored over the course of a few weeks. In 2001 (Engel *et al.* 2005) and 2003 (Avgoustidi 2007; Allgaier *et al.* 2008; Engel *et al.* 2008; Paulino *et al.* 2008), three treatments were used: 180 ppmv (glacial), 370 ppmv (present) and 700 ppmv (IS92a emissions scenario), and the 2005 experiment again compared three: 375 ppmv (present), 750 ppmv (future) and 1150 ppmv (Far future). A summary of some of the results of these experiments is given in the following sections.

3.1.3.1. Photosynthesis and growth rate

During the 2001, the coccolithophore *Emiliana huxleyi* displayed adecreasing net specific growth rate with increasing CO_2, although no significant reduction in biomass was observed relative to low-CO_2 (Engel *et al.* 2005). Many phytoplankton cells experience a lack of pH homeostasis. Therefore as pH is lowered, cells may have to expend more energy maintaining a viable internal cell pH, lowering the overall productivity of the cells (Raven 1980; Dason and Colman 2004). In addition, the reaction rate of enzymes is pH dependent, so any departure from optimum pH may weaken cellular function (Hinga 2002). So it is likely that a number of pH effects work synergistically to reduce photosynthesis, growth rates and cellular productivity. If the conditions experienced by *E. huxleyi* during the mesocosm CO_2 experiments are representative of the future high CO_2 world, a decline in net specific growth rate may diminish the competitive ability of this species, with implications for its abundance and distribution (Engel *et al.* 2005).

3.1.3.2. Phytoplankton calcification and C cycling

The 2003 experiment revealed decreased calcification by coccolithophores, accompanied by an increase in the proportion of misshapen liths and incomplete

coccospheres at elevated CO_2 (Engel *et al.* 2005), a result that is in agreement with single-species laboratory cultures of coccolithophores (Riebesell *et al.* 2000b). Furthermore, during the 2001 mesocosm CO_2 experiment, coccolithophores subjected to low 'glacial' CO_2 concentrations (180 ppmv) produced larger and heavier coccoliths compared with higher CO_2 treatments (Engel *et al.* 2005). Recent work by Rodriguez-Iglesias *et al.* (2008) has produced contradictory results, suggesting that coccolithophores such as *E. huxleyi* may in fact show increased calcification and net primary production under high CO_2 (Iglesias-Rodriguez *et al.* 2008). Returning to the 2003 mesocosm experiment, the observed reduction in calcification rates under the 'Year 2100' high CO_2 treatment, in combination with direct pH effects on cell physiology affected cell division rates, and resulted in lowered population growth rates (Engel *et al.* 2005). In addition, calcification was delayed under these conditions, leading to a reduction in the overall amount of $CaCO_3$ production (Engel *et al.* 2005).

3.1.3.3. Organic C export

The results of the 2001 mesocosm CO_2 experiment revealed increased transparent exopolymer particle (TEP) production at high CO_2 concentrations, resulting in enhanced aggregation of detrital particles. Consequently, under high CO_2 conditions particles sediment out at a greater rate and are characterised by increased C:N ratio and depletions of P (Engel *et al.* 2005). A similar phenomenon has been observed with increased CO_2 concentrations in a study in the Baltic Sea (Engel 2002). Therefore, a shift in organic C export as a result of OA could have important consequences. As TEP formation enhances C export and hence the biological pump (see section 1.1.6), the overall response of *E. huxleyi* represents a negative feedback with respect to rising CO_2 concentrations. If this enhancement of C export is as significant for other phytoplankton groups, and works synergistically with the effects of decreasing biogenic calcification, it could correspond to a major negative feedback to anthropogenic CO_2 (Delille *et al.* 2005).

3.1.3.4. Trace gas production

Trace gas measurements of relevance to this work were conducted during the 2003 and 2005 mesocosm experiments, primarily focusing on DMS, its precursor DMSP, and the associated enzyme DMSP-lyase. Measurements of other volatile trace gases, including CH_2ClI, were made in 2005. During the 2003 experiment Avgoustidi

revealed a significant reduction in the production of dimethyl sulphide (DMS) under high CO_2, compared to the present day CO_2 mesocosms (Avgoustidi 2007). The 2005 experiment produced opposite results. At 2 x CO_2 (750 µatm) there was 22 - 26 per cent more DMS produced relative to present CO_2 (375 µatm), whilst at 3 x CO_2 14 - 18 per cent greater DMS production was observed (Wingenter *et al.* 2007; Vogt *et al.* 2008). Clearly, further experiments are required, so that more definitive conclusions may be drawn regarding the future of the global S cycle in the context of increasing ocean acidity.

During the 2005 mesocosm CO_2 experiment, concentrations of chloroiodomethane (CH_2ClI) were quantified (Wingenter *et al.* 2007). An increase of ~46 per cent was observed in mesocosms exposed to 2 x CO_2 (750 µatm) relative to present CO_2 (375 µatm), whilst under the 3 x CO_2 conditions, a large 131 per cent increase was observed.

3.1.4. Hypotheses and Aims

Clearly, the currently available information on the impact of elevated CO_2 and decreased seawater pH on the production of marine trace gases is of both a limited and a contradictory nature. This chapter describes a mesocosm CO_2 perturbation experiment that was performed in May 2006. The aim of this study was to further our knowledge of the impacts of OA on the concentrations, and hence net production/removal processes for marine trace gases, and attempt to overcome some the existing contradictions, by addressing the following hypotheses:

1. The net production of a range of climatically- and atmospherically-important volatile marine trace gases, including:

    a. *Iodine-containing compounds (Iodocarbons)*
    b. *Bromine-containing compounds (Bromocarbons)*
    c. *DMS, and its precursor DMSP*

    is impacted by elevated CO_2/decreased seawater pH during a mesocosm phytoplankton bloom CO_2 perturbation experiment.

2. The impacts on trace gas production are related to changes in overall phytoplankton/bacterial biomass or community structure.

3.2. Experimental Setup, Material and Methodology

3.2.1. General experimental setup

The mesocosm experiment was carried out at the Marine Biological Station, Espegrend, Bergen, Norway (Raunefjörden, 60.3°N, 5.2°E) from 3 to 23 May 2006. Six reinforced polyethylene mesocosm enclosures (M1 – M6) with a 2 m diameter, 3.5 m depth (0.5 m above surface of the water) and a total volume of around 11,000 m^3 were deployed in the fjord. The mesocosms were covered with lids consisting of a plastic frame covered in high UV- transmitting horticultural polyethylene, attached to the mesocosms through a system of ropes and karabiners. Although the lids were not intended to be leak tight, they reduced exchange of the enclosure headspaces with the atmosphere and prevented rain entering. The transmission of photosynthetically active radiation (PAR) through the polyethylene enclosures was measured at 92 per cent of total PAR. The mesocosm enclosures were attached to the southern side of a raft, with a small floating laboratory, approximately 200 m away from the shore. On 2 May, the enclosures were filled with nutrient-deplete, unfiltered water, pumped directly from the fjord from a depth of 5 m. In order to stimulate the development of a phytoplankton bloom, 0.8 µmol l^{-1} phosphate and 15 µmol l^{-1} nitrate were added to all six mesocosm enclosures on 6 May. The water inside the enclosures was lightly mixed using a pumping system which circulated water from 3 m depth to the surface at a rate of approximately 1000 litre per day.

Two treatments were used in order to assess the effect of high CO_2 on a phytoplankton bloom. M1, M2 and M3 (See Figure 3.1 below) were the "High-CO_2" mesocosms, whilst M4, M5 and M6 were the "Present Day" mesocosms. Fjord water from outside of the mesocosms was also monitored for pCO_2 and pH, in order to act as a control. A CO_2 aeration system was constructed and installed by Phil Nightingale and Malcolm Liddicoat (PML). The high CO_2 bags were aerated with air enriched with CO_2 for 2 days until pH ~7.8 was attained. From this point onwards, only the headspace was flushed with high-CO_2 air rather than the whole water column. This allowed the carbonate system to develop and adjust naturally while just maintaining high CO_2 concentration in the atmosphere of the enclosure headspace. The ambient mesocosms were aerated with air for 1-2 days at start of experiment, purely to ensure

they were exposed to the same physical treatment. Daily sampling commenced on 6 May between 0900 and 1000 (local time).

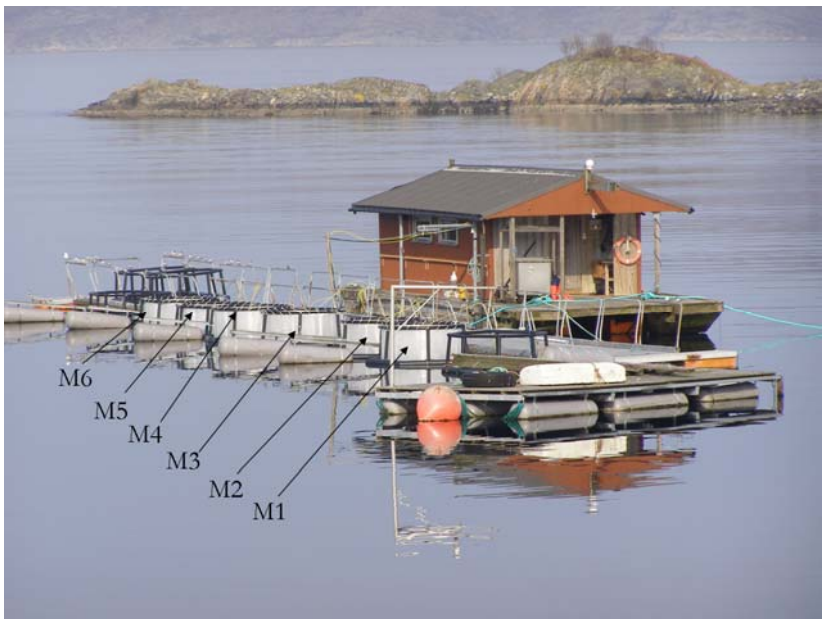

Figure 3.1. The floating laboratory raft with mesocosm enclosures moored on the southern side. M1, M2 and M3 were the "high-CO_2" bags with pCO_2 attaining ~700-800 µatm. M4, M5 and M6 were the "present day" bags which underwent no enhanced CO_2 treatment.

3.2.2. Trace gas analyses

Sample collection for trace gas analyses was undertaken from 6 – 23 May (excluding 17 May due to technical problems). One sample per day was taken from M2, M3, M4 and M5, whilst triplicate samples were taken from M1 and M6 on alternate days. Sampling began at 0900 everyday, and was completed by 1000.

3.2.2.1. Halocarbons

Seawater samples for halocarbon analyses were collected as detailed in Chapter 2, section 2.3.1, using a syringe extension in order to reach over the side of the mesocosm enclosures to the water inside. Immediately after sampling, syringes were placed in a temperature controlled room, set at the *in situ* temperature of the fjord water (9°C), until analysis. Samples were analysed using cryogenic purge and trap, followed by GC-MS, according to the method discussed in Chapter 2.

3.2.2.2. DMS/DMSP

Seawater samples for DMS analysis were collected and analysed by cryogenic purge and trap/GC-FPD at the mesocosm facility as detailed in Chapter 2, section

2.4.1.2. Samples for DMSPp and DMSPd were collected and fixed as described in Chapter 2, section 2.4.1.3 and underwent headspace analysis on return to UEA.

3.2.3. The Carbonate System: pCO_2, Total Alkalinity (TA) and pH

The following analyses were performed by Dorothee Bakker and Gareth Lee (UEA). Discrete aqueous samples for the partial pressure of carbon dioxide (pCO_2) were taken in 500 ml volumetric flasks from 3 to 24 May 2006. The samples were analysed within 14 hours of collection using a UEA-built instrument with infrared detection (Wanninkhof and Thoning 1993). The analysis temperature was within 2°C of the *in situ* temperature. The CO_2 instrument was calibrated twice daily against secondary standards with CO_2 mixing ratios of 0, 258.40, 470.32, 682.72, and 877.19 μmol mol^{-1}. These secondary standards had been calibrated against NOAA CO_2 standards. The program CO2SYS (Mehrbach *et al.* 1973; Dickson and Millero 1987; Lewis and Wallace 1998) and the carbonate constants by Mehrbach et al. (1973), as refitted by Dickson and Millero (1987) were used to correct for the sample headspace and the temperature difference between sampling and analysis (DOE 1994). The accuracy of pCO_2 is estimated as better than 5 μatm. The average difference between 8 replicate samples infers a reproducibility of 3 μatm.

Daily samples for total alkalinity (TA) were taken, filtered and fixed with mercuric chloride from 11 to 20 May. TA (see Section 1.1.4) was determined by potentiometric titration with a Vindta system at UEA. The constants of Mojica Prieto (2002) and multiple least squares fitting were used. Analysis of certified reference material suggests an accuracy and reproducibility of 4 and 2 μmol/kg, respectively. Outliers in TA were replaced by values interpolated from nearby days. TA values for 3 – 10 May have been extrapolated from TA on 11 May and an empirical relationship between TA and coccolithophorid numbers. TA varied little between treatments over this period. pH on the total pH scale was calculated from TA and pCO_2 with CO2SYS (Lewis and Wallace 1998) with the equations of Mehrbach *et al.* (1973) and Dickson and Millero (1987). The variation in calculated pH is dominated by variation in pCO_2 with little effect from changes in TA.

3.2.4. Chlorophyll a

Water samples for chlorophyll *a* were taken from the 5 litre aspirators on sixteen days out of eighteen. 500 ml polycarbonate bottles were filled with seawater,

and returned to the laboratory where they were kept in the dark in the constant temperature room (9°C) until processing within 4 hours of sample collection. The volume of seawater that was filtered varied; as the bloom progressed, and the concentration of phytoplankton cells increased, the filtering volume was reduced. From 6 – 12 May, 500 ml was filtered, 13 – 16 May it was reduced to 350 ml, and reduced again to 300 ml for 17 – 23 May. For the final 3 days, 16 to 18, the volume was increased to 350 ml. Filtering was carried out in low light conditions, in a constant temperature room set at *in situ* temperature. Cellulose acetate membrane filters were used (47 mm, 0.2 μm) on a manifold filtration unit, using a low filtration pressure of < 100 mm Hg. Once the required volume had passed through the membrance, the vacuum pump was switched off, and the filter paper was gently folded up with tweezers, placed in a cryovial and immediately shock frozen in liquid nitrogen. Samples were stored at -80°C until further analysis. In order to extract chlorophyll *a*, the frozen filters were soaked in 20ml of 90% acetone for 24 hours, in darkness and at -20°C. A Turner fluorometer was used to determine the fluorescence of the samples. Phaeopigments were determined by acidification of the acetone extract with 10 percent HCl. Calibration of the fluorometer was performed using serial dilutions of a 1 mg l^{-1} chlorophyll *a* standard.

3.2.5. Phytoplankton community determination

Phytoplankton microscopy counts were carried out by Claire Widdicombe (PML), according to the methods described in Section 2.5.2 (Chapter 2). Samples were taken from M1 and M6 on 9, 11, 12, 13, 14, 15, 18 and 21 May. Cell counts were converted to biomass according to the equations of Menden-Deuer and Lessard (2000). Samples for flow cytometric counts of phytoplankton were taken and analysed daily by Isabelle Mary (NOCS) according to the methods described in Section 2.5.3. (Chapter 2).

3.2.6. Statistical analyses

All trace gas, DMSP and chlorophyll *a* data were analysed using two-sample tests of hypotheses. Initially tests of normality were applied ($p<0.05$ = not normal), and if data failed to fit the assumptions of the test, transformations of the data were performed. Initially square root or logarithmic transformations were applied, and where these failed to produce normally distributed data, Johnson's transformations

were used. The analysis continued from this point, firstly with a test for equal variances (Levene's statistic, $p>0.05$ = equal variances), culminating in a two-sample T-test ($p<0.05$ = significant differences). For those data which still failed to display normality following transformation, non-parametric tests were applied. Data that displayed equal variances underwent a Mann-Whitney test, and for those that were neither normally distributed nor displayed equal variances a Mood's Median test was used. Using this method of statistical analyses, tests are used that decrease in power from T-tests, to Mood's Median, depending on the ability of the data to fit the assumptions of the tests.

Spearman's Rank Correlation Coefficients (ρ), along with associated significance level (95% $p<=0.05$, 98% $p<=0.02$, 99% $p<=0.01$) were calculated to identify relationships between various chemical and biological parameters measured during the experiment.

3.3. Results Description

3.3.1. pCO_2 and pH

Figure 3.2 shows the changes in pCO_2 and pH throughout the course of the experiment. On 3 and 4 May, the effect of bubbling with CO_2 was clear in M1, M2 and M3 with a rapid increase in pCO_2 up to 660-736 µatm, accompanied by a sharp drop in pH to 7.8. Between 11 – 14 May, during a period of rapid phytoplankton growth (See Figure 3.5), the pCO_2 gradually decreased back down to near ambient levels, with a concomitant rise in pH (Fig. 3.2). Consequently on 15 May, the decision was made to re-aerate M1 and M2 with CO_2-enriched air to bring the pH back down to target levels. M3 was left untouched in order to see what would happen if the experiment had continued unaltered.

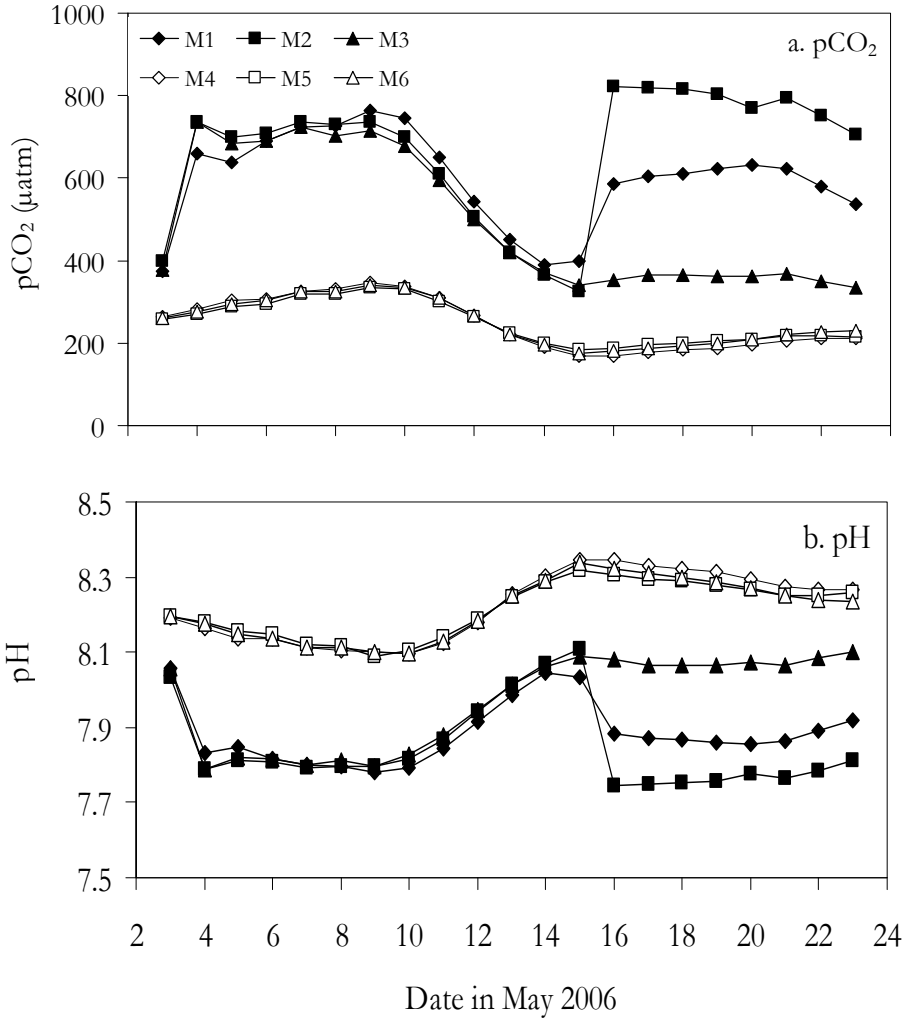

Figure 3.2. The changes in a. pCO_2 (µatm) and b. pH. The sharp increase in pCO_2 and decline in pH mark the point of re-aeration with CO_2 in M1 and M2. Legend in panel a.

The control M4 was also left unaltered, and M5 and M6 were re-aerated with air in order to receive the same physical treatment as M1 and M2. The experiment was continued following this additional treatment until 23 May when sampling ceased. Due to this change in experimental conditions, and as trace gases are driven out of the water phase by aeration, priority is given to data from the unaltered M3 and M4 from 16 May onwards. All data will be presented, although data from M1, M2, M5 and M6 will be plotted in grey from 16 May.

The re-bubbling of M1 and M2 with CO_2-enriched air on 15 May is clearly seen as a sharp rise in pCO_2 up to 823 µatm in M2 in Figure 3.2. The pH dropped to 7.9 and 7.7 in M1 and M2, respectively. pCO_2 and pH in M3 remained stable for the rest of the experiment, with a mean pCO_2 of 358 µatm for this period and a stable pH of

just over 8.1. M3 could still be considered to represent a CO_2-perturbed environment, as pCO_2 levels were on average 80 µatm higher than in the present day mesocosms owing to the headspace still being flushed with high-CO_2 air. Table 3.1 gives a summary of the CO_2/air treatments received by each of the mesocosms over the course of the experiment, and Table 3.2 displays a summary of measurements of pH and pCO_2 in each mesocosm at the beginning of the experiment (4 May), following re-aeration of M1, M2, M5 and M6 (16 May) and at the end of the experiment (23 May).

Table 3.1. Summary of the CO_2/air treatments for each of the mesocosms.

	CO_2/Air aeration 3 May	Air aeration 3 May	CO_2/Air aeration 15 May	Air aeration 15 May
M1	√		√	
M2	√		√	
M3	√			
M4		√		
M5		√		√
M6		√		√

Table 3.2. Summary of pCO_2 and pH. Measured on 4 May after initial aeration, on 16 May after re-aeration of M1, M2, M5 and M6, and at the end of the experiment on 23 May. Mean pCO_2 and pH for the High-CO_2 and ambient CO_2 treatments are also shown.

	4 May pCO_2(µatm) pH	**16 May pCO_2(µatm) pH**	**23 May pCO_2(µatm) pH**	**Mean pCO_2(µatm) pH**
M1	660 7.8	586 7.9	535 7.9	594 7.9
M2	736 7.8	823 7.8	704 7.8	754 7.8
M3	736 7.8	351 8.1	336 8.1	474 8.0
High CO_2 Average	711 7.8	587 7.9	525 7.9	
M4	282 8.2	170 8.4	210 8.2	221 8.3
M5	271 8.2	188 8.3	216 8.3	225 8.3
M6	275 8.2	182 8.3	229 8.2	228 8.2
Present day CO_2 Average	276 8.2	180 8.3	218 8.2	

3.3.2. Meteorological observations

The experiment was undertaken during May 2006 through a period which was characterised by warm, sunny weather for the first week, followed by more typical wet and cool weather for the remainder of the month. Figure 3.3 is a plot of minimum, maximum and mean air temperature measured daily at a weather station situated at Bergen Flesland airport, about 20km from the Marine Biological Station. The 12 year (1996-2008) mean daily temperature is also plotted, and clearly the warm temperatures experienced during the first week of the experiment were far above average for the time of year. Critically, the most sun and warmth was experienced during the early to mid stages of the bloom, including the exponential growth phase and peak of the bloom. Also shown in Figure 3.3 are the recorded temperatures for the mesocosm experiment that was carried out in the previous year (2005). During this experiment, temperatures were much lower than those from this study, and for the majority of the time, temperatures were below average for the time of year.

a. Mesocosm 2006

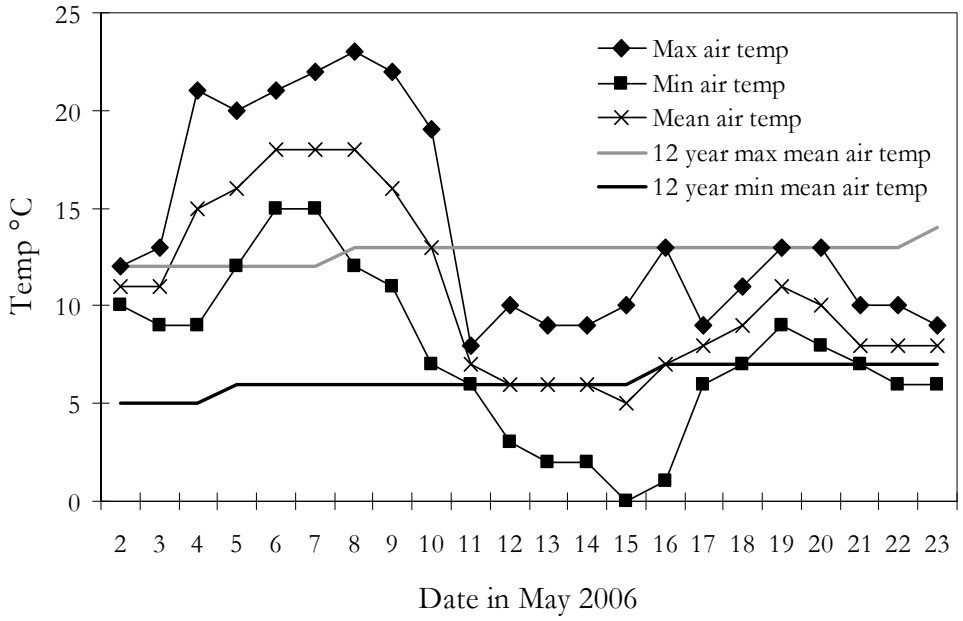

b. Mesocosm 2005

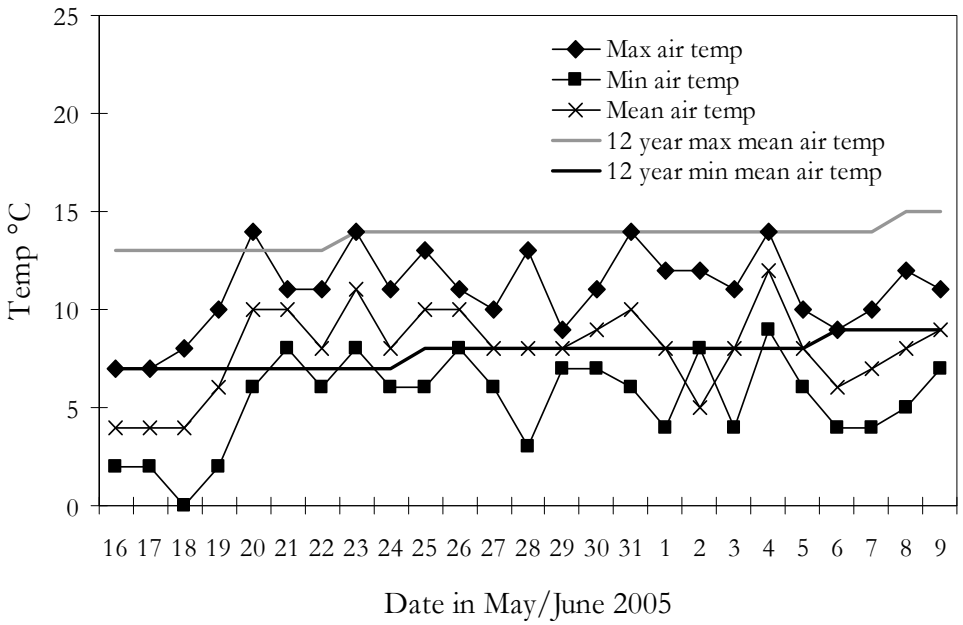

Figure 3.3. Minimum, maximum and mean daily air temperature (°C). Recorded at the Bergen Flesland airport weather station (www.wunderground.com), with the 12 year (1996-2008) mean maximum and minimum daily temperatures for a. 2006 Mesocosm experiment (this study) and b. 2005 Mesocosm experiment. For discussion of the 2005 experiment see Discussion section 6.2.1.

This information will be used later to help explain differences between the two experiments. Chlorophyll *a* measurements, used as a proxy of total phytoplankton biomass, are shown in Figure 3.4. Also shown are phaeopigment concentrations, usually considered a biomarker of grazing or general phytoplankton degradation (Jeffrey 1980). Following the addition of nutrients on 6 May (See Figure 3.4), four days passed before obvious growth began to occur within the mesocosms. However, once the bloom was sufficiently stimulated, exponential growth rapidly proceeded from 11 – 13 May, with the peak of the bloom occurring on 13 - 14 May. The temporal dynamics of the chlorophyll *a* concentrations have been used to divide the experiment up into three phases: **Phase 1 Pre-bloom**, a period before any significant growth occurred (6 – 9 May), **Phase 2 Bloom**, encompassing the period of exponential growth, the peak and decline in chlorophyll *a* (10 – 17 May), and **Phase 3 Post-bloom**, where nutrients had become depleted and opportunistic species began to dominate (18 – 23 May).

3.3.3. Development of the bloom

Nitrate and phosphate concentrations rapidly declined during the period 10 – 15 May, falling from 17 to ~2 μmol l^{-1} and 1.0 to 0.3 μmol l^{-1}, respectively. Following this, chlorophyll *a* concentrations in all mesocosms gradually declined over the period 15 – 18 May, while nutrient concentrations remained stable. During the latter stages of the experiment (19 – 23 May) a secondary increase in chlorophyll *a* occurred in all mesocosms except M6, suggesting some recycling of nutrients and renewed growth. A slight increase in nitrate concentrations during this period (Figure 3.5) may have stimulated growth at this late stage of the experiment.

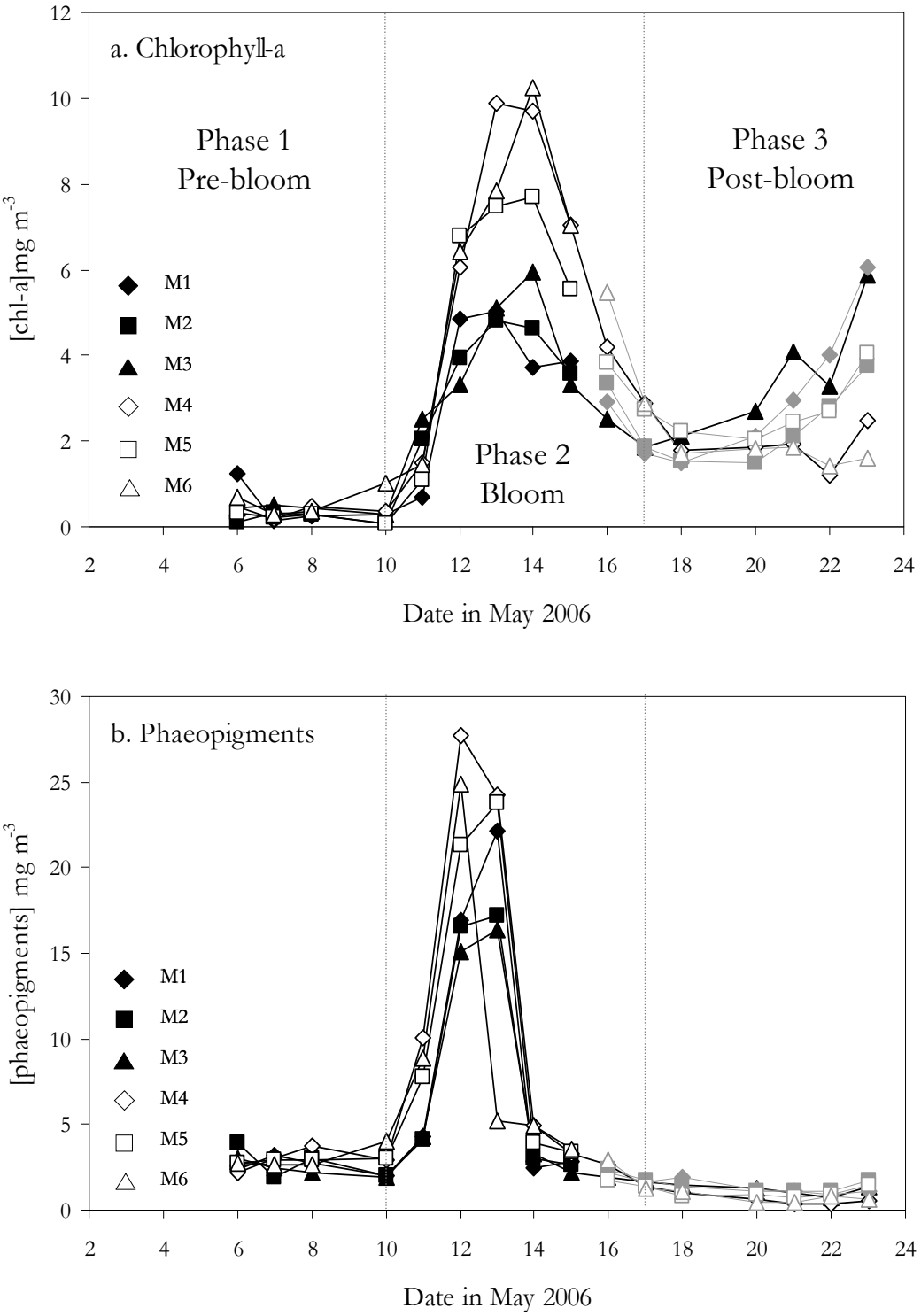

Figure 3.4. Concentrations of a. Chlorophyll *a* (mg m^{-3}) and b. Phaeopigments measured over the course of the experiment. Due to re-aeration and alteration of experimental conditions of mesocosms 1, 2, 5, and 6 on 15 May, data for these mesocosms is shown in grey. The un-altered M3 and M4 are plotted in black for the whole experiment. The experiment is divided into three phases: 1. Pre-bloom phase 6 – 9 May, 2. Bloom phase, 10 – 17 May and 3. Post-bloom phase 18 – 23 May.

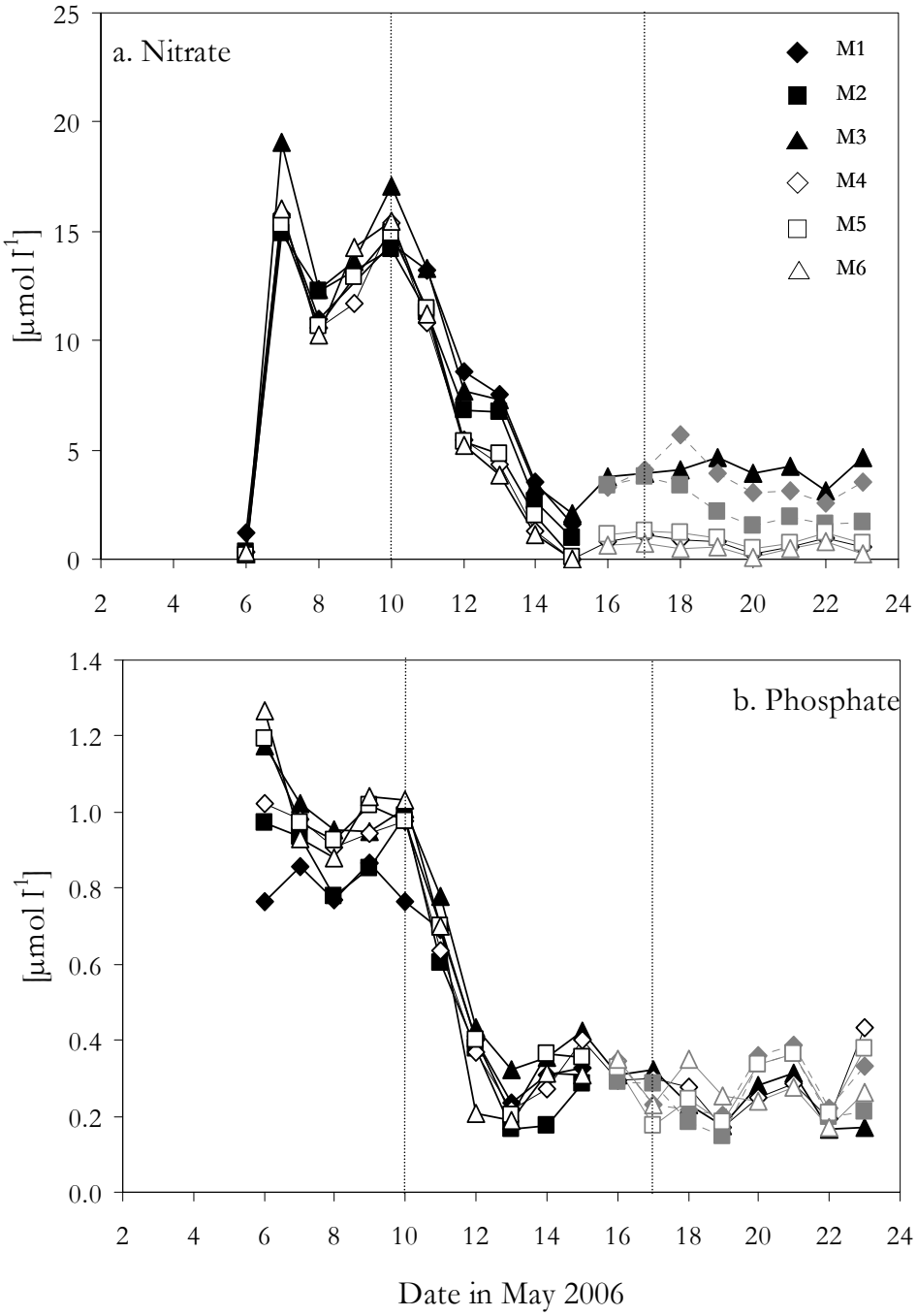

Figure 3.5. a. Nitrate and b. Phosphate concentrations (µmol l^{-1}). Due to re-aeration and alteration of experimental conditions of mesocosms 1, 2, 5, and 6 on 15 May, data for these mesocosms is shown in grey. The un-altered M3 and M4 are plotted in black for the whole experiment. The experiment is divided into three phases: 1. Pre-bloom phase 6 – 9 May, 2. Bloom phase, 10 – 17 May and 3. Post-bloom phase 18 – 23 May. Data courtesy of Ian Joint, Plymouth Marine Laboratory.

Chlorophyll *a* concentrations for the whole experiment (taking into account M3 and M4 only after 15 May) had mean values of 2.5 mg m^{-3} for the high CO_2 treatment, and 3.4 mg m^{-3} for the present day, representing a mean 28% decrease in chlorophyll *a* concentrations under high CO_2. The data was non-normally distributed so underwent a log transformation to improve the distribution of the data (Test for Normality, Anderson-Darling High CO_2 = 0.466, p = 0.237, Present day = 0.329, p=0.505), and did display equal variances (Levene's statistic 0.40, p = 0.527). Therefore the Mann-Whitney test was used and the mean data were found to show no significant differences between treatments (W = 1106.5, p = 0.4182, See Table 3.3 and Appendix 1). When Phase 2 (Bloom period 10 – 17 May – see Figure 3.5) is considered separately, differences between treatments become apparent. There were large differences in mean concentrations between treatments during this period (Present day = 3.12 mg m^{-3}, High CO_2 = 1.78 mg m^{-3}, 43% decrease under high CO_2). The data was found to be normally distributed (Test for Normality, Anderson-Darling High = 0.452, p =0.245, Present day= 0.664, p = 0.070) although it did not display equal variances (Levene's statistic = 7.07, p = 0.011). Therefore a T-test (not assuming equal variances) was performed and this confirmed that there were significant differences in chlorophyll *a* concentrations between treatments during the bloom phase of the experiment (T = 2.45, DF = 28, p = 0.021, See Table 3.3 and Appendix 2).

Figure 3.6 shows microphytoplankton cell counts from flow cytometric analysis. In general, most species showed little increase in abundance until 9 – 11 May. Following the initiation of growth most species peaked in abundance at some stage in Phase 2 between the 12 and 15 May. During Phase 3, most species also experienced a secondary increase in abundance over the final 4 – 5 days of the experiment (19 – 23 May).

The coccolithophores (Fig. 3.6 a) grew in number from <500 cells ml^{-1} at the start of the experiment, to ~3000 cells ml^{-1} in M3, M4, M5 and M6 on 14 May. M1 and M2 failed to reach a peak, with numbers never exceeding about 1000 cells ml^{-1}.

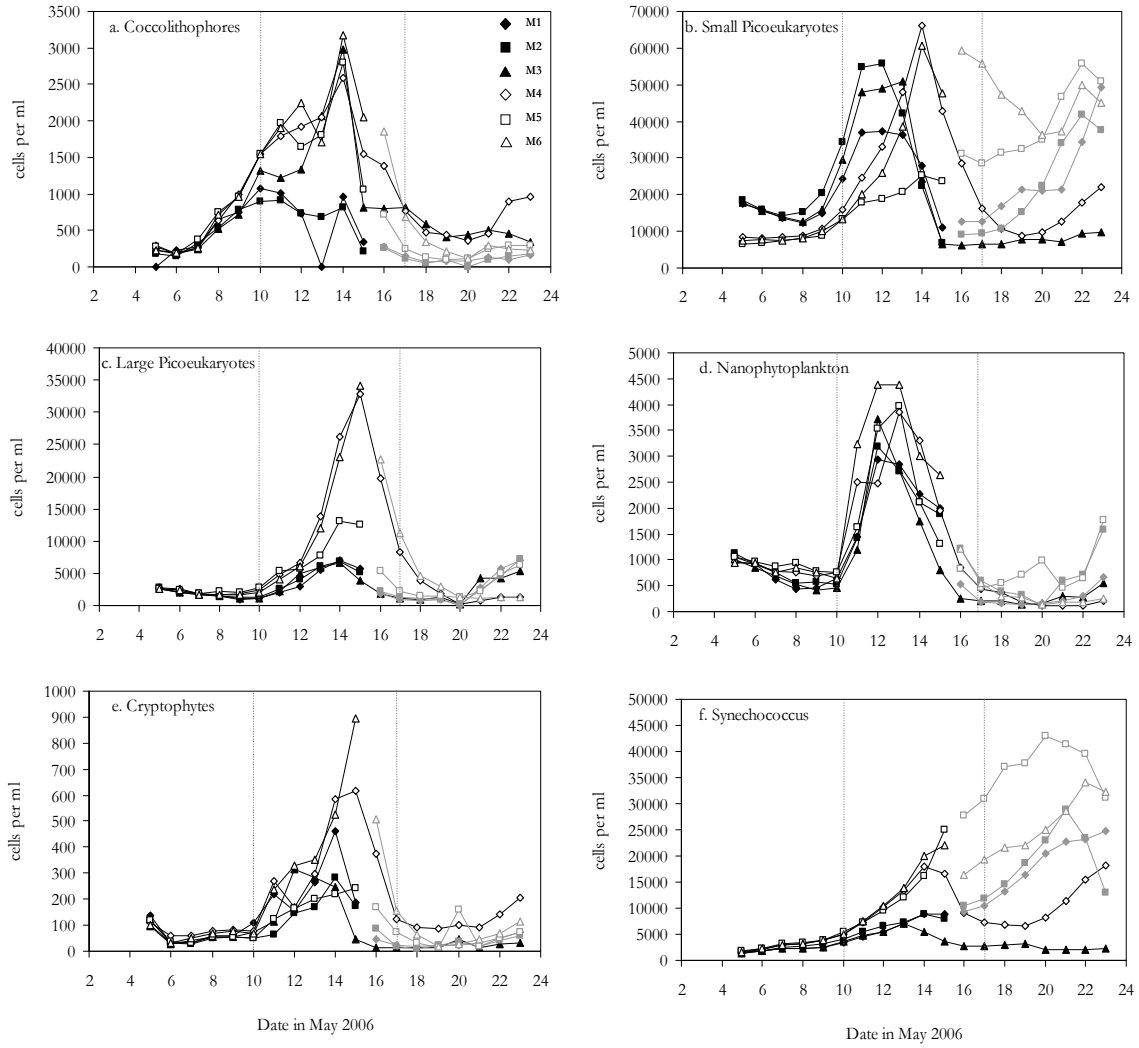

Figure 3.6. Microphytoplankton species cell counts (cell per ml). a. Coccolithophores, b. Small picoeukaryotes, c. Large picoeukaryotes, d. Nanophytoplankton, e. Cryptophytes, f. *Synechococcus*. Data produced by Isabelle Mary (NOCS) from flow cytometric analysis. Due to re-aeration and alteration of experimental conditions of mesocosms 1, 2, 5, and 6 on 15 May, data for these mesocosms is shown in grey. The un-altered M3 and M4 are plotted in black for the whole experiment. Vertical grey lines indicate the 3 phases of the bloom. A summary of the statistical analysis performed on this data is shown in Table 3.3.

From the peak of the bloom, M3 and M4 saw rapid decreases in cell number down to ~1000 cells ml^{-1}, with numbers remaining identical in these two mesocosms between 17 and 21 May. Following this, M4 displayed some renewed growth, with an increase in abundance between 22 and 23 May. However, as a whole, there were large differences in coccolithophore numbers between treatments over the course of the experiment. A statistically significant 42 percent decrease in coccolithophores was observed under high CO_2 ($T = 3.17$, $p = 0.002$, see Table 3.3).

The small picoeukaryotes (Fig. 3.6 b) displayed clear and consistent differences between treatment from the outset, with a starting number of ~20,000 cells ml^{-1} in the high CO_2 M1, M2 and M3, and ~10,000 cells ml^{-1} in M4, M5 and M6. Once the bloom took off, the differences became even more apparent, with highly diverse temporal dynamics between the present day and high CO_2 mesocosms. M1, M2 and M3 peaked at ~60,000 cells ml^{-1} on the 11 – 13 May, with numbers sustaining their maximum values for 2 – 3 days. In contrast, M4 and M6 experienced a sharp peak of >60,000 cells ml^{-1} on 14 May, followed by a quick decline in numbers the following day. Interestingly, M5 failed to reach a peak in small picoeukaryotes, with numbers just gradually rising to the end of the experiment. Numbers in M3 collapsed to <10,000 cell ml^{-1} by 15 May and stabilised at these levels until the end of the experiment. By contrast, M4 reached a minimum of ~10,000 cells ml^{-1} on 19 May, but then showed renewed growth over the period 20 - 23 May, reaching 20,000 cells ml^{-1} by the end of the experiment. Although the temporal development of the small picoeukaryotes population exhibited quite different behaviour between treatments, there was only a small overall difference between treatments and no significant differences (+9 percent under high CO_2, see Table 3.3).

The abundance of large picoeukaryotes (Fig. 3.6 c) in all mesocosms started at low levels of <5000 cells ml^{-1}. However, as soon as growth took off, large differences between treatments became apparent. M1, M2 and M3 reached a modest peak on 14 May of just over 5000 cells ml^{-1}. By stark contrast, M4 and M6 peaked at ~35,000 cells ml^{-1} on 15 May, and M5 had a slightly less dramatic maximum of ~15,000 cells ml^{-1} over 14 – 15 May. For the period of the bloom (Phase 2), mean numbers of large picoeukaryotes were 68 percent lower under high CO_2, a difference found to be significantly different ($T = 4.5$, $p<0.001$, see Table 3.3). During Phase 3 (Post-bloom) differences between treatments remained but reversed in nature. Numbers in M4 stayed low, whilst the high CO_2 M3 displayed renewed growth over 21 – 23 May, re-attaining levels of ~5000 cells ml^{-1}. Overall, mean numbers of large picoeukaryotes were significantly lower under high CO_2 (-60 percent, $T = -2.33$, $p = 0.023$, see Table 3.3).

Table 3.3. Summary of the statistical analysis performed on chlorophyll a and microphytoplankton data. M3 and M4 only are included in the analysis for data after 15 May. For full details of statistical analyses see Appendix 1 and 2.

	Percentage change under high CO_2	**Statistical Test**	**Significant differences ($p<0.05$)**
Chlorophyll a Whole experiment	-28 %	Mann-Whitney W = 1106.5, p = 0.4182	
Chlorophyll a Phase 2 Bloom	-40 %	2-sample T-test T = 2.45, p = 0.021	√
Coccolithophores	-42 %	2-sample T-test T = 3.17, p = 0.002	√
Small Picoeukaryotes	+9 %	Mann-Whitney W = 1431, p = 0.642	
Large Picoeukaryotes	-60 %	2-sample T-test T = -2.33, p=0.023	√
Large Picoeukaryotes Phase 2 (Bloom)	-68 %	2-sample T-test T = 4.5, p<0.001	√
Nanophytoplankton	-25 %	Mann-Whitney W = 1175, p = 0.1188	
Cryptophytes	-44 %	2-sample T-test T = 2.93, p = 0.005	√
Synechococcus	-55 %	Mood's Median X^2 = 9.14, p = 0.003	√

During Phase 1, numbers of nanophytoplankton (Fig. 3.6 d) showed a slight decrease before the bloom took off in Phase 2, with numbers falling from ~1000 cells ml^{-1} to ~500 cells ml^{-1} over 5 to 10 May. However, subsequent to 10 May, growth swiftly ensued in all mesocosms, with peaks of 3000 – 4000 cells ml^{-1} in M1, M2 and M3 on 12 May, and 4000 – 4500 cells ml^{-1} in M4, M5 and M6 on 13 May. Following this maximum, numbers rapidly fell to <1000 cells ml^{-1} in all mesocosm on 17 May. From this point, the abundance of nanophytoplankton in M3 and M4 remained low until the end of the experiment. As a whole, only small differences between treatments were obvious for the nanophytoplankton, e.g. slightly enhanced numbers in M6 during Phase 2. Although a 25 percent decrease in mean numbers was observed under high CO_2, this difference was not found to be statistically significant (See Table 3.3).

The Cryptophytes (Fig. 3.6 e) displayed the lowest abundance over the course of the experiment of the phytoplankton species described here, with numbers never exceeding 1000 cells ml^{-1} and mean values of only 109 cells ml^{-1} under high CO_2 and 195 cells ml^{-1} under the present day treatment. Numbers of Cryptophytes were very

low during Phase 1 in all mesocosms (<100 cells ml^{-1}) and there were no clear difference between treatments. Growth began during Phase 2, and initially with no obvious differences between mesocosms. However, a divergence became apparent on 14 May when Cryptophyte numbers peaked. Numbers in the present day M6 reached 900 cells ml^{-1}. The maximum abundance under high CO_2 was attained on 14 May in M1, with a peak of just under 500 cells ml^{-1}. Numbers in all mesocosms gradually fell after the peak, and stabilised at <200 cells ml^{-1} in M3 and M4 for the first five days of Phase 3. Similarly to the coccolithophores and small picoeukaryotes, numbers started increasing again in M4 towards the end of the experiment. As a whole, a significant mean 44 percent decrease in Cryptophyte numbers was observed under high CO_2 ($T = 2.93$, $p = 0.005$, see Table 3.3).

The nature of the temporal development of *Synechococcus* (Fig. 3.6 e) was quite different to that of the other groups of microphytoplankton described here. In addition, there was also less clear reproducibility between mesocosms within treatments. Initially, reproducibility was good, with low numbers (<5000 cells ml^{-1}) in all mesocosms during Phase 1. By the start of Phase 2 (10 May) a divergence between high and present day CO_2 mesocosms had appeared, with lower numbers under high CO_2. At this point, inter-treatment reproducibility was still good. A shift occurred on 14 – 15 May, with deviations between mesocosms of the same treatment. It is possible this is symptomatic of the re-aeration of M1, M2, M5 and M6. M1 and M2 behave similarly from this point with continuing increasing numbers. In contrast, M3 saw a slight decrease in numbers following a modest peak on 15 May, and then stabilised at ~2000 cells ml^{-1} for the remainder of the experiment. In a similar fashion, M5 and M6 displayed comparable temporal trends during Phase 3 following their re-aeration, whereas following a peak of ~20,000 cells ml^{-1} on 14 May, numbers in M4 dropped to ~10,000 cells ml^{-1} by 17 May. Renewed growth then occurred in M4 towards the end of the experiment, a secondary bloom that was mirrored by the Cryptophytes, small picoeukaryotes and coccolithophores. Statistically, a large and significant difference in *Synechococcus* numbers between treatments was detected, with a 55 percent reduction under high CO_2 (Mood's Median $X^2 = 9.14$, $p = 0.003$).

Further information on the phytoplankton communities of the experiment was derived from phytoplankton microscopy enumeration. Phytoplankton biomass data is shown in Appendix 4, and Figure 3.7 a shows percentage phytoplankton biomass for M1 and M6, with data for the high-CO_2 M1 scaled to the present day control M6. Taken as an average of the whole experiment, total biomass was 32 percent lower

under high-CO_2 in M1, although total biomass under high-CO_2 exceeded that for present day CO_2 on 11 and 14 May (See Figure 3.7). The peak in total biomass occurred on 15 May in both M1 and M6, with a maximum values of 264.5 mg C m^{-3} and 323.2 mg C m^{-3}, respectively (See Appendix 4). Interestingly, this peak was one day after the chlorophyll *a* peak, the concentrations of which had already begun a steep decline by 15 May (Figure 3.5). The overall composition of the community does not show any clear differences between treatments (Figure 3.7 a), with the various components of the phytoplankton community occurring in similar proportions under both treatments, although it is difficult to subject the data to any complex statistical analyses in order to elucidate any differences due to the low number of samples.

In terms of biomass, the communities of both M1 and M6 were dominated by Flagellates, which made up 71 percent of total biomass in M1 and 67 percent in M6 (Appendix 5). Unlike the data for total biomass, the limited available information on the flagellate community does suggest there may be some differences between treatments. In the present day M6, the flagellates are dominated by "Undetermined flagellates 10 μm" with 30 percent of the population, followed by the Cryptophyceae with 20 percent. In contrast, the community of the high CO_2 M1 was dominated by the Cryptophyceae (24 percent), with a 10 percent contribution from "Undetermined Flagellates 10 μm". The temporal dynamics of the flagellate community are shown in Figure 3.8. An initial peak on 14-15 May in both mesocosms was dominated by "undetermined flagellates". Following this was a secondary peak characterised by high Cryptophyceae biomass on 18 May. The Cryptophyceae are typically present in low numbers in natural waters, but sporadically observed in high numbers following the senescence of a previously-dominant bloom species (Stewart and Wetzel 1986). The findings of this study are in agreement with this, as Cryptophyceae numbers rapidly rose following the peak in flagellate biomass, particularly in M6 (Figure 3.8 b). The biomass of Cryptophyceae exhibited two peaks in M1, one on 13 May immediately after a peak in Prymnesiophytes, and the other on 18 May, as in M6.

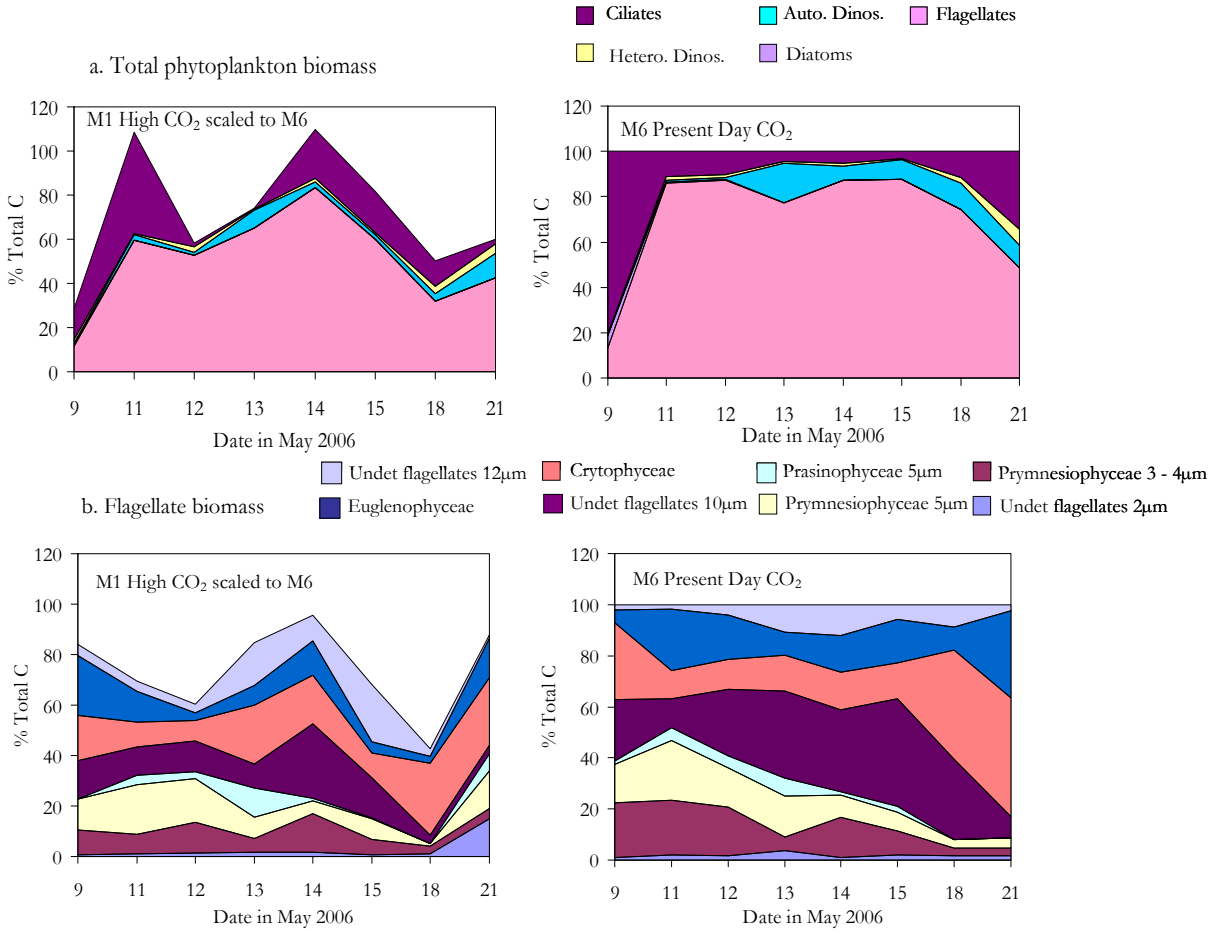

Figure 3.7. Phytoplankton percentage biomass for a. Overall groups (Ciliates, heterotrophic dinoflagellates, autotrophic dinoflagellates, diatoms and flagellates) and b. Flagellates. Counts were made on the following days: 9, 11, 12, 13, 14, 15, 18 and 21 May. Flagellates were the dominant group under both treatments - 71% of total biomass in high CO_2 M1 and 66% in ambient CO_2 M6. The flagellates under high CO_2 were dominated by Crytophyceae (24%) and under the ambient control by "undetermined flagellates 10µm" (30%). Data for the high CO_2 M6 is scaled to the ambient control M1 to show how the total biomass in M1 changed in relation to M6. Phytoplankton microscopy counts performed by Claire Widdicombe, PML.

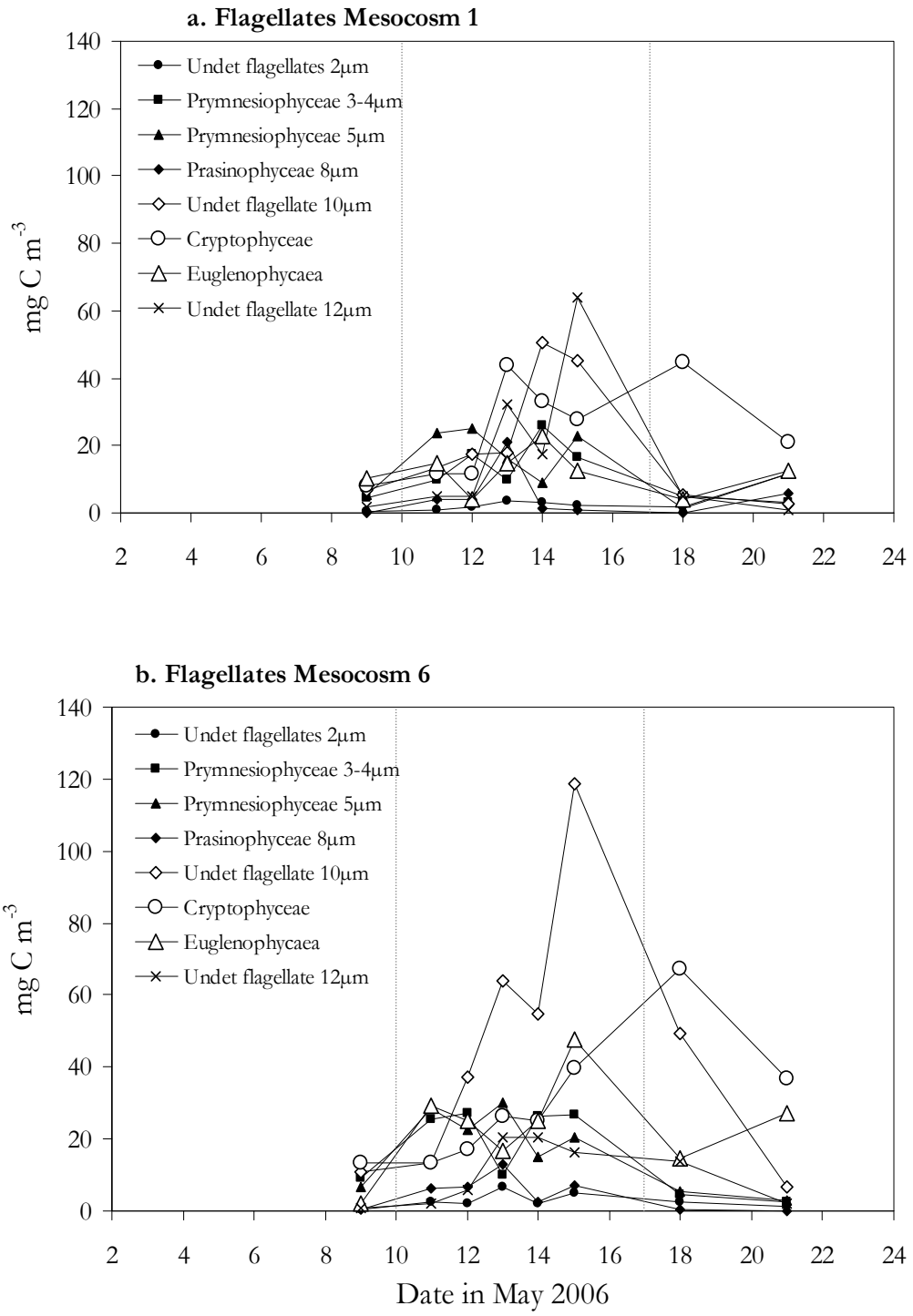

Figure 3.8. Biomass of the individual components of the flagellate community over the course of the experiment in a. High CO_2 Mesocosm 1 and b. Present day Mesocosm 6. Phytoplankton microscopy counts performed by Claire Widdicombe, PML. Vertical grey lines indicate the 3 phases of the bloom.

Coccolithophores are often regarded as a key phytoplankton species in investigations into the impacts of OA. Not only are they key marine calcifiers that have a significant impact on oceanic carbon cycling (Brown and Yoder 1994; Riebesell *et al.* 2000b), they are also prolific producers of the climatically-important trace gas DMS (Malin *et al.* 1992; Liss *et al.* 1997). Therefore, it is important to assess the contribution coccolithophores may have made to the communities of the mesocosms. Unfortunately, due to the methodology used for the phytoplankton microscopy enumeration, preservation of coccolithophores was not possible (Lugol's iodine is corrosive to coccolithophore calcium carbonate tests). Therefore, information was derived from flow cytometry counts, performed by Isabelle Mary (NOCS). Coccolithophore counts (cells per ml) were converted to biomass using the equations of (Menden-Deuer and Lessard 2000). Figure 3.9 shows coccolithophore biomass (solid lines) plotted with total flagellate biomass (dashed lines).

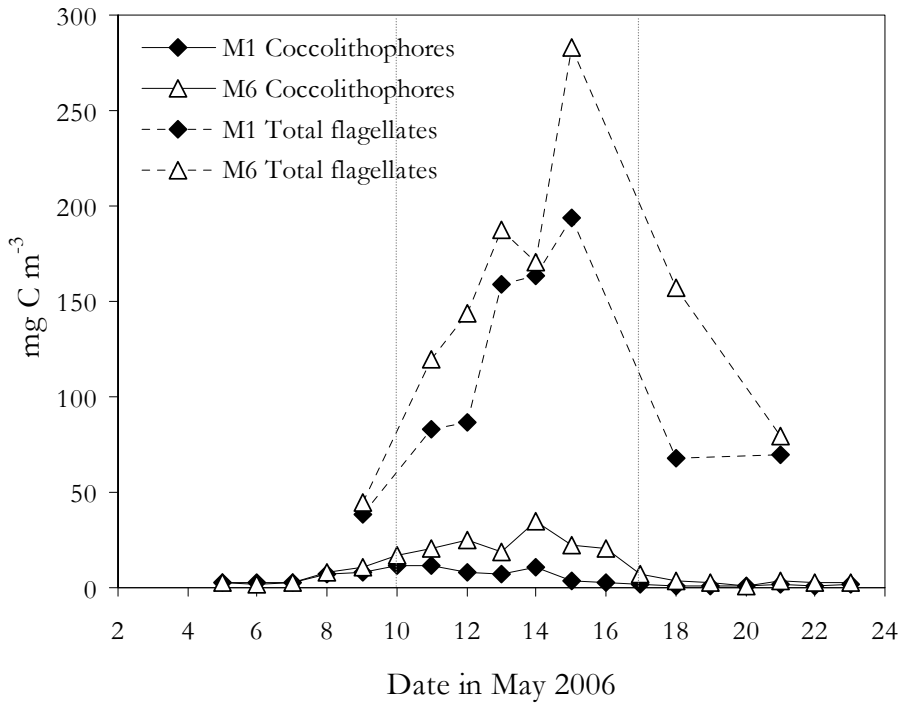

Figure 3.9. Total flagellate biomass (mg C m^{-3}) under high CO_2 (M1 – Open diamonds)) and under the ambient control (M6 – Open triangles), and coccolithophore biomass (mg C m^{-3}) under high CO_2 (M1 – closed diamonds) and under the ambient control (M6 – closed triangles). Contribution of coccolithophores to total flagellate biomass is 6 percent under high CO_2 and 12 percent under the ambient control. Vertical grey lines indicate the 3 phases of the bloom. Coccolithophore counts performed by Isabelle Mary, NOCS.

Clearly, coccolithophores contributed a small fraction to the total flagellate community, suggesting they were not an important component of the total biomass during this experiment. However, there were statistically significant differences in coccolithophore numbers between treatments (T = 3.17, DF = 68, p = 0.002, see Table 3.3), with a mean of 728.9 cells per ml under high CO_2 compared to 1252.0 cells per ml under present day CO_2, a difference of 42 percent.

3.3.4. Halocarbons

3.3.4.1. Iodocarbons

The iodocarbons generally showed similar temporal trends over the course of the experiment, and maximum concentrations were observed during the period 14 – 18 May. The concentrations of the iodocarbons (CH_3I, C_2H_5I, CH_2I_2, CH_2ClI) are shown in Figure 3.10. As M1, M2, M5 and M6 underwent re-aeration on 15 May and these data are plotted in grey from 17 May to the end of the experiment – priority is given to the data from M3 and M4 which underwent no further treatment subsequent to the initial aeration. The temporal dynamics of the iodocarbons suggest an association with biological activity, as all exhibit a period of rapid increase before reaching a peak, then decreasing during the latter stages of the experiment. However, the concentrations do not appear to be directly related to total phytoplankton growth since maximum concentrations occurred generally after the maxima in chlorophyll *a*. Furthermore, the timings of the initial increases in iodocarbons did not coincide with those of chlorophyll *a* (11 May) (Figures 3.5 and 3.10): iodomethane (CH_3I) and iodoethane (C_2H_5I) increased from 8 May whereas diiodomethane (CH_2I_2) and chloroiodomethane (CH_2ClI) concentrations began to rise on 12 and 13 May, respectively. Figure 3.10 clearly shows that lowered pH in the high-CO_2 mesocosms resulted in a reduction in iodocarbon concentrations. For the experiment as a whole, mean concentrations of all iodocarbons were lower under high CO_2. Mean concentrations of CH_3I, C_2H_5I, CH_2I_2 and CH_2ClI under high CO_2 were 5.4 pM, 0.5 pM, 134.6 pM and 136.9 pM, compared to 9.2 pM, 0.7 pM, 200.8 pM and 191.0 pM in the present day mesocosms. During Phase 2, the mean concentrations of CH_3I, C_2H_5I and CH_2I_2 were all lower under high CO_2, with CH_3I displaying significant differences for this period and also over the whole experiment (Whole experiment: T = 2.35, p = 0.022, Phase 2 T = 2.75, DF = 22, p = 0.012 , Table 3.4 and Appendix 1 and 2). During

this period, CH_2ClI showed little difference between treatments, with almost identical concentrations in all mesocosms.

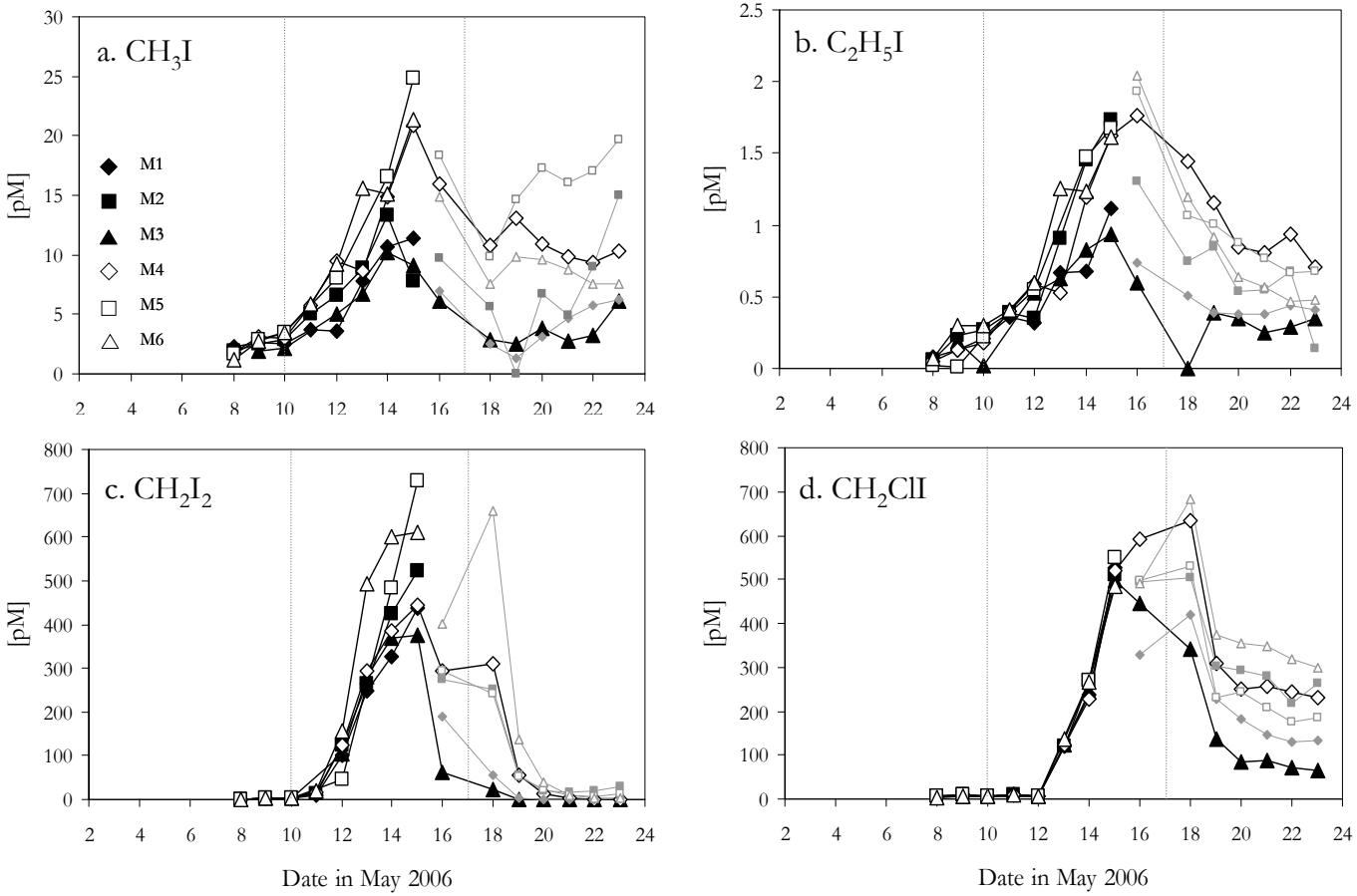

Figure 3.10. Concentrations of a. CH_3I, b. C_2H_5I, c. CH_2I_2 and d. CH_2ClI (pM) over the course of the experiment. Due to re-aeration and alteration of experimental conditions of mesocosms 1, 2, 5 and 6 on 15 May, trace gas data for these mesocosms is shown in grey after this date. Vertical lines indicate the 3 phases of the bloom. The un-altered M3 and M4 are plotted in black for the whole experiment

However, during Phase 3 (Post-bloom 18 – 23 May), all the iodocarbons exhibited an effect of high CO_2 treatment, with average decreases of 67, 73, 93 and 59 percent for CH_3I, C_2H_5I, CH_2I_2 and CH_2ClI, respectively (See Table 3.15). Differences between treatments were maintained in M3 and M4 until the end of the experiment, with the exception of CH_2I_2 which returned to its initial concentrations on 20 May.

Table 3.4. Summary of outcome of statistical analysis on iodocarbon data. Two analysis were performed, one on data for the whole experiment, and one on data from Phase 2 of the experiment (Bloom 10 – 17 May). For all analyses, M3 and M4 only are included after 15 May. Phase 3 could not undergo the same statistical analysis due to lack of replicates.

	Statistical Test	**Significant differences ($p<0.05$)**
CH_3I Whole experiment	Mann-Whitney W = 691, p = 0.0108	√
CH_3I Phase 2 Bloom	2-sample T-test T = 2.75, p = 0.012	√
C_2H_5I Whole experiment	2-sample T-test T = 1.74, p = 0.087	
C_2H_5I Phase 2 Bloom	2-sample T-test T = 1.36, p = 0.182	
CH_2I_2 Whole experiment	Mann-Whitney W = 786, p = 0.2833	
CH_2I_2 Phase 2 Bloom	2-sample T-test T = 1.13, p = 0.265	
CH_2ClI Whole experiment	Mann-Whitney W = 828, p = 0.6746	
CH_2ClI Phase 2 Bloom	Mann-Whitney W = 307.5, p = 0.5944	

Figure 3.11 shows the mean ratios of a. CH_3I, b. C_2H_5I, c. CH_2I_2 and d. CH_2ClI to chlorophyll *a*. During Phase 1 before the bloom had initiated, production of CH_3I and C_2H_5I per chlorophyll *a* was elevated under high CO_2. This trend quickly changed once exponential growth began during Phase 2. For the period 12 - 15 May, less difference in ratios was observed for both CH_3I and C_2H_5I. Following this, large differences between treatments appeared from 16 May which lasted through until the end of the experiment, with much less CH_3I and C_2H_5I per chlorophyll *a* produced under high CO_2. A considerable drop in ratio on 23 May under present day CO_2 was seen for both compounds. Ratios of CH_2I_2 and CH_2ClI to chlorophyll *a* also showed similarities to each other. Little difference between mesocosms was observed

for the first half of the experiment (8 – 15 May), with gradually rising ratios under both treatments. However, the ratios were slightly elevated under high CO_2, suggesting marginally more production of these compounds per chlorophyll *a*. In contrast, large difference between treatments became apparent from 16 May, with rising ratios under present day CO_2 culminating in a peak on 18 May, contrasted by rapidly declining ratios in the high CO_2 treatment. Ratios for CH_2ClI remained higher under present day CO_2 until the end of the experiment, whilst those for CH_2I_2 dropped down to the low levels seen under high CO_2 for the last 2- 3 days of the experiment.

The similar trends observed for CH_3I: chlorophyll *a* and C_2H_5I: chlorophyll *a* over the course of the experiment imply similar production/consumption mechanisms for these two gases. Likewise, the ratios of CH_2I_2: chlorophyll *a* and CH_2ClI: chlorophyll *a* displayed similar temporal dynamics, suggesting their production is also related, but not so closely related to the processes controlling CH_3I and C_2H_5I. However, a sharp drop in ratios on 23 May was recorded for CH_3I, C_2H_5I and CH_2ClI, hinting that there may be some links in their production/removal mechanisms.

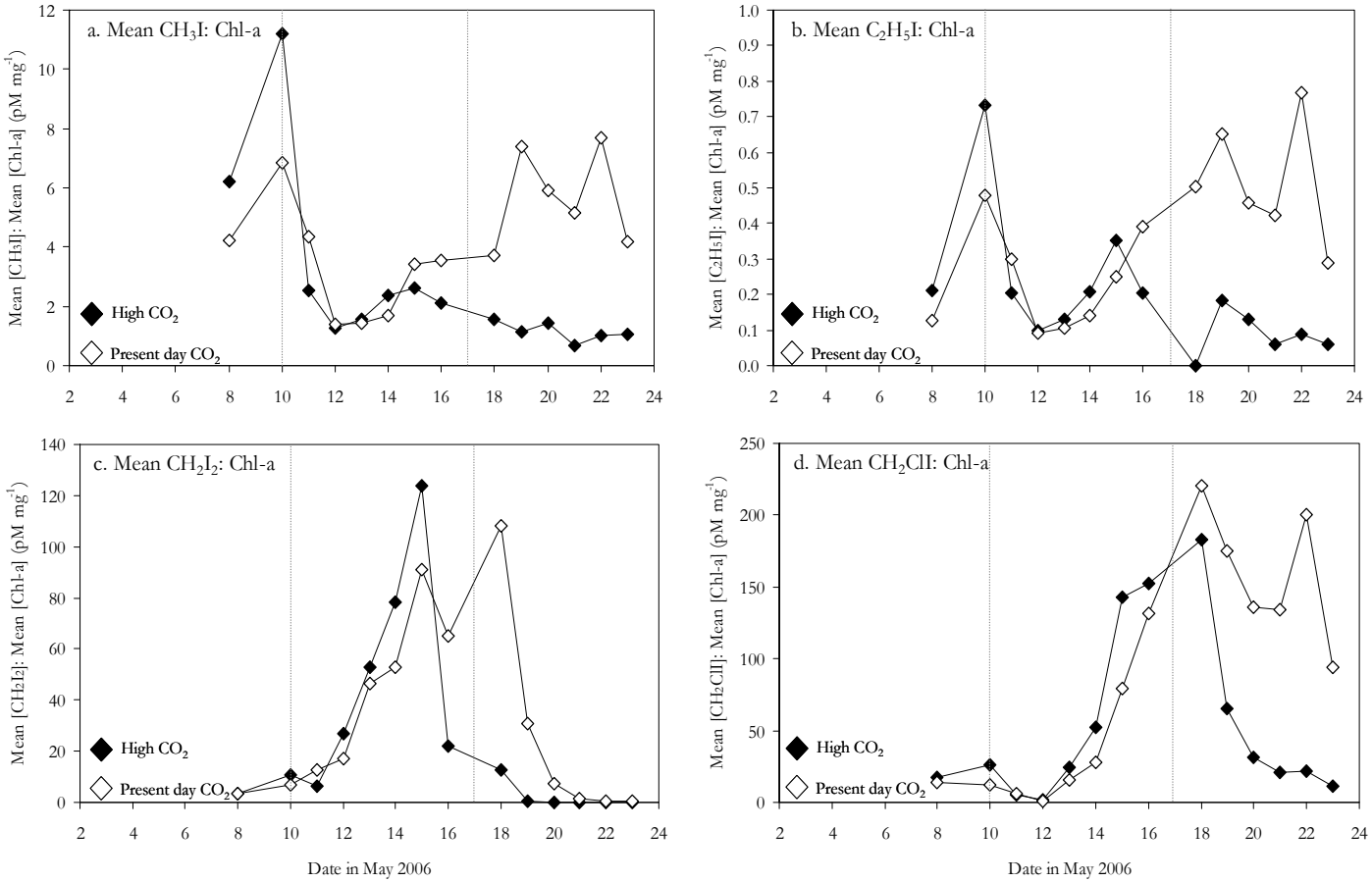

Figure 3.11. Mean ratios of a. CH_3I: Chlorophyll *a*, b. C_2H_5I: Chlorophyll *a*, c. CH_2I_2: Chlorophyll *a* and d. CH_2ClI: Chlorophyll *a* for the present day (open diamonds) and high CO_2 (closed diamonds) treatment. Vertical grey lines indicate the 3 phases of the bloom. M3 and M4 only are taken into consideration after 15 May.

Table 3.5. Selected Spearman's Rank Correlation Coefficients (ρ) and associated significance level for mean CH_3I, C_2H_5I, CH_2I_2, CH_2ClI, chlorophyll *a*, phaeopigments and phytoplankton community components under high CO_2 (M1, M2, M3) and present-day CO_2 (M4, M5, M6). M3 and M4 only are included in the analysis after 15 May. Full results of all Spearman's Rank are shown in Appendix 6.

		CH_3I	C_2H_5I	CH_2I_2	CH_2ClI
C_2H_5I	High CO_2	0.821***	-	-	-
C_2H_5I	Present CO_2	0.914***	-	-	-
CH_2I_2	High CO_2	0.650**	0.632**	-	-
CH_2I_2	Present CO_2	0.686***	0.618**	-	-
CH_2ClI	High CO_2	0.529*	0.514*	NS	-
CH_2ClI	Present CO_2	0.804***	0.900***	NS	-
Chlorophyll *a*	High CO_2	0.654**	0.522*	NS	NS
Chlorophyll *a*	Present CO_2	0.775***	0.555*	0.709***	NS
Phaeopigments High CO_2		0.419	0.543	0.731***	-0.055
Phaeopigments Present CO_2		0.005	-0.115	0.580*	-0.405
Small picoeukaryotes Present CO_2		0.521*	NS	0.557*	NS
Large picoeukaryotes Present CO_2		NS	NS	0.807***	NS
Nanophytoplankton High CO_2		0.543*	NS	0.618**	NS
Nanophytoplankton Present CO_2		NS	NS	0.632**	NS
Cryptophytes High CO_2		NS	0.532*	0.632**	NS
Synechococcus High CO_2		0.532*	0.614**	0.889***	NS
Synechococcus Present CO_2		0.596*	0.525*	NS	NS

* = 95% confidence level (p<=0.05), ** = 98% confidence level (p<=0.02), *** = 99% confidence level (p<=0.01), NS = not significant

Table 3.5 shows significant Spearman's Rank correlations between the iodocarbons (CH_3I, C_2H_5I, CH_2I_2 and CH_2ClI) and biological/community parameters (Chlorophyll *a* and phytoplankton cell counts). Starting with the iodocarbons themselves, CH_3I and C_2H_5I were significantly correlated with all other compounds, with particularly strong relationships between CH_3I and C_2H_5I under

both high and present day CO_2 (n = 16, ρ = 0.821 and 0.914, respectively), and CH_3I and CH_2ClI and C_2H_5I and CH_2ClI under present day CO_2 (n = 16, ρ = 0.804 and ρ = 0.900, respectively). CH_2I_2 and CH_2ClI were correlated with both CH_3I and C_2H_5I, but not with each other.

The iodocarbons showed a wide range of correlations with the biological parameters. Under both high and present day CO_2, CH_3I and C_2H_5I were significantly correlated with both chlorophyll *a* and *Synechococcus* (See Table 3.5). In addition, CH_3I was correlated with nanophytoplankton (ρ = 0.543) and C_2H_5I with Cryptophytes (ρ = 0.532) under high CO_2. Of the iodocarbons, CH_2I_2 showed the greatest number of correlations with biological parameters. It displayed particularly strong relationships with nanophytoplankton under both treatments (ρ = 0.618 Present, ρ = 0.807 High), chlorophyll *a*, and small and large picoeukaryotes under the present day treatment (ρ = 0.709, 0.557, 0.807, respectively), and with *Synechococcus* and coccolithophores under high CO_2 (ρ = 0.889 and 0.532). In addition, CH_2I_2 was found to be significantly correlated with phaeopigments under both treatments, with a particularly strong positive correlation (99% significance level) under high CO_2.

Table 3.6 shows selected significant Spearman's Rank correlation coefficients for the iodocarbons and phytoplankton species biomass, derived from cell microscopy enumeration. Cell enumerations were only carried out for M1 and M6, and on a limited number of days (9, 11-5, 18, 21 May) so the amount of data available for analysis was small. Nevertheless, strong significant correlations were seen between CH_3I, C_2H_5I and CH_2I_2 and the flagellates in both M1 and M6 (See Table 3.6). Autotrophic dinoflagellates also strongly correlated with CH_3I and C_2H_5I in M6 (ρ = 0.738 and 0.833, respectively). When the flagellates were divided into their constituent groups, further relationships were observed. The "undetermined flagellates 10μm" were correlated with CH_3I, C_2H_5I and CH_2I_2 in M6, while "undetermined flagellates 12μm" correlated with the same three compounds in both M1 and M6 (Table 3.6). Interestingly, CH_2ClI displayed no significant positive correlations with any of the biological parameters, although showed one significant negative correlation with small picoeukaryotes under high CO_2 (ρ = -0.629). This lack of correlations implies that concentrations of this compound may not be directly dependent on biological production or consumption processes.

Table 3.6. Selected Spearman's Rank Correlation Coefficients (ρ) and associated significance level for mean CH_3I, C_2H_5I, CH_2I_2, CH_2ClI, and phytoplankton biomass under high CO_2 (M1, M2, M3) and present-day CO_2 (M4, M5, M6). M3 and M4 only are included in the analysis after 15 May. Full results of Spearman's Rank analysis are shown in Appendix 9.

Mesocosm 1: 9,11-15,18,21 May	CH_3I	C_2H_5I	CH_2I_2
C_2H_5I	0.762*	-	-
CH_2I_2	NS	0.762*	-
CH_2ClI	NS	0.857**	NS
Flagellates	0.881***	0.762*	0.881***

Mesocosm 6: 9,11-15,18,21 May			
C_2H_5I	0.929***	-	-
CH_2I_2	NS	0.810	-
Flagellates	0.881***	0.976***	0.833**
Autotrophic dinoflagellates	0.738*	0.833**	NS

FLAGELLATES			
Mesocosm 1: 9,11-15,18,21 May	CH_3I	C_2H_5I	CH_2I_2
Undetermined flagellates 12 µm	NS	0.833**	0.905***

Mesocosm 6: 9,11-15,18,21 May			
Undetermined flagellates 10 µm	0.786*	0.905***	0.762*
Undetermined flagellates 12 µm	NS	0.810*	0.738*

* = 95% confidence level (p<=0.05), ** = 98% confidence level (p<=0.02), *** = 99% confidence level (p<=0.01), NS = not significant

3.3.4.2. Bromocarbons

The temporal changes in the concentrations of the bromocarbon gases (Figure 3.12) were substantially different to those of the iodocarbons. Large peaks on 9 May prior to the development of the bloom were seen in all three bromocarbons, followed by rapid decreases in concentrations. There did appear to be some relationship to biomass over the period of exponential growth (See Figure 3.5 and 3.12), with a slight increasing trend in concentrations of all bromocarbons

over the period 11 – 15 May. In addition, the bromocarbons did tend to show some increase under high CO_2 (Table 3.15), with mean concentrations of all three being elevated under high CO_2. Mean concentrations (and ranges) of $CHBr_3$, CH_2Br_2 and $CHBr_2Cl$ under high CO_2 were 39.8 pM (5.2 – 80.6 pM), 2.4 pM (0.01 – 5.2 pM) and 0.6 pM (0.4 – 1.1 pM), compared to 34.7 pM (3.8 – 59.2 pM), 2.2 pM (1.1 – 4.9 pM) and 0.5 pM (0.3 – 0.7 pM) under present day CO_2. $CHBr_2Cl$ was statistically significantly elevated during the whole experiment (Whole experiment T = -0.328, DF = 55, p – 0.002, Phase 2 Bloom, T = -2.82, DF = 33, p = 0.008 See Table 3.7 and Appendix 1 and 2), and during Phase 3 (Post-bloom) both $CHBr_3$ and $CHBr_2Cl$ showed relatively large percentage increases (14% and 29%, respectively, see Table 3.15).

Table 3.7. Summary of statistical analysis on bromocarbon data.
Two analysis were performed, one on data for the whole experiment, and one on data from Phase 2 of the experiment (Bloom 10 – 17 May). For all analyses, M3 and M4 only are included after 15 May.

	Statistical Test	**Significant differences ($p<0.05$)**
$CHBr_3$ Whole experiment	Mann-Whitney W = 967, p = 0.08	
$CHBr_3$ Phase 2 Bloom	Mann-Whitney W = 381, p = 0.0622	
CH_2Br_2 Whole experiment	2-sample T-test T = -0.08, p = 0.936	
CH_2Br_2 Phase 2 Bloom	2-sample T-test T = 0.44, p = 0.667	
$CHBr_2Cl$ Whole experiment	2-sample T-test T = -3.28, p = 0.002	√
$CHBr_2Cl$ Phase 2 Bloom	2-sample T-test T = -2.82, p = 0.008	√

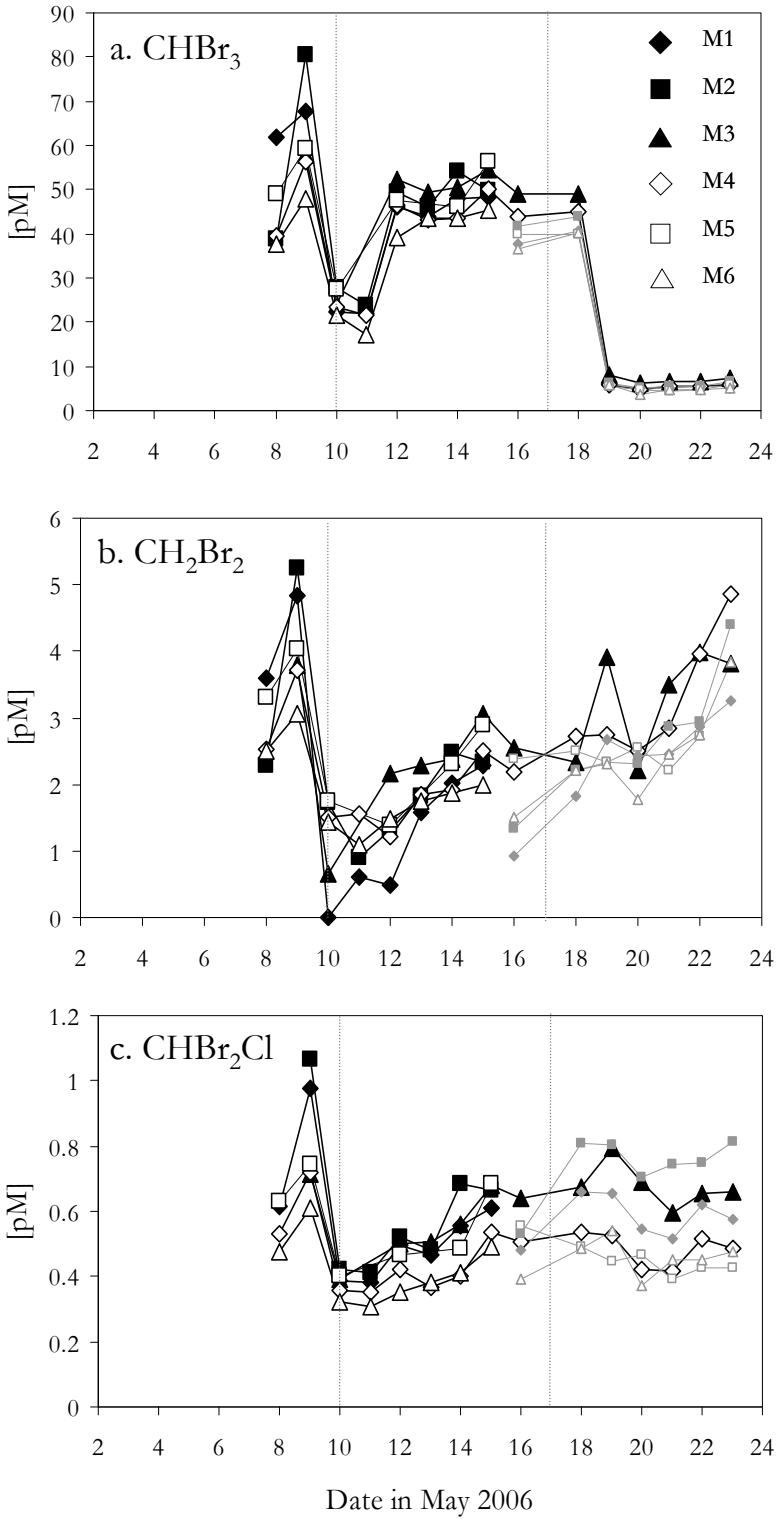

Figure 3.12. Concentrations of a. $CHBr_3$, b. CH_2Br_2 and c. $CHBr_2Cl$ (pM) over the course of the experiment. Due to re-aeration and alteration of experimental conditions of mesocosms 1, 2, 5, and 6 on 15 May, trace gas data for these mesocosms is shown in grey. Vertical grey lines indicate the 3 phases of the bloom. The un-altered M3 and M4 are plotted in black for the whole experiment.

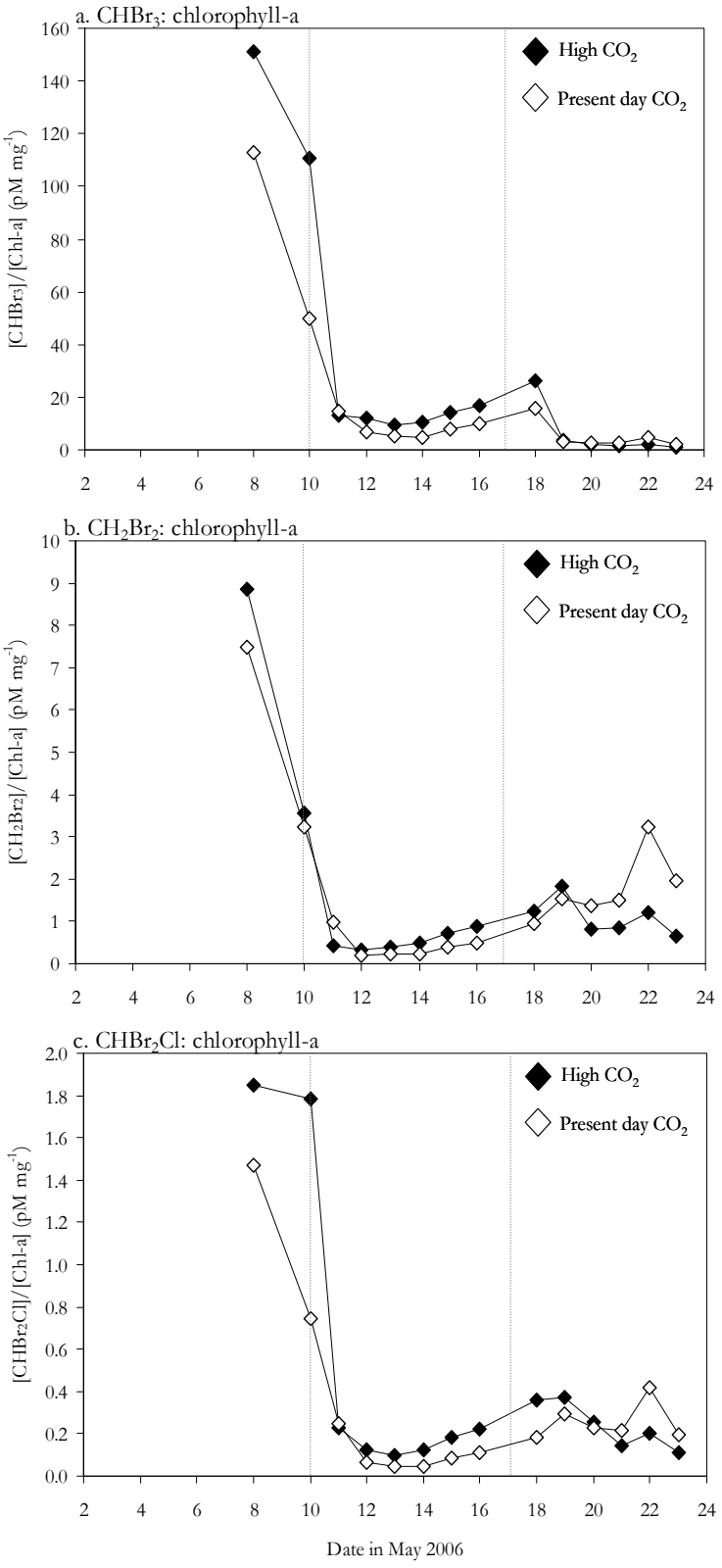

Figure 3.13. Mean ratios of a. $CHBr_3$: Chlorophyll *a*, b. CH_2Br_2: Chlorophyll *a*, and c. $CHBr_2Cl$: Chlorophyll *a* for the present day (open diamonds) and high CO_2 (closed diamonds) treatment. Vertical grey lines indicate the 3 phases of the bloom. M3 and M4 only are taken into consideration after 15 May.

Figure 3.13 shows the mean ratios of a. $CHBr_3$: chlorophyll *a*, b. CH_2Br_2: chlorophyll *a* and c. $CHBr_2Cl$: chlorophyll *a* over the course of the experiment. For all three compounds, the ratio starts relatively high during the pre-bloom phase. However, as soon as the bloom is initiated in Phase 2, the ratios all sharply drop, indicating much less production of bromocarbons per chlorophyll *a* during this period of rapid growth. As the bloom proceeded, the ratios of all three rose gradually, suggesting some increase in production relative to chlorophyll *a*. During Phase 3, $CHBr_3$; chlorophyll *a* dropped to very low levels as there was little production of $CHBr_3$ at this point. By contrast, CH_2Br_2: and $CHBr_2Cl$: chlorophyll *a* experienced a small peak on 22 May, an indication of short-lived enhanced production of these compounds relative chlorophyll *a* at this late stage of the experiment. In general the ratios of bromocarbons to chlorophyll *a* were higher under high CO_2, indicative of a greater amount of bromocarbons produced per chlorophyll *a* under these perturbed conditions. An exception to this is during Phase 3 when ratios were slightly higher under ambient CO_2 conditions, suggesting some shift in the production regime of these compounds.

Table 3.8 shows selected significant temporal correlations between the bromocarbons and biological/community parameters, including chlorophyll *a* and phytoplankton cell counts. Of the bromocarbons, CH_2Br_2 and $CHBr_2Cl$ showed a strong significant positive correlation ($n = 16$, $\rho = 0.802$), whilst $CHBr_3$ was not significantly correlated with either of the other bromocarbons. However, $CHBr_3$ did show strong relationships with a number of phytoplankton species, notably the nanophytoplankton and Cryptophytes under both treatments, as well as coccolithophores, and small and large picoeukaryotes under present day CO_2, and *Synechecoccus* under high CO_2 (see Table 3.8).

In contrast, CH_2Br_2 and $CHBr_2Cl$ did not show any significant positive correlations with any of the phytoplankton groups, although a number of strong negative relationships were observed e.g. CH_2Br_2 and $CHBr_2Cl$ and coccolithophores, High CO_2, $\rho = -0.811$ and -0.807, respectively.

Table 3.8. Selected Spearman's Rank Correlation Coefficients (ρ) and associated significance level for mean $CHBr_3$, CH_2Br_2, $CHBr_2Cl$, chlorophyll *a* and phytoplankton community components under high CO_2 (M1, M2, M3) and present-day CO_2 (M4, M5, M6). M3 and M4 only are included in the analysis after 15 May. Full results of Spearman's Rank analysis are shown in Appendix 7.

	$CHBr_3$	**CH_2Br_2**	**$CHBr_2Cl$**
$CHBr_2Cl$ High CO_2	NS	0.802***	-
Chlorophyll *a* Present CO_2	0.662**	NS	NS
Coccolithophores High CO_2	NS	-0.811***	-0.807***
Coccolithophores Present CO_2	0.710**	-0.618*	NS
Small picoeukaryotes High CO_2	NS	NS	-0.653**
Small picoeukaryotes Present CO_2	0.640*	NS	NS
Large picoeukaryotes High CO_2	NS	NS	NS
Large picoeukaryotes Present CO_2	0.921***	NS	NS
Nanophytoplankton High CO_2	0.600*	NS	-0.587*
Nanophytoplankton Present CO_2	0.842***	-0.662**	NS
Cryptophytes High CO_2	0.640*	NS	-0.600*
Cryptophytes Present CO_2	0.596*	NS	NS
Synechococcus High CO_2	0.771***	-0.552*	NS
Synechococcus Present CO_2	NS	NS	NS

* = 95% confidence level (p<=0.05), ** = 98% confidence level (p<=0.02), *** = 99% confidence level (p<=0.01), NS = not significant

Table 3.9 shows selected Spearman's Rank correlation coefficients for the iodocarbons and phytoplankton species biomass, derived from cell microscopy enumeration. Cell enumerations were only carried out for M1 and M6, and on a limited number of days (9, 11-5, 18, 21 May) so the amount of data available for analysis was small. No significant positive correlations were found between the bromocarbons and the total phytoplankton biomass data, and only two were

identified between the bromocarbons and the flagellate community ($CHBr_3$ and "undetermined flagellates 10μm" M1 ρ = 0.762, CH_2Br_2 and Cryptophytes M6 ρ = 0.857), with the majority of significant correlations being negative.

Table 3.9. Selected Spearman's Rank Correlation Coefficients (ρ) and associated significance level for mean $CHBr_3$, CH_2Br_2, $CHBr_2Cl$, chlorophyll *a* and phytoplankton community components under high CO_2 (M1, M2, M3) and present-day CO_2 (M4, M5, M6). M3 and M4 only are included in the analysis after 15 May. Full results are shown in Appendix 10.

FLAGELLATES			
Mesocosm 1: 9,11-15,18,21 May	$CHBr_3$	CH_2Br_2	$CHBr_2Cl$
Undetermined flagellates 2μm	-0.762*	NS	NS
Prasinophytes 5 μm	NS	NS	-0.874**
Undetermined flagellates 10 μm	0.762*	NS	NS

Mesocosm 6: 9,11-15,18,21 May	$CHBr_3$	CH_2Br_2	$CHBr_2Cl$
Prasinophytes 5 μm	NS	-0.833**	NS
Undetermined flagellates 10 μm	NS	NS	NS
Cryptophytes	NS	0.857**	NS
Euglenophytes	-0.833**	NS	NS

*= 95% confidence level (p<=0.05), ** = 98% confidence level (p<=0.02), *** = 99% confidence level (p<=0.01), NS = not significant

Table 3.10. Spearman's Rank Correlation Coefficients (ρ) and associated significance level for mean $CHBr_3$, CH_2Br_2, $CHBr_2Cl$ and phaeopigment concentrations under high CO_2 (M1, M2, M3) and present-day CO_2 (M4, M5, M6). M3 and M4 only are included in the analysis after 15 May.

	$CHBr_3$	**CH_2Br_2**	**$CHBr_2Cl$**
Phaeopigments High CO_2	0.723***	-0.654**	-0.605*
Phaeopigments Present CO_2	0.743***	-0.756***	-0.279

Bromocarbon concentrations were also correlated with phaeopigment concentrations, using a Spearman's Rank analysis (Table 3.10). All of the bromocarbons under both treatments showed significant correlations, except $CHBr_2Cl$ under present day CO_2. However, the nature of the correlations varied, with $CHBr_3$ displaying strong significant (99% significant level) positive

correlations under both treatments, and CH_2Br_2 and $CHBr_2Cl$ showing a negative response to phaeopigment concentrations.

3.3.5. DMS/DMSP

The results for DMS and its precursor, DMSPp (particulate) and DMSPt (total)[2] are shown in Figure 3.14 a, b and c. In all mesocosms, there was an overall increase in DMS concentrations with time, but the temporal trends observed for the two treatments were markedly dissimilar. Under present day CO_2, both DMS and chlorophyll *a* peaked on 13 – 14 May. In contrast, DMS under high CO_2 displayed only a gentle rise which did not concur with the trend in chlorophyll *a* (Figure 3.5 and 3.14). A large and statistically significant 57 percent reduction in DMS concentrations was observed under high CO_2 for Phase 2 (Bloom) of the experiment ($T = 4.75$, $DF = 24$, $p < 0.001$, and see Table 3.11 and Appendix 1 and 2). During Phase 3 (Post-bloom), DMS concentrations were 63 percent lower in the high CO_2 compared to present-day CO_2 (Table 3.14).

DMSP concentrations were generally lower under high CO_2 (DMSPp -24 percent, DMSPt -23 percent, See Figure 3.14 b and Table 3.14). DMSPt showed statistically significant differences between treatments for the whole experiment ($T = 2.60$, $DF = 70$, $p = 0.011$) and both DMSPp and DMSPt displayed significant differences for the Phase 2 (Bloom) (DMSPp $T = 2.18$, $DF = 28$, $p = 0.038$, DMSPt $T = 2.90$, $DF = 25$, $p = 0.008$). However, the differences between treatment are much less clear than for DMS, there is much greater day-to-day variability, and the peak in DMSP concentrations occurs two days after the peak in DMS (15 May compared to 13 May for DMS) (Figure 3.14 b and c).

[2] Total DMSP (DMSPt) calculated as sum of concentrations of DMSPp and dissolved DMSP (DMSPd).

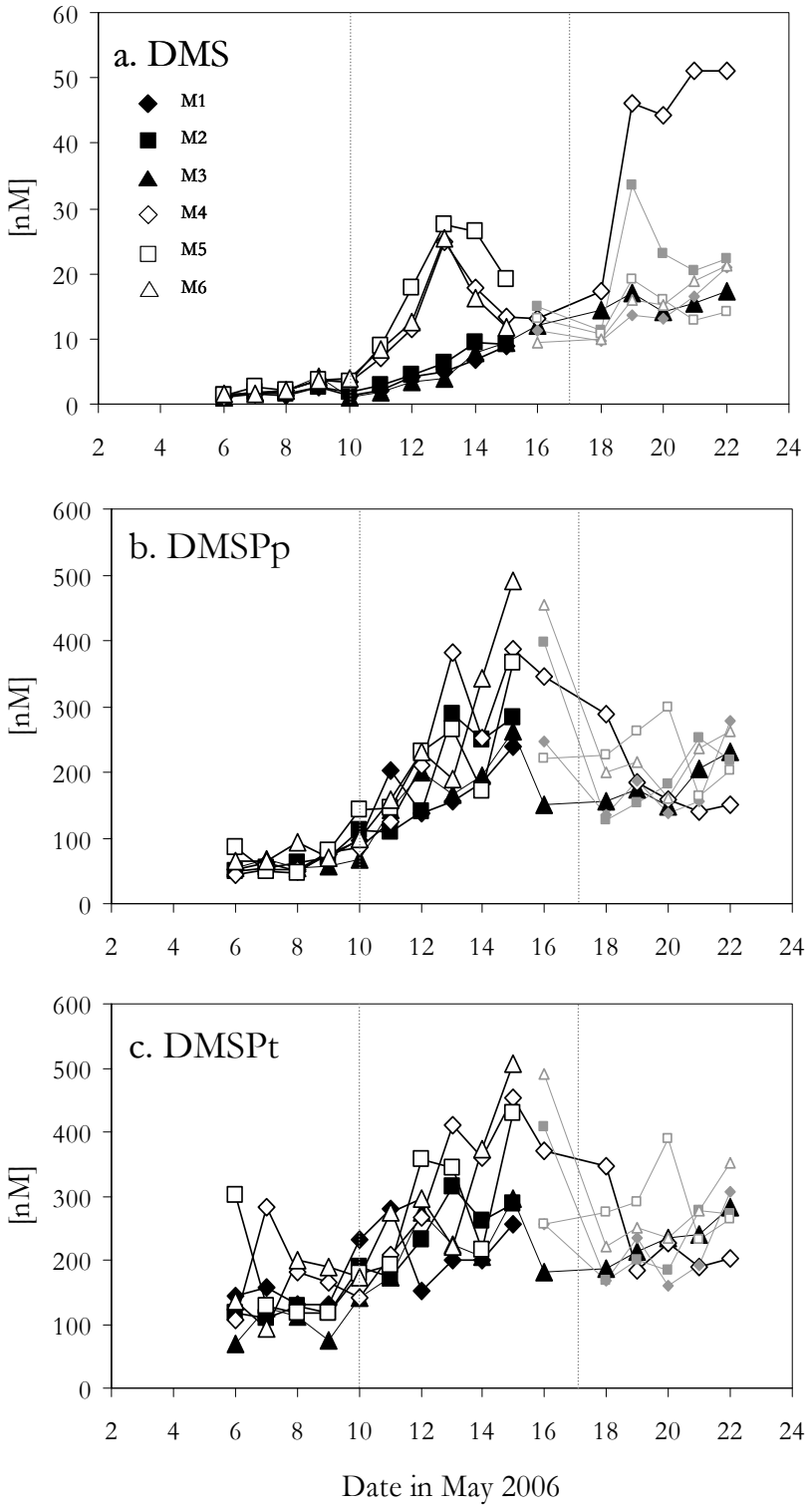

Figure 3.14. Concentrations (nM) of a. DMS, b. particulate DMSP (DMSPp) and c. total DMSP (DMSPt) in all mesocosms over the course of the experiment. Due to re-aeration and alteration of experimental conditions of M1, M2, M5, and M6 on 15 May, data for these mesocosms is shown in grey. The un-altered M3 and M4 are plotted in black for the whole experiment. Vertical grey lines indicate the 3 phases of the bloom.

Table 3.11. Summary of outcome of statistical analysis on DMS/DMSP data. Two analysis were performed, one on data for the whole experiment, and one on data from Phase 2 of the experiment (Bloom 10 – 17 May). For all analyses, M3 and M4 only are included after 15 May.

	Statistical Test	**Significant differences ($p<0.05$)**
DMS Whole experiment	2-sample T-test T = 2.88, p = 0.005	√
DMS Phase 2 Bloom	2-sample T-test T = 4.75, p <0.001	√
DMSPp Whole experiment	Mann-Whitney W = 1225, p = 0.3189	
DMSPp Phase 2 Bloom	2-sample T-test T = 2.18, p = 0.038	√
DMSPt Whole experiment	2-sample T-test T = 2.60, p = 0.011	√
DMSPt Phase 2 Bloom	2-sample T-test T = 2.90, p = 0.008	√

Figure 3.15 shows the ratios of DMS, DMSP*t* and chlorophyll *a* over the course of the experiment. The ratio of DMS to DMSP*t* (Figure 3.15 a) showed large differences between treatments for both Phase 2 and Phase 3, with an average of 57 percent less DMS produced per DMSP*t* under the high CO_2 treatment. However, for two days this trend was reversed (16 and 18 May), with a higher ratio under high CO_2. Following this, the ratio again switched and became very pronounced, with much more DMS produced per DMSP*t* in the present day M4 compared to the high CO_2 M3. The ratio of DMSPt to chlorophyll *a* (Figure 3.15 b) showed much less pronounced differences, particularly during the critical Phase 2.

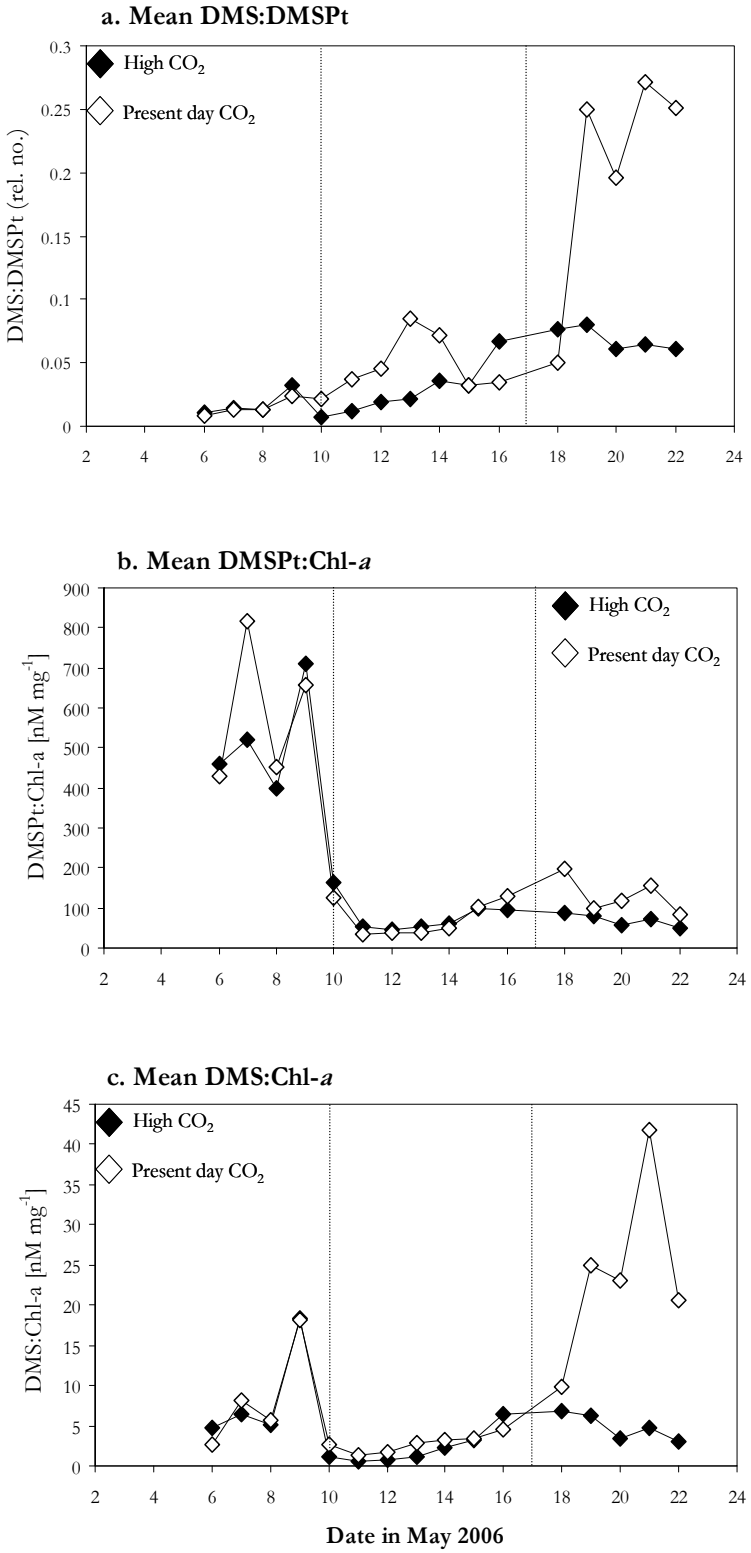

Figure 3.15. Mean ratios of a. DMS to DMSPt, b. DMSPt to chlorophyll *a*, and c. DMS to chlorophyll *a* for the present day (open diamonds) and high CO_2 (closed diamonds) treatment. Vertical grey lines indicate the 3 phases of the bloom. M3 and M4 only are taken into consideration after 15 May.

During this period of maximum growth, there was virtually no difference between treatments, suggesting that there were no major shifts in ecosystem composition during this period that may have impacted on the production of DMSP and resulted in the observed large differences in DMS concentrations between treatments. During the third phase, the ratio became lower under high CO_2 in M3 relative to M4, indicative of lowered production of DMSP per chlorophyll *a*, and suggesting some change in community structure and DMSP production. No difference was observed in the ratio of DMS to chlorophyll *a* (Figure 3.15 c) between treatments until Phase 3 where greatly more DMS per chlorophyll *a* was produced under high CO_2 in M3 compared to M4.

Table 3.12 shows significant Spearman's Rank correlation coefficients for relationships between DMS, DMSPt, chlorophyll *a* and phytoplankton community composition. DMS displayed few significant correlations: with DMSPt and chlorophyll *a* under high CO_2 (n= 16, ρ = 0.624 and 0.521, respectively), and *Synecococcus* under present day CO_2 (n = 16, ρ = 0.712). In addition, two significant negative correlations were identified, with small picoeukaryotes and nanophytoplankton under high CO_2 (n = 16, ρ = -0.635 and -0.550, respectively), suggesting these groups of phytoplankton are associated with low levels of DMS under this treatment. DMSPt displayed a greater range of significant correlations with biological/community parameters. In both the high and present day CO_2 treatments, DMSPt was temporally correlated with chlorophyll *a* (n = 16, ρ = 0.853 and 0.750) and large picoeukaryotes (n = 16, ρ = 0.535 and 0.526). In the present day treatment, small picoeukaryotes, Cryptophytes and Synechococcus were all significantly correlated with DMSPt (n = 16, ρ = 0.700, 0.826 and 0.729, respectively. In addition, chlorophyll *a* displayed more correlations with the community components under present day CO_2 compared to high CO_2 (Present day Chlorophyll *a* vs. coccolithophores, small and large picoeukaryotes, nanophytoplankton and Synechecoccus. High CO_2 Chlorophyll *a* vs. Large picoeukaryotes and Cryptophytes). To summarise, the nature of the correlations for DMS and DMSPt varied between treatments, with a greater number of significant correlations found under present day CO_2. This suggests there was some impact of the perturbed high CO_2 conditions on the communities of the mesocosms, and their ability to produce/consume DMSPt/DMS.

Table 3.12. Selected Spearman's Rank Correlation Coefficients (ρ) and associated significance level for mean DMS, DMSPt, chlorophyll *a* and phytoplankton community components under high CO_2 (M1, M2, M3) and present-day CO_2 (M4, M5, M6). M3 and M4 only are included in the analysis after 15 May. Full results of Spearman's Rank analysis are shown in Appendix 8.

	DMS	**DMSP*t***	**Chl *a***
DMSPt High CO_2	0.624**	-	-
DMSPt Present CO_2	NS	-	-
Chlorophyll *a* High CO_2	0.521*	0.853***	-
Chlorophyll *a* Present CO_2	NS	0.750***	-
Coccolithophores Present CO_2	NS	NS	0.753***
Small picoeukaryotes High CO_2	-0.635**	NS	NS
Small picoeukaryotes Present CO_2	NS	0.700***	0.847***
Large picoeukaryotes High CO_2	NS	0.535*	0.574*
Large picoeukaryotes Present CO_2	NS	0.526*	0.679**
Nanophytoplankton High CO_2	-0.550*	NS	NS
Nanophytoplankton Present CO_2	NS	NS	0.562*
Cryptophytes High CO_2	NS	NS	0.876***
Cryptophytes Present CO_2	NS	0.862***	NS
Synechococcus Present CO_2	0.712***	0.729***	0.779***

*= 95% confidence level (p<=0.05), ** = 98% confidence level (p<=0.02), *** = 99% confidence level (p<=0.01), NS = not significant

Spearman's rank correlations were also performed for DMS/DMSPt and chlorophyll *a* with total phytoplankton biomass data, and flagellate biomass data derived from microscopy cell enumeration. Cell enumerations were only carried out for M1 and M6, and on a limited number of days (9, 11-5, 18, 21 May) so the amount of data available for analysis was small. No significant correlations were found between DMS/DMSPt and phytoplankton biomass, which may be a symptom of the small sample size number for the analysis. However, significant correlations were found between DMS/P and some specific classes of plankton (See table 3.13

and Appendix 8), supporting the notion that plankton species differ in their ability to produce these compounds (see Discussion, section 3.4.4)..

Table 3.13. Spearman's Rank Correlation Coefficients (ρ) and associated significance level for mean DMS, DMSPt and phaeopigment concentrations under high CO_2 (M1, M2, M3) and present-day CO_2 (M4, M5, M6). M3 and M4 only are included in the analysis after 15 May.

	DMS	**DMSPt**
Phaeopigments High CO_2	-0.812***	-0.235
Phaeopigments Present CO_2	-0.459	-0.179

Table 3.13 shows Spearman's Rank correlations between DMS/DMSPt and phaeopigments. Whilst DMS displayed a strong significant negative correlation (99% significance level) under high CO_2, no other significant relationships were identified between these compounds.

3.3.6. Summary of trace gas data

Table 3.14 gives a summary of the mean concentrations and percentage differences between treatments for Phase 2 (Bloom), Phase 3 (Post-bloom) and for the whole experiment. During the bloom phase, concentrations of CH_3I and DMS showed the largest differences between treatments, with decreases of 43 percent and 57 percent under high CO_2, respectively. For the post-bloom phase, only data from M3 and M4 is taken into account, and during this period considerable decreases in concentrations under high CO_2 were seen for all of the iodocarbons (CH_3I -67%, C_2H_5I -73%, CH_2I_2 93%, CH_2ClI 59%), and again for DMS (-63%). For the experiment as a whole, DMS and CH_3I showed the greatest overall declines in concentration under high CO_2 (-60% and -41%, respectively). In contrast to the other trace gases, concentrations of the bromocarbons generally showed small increases under high CO_2, with increases of 13 percent, 8 percent and 22 percent for $CHBr_3$, $CH2Br_2$ and $CHBr_2Cl$, respectively.

Table 3.14. Summary of trace gas, DMSP and chlorophyll *a* data. Means and percentage differences of measured variables for high CO_2 treatment and present day, CO_2 treatment for the Bloom period in all mesocosms, Post-bloom period in mesocosms 3 and 4 and for the whole experiment (M3 and M4 only after 15 May).

	Phase 2 BLOOM 10 – 17 May All Mesocosms			**Phase 3 POST-BLOOM 18 – 23 May Mesocosms 3 and 4**			**WHOLE EXPERIMENT 6 – 23 May (Mesocosms 3 and 4 only after 15 May)**		
	High CO_2	**Present day**	**% diff.**	**High CO_2**	**Present day**	**% diff.**	**High CO_2**	**Present day**	**% diff.**
CH_3I *	6.9	12.1	-43	3.6	10.7	-67	5.4	9.7	-44
C_2H_5I *	0.7	1.0	-32	0.3	1.0	-73	0.5	0.8	-35
CH_2I_2 *	197.4	283.4	-30	4.6	63.9	-93	127.8	175.9	-27
CH_2ClI *	189.3	207.2	-9	131.1	321.7	-59	136.9	179.0	-24
$CHBr_3$ *	41.2	38.1	+7	14	12.1	+14	39.8	34.7	+13
CH_2Br_2 *	1.6	1.9	-17	3.29	3.28	+0.3	2.4	2.2	+8
$CHBr_2Cl$ *	0.5	0.4	+17	0.7	0.5	+29	0.6	0.5	+22
DMS ¥	6.1	14.1	-57	15.7	42.0	-63	5.7	14.1	-60
DMSPt ¥	191.7	252.3	-24	182.9	184.3	-0.8	139.0	182.9	-24
Chl-a ¤	3.2	5.3	-40	3.6	1.8	+49	2.5	3.5	-28

* = pM, ¥ = nM ¤ = mg m^{-3}

3.4. Discussion

3.4.1. Comparison to previous mesocosm experiments and the open ocean

A number of previous mesocosm studies performed at the Marine Biological Station in Bergen have reported values for DMS, DMSP and chlorophyll *a* under present day CO_2 conditions (Levasseur *et al.* 1996; Williams and Egge 1998; Wilson *et al.* 1998; Steinke *et al.* 2007), whilst more recently Avgoustidi (2007), Vogt *et al.* (2008) and Wingenter *et al.* (2007) reported these values for experiments using both present day, glacial, future and far future CO_2 conditions. Overall, chlorophyll *a* concentrations for the studies mentioned above ranged from 0 – 16 mg m^{-3}, DMS ranged from 0 – 120 nM, and DMSP from around 20 – 800 nM. The concentrations of chlorophyll *a* (0 – 10 mg m^{-3}), DMS (0 – 50 nM) and DMSP (100 – 500 nM) for this study fell well within this range of values. In terms of phytoplankton community composition, this experiment did differ from others, as the blooms in this study were generally flagellate-dominated but with low numbers of

coccolithophores (0 – 3000 cells ml^{-1}). Previous experiments were characterised by coccolithophore-dominated (*E. huxleyi*) blooms, with 5.5 x 10^6 cells ml^{-1} reported for the 2003 experiment (Avgoustidi 2007), and a somewhat higher 56 x 10^6 cells ml^{-1} for the 2005 experiment (Wingenter *et al.* 2007; Vogt *et al.* 2008).

In general, the concentrations of chlorophyll *a*, DMS and DMSP reported in mesocosm studies, including this one, are well above those values usually encountered in the open ocean. Measurements made along the Atlantic Meridional Transect (Aiken *et al.* 2000; Chuck *et al.* 2005) give chlorophyll *a* concentrations of ~0.05 – 0.07 mg m^{-3} in the Atlantic gyres, with values only exceeding 1 mg m^{-3} in the highly productive West African upwelling regions. Using a comparison of global ocean measurements of DMS concentrations, it has been estimated that 95 percent of open ocean DMS measurements are less than 5 nmol l^{-1} (Kettle and Andreae 2000). Therefore the conditions created within the mesocosms are most comparable to highly productive regions experiencing strong phytoplankton blooms. Such regions make up a small percentage of the total surface area of the oceans. For example, it has been estimated that blooms of *E. huxleyi* annually cover an average of 1.4 x 10^6 km^2, which represents a small 0.4 percent of the total surface area of the oceans (Brown and Yoder 1994). When coccolithophore blooms do occur in the open ocean, chlorophyll *a* concentrations are much lower than those reported for mesocosm experiments, with mean concentrations generally less than 2 mg m^{-3} (Holligan *et al.* 1983; Turner *et al.* 1988; Balch *et al.* 1991; Malin *et al.* 1993). However, DMS and DMSP concentrations during such blooms have been reported to be comparable to those experienced in mesocosms. As an example, Malin *et al.* (1993) observed a range of 1.06 – 93.8 nmol l^{-1} for DMS and 10.8 – 280 nmol l^{-1} for DMSPp during a North East Atlantic coccolithophore bloom.

In the oceans, high chlorophyll *a* concentrations of the order seen during mesocosm experiments are more often associated with coastal areas that experience high nutrient loading and high phytoplankton biomass, such as the coastal waters of the North Sea during the Spring bloom. At this time of year, surface chlorophyll *a* concentrations of ≥ 8 mg m^{-3} have been measured over most of the eastern North Sea, and in UK coastal waters (Turner *et al.* 1988; Joint and Pomroy 1993). Where the dinoflagellate *Gyrodinium auereolum* was seen to dominate the phytoplankton community, Turner *et al.* (1988) measured chlorophyll *a* concentrations of up to 40 mg m^{-3}.

Only one previous study has reported concentrations of halocarbons from a mesocosm experiment. Wingenter *et al.* (2007) measured the concentrations of CH_2ClI during the 2005 CO_2 mesocosm experiment. The reported concentrations were rather lower than those for this study, ranging from approximately 5 – 30 fM (compared to 0 – 680 pM), although large differences between treatments were also observed. Increases in concentration of 46 percent for double CO_2 and 118 percent for triple CO_2 were reported (Wingenter *et al.* 2007). In addition, the peak in CH_2ClI occurred 6 – 10 days after the chlorophyll *a* peak.

3.4.2. Iodocarbons

3.4.2.1. Overview

CH_3I and C_2H_5I concentrations under both treatments fell within open ocean and coastal seawater measurements (Abrahamsson *et al.* 2004a; Chuck *et al.* 2005; Archer *et al.* 2007). The latter is a minor iodocarbon component of seawater (Archer *et al.* 2007) and in this study it made up <1 percent of the total iodocarbon pool. CH_2I_2 and CH_2ClI concentrations were somewhat elevated compared to most (but not all) oceanic measurements (Klick and Abrahamsson 1992; Abrahamsson *et al.* 2004a) and they dominated the iodocarbon pool, in common with a number of other studies (Abrahamsson *et al.* 2004a; Archer *et al.* 2007; Carpenter *et al.* 2007). During this study, the concentrations of all of the iodocarbons experienced some reduction under high CO_2. Thus for the highly productive mesocosm environment, the processes controlling net iodocarbon production do appear to be susceptible to lowered pH.

3.4.2.2. CH_3I and C_2H_5I

CH_3I production is often referred to as biogenic (Moore and Zafiriou 1994): directly produced by macroalgae and phytoplankton (Archer *et al.* 2007) and indirectly through a photochemical reaction with organic matter (Laturnus 1995). In addition, observations of CH_3I in surface waters and the atmosphere suggest a photochemical production pathway, particularly in open tropical oligotrophic regions (Richter and Wallace 2004). Within highly productive systems such as the mesocosm, a direct input from biological production through methyltransferase enzyme activity of both phytoplankton and/or bacteria is likely (Amachi *et al.* 2001; Archer *et al.* 2007). Indirect biological production of CH_3I has also been proposed,

through a radical recombination mechanism from the photolytic reaction of a humic-derived methyl radical and seawater iodide ions (Moore and Zafiriou 1994). If the production of CH_3I is controlled by the availability of the reactants, high dissolved organic matter (DOM) concentrations may therefore be conducive to greater rates of production. Again, in the highly productive mesocosm, DOM levels are likely to be high, leading to production of CH_3I that is directly or indirectly in synchrony with changes in biological activity.

Further information on the controls on CH_3I production can be derived from information on the concentration of nitrate (NO_3^-) in the seawater. Figure 3.16 shows the relationship between NO_3^- and CH_3I, for both the high CO_2 and present CO_2 treatments a strong statistically significant negative relationship is observed.

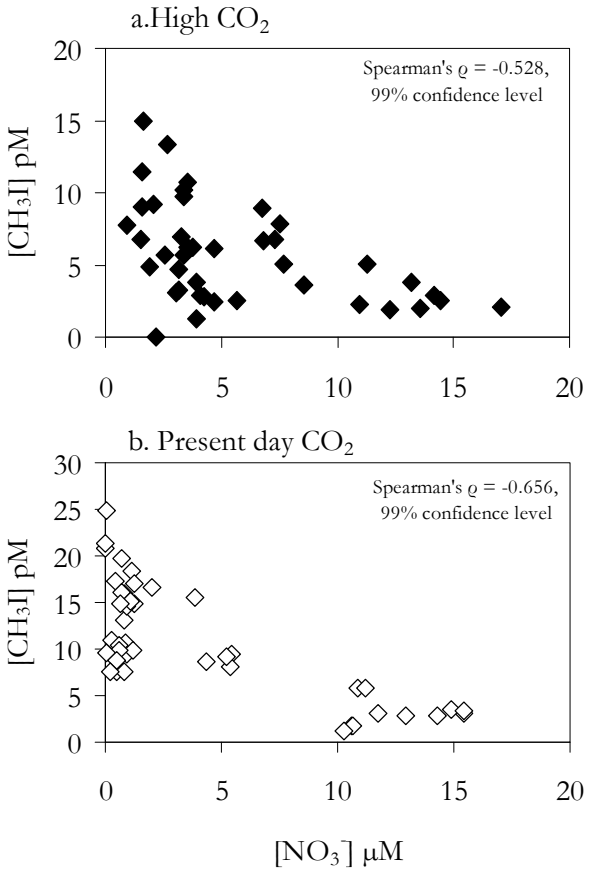

Figure 3.16. Correlations between nitrate concentrations (µM) and CH_3I concentrations (pM) under a. High CO_2 and b. Present day CO_2. Spearman's rank analysis was performed on the data; values of ρ and associated confidence level are shown.

This trend has also been observed by Chuck *et al.* (2005) in Atlantic and Southern Ocean waters, and Campos *et al.* (1999) reported a similar inverse relationship between $[I^-]$ and $[NO_3^-]$ in the Weddell Sea. It has been suggested that

this points to an association between CH_3I production and nitrate reductase activity (Campos *et al.* 1999; Chuck *et al.* 2005). Nitrate reductase is used by phytoplankton to take up iodate, as well as nitrate, leading to the formation of I^- within the cells (Campos *et al.* 1999). This reduced iodine is released to seawater from the cell and could contribute to the indirect production of compounds such as CH_3I. However, when NO_3^- levels are high, nitrate reductase preferentially reduces nitrate, resulting in lowered production of I^- as a result of chemical competition (Campos *et al.* 1999).

In the early stages of the mesocosm experiment when NO_3^- levels were very high, this may have resulted in diminished CH_3I formation. The increase in CH_3I seen during the post-bloom phase may have been in response to low NO_3^- levels. The correlation between CH_3I and NO_3^- was slightly weaker under high CO_2, due to less production of CH_3I under these altered conditions. It is possible that during the post-bloom phase when iodate reduction was favoured due to low NO_3^- levels, the activity of nitrate reductase was impacted by the high CO_2 and lowered pH of M3, resulting in a drop in production of this compound. In addition, when nutrient levels are lower after blooms of plankton, smaller-celled plankton species such as *Synechococcus* and small picoeukaryotes are able to opportunistically dominate due to low surface area to volume ratios (Partensky *et al.* 1999) – this was clearly seen during this experiment (Figure 3.6). The production of CH_3I also showed some recovery during the post-bloom phase (Figure 3.10). Furthermore, *Synechococcus* and small picoeukaryotes were significantly positively correlated with CH_3I. Thus, there appears to be a degree of coupling between nitrate levels, the abundance of smaller-celled plankton species, and the production of CH_3I.

There is little available information on the sources and sinks of C_2H_5I; however previous studies have found significant correlations between C_2H_5I and CH_3I suggesting similar production/removal mechanisms involved in controlling their concentrations (Makela *et al.* 2002; Richter and Wallace 2004; Archer *et al.* 2007). Information derived from this study further supports this notion.

Concentrations of both CH_3I and C_2H_5I were lower under high CO_2 (41 percent and 32 percent, respectively), and they were also significantly correlated with each other (High CO_2 Pearson's Correlations Coefficient = 0.839, $p<0.001$, Present day CO_2 Pearson's Correlation Coefficient = 0.849, $p<0.001$). CH_3I was significantly lower for both the experiment as a whole, and during the bloom phase. Although the decrease in C_2H_5I was not found to be statistically significant, a

decrease of one third was seen over the course of the experiment. In addition, both compounds were significantly correlated with chlorophyll *a* concentrations, strongly alluding to either a direct or indirect biological source. Support for a biological source is further enhanced by statistically significant correlations with the cyanobacteria *Synechococcus* under both high and present day CO_2. Taking the above information into account, it is likely that the observed reductions in concentrations of these iodocarbons may be a result of an impact of high CO_2/lowered pH on their biological production, with evidence that *Synechococcus* may have a large impact on concentrations of these iodocarbons. *Synechococcus* are a prevalent unicellular marine cyanobacterium, representing a chief component of the prokaryotic autotrophic picoplankton (Manley and Cuesta, 1997). In terms of the open ocean, *Synechococcus* numbers are thought to range from 5×10^2 cells ml^{-1} to 1.5×10^6 cells ml^{-1} (Partensky *et al.* 1999); the range of $<5 \times 10^3$ cells ml^{-1} to $\sim 4.5 \times 10^3$ cells ml^{-1} observed during this experiment is therefore realistic for open ocean abundances. Although one previous study on axenic cultures of *Synechococcus* showed no production of CH_3I (Manley and Cuesta 1997), CH_3I production in the oceans has been attributed to the closely-related cyanobacterium *Prochlorococcus* (Smythe-Wright *et al.* 2006). In this study, numbers of *Synechococcus* experienced a statistically significant 55 percent reduction under high CO_2. This may explain a large proportion of the decrease in concentrations of CH_3I and C_2H_5I. Furthermore, the main photosynthetic pigment of *Synechococcus* is chlorophyll *a* (Waterbury *et al.* 1979), and this may have strengthened the correlation between chlorophyll *a* and these iodocarbons.

3.4.2.3. CH_2I_2 and CH_2ClI

CH_2I_2 is considered to be produced biogenically through iodoperoxidase activity (Moore and Zafiriou 1994; Archer *et al.* 2007). This is supported by data from this study, with correlations between CH_2I_2 and nanophytoplankton under both treatments, and flagellate biomass in M1 and M6, and with chlorophyll *a* under present CO_2 conditions. The lack of significant correlation with chlorophyll *a* under the high CO_2 conditions may be indicative of an ecosystem shift towards species that are less prolific producers of CH_2I_2, a response also observed for DMS (see section 3.4.4.3). As well as displaying different correlations, the temporal development of CH_2I_2 was quite different to that for CH_3I and C_2H_5I. Thus the production of these two groups of halocarbons may be through distinct processes,

and/or by different taxonomic groups of phytoplankton and bacteria. As well as being associated with biological productivity, there is evidence that CH_2I_2 may be a by-product of the breakdown/senescence of the bloom. A positive correlation was observed between this compound and phaeopigment concentrations, a relationship that was particularly strong under high CO_2. Phaeopigments are degradation products of chlorophyll *a* and are often used as indicators of grazing activity (Jeffrey 1980). Therefore, it is possible that CH_2I_2 is released from phytoplankton cells as they are grazed by zooplankton, or from the faecal pellets of the grazers. A more significant relationship between these two compounds under high CO_2 may suggest that grazing is a stronger source of CH_2I_2 under high CO_2 due to a higher level of senescence.

Following release into the water column, CH_2I_2 is subject to rapid photolysis in seawater (photolytic lifetime of ~12 minutes), with strong evidence that this reaction produces CH_2ClI with a yield of 25 – 35 percent (Jones and Carpenter 2005; Martino *et al.* 2005). During this study, CH_2ClI was not found to be positively correlated with any of the phytoplankton groups, or associated biological parameters. This evidence strongly supports an inorganic production pathway for this compound. Following production of CH_2I_2 by phytoplankton, a photochemically catalysed reaction between CH_2I_2 and Cl^- leads to the formation of CH_2ClI. Oceanic depth profiles also provide evidence for this, with high levels of CH_2I_2 occurring at greater depth than maxima in CH_2ClI concentrations, indicative of production of CH_2I_2 by phytoplankton at the chlorophyll maximum, followed by photochemical production of CH_2ClI at shallower depths (Moore and Tokarczyk 1993; Yamamoto *et al.* 2001).

3.4.3. Bromocarbons

3.4.3.1. Overview

Concentrations of all the bromocarbons fell within the range of previous measurements from open ocean and coastal environments. In Quack and Wallace (2004) a review of 38 studies which include measurements of seawater $CHBr_3$ concentrations from a range of oceanic locations, the mean $CHBr_3$ concentrations ranged from 0.4 pM to 2770 pM. Similarly, Chuck *et al.* (2005) reviewed data from 11 studies of open ocean measurements, with a range of 3.1 – 38 pM, very similar to the range seen during mesocosm experiment. In terms of location, the values measured during the mesocosm are more comparable to open ocean measurements,

as opposed to the often extremely elevated concentrations experienced in coastal areas with extensive beds of macroalgae. Concentrations of all of the bromocarbons were slightly elevated under high CO_2, with $CHBr_2Cl$ displaying significant differences between treatments. However, it is not clear whether the observed differences between treatments in bromocarbons concentrations can be attributed to an effect of pCO_2. Unlike chlorophyll *a*, DMS/P and iodocarbons, which all show similar temporal trends in response to high CO_2, the bromocarbons do not appear to show the same effect of treatment. Despite significant differences between treatments for $CHBr_2Cl$ during the bloom phase, there is no clear evidence for difference between treatments when taking all three mesocosm replicates into consideration. There are obvious differences seen between M3 and M4 during the post-bloom phase; however $CHBr_3$ concentrations, for example, are greater in M3 that M4 even when there was no overall difference between all six mesocosms during the bloom phase. It seems that there were considerable differences in concentrations of bromocarbons between the mesocosms from the start of the experiment, differences that are not easy to explain or understand. Therefore, the apparent differences between treatments may in fact be a result of inherent inter-mesocosm variability that has a greater impact on bromocarbon concentrations than any effect of high CO_2.

3.4.3.2. $CHBr_3$

Despite the lack of response to high CO_2, the bromocarbons do show a number of interesting correlations with a range of biological parameters, providing some indication of the possible sources of these compounds. $CHBr_3$ showed the greatest number of correlations, with significant correlations between this compound and nanophytoplankton and Cryptophyte numbers under both treatments, chlorophyll *a*, coccolithophore and small and large picoeukaryotes under present day CO_2, and *Synechococcus* under high CO_2. Correlations with chlorophyll *a* have been reported in previous studies (Krysell 1991; Moore and Tokarczyk 1993). The correlations found in this study provide evidence that this compound may be derived directly from a phytoplankton source. While the production of $CHBr_3$ by macroalgae is generally widely accepted (Krysell 1991; Nightingale *et al.* 1995; Laturnus 1996; Carpenter and Liss 2000; Quack and Wallace 2004), direct production by phytoplankton is less well documented. The ubiquitous occurrence of $CHBr_3$ in the surface oceans and decreasing

concentrations of $CHBr_3$ with depth has been attributed to possible production by phytoplankton (Quack and Wallace 2004). The relationships identified here suggest that at least some of the production of $CHBr_3$ originates from a phytoplankton source. The observed discrepancies in significant correlations between treatments may be the result of the ecosystem shifts under the high CO_2 regime, with significant decreases in abundances of coccolithophores, large picoeukaryotes, nanophytoplankton, Cryptophytes and *Synechococcus* (See Table 3.3). A strong positive correlation was observed between $CHBr_3$ concentrations and phaeopigments, a relationship also observed by Quack *et al.* (2007) in the Mauritanian upwelling. Phaeopigments are associated with the senescence of a bloom, and are also indicative of the grazing activity of zooplankton (Jeffrey 1980). Therefore this correlation alludes to an association between production of $CHBr_3$ and phytoplankton degradation, senescence and grazing by zooplankton. A similar relationship was reported by Quack *et al.* (2007) in the productive waters of the Mauritanian upwelling.

3.4.3.3. CH_2Br_2 and $CHBr_2Cl$

Concentrations of CH_2Br_2 and $CHBr_2Cl$ were not correlated with $CHBr_3$, a phenomenon that has been previously observed by Chuck *et al.* (2005). In addition, concentrations of CH_2Br_2 and $CHBr_2Cl$ did not show any positive correlations with phytoplankton numbers or biomass, although they did show a range of significant negative correlations (See Table 3.9). This implies that CH_2Br_2 and $CHBr_2Cl$ are being produced indirectly through reactions such as the reductive dehalogenation of $CHBr_3$ (Goodwin *et al.* 1997a; Quack and Wallace 2004), or as break down products of components of the bloom i.e. concentrations of these compounds increase in response to decreasing phytoplankton numbers as cells are grazed or senesce. However and again in contrast to $CHBr_3$, both compounds were negatively correlated with phaeopigment concentrations. So it is possible that CH_2Br_2 and $CHBr_2Cl$ are indicative of the degradation of phytoplankton cells, but less so as an artifact of grazing. This difference in relation to phaeopigments again points to distinct production and consumption processes that separate $CHBr_3$ from CH_2Br_2/$CHBr_2Cl$.

3.4.3.4. CH_2Br_2:$CHBr_3$

The ratio of CH_2Br_2 to $CHBr_3$ showed a large range over course of the experiment (Figure 3.17), from <0.1 from 8 – 18 May to 0.4 – 0.8 for remainder of

experiment. The low ratios during the highly productive bloom phase of the experiment are indicative of elevated concentrations of $CHBr_3$, and ratios of this order are usually encountered in coastal areas which experience strong sources of this compound (e.g (Moore and Tokarczyk 1993; Krysell and Nightingale 1994; Carpenter *et al.* 2003). The higher ratio seen during the post-bloom phase is more usual of the open ocean (Butler *et al.* 2007; Quack *et al.* 2007a). The increase in ratio during the post-bloom phase suggests an additional source of CH_2Br_2 during this period, which could be the result of biologically-mediated reductive dehalogenation of $CHBr_3$ (Quack and Wallace 2004; Quack *et al.* 2007a). Furthermore, enhanced loss of $CHBr_3$ through air-sea exchange is possible, as although the transfer coefficients of the two compounds are similar, a greater concentration gradient between the sea and air generally exists for $CHBr_3$ resulting in a larger flux of $CHBr_3$ to the atmosphere (Quack *et al.* 2007a). If biological production of $CHBr_3$ had become negligible by this stage of the experiment, this loss due to ventilation to the atmosphere may have caused the large depletions in $CHBr_3$ seen towards the end of the experiment.

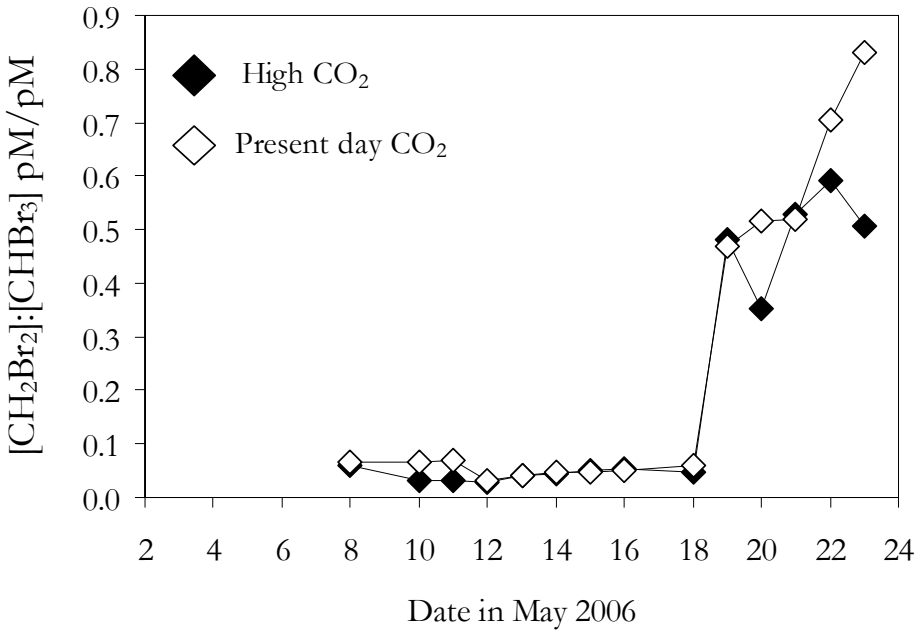

Figure 3.17. Ratio of CH_2Br_2 to $CHBr_3$ over the course of the experiment. M3 and M4 only are taken into consideration after 15 May.

3.4.4. DMS/DMSP

3.4.4.1. Overview

The concentrations of DMS, DMSPp and DMSPt were all significantly lower under high CO_2 during this mesocosm experiment, and these differences were particularly pronounced during the period of rapid growth during the bloom phase. Furthermore, there was good reproducibility between mesocosms (mean coefficient of variation for DMS between mesocosms <18 percent – see Appendix 11), suggesting the communities of each mesocosm were behaving similarly over the course of the bloom.

Chlorophyll *a* was correlated with DMSPt under both treatments, whilst it was only correlated DMS under high CO_2. Poor correlations between DMS and chlorophyll *a* has been reported previously and has been attributed to the differing abilities of various phytoplankton species to produce both chlorophyll *a* and DMSP, and the complex cycling of DMSP to DMS (Turner *et al.* 1988; Matrai *et al.* 1993; Kwint and Kramer 1995; Liss *et al.* 1997). Strong negative correlations were also observed between DMS and phaeopigments, particularly under high CO_2. If phaeopigments are considered to be an indication of grazing activity and senescence (Jeffrey 1980), this suggests that DMS production may not be directly related to such processes, and maximum DMS production may occur before senescence begins.

The DMS and DMSP concentrations measured during this experiment were comparable to summertime measurements from nearshore UK waters (Turner *et al.* 1988), and were well within the range of measurements during NE Atlantic coccolithophore blooms (Malin *et al.* 1993). The overall decrease in DMS concentrations was much more pronounced than for DMSPt and DMSPp, suggesting that there may be more impact on the conversion of DMSP to DMS than the initial production of DMSP.

3.4.4.2. Comparison to previous studies

The results of this study are in strong agreement with the mesocosm study in 2004 (Avgoustidi 2007) that also showed substantially lower DMS production under high CO_2 (later confirmed by a series of *in vitro* studies with single species cultures of *E. huxleyi*). However, DMS data from both studies differs with those from a mesocosm experiment in 2005 which showed only small differences in DMS

between elevated and normal CO_2 treatments (Wingenter *et al.* 2007; Vogt *et al.* 2008). Unusually low temperature and light intensities for the time of year were experienced during the 2005 study (Vogt *et al.* 2008 and see Figure 3.3) which may have influenced the development of the bloom and subsequent DMS production/removal mechanisms. Although the overall outcomes of the experiments differed somewhat, the DMSP and DMS characteristics of the three experiments were comparable. DMS and DMSP concentrations exhibited similarities in range, with maximum concentrations during the bloom phases of each experiment of 30 nM and ~500 nM, respectively (this study), 35 nM and 250 nM (2004), and 35 nM and 500 nM (2005) (Avgoustidi 2007; Vogt *et al.* 2008).

3.4.4.3. DMS/DMSP production and phytoplankton communities

In recent years, a large amount of research has focussed on the impact of OA on coccolithophores, due the expected effect of lowered pH on the calcification of these organisms, and the associated biogeochemical consequences (Riebesell *et al.* 2000b; Engel *et al.* 2005; Leonardos and Geider 2005; Iglesias-Rodriguez *et al.* 2008). However this group of phytoplankton is less relevant to this work as coccolithophores comprised only a small proportion of the phytoplankton biomass in the mesocosms, contributing 6 percent to the dominant flagellate biomass under high CO_2, and 12 percent under present day CO_2. To further support this, no correlations were found between DMS/DMSP and coccolithophore numbers. In comparison to the two previous CO_2 mesocosm studies, coccolithophores were present in much lower numbers. Avgoustidi (2007) saw *E. huxleyi* numbers reach 56 x 10^6 cells ml^{-1}, whilst Vogt *et al.* (2008) saw a more modest maximum of around 5 x 10^6 cells ml^{-1}. In this study, *E. huxleyi* numbers reached a maximum only of 3 x 10^3 cells ml^{-1}. This suggests that during this study, other species were responsible for the majority of DMSP production. Concentrations of chlorophyll *a* also showed some variation between experiments. This study saw maximum concentrations during the bloom of 10 mg m^{-3} whilst Vogt *et al.* (2008) reported a maximum of 13 mg m^{-3}. In contrast, Avgoustidi (2007) saw much lower concentrations, with a maximum of 5 mg m^{-3}, despite experiencing a strong coccolithophore bloom. However, open ocean *E. huxleyi* blooms have been associated with chlorophyll *a* levels that are not exceptionally elevated (Holligan *et al.* 1983; Balch *et al.* 1991; Malin *et al.* 1993).

The ratios of DMS:chlorophyll *a* and DMSPt:chlorophyll *a* (Figure 3.15) provide a good indication of the relative strength of DMS and DMSP production by the phytoplankton assemblage at different stages of the experiment, and can highlight where ecosystem shifts may have occurred. During Phase 1, DMSPt:chlorophyll *a* was high, indicating that the communities of the mesocosms under both treatments were strong DMSP producers. Once exponential growth began, the ratio rapidly decreased under both treatments, suggesting that the dominant bloom-forming species were low- or non-DMSP producers. Following the bloom, the ratio increased again in the present day treatment, whereas it remained low under high CO_2, signifying the development of two distinct communities under the two treatments, with weaker DMSP production under high CO_2. In contrast, the DMS: chlorophyll *a* ratio showed no difference between treatments during Phases 1 and 2, suggesting no difference in DMS production in terms of the phytoplankton community. As large differences in DMS were observed, this points to an impact of high CO_2 on a process separate to direct production by phytoplankton. During the post-bloom phase, a shift appeared to occur, with elevated DMS:chlorophyll *a* under present day CO_2. Under the perturbed conditions of M3, this may be evidence of a community dominated by non-DMS producers, or a decline in DMS production mechanisms relative to the unperturbed M4.

Concentrations of DMS, DMSPt and chlorophyll *a* were found to be significantly correlated with *Synechococcus* numbers under present day CO_2, indicating that this species may be a strong source of these compounds under unperturbed conditions. Wilson *et al*. (1998) also reported correlations between this species and DMSP during an earlier ambient CO_2 mesocosm experiment, and came to similar conclusions about the production of DMSP. The lack of correlation between this species and DMS/DMSP under high CO_2 may be a result of the drastic fall in both numbers of *Synechococcus* and DMS concentrations under high CO_2 (-55 and -60 percent, respectively), resulting in their decoupling. In addition and this time under both treatments, DMSPt was significantly correlated with large picoeukaryotes, suggesting a further strong phytoplankton source. Similarly to DMS and DMSPt, a large drop in large picoeukaryotes numbers was seen under high CO_2 (-60 percent), implying that this taxonomic group were directly responsible for a large proportion of the DMSP/DMS production during this experiment.

Therefore it is likely that DMSP and DMS are originating from a variety of biological sources, with the differences in correlation between treatments indicative of ecosystem shifts caused by the perturbed conditions.

3.4.4.4. Conversion of DMSP to DMS

The main feature of this study in terms of DMS was the great difference in temporal yield of this compound under high CO_2 compared to the present day treatment. It is possible that ecosystem shifts are largely responsible for this difference, as explained in the section above. As the differences in concentration and temporal development were less dramatic for DMSPt, it appears that the impact of high CO_2 may be on the conversion of DMSP to DMS, rather than the initial production of DMSP itself. The DMS: DMSP ratio (Figure 3.15) gives a good indication of the ability of the system to convert DMSP to DMS. This ratio showed no difference between treatments during Phase 1 of the experiment, suggesting the presence of similar communities and production/removal mechanisms under both treatments, capable of producing equal amounts of DMS per DMSP. The ratio changed as soon as the bloom initiated in Phase 2, with less DMS produced per DMSP under high CO_2, and these differences remained until the end of the experiment. This reinforces that there may have been some impact of high CO_2 on the process of conversion of DMSP to DMS.

DMS is produced in seawater by the breakdown of DMSP, a reaction that is catalysed by both intra- and extra-cellular DMSP-lyase (Stefels *et al.* 1996; Steinke *et al.* 1996). A number of factors can exert a great affect on this process. Grazing by protozoans and zooplankton initiates the mixing of DMSP and DMSP-lyase as cells are broken apart by the grazing action (Wolfe *et al.* 1997). Similarly, viral lysis of infected phytoplankton cells encourages the catalysis of DMSP, resulting in the production of DMS (Malin *et al.* 1998; Wilson *et al.* 1998). Further DMS production is possible through the bacterial consumption of DMSP. DMSP is thought to be one of the most significant substrates for heterotrophic bacteria in the marine environment, and bacterial DMS production is a key control on seawater concentrations of this compound (Kiene and Bates 1990; Kiene *et al.* 2000; Vila-Costa *et al.* 2006). In addition to bacteria, cyanophytes such as *Prochlorococcus* and *Synechococcus*, and diatoms, are able to take up and assimilate DMSP, thus contributing to the overall DMS production in the water column (Vila-Costa *et al.*

2006). Therefore, an impact on one or more of these processes as a result of the perturbed conditions in the high CO_2 mesocosms may have resulted in the observed lowered DMS concentrations.

3.4.4.5. Direct impacts on DMS

It is also possible that there was an impact of the high CO_2 conditions on the DMS itself, rather than on the conversion of DMSP to DMS. The bacterial consumption of DMS is a recognised process, and one which if rapid enough, can result in no increase in seawater DMS concentrations, and can dominate over the sea-air exchange of DMS (Kiene and Bates 1990). The major microbial degradation pathways involve DMS monooxygenase and methyltransferase, as well as oxidation via DMS dehydrogenase (Stefels *et al.* 2007). In the high CO_2 mesocosms, there may have been enhanced activity of these processes due to higher numbers of DMS-degrading bacteria as a result of ecosystem shifts, resulting in rapid consumption in DMS and diminished concentrations compared to the present day mesocosms. The significance of bacterial DMS consumption is a function of the strength of other competing processes (Stefels *et al.* 2007), therefore it is feasible that the elevated CO_2 and lowered pH weakened other DMS removal mechanisms, providing an opportunity for bacterial activity to dominate and rapidly consume the DMS. Unfortunately, information on the DMS-utilising bacterial communities under the different CO_2 treatments of the experiment is not available, so it is only possible to speculate.

3.4.4.6. Contextualisation in terms of the open oceans

The concentrations of DMS and DMSP observed during this and other mesocosm experiments are considered to be unrepresentative of those encountered in the majority of the open ocean. Although such concentrations may exist for short periods of time during spring bloom conditions and in highly productive coastal waters (Turner *et al.* 1988; Malin *et al.* 1993), the majority (>95 percent) of open ocean DMS measurements are <5 nM (Kettle and Andreae 2000). Furthermore, the flux of DMS from the ocean to the atmosphere is most important in remote regions such as the Southern Ocean (Kettle *et al.* 1999; Kettle and Andreae 2000) where chlorophyll *a* concentrations are much lower than experienced during this study. This makes it difficult to extrapolate results of mesocosm studies to the global scale. At this stage it is hard to predict what the consequences for future

oceans will be in terms of the net production of climatically-important trace gases, as extrapolation with the limited available data is likely to be unreliable.

3.4.5. Limitations of mesocosm experiments

Despite extensive use of mesocosms in studies of marine pelagic communities, and a large body of published literature on their use, there is an appreciation that mesocosms have a number of limitations when attempting to represent open ocean conditions (Kwint and Kramer 1995; Watts and Biggs 2001; Vogt *et al.* 2008). The physical size (depth and volume) of mesocosms has proved contentious. As most mesocosm experiments involve only a few tens of cubic metres of seawater, this has raised difficulties with scaling up to the global oceans. Further, it seems that due to their limited size, mesocosm tend to be more susceptible to outside environmental influences than the open ocean, such as temperature and light availability (Watts and Biggs 2001). The construction material of mesocosm enclosures is also something that requires close consideration, as sufficient light must be able to enter the mesocosms to achieve photosynthesis at a similar rate to that in the natural setting (Williams and Egge 1998; Watts and Biggs 2001). However, the most recent mesocosm experiments have used transparent polyethylene, which allows transmittance of >90 percent photosynthetically active radiation (PAR) (Barlow *et al.* 1998; Sanders and Purdie 1998; Williams and Egge 1998; Engel *et al.* 2004; Wingenter *et al.* 2007; Hopkins *et al.* 2010). Problems associated with inappropriate mixing regimes and artificial sedimentation have also been raised (Watts and Biggs 2001).

An important limitation of mesocosms is considered to be the unnatural side effects introduced by the containing walls which are not present in natural systems (Vallino 2000; Passow and Riebesell 2005). Not only are the walls restrictive to mixing and sedimentation, artificial loss of nutrients is thought to occur through algal wall growth (Watts and Biggs 2001). Furthermore, there is the question of whether the ecosystem succession seen in a mesocosm experiment is truly representative of what occurs in the natural environment, or is an artefact of the forced conditions within a mesocosm, particularly as higher trophic organisms are excluded (Watts and Biggs 2001; Passow and Riebesell 2005).

The majority of past mesocosm experiments, including this study, have used replicate (either triplicate or quadruplicate) mesocosms to represent different treatments. However, questions have been raised as to the usefulness of replicates

in a mesocosm situation (Wilson *et al.* 1998). Some studies have found large differences between replicate enclosures, raising the question of whether they could therefore be considered true replicates. Thus, some of this variability may be caused by small differences in starting conditions between individual mesocosms (Passow and Riebesell 2005). For example, the combination of high reproductive rates and small differences in initial numbers of bacteria and/or substrates can lead to significantly large effects (Kwint and Kramer 1995). Kwint and Kramer (1995) suggested a number of reasons as to why DMS concentrations varied so much between replicate mesocosms in their experiment, and came up with a number of possibilities including, differences in phytoplankton species distribution (regardless of similar chlorophyll *a* concentrations), differences in zooplankton grazing demands, and differential loss of DMS through photochemical conversion, diffusion through the mesocosm walls, output to the atmosphere and bacterial consumption. During this study, the triplicate mesocosms displayed reasonably similar temporal dynamics in terms of trace gases up until the point of re-aeration of M1, M2, M5 and M6 on 15 May, but did show some degree of variation. Coefficients of variation (CoVs) for the triplicate mesocosm are shown in Appendix 11. For the iodocarbons, CoVs ranged from 7 – 33 percent, for the bromocarbons 8 – 37 percent, and DMS/ DMSP 15 – 28 percent. Kwint and Kramer (1995) suggest that analytical error could cause some of the variation seen between mesocosms. With analytical errors of 10 – 18 percent for the iodocarbons, 5 – 16 percent for the bromocarbons and 7 – 22 percent for DMS/DMSP (see Appendix 12) it is likely that some of the variation seen between replicate mesocosms in this experiment can be explained by this. The remaining percentage variation would then be quite small suggesting that differences in production/removal mechanisms of trace gases between replicate mesocosms was relatively minor.

The timescale of mesocosm experiments is considered a major limitation, particularly in the context of OA. Abrupt changes to carbonate chemistry experienced over 1 – 2 days provide the opportunity to examine short term reactions to strong and rapid perturbations. This eliminates any possibility of evolutionary adaptation or migration of species better adapted to the perturbed conditions, and reduces the feasibility of extrapolation to future environments (Passow and Riebesell 2005). The progression of future OA will occur at a slower rate, the effects of which are hard to simulate, and potential consequences difficult to predict.

3.5. Summary and Conclusions

3.5.1. Iodocarbons

During this experiment, the concentrations of a number of marine trace gases appeared to show some impact of high CO_2/ lowered seawater pH during a mesocosm CO_2 perturbation experiment. For the iodocarbons, large percentage decreases in mean concentrations of between 28 and 41 percent were observed, with the decrease in CH_3I found to be statistically significant. The results indicate that the direct and indirect biogenic production of CH_3I and C_2H_5I in the highly productive mesocosms was likely due to correlations with a number of biological parameters. *Synechococcus* appeared to be a particularly strong potential source, and the large decrease in *Synechococcus* numbers under high CO_2 could explain some of the decrease seen in concentrations of these compounds under this treatment. Therefore the impact of high CO_2 and lowered pH may have caused an ecosystem shift, directly impacting on the concentrations of CH_3I and C_2H_5I. There was evidence that CH_2I_2 was also being produced biogenically, but there was evidence that the source differed to that for CH_3I and C_2H_5I, as CH_2I_2 appeared to be more closely related to the nanophytoplankton. In addition, this compound showed some relationship to the grazing and/or senescence of the bloom, a relationship that was stronger under high CO_2. Potentially, this can be attributed to a greater level of senescence in an ecosystem that is under more stressful conditions. There was no direct evidence that CH_2ClI was being produced biogenically, and is it likely that it was being created *via* a photochemical pathway through the degradation of CH_2I_2.

3.5.2. Bromocarbons

The mean concentrations of the bromocarbons were slightly elevated under high CO_2, significantly so in the case of $CHBr_2Cl$. However, there was no strong evidence that this was the result of an impact of high CO_2/ lowered pH. The apparent differences in concentration between treatments existed from the start of the experiment, and were maintained throughout. Therefore, it is more likely that this is a result of inter-mesocosm variability, rather than any effect of treatment. Due to a number of correlations with biological parameters, there was evidence that $CHBr_3$ was derived from a biological source. Discrepancies in some of these

correlations between treatments may be indicative of ecosystem shifts, with some populations being stronger producers of $CHBr_3$. Additionally, this compound displayed an association with grazing/senescence, suggesting that it is produced as a breakdown product of phytoplankton. CH_2Br_2 and $CHBr_2Cl$ were not correlated with $CHBr_3$, implying a different source, and one that is not directly associated with biological activity. Evidence for the lack of a direct link to biology came from numerous negative correlations between these two compounds and a range of biological parameters. Therefore it is possible that they are produced indirectly through reactions involving $CHBr_3$, or as breakdown products of the bloom.

3.5.3. DMS/DMSP

The mean concentrations of both DMS and DMSPt were significantly lower under high CO_2, with mean decreases of 60 percent and 24 percent, respectively. These results were in agreement with the 2004 mesocosm study (IPCC, 2007), although differed somewhat to the results of the 2005 experiment (IPCC, 2007). These discrepancies highlight the recognised inconsistent behaviour of CO_2 perturbation studies. In contrast to previous mesocosm experiments, coccolithophores comprised a minor component of the phytoplankton community, and thus were unlikely to be responsible for the majority of DMSP/DMS production. *Synechococcus* and picoeukaryotes appeared to be strong sources of these compounds, although the correlations were weaker under high CO_2. Again, this may be indicative of a species shift under the future high CO_2 regime. As the impacts on DMSP was rather less marked than that for DMS, it appears that there was greater influence of the changed CO_2 regime on the conversion of DMSP to DMS, rather than the initial production of the precursor. A number of processes are involved in the breakdown to DMS, including grazing, viral lysis, bacterial and phytoplankton production/uptake, so an effect of high CO_2/lowered pH on any one or more of these may have contributed to the large decrease in DMS. Furthermore, an impact on the processes controlling seawater DMS concentrations may have been affected. The bacterial consumption of DMS is an important process, and it is possible that the lowered concentrations of this compound under high CO_2 were in part a result of enhanced bacterial uptake of DMS in these perturbed conditions.

3.5.4. Extrapolation to the real world

Mesocosm experiments are currently the best way of exploring the impact of changes to pCO_2 on complex pelagic communities, in relatively large volumes of water (compared to laboratory studies), under quasi- natural meteorological and oceanic conditions. In addition, they provide a vital compromise between small-scale single-species laboratory culture studies and large-scale complex open ocean experiments (Passow and Riebesell 2005).

If the results of short-term (tens of days) and limited size mesocosm studies represent decadal global ocean changes, future OA has the potential to impact the production of globally-important marine trace gases. Since CO_2 emissions are expected to continue to increase (I.P.C.C. 2007), these results indicate that the sea-air fluxes of compounds such as DMS and iodocarbons could halve by the end of this century. In order to assess the impact on radiative forcing and the atmosphere's oxidative capacity, the complexity of the ocean-atmosphere system must be taken into account. The future oceans will not only be subjected to lowered pH, but there will also be global changes to other parameters, such as biological productivity and nutrient regimes, with as-yet unidentified feedbacks (I.P.C.C. 2007). Combined with physical changes to the climate and ocean system, all could impact on the sea-to-air flux of trace gases (Raven *et al.* 2005; I.P.C.C. 2007). These findings reveal novel effects that need to be addressed in global ocean-atmosphere modelling studies to improve prediction of the earth's future climate and atmospheric chemistry. However, further research is required in order to facilitate a greater understanding of how marine trace gas production may be impacted in a future high CO_2 world. This issue will be investigated further in the following chapters.

CHAPTER 4

High-CO_2 Seawater Laboratory Incubation Experiments

4.1. Introduction

The mesocosm CO_2 perturbation experiment (Chapter 3) revealed a strong effect of high CO_2/lowered seawater pH on the seawater concentrations of a range of iodine- and bromine-containing halocarbons. A large reduction in concentrations of iodocarbons was observed, accompanied by a less definitive but still intriguing impact on the bromocarbons. However, these results mark only the beginning of our understanding of the future impacts of OA on marine halocarbons and their sea-to-air flux. The data is very specific to one situation, and one community of plankton. The communities of the mesocosms were dominated by flagellates and ciliates, and in particular species that are adapted to a fjord setting rather than the open ocean, so this raises a number of questions:

1. Would it be possible to replicate the results of the mesocosm experiment on a smaller-scale and in a more controlled environment?

2. How would coastal/open ocean/seasonal communities dominated by other species/taxa react to the changed pCO_2 conditions?

3. What would this mean for the net production of biogenic trace gases?

The following chapter describes two incubation experiments that were designed to address these questions.

4.1.1. Sampling Site

Seawater samples for incubation were collected from the L4 Western Channel Observatory time series station. L4 is located in the Western English Channel about 10 nautical miles south west of Plymouth, Devon (50° 15.00' N, 4° 13.02') (See Figure 4.1). Since 1988, weekly monitoring of a range of physical, chemical and biological

parameters has been performed, and the site is considered important as it represents ocean-influenced and coastal waters, within a reasonable distance of Plymouth. As it is located at temperate latitudes, L4 experiences typical seasonal planktonic succession, with dominance by different species/taxa varying throughout the year. This phenomenon is under the control of physical (temperature and light) and chemical (nutrient concentrations) restraints on phytoplankton growth which allow for the coexistence of many species. As these restraints on growth vary according to the seasons, successive changes in the relative abundances of the component species can occur. Therefore certain species will prosper at particular times of the year depending on their species-specific growth rates and responses to nutrients (Lalli and Parsons 1997). At L4, records show that the autumn and winter plankton biomass is dominated by bacteria and flagellates. In early Spring, a diatom bloom occurs, shifting the ecosystem composition in favour of these organisms. May through to August sees a dominance by both autotrophic and heterotrophic dinoflagellates, accompanied by an abundance of ciliates (Rodriguez *et al.* 2000). With this information in mind, a further question was posed:

4. Would the response of trace gas production of natural phytoplankton assemblages vary in response to high pCO_2 according to changes in seasonal community assemblages dominated by different groups of phytoplankton?

Samples were collected from L4 at two different times, the first in late Spring (4 June) and the other in late Summer (30 July). These dates were chosen in order to test the response of phytoplankton communities dominated by varying species. The following chapter details the experimental setup and the results of two high CO_2 natural seawater incubation experiments that were performed during 2007.

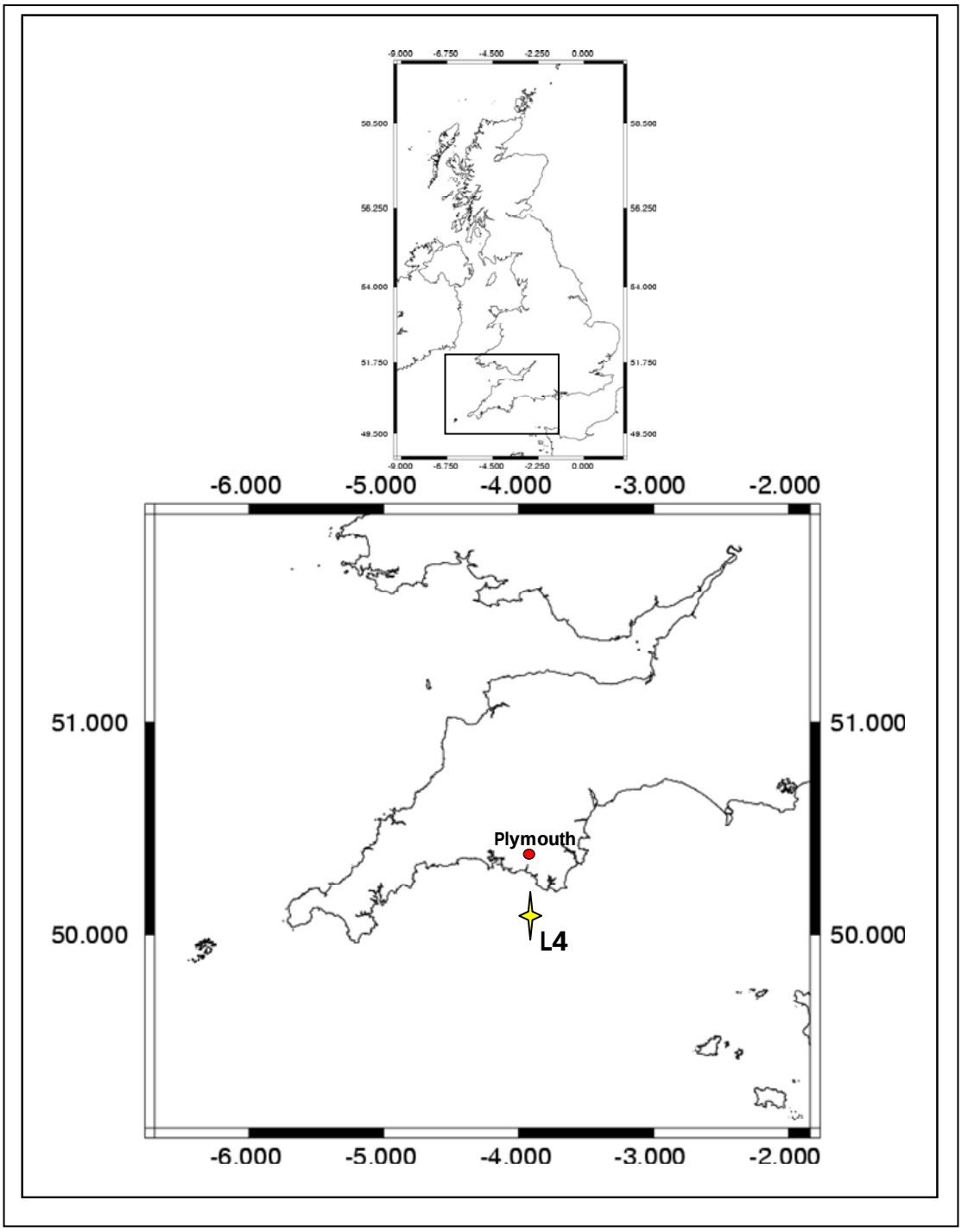

Figure 4.1. Location map of the L4 Western Channel Observatory time series station in the Western English Channel.

4.2. Experimental Setup and Methodology

4.2.1. Incubation setup

To address the questions in Section 4.1, two laboratory systems were constructed: one for incubating seawater at future high CO_2 levels, and another system to act as a present day control. Natural marine phytoplankton assemblages underwent incubation, and in principle the experiment was similar in nature to the mesocosm experiment: Nutrients were added to the incubations at the start of the experiment to stimulate a strong phytoplankton bloom, allowing the concentrations of relevant trace gases to be monitored over the rapid growth and decline of the bloom. The experiments were performed in a temperature and light controlled culture room, with a 16:8 hour light-dark cycle, creating much more uniform and controlled conditions than those experienced in the fjord during mesocosm experiments, where light and temperature can fluctuate over the course of few hours.

During the Spring and Summer of 2007, two 16 – 17 day laboratory seawater CO_2 incubation experiments were performed at Plymouth Marine Laboratory, using natural seawater samples from the L4 Western Channel Observatory time series station (See Figure 4.1). Surface seawater was collected with a stainless steel bucket and transferred to acid-washed 10 litre carboys. Water samples for Experiment 1 were collected on 4 June, and for Experiment 2 on 31 July, during the routine weekly L4 sampling. The temperature of the samples at the time of collection were 14°C for Experiment 1, and 15.5°C for Experiment 2. The satellite images below show time integrated surface chlorophyll *a* concentrations (mg m^{-3}) (Figures 4.2A and 4.3 A) and sea surface temperature (Figures 4.2B and 4.3 B) for the days prior to, and including sampling days. At the time of sampling for Experiment 1 (Fig. 4.2A) there was evidence of areas of high surface chlorophyll *a* concentrations in excess of 5 mg m^{-3} in several extensive patches. One particularly large patch was associated with cooler waters SW of the Cornish peninsula. An intense area of biological activity was detected close to the L4 sampling site, with concentrations ranging from 20 to 40 mg m^{-3}.

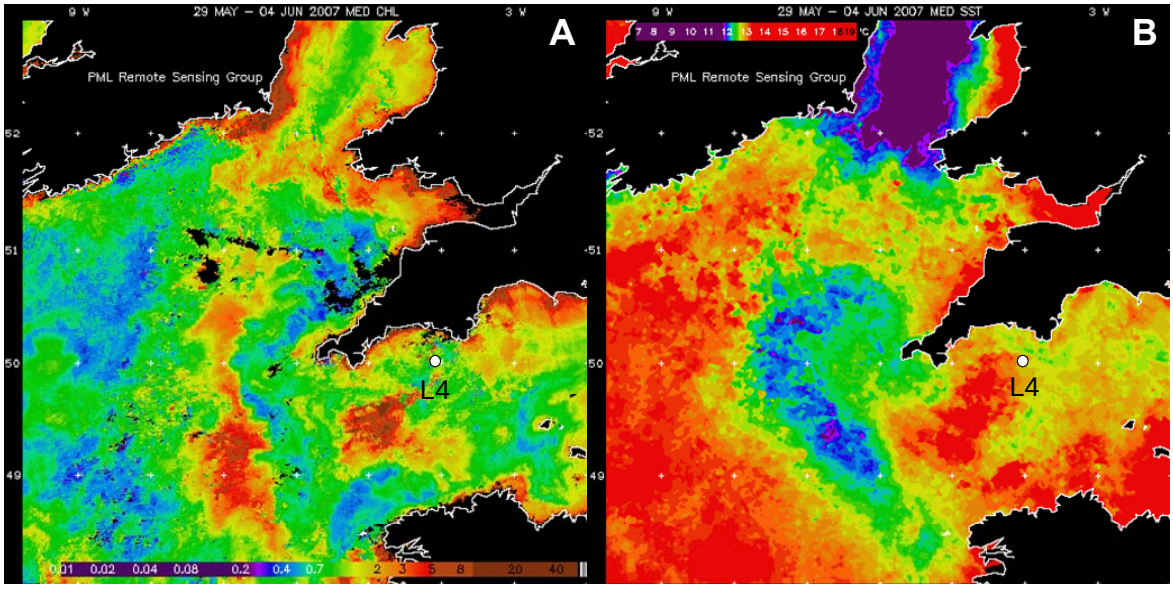

Figure 4.2. Satellite images showing average values of A. Chlorophyll (OC3M, MODIS Aqua) and B. Sea surface temperature (11 µm, AVHRR) for the period 29 May to 4 June 2007. Sampling for Experiment 1 took place on 4 June.

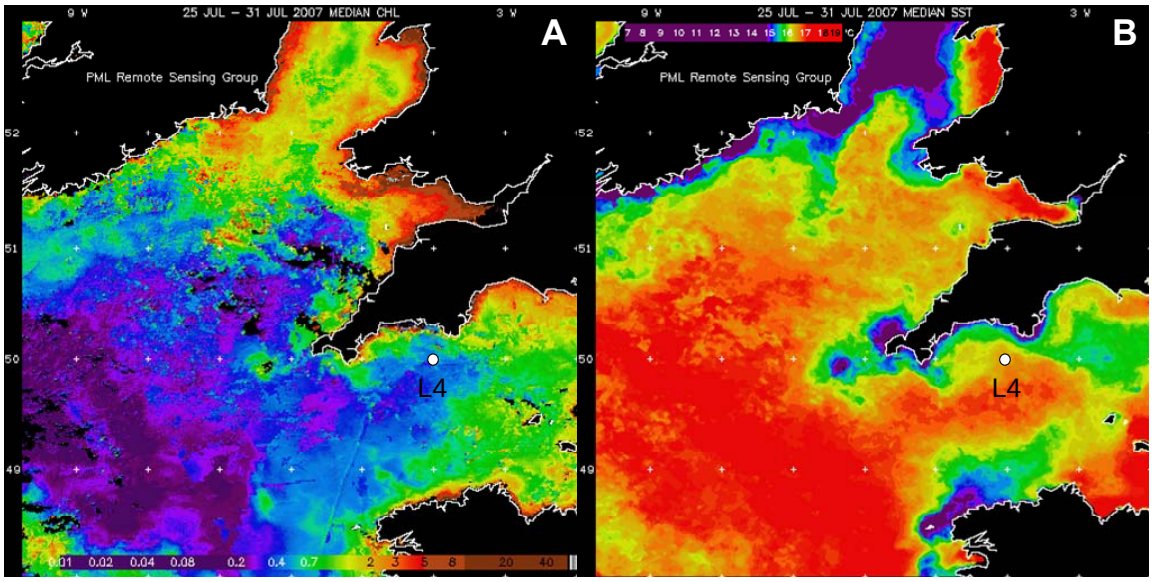

Figure 4.3. Satellite images showing average values of A. Chlorophyll (OC3M, MODIS Aqua) and B. Sea surface temperature (11 µm, AVHRR) for the period 25 to 31 July 2007. Sampling for Experiment 2 took place on 31 July. Images courtesy of Plymouth Marine Laboratory Remote Sensing Group.

The conditions during the sampling for Experiment 2 were quite different, with much lower chlorophyll *a* concentrations of less than 0.7 mg m^{-3} over much of the open sea, with only the coastal areas retaining high levels of chlorophyll *a*. As it was later in the Summer, sea surface temperature was higher, and more homogenous.

Within the vicinity of L4, chlorophyll *a* concentrations were low, with values not exceeding 0.4 mg m^{-3}.

On return to the laboratory, 4.5 litres of seawater was siphoned directly through a 50µm mesh to remove all large grazers, and into acid-washed 5 litre glass Duran flasks. Nylon bungs were modified in house at UEA for the Duran flasks. The bungs had two ¼" holes drilled in them, through which two lengths of ¼" nylon tubing was inserted to operate as an inlet and an outlet. The outlet was fitted with a sterile inline filter with cellulose acetate membrane (0.2 µm) in order to prevent any particulates or bacteria entering the incubations. The inlet to the incubation vessel again comprised a sterile inline filter, along with a 3-way stopcock with luer fittings and a Swagelok stainless steel metering valve to accurately control the flow of gas into the incubations. A diagram of the incubation setup is shown in Figure 4.4 and a detailed photograph of the apparatus is shown in Figure 4.5 a and b.

The experiments were performed in a constant-temperature culture room (~15 °C), with light levels of 72.90 µmol m^{-2} s^{-1}. The incubation vessels were connected to the gas supply with 1/8" nylon tubing. To simulate those condition predicted for the Year 2100, four of the vessels were incubated with an air/CO_2 mixture of 750ppmv (BOC) at a flow rate of ~100 ml/min until the target pH of 7.7-7.87 was achieved. Once this pH was achieved (after 2 days) flow rates were reduced to ~40 ml/min, and nutrients (Starting concentrations [NO_3^-] = 10 µmol l^{-1} and [PO_4^{3-}] = 0.625 µmol l^{-1}, approximate UK waters winter values) were added to the incubation vessels to stimulate the development of a phytoplankton bloom. The four remaining incubation vessels acted as a control, and were aerated with laboratory air, using a Millipore vacuum pump. Figure 4.5 c shows the glass gas diffuser submerged in seawater in an incubation vessel. At a flow rate of ~40 ml min^{-1} disturbance to the water is minimal, whilst allowing equilibration of the seawater and CO_2.

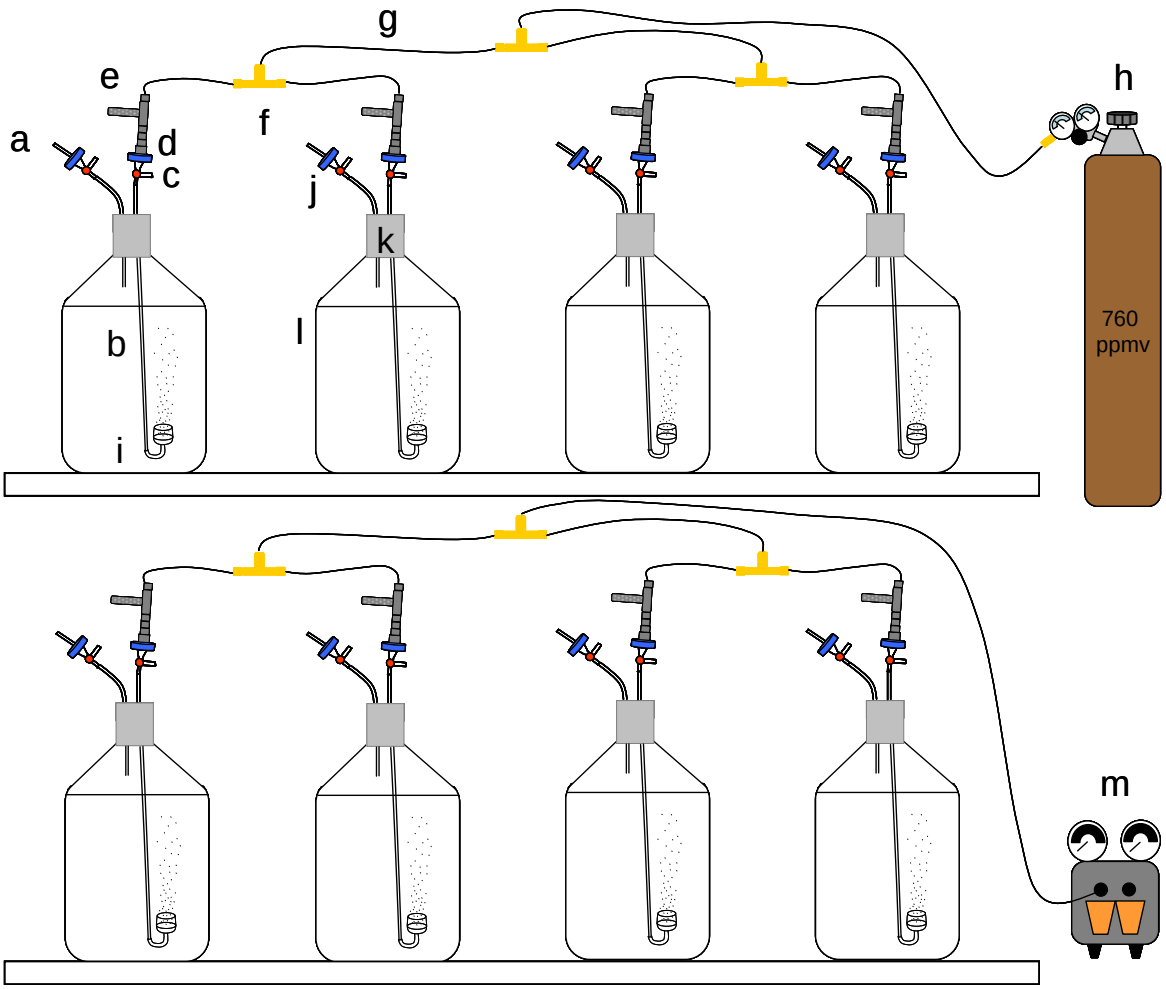

Figure 4.4. Diagrammatic representation of the L4 CO_2 incubation experimental setup. a. Vent, b. ¼" nylon tubing, c. 3-way stopcock with luer connections, d. Swagelok ¼" – 1/8" SS reducing union, e. Swagelok SS metering valve, f. Swagelok brass t-piece, g. 1/8" nylon tubing, h. BOC CO_2/Air mixture 760 ppmv, i. Glass gas diffuser, j. 0.2µm air filter, k. Nylon bung, l. 5 litre glass Duran flask, m. Millipore vacuum pump. (SS = stainless steel).

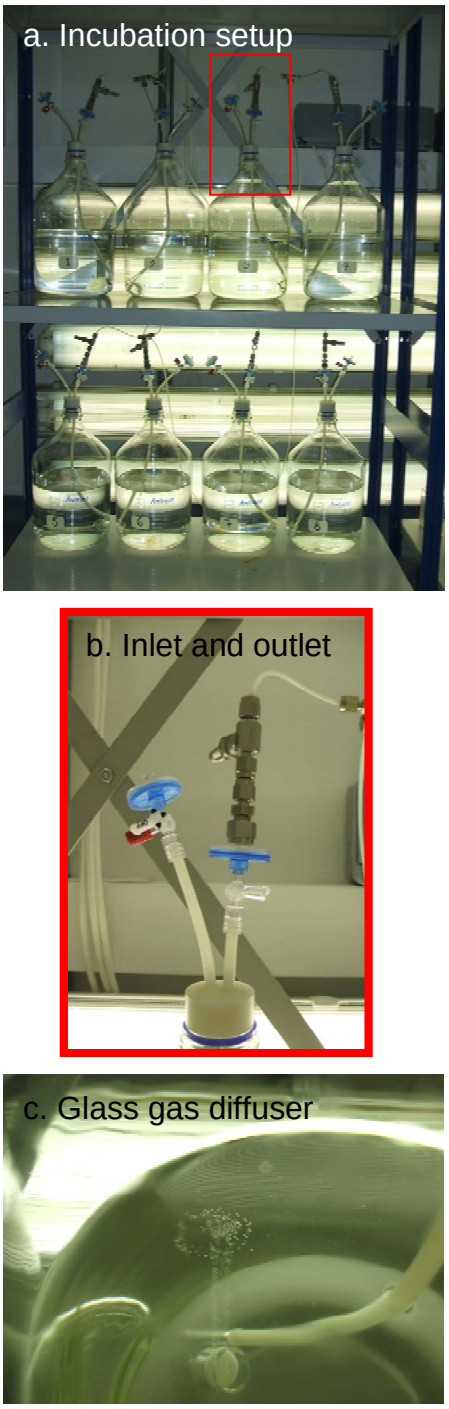

Figure 4.5. Photographs of the incubation setup. a. Photograph of the incubation setup, b. Detailed view of the inlet and outlet of each incubation vessel, c. View of the degree of bubbling resulting from the aeration of the vessels (40-50ml/min). Disturbance of the surface of the water was minimal.

The CO_2 concentration of the air coming through the Millipore pump was monitored over a three day period during the second experiment, using a CO_2 gas analyser (Li-Cor Biosciences), in order to ensure that the present day CO_2 vessels were receiving the desired CO_2 treatment. As shown by Figure 4.6, the CO_2 of the air showed some small fluctuations. The peaks seen at ~20 hours and ~45 hours occur immediately after the daily sampling time, when up to 45 minutes may have been spent in the culture room. It is possible that the increase in pCO_2 was a result of human respiration on the CO_2 concentration in the culture room. However, the CO_2 levels rapidly dropped back down once the incubation room had been left empty for a few hours. With a mean CO_2 concentration of 363.3 ppmv (± 27.8 (SD)) the control incubations can be considered to have experienced the equivalent of present day atmospheric CO_2 concentrations over the global oceans.

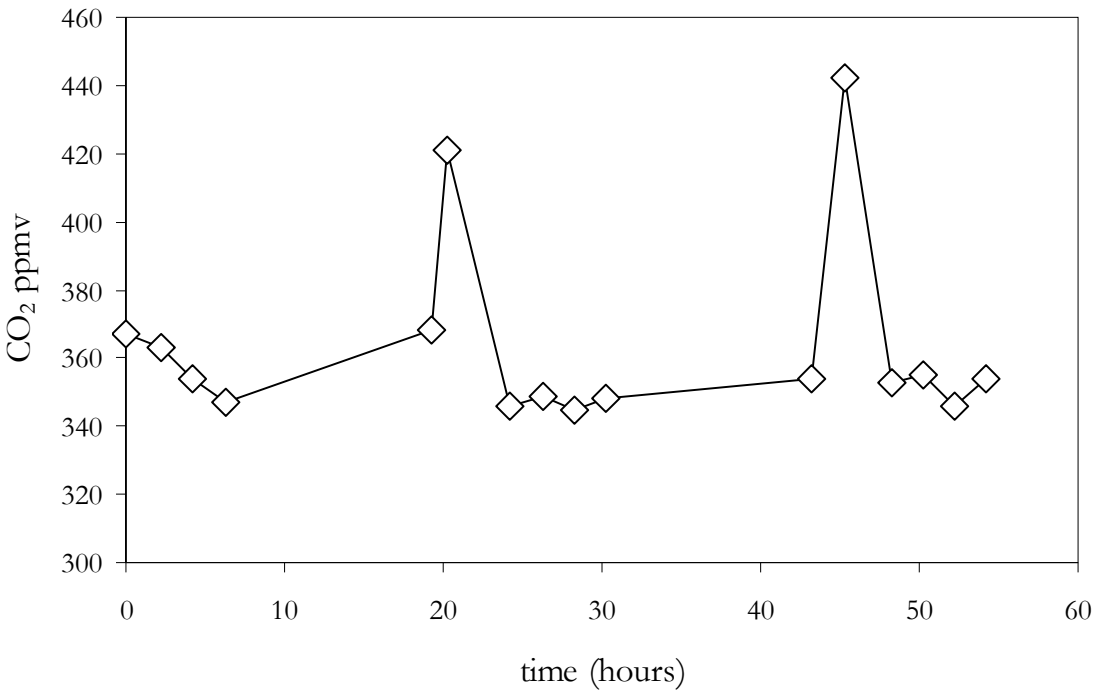

Figure 4.6. CO_2 concentrations (ppmv) of the laboratory air used to aerate the control incubations over a three day period during Experiment 2.

4.2.2. pH measurements

pH measurements were taken daily, immediately following sampling, using a Jenco pH/mV/temperature probe and meter. The air-tight bungs were removed from

the incubation vessels and the probe was inserted directly into the seawater, and held in place for around one minute, or until the signal stabilised. The pH probe was calibrated daily using NBS calibration buffer standards of pH 4.0, 7.0 and 10.0 (Fisher Scientific).

4.2.3. Halocarbon analyses

Seawater samples for halocarbon analyses were taken with a 100ml glass syringe, by removing the filter and inserting a 1/8" nylon syringe extension through the ¼" vent of the incubation vessel. This ensured that the vessels did not have to have their bungs removed, therefore maintaining the desired atmosphere inside the vessel. Immediately after sampling, syringes were placed in cool-box until analysis. All samples were processed with 2.5 hours of sampling. Samples were analysed using purge and trap with Markes sorbent tubes held in a chiller, followed by TD-GC-MS, according to the method discussed in Section 2.3.1.3 (Chapter 2).

4.2.4. Chlorophyll a determination

Water samples for chlorophyll *a* were taken from the incubations on a daily basis. 100 ml of seawater was drawn up into a glass syringe, and then transferred to a 100 ml glass Duran bottle. Samples were kept in the dark until processing 2-3 hours later. 47 mm diameter GF/F filters (0.7 µm poresize) were used, with a low filtration pressure of < 100 mm Hg. Once the required volume had passed through the filter paper, the vacuum was released, and the filter paper was gently folded up with tweezers, wrapped in Aluminium foil and placed in a -80°C freezer. In order to extract chlorophyll *a*, the frozen filters were soaked in 20ml of 90% acetone for 24 hours, in darkness and at -20°C. After 24 hours, the samples were centrifuged for 3 minutes at 4000 rpm in order to remove any particles from the acetone/chlorophyll *a* solution. A Turner fluorometer was used to determine the fluorescence of the samples. Calibration of the fluorometer was performed using serial dilutions of a 1 mg l^{-1} chlorophyll *a* standard.

4.2.5. Phytoplankton community determination

4.2.5.1. Flow cytometry

Samples for flow cytometric counts of microphytoplankton were taken and analysed daily according to the methods described in Section 2.5.3. (Chapter 2).

4.2.5.2. Phytoplankton microscopy counts

Phytoplankton microscopy counts were carried out by Claire Widdicombe (PML), according to the methods described in Section 2.5.2 (Chapter 2). Samples from all 8 vessels on days 3 and 16 in Experiment 1, and days 4 and 17 in Experiment 2 were analysed. Cell counts were converted to biomass according to the equations of Menden-Deuer and Lessard (2000).

4.2.6. Statistical analyses

All halocarbon, chlorophyll *a* and microphytoplankton data from all vessels were analysed using two-sample tests of hypotheses. Initially tests of normality were applied ($p<0.05$ = not normal), and if data failed to fit the assumptions of the test, linearity transformations of the data were performed (square root or logarithmic transformations). The analysis continued from this point, firstly with a test for equal variances (Levene's statistic, $p>0.05$ = equal variances), culminating in a two-sample T-test ($p<0.05$ = significant differences). For those data which still failed to display normality following transformation, non-parametric tests were applied. Data that displayed equal variances underwent a Mann-Whitney test. Using this method of statistical analyses, tests are used that decrease in power, depending on the ability of the data to fit the assumptions of the tests.

Spearman's Rank Correlation Coefficients (ρ), along with associated significance level (95% $p<=0.05$, 98% $p<=0.02$, 99% $p<=0.01$) were calculated to identify relationships between various chemical and biological parameters measured during the experiment.

4.3. Results

4.3.1. Experiment 1

4.3.1.1. pH and Chlorophyll *a*

The pH of the seawater before treatment was approximately 8.0, a value that is slightly lower than surface seawater in equilibrium with current atmospheric CO_2 concentrations (Raven *et al.* 2005). The rapid aeration of the incubation vessels for the first two days of the experiment caused a large drop in pH in the high CO_2 vessels, and by day 3 the pH was down to 7.6 in the high CO_2 vessels, as shown in Figure 4.7.

The addition of nutrients on day 3 was followed by the initiation of rapid phytoplankton growth (See Figure 4.8), causing the pH in all mesocosms to begin to increase. By day 5 the high CO_2 vessels rose to ~7.9, with the exception of V1 that had increased to only ~7.7. The pH of high CO_2 V2, V3 and V4 appeared to stabilise on day 8, at around pH 8.0, before dropping down again on day 14 to 7.7 – 7.8, as growth began to diminish in the vessels. V1 behaved quite differently to the other high CO_2 vessels in terms of pH, with much lower values during the majority of the experiment. Overall, there was a statistically significant difference between the mean pH of 7.86 under high CO_2 and the mean of 8.08 for the present day CO_2 vessels (See Table 4.1 and Appendix 13).

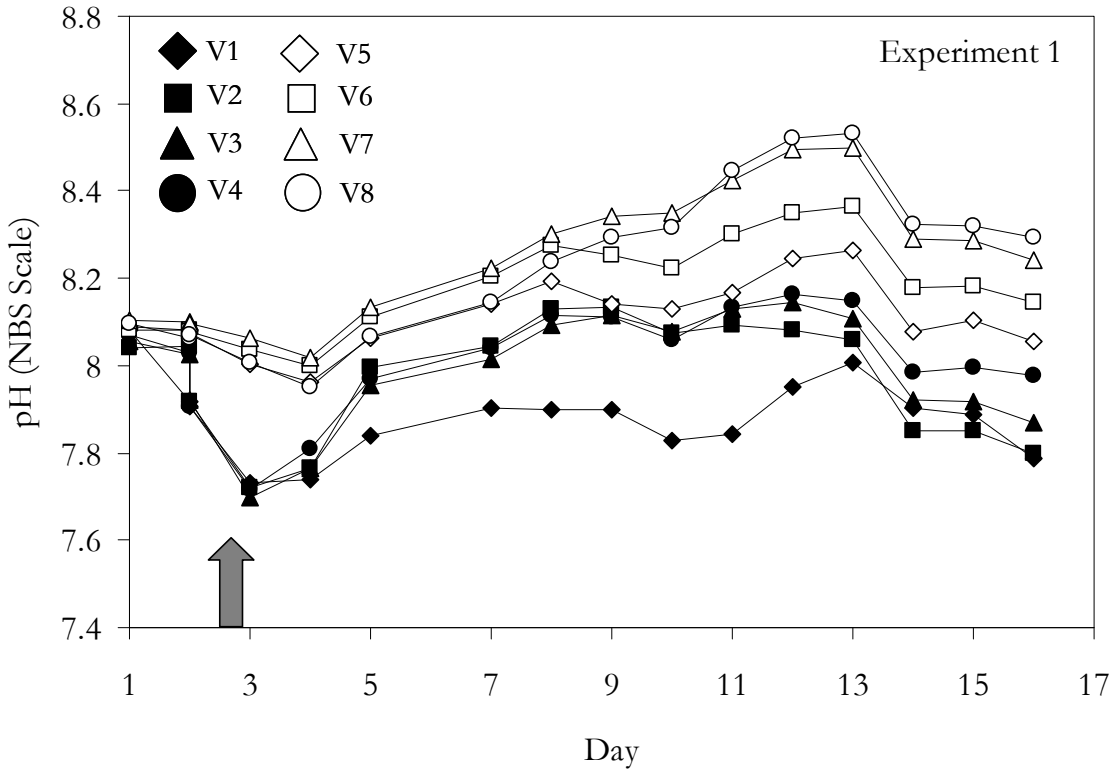

Figure 4.7. Daily pH measurements (NBS Scale) made during Experiment 1. V1 – V4 = High CO_2, V5 – V8 = Present day CO_2. Arrow indicates nutrient addition.

Following the addition of nutrients, a strong phytoplankton bloom proceeded in all vessels. On day 3 chlorophyll *a* concentrations reached between 5 and 10 mg m^{-3}; this rapid growth continued in all vessels (except V1), with rising concentrations that reached a sharp peak on day 8 of 40 to >60 mg m^{-3}. V1 behaved quite differently during this period of the experiment. Until day 5, the chlorophyll *a* in this vessel increased in step with the others, but displayed a sudden halt in growth following this

point, failing to reach the pinnacle of growth shown by all others. By day 8 concentrations began to recover, with a "peak" in chlorophyll *a* on day 9 of 34.2 mg m^{-3}. The pH of this vessel reflected the lower chlorophyll *a* biomass, with a weaker response to changes in pCO_2 and chlorophyll *a* compared to the other high CO_2 vessels.

.

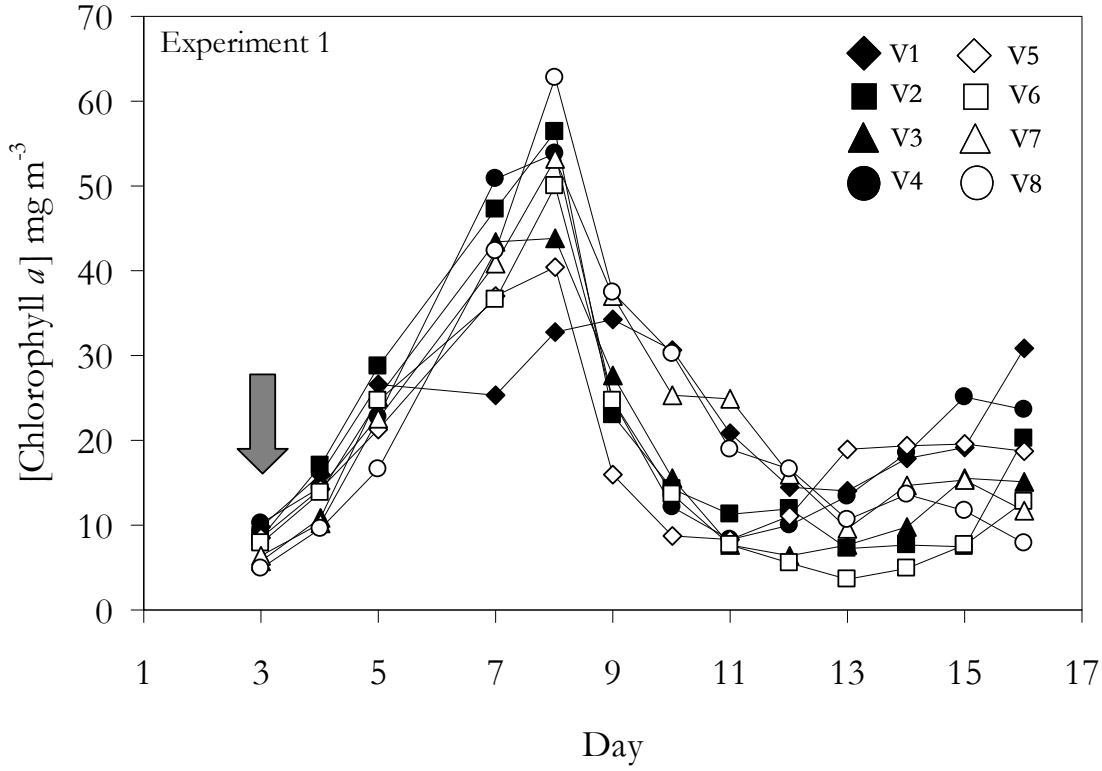

Figure 4.8. Daily chlorophyll *a* concentrations during Experiment 1.
V1 – V4 = High CO_2, V5 – V8 = Present day CO_2. Arrow = Nutrient addition.

Following the peak on day 8, chlorophyll *a* concentrations in V2 – V8 experienced a rapid decrease. This was most pronounced in V2, V3, V4, V5 and V6. By day 13, most vessels reached a minimum, followed by a secondary increase in chlorophyll *a* in some vessels (particularly V1, but also V2 and V6) over the last 3 – 4 days of the experiment, whilst the remaining vessels appeared to stabilise or show some further decrease in concentrations. There were not found to be any statistically significant differences between treatments for mean chlorophyll *a* concentrations (T-test T = -0.68, p = 0.496) (See Table 4.1).

4.3.1.2. The phytoplankton community

4.3.1.2.1. Cell numbers from flow cytometry

Numbers of nanophytoplankton in all vessels started at <5000 cells ml^{-1}, with growth rapidly after the addition of nutrients (Figure 4.9a), and all showed similar temporal development for the first three days of the experiment, with numbers reaching ~6000 cells ml^{-1}. Following this, differences between vessels began to become apparent, and by day 8 most vessels were exhibiting great variation in numbers. The high CO_2 vessels displayed a modest peak on day 9 (8000 – 11000 cells ml^{-1}), whilst between days 7 and 10, numbers decreased rapidly, falling to ~2300 cells ml^{-1}. During this period, V8 behaved quite differently to all the other vessels, reaching a large peak on day 9 (16000 cells ml^{-1}) before numbers gradually dropped off. A number of the vessels (V1, V4, V5, V6, V7) experienced a secondary phase of nanophytoplankton growth over the last 4 days of the experiment, particularly in V5 which reached 27000 cells ml^{-1} by the end of the experiment. Overall, mean nanophytoplankton numbers increased by 7.4 percent under high CO_2. However, the lack of consistency in temporal development within vessels of the same treatment, and large variability between vessels of the same treatment meant that there was no significant difference in nanophytoplankton numbers between treatments (T-test $T = 1.50$, $p = 0.136$, See Table 4.1 and Appendix 13). Numbers of nanophytoplankton were found to be correlated with chlorophyll *a* only under the present day CO_2 treatment (Spearmans's $\rho = 0.472$, $p<0.05$, see Table 4.2 and Appendix 18).

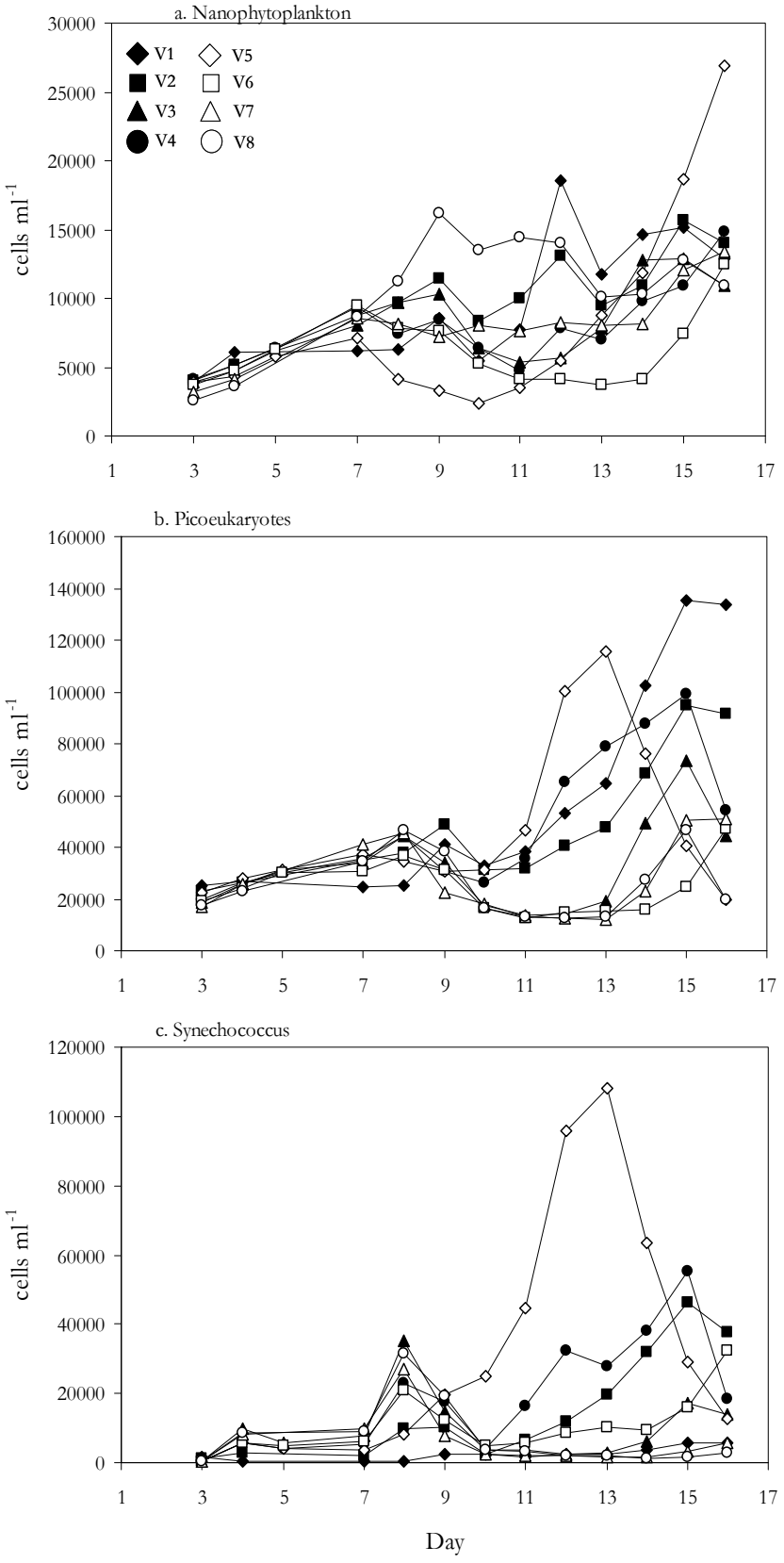

Figure 4.9. Microphytoplankton species cell counts (cell per ml) during experiment 1. a. Nanophytoplankton, b. Picoeukaryotes, c. *Synechococcus*. V1 – V4 = High CO_2, V5 – V8 = Present day CO_2.

Table 4.1. Summary of the statistical analysis on chlorophyll *a* and microphytoplankton data.

	Mean High CO_2	Mean Present day CO_2	% change under high CO_2	Statistical test	Significant differences ($p<0.05$)
pH	7.86	8.08	N/A	Mann Whitney W =2582.5, p<0.001	√
Chlorophyll *a* mg m^{-3}	21.5	20.5	+4.8%	T-test T = -0.68, p = 0.496	
Nanophytoplankton cells ml^{-1}	8897	8243	+7.4%	T-test T = 1.50, p = 0.136	
Picoeukaroytes cells ml^{-1}	46675	31480	+32.6%	T-test T = 3.53, p = 0.001	√
***Synechococcus* cells ml^{-1}**	11668	14334	-18.6%	T-test T =-0.37, p = 0.711	
Diatoms µg l^{-1}	5.36	2.87	+46.5%	T-test T = -1.74, p = 0.105	
Auto. Dinoflagellates µg l^{-1}	4.48	3.63	+18.9%	T-test T = -1.74, p = 0.105	
Flagellates µg l^{-1}	7.97	8.90	-10.5%	T-test T = 0.67, p = 0.517	
Hetero. Dinoflagellates µg l^{-1}	84.90	85.10	-0.2%	T-test T = 0.01, p = 0.993	
Ciliates µg l^{-1}	4.68	4.41	+5.8%	T-test T = -0.11, p = 0.916	
Total Biomass µg l^{-1}	107.4	91.8	+14.5%	T-test T = -3.58, p = 0.0012	

The temporal dynamics of the picoeukaryotes (Figure 4.9b) were similar to the nanophytoplankton for the first 7 days of the experiment. There were little differences between vessels during this period, although similarly to the nanophytoplankton, numbers in V1 were slightly lower than the rest. The picoeukaryotes started at around 20,000 cells ml^{-1}, doubling to 40,000 by day 8. A small peak was attained on

days 8 – 9 in most vessels, followed by a decline in numbers. From day 10 onwards, large differences between vessels began to appear. V1, V2, V4 and V8 saw rapid increases in numbers, whilst V3, V5, V6 and V7 continued to decrease. Numbers in V8 rapidly decreased on day 14, from 120,000 cells ml^{-1} to 70,000 cells ml^{-1} within 24 hours, and continued to fall until reaching 20,000 cells ml^{-1} at the end of the experiment. The high CO_2 vessels V2 and V4 reached an almost identical maximum of 95 – 100,000 cells ml^{-1} on day 15, before declining on day 16. The present CO_2 V6, V7 and V8, as well as the high CO_2 V3 showed growth over the last 3 days of the experiment, although this growth was greatest in V3. By the end of the experiment, numbers in V3, V4 V6 and V7 were quite similar, at around 44 – 54,000 cells ml^{-1}, whilst V5 and V8 ended with much lower numbers of ~20,000 cells ml^{-1}. V2 behaved quite differently, retaining high numbers in excess of 90,000 cells ml^{-1} at the end of the experiment. Despite a certain amount of within-treatment variability, the difference in mean number of picoeukaryotes under high CO_2 were found to be significantly higher than under the present day treatment (T-test, $T = 3.53$, $p<0.001$, see Table 4.1 and Appendix 13). Picoeukaryote numbers found to be significantly correlated with chlorophyll *a*, but in the same way as the nanophytoplankton, only under the present day CO_2 treatment (Spearman's $\rho = 0.319$, $p<0.05$, see Table 4.2 and Appendix 18).

Numbers of *Synechococcus* began low in all vessels (<10,000 cells ml^{-1}) and showed only small differences between vessels up to day 7 (Figure 4.9c). On day 8, five of the vessels (V3, V4, V6, V7, V8) reached a peak of 20 – 40,000 cells ml^{-1}, which also coincided with the peak in chlorophyll *a* (Figure 4.8). Despite this, no significant correlations were found between *Synechococcus* numbers and chlorophyll *a* concentrations (Table 4.2 and Appendix 18). Following this, numbers in these vessels fell, reaching a minimum on day 10. Numbers in V2 and V5 did not peak on day 8, but instead rose more steadily. However, V2 ceased to rise on day 9 and dropped to a minimum, as seen in all other vessels apart from V5. In a similar fashion to the picoeukaryotes, numbers of *Synechococcus* in V5 rapidly rose, going from <30,000 cells ml^{-1} to just under 105,000 cells ml^{-1} in 3 days. The highest numbers were achieved on day 13, in common with the peak in picoeukaryote numbers in this vessel. In the remaining vessels, once the minimum on day 10 had been passed, differences between vessels became apparent, although it is not clear if the differences can be attributed to CO_2 treatment.

Table 4.2. Spearman's Rank Correlation Coefficients (ρ) and associated significance level for mean chlorophyll *a* and microphytoplankton community components under high CO_2 (V1, V2, V3, V4) and present-day CO_2 (V5, V6, V7, V8).

	Nanophytoplankton	Picoeukaryotes	Synechococcus
Chl *a* High CO_2	0.221	0.233	0.077
Chl *a* Present CO_2	0.472	0.319	0.239

N = 48, shaded in grey = significant, critical value at 0.05 significance level = 0.286.

V1, V7 and V8 showed no further growth, with numbers remaining <6000 cells ml^{-1}. *Synechococcus* numbers in V2 and V4 behaved in the same way to the picoeukaryotes, with rapid growth between days 11 – 15, then numbers slightly declining on day 16. V3 showed little growth until day 15, but did not exceed 20,000 cells ml^{-1}. Following the large peak in V5 on day 13, numbers in this vessel rapidly crashed, reaching similar levels to V3 by day 16. V6 displayed similar temporal development to that of the picoeukaryotes, with the majority of growth occurring over days 14 – 16. Although an overall mean decrease in *Synechococcus* numbers of 18.6 percent was seen under high CO_2, the high amount of variability between vessels of the same treatment meant that no significant differences were identified (T-test, T = -0.37, p = 0.711, see Table 4.1 and Appendix 13).

4.3.1.2.2. Biomass

Carbon biomass (μg C l^{-1}) in terms of individual taxonomic groups of plankton (Figure 4.10a-e) and total plankton biomass (Figure 4.10f) showed variability both temporally, between treatments, and between vessels of the same treatment. The biomass on day 0 acts as a starting point, and is representative of one sample taken from the L4 sampling station, and immediately preserved, with no further processing or treatment. By day 3, diatom biomass (Figure 4.10a) began to show large differences between treatments, with significantly higher levels under high CO_2 (T = -5.09, p = 0.015, see Table 4.1 and Appendix 14), and reasonable replication between vessels of the same treatment, particularly the present day vessels (Relative SD = 35%, compared to 72% under high CO_2, see Table 4.3). By day 16, the differences between treatments had become less clear as a result of increased variability between the present CO_2 vessels (RSD 107%, see Table 4.3).

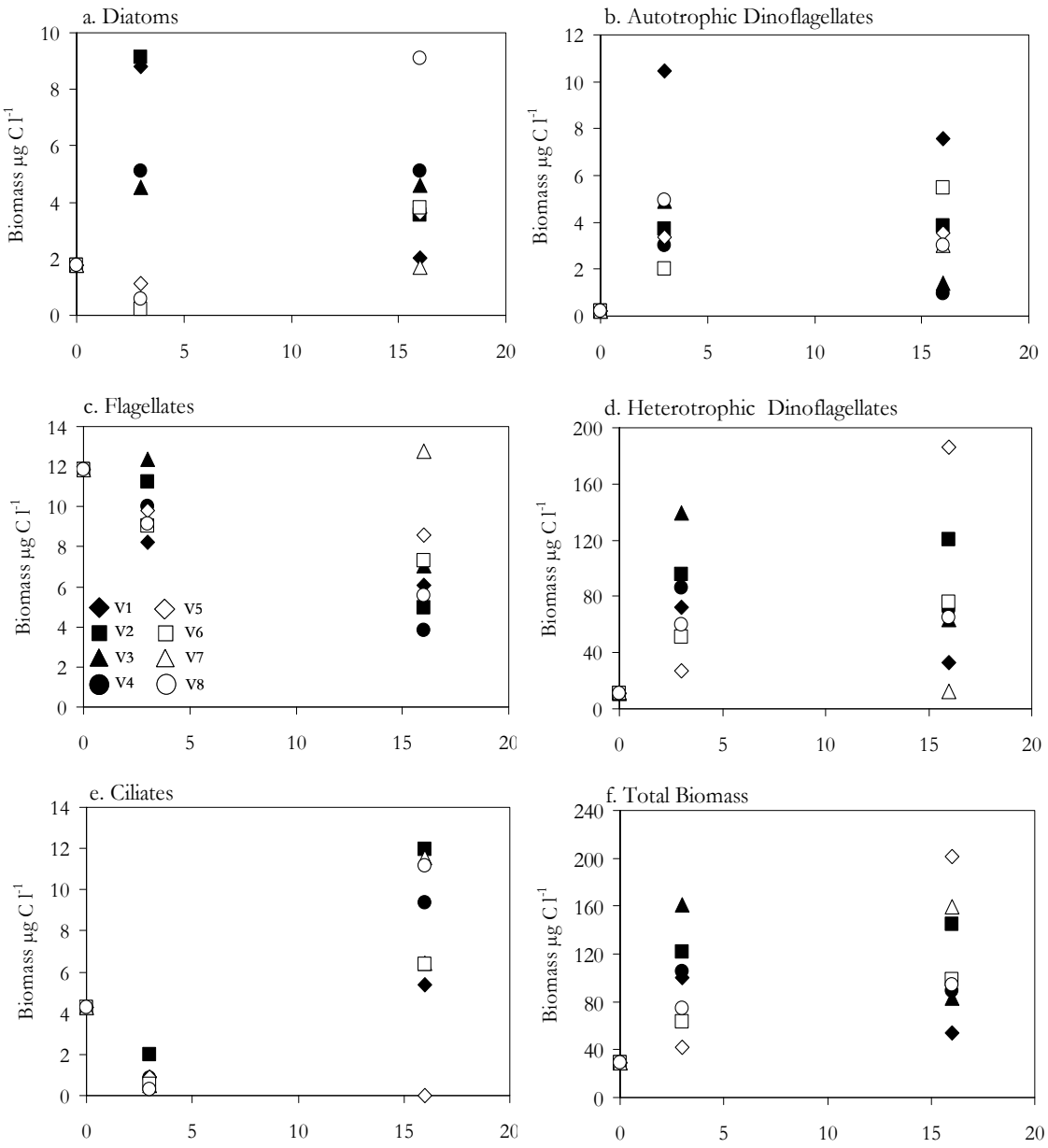

Figure 4.10. Plankton carbon biomass (µg C l^{-1}) on days 0 (water collection), 3 and 16. Each point is representative of measurement from one vessel. a. Diatoms b. Autotrophic dinoflagellates, c. Flagellates, d. Heterotrophic dinoflagellates, e. Ciliates, f. Total biomass. Legend is shown in panel c.

Overall, there was an increase in mean diatom biomass over the course of the experiment in the present day vessels, and a decrease under high CO_2. Autotrophic dinoflagellate biomass did not show any clear affect of treatment at any stage (Figure 4.10b). A drop in biomass was observed under high CO_2 (Mean Day 3 - 5.5 µg C l^{-1}, Day 16 - 3.4 µg C l^{-1}) whilst a small increase was seen under present day CO_2 (3.4 µg C l^{-1} to 3.8 µg C l^{-1}, see Appendix 14 for further details). Flagellate biomass (Figure 4.10c) started at similar levels of around 8 – 13 µg C l^{-1}in all vessels. Between days 3

and 16, mean biomass under high CO_2 halved (10.5 – 5.5 µg C l^{-1}), whilst only a small drop was seen under present CO_2 conditions (9.3 – 8.6 µg C l^{-1}). So although this clear difference in temporal development was observed, no significant differences between treatments in flagellate biomass were detected.

The heterotrophic dinoflagellates (Figure 4.10d) displayed some growth under present CO_2 between days 3 and 16 (46.1 – 114.3 µg C l^{-1}) whilst in contrast, the mean biomass under high CO_2 fell from 98.2 to 71.5 µg C l^{-1}. Data for day 3 did show significant differences between treatments (T = -2.75, p = 0.040, see Table 4.1 and Appendix 14) although by day 16 this consistent difference between treatments had lessened.

Ciliate biomass in all vessels (except V5) (Figure 4.10e) showed a large increase between days 3 and 16, from 1.1 to 8.3 µg C l^{-1} under high CO_2, and 0.6 – 7.3 µg C l^{-1} under present conditions. Although biomass did appear to be slightly elevated under high CO_2, no significant differences were detected (See Table 4.1). In terms of total biomass (Figure 4.10f) the high CO_2 vessels generally displayed higher levels on day 3, a difference between treatments that was found to be significant (T = -3.58, p = 0.012, see Table 4.1). By day 16, this difference had diminished, as a result of the greatly increased variability between replicate vessels. The relative standard deviation of measurements from replicate vessels is shown in Table 4.3. The ciliates showed the greatest variability between replicate vessels, of 93 percent under high CO_2, and 119 percent under the present CO_2 treatment.

Table 4.3. Relative standard deviation (RSD) of plankton biomass from replicate vessels.

	High CO_2 RSD	Present Day CO_2 RSD
Diatoms	46%	107%
Auto. Dinoflagellates	71%	33%
Flagellates	38%	25%
Hetero. Dinoflagellates	40%	64%
Ciliates	93%	119%
Total Biomass	32%	70%

Figure 4.11 shows bar charts of percentage biomass contribution of individual plankton taxa under a. High CO_2, and b. Present day CO_2. The data for the high CO_2 treatment has been scaled to the present CO_2 data to show the relative changes in biomass under the high CO_2 conditions. By day 3, the biomass under high CO_2 was double that in the control vessels, and this difference was mainly attributable to

greater heterotrophic dinoflagellates biomass. By day 16, the biomass under high CO_2 crashed relative to the present day treatment, with decline of almost a third. Again, this was mainly due to changes in heterotrophic dinoflagellates biomass.

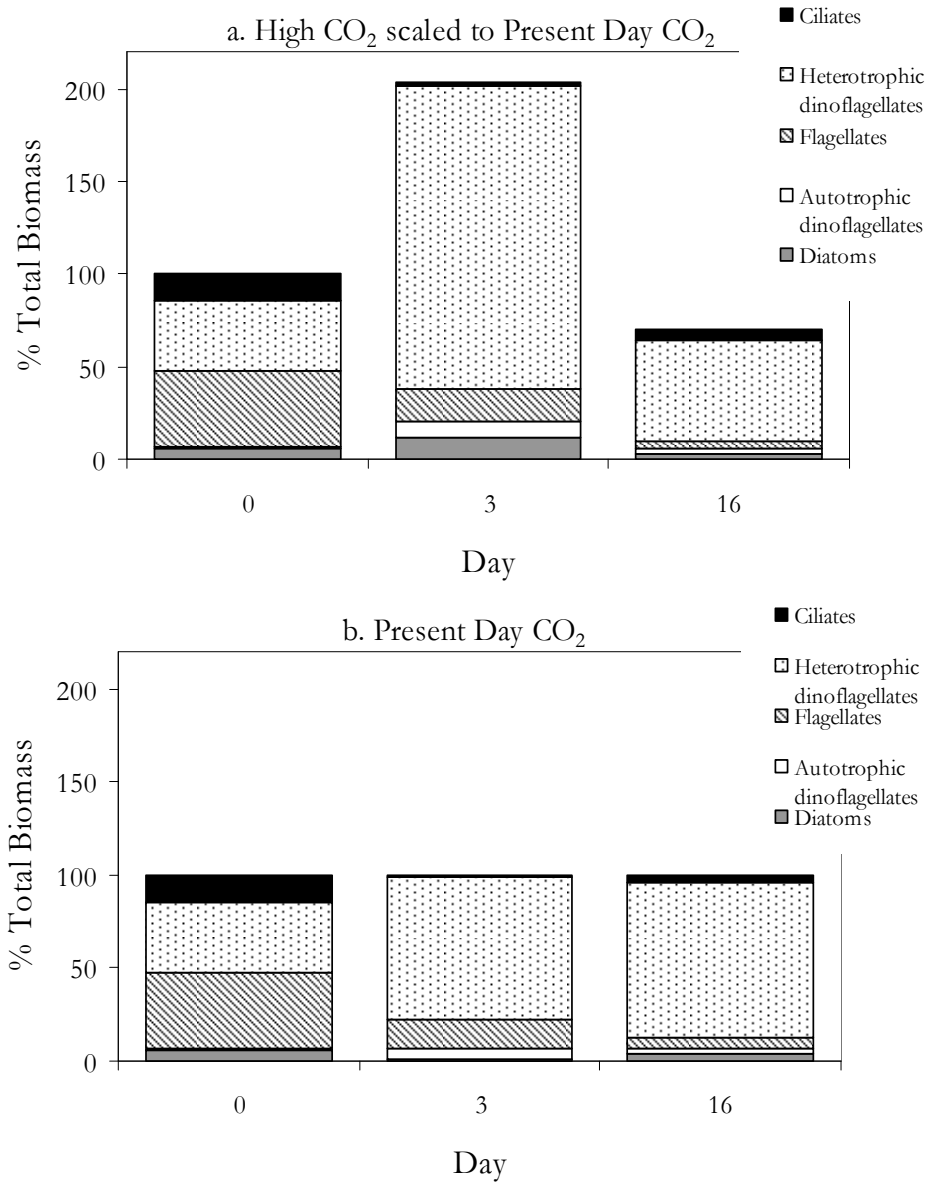

Figure 4.11. Mean percentage total biomass contribution of diatoms, autotrophic dinoflagellates, flagellates, heterotrophic dinoflagellates and ciliates to the phytoplankton populations. a. High CO_2 vessels, scaled to the present CO_2 vessels, and b. Present day CO_2 vessels, on days 0 (4 June – water collection day), 3 (7 June) and 16 (20 June). Mean percentage calculated from 4 replicate vessels for each CO_2 treatment.

4.3.1.3. Iodocarbons

4.3.1.3.1. Overview

The temporal dynamics of the iodocarbons were quite variable, as shown in Figure 4.12. The majority of these compounds appeared to show no direct relationship to biological activity, with the exception of C_2H_5I that peaked in concentration on the same day as the peak in chlorophyll *a* (Day 8, see Figure 4.8). Concentrations of CH_3I and 2-C_3H_7I showed little variation over the course of the experiment, with similar mean values on the first and last days (Day 3 and 16, CH_3I 3.40 and 3.42 pM, 2-C_3H_7I 0.38 and 0.45 pM), and some evidence for a difference between treatments. CH_2I_2 and CH_2ClI showed similar trends, with gradually decreasing concentrations, no obvious peaks or troughs, and no significant differences between treatments. Due to the similarities between some iodocarbons, and differences with others, it appears that a number of distinct production/removal processes appear to be responsible for net iodocarbon concentrations. Concentrations of CH_3I, C_2H_5I and 2-C_3H_7I fell within previous measurements from L4 seawater samples and other open ocean studies, whereas CH_2ClI was somewhat elevated in comparison (Abrahamsson *et al.* 2004a; Archer *et al.* 2007). Due to contamination in the analytical system, CH_2I_2 could not be calibrated during this study and therefore qualitative information is not available, so cannot be compared to previous measurements.

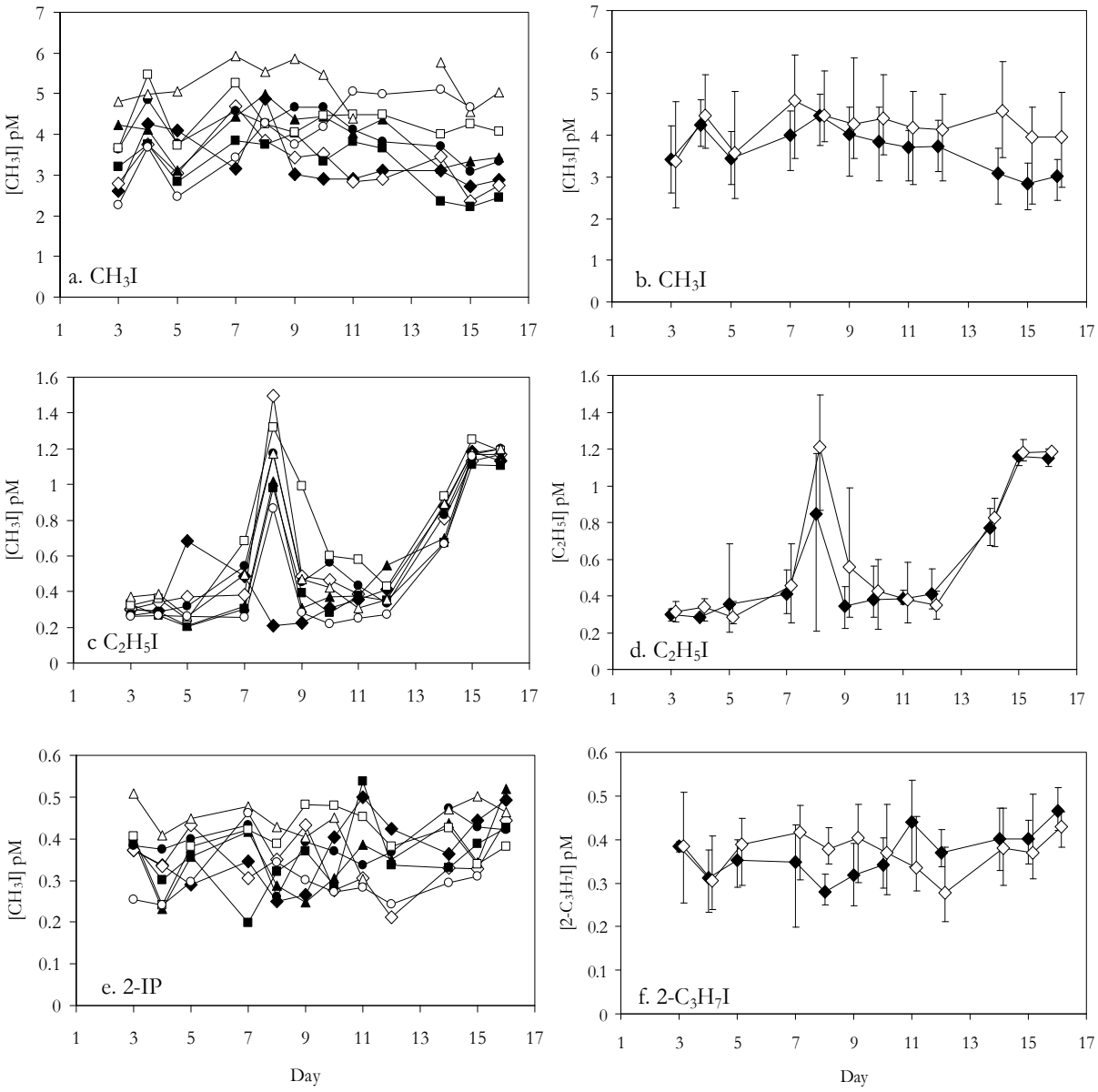

Figure 4.12. Continued on next page.

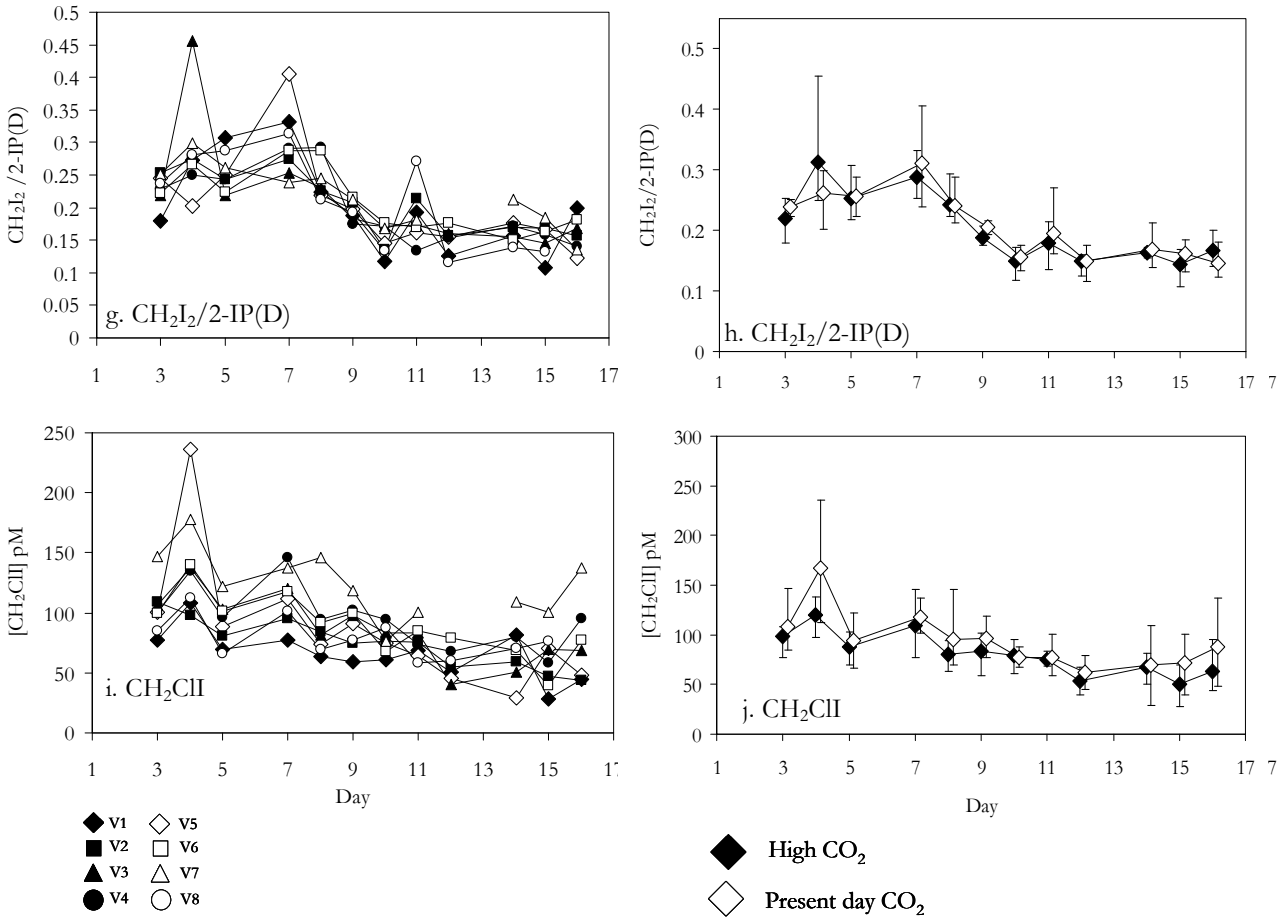

Figure 4.12. Total concentrations, and mean concentrations ± range of iodocarbons (pM) during Experiment 1. a. CH_3I, b. Mean CH_3I, c. 2-C_3H_7I, d. Mean 2-C_3H_7I, e. C_2H_5I, f. Mean C_2H_5I, g. CH_2I_2/2-IP(D), h. Mean CH_2I_2/2-IP(D), i. CH_2ClI, j. Mean CH_2ClI. V1 – V4 = High CO_2, V5 – V8 = Present day CO_2. Error bars indicate maximum and minimum values from replicate vessels.

4.3.1.3.2. CH_3I and 2-C_3H_7I

As shown by Figure 4.12a, b, c and d concentrations of CH_3I and 2-C_3H_7I showed little variation within vessels over the duration of the experiment. However, both compounds did show some difference between treatments, despite the lack of temporal variability. Mean concentrations of CH_3I (Fig. 4.12b) decreased by 12.8 percent under high CO_2, compared to the present day CO_2 vessels, a difference that was found to be significant (T-test T = -3.06, p = 0.003, see Table 4.4, and Appendix 13). Differences in mean concentrations of 2-C_3H_7I (Fig. 4.12d) were most pronounced during the first half of the experiment (days 3 – 10), again with significantly lower concentrations under high CO_2 during this period (T-test T = -2.30, p = 0.025 see Table 4.4, and Appendix 13). Figure 4.13a and b shows plots of the ratio of CH_3I and 2-C_3H_7I to chlorophyll *a* concentrations. When the data is normalised in this way, most differences between treatments are almost eliminated, with the exception of CH_3I: chlorophyll *a* over the last three days of the experiment, where the ratio was diminished under high CO_2. In general, the ratio was much lower during the peak of bloom activity (days 5 – 10, see Figure 4.8), but increased again during the later stages of the experiment as the main bloom broke down.

Spearman's rank correlations were performed on the data to identify significant relationships between the iodocarbons and other chemical and biological parameters. The results of these analyses are shown in Table 4.5, with further details in Appendix 16. CH_3I displayed a number of significant correlations – with all the iodocarbons, except C_2H_5I, and also with CH_2Br_2 under high CO_2 and with CH_2ClI and CH_2Br_2 under present CO_2. When compared to biological parameters, it was significantly correlated with both nanophytoplankton and picoeukaryotes under high CO_2 and *Synecococcus* in the present CO_2 treatment. 2-C_3H_7I was correlated with CH_3I, CH_2I_2 and CH_2BrCl under high CO_2, CH_2ClI under present CO_2 and C_2H_5I under both treatments, and nanophytoplankton and picoeukaryotes under high CO_2.

4.3.1.3.3. C_2H_5I

The temporal development of concentrations of C_2H_5I was quite different to all the other iodocarbons, and appeared to show the most association with biological parameters (Figure 4.12 e and f). With the exception of V1, the concentration in all vessels rose from <0.4 pM at the start of the experiment to a sharp peak of 0.9 – 1.5

pM on day 8, coinciding with the peak in chlorophyll *a* (Figure 4.8). Concentrations then rapidly crashed to pre-peak levels by the following day. After a period of stabilisation (days 10 – 12) concentrations in all vessels rapidly rose again over the last 3 days of the experiment. V1 behaved quite differently during the first half of the experiment, reaching relatively high concentrations of 0.7 pM on day 5 before dropping down to 0.2 pM on day 8 whilst the other vessels were experiencing their peak in concentrations. However, during the second half of the experiment, this vessel acted very similarly to the others. Overall, no significant differences in mean concentrations of C_2H_5I between treatments were observed (Mann Whitney, W = 2187, p = 0.4842, see Table 4.4).

Ratios of C_2H_5I to chlorophyll *a* also showed no difference between treatments (Figure 4.13c and Table 4.4), and were low and reasonably stable for the first half of the experiment, before increasing slightly during the latter half. The Spearman's Rank analysis revealed a wide range of correlations between this compound and other chemical and biological parameters (Table 4.5). It was significantly correlated with CH_2I_2, 2-C_3H_7I, $CHBr_3$ and CH_2BrCl under both treatments, and with CH_2ClI under high CO_2. This compound also displayed significant correlations with picoeukaryotes and *Synechococcus* under both treatments, and nanophytoplankton under high CO_2.

Table 4.4. Summary of the statistical analysis performed on all iodocarbon concentration data and all iodocarbon : chlorophyll *a* ratio data.

pM	Mean High CO_2	Mean Present day CO_2	% change under high CO_2	Statistical test	Significant differences ($p<0.05$)
CH_3I	3.65	4.19	-12.8%	T-test T = -3.06, p = 0.003	√
C_2H_5I	0.57	0.62	-8.6%	Mann Whitney W = 2187, p = 0.4842	
CH_2I_2/2-IP(D)	0.247	0.2103	-2.7%	T-test T = -0.53, p = 0.595	
CH_2ClI	80.73	94.45	-14.5%	T-test T = -1.84, p = 0.069	
2-IP	0.368	0.371	-0.8%	T-test T = -0.19, p = 0.848	
2-IP (Days 3 – 10)	0.334	0.378	-11.6%	T-test T = -2.30, p = 0.025	√
CH_3I:Chl *a*	0.237	0.295	-19.7%	T-test T = 1.55, p = 0.124	
C_2H_5I:Chl *a*	0.035	0.042	-16.7%	T-test T = 0.88, p = 0.381	
CH_2I_2/2-IP(D):Chl *a*	0.013	0.015	-13.3%	T-test T = 0.81, p = 0.418	
CH_2ClI:Chl *a*	5.164	6.768	-23.7%	T-test T = 1.48, p = 0.142	
2-C_3H_7I:Chl *a*	0.024	0.027	-11.1%	T-test T = 0.54, p = 0.590	

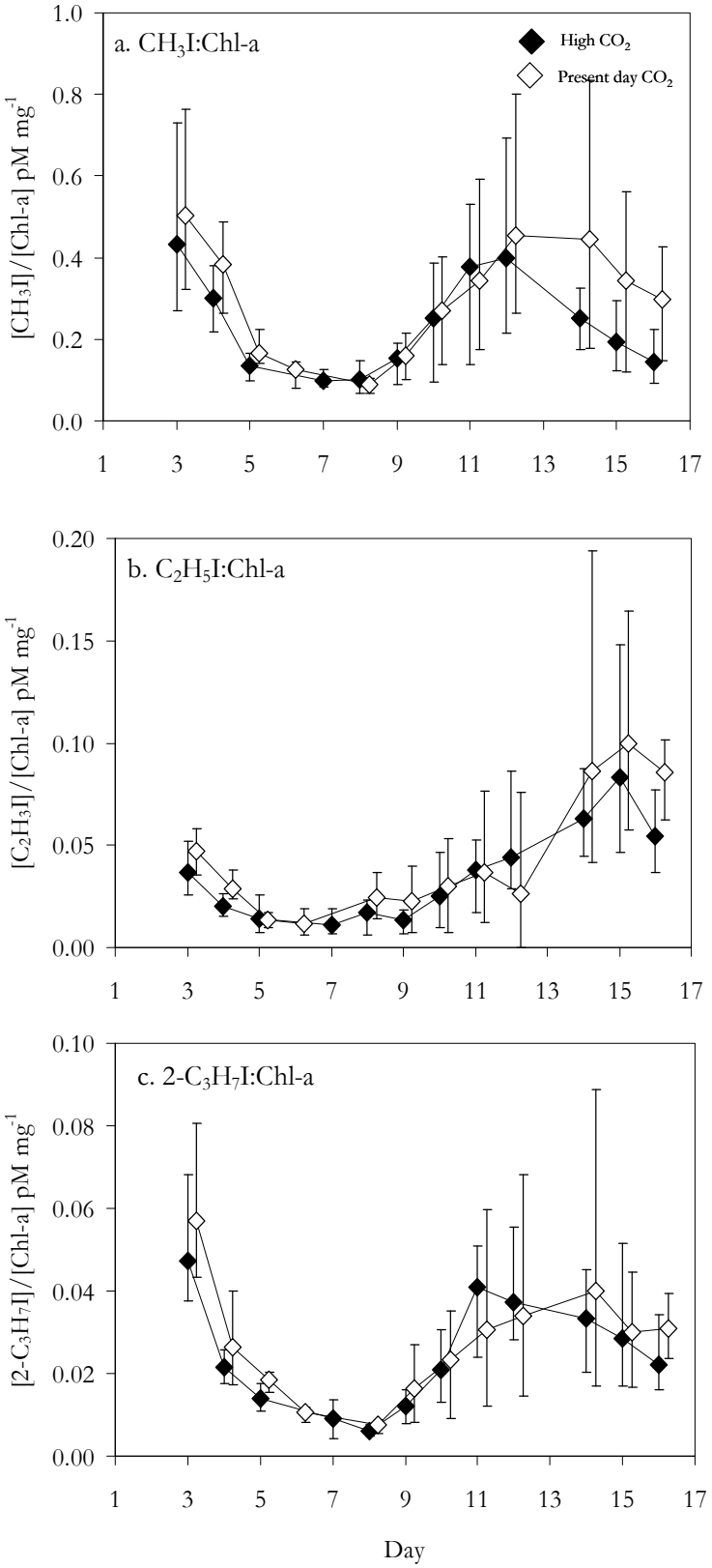

Figure 4.13. Continued on next page.

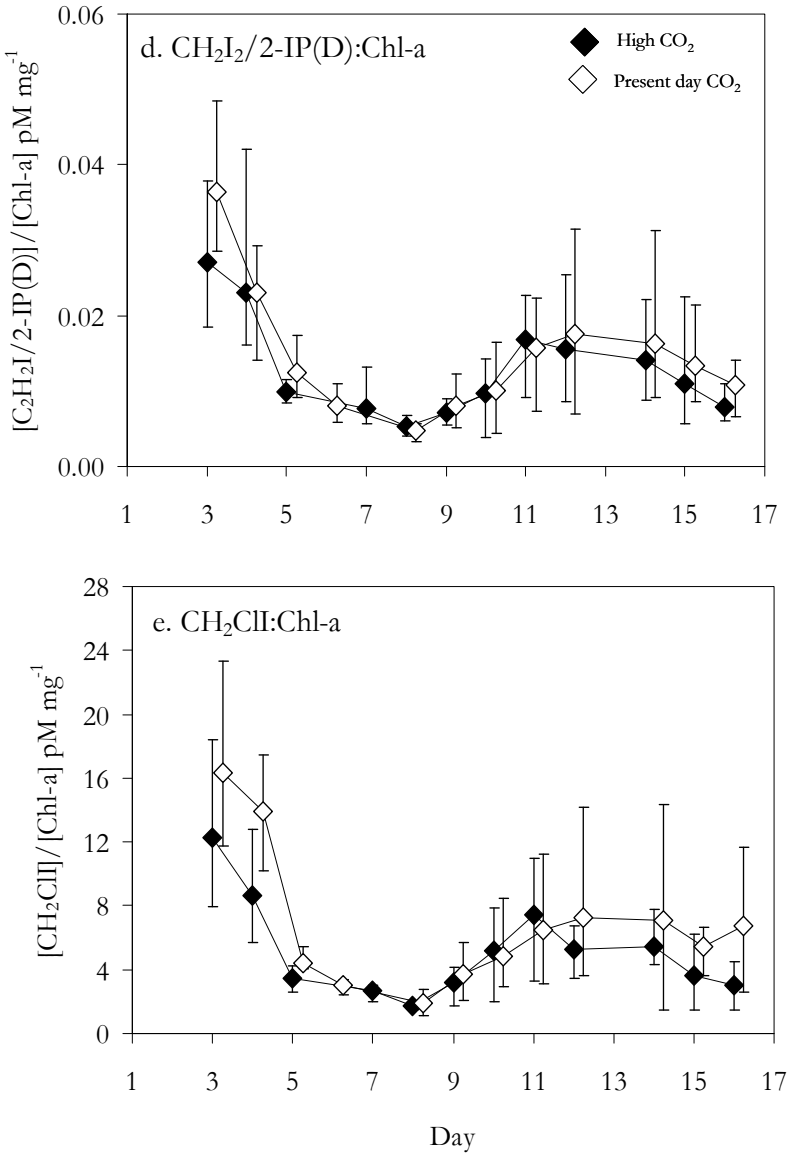

Figure 4.13. Mean ratios of iodocarbons to chlorophyll *a* duringExperiment 1. a. CH_3I:Chl *a*, b. 2-C_3H_7I:Chl *a*, c. C_2H_5I:Chl *a*, d. CH_2I_2/2-IP(D):Chl *a*, e. CH_2ClI:Chl *a* (Error bars show range).

4.3.1.3.4. CH_2I_2 and CH_2ClI

Plots of CH_2I_2/2-IP(D) and CH_2ClI concentrations are shown in Figure 4.12 g, h, i and j. These compounds showed somewhat similar temporal trends, with gradually decreasing concentrations over the course of the experiment, although lacking in any clear correspondence between the compounds within the same vessels. It should be noted that quantification of CH_2I_2 was not possible during this experiment due to contamination of the GC-MS, so the data shown may not be

accurately representative of CH_2I_2 concentrations in the vessels. Both compounds showed a slight peak on day 4, a feature in common with CH_3I. Due to a high degree of inter-vessel variability, there did not appear to be any differences between treatments, and no significant differences were identified (CH_2I_2 T-test T = -0.53, p = 0.595, CH_2ClI T = -1.84, p = 0.069), although mean concentrations were lower under high CO_2 (CH_2I_2 -2.7 percent, CH_2ClI -14 percent). When normalised to chlorophyll *a* concentrations (Figure 4.13d and e), both compounds showed comparable patterns, with elevated ratios for the first two days, followed by a decrease during the bloom period (days 5 – 9), then a slight rise and fall in ratio towards the end of the experiment. The mean ratio to chlorophyll *a* for both compounds was lower under high CO_2 for the first 3 and last 5 days of the experiment, but showed no discernable differences during the bloom.

The Spearman's Rank analyses (Table 4.5) revealed that CH_2I_2 and CH_2ClI were significantly correlated with each other under both treatments, and 2-C_3H_7I with CH_2I_2 under high CO_2 and with CH_2ClI under present CO_2, and both with CH_2BrCl under both treatments. Unlike all the other iodocarbons, CH_2I_2 showed a significant correlation with chlorophyll *a*, under both treatments, as well as with nanophytoplankton, picoeukaryotes and *Synechococcus* under high CO_2. By contrast, CH_2ClI was negatively correlated with nanophytoplankton and picoeukaryotes under high CO_2.

Table 4.5. Spearman's Rank Correlation Coefficients (ρ) and associated significance level for mean iodocarbons concentrations, with bromocarbons concentrations, chlorophyll *a* and microphytoplankton community components under high CO_2 (V1, V2, V3, V4) and present-day CO_2 (V5, V6, V7, V8).

		CH_3I	C_2H_5I	CH_2I_2	CH_2ClI	2-C_3H_7I
CH_2I_2	High CO_2	0.400	-0.360	-	-	-
CH_2I_2	Present CO_2	0.098	-0.317	-	-	-
CH_2ClI	High CO_2	0.544	-0.411	0.641	-	-
CH_2ClI	Present CO_2	0.416	-0.165	0.559	-	-
2-C_3H_7I	High CO_2	-0.339	0.364	-0.315	-0.211	-
2-C_3H_7I	Present CO_2	0.279	0.386	0.141	0.361	-
$CHBr_3$	High CO_2	-0.089	0.450	-0.104	-0.064	0.098
$CHBr_3$	Present CO_2	0.050	0.344	-0.181	0.021	0.116
CH_2Br_2	High CO_2	0.287	-0.073	0.122	0.139	-0.146
CH_2Br_2	Present CO_2	0.606	-0.239	0.150	0.363	0.190
CH_2BrCl	High CO_2	0.043	0.554	-0.487	-0.398	0.356
CH_2BrCl	Present CO_2	0.042	0.391	-0.351	-0.457	0.118
Chl *a*	High CO_2	0.121	0.058	0.367	0.139	-0.159
Chl *a*	Present CO_2	0.220	0.028	0.303	0.149	0.106
Nanophytoplankton High CO_2		-0.374	0.663	-0.483	-0.533	0.290
Picoeukaryotes High CO_2		-0.504	0.664	-0.475	-0.538	0.306
Picoeukaryotes Present CO_2		-0.143	0.478	0.040	0.029	0.036
Synechococcus Present CO_2		-0.298	0.408	-0.093	-0.273	-0.071

N = 48, shaded in grey = significant, critical value at 0.05 significance level = 0.286.

4.3.1.4. Bromocarbons

4.3.1.4.1. Overview

The dynamics of the concentrations of the three bromocarbons (Figure 4.14) showed a number of differences, and a high degree of inter-vessel variability. $CHBr_3$ displayed spikes of higher concentrations, some of which occurred in a number of vessels concurrently, whilst others appeared more random. The general trend showed little connection with biological activity. Concentrations of CH_2Br_2 were significantly

high under high CO_2, although again this compound did not show any obvious association with the growth of phytoplankton in the vessels. Concentrations of CH_2BrCl gradually rose over the duration of the experiment, and exhibited a mean percentage decrease under high CO_2. The concentrations of $CHBr_3$ and CH_2Br_2 measured during this study were similar to those measured previously in L4 seawater (Archer *et al.* 2007) as well as in other open ocean waters (Abrahamsson *et al.* 2004a; Quack *et al.* 2004; Chuck *et al.* 2005), whilst concentrations of CH_2BrCl were much lower than other previously reported measurements from the Southern Ocean (Abrahamsson *et al.* 2004a; Abrahamsson *et al.* 2004b).

Table 4.6. Summary of the statistical analysis performed on bromocarbons concentrations and bromocarbon : chlorophyll *a* ratios.

pM	Mean High CO_2	Mean Present day CO_2	% change under high CO_2	Statistical test	Significant differences ($p<0.05$)
$CHBr_3$	2.58	3.73	-30.8%	Mann-Whitney W = 1910, p = 0.3345	
CH_2Br_2	11.23	7.08	+36.9%	Mann Whitney W = 3035, p<0.001	√
CH_2BrCl	3.83	4.28	-10.5%	T-test T = -1.39, p = 0.167	
$CHBr_3$:Chl *a*	0.156	0.238	-34.5%	T-test T = 1.16, p = 0.247	
CH_2Br_2:Chl *a*	0.716	0.446	+60.5%	T-test T = -3.00, p = 0.003	√
CH_2BrCl:Chl *a*	0.250	0.310	-19.4%	T-test T = 0.95, p = 0.344	

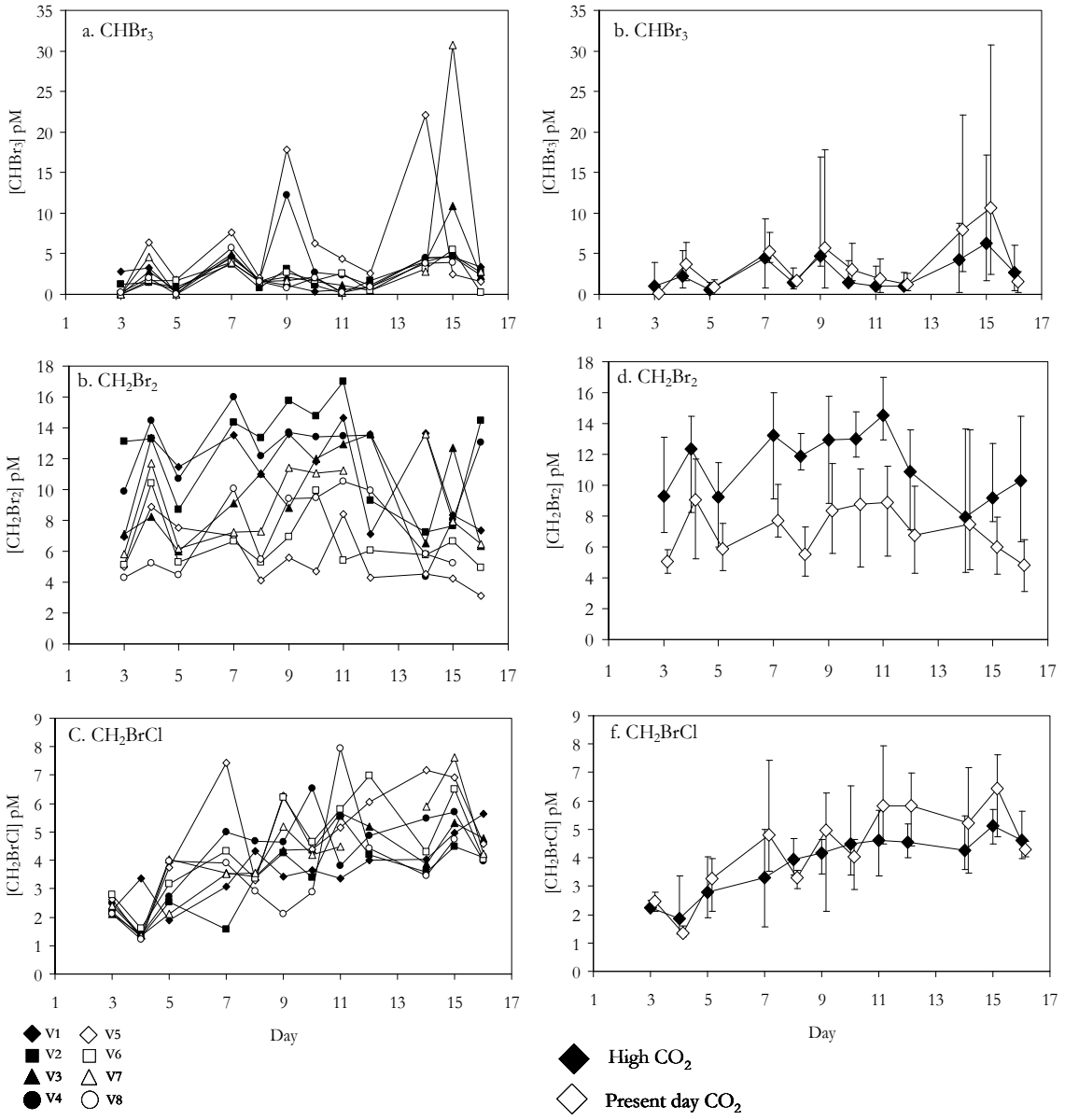

Figure 4.14. Total concentrations (a, c, e) and mean concentrations (± range) (b, d, f) of bromocarbons (pM) during Experiment 1. a. $CHBr_3$, b. Mean $CHBr_3$, c. CH_2Br_2, d. Mean CH_2Br_2, e. CH_2BrCl, f. Mean CH_2BrCl. V1 – V4 = High CO_2, V5 – V8 = Present day CO_2.

4.3.1.4.2. $CHBr_3$

Concentrations of $CHBr_3$ (Fig. 4.14 a and b) showed no clear pattern over the course of the experiment, and were characterised by a number of peaks in all (days 4, 7 and 15), or some vessels (V4 and V5 day 9, V1 day 14). V5 generally experienced higher concentrations than all other vessels, with a mean of 6.2 pM compared to 1.9 – 4.6 pM for all others. However, V7 displayed the highest single concentration on day

15 of 30.7 pM, though this was quite uncharacteristic of this vessel in terms of the experiment as a whole. In general, differences between treatments were not immediately obvious, and although a 30.8 percent decrease in mean concentrations was seen under high CO_2, this difference was not statistically significant (See Table 4.6).

The plot of mean $CHBr_3$: chlorophyll *a* (Figure 4.15a) makes the difference between treatments clearer, although the wide range of the data is also noticeable. The ratio in all vessels was relatively low until day 9, when it increased slightly, revealing the differences between treatment, with a diminished ratio under high CO_2. This 34.5 percent decrease in ratio was not found to be statistically significant (See Table 4.6). Spearman's Rank analyses showed that $CHBr_3$ was significantly correlated with C_2H_5I, CH_2BrCl, picoeukaryotes and *Synechococcus* under both treatments, and nanophytoplankton under high CO_2. Results of the analyses are shown in Table 4.7 and Appendix 17.

4.3.1.4.3. CH_2Br_2

The temporal development of CH_2Br_2 concentrations (Figure 4.14 c and d) was typified by elevated concentrations under high CO_2 for the majority of the experiment. Differences between treatments were present from the start, and were maintained in most vessels until day 12. Concentrations in all vessels showed daily variability, and the spike on day 4 was the only such event that was echoed in the majority of vessels. A peak in concentrations on this day was also observed for CH_3I, CH_2ClI and $CHBr_3$, suggesting some link between the production of these compounds.

Of the high CO_2 vessels, V3 displayed concentrations that were more comparable to those seen in the present CO_2 vessels. The mean in V3 was 9.5 pM, compared to means of >11 pM in V1, V2 and V4. V5 exhibited the lowest concentrations of CH_2Br_2, with a mean of 5.6 pM, despite this vessel having the highest mean concentration of $CHBr_3$. The concentrations in the high CO_2 vessels appeared to follow an increasing trend over days 3 – 11, after which all experienced a drop to levels more analogous to the present CO_2 treatment. The concentration recovered over the last two days in V2 and V4 whilst V1 and V3 remained at lower levels. By contrast, concentrations in the present day vessels exhibited a decreasing trend towards the end of the experiment.

The rather obvious differences in CH_2Br_2 concentrations between treatments were found to be statistically significant (Mann Whitney W = 3035, $p<0.001$), with a 36.9 percent increase in this compound under high CO_2. Normalising the data to chlorophyll *a* (Figure 4.15b) exaggerated this difference between treatments further, resulting in a significant 60.5 percent increase in mean CH_2Br_2: chlorophyll *a* under high CO_2 (T-test, T = -3.00, p = 0.003). The ratio showed the greatest difference between treatments over days 9 – 12 following the crash in chlorophyll *a*.

No significant correlations between CH_2Br_2 and any of the biological parameters were identified (See Appendix 17). However, this compound was correlated with CH_3I under both treatments and CH_2ClI under present day CO_2 (Table 4.5).

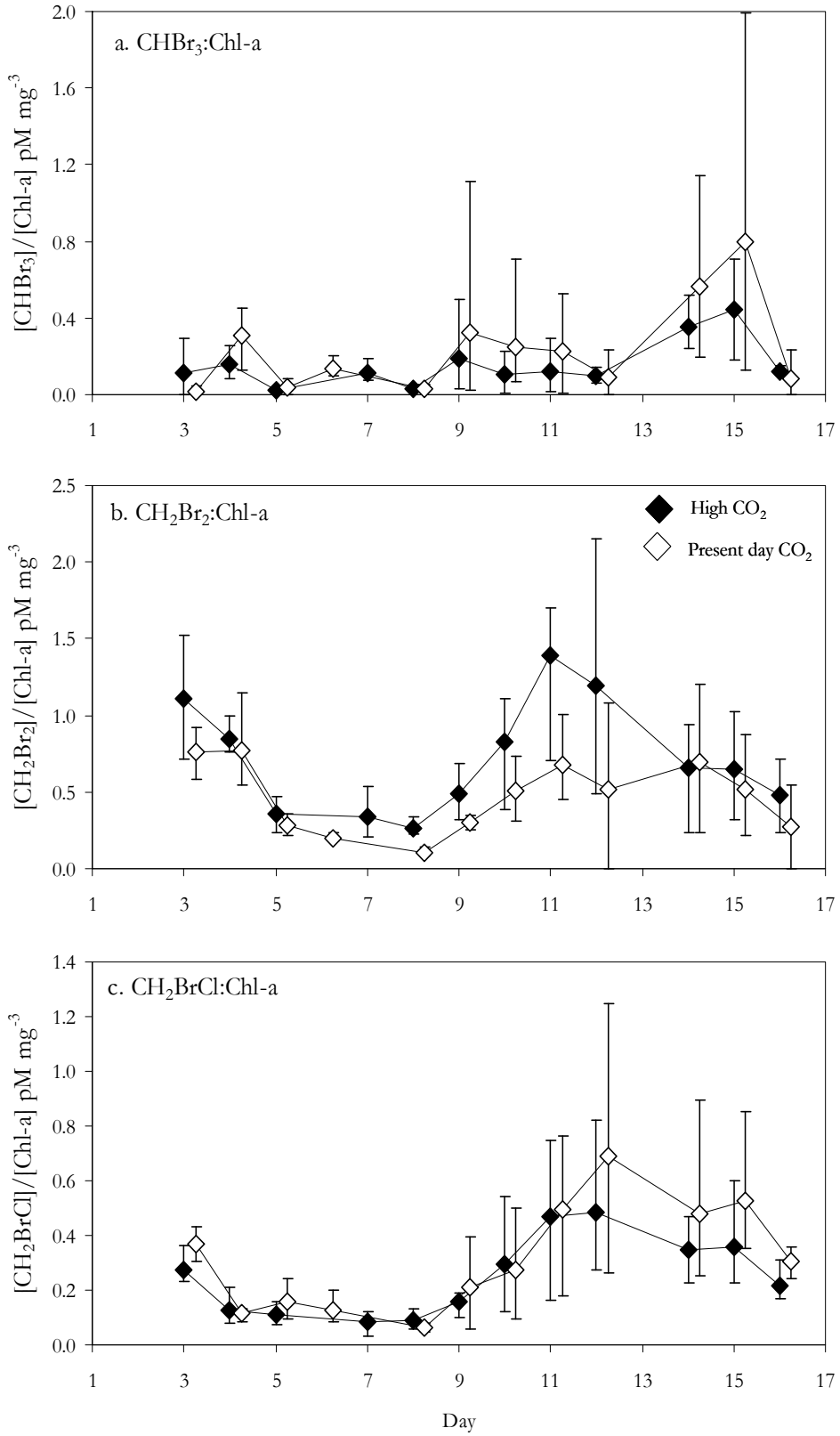

Figure 4.15. Mean ratios of bromocarbons to chlorophyll *a* during Experiment 1. a. $CHBr_3$:Chl *a*, b. CH_2Br_2:Chl *a*, c. CH_2BrCl:Chl *a* (Error bars show range).

Table 4.7. Spearman's Rank Correlation Coefficients (ρ) and associated significance level for mean bromocarbons concentrations, chlorophyll *a* and microphytoplankton community components under high CO_2 (V1, V2, V3, V4) and present-day CO_2 (V5, V6, V7, V8).

		$CHBr_3$	CH_2BrCl
CH_2Br_2	High CO_2	-0.067	
CH_2Br_2	Present CO_2	0.146	
CH_2BrCl	High CO_2	0.305	
CH_2BrCl	Present CO_2	0.362	
Chlorophyll *a*	High CO_2	0.119	-0.020
Chlorophyll *a*	Present CO_2	0.012	-0.021
Nanophytoplankton	High CO_2	0.441	0.484
Nanophytoplankton	Present CO_2	0.012	0.271
Picoeukaryotes	High CO_2	0.461	0.393
Picoeukaryotes	Present CO_2	0.442	0.101
Synechococcus	High CO_2	0.381	0.455
Synechococcus	Present CO_2	0.298	0.197

N = 48, shaded in grey = significant, critical value at 0.05 significance level = 0.286.

4.3.1.4.4. CH_2BrCl

The concentrations of CH_2BrCl showed a general increasing trend in all vessels over the course of the experiment (Fig. 4.14 e and f). Concentrations began at very similar levels on day 3 in all 8 vessels (2.1 – 2.8 pM) and differences between vessels started to become most obvious from day 5 onwards. A drop in concentrations on day 4 was observed in all but V1, an opposite trend to that seen on this day for CH_3I, CH_2ClI, $CHBr_3$ and CH_2Br_2. Similarly to CH_2Br_2, the temporal dynamics of CH_2BrCl were characterized by a large amount of daily variability, making it difficult to visually identify any differences between treatments. The present day vessels showed quite erratic concentrations, particularly V5 and V8, which displayed large peaks and troughs on days 4 and 7 in V5, and days 9 and 11 in V8. A peak in concentrations in most vessels occurred on day 15, and concentrations of the majority of the present day vessels exceeded those under high CO_2. Following this, concentrations then sharply dropped in all vessels (except V1) and ended the experiment at similar levels (4.0 –

4.8 pM), with the previously highly variable nature of concentrations seemingly ceasing.

The CH_2BrCl: chlorophyll *a* ratio (Figure 4.15c) showed little difference between treatments from days 3 – 11, subsequent to which the ratio under high CO_2 became diminished compared to the present day CO_2 treatment during the final stages of the experiment. Although some differences between treatments were apparent for concentrations of this compound (10.5 percent decrease under high CO_2) and its ratio to chlorophyll *a* (19.4 percent decrease under high CO_2), these differences were not found to be significant (Table 4.6 and Appendix 13 and 15).

CH_2BrCl showed a number of strong relationships with the iodocarbon compounds, as reflected by the Spearman's Rank analyses. It was significantly correlated with C_2H_5I, CH_2I_2 and CH_2ClI, as well as $CHBr_3$ under both treatments and 2-C_3H_7I under high CO_2 (Table 4.5 and 4.7). In addition, close associations with nanophytoplankton, picoeukaryotes and *Synechococcus* were identified under high CO_2 (See Table 4.7 and Appendix 17).

4.3.2. Experiment 2

4.3.2.1. pH and Chlorophyll *a*

The pH of the seawater in the vessels (Figure 4.16) started at about 8.0, and after 24 hours of aeration, had fallen to around 7.8 in the high CO_2 vessels, and to 7.9 in the present day vessels. Aeration was performed for longer than during Experiment 1 (4 days as opposed to 3 days) as the pH did not drop as rapidly or to as low levels. In fact the pH started going up in all vessels (except V1), suggesting growth had proceeded before the addition of nutrients. Indeed, this was supported by the chlorophyll *a* data (Figure 4.17), showing that concentrations were already relatively high before nutrients were added to the incubations on day 2. Chlorophyll *a* at this stage ranged from 6 – 21 mg m^{-3}, a clear indication of growth. After addition of nutrients on day 4, the pH continued to rise in all vessels (slightly delayed in V1) accompanied by rapidly increasing chlorophyll *a* concentrations, with some vessels showing a 2- to 3-fold increase over 2 days. V6 was the first vessel to peak in chlorophyll *a* concentrations, on day at 49 mg m^{-3}. Following this, V1, V2, V3, V4 and V7 peaked on day 6, with a maximum of 83 mg m^{-3} in V2, although V1 only attained 29 mg m^{-3}. V8 peaked a day later at 40 mg m^{-3}.

Subsequent to this sharp chlorophyll *a* peak, concentrations rapidly fell, and all but V1 were <12.2 mg m^{-3} by day 9. V1 crashed to 6 mg m^{-3} on the following day. The present day CO_2 vessels showed little further increase in chlorophyll *a*, not exceeding 5 mg m^{-3} in any of the vessels through to the end of the experiment. The high CO_2 vessels all showed some additional growth past this point, particularly V2 which re-attained and maintained concentrations of >13 mg m^{-3} until the end of the incubation period. This resulted in V2 experiencing the highest pH of 8.03 of the high CO_2 vessels for most of the experiment. The lower chlorophyll *a* concentrations seen in V1 were reflected in the lower pH levels for this vessel.

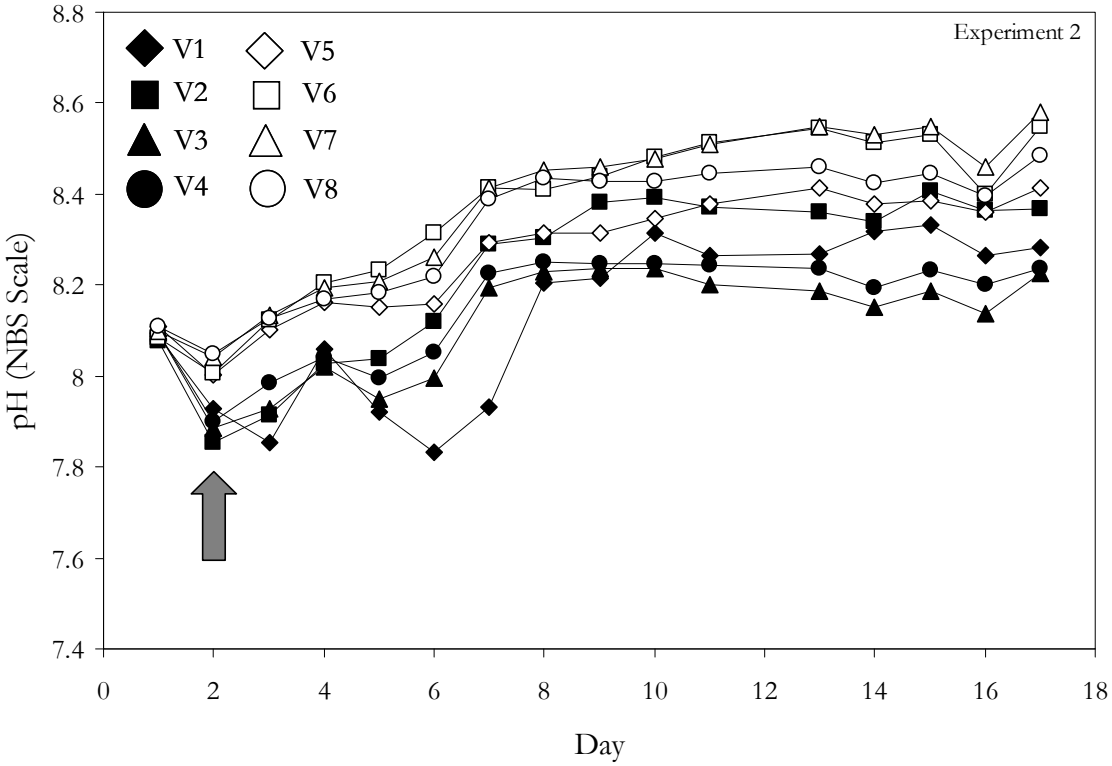

Figure 4.16. Daily pH measurements (NBS scale) made during Experiment 2. V1 – V4 = High CO_2, V5 – V8 = Present day CO_2. Arrow = nutrient addition.

The mean difference in pH between the two treatments was found to be significant (Mann Whitney, W = 3014, p<0.001, see Table 4.8 and Appendix 20). Over the course of the experiment, a 34 percent increase in mean chlorophyll *a* concentrations under high CO_2 was observed, a difference that was found to be statistically significant (Mann Whitney, W = 3095, p = 0.0178, see Table 4.8 and Appendix 20).

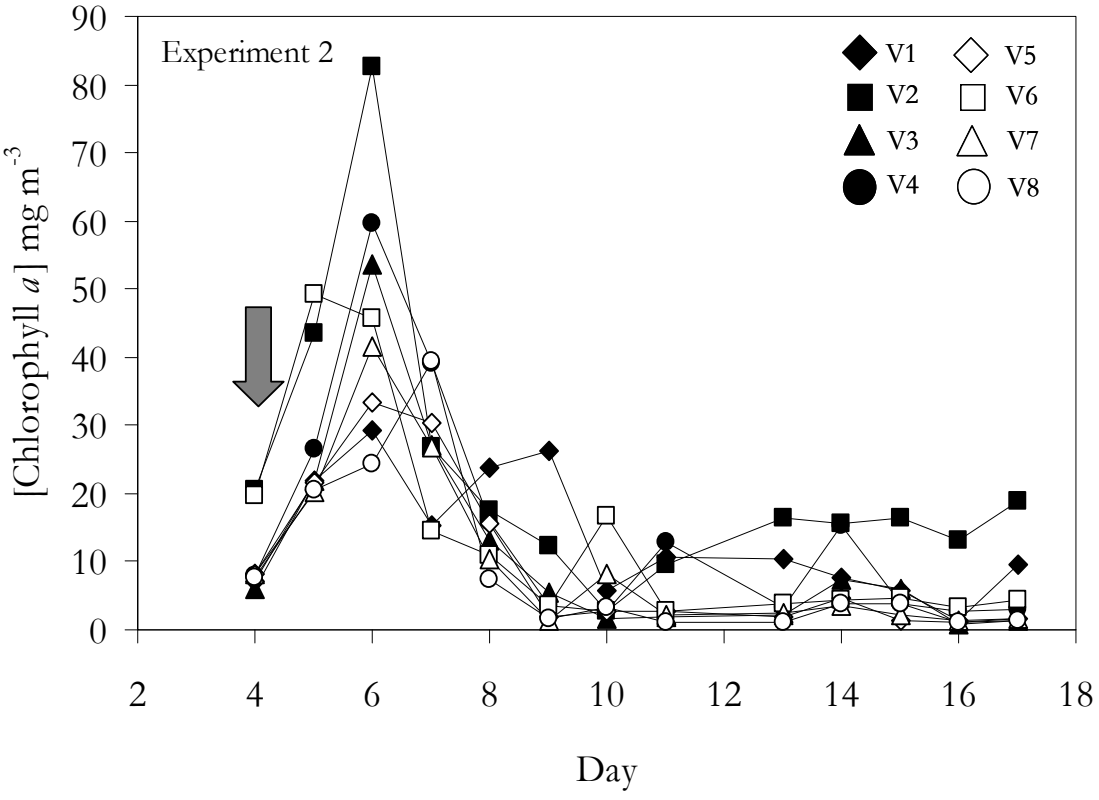

Figure 4.17. Daily chlorophyll *a* concentrations during Experiment 2. V1 – V4 = High CO_2, V5 – V8 = Present day CO_2. Arrow = nutrient addition.

4.3.2.2. The Phytoplankton community

4.3.2.2.1. Cell numbers from flow cytometry

Numbers of nanophytoplankton began relatively high in all vessels in comparison to Experiment 1, supporting the notion that growth had commenced even before addition of nutrients. As shown by Figure 4.18a, V2 and V6 were particularly high with numbers in excess of 21,000 cells ml^{-1}, whilst the remaining vessels started at around 10 – 14,000 cells ml^{-1}. By contrast numbers in Experiment 1 only exceeded 20,000 cells ml^{-1} on one day in one vessel.

Numbers increased rapidly following the addition of nutrients, particularly in V2 and V6, and the majority of vessels peaked on day 6, corresponding to the peak in chlorophyll *a* concentrations. Nanophytoplankton numbers were found to be significantly positively correlated with chlorophyll *a* concentrations (See Table 4.9).

The maximum numbers of nanophytoplankton were recorded in V6 with 45,000 cells ml^{-1} whilst V1 reached a peak of only 15,000 cells ml^{-1}. Following the sharp peak, V2 and V6 experienced a rapid crash, and numbers in the remaining vessels declined more steadily. By day 8, the majority of the vessels were seeing a decline in numbers, but in contrast, V2 and V6 rose again, reaching a secondary peak on day 11 of 18,000 and 30,000 cells ml^{-1}, respectively. Numbers in the remaining vessels stabilised over the last 7 days of the experiment, although some decrease was seen in V1 that was not echoed in the others. The data suggests that V2 and V6 were behaving quite similarly in terms of nanophytoplankton dynamics, whilst numbers in the other 6 vessels were controlled by other, distinct, processes. Overall, only a small 6.5 percent decrease in mean nanophytoplankton numbers was measured under high CO_2, a difference that was not found to be significant (T-test, T = -0.2, p = 0.841, see Table 4.8 and Appendix 20).

Synechecoccus numbers did not exceed 9000 cells ml^{-1} in any of the vessels until day 9, when growth began. This is similar to Experiment 1, where numbers remained low for the first 5 days. As shown by Figure 4.18b, the level of growth varied greatly between vessels, and in general, the high CO_2 vessels saw more growth than the present day CO_2 (Means, High CO_2 29599 cells ml^{-1}, Present CO_2 26921 cells ml^{-1}, see Table 4.8). Of the high CO_2 vessels, V2 saw the least growth, reaching a maximum of 32,000 cells ml^{-1} on day 16, whilst V4 peaked at 41,000 cells ml^{-1} on day 13. *Synechococcus* were most successful in V1 and V3, both peaking on day 15, with the peak of >200,000 cells ml^{-1} in V1 almost double that of V3. Numbers in V6 and V7 remained low throughout, not exceeding 27,000 cells ml^{-1}. In contrast, V5 and V8 showed much greater abundance of *Synechococcus,* although the peak of 84,000 cells ml^{-1} in V8 on day 15 was dwarfed by the maximum of >250,000 cells ml^{-1} in V5. All vessels saw a decline in numbers of the last day of the experiment. Despite a mean 9 percent increase in *Synechococcus* numbers under high CO_2, no significant differences between treatments were identified (Mann Whitney W = 2877, p = 0.3409, see Table 4.8 and Appendix 20 Additionally, *Synechococcus* numbers were found to possess a significant negative correlation with chlorophyll *a* concentrations (See Table 4.9).

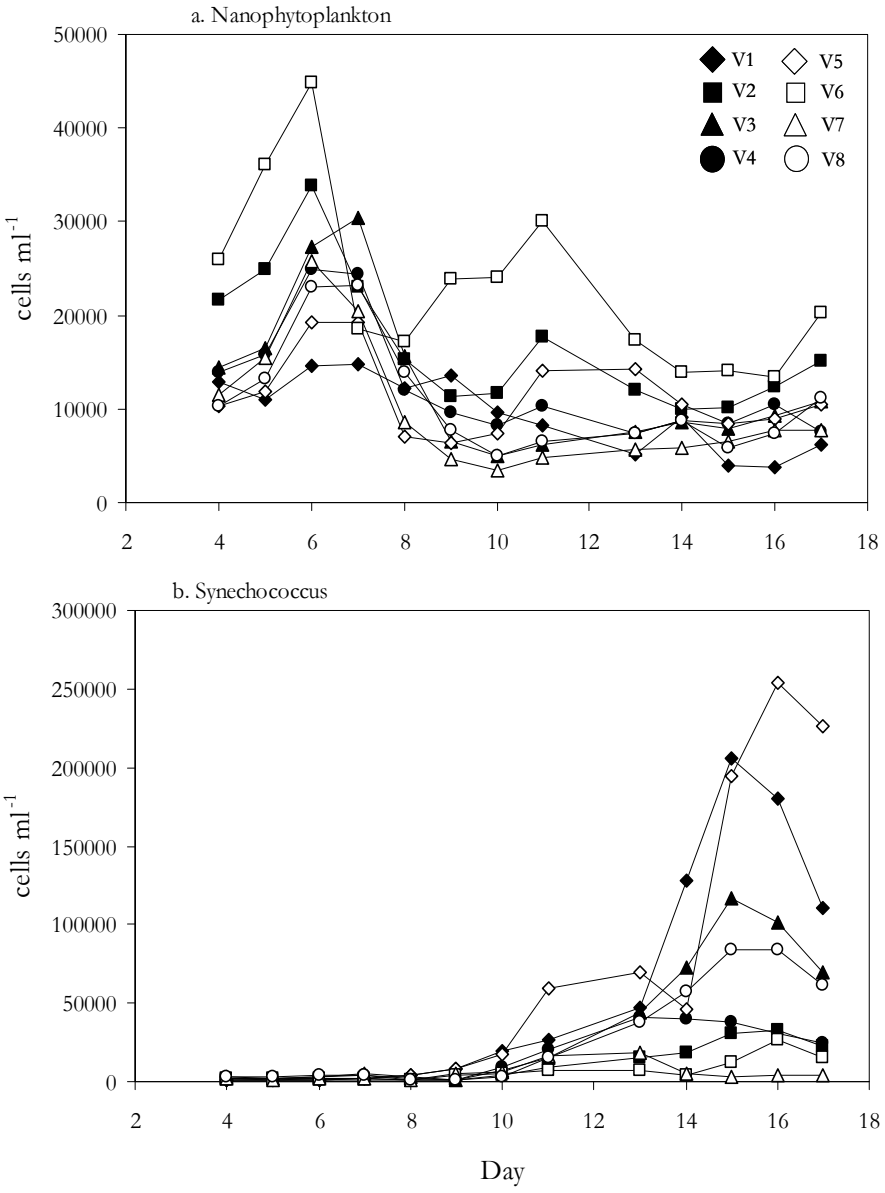

Figure 4.18. Microphytoplankton species cell counts (cell per ml) during Experiment 2. a. Nanophytoplankton, b. *Synechococcus* . V1 – V4 = High CO_2, V5 – V8 = Present day CO_2.

Table 4.8. Summary of the statistical analysis on chlorophyll *a* and microphytoplankton data.

	Mean High CO_2	Mean Present day CO_2	% change under high CO_2	Statistical test	Significant differences ($p<0.05$)
pH	8.05	8.22	N/A	Mann Whitney W = 3014, p<0.001	√
Chlorophyll *a* mg m^{-3}	15.7	10.7	+31.6%	Mann Whitney W = 3127, p = 0.0099	√
Nanophytoplankton cells ml^{-1}	12924	13828	-6.5%	T-test T = -0.20, p = 0.841	
***Synechococcus* cells ml^{-1}**	29599	26921	+9.1%	Mann Whitney W = 2877, p = 0.3409	
Diatoms µg l^{-1}	4.79	0.99	+79.3%	T-test T = -0.92, p = 0.373	
Auto. Dinoflagellates µg l^{-1}	5.34	2.86	+46.4%	T-test T = -0.44, p = 0.670	
Flagellates µg l^{-1}	40.80	48.80	-16.4%	T-test T = 0.70, p = 0.497	
Hetero. Dinoflagellates µg l^{-1}	2.21	2.56	-13.7%	T-test T = 0.52, p = 0.609	
Ciliates µg l^{-1}	3.01	2.52	+16.3%	Mann Whitney W = 71.0, p = 0.7929	
Total Biomass µg l^{-1}	56.2	57.7	-2.6%	Mann Whitney W = 62.0, p = 0.5635	

Table 4.9. Spearman's Rank Correlation Coefficients (ρ) and associated significance level for mean chlorophyll *a* and microphytoplankton community components under high CO_2 (V1, V2, V3, V4) and present-day CO_2 (V5, V6, V7, V8).

	Nanophytoplankton	Synechococcus
Chlorophyll *a* High CO_2	0.752	-0.502
Chlorophyll *a* Present CO_2	0.615	-0.694

N = 48, shaded in grey = significant, critical value at 0.05 significance level = 0.286

4.3.2.2.2. Biomass

Similarly to Experiment 1, the biomass of individual phytoplankton taxa showed a high degree of variability between both treatments and replicates of treatments (Figure 4.19 a – e). Total biomass, shown in Figure 4.19f, showed great similarity under both treatments on day 4 whilst the replication became less robust by day 17. In the same way as Experiment 1, Day 0 represents the biomass from one sample taken from the L4 sampling station, with no further processing. Between this initial sampling and day4, following 3 days of aeration in the vessels, diatom numbers fell sharply from 23 µg C l^{-1} to <1 µg C l^{-1} in all vessels (Figure 4.19 a). By day 17, the majority of vessels showed only small recovery in diatom biomass, with levels still <5 µgC l^{-1}. V1 was an exception to this, with biomass reaching 29 µg C l^{-1} on day 17. Overall, no significant differences between treatments were detected (Table 4.8). Autotrophic dinoflagellate biomass (Figure 4.19b) displayed similar temporal behaviour to the diatoms, with low numbers in all vessels on day 4, although with a slightly higher mean biomass under high CO_2 (1.5 µg C l^{-1}compared to 1.0 µg C l^{-1} under present CO_2). Most vessels showed some growth by day 17, and in general this growth was slightly greater under present CO_2. Again, the exception to this was V1, which showed much greater growth than all the other vessels, reaching 29 µg C l^{-1}. Despite this, there were no significant differences between treatments. Flagellate biomass (Figure 4.19c) showed little change between the initial sampling on day 0 and day 4. Furthermore, little difference between treatments was evident at this stage. In a trend that seems typical of these experiments, great variability between vessels of both the same and different treatments emerged by day 17 (See Table 4.10), resulting in no clear differences between treatments. The flagellate biomass exhibited a wide

range between vessels, from <16 μg l^{-1} in V1, V3 and V5, up to 160 – 180 μg l^{-1} in V2 and V6.

Table 4.10. Relative standard deviation (RSD) of phytoplankton biomass from replicate vessels.

	High CO_2 RSD	Present Day CO_2 RSD
Diatoms	206%	98%
Auto. dinoflagellates	178%	84%
Flagellates	125%	114%
Hetero. dinoflagellates	47%	63%
Ciliates	93%	74%
Total Biomass	89%	96%

The heterotrophic dinoflagellates (Figure 4.19d) did not show an overall increase in biomass between day 4 and 17 under either treatment, and only V7 showed an increase in biomass. No differences between treatments were observed. Ciliate biomass (Figure 4.19e) fell from ~16 μg C l^{-1} on day 0, to <9 μg C l^{-1} on day 4. Large variability between replicate vessels was also evident at this stage (See Table 4.10), with no obvious difference between treatments. Mean biomass fell under both treatments by day 17, from 4.2 to 1.8 μg C l^{-1} under high CO_2, and 3.5 to 1.5 μg C l^{-1} under present CO_2. Although in general the biomass was lower under present CO_2, no significant differences between treatments were revealed. In terms of total biomass (Figure 4.19f) a small decrease was observed under high CO_2 (-2.6 percent) relative to the present day vessels. Similarly to Experiment 1, any differences between treatments that may have existed were overshadowed by large variability between replicate vessels (Table 4.10). The diatoms showed the greatest variability (RSD = 205 percent under high CO_2), whilst the heterotrophic dinoflagellates showed the least (47 percent high CO_2, 63 percent present CO_2).

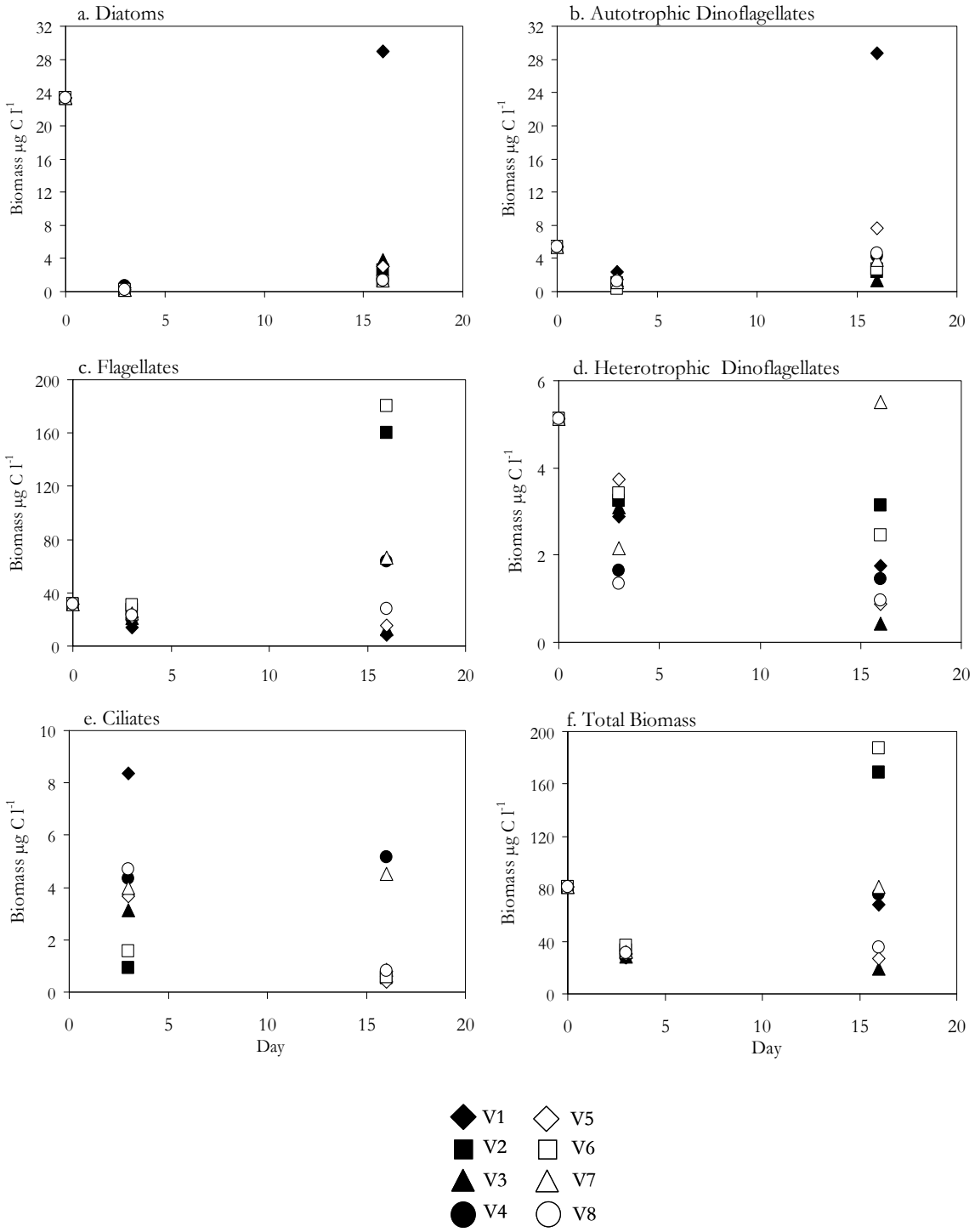

Figure 4.19. Phytoplankton carbon biomass (µg C l^{-1}) on days 0 (water collection), 4 and 17. Each point is representative of measurement from one vessel. a. Diatoms b. Autotrophic dinoflagellates, c. Flagellates, d. Heterotrophic dinoflagellates, e. Ciliates, f. Total biomass. Legend is shown in panel c.

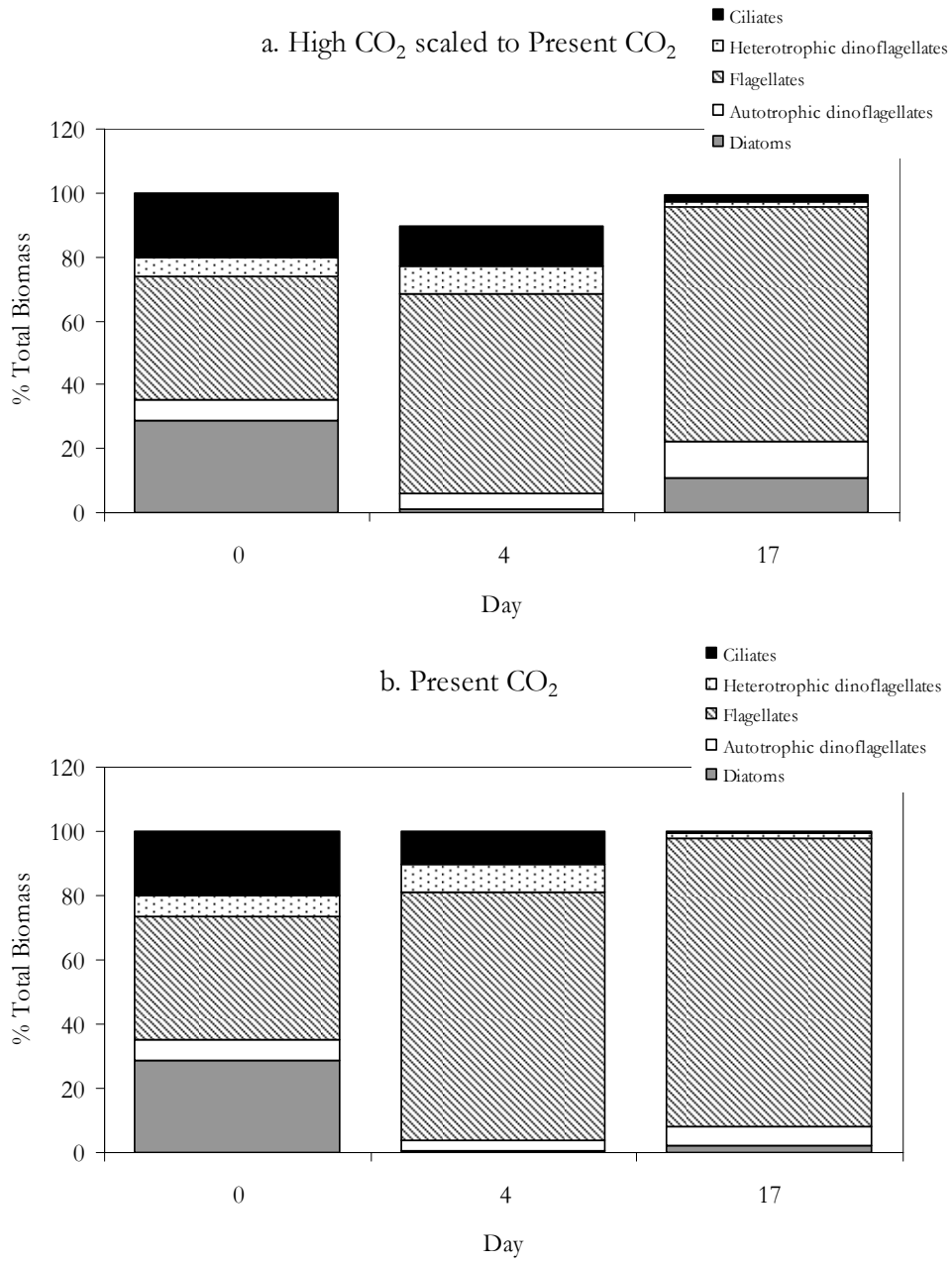

Figure 4.20. Percentage total carbon biomass contribution of diatoms, autotrophic dinoflagellates, flagellates, heterotrophic dinoflagellates and ciliates to the phytoplankton populations. a. High CO_2 vessels, scaled to the present CO_2 vessels, and b. Present day CO_2 vessels, on days 0 (water collection), 4 and 17.

Figure 4.20 shows bar charts of percentage biomass contribution of individual phytoplankton taxa under a. High CO_2 and b. Present day CO_2, with the data for high CO_2 scaled to the present, in order to show relative changes in biomass. Unlike Experiment 1, biomass did not vary that greatly between treatments, with only a 10

percent drop in biomass on day 4 under high CO_2. By day 17, although there was a <1 percent difference in biomass between treatments, the relative proportions of some taxa showed some variation. The population showed a greater contribution from autotrophic dinoflagellates, diatoms and ciliates on day 17 under high CO_2. Despite this, no significant differences in total biomass between treatments were observed (See Table 4.8 and Appendix 21).

4.3.2.3. Iodocarbons

4.3.2.3.1. Overview

The temporal dynamics of the iodocarbons were variable, as shown by Figure 4.21. Most of the compounds appeared to show some association with biological parameters. For example, CH_3I (Fig. 4.21a) displayed a period of increasing concentrations followed by a decline, perhaps echoing the growth and senescence of phytoplankton, and C_2H_5I (Fig. 4.21b) experienced a sharp peak on day 7, one day after the chlorophyll *a* maximum (see Fig. 4.17). The remaining iodocarbons (2-C_3H_7I, CH_2I_2 and CH_2ClI) showed a generally increasing trend in concentrations towards the end of the experiment, a pattern reflected in the data for *Synechococcus*, numbers of which greatly increased over the second half of the experiment (Figure 4.18). CH_2I_2 concentrations in Experiment 2 ranged from 20 – 100 pM, values that are somewhat elevated compared to both L4 seawater measurements and other oceanic measurements (Archer *et al.* 2007; Carpenter *et al.* 2007), although such concentrations have been reported previously (Klick 1992; Klick and Abrahamsson 1992; Abrahamsson *et al.* 2004b). However, it is common to encounter CH_2I_2 as the dominant species in the iodocarbon pool (Klick 1992; Abrahamsson *et al.* 2004b; Archer *et al.* 2007).

4.3.2.3.2. CH_3I

Concentrations of CH_3I, shown in Figure 4.21 a and b ranged from 3 – 35 pM and displayed some temporal variability. All vessels exhibited an increase in concentrations between days 4 and 9, with days 8 - 9 representing the peak in CH_3I concentrations. This peak occurred 2 – 3 days after the peak in chlorophyll *a* (See Figure 4.17). Vessels belonging to different treatments displayed a degree of similarity.

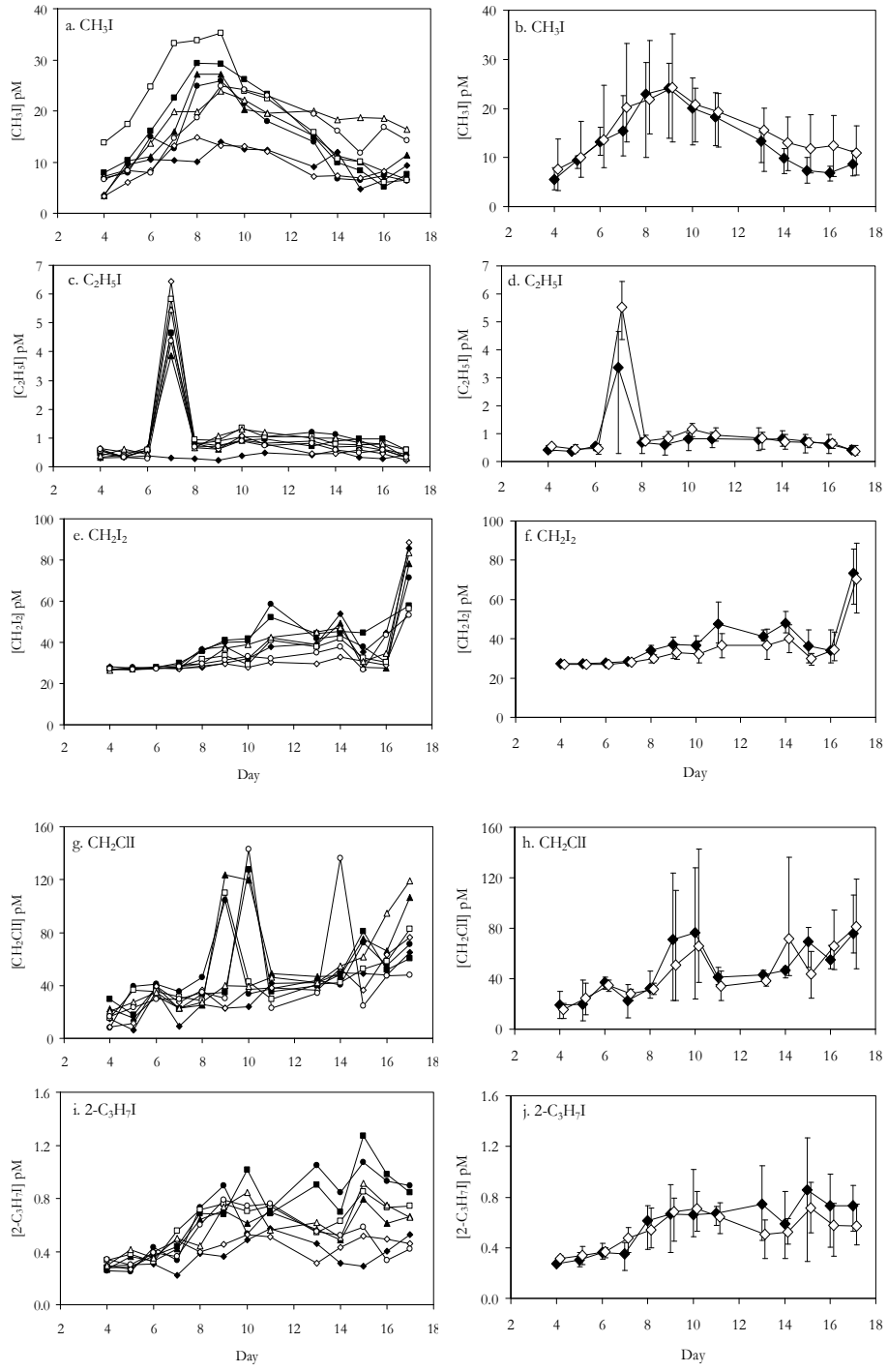

Figure 4.21. Total and mean concentrations of iodocarbons (pM) during Experiment 2. a. CH_3I, b. Mean CH_3I, c. C_2H_5I, d. Mean C_2H_5I, e. CH_2I_2, f. Mean CH_2I_2, g. CH_2ClI, h. Mean CH_2ClI, i. 2-C_3H_7I, j. Mean 2-C_3H_7I. V1 – V4 = High CO_2, V5 – V8 = Present day CO_2. Error bars indicate maximum and minimum values from replicate vessels.

For example, V1 and V5 followed a very similar pattern of concentrations, with concentrations that were somewhat lower than the other vessels from day 4 to 14. V2 and V6 also behaved in a comparable manner, with a steep rise in concentrations over the first four days, followed by a rapid fall towards the end of the experiment. The present CO_2 V7 and V8 showed similar temporal dynamics, and ended the experiment with the highest CH_3I concentrations of all vessels. Overall, mean concentrations of CH_3I (Fig. 4.21 b) were 13 percent lower under high CO_2, a result that was consistent with Experiment 1, where a fall of 13 percent was also recorded. However unlike Experiment 1, due to the variability between vessels of the same treatment, this difference was not found to be statistically significant (See Table 4.11 and Appendix 20). Figure 4.22 a shows plots of the mean ratio of CH_3I to chlorophyll *a* (± max. and min. values) over the course of the experiment, and when the data is normalised in this way, differences between treatments become more apparent. Initially there was little difference in the ratio between treatments (days 4 – 8), but subsequent to this, the ratio was diminished under high CO_2, revealing much lower production of CH_3I per mg of chlorophyll *a*. This difference, which amounted to a 51 percent decrease under high CO_2, was found to be statistically significant (Mann Whitney W = 2332, p = 0.0090, see Table 4.11 and Appendix 20). Spearman's Rank analyses revealed that CH_3I was not closely correlated with many of the other measured parameters. Significant correlations were identified with C_2H_5I under both treatments, 2-C_3H_7I under present CO_2, and it exhibited a significant negative correlation with *Synechococcus* numbers under high CO_2 (see Table 4.12).

4.3.2.3.3. C_2H_5I

The temporal development of C_2H_5I concentrations (Figure 4.21 c and d) was dominated by a very large, anomalous peak in seven of the vessels on day 7. For the majority of the experiment, concentrations did not exceed 1.4 pM in any vessel, but day 7 saw concentrations in all (but V1) exceed 3.8 pM, with a maximum of 6.4 pM in the high CO_2 V5. This event occurred a day after the peak in chlorophyll *a*. Concentrations in V1 were generally lower than the other vessel. Mean concentrations were 21 percent lower under high CO_2, although this difference was not found to be statistically significant (See Table 4.11). Similarly to CH_3I, greater differences between treatments were revealed when the data was normalised to chlorophyll *a* (Figure 4.22b). The ratio was similar under both treatments for the first three days, but after this differences became apparent, with a tendency for lower

ratios under high CO_2. Interestingly, the temporal development of C_2H_5I: chlorophyll *a* was similar to that of CH_3I: chlorophyll *a*. In addition, the 46 percent reduction in C_2H_5I: chlorophyll *a* under high CO_2 was found to be statistically significant (Mann Whitney W = 2263, p = 0.0024, see Table 4.11). Also in common with CH_3I, this compound did not display many correlations with other parameters. In fact it was only found to be significantly correlated with CH_3I and 2-C_3H_7I (See Table 4.12).

Table 4.11. Summary of the statistical analysis performed on iodocarbon concentrations and iodocarbon : chlorophyll *a* ratios.

pM	Mean High CO_2	Mean Present day CO_2	% change under high CO_2	Statistical test	Significant differences (p<0.05)
CH_3I	13.46	15.53	-13.3%	Mann Whitney W = 2518, p = 0.1619	
C_2H_5I	0.85	1.07	-20.5%	Mann Whitney W = 2542, p = 0.2229	
CH_2I_2	39.41	35.96	+8.8%	Mann Whitney W = 2378, p = 0.1337	
CH_2ClI	46.77	44.98	+3.8%	T-test T = 0.16, p = 0.876	
2-C_3H_7I	0.58	0.54	+7.8%	T-test T = 0.39, p = 0.696	
CH_3I: Chl *a*	2.48	5.01	-50.5%	Mann Whitney W = 2332, p = 0.0090	√
C_2H_5I: Chl *a*	0.13	0.24	-45.8%	Mann Whitney W = 2263, p = 0.0024	√
CH_2I_2: Chl *a*	8.29	13.53	-38.7%	T-test T = 2.21, p = 0.030	√
CH_2ClI: Chl *a*	12.03	16.00	-24.8%	Mann Whitney W = 2486, p = 0.1134	
2-C_3H_7I: Chl *a*	0.12	0.18	-33.3%	Mann Whitney W = 2473, p = 0.0941	

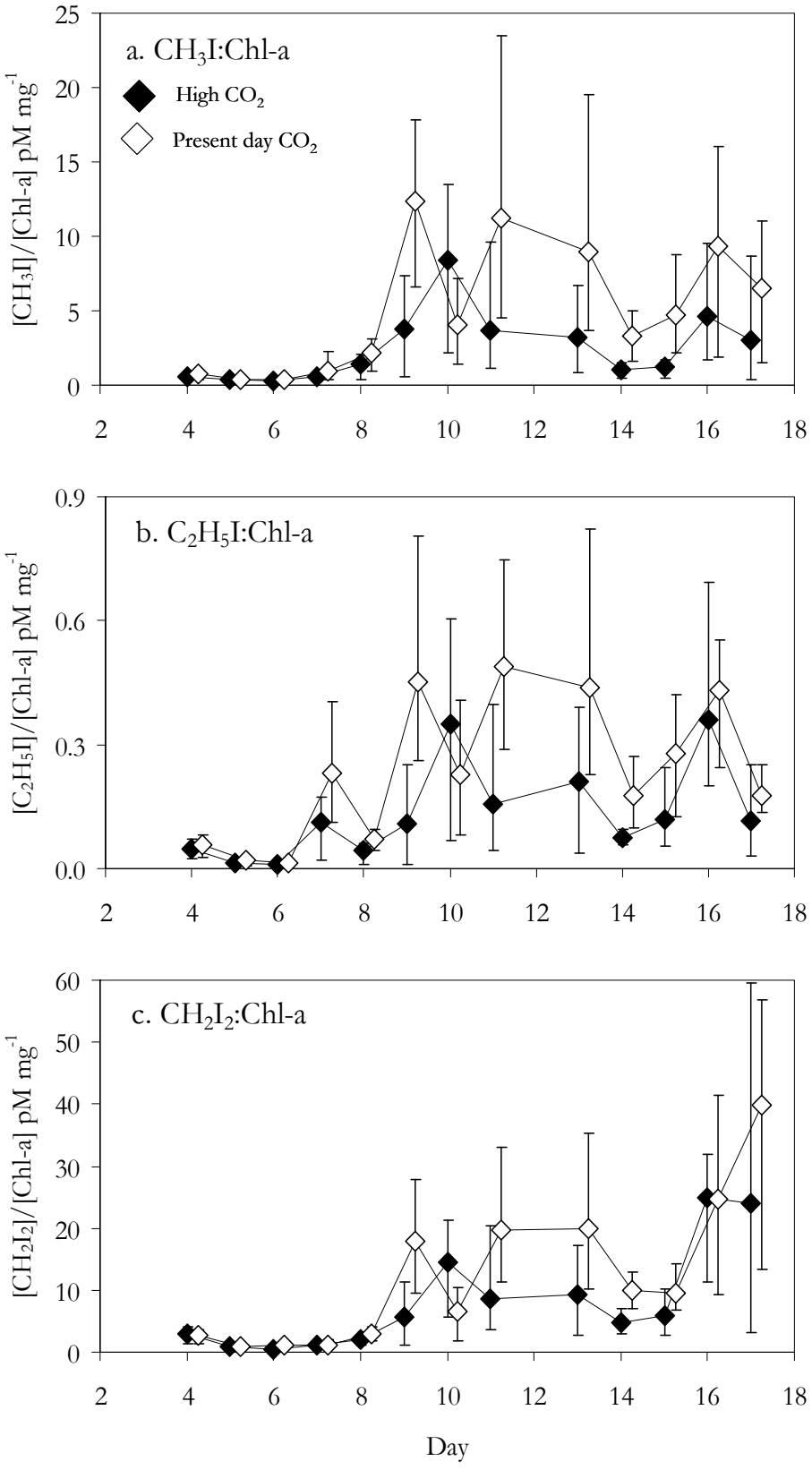

Figure 4.22. Continued on next page.

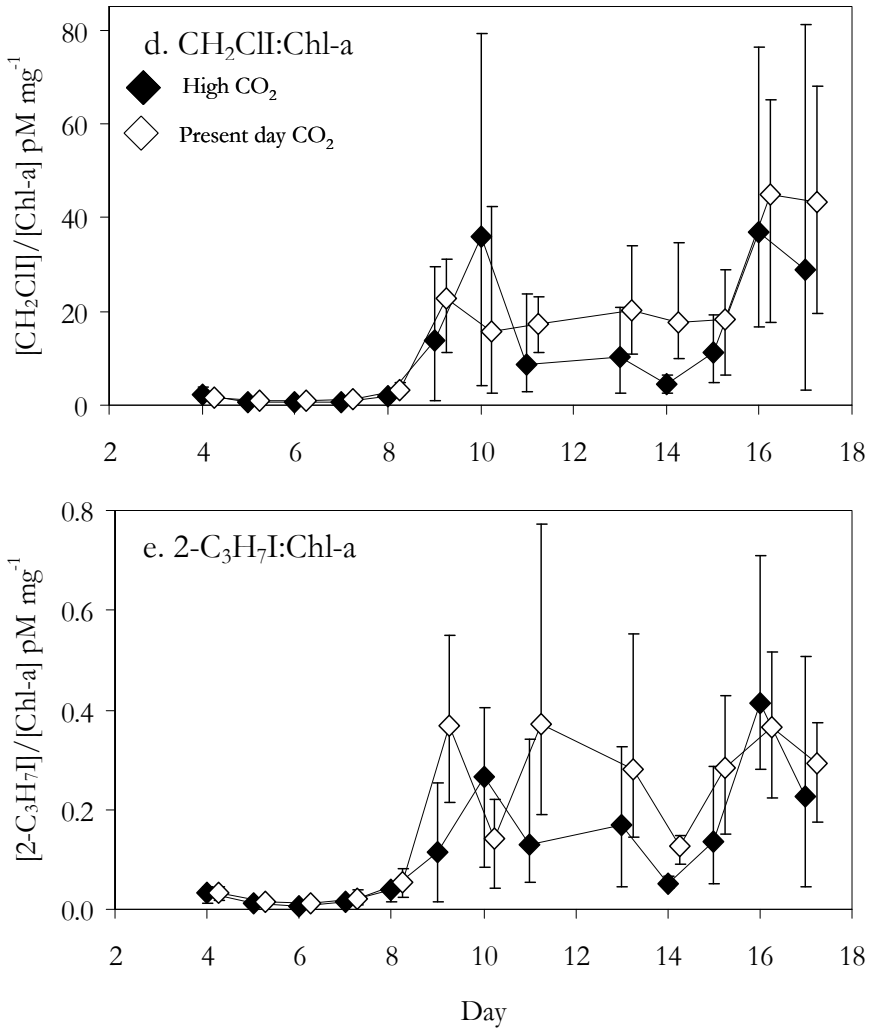

Figure 4.22. Mean ratios of iodocarbons to chlorophyll *a* during Experiment 2. a. CH_3I: Chl *a*, b. C_2H_5I: Chl *a*, c. CH_2I_2/2-IP(D): Chl *a*, d. CH_2ClI: Chl *a*, e. 2-C_3H_7I: Chl *a*. (error bars show range).

4.3.2.3.4. CH_2I_2 and CH_2ClI

Concentrations of CH_2I_2 and CH_2ClI (Figure 4.21 e, f, g and h) displayed a similar range of means (See Table 4.11) and both experiencing gradually increasing concentrations over the course of the experiment. CH_2I_2 concentrations were very similar in all vessels until day 8, when differences between treatments merged. Day 8 and 9 saw higher concentrations under high CO_2 in V2, V3 and V4, whilst concentrations in V1 were more comparable to those in the present day vessels. V3 dropped to such levels on day 10. In addition, V2 and V4 peaked on day 11, whilst V1 and V3 peaked three days later. By contrast, the present day vessels did not exhibit such clear peaks in concentration. The final day of the experiment saw maximum

concentrations in almost all vessels, reaching 70 – 90 pM in V1, V3, V4, V5 and V7, and 53 – 58 pM in the remaining vessels. Concentrations of CH_2ClI followed a similar temporal trend, although the dynamics of this compound were characterised by random, sharp peaks in concentration in some vessels. V8 exhibited two such peaks on days 10 and 14, increasing from <40 pM to >135 pM, and back down again, over the course of three days. Other vessels to experience such peaks included V4 and V6 on day 9, V3 on days 9 – 10, and V2 on day 10. In common with CH_2I_2, concentrations in the majority of vessels showed some increase on the final day of the experiment, although this feature was not as prominent as for CH_2ClI. Overall, mean concentrations of both compounds exhibited a small increase under high CO_2, of 9 percent for CH_2I_2 and 4 percent for CH_2ClI, but these differences were not significant (See Table 4.11).

The plots of the ratios of CH_2I_2: and CH_2ClI: chlorophyll *a*, shown in Figure 4.22 c and d, reveal more interesting information about the data. Both compounds showed very similar temporal development to the ratios for CH_3I and C_2H_5I, again with little difference between treatments until day 9, from when the ratio under high CO_2 lessened relative to the present CO_2. For CH_2I_2: chlorophyll *a*, a significant 39 percent decrease was observed (T-test, T = 2.21, p = 0.030), but the 25 percent decrease for CH_2ClI was not found to be significant (See Table 4.11). Spearman's Rank analyses revealed that CH_2I_2 and CH_2ClI were significantly correlated with almost all other measured parameters, including each other, the bromocarbons, chlorophyll *a*, and numbers of nanophytoplankton and *Synechococcus*. The strongest correlations were with both $CHBr_3$ and CH_2Br_2, and the relationships with chlorophyll *a* and nanophytoplankton were negative in nature. CH_2I_2 and CH_2ClI were not significantly correlated with either CH_3I or C_2H_5I (Table 4.12).

4.3.2.3.5. 2-C_3H_7I

Concentrations of 2-C_3H_7I (Figure 4.21 i and j) were low (<1.4 pM) and variable with time. In general, there was an increasing trend in concentrations, with all vessels starting similarly at <0.4 pM, and finishing within a range of 0.4 – 0.9 pM on day 17. V2 achieved maximum concentrations on day 10 (1.0 pM) and day 15 (1.3 pM), whilst V1 generally experienced the lowest concentrations (<0.6 pM for the whole experiment). The mean concentrations of 0.58 pM and 0.54 pM under high and present CO_2, respectively, represented a small 8 percent increase under high CO_2

conditions, which was not found to be significant (See Table 4.11). The ratio of 2-C_3H_7I: chlorophyll *a* (Figure 4.22e) was again comparable to the other iodocarbons, particularly CH_3I and C_2H_5I, to which the temporal trends were very similar. However, the decrease in ratio of 33 percent was not found to be significant (Table 4.11). As in the case of CH_2I_2 and CH_2ClI, 2-C_3H_7I was found to be significantly correlated with a wide range of measurements, including CH_2I_2, CH_2ClI, C_2H_5I, chlorophyll *a*, nanophytoplankton and *Synechococcus*, and was most strongly correlated with the bromocarbons.

Table 4.12. Spearman's Rank Correlation Coefficients (ρ) and associated significance level for mean iodocarbons concentrations, with chlorophyll *a*, bromocarbon concentrations and microphytoplankton community components under high CO_2 (V1, V2, V3, V4) and present-day CO_2 (V5, V6, V7, V8).

		CH_3I	**C_2H_5I**	**CH_2I_2**	**CH_2ClI**	**2-C_3H_7I**
C_2H_5I	High CO_2	0.435	-	-	-	-
C_2H_5I	Present CO_2	0.561	-	-	-	-
CH_2I_2	High CO_2	0.084	0.213	-	-	-
CH_2I_2	Present CO_2	0.227	0.084	-	-	-
CH_2ClI	High CO_2	-0.014	0.243	0.518	-	-
CH_2ClI	Present CO_2	0.134	0.034	0.662	-	-
2-C_3H_7I	High CO_2	0.222	0.609	0.575	0.665	-
2-C_3H_7I	Present CO_2	0.512	0.521	0.462	0.489	-
$CHBr_3$	High CO_2	-0.192	0.176	0.645	0.576	0.478
$CHBr_3$	Present CO_2	0.041	0.098	0.702	0.747	0.444
CH_2Br_2	High CO_2	-0.212	0.063	0.661	0.604	0.514
CH_2Br_2	Present CO_2	-0.035	0.022	0.692	0.728	0.509
CH_2BrCl	High CO_2	-0.199	0.266	0.573	0.654	0.604
CH_2BrCl	Present CO_2	0.166	0.214	0.597	0.668	0.529
Chlorophyll *a*	High CO_2	0.099	-0.084	-0.402	-0.567	-0.418
Chlorophyll *a*	Present CO_2	-0.089	-0.006	-0.582	-0.417	-0.439
Nanophytoplankton	High CO_2	0.132	-0.005	-0.474	-0.600	-0.384
Nanophytoplankton	PresentCO_2	-0.095	-0.101	-0.311	-0.206	-0.293
Synechococcus	High CO_2	-0.356	0.066	0.500	0.531	0.334
Synechococcus	Present CO_2	-0.250	-0.093	0.436	0.482	0.212

N = 48, shaded in grey = significant, critical value at 0.05 significance level = 0.286.

4.3.2.4. Bromocarbons

4.3.2.4.1. Overview

The concentrations of the bromocarbons (Figure 4.23) exhibited similar temporal dynamics, with a trend of increasing concentrations as the experiment progressed. As such, the concentrations appeared to show some association with biological activity, increasing in response to decreasing chlorophyll *a* and nanophytoplankton numbers, and increasing with increased growth of *Synechococcus* (See Table 4.13). Mean concentrations of $CHBr_3$ and CH_2Br_2 were slightly elevated under high CO_2, whereas CH_2BrCl showed a mean decrease in concentrations in the perturbed vessels (Table 4.14). In comparison to Experiment 1, despite lower maximum concentrations, mean concentrations of $CHBr_3$ were higher (7.2 pM compared to 3.1 pM) and less erratic in behaviour. In contrast, CH_2Br_2 and CH_2BrCl experienced lower concentrations during Experiment 2 (CH_2Br_2 6.4 pM compared to 9.2 pM, CH_2BrCl 0.7 pM compared to 4.1 pM). Overall, the temporal progression of the bromocarbons was more consistent than in Experiment 1, with the compounds sharing a number of similarities. Again, the concentrations of $CHBr_3$ and CH_2Br_2 were similar to those measured previously in L4 seawater (Archer *et al.* 2007) as well as in other open ocean waters (Abrahamsson *et al.* 2004a; Quack *et al.* 2004; Chuck *et al.* 2005), whilst concentrations of CH_2BrCl were far lower than other previously reported measurements from the Southern Ocean (Abrahamsson *et al.* 2004a; Abrahamsson *et al.* 2004b).

4.3.2.4.2. $CHBr_3$

$CHBr_3$, shown in Figure 4.23 a and b, exhibited generally increasing concentrations over the course of the experiment, and maximum concentrations were attained on day 16 in most vessels, although V1 and V5 peaked two days earlier. No clear differences between treatments were evident, with only a small 0.8 percent increase in concentrations under high CO_2 (See Table 4.14).

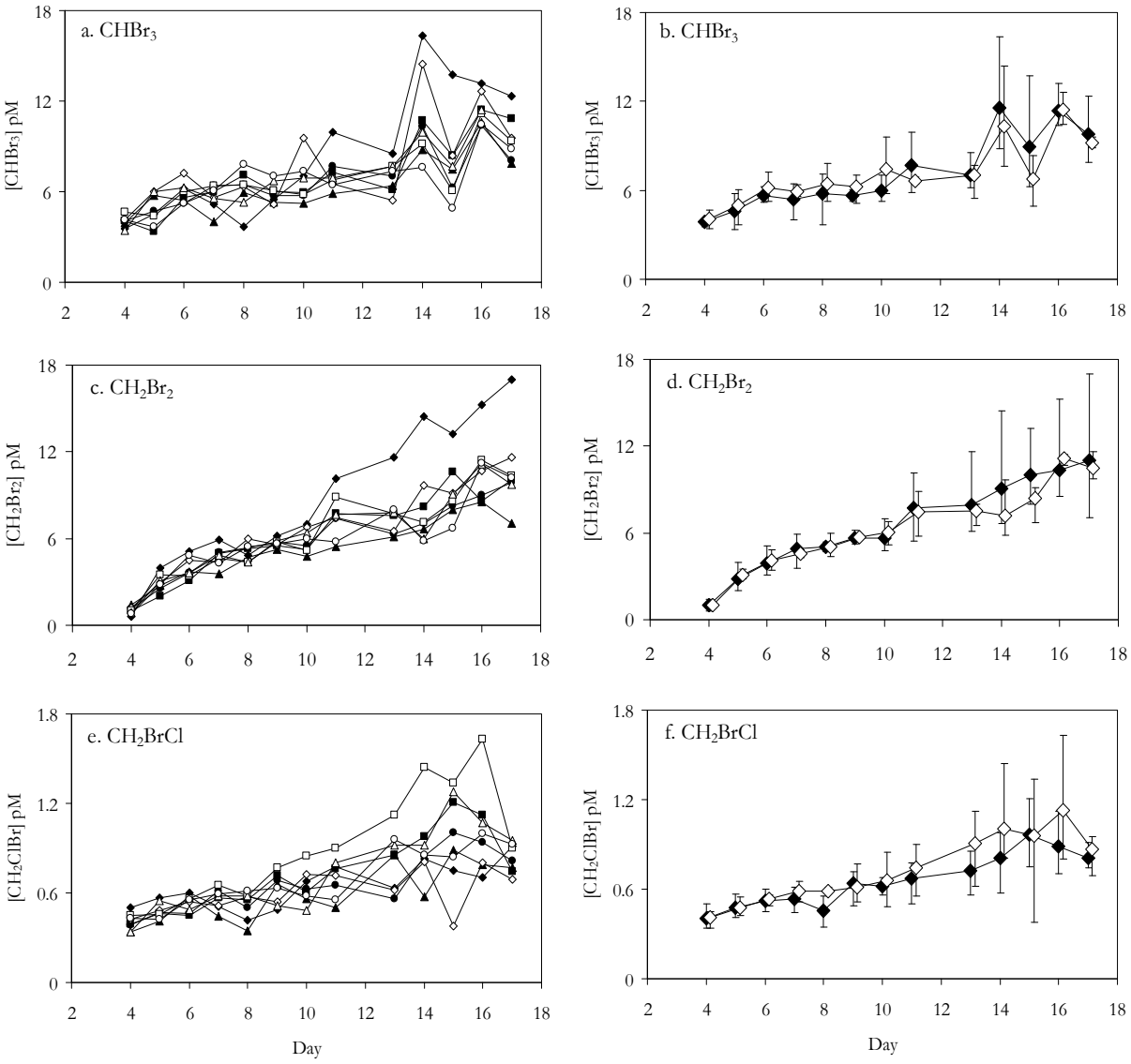

Figure 4.23. Concentrations of bromocarbons (pM) during Experiment 2. a.$CHBr_3$, b. CH_2Br_2, c. CH_2BrCl. V1 – V4 = High CO_2, V5 – V8 = Present day CO_2. Error bars indicate maximum and minimum values from replicate vessels.

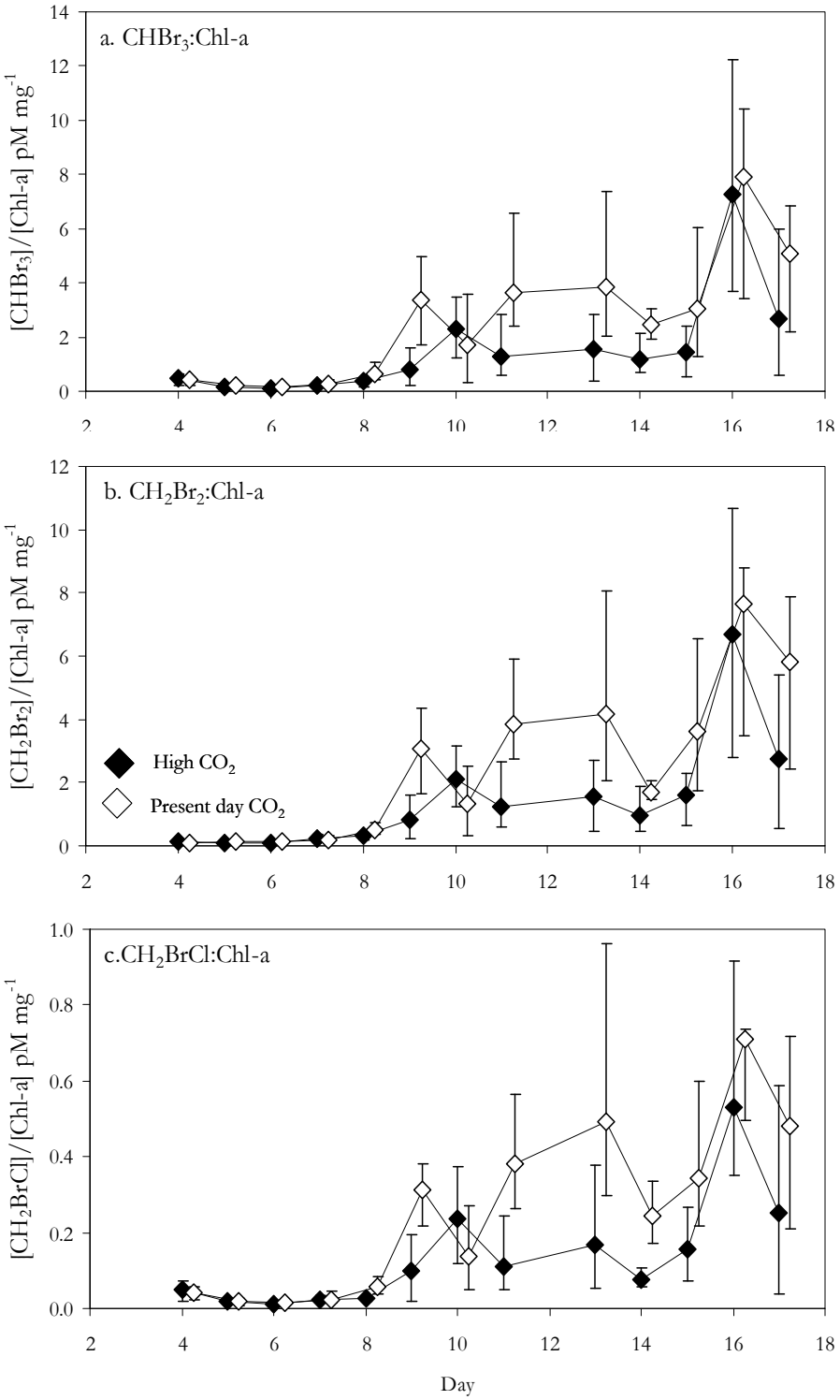

Figure 4.24. Mean ratios of bromocarbons to chlorophyll *a* over the course of Experiment 2. a. $CHBr_3$: Chl *a*, b. CH_2Br_2:Chl *a*, c. CH_2BrCl:Chl *a*. (Error bars show range).

When the data was normalised to chlorophyll *a* (Figure 4.24 a), differences in between mean ratios become apparent, revealing a pattern very similar in nature to that for the iodocarbon: chlorophyll *a* ratios (See Figure 4.22). There was little

difference in ratio from day 4 to 8, after which differences became apparent with generally lower ratios under high CO_2. This difference, amounting to a 40 percent decrease in mean ratio under high CO_2, was found to be statistically significant (Mann Whitney W = 2409, p = 0.0372). Following Spearman's Rank analyses, $CHBr_3$ was found to be significantly correlated with CH_2I_2, CH_2ClI, 2-C_3H_7I, all the bromocarbons, chlorophyll *a*, nanophytoplankton and *Synecheococcus* (Table 4.13). Correlations with chlorophyll *a* and nanophytoplankton were negative in nature, and $CHBr_3$ was most strongly correlated with CH_2Br_2 suggesting closely related production.

4.3.2.4.3. CH_2Br_2

Similarly to $CHBr_3$, concentrations of CH_2Br_2 gradually increased over the course of the experiment (Figure 4.23 c and d). However, the rate of increase for this compound was greater, with concentrations climbing from <1.2 pm to 7 – 17 pM by day 17. A 4 percent increase in CH_2Br_2 was observed under high CO_2, but no significant differences between treatments were detected (See Table 4.14). V1 experienced the highest and most rapidly increasing concentrations, whilst its high CO_2 replicate V3 produced the lowest concentrations.

The ratio of CH_2Br_2: chlorophyll *a* produced a plot very similar to that for the iodocarbons and $CHBr_3$, with reduced ratios under high CO_2 for days 9 – 17 (Figure 4.24 b). However, the difference for this compound was not found to be significant (See Table 4.14). As for $CHBr_3$, CH_2Br_2 was correlated with a wide range of other measured parameters, again with significant negative correlations with chlorophyll *a* and nanophytoplankton, and particularly strong positive correlations with the other bromocarbons, and also with *Synechococcus* (See Table 4.13).

Table 4.13. Spearman's Rank Correlation Coefficients (ρ) and associated significance level for mean bromocarbons concentrations, chlorophyll *a* and microphytoplankton community components under high CO_2 (V1, V2, V3, V4) and present-day CO_2 (V5, V6, V7, V8).

		$CHBr_3$	CH_2Br_2	CH_2BrCl
CH_2Br_2	High CO_2	0.896	-	-
CH_2Br_2	Present CO_2	0.809	-	-
CH_2BrCl	High CO_2	0.767	0.833	-
CH_2BrCl	Present CO_2	0.659	0.759	-
Chlorophyll *a*	High CO_2	-0.374	-0.441	-0.432
Chlorophyll *a*	Present CO_2	-0.565	-0.737	-0.477
Nanophytoplankton	High CO_2	-0.507	-0.636	-0.536
Nanophytoplankton	Present CO_2	-0.326	-0.372	-0.136
Synechococcus	High CO_2	0.760	0.795	0.628
Synechococcus	Present CO_2	0.509	0.781	0.490

N = 48, shaded in grey = significant, critical value at 0.05 significance level = 0.286

4.3.2.4.4. CH_2BrCl

The concentrations of CH_2BrCl showed similar trends to the other bromocarbons, with an increasing trend in concentrations as the experiment progressed (Figure 4.23 e and f). However, in contrast to $CHBr_3$ and CH_2Br_2, mean concentrations were lower under high CO_2, with a mean 10 percent decrease. Following statistical analysis, this difference was not found to be significant (See Table 4.14). Also unlike to the other bromocarbons, maximum concentrations of CH_2BrCl of 1.6 pM were encountered in the present day V6, as opposed to the high CO_2 V1.

The ratio of CH_2BrCl: chlorophyll *a* over time (Figure 4.24 c) was again very similar to the iodocarbons and the other bromocarbons, with a great reduction in the ratio after day 9 under high CO_2, amounting to a mean 44 percent decrease which was found to be significant (Mann Whitney W = 2377, p = 0.0219, see Table 4.14 and Appendix 22). Spearman's Rank analyses revealed that CH_2BrCl was significantly correlated with CH_2I_2, CH_2ClI, 2-C_3H_7I, the other bromocarbons, and *Synechococcus*,

and displayed significant negative correlations with chlorophyll *a* under both treatments, and with nanophytoplankton under high CO_2.

Table 4.14. Summary of the statistical analysis performed on bromocarbons concentrations and bromocarbon : chlorophyll *a* ratios.

pM	Mean High CO_2	Mean Present day CO_2	% change under high CO_2	Statistical test	Significant differences ($p<0.05$)
$CHBr_3$	7.18	7.12	+0.8%	T-test T = -0.23, p = 0.822	
CH_2Br_2	6.54	6.28	+4.0%	Mann Whitney W = 2731, p = 0.9974	
CH_2BrCl	0.66	0.73	-10.1%	Mann Whitney W = 2565, p = 0.2849	
$CHBr_3$: Chl *a*	1.52	2.53	-39.9%	Mann Whitney W = 2409, p = 0.0372	√
CH_2Br_2: Chl *a*	1.43	2.84	-49.7%	Mann Whitney W = 2451, p = 0.072	
CH_2BrCl: Chl *a*	0.13	0.23	-43.5%	Mann Whitney W = 2377, p = 0.0219	√

4.4. Discussion and conclusions

4.4.1. Experiment 1

4.4.1.1. Biological parameters

Chlorophyll *a* concentrations and total biomass showed small increases under high CO_2 during Experiment 1. During the early stages of experiment, there is evidence that the CO_2 addition relieved carbon limitation and resulted in an increase in biomass: on day 3 biomass in the high CO_2 vessels was almost double that in the present day vessels. However, by day 16 the biomass had crashed to levels far below

the present day treatment, suggesting that the level of biomass achieved in the first half of the experiment was not sustainable. An enhancement of phytoplankton growth under elevated CO_2 concentrations is a widely reported phenomenon (Hein and Sand-Jensen 1997; Wolf-Gladrow *et al.* 1999; Riebesell 2004; Schippers *et al.* 2004; Leonardos and Geider 2005; Fei-Xue Fu *et al.* 2007). However, the effect is only expected to occur in phytoplankton species that lack carbon concentrating mechanisms (CCMs), so that the communities of the future high-CO_2 oceans will shift in favour of these organisms, as well as those with a high overall C demand, and/or low surface area to volume ratio (Wolf-Gladrow *et al.* 1999). In the high CO_2 vessels, numbers of picoeukaryotes showed a significant increase, and there was 46 percent higher diatom biomass after 3 days of incubation, as well as higher heterotrophic dinoflagellate biomass, although not significantly so. In addition, *Synechococcus* numbers were 19 percent lower under high CO_2. These differences in communities between treatments suggest that some shift may have occurred in response to the altered conditions. Diatoms are known to operate CCMs, which provide them with equilibrium CO_2 concentrations around RUBISCO (See Chapter 1, Section 1.6.2.2), higher than that in the surrounding medium (Roberts *et al.* 2007). There is also evidence that diatoms can switch to an alternative CO_2 storage pathway, enabling efficient uptake of CO_2 when CCMs cannot operate effectively (Reinfelder *et al.* 2000; Riebesell 2000). In addition, two species of diatom (*Thalassiosira weissflogii* and *Phaeodactylum tricornutum*) have been shown to energetically favour the uptake of CO_2 over HCO_3^- if it is present at high enough concentrations, with CO_2 acting as an important substrate for photosynthesis (Burkhardt *et al.* 2001). Thus diatoms are capable of coping with environmental variability, when other organisms may be disadvantaged (Riebesell 2000). As a result, they may experience some enhancement of photosynthetic CO_2 fixation or growth when the seawater CO_2 concentrations increase. The large increase in diatom biomass seen in the high CO_2 vessels after the first three days of the experiment may be a result of CO_2 enrichment. A previous study found that diatoms were the only taxa to increase in abundance after 24 hours of incubation (at ambient temperature and CO_2) (Venrick *et al.* 1977), suggesting this group may also be less susceptible to the negative effects of filtration and containment.

The response of *Synechococcus* is in agreement with a number of other studies into the effects of high CO_2 on phytoplankton communities (Rochelle-Newall *et al.*

2004; Paulino *et al.* 2008). In this study and others (Rochelle-Newall *et al.* 2004; Paulino *et al.* 2008), *Synechococcus* was the only population that displayed higher biomass under the lower CO_2 treatment, a difference that was more visible towards the end of the experiment when nutrients would have been depleted and production dependent on re-mineralized nutrients. *Synechococcus*, and cyanobacteria in general, are known to operate effective CCMs (Hassidim *et al.* 1997; Badger and Price 2003; Fei-Xue Fu *et al.* 2007), and have not demonstrated greatly enhanced growth under high CO_2 regimes during laboratory culture experiments (Fei-Xue Fu *et al.* 2007). Consequently, competition, and the resulting relative abundances of *Synechococcus* and picoeukaryotes may be a result of their differing requirements for dissolved inorganic carbon. If picoeukaryotes growth is DIC limited, and *Synechococcus* growth not, this would increase the success of picoeukaryotes under high CO_2 at the expense of *Synechococcus,* as was the case during this study.

4.4.1.2. Trace gases

Experiment 1 saw modest decreases in all mean trace gas concentrations (except CH_2Br_2) under high CO_2, suggesting some negative impact on the net production of these compounds. Interestingly, all measured biological parameters, except *Synechococcus*, showed an increase under high CO_2, suggesting that although growth was perhaps more favourable, the production of halocarbons was somewhat suppressed. It is possible that some of the decrease in *Synechococcus* numbers (-19 percent) may be responsible for the reduction in halocarbon concentrations. However, in terms of the iodocarbons, there is little evidence for this as *Synechococcus* showed few significant correlations with these compounds (Table 4.5).

4.4.1.2.1. Iodocarbons

Concentrations of CH_3I and C_2H_5I were of a similar order to those measured during the mesocosm experiment (Chapter 3) and also fall within the range of open ocean and coastal seawater measurements (Abrahamsson *et al.* 2004a; Chuck *et al.* 2005; Archer *et al.* 2007). An overview of seawater production processes for CH_3I is given in Chapter 3, Section 3.4.2.2. Similarly to the mesocosm experiment, the communities of the incubations were highly productive, with chlorophyll *a* concentrations of up to 60 mg m^{-3}, well above open ocean, and even most coastal measurements. Therefore it is likely that some of the production of CH_3I may be derived directly from one or several biological sources. These may include direct

production by phytoplankton (Archer *et al.* 2007) and/or bacteria (Amachi *et al.* 2001), 2001), or indirect production through photochemical reactions between organic matter and iodide ions (Moore and Zafiriou 1994; Laturnus 1995). Less is known about the production of C_2H_5I, although strong correlations with CH_3I in a number of studies (Makela *et al.* 2002; Richter and Wallace 2004; Archer *et al.* 2007), and during the mesocosm study (Chapter 3) point to a common source of these compounds. However, CH_3I and C_2H_5I were not significantly correlated during this experiment. The dynamics of C_2H_5I suggest this compound may be closely related to biological activity, with a period of increasing concentrations, followed by a peak and decline. Although not correlated with chlorophyll *a*, it was significantly correlated with picoeukaryotes and *Synechococcus* under both treatments, placing these organisms as a potential source. Picoeukaryotes increased by 33 percent under high CO_2, but this does not help explain the reduction in C_2H_5I if these organisms were directly producing this compound. The observed 19 percent decrease in *Synechococcus* may explain some of the reduction on C_2H_5I concentrations. However, there is no current available information on whether it does produce this compound, although there is currently no evidence that *Synechococcus* produce CH_3I (Manley and Cuesta 1997).

A further source of mono-halogenated iodocarbons has recently been described. Degradation products of intense phytoplankton growth, such as aggregates and mucilage have been identified as potential strong sources of CH_3I, C_2H_5I and 2-C_3H_7I (Hughes *et al.* 2008). If growth was favoured under high CO_2, resulting in a healthier, more sustained population, there may have been less rapid senescence and degradation compared to the present day treatment. This would lead to a weaker source of iodocarbons from these degradation products, accounting for the lowered concentrations under high CO_2 relative to the present day treatment. In support of this, the decrease in CH_3I concentrations under high CO_2 became most apparent over the last 8 days of the experiment, during the period of nutrient depletion and the breakdown of the bloom.

CH_2I_2 and 2-C_3H_7I showed only small decreases under high CO_2, suggesting their production was not greatly affected by the high CO_2 conditions. CH_2ClI, however, decreased by 15 percent under high CO_2, although this decrease was not found to be significant. This compound is generally considered to be produced indirectly in seawater, through the photolysis of biogenically-produced CH_2I_2 (Jones and Carpenter 2005; Martino *et al.* 2005). A lack of significant positive correlations

between this compound and any of the biological parameters provides support for this. However, CH_2ClI was significantly negatively correlated with nanophytoplankton and picoeukaryotes under high CO_2, suggesting that this compounds is associated with the degradation of the bloom, a process that may have been stronger under the perturbed CO_2 conditions. During the mesocosm experiment (Chapter 3) CH_2I_2 was found to be correlated with phaeopigments, and thus likely to be associated with the bloom degradation. Therefore if CH_2I_2 production increased during the senescent phase of the bloom, the photolytic production of CH_2ClI would also increase during this period. The data for CH_2I_2 for this experiment is unquantified as the GC-MS was experiencing contamination of this compound, making calibration difficult. Therefore there is only limited data in support of this production mechanism for CH_2ClI.

4.4.1.2.2. Bromocarbons

Concentrations of the bromocarbons fell within the range of previous seawater measurements, although were more comparable to open ocean measurements than highly elevated concentrations found in the vicinity of macroalgal beds (Ekdahl *et al.* 1998; Quack and Wallace 2004; Chuck *et al.* 2005; Quack *et al.* 2007b). Concentrations of $CHBr_3$ and CH_2BrCl were reduced under high CO_2, with reductions of 31 percent and 11 percent, respectively. By contrast, CH_2Br_2 showed a large and significant 37 percent increase under high CO_2.

$CHBr_3$ displayed strong correlations with *Synechococcus* and picoeukaryotes under both treatments and with nanophytoplankton under high CO_2, suggesting a direct biological source for this compound. $CHBr_2Cl$ was correlated with these groups of phytoplankton only under the high CO_2 treatment, perhaps reflecting community shifts under the high CO_2 treatment. These compounds were strongly correlated with each other under both treatments, implying a common source, and both showed a decrease under high CO_2. Therefore some of the decrease in concentrations of these compounds under high CO_2 may have been caused by the decrease in numbers of *Synechococcus*. Furthermore, $CHBr_3$ production has previously been attributed to the presence of *Synechococcus* (Quack *et al.* 2007b). Unfortunately, the sources of CH_2BrCl are less well documented, but are thought to include biological sources such as rhodophytes (Kladi *et al.* 2004), and chemical sources including from the photolysis of CH_2BrI (Jones and Carpenter 2005) and halogen exchange of CH_2I_2 or CH_2Br_2 (Ballschmiter 2003). Direct production by phytoplankton has not been previously

reported, although the results of this study provide some evidence that these organisms may be a source of CH_2BrCl.

CH_2Br_2 was the exception to all other halocarbons in Experiment 1, experiencing a 37 percent increase in concentrations under high CO_2. However, as shown by Figure 4.14, the levels of CH_2Br_2 were consistently higher under high CO_2 from the start to the end of the experiment. Although it is possible that the communities of V1 – V4 had higher net production of this compound, it is also very feasible that this result is caused by contamination of the high CO_2 vessels. The most likely source of this contamination is from the CO_2/air mixture that was used to aerate the incubations and adjust the pH. Further evidence for a non-biological source comes from a lack of significant correlations with any of the measured biological parameters, whereas both $CHBr_3$ and CH_2BrCl displayed a number of such relationships (See Table 4.7).

Whilst it is acknowledged that the net concentrations of trace gases in seawater are dictated by a fine balance between production and consumption processes, there is currently no available information on the biological uptake of the halocarbons compounds reported here. A number of studies have assessed the bacterial consumption of $CHBr_3$ using both stable- ($^{13}CHBr_3$) and radio-isotope ($^{14}CHBr_3$) techniques (Goodwin *et al.* 1997a; King and Saltzman 1997; Goodwin *et al.* 1998). This suggests that bacteria are very likely to play an important, but currently unquantified, role in the fate of iodocarbons.

4.4.2. Experiment 2

4.4.2.1. Biological parameters

During Experiment 2, all vessels experienced a rapid increase in chlorophyll *a* concentrations over the first three days of the experiment. There is evidence that this growth began even before nutrients were added to the incubations. The satellite-derived surface chlorophyll *a* images (Figure 4.3A) show that concentrations were low at L4 when the water was collected (~0.4 mg m^{-3}), but on the day the nutrients were added to the vessels, they already between 6 and 21 mg m^{-3}. It was observed that when the samples were collected for the experiment, there was a high density of copepods present. By removing these large grazers from the seawater before entering

the incubation vessels, it may have allowed this rapid growth of phytoplankton to commence.

The phytoplankton communities of the high CO_2 vessels generally experienced an enhancement of growth. Chlorophyll *a* showed a significant 32 percent increase under high CO_2, accompanied by 9 percent increase in *Synechococcus*, 16 percent increase in ciliates, 46 percent increase in autotrophic dinoflagellates and a large 79 percent increase in diatom biomass. Although the remaining measured biological parameters decreased, the large observed increases do suggest that the communities of the incubations may have been C-limited, and as a result, benefited from the CO_2 enrichment. The potential enrichment effect of CO_2 on diatoms was discussed above in the context of Experiment 1, and is also relevant to the discussion here. However, although diatom biomass greatly increased under high CO_2, the diversity of the diatom community greatly diminished, as shown by Figure 4.25 below. On day 4, the diatom community was not dominated by one particular species, and there were no clear differences between treatments. By day 17, a large number of diatoms had disappeared from the communities of most vessels, and two taxa dominated most vessels (*Thalassiosira* 10µm, *Pseudo-nitzschia delicatissima*). In contrast to all other vessels, V5 was almost entirely dominated by *Thalassionema nitzschioides*. There also appeared to be some distinction in diatom community composition between treatments, with *Thalassiosira* making up between 59 and 99 percent of the total diatom biomass under high CO_2, compared to between 19 and 68 percent under present day CO_2, whilst *P. delicatissima* contributed between 20 to 79 percent. Two possible conclusions can be drawn from this information: 1. The diatom species that dominated at the end of the experiment were more robust and able to thrive in the artificial incubation environment, or 2. The diatom species that dominated at the end of the experiment were less susceptible to changes in pCO_2 and pH, or benefited from enhanced CO_2 through stimulation of photosynthesis.

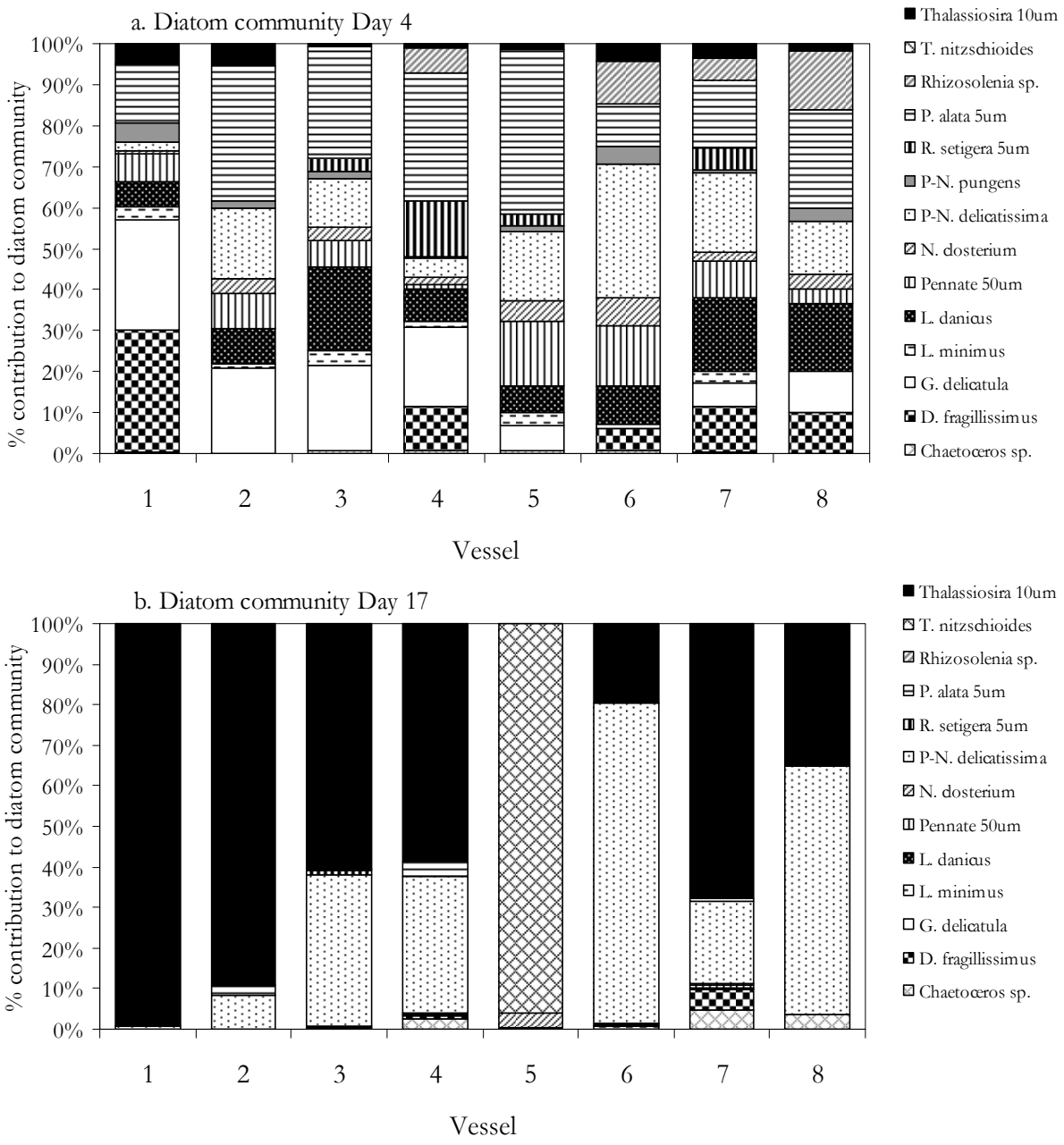

Figure 4.25. Percentage contribution of components of the diatom community to total diatom biomass on a. Day 4 and b. Day 17 of Experiment 2. Data courtesy of Claire Widdicombe, PML. Diatom species: *Chaetoceros* sp., *Dactyliosolen fragillissimus*, *Guinardia delicatula*, *Leptocylindrus minimus*, *Leptocylindrus danicus*, Pennate 50µm, *Nitzschia closterium*, *Pseudo-nitzschia delicatissima*, *Pseudo-nitzschia pungens*, *Proboscia alata* 5µm, *Rhizosolenia setigera* 5µm, *Rhizosolenia* sp 5µm, *Thalassionema nitzschioides*, *Thalassiosira* 10µm.

Diatoms have previously been shown to be better able to cope with incubation experiments than other species of phytoplankton (Venrick *et al.* 1977) and this may partly explain why they appeared to thrive during this experiment. The ability of diatoms to operate both CO_2 and HCO_3^- uptake and storage systems may cause an enhancement of photosynthesis and growth at elevated CO_2 (Reinfelder *et al.* 2000;

Riebesell 2000; Burkhardt *et al.* 2001), as seen during these experiments. Despite the large change in diatom biomass, the total biomass showed little difference between treatments, and in fact, a small decrease in biomass was seen under high CO_2 after the first 4 days of the experiment. This suggests there was not an overall beneficial effect of high CO_2 on the community.

4.4.2.2. Trace gases

4.4.2.2.1. Iodocarbons

Mean concentrations of CH_3I and C_2H_5I were somewhat higher than those measured during Experiment 1 (CH_3I 73 percent, and C_2H_5I 37 – 44 percent). However, these values are of the order that has previously been measured at the L4 sampling station at the time of year the samples for this experiment were taken (Archer*, et al.*, 2007). In common with the mesocosm experiment (Chapter 3) and L4 Experiment 1, concentrations of both of these compounds were lower under high CO_2, although for this experiment the differences were not statistically significant. In contrast, the remaining iodocarbons (CH_2I_2, CH_2ClI, 2-C_3H_7I) showed small mean increases in the high CO_2 vessels.

Spearman's Rank correlations revealed that CH_3I and C_2H_5I were significantly correlated with each other, suggesting these compounds originate from a common production mechanism. Furthermore, neither was correlated with any of the measured biological parameters. This lack of association with biological processes could allude to a indirect photochemical production pathway for CH_3I (and C_2H_5I) during this experiment (Moore and Zafiriou 1994; Richter and Wallace 2004). If this was the case, it suggests that this process is in some way sensitive to changes in pH/pCO_2. Chlorophyll *a* concentrations were significantly higher under high CO_2, suggesting that the communities under these perturbed conditions were more productive. High productivity might be expected to lead to higher DOM, thus providing more ingredients for the photochemical formation of iodocarbons (Moore and Zafiriou 1994). If this were the case, concentrations of CH_3I and C_2H_5I might have been expected to be higher under high CO_2. However, as in Experiment 1, the production of these compounds through degradation processes (Hughes *et al.* 2008) may be of more importance. If the populations of the high CO_2 vessels were healthier and more productive, there may have been less degradation and thus a lower rate of production of the precursors necessary for iodocarbon formation.

Mean concentrations of the remaining iodocarbons (CH_2I_2, CH_2ClI, 2-C_3H_7I) all showed some increase under high CO_2, a finding that contradicts most of the data for these compounds from the mesocosm experiment (Chapter 3) and L4 Experiment 1. In addition, they were not correlated with CH_3I and C_2H_5I, but were correlated with all biological parameters, suggesting that they were produced via biogenic-processes distinct from those leading to the net production of CH_3I and C_2H_5I. Furthermore, the correlations with chlorophyll *a* and nanophytoplankton were negative in nature, implying that these compounds are associated with the decline of the bloom. However, the degradation products of intense phytoplankton activity are thought to only include mono-halogenated iodocarbons (Hughes *et al.* 2008), so this production pathway does not necessarily explain the formation of CH_2I_2 and CH_2ClI. However, a significant link between CH_2I_2 and phaeopigments during the mesocosm experiment (Chapter 3) implied an associated between this compound and grazing/degradation processes. Although it is difficult to explain the exact origin of these compounds, it does appear that they are produced from a biogenic source. As biomass (as chlorophyll *a*) was so elevated under high CO_2, the increase in concentrations of biogenically-produced CH_2I_2, CH_2ClI and 2-C_3H_7I may be a result of this.

4.4.2.2.2. Bromocarbons

Mean concentrations of $CHBr_3$ and CH_2Br_2 showed very small, insignificant increases under high CO_2. In contrast CH_2BrCl decreased by 10 percent, a result very similar to Experiment 1. The bromocarbons displayed many significant correlations: 1. with each other, pointing to a common source, 2. with CH_2I_2, CH_2ClI, 2-C_3H_7I, and 3. with all measured biological parameters. These relationships suggest that the production of these compounds is from a biological source, and one that may be common to the above mentioned iodocarbons. Similarly to CH_2I_2 and CH_2ClI, correlations with chlorophyll *a* and nanophytoplankton were negative, as concentrations of these compounds generally increased during degradation phase of the bloom. Again, as there was an overall increase in productivity (as chlorophyll *a*) under high CO_2, this may have resulted in the increase in net production of $CHBr_3$ and CH_2Br_2. The observed decrease in CH_2BrCl is difficult to explain in terms of the available biological data for the incubations. The concentrations of this compound were very low throughout the experiment (Mean High CO_2 0.66 pM, Mean Present CO_2 0.73 pM) and at such low concentrations the margin of error becomes greater. For this compound using this method of analysis the analytical error has been calculated

at 7 percent (See Chapter 2, Table 2.3). Therefore some of the error inherent to the method may account for this seemingly large difference between treatments.

4.4.2.2.3. Trace gas: chlorophyll *a* ratios

As explained above, the differences in trace gas concentrations between treatments were not found to be statistically significant, suggesting a degree of resilience of the community to the high CO_2 conditions in terms of trace gas production. However, the various components of the phytoplankton community showed a range of responses. There was a significant decrease in numbers of nanophytoplankton. By contrast, chlorophyll *a* concentrations showed a significant increase under high CO_2, accompanied by a significant increase in diatom biomass and an increase in *Synechococcus* numbers. The large increase in chlorophyll *a*, along with only modest changes in trace gas concentrations, resulted in dramatic, and in the majority of cases, significant decreases in the halocarbon: chlorophyll *a* ratio. Furthermore, the ratios all showed very similar temporal dynamics. As chlorophyll *a* was constant, these similarities were driven by the relationship between the trace gases, which may further support a common source or route of production. Most interesting are the differences in halocarbon: chlorophyll *a* ratios between treatments. The decrease in ratio under high CO_2 ranged from 24 – 52 percent, with the decreases for CH_3I, C_2H_5I, CH_2I_2, $CHBr_3$ and CH_2BrCl found to be statistically significant. This suggests that the communities' ability to produce trace gases was affected by the high CO_2 treatment, despite a significant 32 percent increase in chlorophyll *a*. The differences are most clear during the degradation phase of the bloom - in fact for most of the halocarbons, little differences in ratio between treatments were visible until day 9, three days after the peak in chlorophyll *a*. This further supports the notion that the strength of halocarbon production increases during the latter stages of a phytoplankton bloom, when there is an increase in grazing and degradation processes. Overall, trace gas production by the community was less favourable under high CO_2 and lowered seawater pH conditions.

4.4.3. Inter-vessel variability

Four replicate vessels were used for each treatment during the L4 incubation experiments, and for each experiment, it is clear that for some parameters at least one of the replicates behaved differently to the others. Poor replication between incubation vessels has been reported previously, and as in this study, the variability

in taxonomic composition in terms of abundance and biomass increased over the course of the incubations (Venrick *et al.* 1977). The relative standard deviations in terms of the replicates for the biomass data has been discussed earlier (Table 4.3 and 4.10), and were shown to display a large range.

Table 4.15. Significantly different relationships between vessels of the same treatment. Where one vessel is significantly different to all others of same treatment, highlighted in grey. See Appendix 27 and 28 for full details of statistical analyses.

Parameter		Experiment 1	Experiment 2
pH	High CO_2	V1 vs. V2, V3, V4	V2 vs. V1, V3
pH	Present day CO_2	V5 vs. V7, V8	V5 vs. V7
Chlorophyll *a*	High CO_2	-	V2 vs. V3
Chlorophyll *a*	Present day CO_2	-	-
Nanophytoplankton	High CO_2	-	V1 vs. V3
Nanophytoplankton	Present day CO_2	V8 vs, V6, V7	V6 vs. V5, V6, V7
Picoeukaryotes	High CO_2	V3 vs. V1, V2	-
Picoeukaryotes	Present day CO_2	V5 vs. V6, V7, V8	-
Synechococcus	High CO_2	V1 vs. V2, V3, V4	-
Synechococcus	Present day CO_2	V5 vs. V7, V8, V6 vs. V7	V5 vs, V6, V7

Table 4.15 shows a summary of the results of statistical analyses on other biological measurements from both Experiment 1 and 2. Where significant differences between vessels of the same treatment were found, this is reported in the table. Those boxes highlighted in grey indicate that one vessel was different from the remaining three replicate vessels of that treatment. V1 from Experiment 1 stood out from the other high CO_2 vessels, with significantly lower pH, and *Synechococcus* numbers. For the present day CO_2 treatment, V5 behaved differently to the rest, with significantly different picoeukaryote numbers. During Experiment 2, there was less variability between vessels of the same treatment, although numbers of nanophytoplankton in V6 were significantly different from the other replicates. It is possible that slight differences in starting conditions between vessels can magnify up to large differences between vessels later on (Venrick *et al.* 1977). This could potentially mean that CO_2 is not the only factor that is different between treatments. Additionally, if one vessel behaves very differently from others, this may affect statistical analyses. Where differences between treatments may exist, this effect is masked by within-treatment variability.

The causes of within-treatment variability can come from a number of sources. As stated above, small differences in starting conditions can reduce the similarity of replicates (Passow and Riebesell 2005). The starting community may unintentionally vary between vessels. For example, copepod eggs are small enough to fit through the 50μm mesh net that was used to screen the seawater before incubation, so although the intention was to remove all large grazers, some may have been introduced into some of the vessels. This can cause great variability between vessels in terms of the phytoplankton community (Venrick *et al.* 1977). "Bottle effects" are a well reported potential source of bias during laboratory incubation experiments (Venrick *et al.* 1977; Ferguson *et al.* 1984; Fogg and Calvario-Martinez 1989; Hughes *et al.* 2008). Such effects are caused by the unnatural side-effects of containment of seawater samples, and include large differences in mixing and sedimentation to the natural setting, artificial loss of nutrients to the container walls which can strongly affect the community dynamics, and the damaging effects of the solid walls to fragile plankton species (Venrick *et al.* 1977; Ferguson *et al.* 1984; Fogg and Calvario-Martinez 1989). Impacts such as these can alter the balance of the phytoplankton communities contained within, and lead to large differences between vessels which started with seemingly identical conditions.

4.4.4. Advantages and limitations of incubation experiments

The net production of halocarbons is the result of a number of complex interactions between dissolved organic matter, availability of halogen ions, bacterial and phytoplankton activity, and abiotic photochemical reactions in surface seawater. Therefore, it is important to gain an understanding of the characteristics of the planktonic community when attempting to determine the factors affecting trace gas production. Batch culture experiments have regularly been used to assess the net production of halocarbons by single-species cultures of phytoplankton (Moore *et al.* 1996; Scarratt and Moore 1996; Manley and Cuesta 1997; Saemundsdottir and Matrai 1998; Scarratt and Moore 1998; Hughes *et al.* 2006). However, in order to accurately understand the potential effects, the conditions of experiments need to be as close to natural as possible. For a number of reasons, single-species batch cultures may be considered to be less representative of the natural setting (Manley and Cuesta 1997):

1. Phytoplankton species used in cultures may be "lab rat", and thus not wholly representative of "wild" algae. It may have lost wild traits, e.g.

unicellular growth pattern instead of colonial (Anderson 2005), or may not be typical of open ocean communities (Tait and Moore 1995).

2. The high cell density experienced batch cultures may favour dominance of bacteria that are not usually abundant in natural seawater communities (Tait and Moore 1995).

3. Cultures used are often axenic, and not all algae grow successfully axenically. As bacteria are potentially very important contributors to halocarbon production (Amachi *et al.* 2001; Hughes *et al.* 2008), this removes a potentially important component of the process.

Therefore, the use of "natural" seawater samples in incubation studies provides the opportunity to investigate trace gas production in a more realistic way. It allows an assessment of the response a whole community assemblage to decreasing pH, over the period of 2 – 3 weeks and during the growth and decline of a phytoplankton bloom, taking account of some of the complex interactions within planktonic communities. Furthermore, as it is predicted that there is likely to be a species shift in response to rising pCO_2 in the oceans (Wolf-Gladrow *et al.* 1999), it enables the acquisition of information on changes to the composition and succession of whole phytoplankton communities.

Despite these clear advantages, it is important to take into account the possible limitations of such experiments, which are mainly a result of "bottle effects" that create biases in results and may make extrapolation to the natural environmental difficult (Venrick *et al.* 1977; Ferguson *et al.* 1984):

1. *Ability of the incubations to reflect natural conditions.* The confinement of seawater induces general changes to communities (altered light and turbulence regimes, changes to biological interactions, isolation from a range of chemical, physical and biological factors, enhancement of contact with others) (Venrick *et al.* 1977).
2. *Physical damage to organisms through rough handling/filtration/contact with container walls.* This may cause decline of some less tolerant species, change composition of community, reduce grazing and cause biomass to increase (Venrick *et al.* 1977; Price *et al.* 1994). However, in terms of the

screening that was performed to remove grazers from the seawater before incubation, a previous study found no evidence that this would cause a decline in community composition (Venrick *et al.* 1977).

3. *Absorption of organic substrates onto container walls*. This may result in a reduction in the activity of bacterioplankton. Bacteria that are absorbed onto glass may rapidly proliferate, changing nutrient dynamics and ecosystem composition (Fogg and Calvario-Martinez 1989).

Our ability to understand the impacts future OA may have on biogenic trace gas production by planktonic communities depends on gaining an understanding of how the whole ecosystem may react to the altered seawater chemistry. The complete acclimation of an organism to environmental changes is defined as its ability to grow and reproduce under the altered conditions (Levitan *et al.* 2007). Although the incubation experiments described here do not achieve this, they represent the beginning of our understanding of which species may be more tolerant, and the implications this will have for trace gas production.

Blank Page

CHAPTER 5

A Natural Analogue to Ocean Acidification?

Marine CO_2 Vents, Ischia, Italy.

5.1 Introduction

Short term OA laboratory and mesocosm experiments have proved to be a valuable tool in assessing the impacts of future low pH conditions on complex marine pelagic ecosystems (Engel *et al.* 2005; Avgoustidi 2007; Wingenter *et al.* 2007; Vogt *et al.* 2008; Hopkins *et al.* 2010), but such experiments have a number of limitations. Firstly, the changes to pCO_2 experienced by the organisms are too rapid to be representative of future oceanic changes (Passow and Riebesell 2005). Thus the organisms cannot adapt to the changed conditions over a significant period of time and may display a "toxic shock" response rather than an evolutionary response to increased CO_2. Such experiments also only focus on a single species, a limited number of species or only a small part of marine ecosystem, and may fail to give any indication of the response of whole ecosystems to the perturbed conditions (Watts and Biggs 2001; Passow and Riebesell 2005). In practical terms, pCO_2 is inherently difficult to control in artificial conditions, particularly when using highly productive phytoplankton cultures, leading to larger fluctuations in pH than will be experienced in the future oceans. Finally, as with any type of incubation or mesocosm experiment, the results may be biased by the effects of enclosure – the "bottle effects" (Venrick *et al.* 1977; Ferguson *et al.* 1984), as discussed in Chapter 4, section 4.4.4.

It has recently been recognised that the problems associated with artificial OA experiments may be overcome with the use of naturally low pH areas, such as upwelling regions and marine CO_2 vent sites. These natural analogues to future OA may enable researchers to gain insights into long-term ecosystem responses to low pH environments, allowing individuals and populations living in ambient seawater to be compared with those living in and adapted to low pH regimes (Orr *et al.* 2009).

Marine volcanic CO_2 vents might lend themselves as ideal natural laboratories for studying the effects of OA on whole marine ecosystems. The Mediterranean is especially abundant with such sites, although the vent emissions of many contain toxic sulphur compounds, and are at high temperatures, rendering them unsuitable for such studies (Hall-Spencer *et al.* 2008). However, those CO_2 vents that are at ambient temperature and lack toxicity offer a much more valuable opportunity for research. Such vent sites can exist for tens to thousands of years, enabling marine ecosystems to adapt and evolve to high CO_2 conditions over realistic periods of time (Hall-Spencer *et al.* 2008).

5.1.1. Study Site Location

The island of Ischia, in the Gulf of Naples, Italy (See Figs. 5.1 and 5.2) is situated in a region known as the Phlegraean Fields – "Phlegraean" meaning fiery, and the reason for this name is clearly visible in the region and on Ischia itself. For thousands of years the area experienced widespread volcanic eruptions and earthquakes, some fierce and devastating, and Ischia saw its fair share of this seismic activity. The island's geology is now much more benign, but there are constant reminders of its violent volcanic origins manifested as hot springs, fumaroles, and shallow marine CO_2 vents. The study site comprises CO_2 vents that diffuse through the seabed at ambient temperature down a stretch of shallow subtidal rocky shore along the north and south sides of the Castello d'Aragonese, situated on the east coast of the island (Fig. 5.2 and 5.4). This site has revealed novel data on the response of rocky shore and seagrass macrofaunal communities to OA (Hall-Spencer *et al.* 2008). The aim of the current work is to determine how useful this site is for investigating the impacts on the pelagic community and the climatically-important trace gases that they produce.

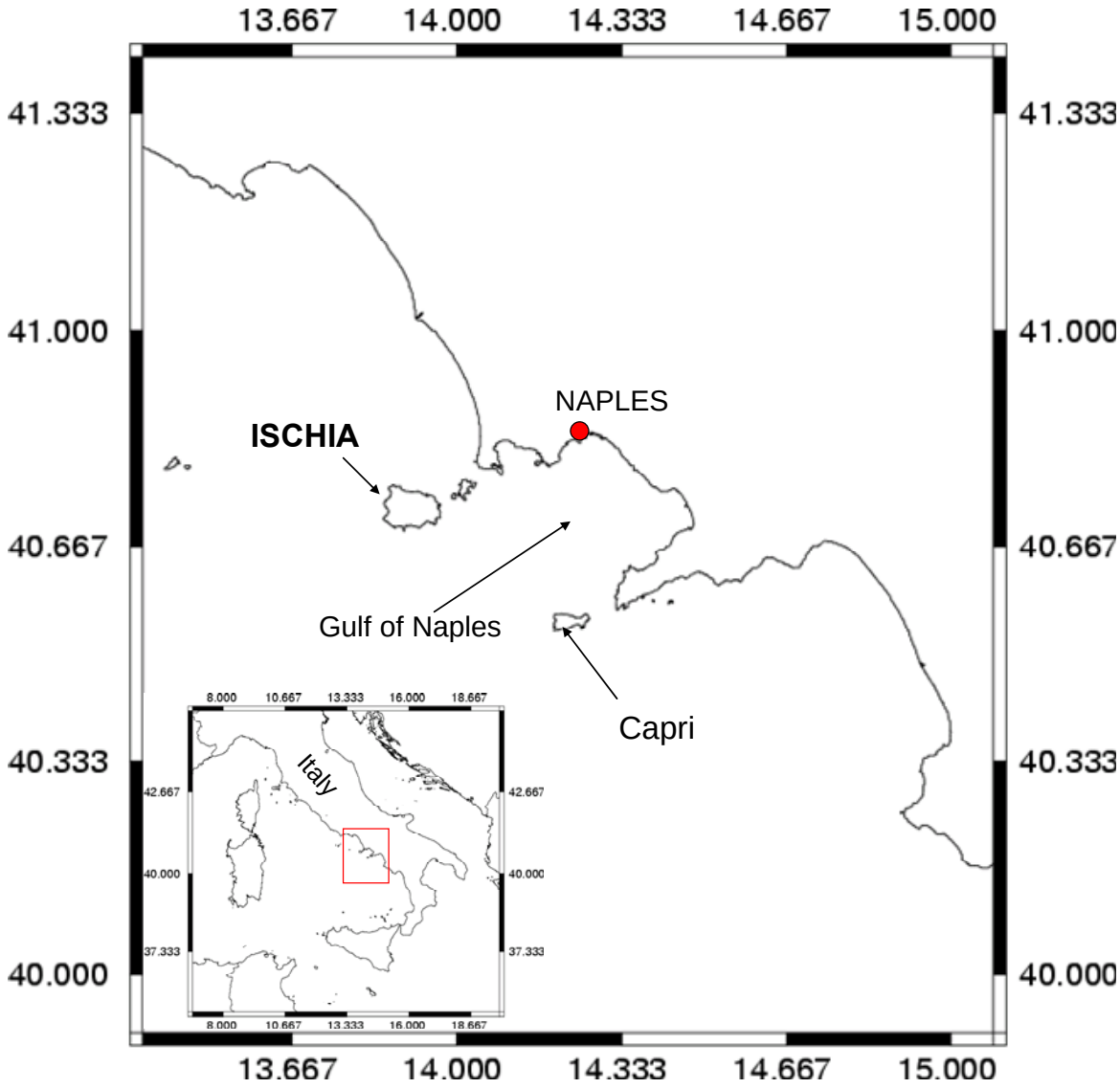

Figure 5.1. Map showing the location of Ischia in the Gulf of Naples (Insert – map of Italy).

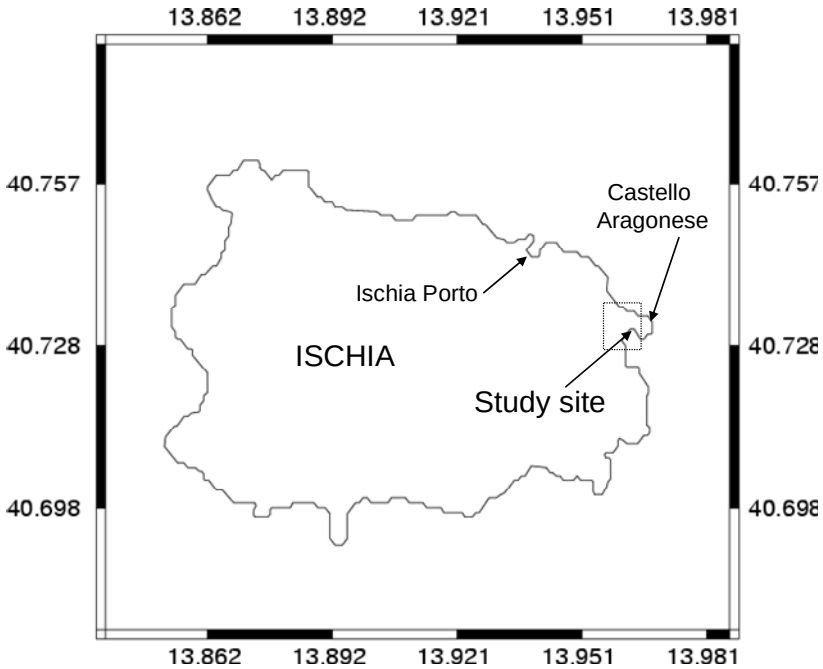

Figure 5.2. Map showing location of study site on the east coast of the island of Ischia.

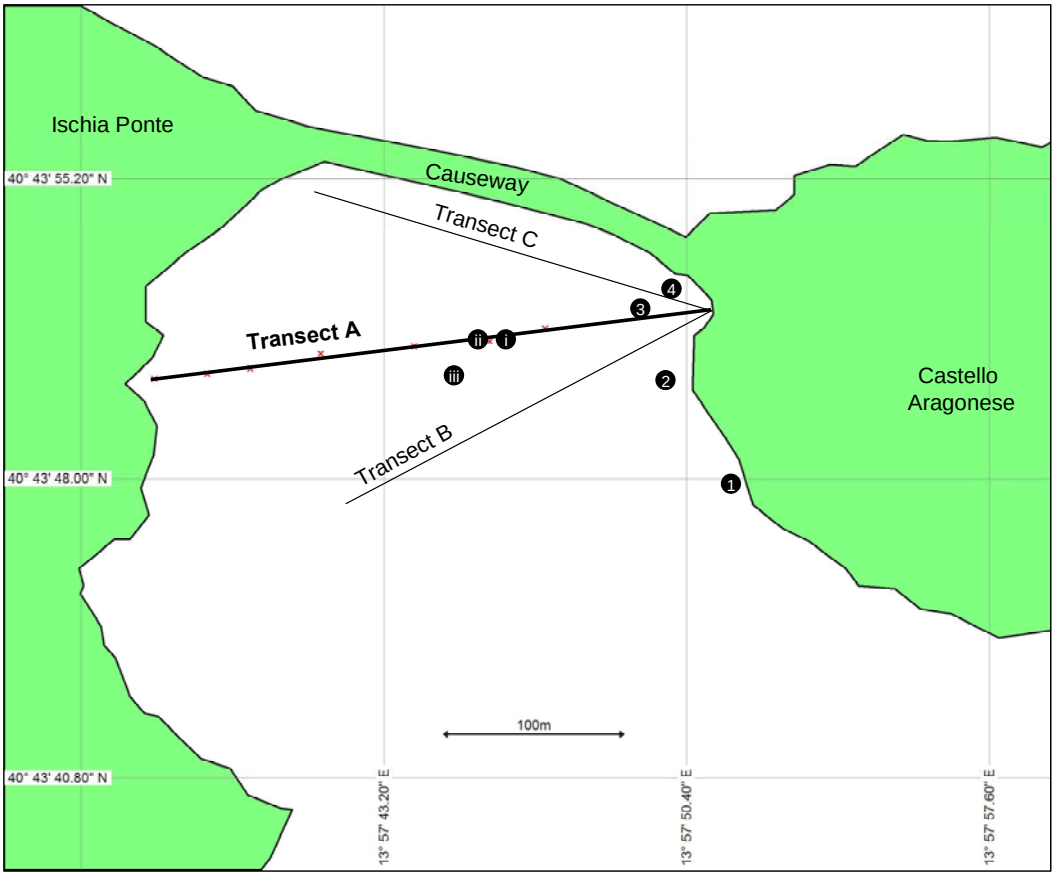

Figure 5.3. Map of the study site.
The locations of Transects A, B and C are indicated by solid lines. Sites 1, 2, 3 and 4 are also shown. i, ii and iii represent sites that were used as background control sites. This area is highlighted by the dashed-line box in Figure 5.2.

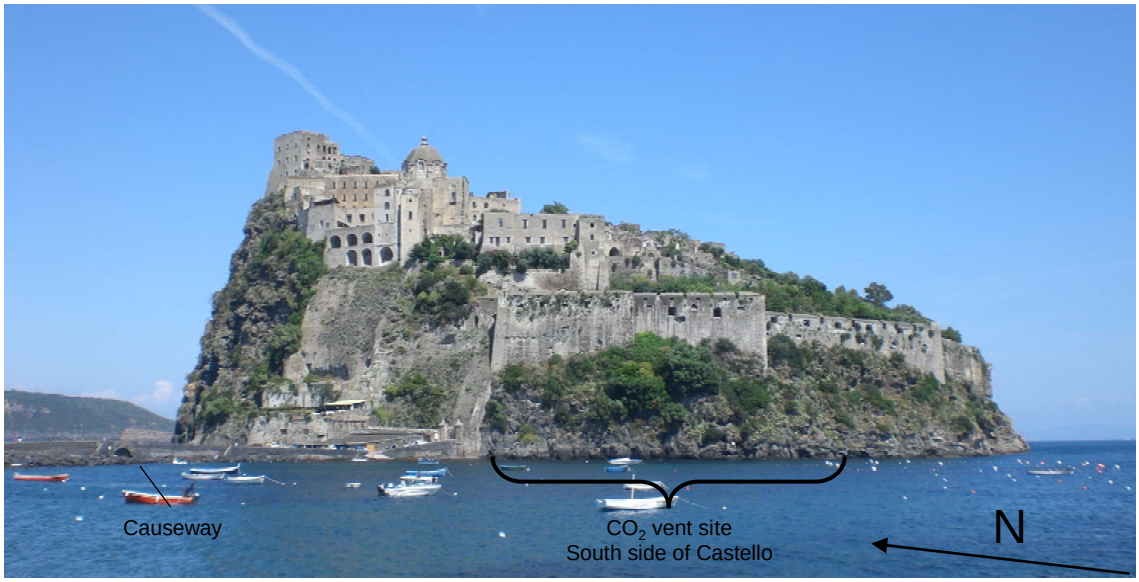

Figure 5.4. Castello d'Aragonese showing location of the CO_2 vent site situated on the south side of the Castello.

5.2 Materials and Methods

Two field campaigns were undertaken in order to produce an assessment of this site: 1. Autumn: 25th October – 22nd November 2007, 2. Spring: 3rd – 31st May 2008. A full description of all methods used during the campaigns is given in the following section.

5.2.1. Temperature, Salinity, pH and Position

Seawater temperature, salinity and pH measurements were taken using a hand-held YSI 556 MPS (multi-parameter system) instrument with a temperature precision thermistor (Accuracy ± 0.15°C), a 4-electrode cell auto-ranging conductivity sensor (Accuracy 1.0%), and a glass combination pH electrode (Accuracy ±0.2 units). pH was calibrated on a regular basis during the field campaigns (daily to every 3 days) using either commercially- or laboratory-prepared pH standards. During autumn, regular pH buffers were used (pH 4, 7 and 10 (Fisher Scientific)), giving pH measurements that were on the NBS scale, and although not ideal for seawater pH measurements (See Chapter 2, Section 2.5.4.), allows relative changes in pH to be assessed. During the spring field campaign the probe was calibrated using laboratory-prepared seawater pH standards, allowing pH measurements on the total scale to be taken. The data were converted from free scale to total scale using the

method described in Chapter 2, Section 2.5.4. Sampling positions were determined using a hand-held Garmin eTrex Venture GPS Navigator.

5.2.2. Trace Gases

Samples for halocarbon determination were taken using 100 ml glass syringes. Surface samples were taken directly from a small boat. A Niskin bottle was used to collect samples from depth. Once back on board the boat, the Niskin was cocked open and halocarbon samples were drawn up into 100 ml glass syringe using a section of nylon tubing. The glass syringes were placed inside a black polythene bag inside a coolbox for transportation to the laboratory. Details of specific sampling procedures used during certain experiments at the site are given in the relevant sections of this chapter.

On return to the laboratory, samples were processed as described in Chapter 2, section 2.3.1.3, with purge and trap, and Markes sorbent tubes. Subsequent to trapping, the tubes were capped off and stored at -20°C until being analysed by GC-MS on return to UEA (within 2 months of sample collection).

Samples for DMS analysis were taken with: 1. The inverted aspirator technique (surface samples) (Chapter 2, Section 2.4.1.1), 2. By manually lowering a Niskin bottle down through the water column and firing with a messenger at the required depth (depth samples). Once full, a length of Taigon tubing was attached to the valve on either the aspirator or Niskin. The tube was then placed to the bottom of a 500 ml glass-stoppered bottle, and a large aliquot taken which was shaken around the bottle to rinse it, and then rejected. Water was then allowed to fill from the bottom of the bottle and to overflow for an estimated 3 times the volume of the bottle. The glass-stopper was firmly placed onto the bottle, ensuring the absence of headspace and bubbles. The bottles were placed in a dark cool box until return to the laboratory on the island.

5.2.3. Chlorophyll a and Phaeopigments

Seawater samples were collected by either the inverted aspirator technique, or using a Niskin bottle. 100 ml of seawater was filtered though 47 mm GF/F filters, then folded up, wrapped in tin foil and stored at -80°C. The samples were analysed on return to UEA using the methods described in Chapter 2, section 2.5.1.

5.2.4. FIRe - Fluorescence Induction and Relaxation

Following dark adaptation (>1 hour), 1 – 3 ml subsample of seawater was transferred to a quartz cuvette and analysed on a Fluoresence Induction and Relaxation fluorometer system (FIRe, Satlantic Inc.) in order to assess the level of environmental stress experienced by phytoplankton in response to the high CO_2 conditions.

Using high luminosity blue (450 nM) and green (530 nM) light emitting diodes (LEDs) to excite chlorophyll a *in vivo*, the FIRe techniques works on the principle of active stimulation and detection of the induction and subsequent relaxation of chlorophyll fluorescence yields on micro- and millisecond time scales (Satlantic Incorporated, 2005).

The FIRe measurement protocol consists of 4 phases (Satlantic Inc, 2005):

1. Strong short pulse of 80 μs (Single Turnover Flash STF) to cumulatively saturate Photo System II (PSII). Provides: $\mathbf{F_0}$ (minimum fluorescence), $\mathbf{F_M}$ (maximum fluorescence STF), $\mathbf{F_V/F_M}$ (maximum quantum yield of photochemistry in PSII, $FV = F_M - F_0$), $\boldsymbol{\sigma_{PSII}}$, (functional absorption cross section of PSII), **p** (connectivity factor – excitation energy transfer between individual photosynthetic units.
2. Weak modulated light applied to record relaxation kinetics of fluorescence yield on timescale of 500 ms.
3. Strong long pulse of 24 ms duration (Multiple Flash Turnover MFT) to saturate PSII and plastoquinine pool (PQ). Provides: $\mathbf{F_M}$ (MTF) and $\mathbf{F_V/F_M}$ (MTF).
4. Weak modulated light to record kinetics of the PQ pool re-oxidation.

Values of F_V/F_M were of interest in this study, as they would provide information on the photosynthetic efficiency of the phytoplankton community, and hence give some indication of the level of stress being experienced by the community. Due to software problems only a limited amount of data were collected.

5.2.5. Currents

Current speed and direction were measured using a Nortek Aquadopp Acoustic Doppler Current Profiler (ADCP) (Nortek AS, www.nortek.no) moored to the seabed in an upward-facing position. The profiler was placed in a stainless steel bucket and

held in an upright position using ballast material comprising gravel and rocks. The bucket was moored to the seabed using rock weights attached to the bucket with cord (Figure 5.5). The Aquadopp Profiler is capable of producing a range of data, including full current profiles, sensor tilt, pressure (proxy of depth), seawater temperature and wave data. Current profile and pressure data was used to derive information on the hydrodynamics experienced at the site.

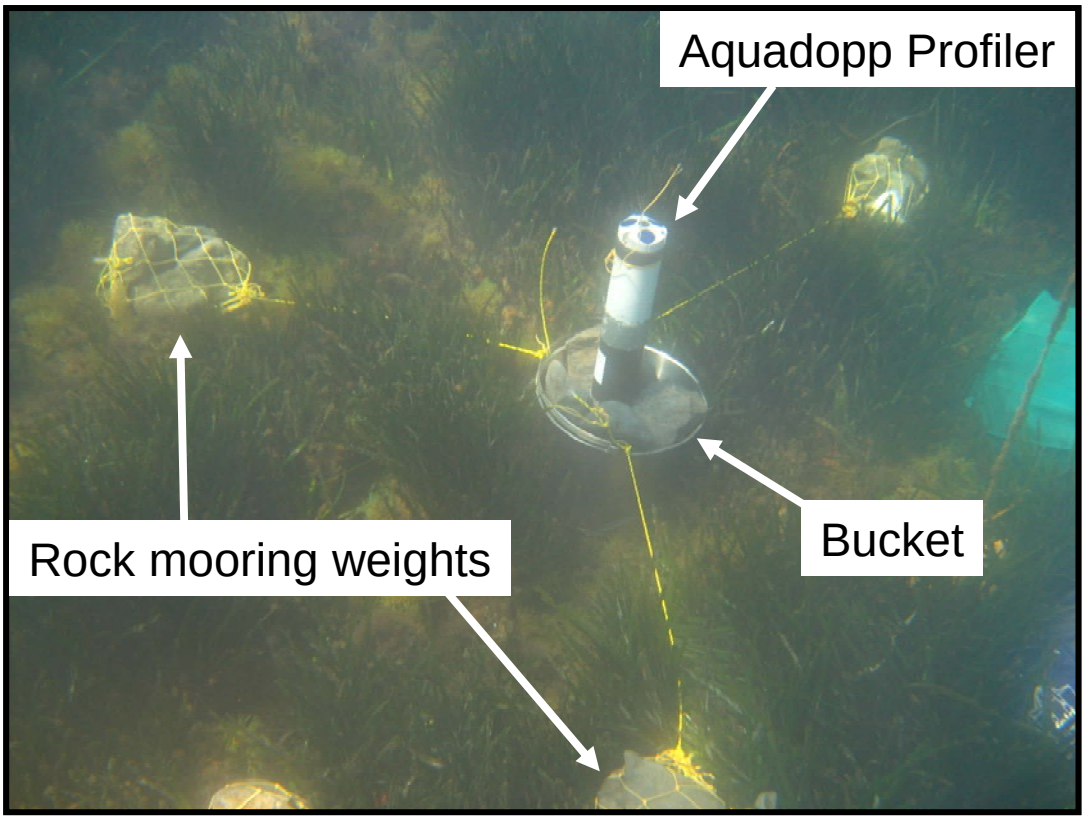

Figure 5.5. The Aquadopp Current Profiler, moored to the seabed in an upward facing position.

5.3 Site Characterisation

5.3.1. The CO_2 Vents

Hall-Spencer *et al.* (2008) performed an initial assessment of the site during Spring 2007. The CO_2 vents on the south side of Castello d'Aragonese percolate through an area of seabed covering ~3000 m^2, at a rate of approximately 1.4 x 10^6 litre CO_2 day^{-1}. No tidal or diurnal variation in gas flow rates was observed (Hall-Spencer

et al. 2008). Vent gases were analysed to confirm they were composed predominantly of CO_2. The results of this analysis are shown in Table 5.1.

Table 5.1. Composition of the gas (%) emitted from volcanic vents at the Castello d'Aragonese. Data from Hall-Spencer *et al.* (2008).

Component	% of total
CO_2	90.1 - 95.3
N_2	3.2 - 6.6
O_2	0.6 - 0.8
Ar	0.08 - 0.1
CH_4	0.2 -0.8

The vent gases were also analysed for this study, as the concentrations of halocarbons were unknown. It was important to determine whether *in situ* halocarbon concentrations might be influenced by sediment and/or vent sources. Vent gas samples were collected using 5-litre Tedlar gas sampling bags (SKC Ltd.) with stainless steel valves. Before sample collection, the bags were purged with high purity nitrogen, evacuated of all air, and the stainless steel valves were tightly closed. Once at the sampling site, an inverted glass funnel was used to accumulate vent gases, whilst a length of ¼" nylon tubing was used to direct the gas into the Tedlar bag. A small section of Tygon tubing was attached to the nylon tubing, and then attached to the inlet on the bag to create a gas tight seal. Once the bag was full, the tubing was removed and all the valves closed. On return to the laboratory, 1500ml of vent gas sample was trapped onto each of 4 Markes sorbent tubes by drawing across the Markes tubes using a 100ml glass syringe. Finally, the Markes tubes were sealed with brass caps and stored at -20°C until analysis at UEA within 2 months of sample collection. When analysed, the vent gas were found to contain no detectable halocarbons.

5.3.2. Meteorology

5.3.2.1. Autumn 2007

Meteorological conditions during the autumn field campaign in 2007 are shown in Figure 5.6 a and b. Air temperatures were almost always lower than seawater temperatures and winds alternated between NE to NNE and S/SW. Daily mean

seawater temperatures (Figure 5.5 a) gradually fell over the month from 19.7°C to 17.6°C in response to the falling air temperatures.

5.3.2.2. Spring 2008

Meteorological conditions during the spring field campaign in 2008 are shown in Figure 5.7 a and b. Mean daily seawater temperatures were lower than daytime air temperatures. Wind direction was much more variable than during autumn, although NE was perhaps the most common direction. A period characterised by high wind speeds was experienced between 19 and 21 May, with a maximum of 17 km/h recorded on 20 May. The final phase of the campaign saw a dramatic shift in weather conditions, with a hot, dry SW wind, resulting in rapidly increasing air temperatures, and decreasing humidity. On 27 May air temperatures peaked at 36°C.

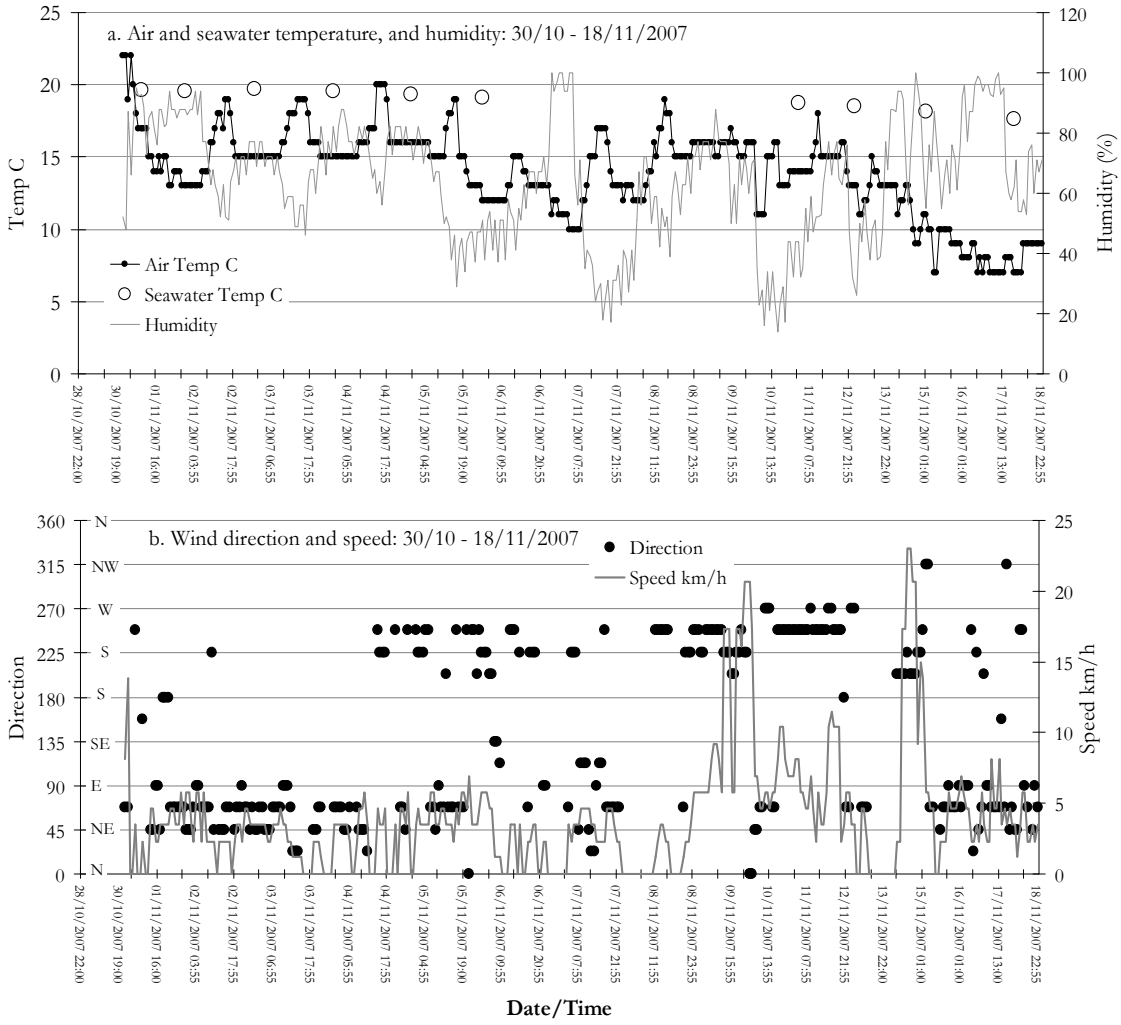

Figure 5.6. a. Air temperature (solid circles), seawater temperature (open circles) (°C), and humidity (%) and b. Wind direction (degrees) and speed (km/h) for the period 30 October – 18 November 2007, during the Autumn fieldwork campaign. Weather data is from weather station 16294 on the island of Capri (See Figure 5.1).

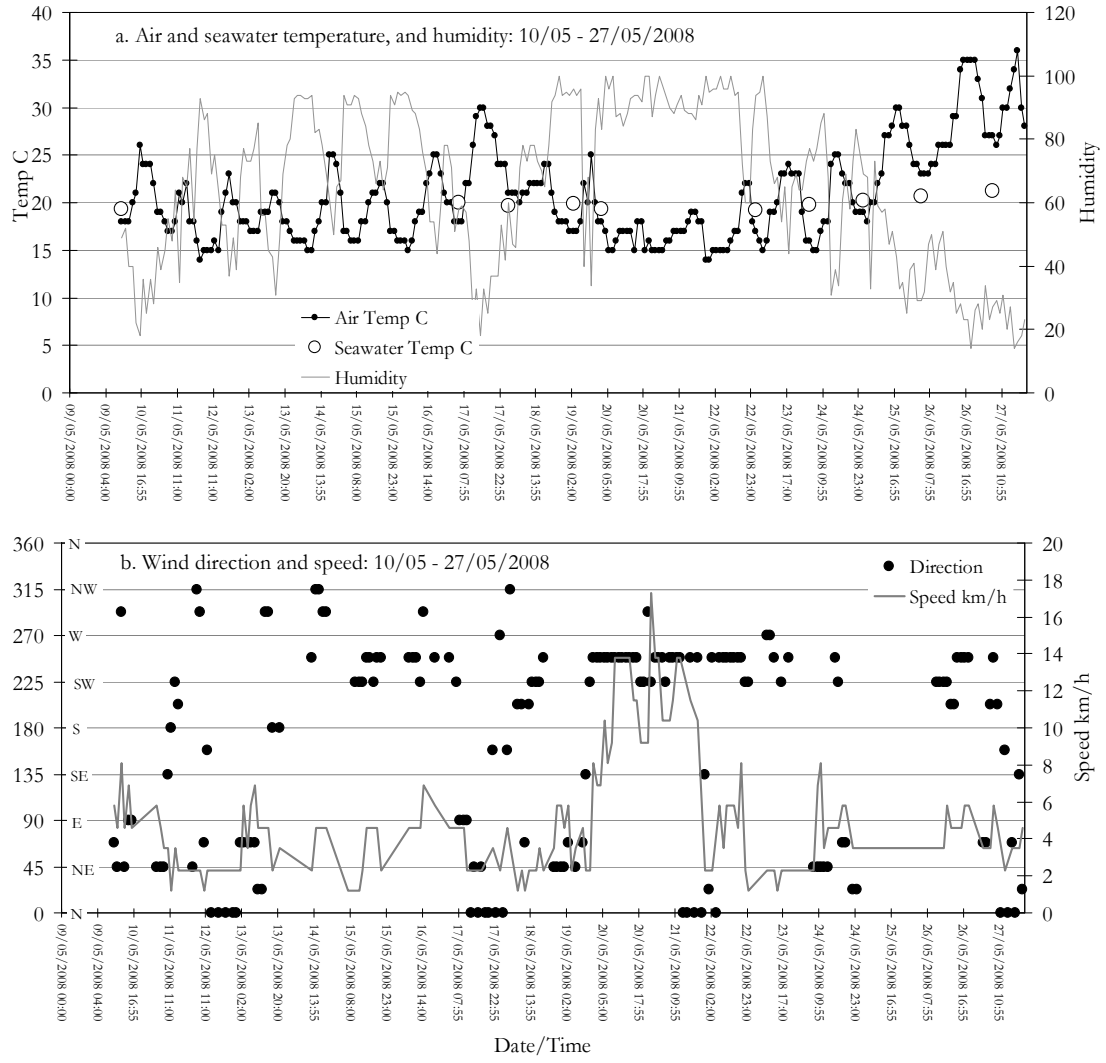

Figure 5.7. a. Air temperature (solid circles), seawater temperature (open circles) (°C), and humidity (%) and b. Wind direction (degrees) and speed (km/h) for the period 10 – 27 May 2008, during the Spring fieldwork campaign. Weather data is from weather station 16294 on the island of Capri (See Figure 5.1).

5.3.3. Bathymetry

Seawater depth measurements were taken manually at the study site along the lines of transects A, B and C (See Figure 5.3) using a plumb line and metered rope, and used to create depth profiles of each of the transects (Figure 5.8). The site was characterised by a 1 – 2m deep trough that ran parallel to the cliff edge, and can be seen on the depth profiles between 1 m and 3 m on A, 0 and 1m on B and 1 m to 5m on C. Transects A and C then crossed a plateau, with depths of <1m. Following the plateau (10m transect A, 13m Transect C), another sandy-bottomed trough was encountered and depths increased to >2.5m. The depth profile of Transect B did not cross the plateau, but instead gently increased in depth and levelled out at around 2m depth at 15m along the transect. Once past the second trough, the seabed of the study site gently sloped down and levelled out on a sandy seagrass bed. Various depth measurements taken in this area indicated that the maximum depth at the sampling sites was 6m, with an average depth of 1.4m. The background control sites i, ii and iii (See Figure 5.3) had depths of 5m, 5.5m and 4m, respectively.

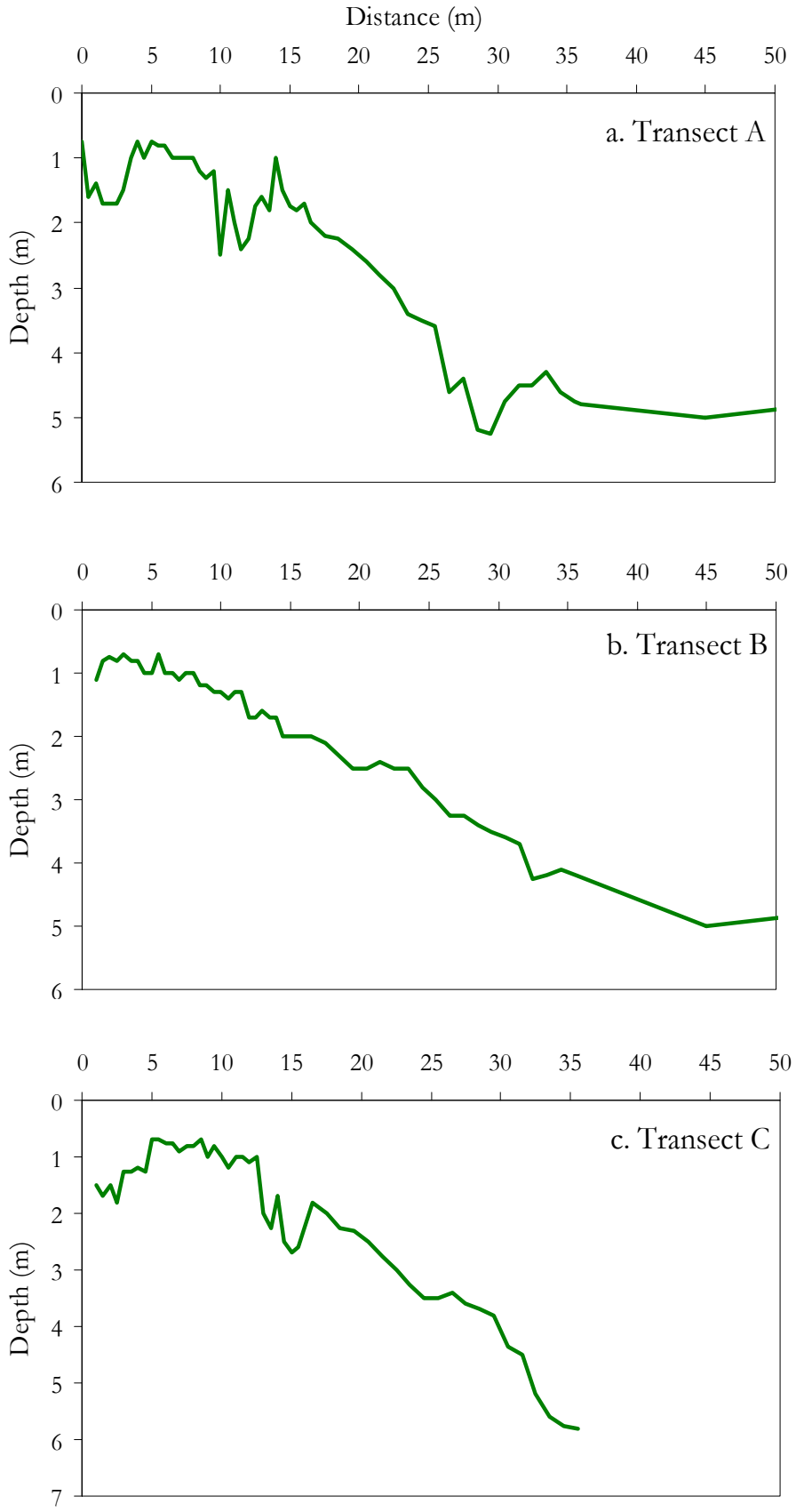

Figure 5.8. Depth profiles of the first 16.5m of a.Transect A, b. Transect B and c. Transect C.

5.3.4. Salinity

Salinity measurements taken at sampling sites are shown in Figure 5.9, a. autumn 2007 and b. spring 2008. Mean salinity values for both field campaigns were similar, with 37.79 for autumn and 37.76 for spring, although the range and variability of data differed between seasons. These values of salinity are in agreement with a previous study from the Gulf of Naples (Stabile *et al.* 2007). Mean salinity values in Autumn were relatively stable over the course of the field campaign, and the consistent nature of the data was reflected in the small range of 0.28 (37.61 to 37.89), and a standard deviation of 0.05. In contrast, spring salinity values showed much greater variability (Figure 5.9 b), with a range of 0.63 (37.42 to 38.05), accompanied by a standard deviation of 0.11.

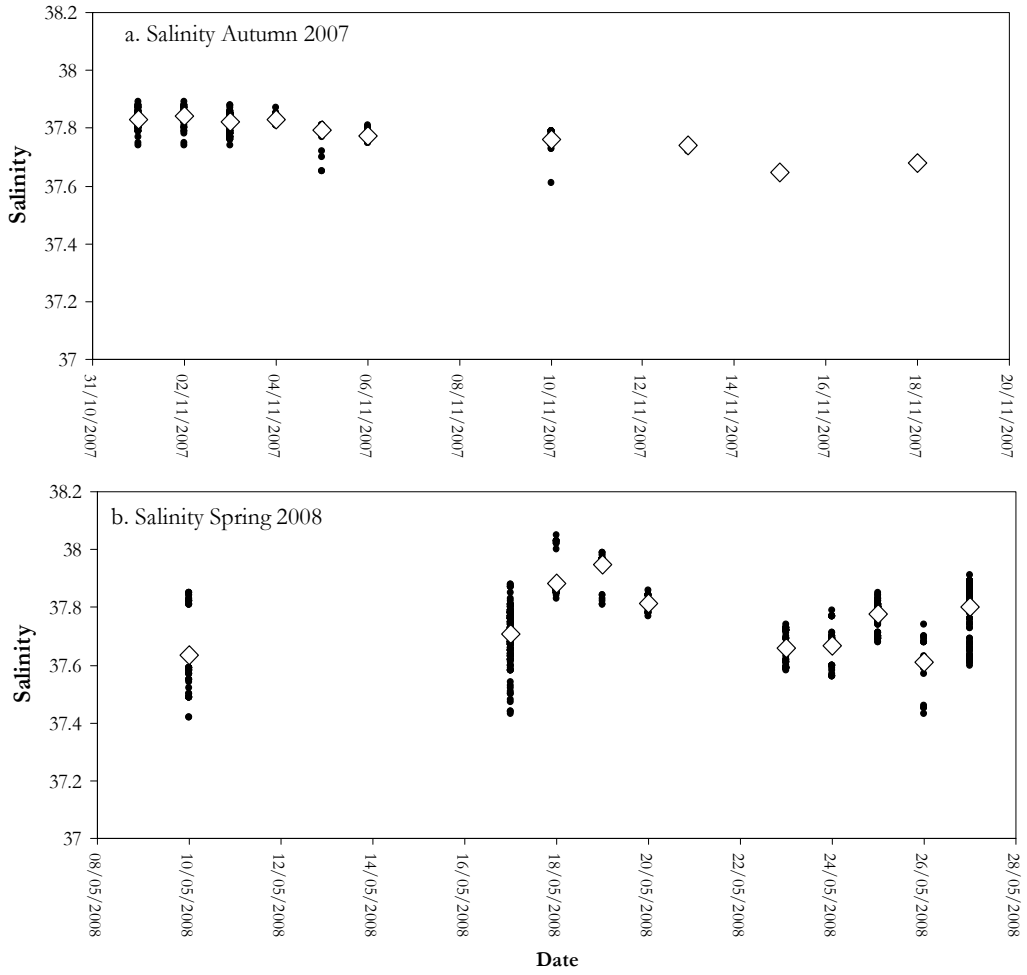

Figure 5.9. Surface salinity with time (date) taken at all sampling sites during a. Autumn 2007 and b. Spring 2008. Closed circles represent individual measurements and open diamonds are the daily mean.

Some of the variability in overall salinity values during the spring field campaign can be attributed to variation in salinity along Transect A. Figure 5.10 shows salinity values along this transect on certain days during a. autumn 2007 and b. spring 2008. During autumn, salinity values were quite consistent along Transect A, with no effect of distance. However, on some days during the spring campaign, an increase in salinity with increasing distance along transect is apparent. Salinity values appear to peak between 30 – 50m along the transect and decrease again at the further station e.g. 17 and 27 May, Figure 5.10 b. However, this phenomenon was not observed consistently, e.g. on 25 May there was less difference in salinity along the transect, although salinity was still lower at the furthest point along the transect.

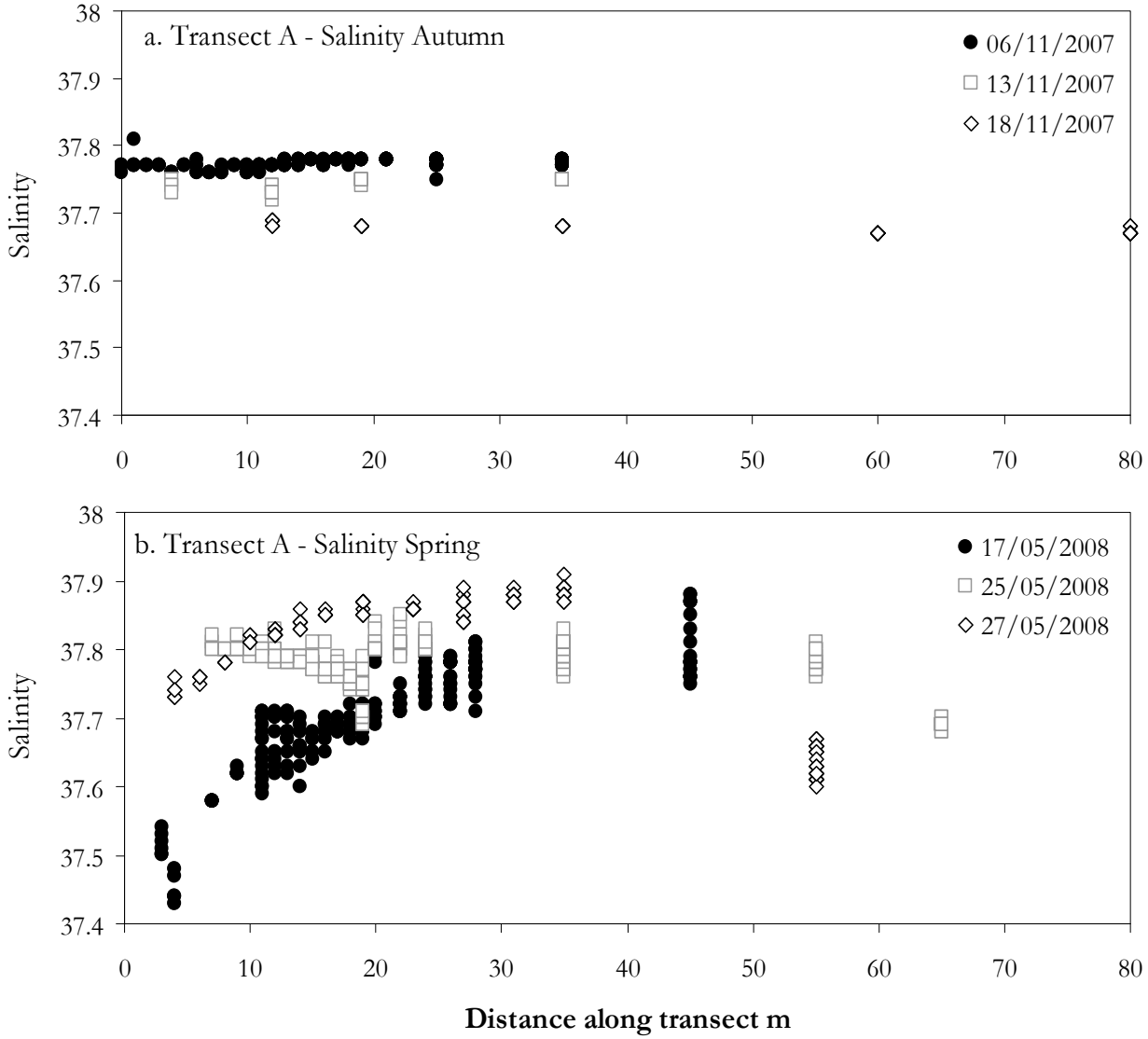

Figure 5.10. Salinity (all measurements) with distance along transect A on a. 6, 13, 18 November, Autumn 2007, and b. 17, 25 and 27 May, Spring 2008.

The causes of the variability in salinity along Transect A on 17 and 27 May may be explained by the weather conditions on these days. These days experienced the highest temperatures of the field campaign, of 30°C and 36°C, respectively, as well as light northerly winds. Temperature and salinity data, presented in Figure 5.11, show that due to these hot, settled conditions, the water column was able to form some structure. A warm water layer developed at the surface, with up to 2°C cooler water at depth. The denser, higher salinity water formed by evaporation at the surface appears to have sunk in the water column, with lower salinity values at the surface compared to deeper down. The resulting thermoclines and haloclines produced by these conditions resulted in variation in salinity values across Transect A.

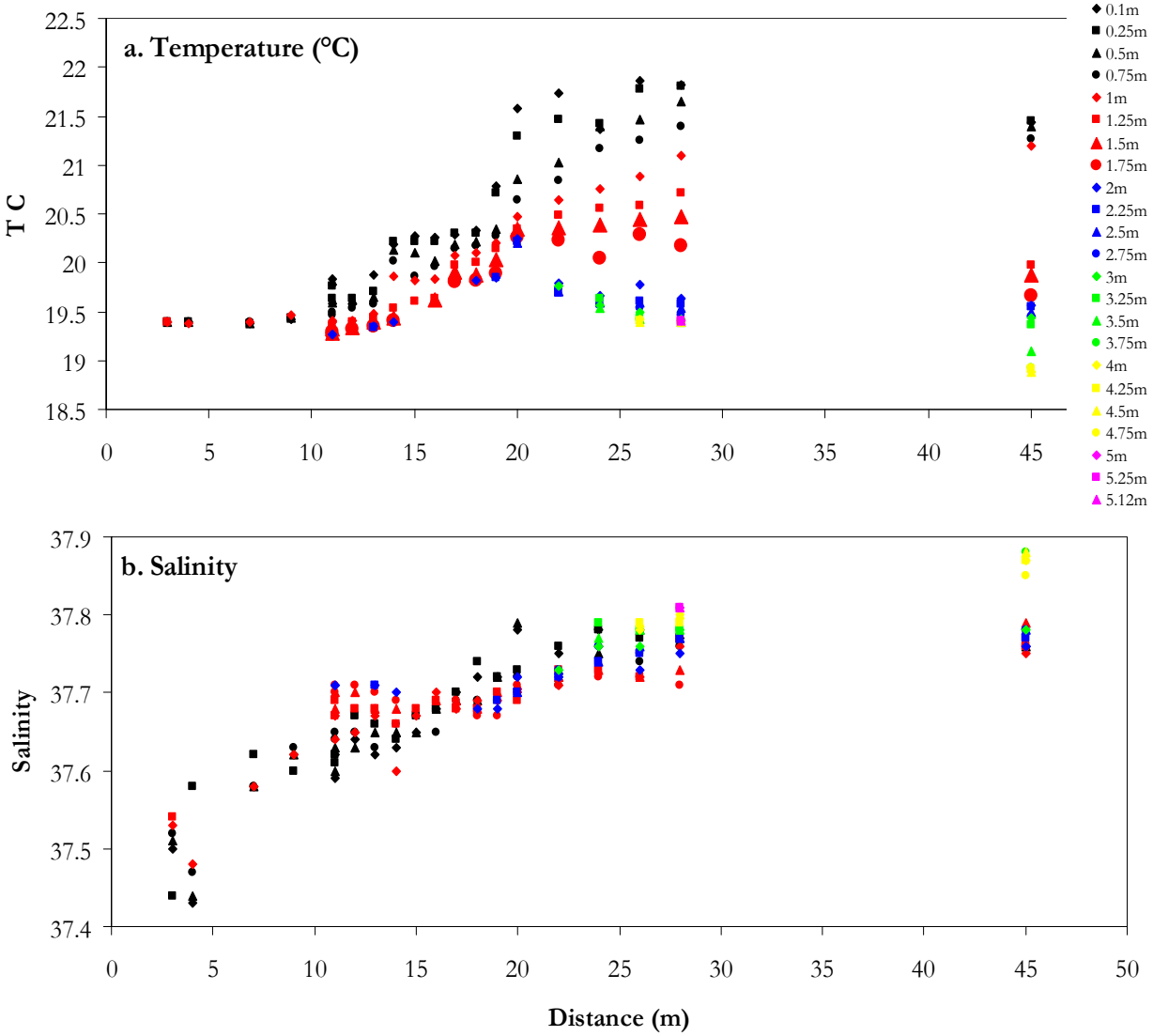

Figure 5.11. a. Seawater temperature (°C) and b. Salinity along transect A on 17 May 2008. Black symbols = 0 - 1m depth, red symbols = 1 – 2m depth, blue symbols = 2 – 3m depth, green symbols = 3 – 4m depth, yellow symbols = 4 – 5m depth and pink symbols = 5 – 6m depth.

Figure 5.12 shows the equivalent data collected during the autumn field campaign. As air temperatures were much cooler in autumn, such water column structure could not form, resulting in a more well-mixed regime, with less variability in salinity. The increase in temperature seen with increasing distance along the transect is the result of the shadow of the Castello on the site. The sites closest to the cliff were still in shade when measurements were taken and as the sun rose and moved around the Castello, a warming effect on the water is observed. Salinity showed very little variation along the transect (Figure 5.12 b), greatly contrasting with the data collected on hot, still days in spring.

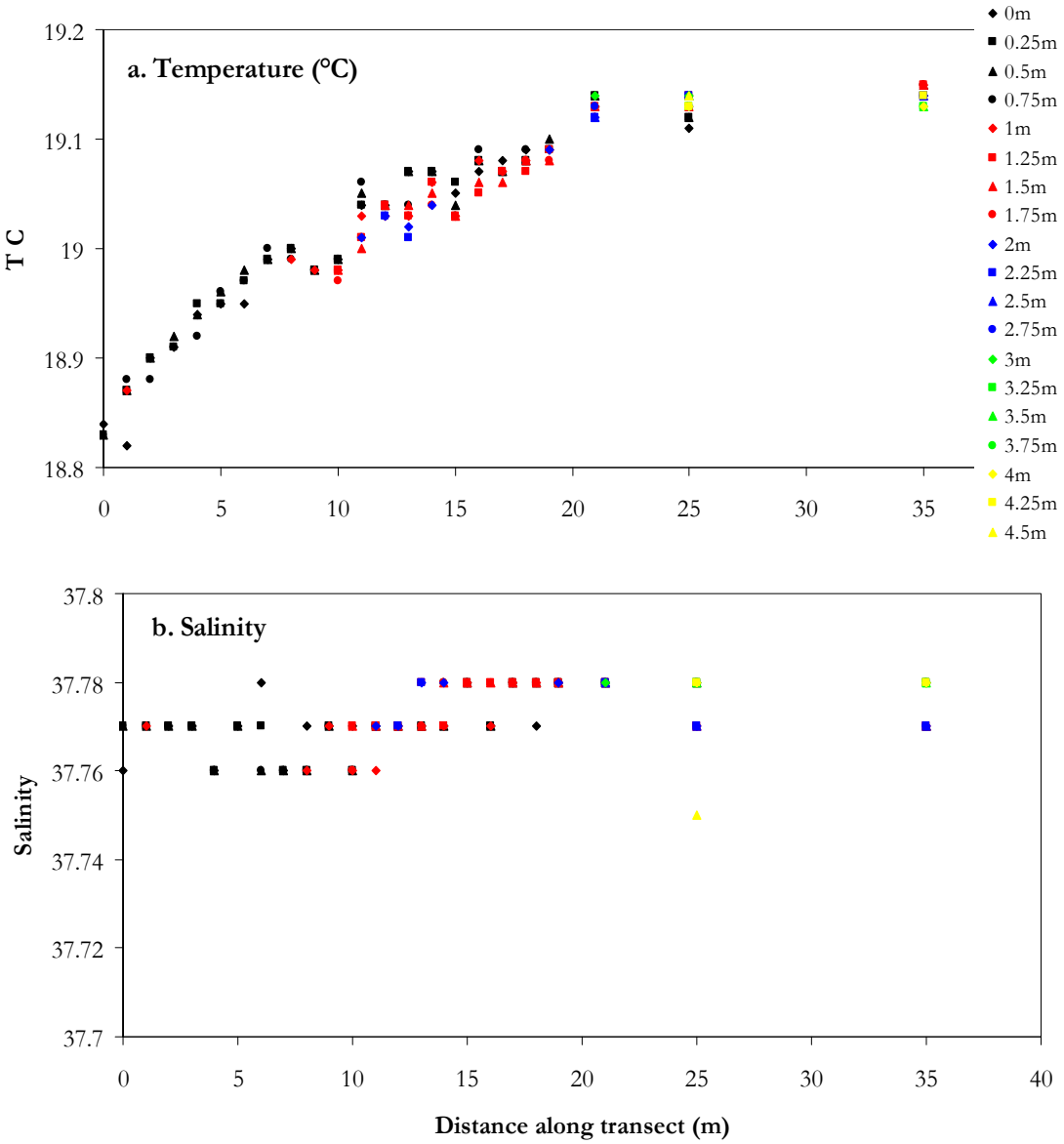

Figure 5.12. a. Seawater temperature (°C) and b. Salinity along transect A on 6 November 2007. Black symbols = 0 - 1m depth, red symbols = 1 – 2m depth, blue symbols = 2 – 3m depth, green symbols = 3 – 4m depth, yellow symbols = 4 – 5m depth and pink symbols = 5 – 6m depth.

5.3.5. Tides

The tides at Ischia are typical of the Mediterranean in general, being semidiurnal in nature and possessing a relatively small tidal range. Tidal heights for Ischia Porto (see Figure 5.3) for the period 17 – 27 May 2008 are shown in Figure 5.13, with a range of between 15 and 30 cm. The maximum tidal range of 25 – 30 cm was recorded from 17 to 21 May, during the spring tidal phase. The tidal range became smaller from 23 May as it entered the neap phase, with a difference between high and low tide of only 10 – 15 cm.

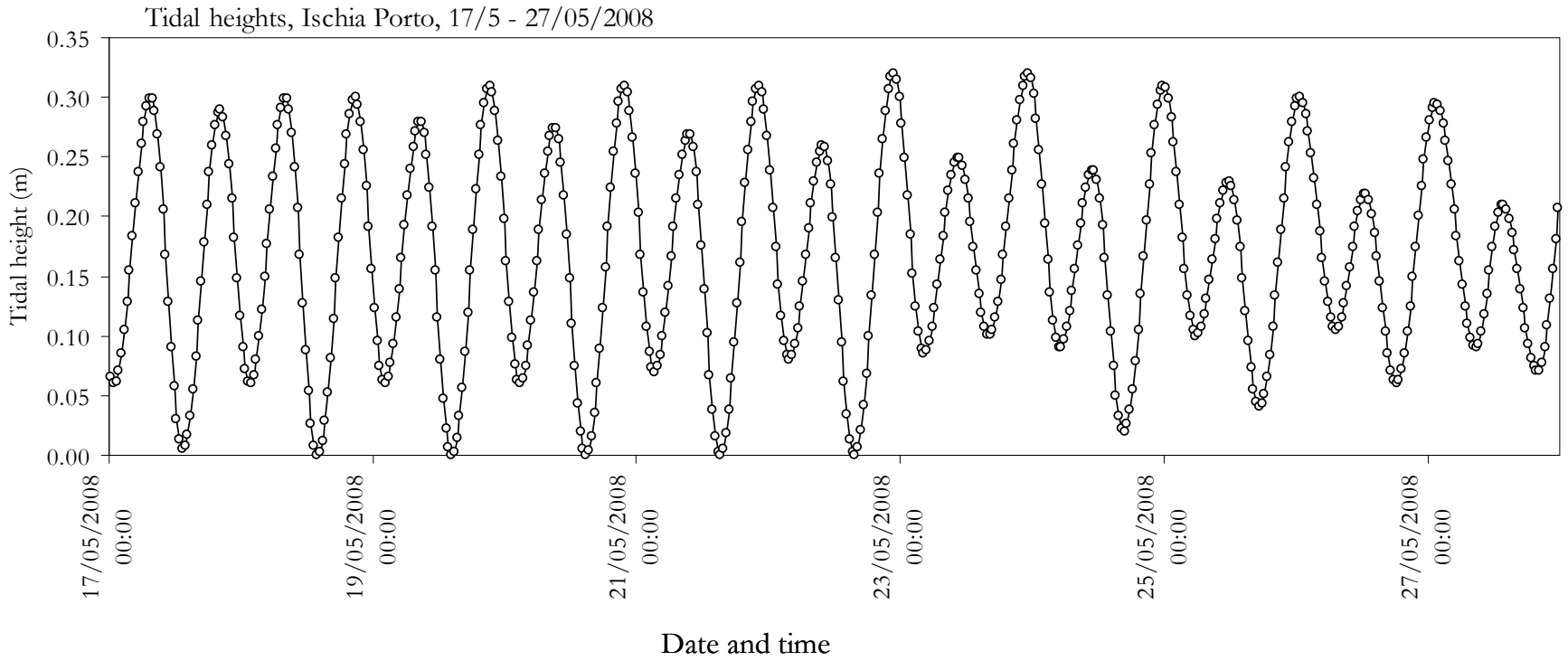

Figure 5.13. Tidal height data (m) for Ischia Porto, 17 – 27 May 2008

5.3.6. Currents

Due to instrumentation problems it was only possible to collect current data at one site (Site 2 – see Figure 5.3) for a 10 hour period. Although limited, this data provides important information on the hydrodynamics of the study site.

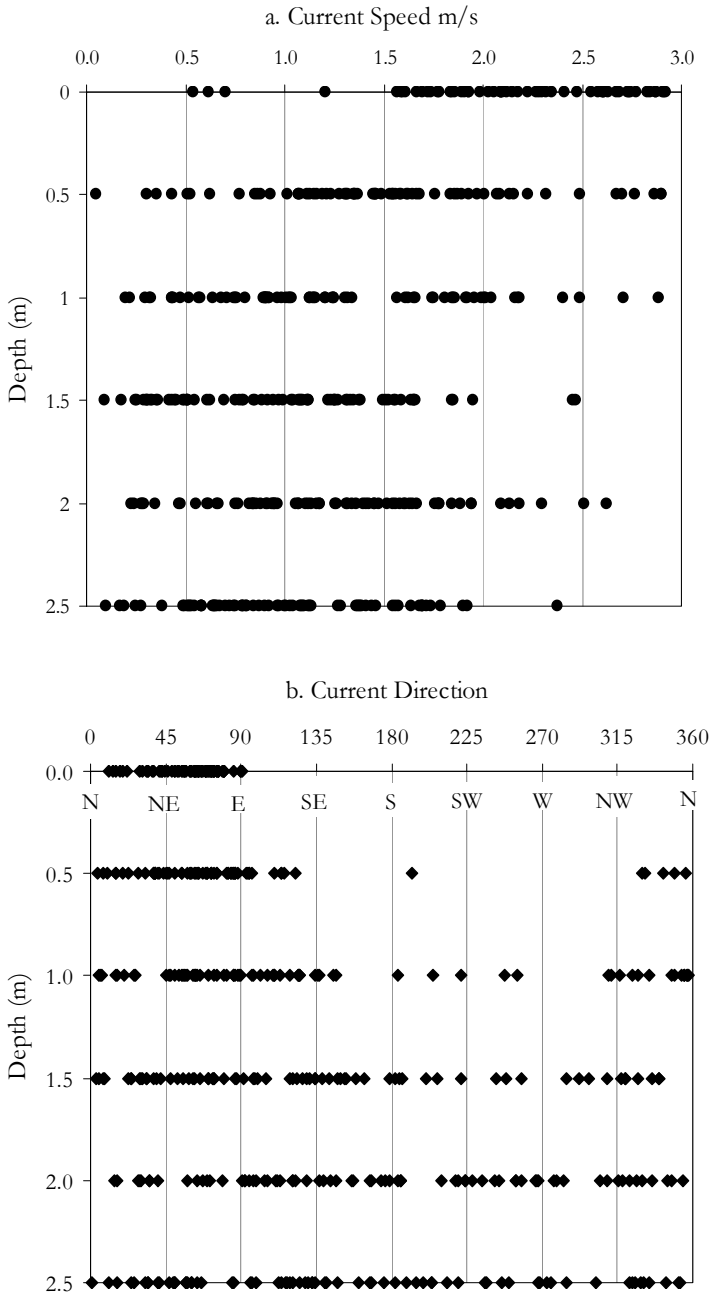

Figure 5.14. ADCP-derived depth profiles of a. Current speed, and b. Current direction over a 10 hour period on 15 May 2008 at Site 2 (see Figure 5.3 for location).

Figure 5.14 shows that current speeds were highest at the surface, and generally fell within the range 1.5 – 3 m/s. Speeds showed a general decreasing trend with depth, and at 2.5 m depth speeds ranged from 0.1 – 2 m/s. Surface currents were dominated by flow from one direction (NE-E). Although the top 1m of water was also influenced by this direction of flow, current direction became much more variable with increasing depth, and by 1.5 to 2.5 m depth all directions of current flow had been experienced in the 10 hour period. From this data it can be concluded that surface currents at the site are primarily controlled by the wind. On 15 May, meteorological data showed that the winds were coming from a SW-SSW direction (See Figure 5.7 b), and it is likely that these winds were causing the NE-E surface current flow

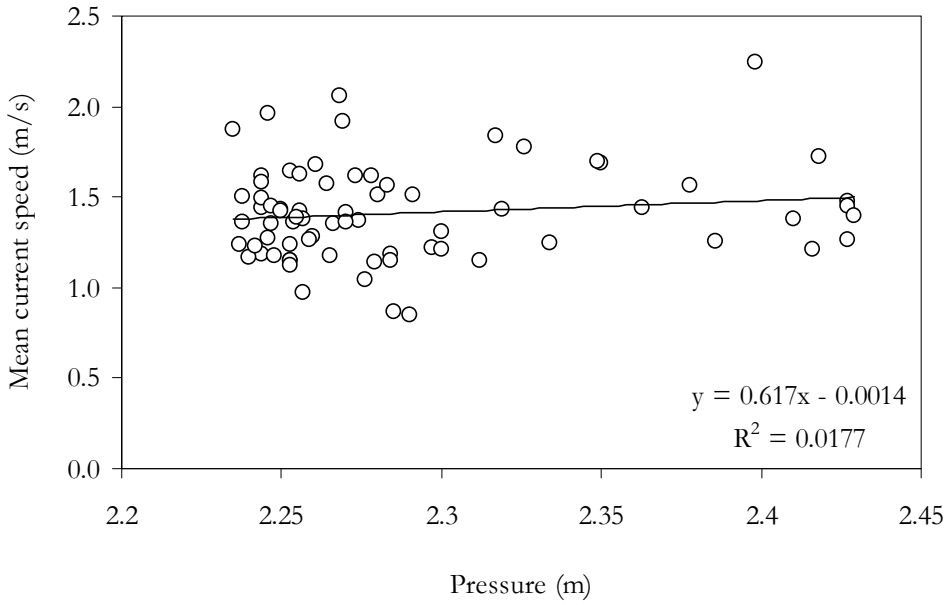

Figure 5.15. Relationship between pressure (m) as a proxy of tidal height, and mean current speed at Site 2 over a 10 hour period on 15 May 2008.

The relationship between tidal movement and current speed was assessed by plotting the pressure sensor reading from the ADCP (which acts as a proxy of tidal height) and mean current speed for the 10 hour period. Figure 5.15 shows there was no relationship between these two parameters, suggesting that tidal movements at the study site have little impact on current speeds. As a result, it is likely that wind has the greatest influence on water movement.

5.4 Seawater pH: Trends and Characteristics

5.4.1. Introduction

One of the main objectives of this study was to determine whether this site represented a good natural analogue of OA, and how useful a tool it may be to investigate of the impacts on the pelagic community. Therefore, it was important to characterise the temporal and spatial variability in seawater pH, and determine whether the pH values were in the range if those expected to be experienced by the surface oceans over the coming centuries. Table 5.2 gives mean, standard deviation and maximum and minimum pH values for surface measurements only, and all measurements taken during the autumn and spring field campaigns. Due to different pH scales used, only the variability in pH data can be compared between seasons.

Table 5.2. Mean, standard deviation, and maximum and minimum values for all pH measurements and surface pH measurements made during the autumn 2007 and spring 2008 field campaigns.

	Autumn 2007 (NBS Scale)		**Spring 2008 (Total Scale)**	
	All measurements	**Surface measurements**	**All measurements**	**Surface measurements**
Mean	7.31	7.21	7.34	7.47
± St. Dev.	0.52	0.64	0.66	0.66
Maximum	7.98	7.98	8.23	8.23
Minimum	5.52	6.03	5.32	5.32
n	918	78	896	88

5.4.2. Overview of seawater pH

Figure 5.16 shows plots of surface pH measurements along Transect A on various dates during a. autumn 2007 and b. spring 2008, with variability over small spatial scales, and over temporal scales both to a daily and seasonal degree. The general change in pH along the transects can be seen for both seasons, with values gradually rising with distance along the transect. Repeated measurements were taken at 4 m, 6 m, 12 m, 18 m, 19 m and 35 m, and the day to day variability in pH

can clearly be seen at these stations. The greatest variation was observed at 12 m, where the pH ranged from 6.97 to 7.94. The daily variability in pH was much greater during Spring; for example, for the period 10 – 27 May the pH ranged from 5.32 to 8.23, and pH characteristics along the transect showed some rapid spatial changes. However, on some days (e.g. 18 and 27 May) rapid changes were not observed, with much more gradual increases in pH along the transect. On most days, background pH levels were not reached until the furthest station at 35 m. However on 25 May, pH levels exceeded 8.0 from 11 m onwards, highlighting the temporal variability in the pH gradient experienced at this site.

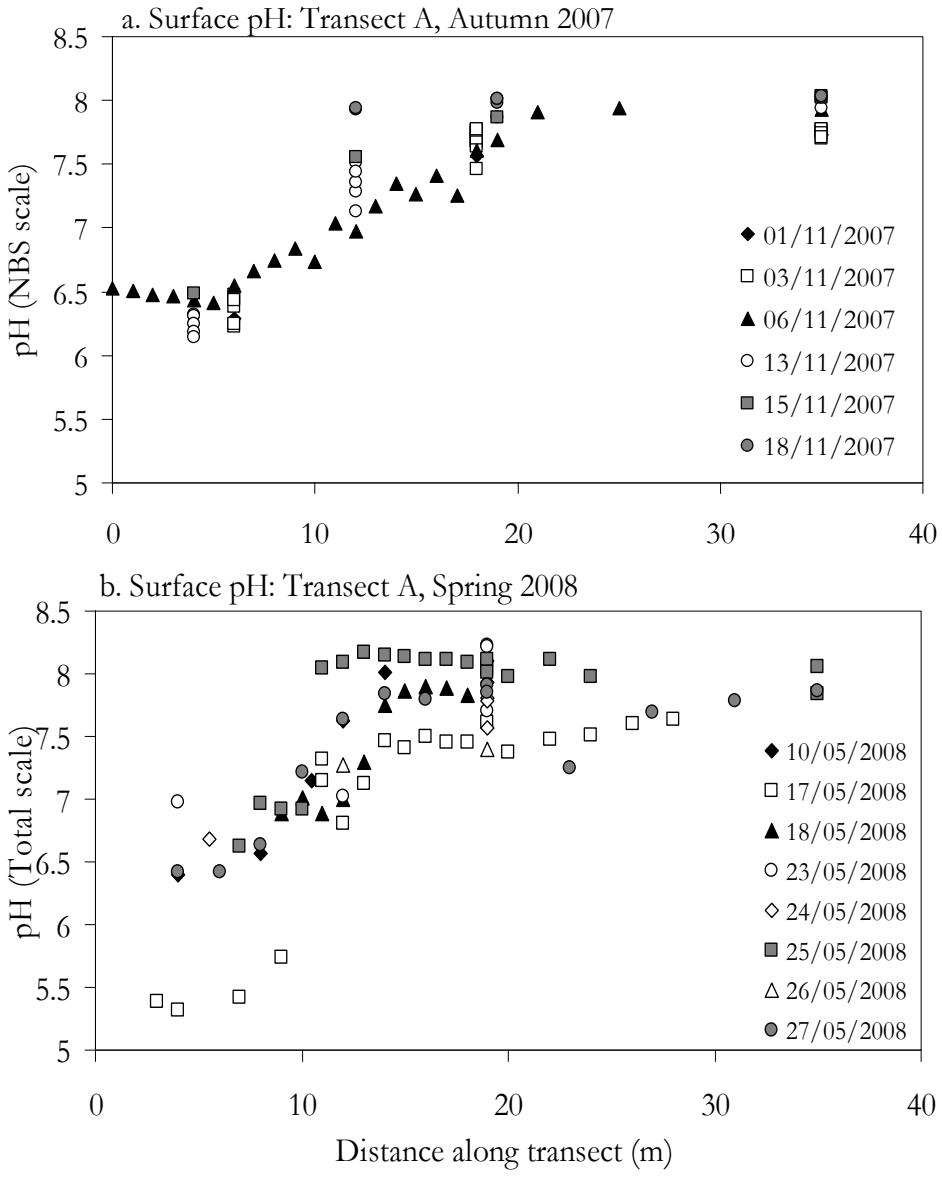

Figure 5.16. Surface pH readings along Transect A on different days during a. Autumn 2007 and b. Spring 2008.

5.4.3. Variability of pH with depth

Variability in pH was also observed with depth in the water column. Figure 5.17 (a – e) shows contour plots of pH along Transect A, using data from the period 10 – 27 May 2008 (Plots provided by S. Turner). The white lines indicate deployment of the YSI sonde, with each white point representing a data point. On 10 May, background pH levels were observed throughout the water column from a distance of only 14 m along the transect. The situation had greatly changed by 17 May, with a protrusion of low pH water extending out at depth to a distance of 24 m along the transect. Despite near background pH levels at the surface, the lower pH water was still detectable lower in the water column. One day later, the low pH feature visible the previous day had disappeared, suggesting some breakdown in the structure of the water column. However, there was a return to more structured conditions on 25 May, with low pH water again extending out at depth along the transect, with low pH water detectable in the bottom waters at 35 m. Two days later, on 27 May, the low pH water extended even further into the bay, detectable through the whole water column at 30 m, and even as far out as 55 m pH levels of around 7.7 – 7.8 were recorded. Therefore the temporal and spatial variability seen in surface pH measurements was also clearly seen in depth profiles, a demonstration of the highly dynamic nature of seawater pH at this site.

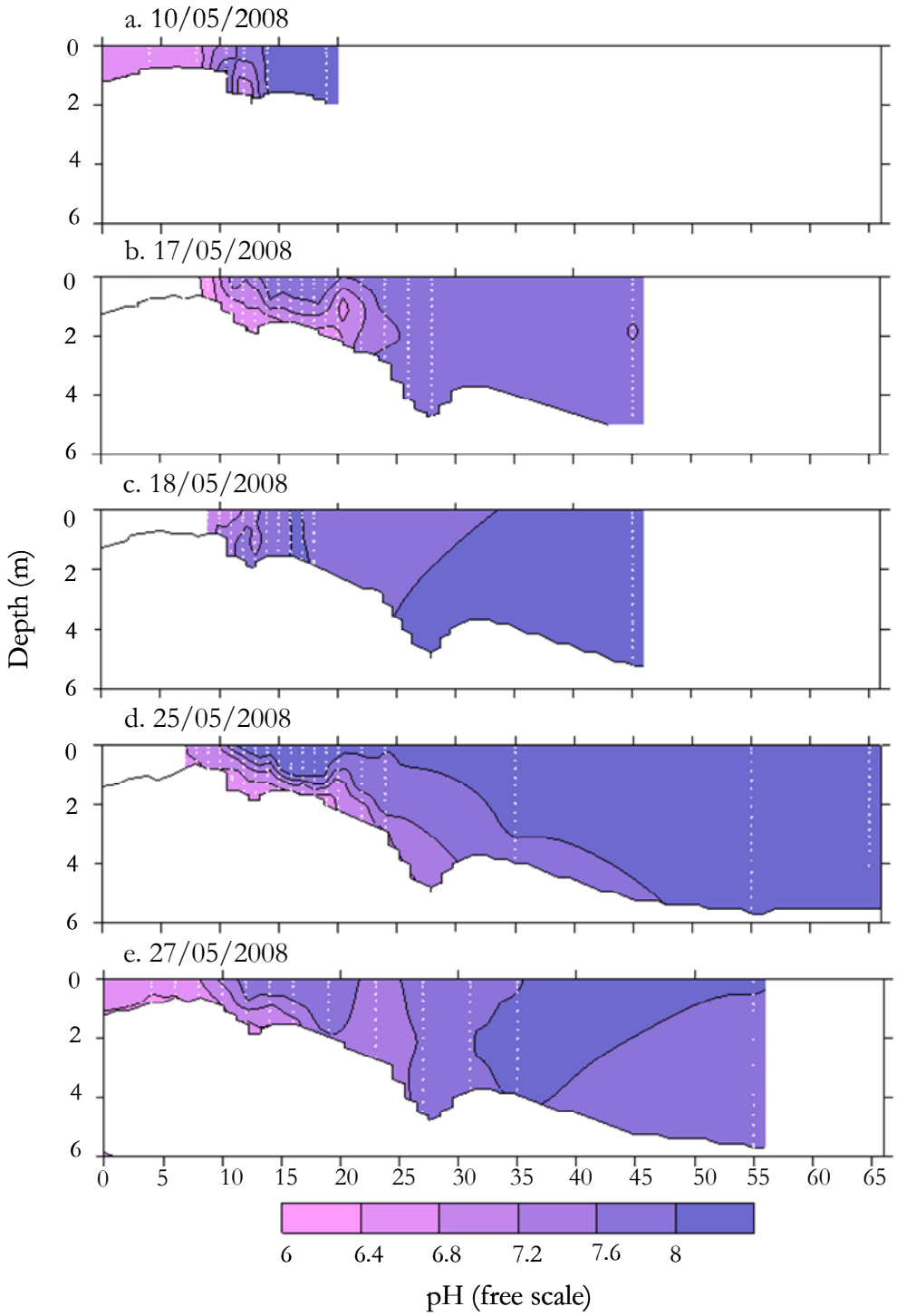

Figure 5.17. pH (Free scale) depth profiles along Transect A on a. 10/05, b. 17/05, c. 18/05, 25/05 and e. 27/05 during the Spring 2008 field campaign. White dotted lines indicate sonde deployment.

5.4.4. Variability of pH with time

During the Spring field campaign, the 19 m station on Transect A was selected as a regular sampling site as the pH measurements suggested that this station may

experience conditions that were representative of Year 2100 scenarios for OA (Caldeira and Wickett 2005; Raven *et al.* 2005). Table 5.3 shows mean pH measurements (± SD) at the 19 m station from both the autumn and spring field campaigns.

Table 5.3. Mean (± Standard deviation) of all pH readings made at 19m, Transect A during the Autumn 2007 field campaign, and all readings prior to Experiment 2 made during Spring 2008.

Season	Mean (± SD)	n
Autumn 2007	7.71 (± 0.28)	86
Spring 2008	7.70 (± 0.53)	54

Full depth profiles of temperature, salinity and pH were taken on seven days between 10 and 27 May at 19 m and contour plots of the profiles with time are shown in Figure 5.18 a, b and c. Overall, temperature ranged from 19.0°C to 21.5°C, and showed some variability with depth. Salinity showed only small variation (37.7 – 37.9).

pH depth profiles at 19 m (Figure 5.18 c – shown here in Freescale) also displayed variability over the course of May. For example, while background pH levels were observed on 10 May, by 17 May a protrusion of low pH water was seen at depth, and such variability was observed throughout the month. So although this station was selected to be representative of predicted Year 2100 surface pH levels, a large degree of temporal variability was observed during the Spring field campaign.

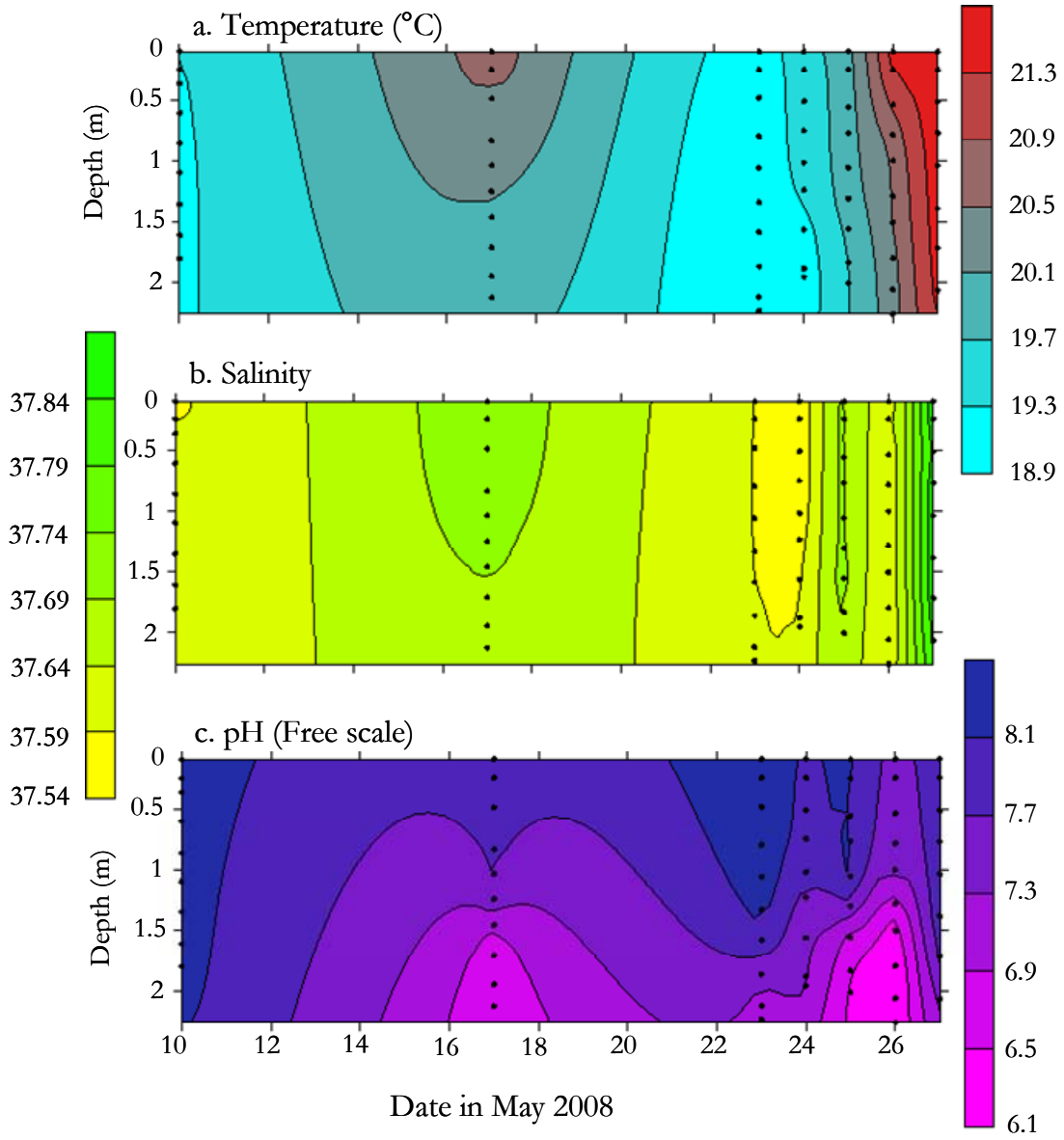

Figure 5.18. Depth profile contour plots of a. Temperature (°C), b. Salinity and c. pH (Free scale) against time, taken at 19m (Transect A).
Profiles were taken on 10/05, 17/05, 23/05, 24/05, 25/05, 26/05 and 27/05 during the Spring 2008 field campaign (indicated by black dots)

5.4.5. Summary and Conclusions

Following the assessment of the pH characteristics of the site, the following conclusions can be drawn:

- A clear horizontal pH gradient exists at this site, with increasing pH with distance along the transect away from the CO_2 vents. In this study, a maximum pH range of 5.6 – 8.1 was recorded during autumn 2007, and 5.3 – 8.2 during spring 2008 over a distance of <100 m.

- The general pH gradient is additionally characterised by hourly, daily, weekly, monthly and seasonal variability.
- The 19 m station on Transect A was chosen as a regular sampling site because it had a mean pH that is representative of Year 2100 scenarios for OA. However this station also experienced changes to pH both on short (minutes to weeks) and long (seasonal) time scales.
- Therefore, this site is not an ideal natural analogue of OA for assessing the impacts on the pelagic community. The hydrodynamics of the site lead to highly variable seawater pH, not enabling the pelagic community to adapt to the high CO_2 conditions. Additionally, there was evidence that the site is influenced by wind driven currents, from a predominantly S/SW direction. These currents bring fresh, unperturbed water, and pelagic organisms that are not adapted to high CO_2/low pH water to the site.

5.5 Biological Characteristics: Chlorophyll *a* and Phaeopigments

5.5.1. Chlorophyll a and Phaeopigments

Seawater samples for chlorophyll *a* and phaeopigment analysis were taken in conjunction with samples for trace gas analysis. As shown in Figure 5.19 a, chlorophyll *a* concentrations during the autumn field campaign ranged from 0.18 – 1.1 mg m^{-3}, with a mean of 0.52 mg m^{-3}. In addition chlorophyll *a* showed variation both on spatial and temporal scales. A general trend for increasing concentration with distance along the transect was observed, particularly on 13 and 15 November. On 18 November concentrations peaked at 12 m, with lower concentrations either side of this station along the transect. Chlorophyll *a* also exhibited some variation on different days. Concentrations were lowest on 13 November; on 15 and 18 November concentrations were of a more similar order, with the exception of 35 m and 100 m on 15 November where concentrations reached their maximum values.

During the autumn campaign, phaeopigment concentrations were low (<0.2 mg m^{-3}), or not detectable (Figure 5.19 b). At the 100 m station and at all sites on 18 November, no phaeopigments were detected. Where phaeopigments were observed, concentrations were found to be highest at 4 m, in very low pH waters, and progressively decreased with distance along the transect.

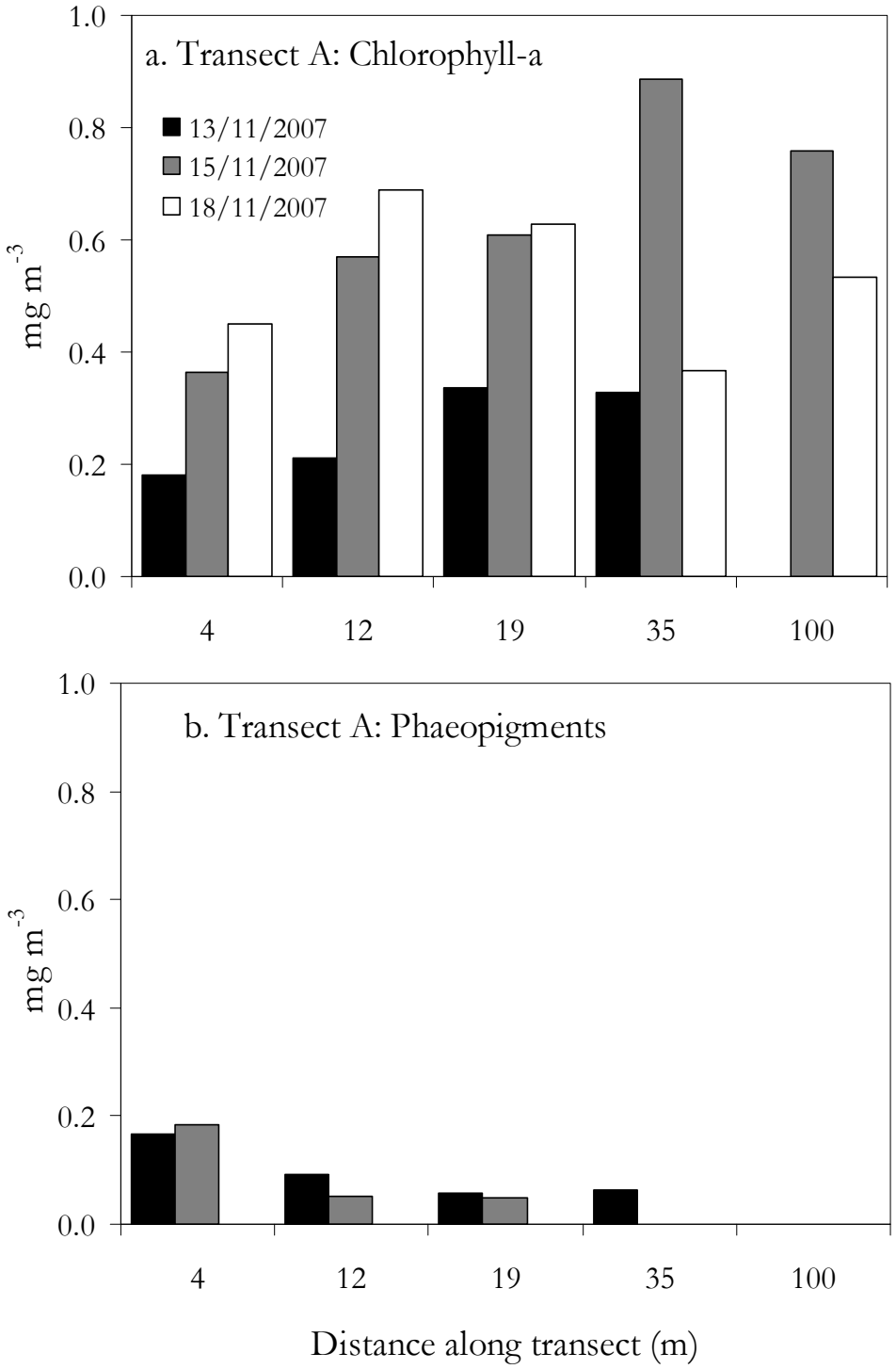

Figure 5.19. Surface concentrations of a. Chlorophyll *a* and b. Phaeopigments (mg m^{-3}) at 4m, 12m, 19m, 35m and 100m along Transect A. Measurements taken on 13, 15 and 18 November 2007. Legend shown in panel a. Phaeopigments were not detected on 15 November at 35 m, or on 18 November at all stations. No data was collected on 13 November at 100 m.

Chlorophyll *a* concentrations measured during the spring field campaign (Figure 5.20 a) were lower than those encountered during autumn, with a range of 0.1 – 0.5 mg m^{-3} and a mean of 0.29 mg m^{-3}. Also in contrast to the autumn data, there was no obvious trend along the pH gradient, and there was less temporal variability in concentrations.

Interestingly, phaeopigment concentrations (Figure 5.20 b) were generally higher than chlorophyll *a*, although there was a greater degree of temporal and spatial variability. Concentrations were highest on 18 November, also coinciding with some of the highest chlorophyll *a* concentrations. Again there were no clear trends in phaeopigment concentration along the transect with respect to changes in pH.

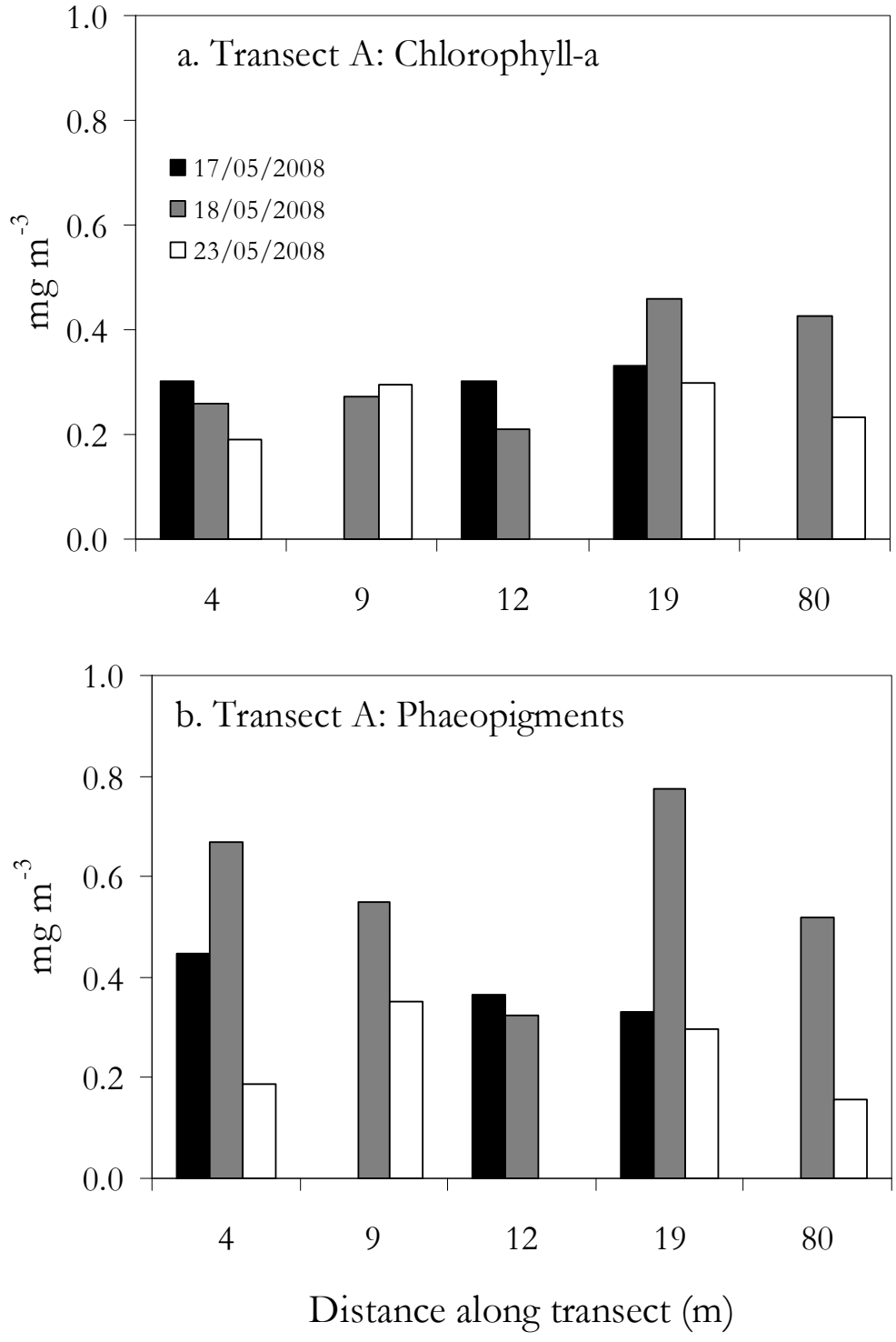

Figure 5.20. Surface concentrations of a. Chlorophyll *a* and b. Phaeopigments (mg m^{-3}) at 4m, 12m, 19m, 35m and 100m along Transect A. Measurements taken on 17, 18 and 23 May 2008. Legend shown in panel a.

5.5.2. Conclusions

The chlorophyll *a* concentrations measured at this site were low in comparison to a previous study of mean surface chlorophyll *a* concentrations from elsewhere in the Gulf of Naples for the period 1984 – 2000. Ribera d'Alcalà *et al.* (2007) reported a mean for May of ~6 mg m^{-3}, and this month also generally saw the highest concentrations of the year. Furthermore, mean concentrations of ~ 1 mg m^{-3} for November were reported. During this study, autumn concentrations did not exceed 1 mg m^{-3} and concentrations were even lower during the spring field campaign (0.2 – 0.5 mg m^{-3}). This suggests that in comparison to the Gulf of Naples as a whole, phytoplankton communities were far less prolific at this site.

5.6 Impacts of pH on the Pelagic Community: "Transplantation" Experiments

5.6.1. Introduction

During the assessment of this site it was important to determine whether the pelagic community was showing adaptation to the high CO_2/low pH conditions. Alternatively were they subject to tidal and wave-driven currents that rapidly washed them into and out of the high CO_2 zone, subjecting them to a toxic shock effect? A previous study reported that growth rates of a number of diatoms dropped by between 70 and 100 percent when pH was lowered from ambient seawater pH levels to 6.0 (Hinga 2002). Therefore, would any changes in trace gas concentrations along the pH gradient be a sign of adaptation and changing production mechanisms, or simply an indicator of a stressed phytoplankton population?

To test these hypotheses, two replicate phytoplankton "transplantation" experiments were carried out. Sections of dialysis tubing were used to incubate seawater samples (BioDesign Inc. Cellulose, 8kDa). Dialysis tubing was chosen for these experiments as it allows water and gas to pass through, but does not allow the passage of particles greater than 8 kDa. Therefore phytoplankton collected from background pH levels would be exposed to altered seawater chemistry over the course of the incubation. The dialysis tubing was cut into 100cm sections and knots were tied in one end. 6 sections of tubing were filled with seawater from the background pH site iii (Figure 5.3) and a knot tied in the other end to seal them. Two were moored at 30 –

50 cm depth at the background pH site in order to act as a control. A further two were moored at the same depth at the 19 m station on Transect A. In Experiment 1, the final two were moored at 5m along Transect A, in extremely low pH of about 6. However, in Experiment 2 the 12 m station on Transect A was selected, as it was deemed to be more representative of future seawater pH conditions than the 5 m stataion. The dialysis bags were left for 24 hours. Samples were taken at T_0 and T_{Final} for chlorophyll *a* extraction, and FIRe analysis.

5.6.2. Experiment 1: 24 – 25 May 2008

5.6.2.1. Seawater pH and temperature

The seawater pH of the three chosen sites for the first dialysis experiment varied greatly, both between sites, and also within individual sites. At 5m on Transect A, with a depth of 0.5m, the pH at T_0 was 6.7 at the surface and 6.4 at the bottom. 24 hours later, at T_F, the pH had not changed greatly, with readings of 6.6 at the surface and 6.4 at the bottom. At 19m on Transect A, quite wide variation in pH was observed over the course of the experiment, as shown on Figure 5.21. At T_0, readings of 7.8 at the surface and 7.5 at the bottom were recorded. At T_{Final}, surface pH levels were 8.03, with a large gradient in pH with increasing depth in the water column, down to 6.35 at the bottom. The background control site (iii) displayed background pH levels of between 8.0 and 8.2 that were well mixed down the water column (See Figure 5.21, solid circles).

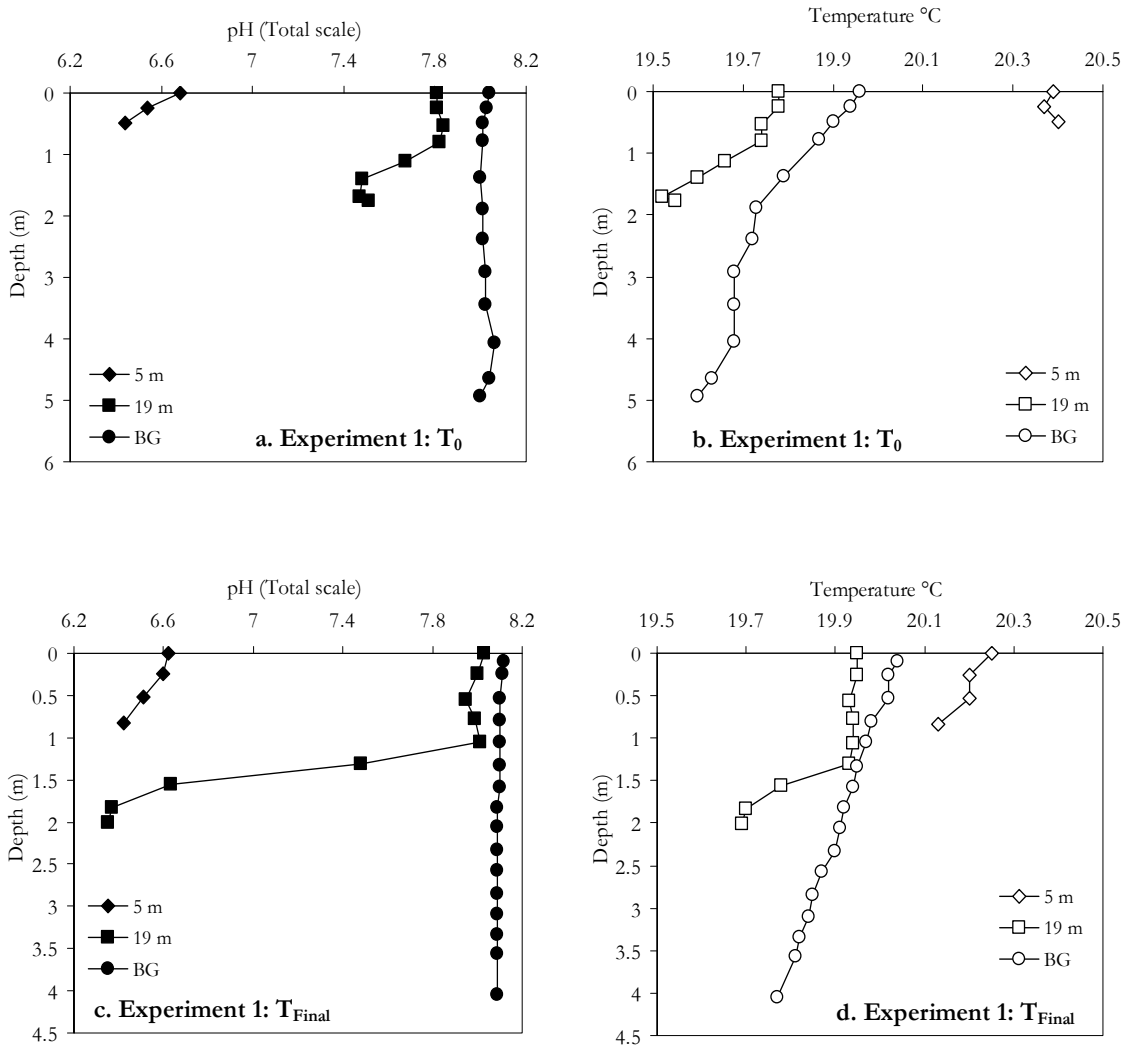

Figure 5.21. Profiles of pH (Total scale) and Temperature (°C) at 5m, 19m and a background (BG) control site (iii) on Transect A, at T_0 (a and b) and T_{Final} (c and d) for dialysis Experiment 1, 24 – 25 May 2008.

5.6.2.2. Chlorophyll *a* and Photosynthetic Efficiency

Figure 5.22 a shows T_0 and T_{Final} chlorophyll *a* and phaeopigments concentrations, and Figure 5.22 b shows the same data points for Fv/Fm. Chlorophyll *a* concentrations measured at T_0 were 0.29 mg m^{-3} and phaeopigments were 0.16 mg m^{-3}. After 24 hours of incubation in low pH conditions at 5 m, chlorophyll *a* and phaeopigments levels had fallen by an average of 64 percent and 52 percent, respectively (See Table 5.4). No information is available on the changes in Fv/Fm at this site as the data was lost.

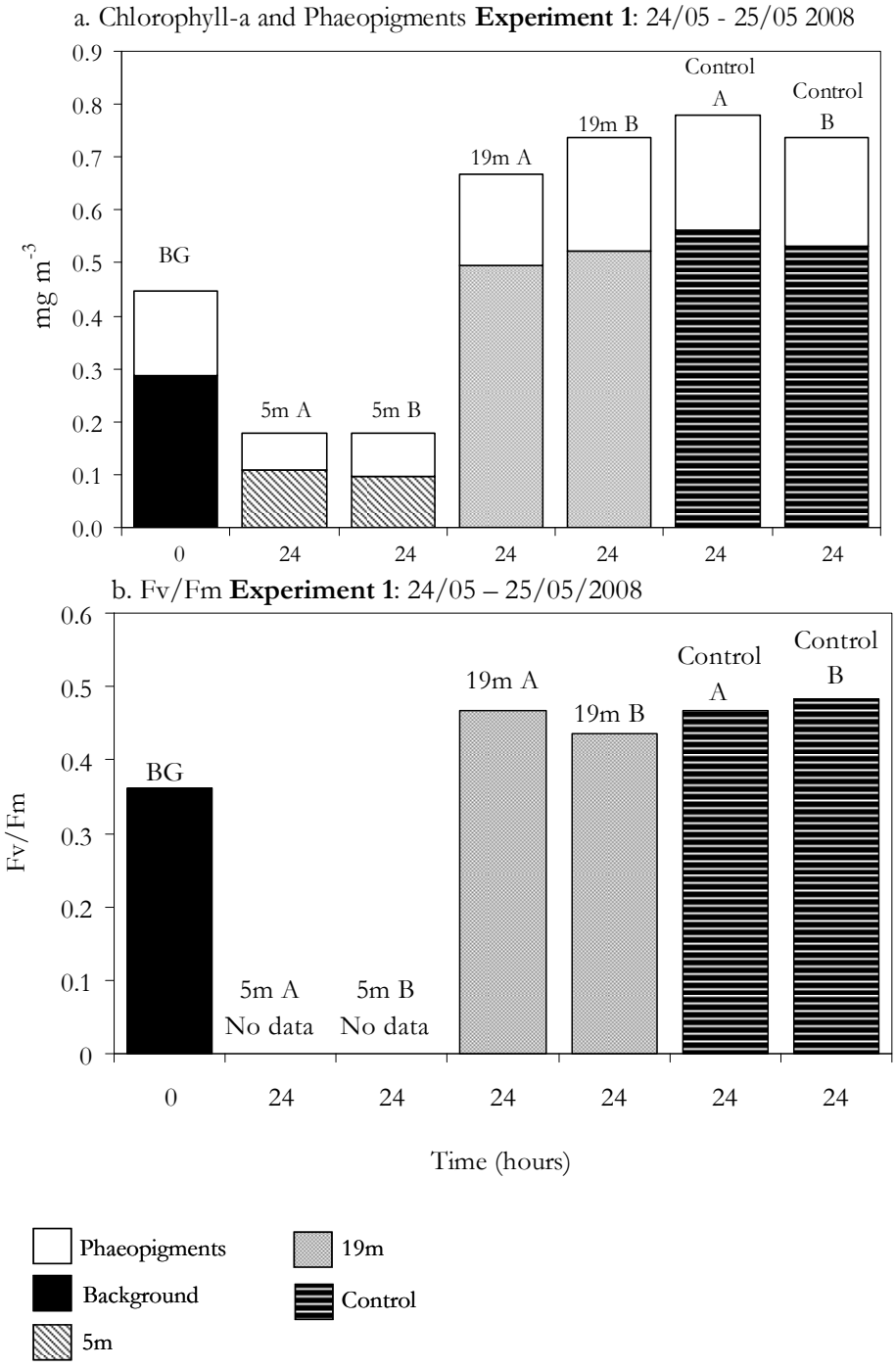

Figure 5.22. a. Chlorophyll *a* and Phaeopigment concentrations (mg m^{-3}) and b. Fv/Fm over the course of the dialysis Experiment 1 24 – 25 May 2008. T_0 are the values at background pH levels. A and B represent replicate dialysis tubes.

At 19m, both chlorophyll *a* and phaeopigments increased in concentration after 24 hours, with mean increases of 43 percent and 17 percent, respectively (Figure 5.22 a and Table 5.4). Similarly, an increase in photosynthetic efficiency was observed (Figure 5.22 b and Table 5.5). At the control site iii, the greatest increases in both chlorophyll *a* and phaeopigments were observed. Chlorophyll *a* increased by an

average of 47 percent, whilst phaeopigments went up by an average of 26 percent. Photosynthetic efficiency did not increase by as much as at the 19 m site.

Table 5.4. Summary of Dialysis Experiment 1: Chlorophyll *a* and phaeopigments concentrations at T_0 and T_{Final}, and percentage changes.

Site	Time (hours)	Chlorophyll *a* µg l^{-1}	% Change	Phaeopigments µg l^{-1}	% Change
Background	0	0.288	-	0.158	-
5m A	24	0.108	**-62.5**	0.069	**-56.3**
5m B	24	0.097	**-66.3**	0.082	**-48.1**
19m A	24	0.496	**+41.9**	0.173	**+8.7**
19m B	24	0.524	**+45.0**	0.213	**+25.8**
Control A	24	0.561	**+48.7**	0.219	**+27.9**
Control B	24	0.531	**+45.8**	0.206	**+23.3**

Table 5.5. Summary of Dialysis Experiment 1: Fv/Fm at T_0 and T_{Final}, and percentage changes.

Site	Time (hours)	Fv/Fm	% Change
Background	0	0.362	-
5m A	24	NO DATA	-
5m B	24	NO DATA	-
19m A	24	0.467	**+22.5**
19m B	24	0.436	**+25.1**
Control A	24	0.468	**+22.6**
Control B	24	0.483	**+17.0**

5.6.3. Experiment 2: 26 – 27 May 2008

5.6.3.1. Seawater pH and temperature

Figure 5.23 shows profiles of pH (Total scale) (a and c) and temperature (°C) (b and d) at T_0 and T_{Final} for the second dialysis experiment. At T_0 only surface measurements are available for the background site (solid and open circles). Full profiles were made at T_{Final}. The pH at T_0 showed some similarity at the 12m and 19m sites, with surface values of 7.3 – 7.4, followed by a strong decreasing gradient down the water column to 5.9 – 6.03 at the bottom. The background control site displayed a much higher surface pH of 8.16. The water depth at the three sites varied, with 2m at 12m, 1.8m at 19m and 5.4m at the background site.

By T_{Final}, the pH at 12m and 19m had increased, and the gradient down the water column less pronounced. At 12m it ranged from 7.6 at the surface to 6.6 at the bottom, while at 19m from 7.9 to 7.3. By contrast, the background site displayed relatively uniform pH levels down the water column, ranging from 7.7 – 7.9. However, these pH readings were somewhat lower than the surface reading taken at T_0.

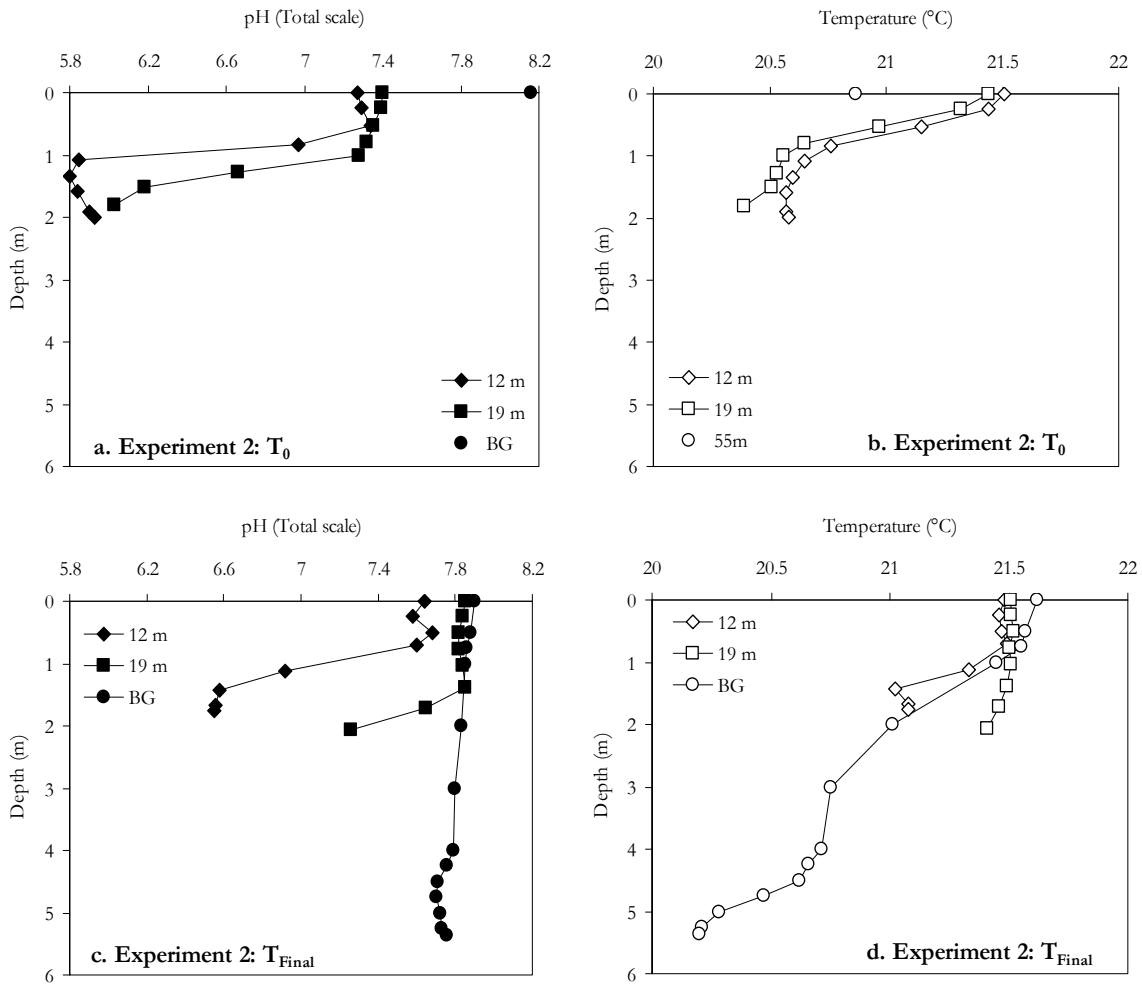

Figure 5.23. Profiles of pH (Total scale) and Temperature (°C) at 12m and 19m on Transect A, at T_0 (a and b) and T_{Final} (c and d) for dialysis Experiment 1, 26 – 27 May 2008.

5.6.3.2. Chlorophyll *a* and Photosynthetic Efficiency

During the second dialysis experiment, a number of samples were lost as they came free of their moorings and drifted away during the night. As a result chlorophyll *a* data is available for the only the background T_0 reading, and for T_{Final}, duplicate samples at 12m, and a single sample at 19m. In addition, Fv/Fm measurements were lost due to an instrumentation error.

Similarly to Experiment 1, the 19m station saw increases in the concentrations of chlorophyll *a* and phaeopigments over the course of the incubation, relative to the T_0 background concentrations (Figure 5.24). As shown in Table 5.6, both chlorophyll *a* and phaeopigments showed an increase. The 12m station gave quite opposing results,

with a mean decrease in chlorophyll *a* concentrations, accompanied by a decrease in phaeopigments.

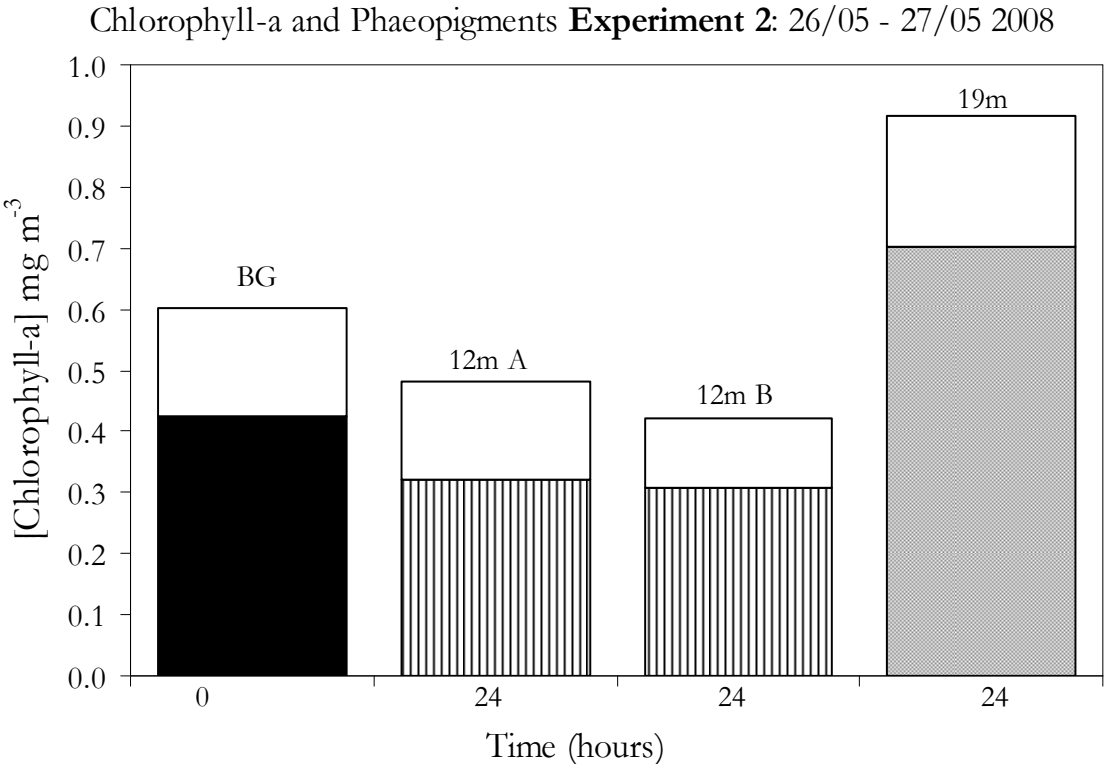

Figure 5.24. Chlorophyll *a* and Phaeopigment concentrations (mg m^{-3}) over the course of the dialysis Experiment 2 26 – 27 May 2008
T_0 are the values at background pH levels.

Table 5.6. Summary of Dialysis Experiment 2: Chlorophyll *a* and phaeopigments concentrations at T_0 and T_{Final}, and percentage changes.

Site	Time (hours)	Chlorophyll *a* µg l-1	% Change	Phaeopigments µg l-1	% Change
Background	0	0.424	-	0.179	-
12m A	24	0.321	**-24.3**	0.160	**-10.6**
12m B	24	0.308	**-27.4**	0.114	**-36.3**
19m	24	0.702	**+39.6**	0.215	**+16.7**

5.6.4. Summary and Conclusions

Two incubation experiments were performed using dialysis membrane tubing to determine the impact of sudden exposure to low pH conditions on the pelagic community at the study site. During Experiment 1, samples were incubated at 5 m, 19 m and at a control site on Transect A. For Experiment 2, incubations were performed at 12 m, 19 m and a control site.

After 24 hours of incubation during Experiment 1, samples at the 5 m site (pH 6.4 – 6.7) saw a pronounced drop in concentrations of chlorophyll *a* and phaeopigments (64 percent and 52 percent, respectively), implying that these conditions were not conducive to growth and survival of phytoplankton. By contrast, at the 19m site (pH 6.3 – 7.8) the planktonic community appeared to benefit from a variable pH regime, with increased chlorophyll *a*, phaeopigments and Fv/Fm (43 percent, 17 percent and 24 percent, respectively), suggesting a healthy and thriving population. Conditions were most favourable at the control site, with the greatest increases in chlorophyll *a* and phaeopigments (mean 47 percent and 26 percent, respectively) and a mean 20 percent increase in Fv/Fm.

Growth was clearly diminished in the communities incubated in the extremely low pH conditions at 5 m, and the organisms were likely to be experiencing a toxic shock effect when washed into this region of the site. Despite the relatively low and fluctuating pH experienced by the organisms at the 19 m station, the available data suggests that the community were able to cope and even thrive in these perturbed conditions. However, the overall health of the population was reduced in comparison to the organisms that were incubated at background pH levels.

Although less data are available for Experiment 2, the 19 m station showed a similar response to Experiment 1. Both chlorophyll *a* and phaeopigments increased (40 percent and 17 percent, respectively), despite the community potentially being exposed to low and wide ranging pH levels over the course of the 24 hour incubation (pH 6.0 – 7.9). Only a few metres away at the 12 m station, the results were quite different. Although the pH experienced by the organisms at T_0 and T_{Final} was only slightly lower (pH 5.8 – 7.7), both chlorophyll *a* and phaeopigments decreased by 26 percent and 23 percent, respectively. This suggests that the conditions experienced at 12 m were less conducive to healthy phytoplankton populations.

This experimental data suggests that if phytoplankton are washed into the very low pH conditions such as those seen at 5 m on Transect A, they are likely to become stressed and unhealthy very quickly, and cannot thrive in these conditions.

Despite a slightly lowered pH at 19m, data from two incubation experiments suggests that phytoplankton are not adversely affected by such conditions. Only a few metres further into the low pH zone (12 m), conditions are less favourable for phytoplankton growth.

It must be considered that these incubations were not performed in ideal conditions as the pH showed variability between T_0 and T_{Final}, making it difficult to predict what pH may have been experienced during the 24 hours they were *in situ*. However, there does appear to be some effect of the general pH regime experienced by the organisms.

The results of these incubations suggest that the highly variable seawater pH at this site renders it non-ideal for trace gas studies on the pelagic ecosystem. Nevertheless, perhaps in a non-ocean acidification context, there is information to be gained on the production of trace gases by the benthic communities found at this site.

5.7 Biogenic Trace Gases: Trends and Characteristics

5.7.1. Temporal and Spatial Trends

5.7.1.1. Iodocarbons, Autumn 2007

Surface iodocarbon concentrations during the autumn field campaign displayed both temporal and spatial variability. Figure 5.25 shows surface concentrations of a. 2-C_3H_7I, b. 1-C_3H_7I, c. CH_2I_2 and d. CH_2ClI on 13, 15 and 18 November 2007 at stations 4, 12, 19, 35 and 100 m along Transect A. Concentrations of iodocarbons were < 4 pM. 2-C_3H_7I and CH_2I_2 generally decreased with distance along Transect A, although this trend was not consistent, and some variability between sampling days was observed. Surface concentrations of 1-C_3H_7I and CH_2ClI showed less variation along the transect and no obvious trends were observed.

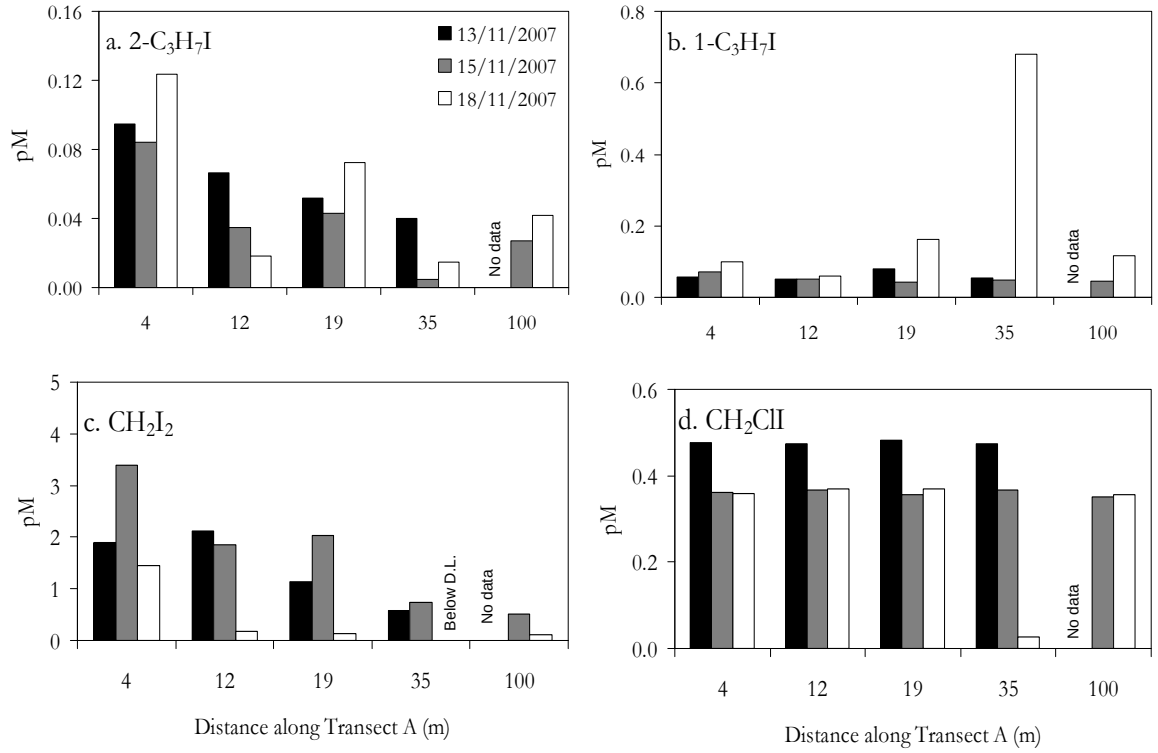

Figure 5.25. Surface concentrations of a. 2-C_3H_7I, b. 1-C_3H_7I, c. CH_2I_2, d. CH_2ClI (pM) at 4m , 12m, 19m, 35m and 100m on Transect A. Measurements were taken on 13 (Black), 15 (Grey) and 18 November 2007 (White). Legend is shown in panel a. No data was collected at 100 m on 13 November. CH_2I_2 at 35 m on 15 November was below the detection limit (D.L.) of 0.3 pM (see Chapter 2, Table 2.3). Data is based on analysis of single samples.

5.7.1.2. Iodocarbons, Spring 2008

Figure 5.26 shows surface and bottom concentrations of a range of iodocarbons at 4 m, 12 m, 19 m, 35 m and 80 m along Transect A during May 2008. Concentrations of 2-C_3H_7I (a and b) ranged from below detection limit to 4.3 pM, with maximum concentrations recorded at 19 m on 27 May at the bottom. However, this maximum appeared to be anomalous, and concentrations on most other days were higher in surface waters than at the bottom. Concentrations of 1-C_3H_7I in surface waters (c) were below DL on most days, but was detected in some bottom samples. CH_2ClI was detected in all samples along Transect A, with similar mean concentrations in surface and bottom waters. CH_2I_2 (g and h) was below DL in all surface samples, and only detectable in two bottom samples. No clear changes in concentrations of iodocarbons with respect to the pH gradient were observed.

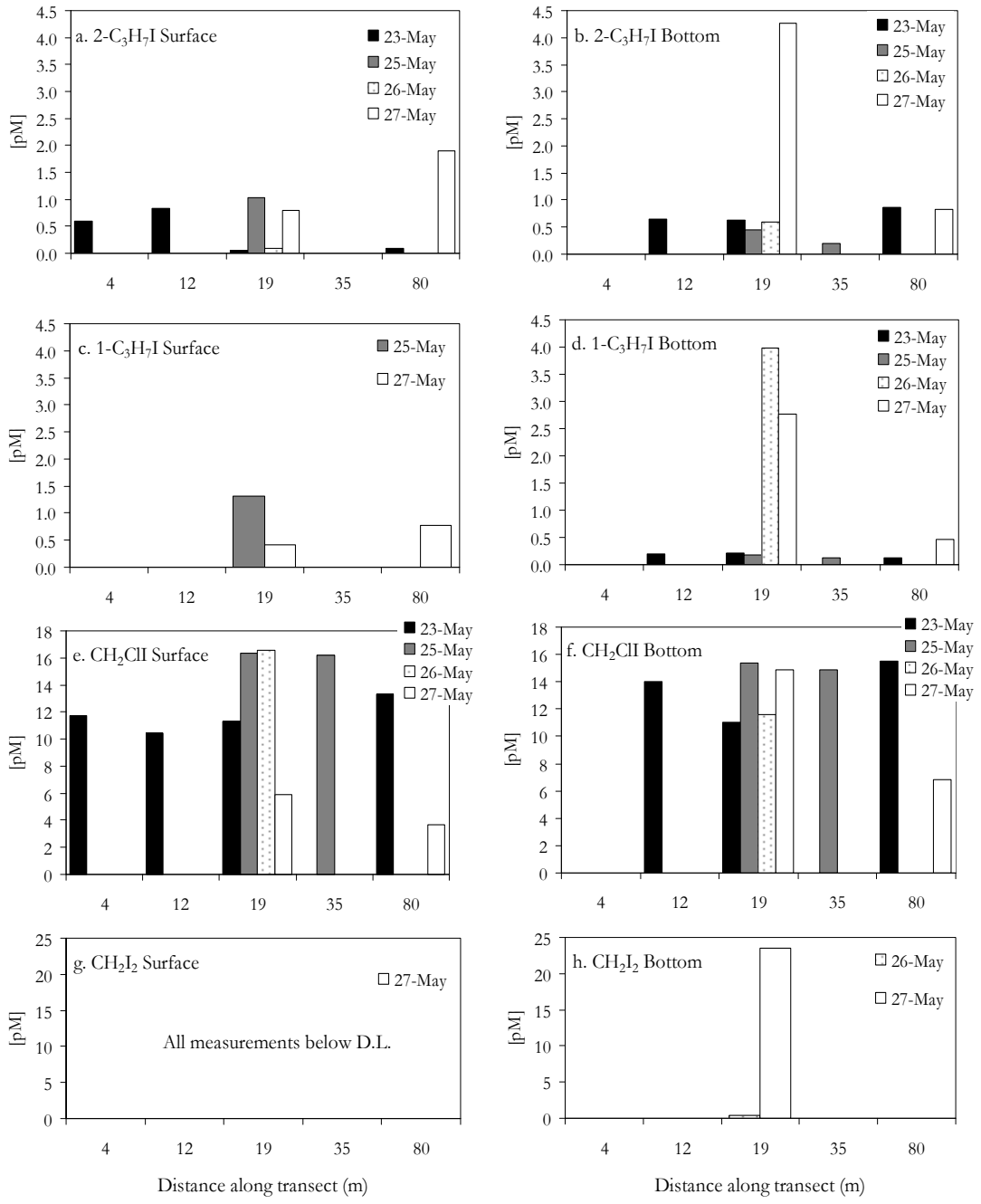

Figure 5.26. Concentrations (pM) of a. 2-C_3H_7I Surface, b. 2-C_3H_7I Bottom, c. 1-C_3H_7I Surface , d. 1-C_3H_7I Bottom, e. CH_2ClI Surface, f. CH_2ClI Bottom, g. CH_2I_2 Surface and h. CH_2I_2 Bottom at 4m , 12m, 19m, 35m and 80m on Transect A. Measurements were taken on 23, 25, 26 and 27 May 2008. CH_2I_2 was below D.L. for all surface samples, and for bottom measurements on 23 May at 12 m and 80 m, and on 25 May at 19 m and 35 m. 1-C_3H_7I was below D.L. for surface samples on 23 May at 12 m, 19 m and 80 m , and on 26 May at 19 m and 35 m (CH_2I_2 D.L = 0.3 pM, 1-C_3H_7I D.L. = 0.1 pM, see Table 2.3). Remaining missing data = no data collected.

5.7.1.3. Bromocarbons, Autumn 2007

Surface concentrations of $CHBr_3$ and CH_2Br_2 showed a high degree of spatial similarity (Figure 5.27), although concentrations of CH_2Br_2 were approximately 10-fold lower than $CHBr_3$. Both showed variation between sampling days and with distance along the transect. No clear trends with distance along the transect were observed, with the variability between sampling days dominating the data.

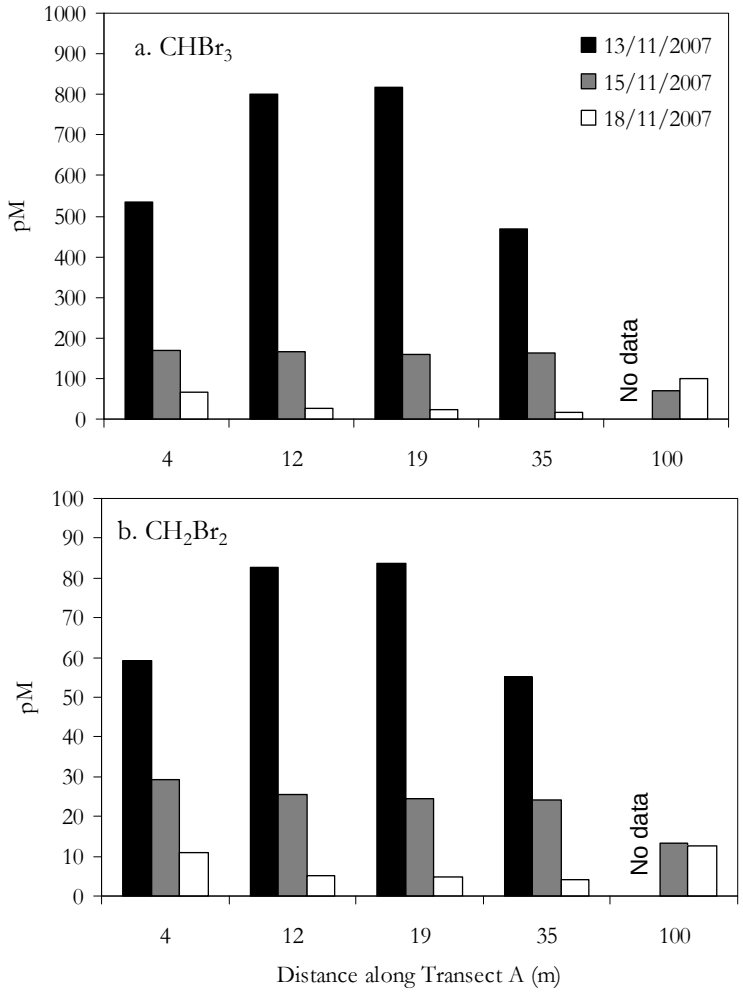

Figure 5.27. Surface concentrations of a. $CHBr_3$, and b. CH_2Br_2 (pM) at 4m , 12m, 19m, 35m and 100m on Transect A. Measurements were taken on 13 (Black), 15 (Grey) and 18 November 2007 (White). Legend is shown in panel a. No data was collected at 100 m on 13 November.

5.7.1.4. Bromocarbons, Spring 2008

Figure 5.28 shows surface and bottom concentrations of bromocarbons along Transect A on 23, 25, 26 and 27 May 2008. As a whole, concentrations were higher in bottom waters compared to surface waters (See Table 5.7). Concentrations in both surface and bottom waters were generally lowest at 80 m, although low

concentrations were also recorded at 19 m on 27 May. Despite lower concentrations at 80 m, no clear trends in concentrations with distance along the pH gradient were observed. Concentrations of CH_2Br_2 (c and d) were around 10-fold lower than $CHBr_3$, a trend repeatedly observed at this site. Similarly to $CHBr_3$, although the lowest concentrations were seen at 80 m, no clear trends with respect to the pH gradient were observed. In common with the other bromocarbons, mean concentrations of $CHBr_2Cl$ were elevated in bottom waters (Mean 21.1 pM compared to 15.4 pM) and despite lower concentrations at 80 m, no obvious changes in concentrations along the transect were observed. CH_2BrI was only detected in one surface sample along Transect A (19 m), and in four bottom samples.

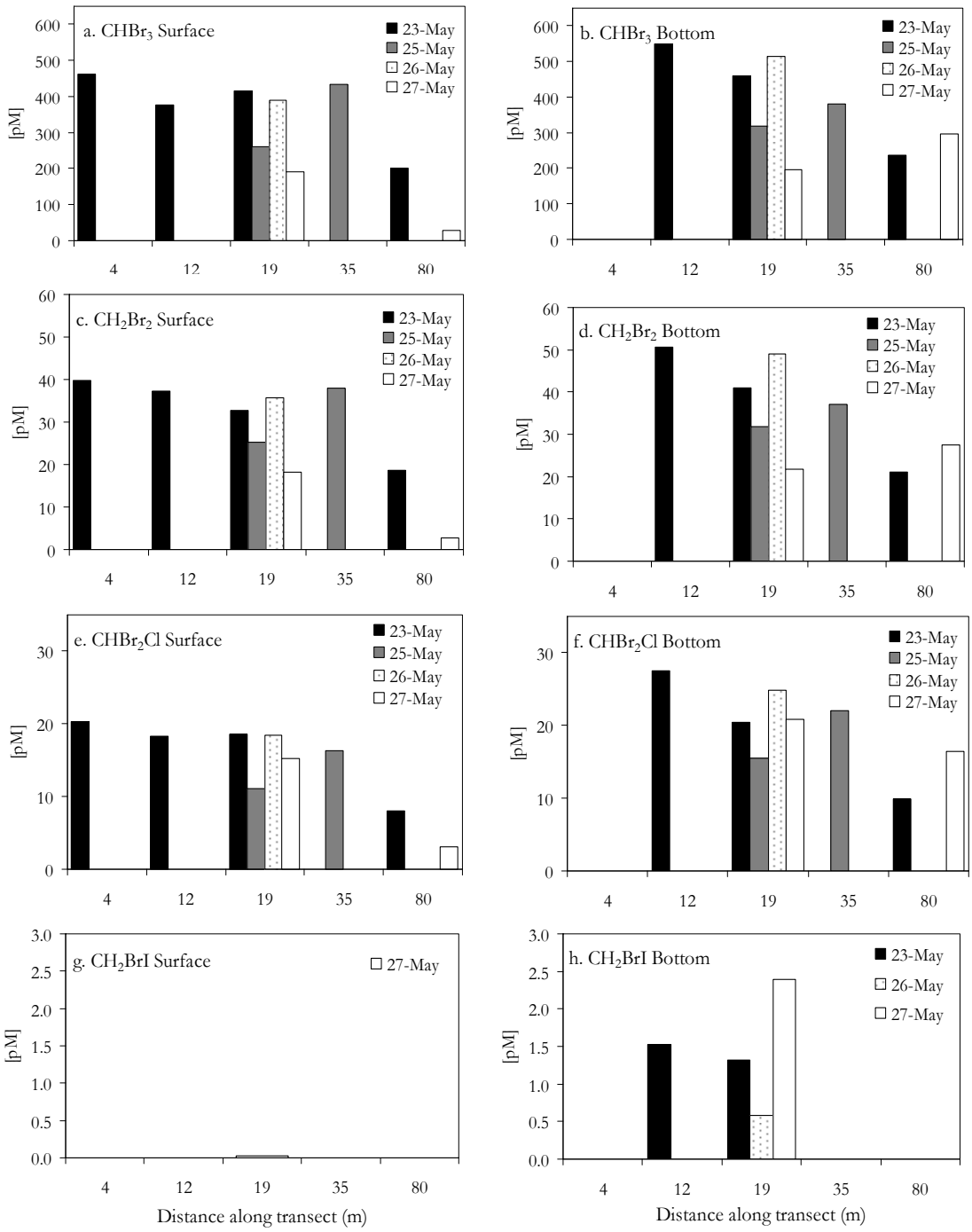

Figure 5.28. Concentrations (pM) of a. $CHBr_3$ Surface, b. $CHBr_3$ Bottom, c. CH_2Br_2 Surface , d. CH_2Br_2 Bottom, e. $CHBr_2Cl$ Surface, f. $CHBr_2Cl$ Bottom, g. CH_2BrI Surface and h. CH_2BrI Bottom at 4m , 12m, 19m, 35m and 80m on Transect A.
Measurements were taken on 23, 25, 26 and 27 May 2008. CH_2BrI was below D.L. for all surface samples on 23, 25, 26 May, and at 80 m on 27 May, and for bottom measurements on 23 May at 80 m, all samples on 25 May and 80 m on 27 May. CH_2BrI D.L = 1 pM. Remaining missing data = no data collected.

5.7.2. Seasonal Variability

Some variability was observed in concentrations of halocarbons between autumn and spring, indicating a degree of seasonal variability. Table 5.7 shows mean surface and bottom concentrations (± standard deviation) for autumn and spring. Mean concentrations of iodocarbons were higher in both surface and bottom waters during spring, suggesting that production of these compounds is elevated at this time of year. Similarly, mean concentrations of $CHBr_3$ were higher during Spring. Concentrations of CH_2Br_2 did not display much seasonal variability, with similar concentrations in both surface and bottom waters during both seasons. $CHBr_2Cl$ and CH_2BrI were only quantified during the Spring field campaign so no comparisons can be drawn.

Table 5.7. Mean concentrations (pM) ± standard deviation (SD) from surface and bottom water samples along Transect A during the Autumn 2007 and Spring 2008 field campaigns.

	Surface Concentrations (pM) Mean (±SD)		**Bottom Concentrations (pM) Mean (±SD)**	
	Autumn 2007	**Spring 2008**	**Autumn 2007**	**Spring 2008**
2-C_3H_7I	0.1 (±0.04)	0.5 (±0.6)	0.04 (±0.02)	0.93 (±1.1)
1-C_3H_7I	0.1 (±0.2)	0.2 (±0.4)	0.2 (±0.3)	1.8 (±3.6)
CH_2ClI	0.4 (±0.1)	12.9 (±4.6)	0.4 (±0.2)	12.6 (±5.2)
CH_2I_2	1.3 (±1.0)	-	1.2 (±0.9)	2.2 (±7.0)
$CHBr_3$	243.0 (±275.3)	327.9 (±133.0)	368.7 (±251.9)	407.9 (±129.3)
CH_2Br_2	27.6 (±27.4)	29.6 (±11.3)	40.3 (±19.1)	38.8 (±11.8)
$CHBr_2Cl$	-	15.4 (±5.4)	-	21.1 (±5.3)
CH_2BrI	-	0.002 (±0)	-	0.7 (±1.5)

5.7.3. Temporal variability at 19 m, Transect A

As described previously in Section 5.4.5, the 19 m station on Transect A was selected as a regular sampling site as pH measurements from the autumn campaign suggested that this site may experience conditions that were representative of Year 2100 scenarios for OA. pH, temperature, salinity and trace gas measurements

(surface and bottom) were made at this station on a number of days over the course of May 2008 in an attempt to characterise this potential OA analogue site.

Concentrations of iodocarbons showed some variation over the course of 23 – 27 May 2008. Daily mean concentrations of a. 2-C_3H_7I, b. 1-C_3H_7I, c. CH_2I_2 and d. CH_2ClI at the surface (Solid circles) and bottom (Open squares) at 19 m are plotted in Figure 5.29, with daily replicate samples shown as smaller symbols. Concentrations of 2-C_3H_7I and 1-C_3H_7I were generally higher at the bottom, with the exception of 25 May when surface concentrations were greatest. Surface concentrations of 2-C_3H_7I and 1-C_3H_7I also showed similar temporal trends. Concentrations of CH_2ClI were generally higher at the surface than the bottom. Both maximum and minimum concentrations were recorded on 26 May, demonstrating the variable nature of the seawater concentrations over small time scales. On 27 May, concentrations at the bottom exceeded those at the surface, a contradiction to the trend seen on previous days. CH_2I_2 concentrations were very low or below DL for the whole period, with the exception of 27 May when an anomalous concentration of 23.4 pM was recorded in a bottom water sample.

Concentrations of bromocarbons at the 19 m station, shown in Figure 5.30, also displayed some variation over the course of 23 – 27 May. Concentrations of all bromocarbons were higher at the bottom than the surface waters and the difference was found to be statistically significant for CH_2BrCl (T-test, T = 2.82, p = 0.015). CH_2Br_2, $CHBr_2Cl$ and $CHBr_3$ displayed similar trends. Concentrations of CH_2BrI in surface waters were below DL, while concentrations ranging between below DL and 2.4 pM were measured at the bottom.

In summary, concentrations of halocarbons at 19m on Transect A varied both with depth in the water column, and on a day-to-day basis. Concentrations of iodocarbons were generally higher at the surface, while the opposite was true for the bromocarbons. Similar temporal trends were seen for 2-C_3H_7I and 1-C_3H_7I, and for CH_2Br_2, $CHBr_2Cl$ and $CHBr_3$.

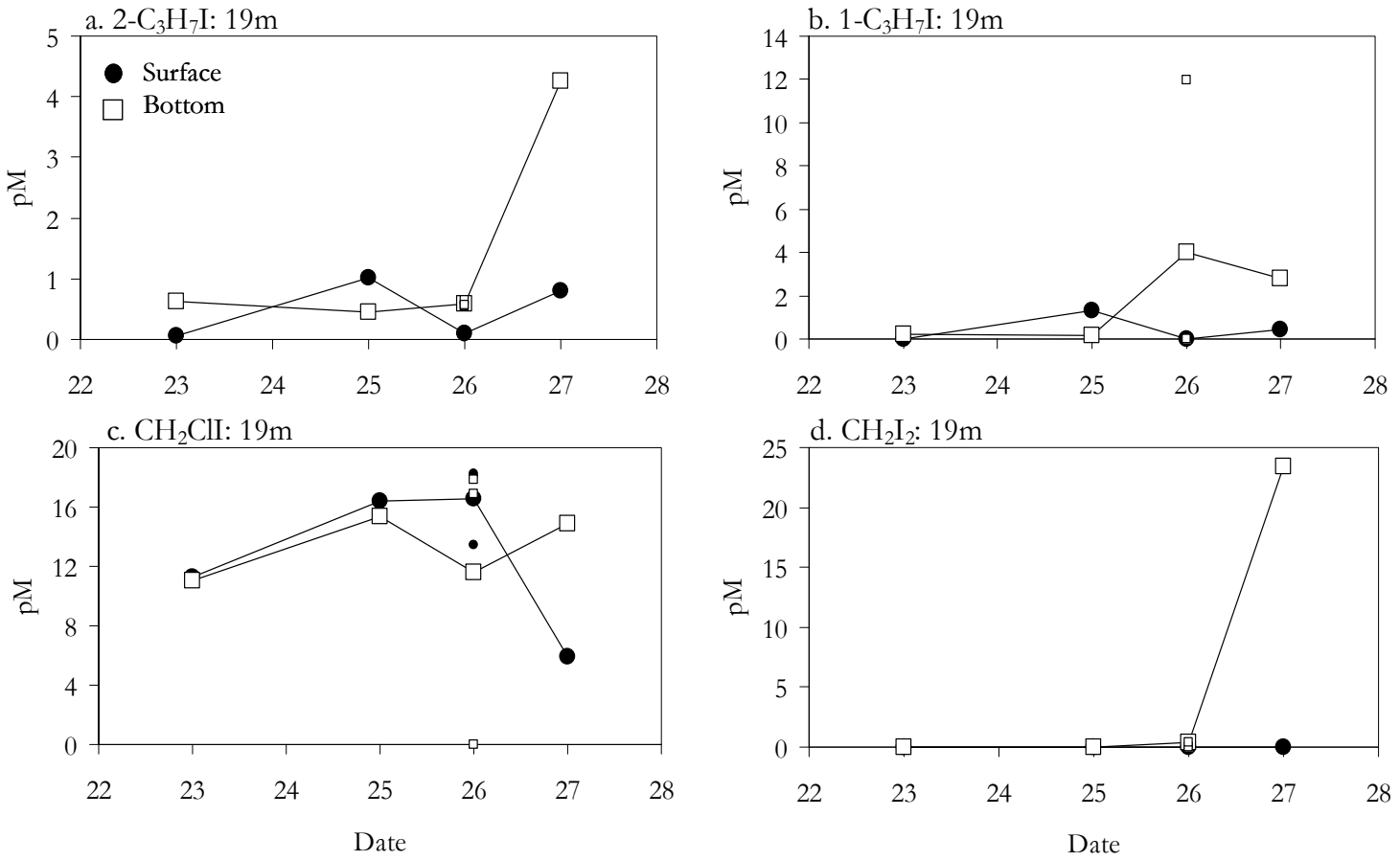

Figure 5.29. Surface (solid circles) and bottom (open square) concentrations of a. 2-C_3H_7I, b. 1-C_3H_7I, c, CH_2ClI, and d. CH_2I_2 at 19m on Transect A between 23 and 27 May 2008. On 26 May 3 measurements were taken: the average is included in the main plot with the replicate samples shown with smaller symbols.

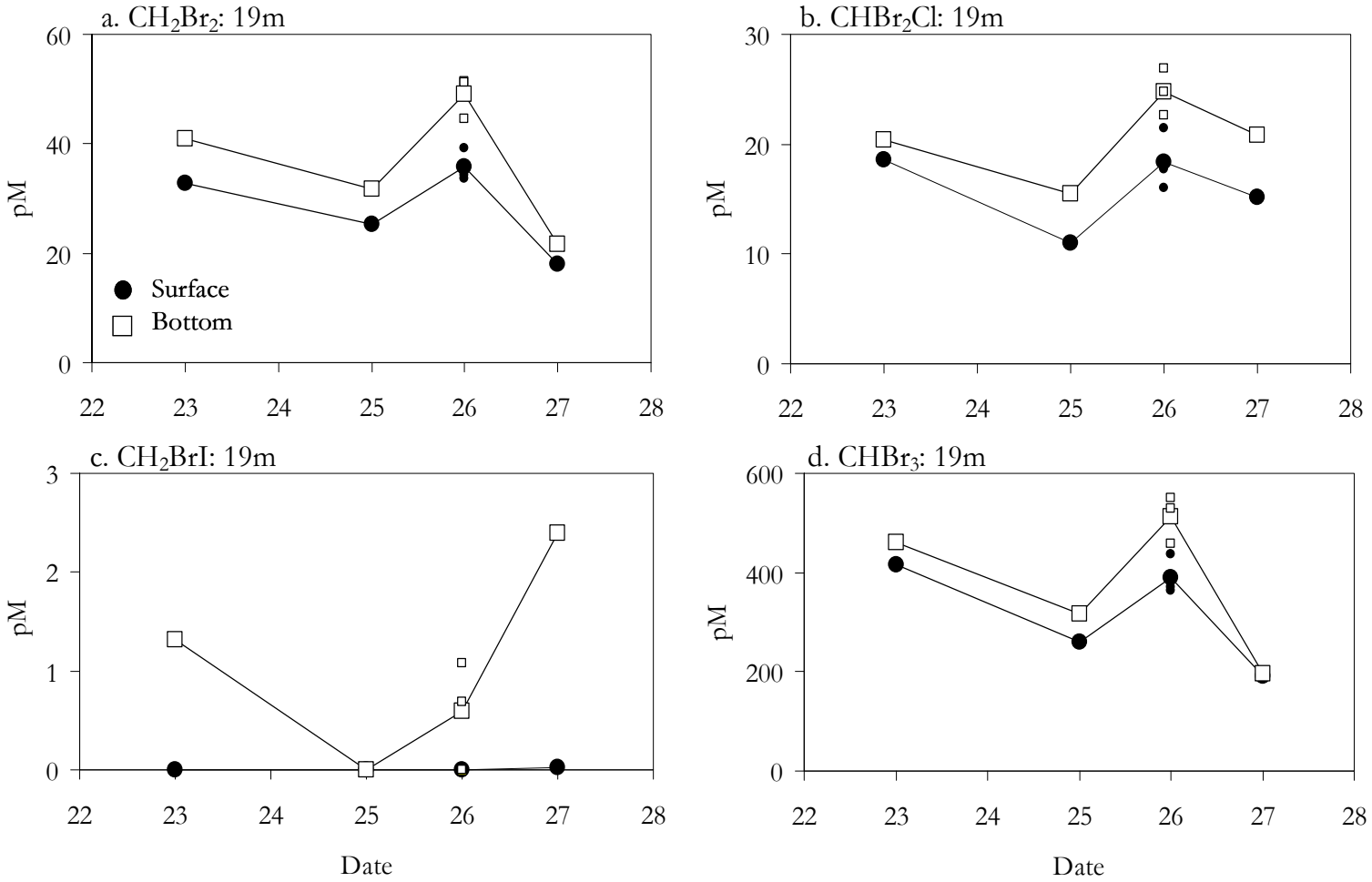

Figure 5.30. Surface (solid circles) and bottom (open square) concentrations of a.CH_2Br_2, b. $CHBr_2Cl$, c, CH_2BrI, and d. $CHBr_3$ at 19m on Transect A between 23 and 27 May 2008. On 26 May 3 measurements were taken: the average is included in the main plot with the replicate samples shown with smaller symbols.

5.7.4. DMSP, Autumn 2007

Samples for particulate DMSP analysis were collected at stations along Transect A during the autumn field campaign. Figure 5.31 shows surface concentrations at 4 m, 12 m, 19 m, 35 m and 100 m on 13, 15 and 18 November 2007. Levels were not detectable at 4 m on any of the sampling days, or at 12 m on 13 and 15 November. Where particulate DMSP was detected, it ranged in concentration from 5.9 – 10.1 nM, with minimum concentrations (other than those below DL) observed at 19 m on 13 and 15 November, and the highest value seen at 12 m on 18 November. In terms of the pH gradient, no clear trends in DMSPp concentration were observed.

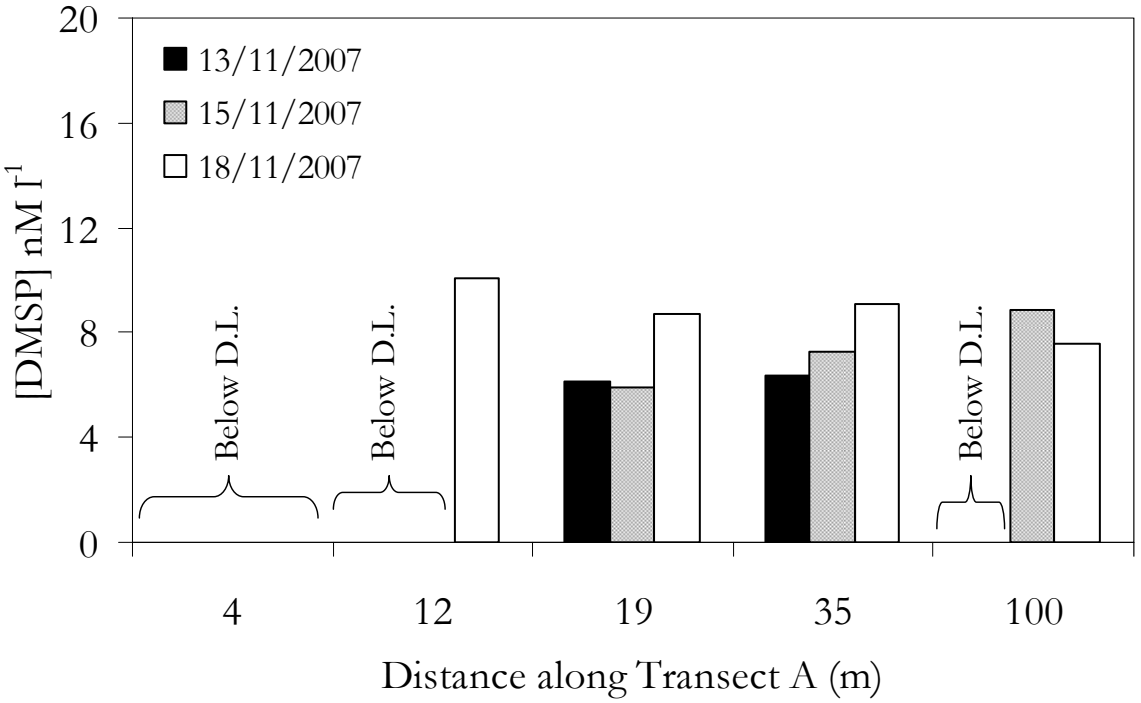

Figure 5.31. Surface concentrations of DMSP (particulate) (nM l^{-1}) at 4m, 12m, 19m, 35m and 100m on Transect A. Measurements were taken on 13 (Black), 15 (Grey) and 18 November 2007 (White). Measurements at 4m on all days, 12m on 13 and 15 November and 100m on 13 November were below the method detection limit (D.L.).

5.7.5. DMS, Spring 2008

Surface and bottom measurements of seawater DMS concentrations at stations along Transect A were performed by Sue Turner (UEA) during the spring field campaign. The data is shown in Figure 5.32, with surface measurements in the top panel (a) and bottom measurements below (b). Surface DMS concentrations ranged from 2.8 – 12.9 nM l^{-1}, with a mean of 6.8 nM l^{-1}. Both the highest and lowest

concentration was recorded at 19 m, emphasising the daily variability in concentrations within sampling stations. There were no clear trends in surface DMS concentrations with distance along the transect.

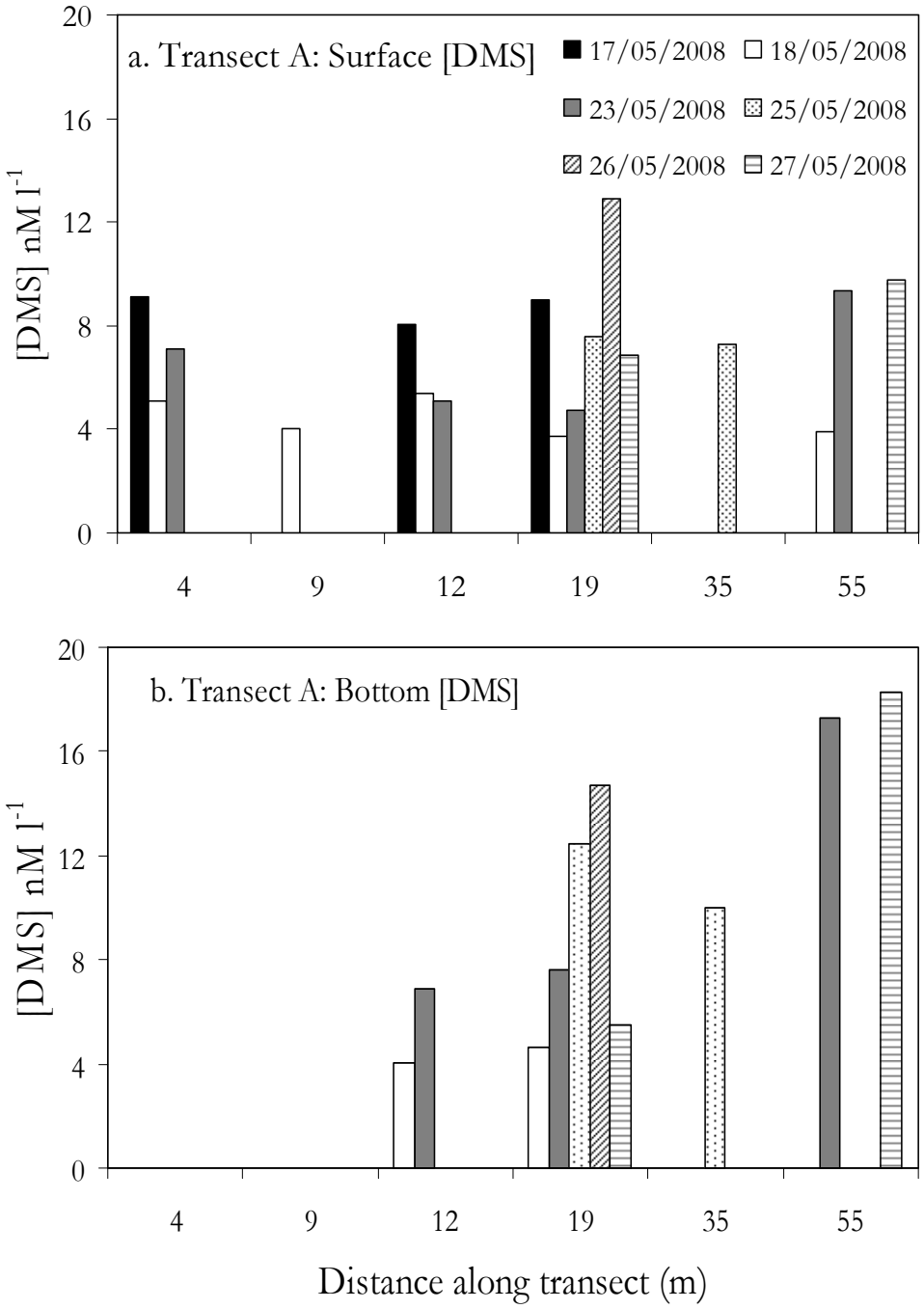

Figure 5.32. a. Surface and b. bottom concentrations of DMS (nM l^{-1}) along Transect A. Measurements taken on 17, 19, 23, 25, 26 and 27 May 2008. Legend shown in panel a.

DMS concentrations from the bottom of the water column were generally higher than those from the surface, and showed a greater range. A maximum value of

18.3 nM l^{-1} was recorded at 55 m and a minimum of 3.4 nM l^{-1} at 12 m. Bottom samples could not be collected at 4 m and 9 m as these sites were too shallow to allow use of the Niskin bottle. In contrast to surface DMS, concentrations at the bottom did show a tendency to increase with increasing distance along the transect. Despite this, the data at 19 m again highlight the large amount of daily within-station variability in concentrations, with a range of 10.1 nM l^{-1}.

5.8 Seawater pH: Relation to Other Parameters

5.8.1. Introduction

Spearman's Rank analysis was used to assess the relationships between concentrations of trace gases at the study site and accompanying seawater pH measurements.

5.8.2. Results of Correlation Analyses

Figure 5.34 shows plots of trace gases and pH during the Autumn campaign. 2-C_3H_7I and CH_2I_2 displayed significant negative correlations with pH (Spearman's ρ = -0.715 and -0.643, respectively, $p<0.01$ for both), whilst no further significant relationships were identified. Relationship between trace gases and pH during the spring campaign are shown in Figure 5.35, with no significant relationships with the iodocarbons identified, and instead $CHBr_3$, CH_2Br_2 and $CHBr_2Cl$ all significantly correlated with pH (Spearman's ρ = -0.607, -0.634, -0.712 respectively, all $p<0.01$).

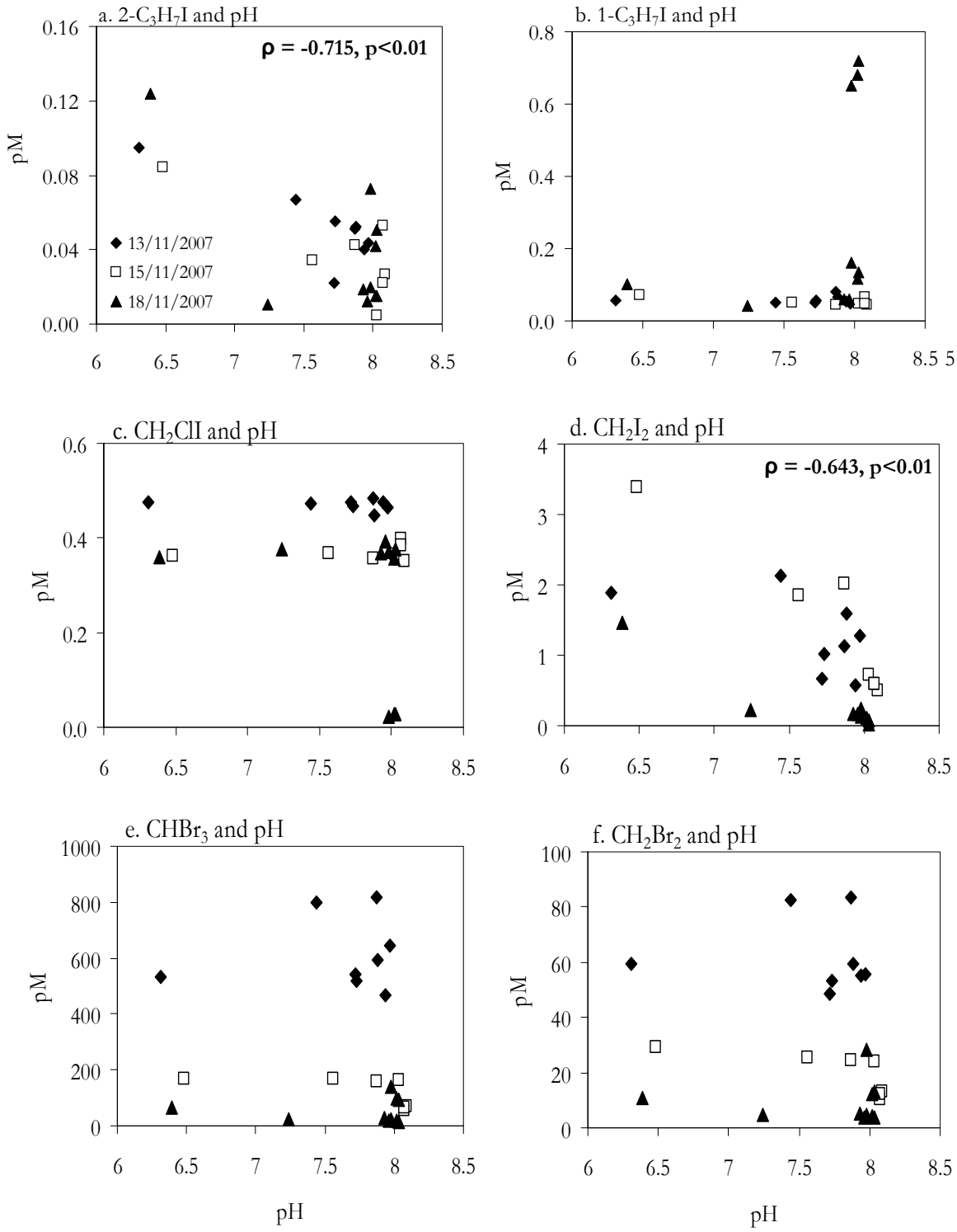

Figure 5.33. Relationships between halocarbons (pM) and pH (Total Scale) measured on 13, 15 and 18 November during the Autumn 2007 field campaign. a. CH_3I, b. C_2H_5I, c. 2-C_3H_7I, d. 1-C_3H_7I, e. CH_2ClI, f. CH_2I_2, g. $CHBr_3$, h. CH_2Br_2. Legend in shown in panel a. Significant correlations with pH were identified for 2-C_3H_7I and CH_2I_2.

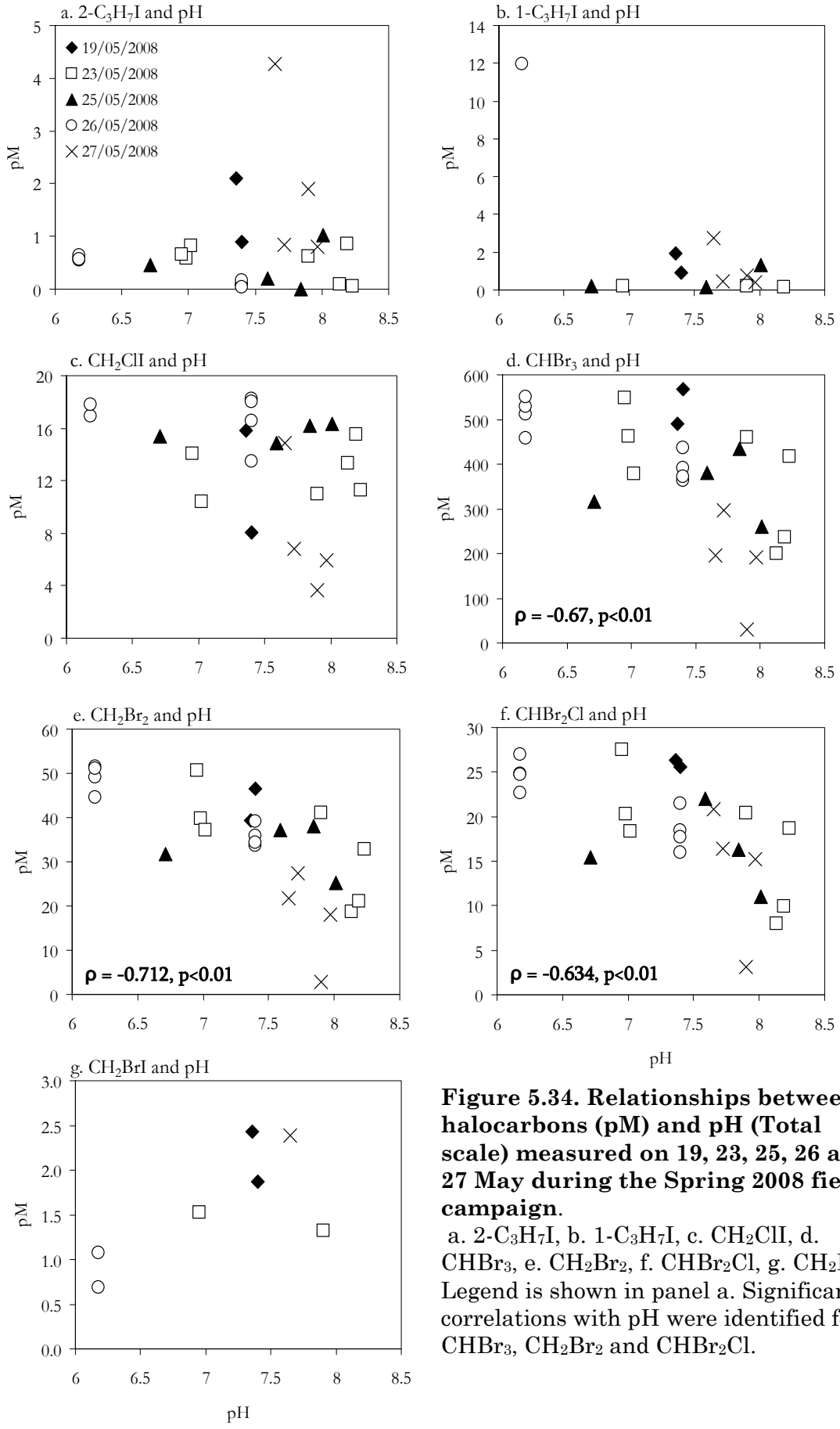

Figure 5.34. Relationships between halocarbons (pM) and pH (Total scale) measured on 19, 23, 25, 26 and 27 May during the Spring 2008 field campaign.
a. 2-C_3H_7I, b. 1-C_3H_7I, c. CH_2ClI, d. $CHBr_3$, e. CH_2Br_2, f. $CHBr_2Cl$, g. CH_2BrI. Legend is shown in panel a. Significant correlations with pH were identified for $CHBr_3$, CH_2Br_2 and $CHBr_2Cl$.

The relationships between trace gas concentrations and a range of ancillary measurements were also assessed using Spearman's Rank analysis. The results for Autumn 2007 are shown in Table 5.8, and those for Spring 2008 in Table 5.9. Significant correlations are highlighted with grey shading, and the asterisks indicate the level of significant (* = p<=0.05, ** = p<=0.02, *** = p<=0.01).

Table 5.8. Selected Spearman's Rank Correlation Coefficients (ρ) and associated significance level for correlations between halocarbon concentrations and various other parameters. Data from Autumn 2007. * = 95% confidence level (Critical value = 0.409, p<=0.05), ** = 98% confidence level (Critical value = 0.485, p<=0.02), *** = 99% confidence level (Critical value = 0.537, p<=0.01). Full details of Spearman's Rank analyses in Appendix 29.

	$2C_3H_7I$ pM	**$1C_3H_7I$ pM**	**CH_2ClI pM**	**CH_2I_2 pM**	**$CHBr_3$ pM**	**CH_2Br_2 pM**	**pH**	**Chl a mg m^{-3}**	**Phaeo. mg m^{-3}**
Temp. °C	0.121	-0.429 *	0.597 ***	0.477 *	0.812 ***	0.818 ***	-0.028	-0.294	0.578 ***
Salinity	0.140	-0.127	0.425 *	-0.008	0.789 ***	0.716 ***	-0.028	-0.655 ***	0.248
Depth m (water)	-0.496 **	0.502 **	-0.438 *	-0.594 ***	-0.124	-0.136	0.714 ***	0.121	-0.511 **
pH	-0.715 ***	0.217	-0.215	-0.643 ***	-0.133	-0.180	-	0.428 *	-0.630 ***
Chl-a mg m^{-3}	-0.417 *	-0.145	-0.087	-0.399	-0.612 ***	-0.616 ***	0.428 *	-	-0.568 ***
Phaeo. mg m^{-3}	0.539 ***	-0.268	0.362	0.842 ***	0.538 ***	0.608 ***	-0.630 ***	-0.568 ***	-
Wind direction °	-0.089	0.488 **	-0.534 ***	-0.688 ***	-0.695	-0.748	0.079	0.159	-0.658 ***
Wind speed km/h	-0.112	0.540 ***	-0.462 *	-0.416 *	-0.005	-0.032	0.301	-0.133	-0.275

Table 5.9. Selected Spearman's Rank Correlation Coefficients (ρ) and associated significance level for correlations between halocarbon concentrations and various other parameters. Data from Spring 2008. * = 95% confidence level (Critical value = 0.364, p<=0.05), ** = 98% confidence level (Critical value = 0.432, p<=0.02), *** = 99% confidence level (Critical value = 0.478, p<=0.01). Full details of Spearman's Rank analyses in Appendix 31.

	2C_3H_7I pM	**CH_2I_2 pM**	**CH_2Br_2 pM**	**$CHBr_2Cl$ pM**	**CH_2BrI pM**	**$CHBr_3$ pM**	**pH**	**Chl-a mg m^{-3}**	**Phaeo. mg m^{-3}**
Temp. °C	0.180	-0.082	-0.298	-0.182	-0.123	-0.349	-0.002	0.418 *	-0.396 *
Salinity	0.469 **	0.230	-0.218	0.021	0.481 ***	-0.149	0.304	-0.381 *	-0.357
Depth m (water)	-0.364 *	0.189	-0.682 ***	-0.711 ***	-0.531 ***	-0.657 ***	0.486 ***	-0.223	-0.578 ***
pH	0.089	0.135	-0.712 ***	-0.634 ***	0.683	-0.607 ***	-	-0.035	-0.192
Chl-a mg m^{-3}	-0.417*	-0.145	-0.087	-0.399	-0.612 ***	-0.616 ***	-0.035	-	0.164
Phaeo. mg m^{-3}	0.374 *	-0.176	0.691 ***	0.617 ***	0.500 ***	0.610 ***	-0.192	0.164	-
Wind direction °	-0.627 ***	-0.482 ***	-0.061	-0.293	-0.864 ***	-0.247	-0.304	0.407 *	0.513 ***
Wind speed km/h	0.800 ***	0.645 ***	-0.492 ***	-0.275	0.460 ***	-0.353	0.593 ***	-0.657 ***	-0.886 ***
Tidal height m	-0.458 **	-0.470 **	0.032	-0.221	-0.441 **	0.006	0.189	0.036	0.337

During the autumn field campaign, all halocarbons were significantly correlated with at least four of the other measured parameters. All, except 2-C_3H_7I, were significantly correlated with seawater temperature, although 1-C_3H_7I was an exception to the others as it displayed a negative relationship while the other compounds were positively correlated. Water depth at the sampling station was significantly correlated with all iodocarbons, and again 1-C_3H_7I differed from the others, being positively correlated. All halocarbons displayed negative correlations with chlorophyll *a* (statistically significant for $CHBr_3$, CH_2Br_2 and 2-C_3H_7I), while phaeopigments were positively correlated with all halocarbons except 1-C_3H_7I and

CH_2ClI. All iodocarbons, except 2-C_3H_7I, were significantly correlated with wind speed and direction. Although the relationship was negative in nature with CH_2I_2 and CH_2ClI, it was positive for 1-C_3H_7I. Chlorophyll *a* displayed a significant positive relationship with seawater temperature, and phaeopigments showed the opposite trend. In addition both chlorophyll *a* and phaeopigments positively co-varied with wind direction, and negatively with wind speed.

In contrast to autumn, the trace gases during the spring field campaign showed no relationship to seawater temperature, despite a significant positive correlation between temperature and chlorophyll *a*, and a significant negative correlation with phaeopigments. Trace gas concentrations did seem to show a degree of coupling to water depth, with all but CH_2I_2 displaying significant negative relationships, indicating a decrease in concentrations with increasing water depth. Chlorophyll *a* concentrations were not positively correlated with any of the halocarbons (see Appendix 32). By contrast phaeopigments concentrations showed significant positive correlations with all of the bromocarbons and also with 2-C_3H_7I. Wind direction and speed seemed to influence the concentrations of a number of the halocarbons although the relationships were most pronounced for the iodocarbons. Finally, tidal height was significantly correlated with only 3 halocarbons (2-C_3H_7I, CH_2I_2 and $CHBr_2I$).

Information on DMS is only available for the spring field campaign and some of the relationships that were identified are shown in Figure 5.36, with further information in Table 5.10 and Appendix 33. DMS was not correlated with either pH or chlorophyll *a*. However significant correlations with water depth ($\rho = -0.534$, $p<=0.01$) and phaeopigment concentrations ($\rho = -0.467$, $p<=0.02$) were identified. Additionally, DMS was strongly correlated with the depth at which the sample was taken, indicating that concentrations increased with increasing depth in the water column.

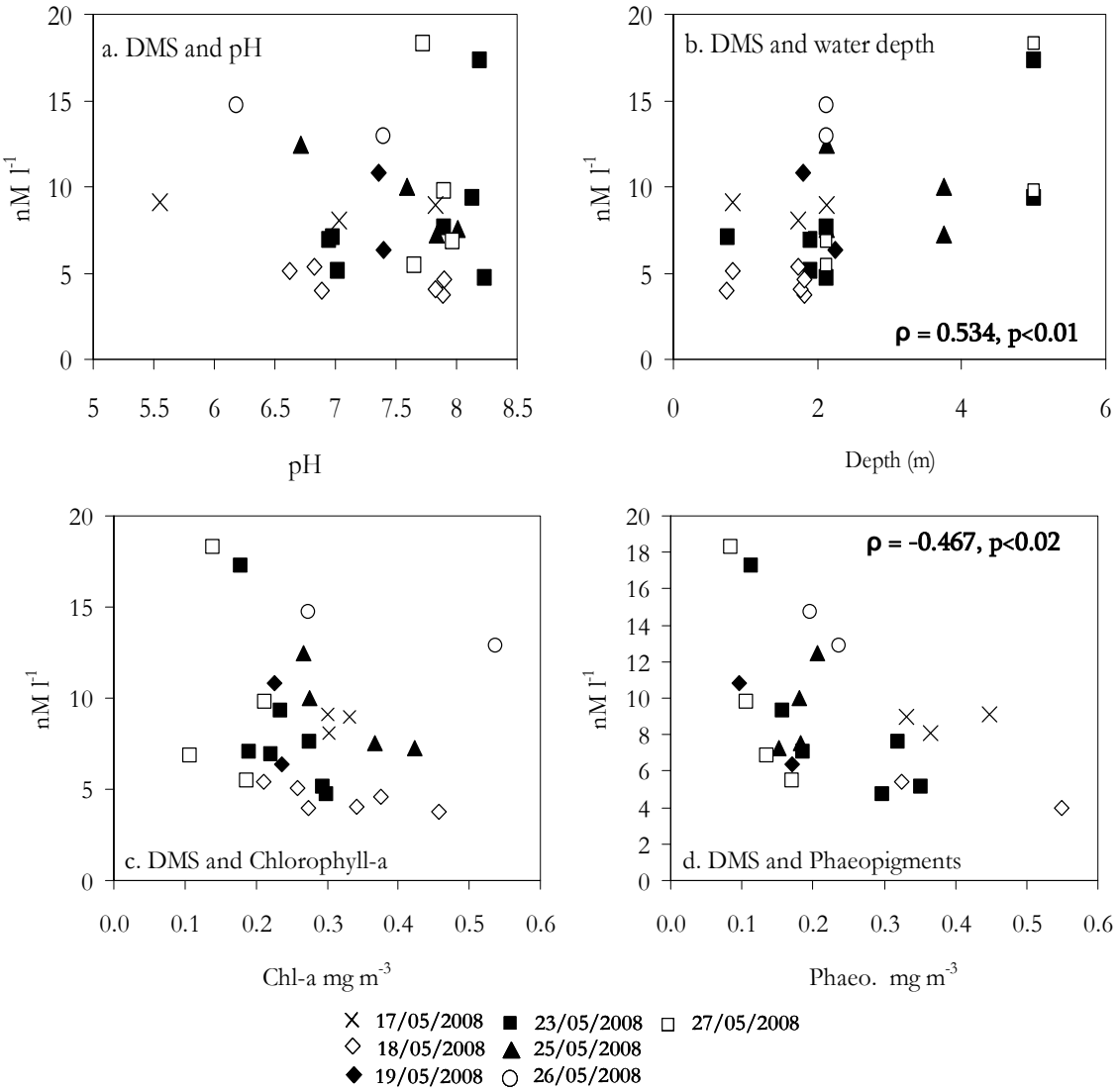

Figure 5.35. Relationships between DMS concentrations (nM) and a. pH (Total scale), b. Water depth (m), c. Chlorophyll *a* (mg m^{-3}) and d. Phaeopigments (mg m^{-3}) during the Spring 2008 field campaign. Significant correlations were found between DMS and water depth, and DMS and phaeopigments.

Table 5.10. Selected Spearman's Rank Correlation Coefficients (ρ) and associated significance level for correlations between DMS concentrations and various other parameters. Data from Spring 2008. n = 30, * = 95% confidence level (Critical value = 0.364, p<=0.05), ** = 98% confidence level (Critical value = 0.432, p<=0.02), *** = 99% confidence level (Critical value = 0.478, p<=0.01). Full details of Spearman's Rank analyses in Appendix 33.

	DMS (nmol l^{-1})	**pH**	**Chlorophyll *a* (mg m^{-3})**	**Phaeopigments (mg m^{-3})**
Temp. °C	0.248	0.222	0.046	-0.460 **
Salinity	-0.367 *	0.323	-0.076	0.072
Depth m (sample)	0.602 ***	0.208	-0.240	-0.082
Depth m (water)	0.534 ***	0.549 ***	-0.217	-0.532 ***
pH	-0.040	-	0.043	-0.220
Chlorophyll *a* mg m^{-3}	-0.103	0.043	-	0.400 *
Phaeopigments mg m^{-3}	-0.467 **	-0.220	0.400 *	-
Tidal Height m	-0.413 *	-0.204	0.354	0.354

5.8.3. Possible causes of observed relationships

5.8.3.1. Correlations with pH and water depth

Seawater pH was significantly correlated with only a small number of trace gases, in autumn with 2-C_3H_7I and CH_2I_2, and in Spring with $CHBr_3$, CH_2Br_2 and $CHBr_2Cl$. All of these were negative relationships, implying that concentrations of these gases increased with decreasing pH. However, this not necessarily evidence of cause and effect. A number of other important parameters were also significantly correlated with pH. Thus it is possible that the correlations seen with the trace gases may be artefacts of these other, more direct, relationships.

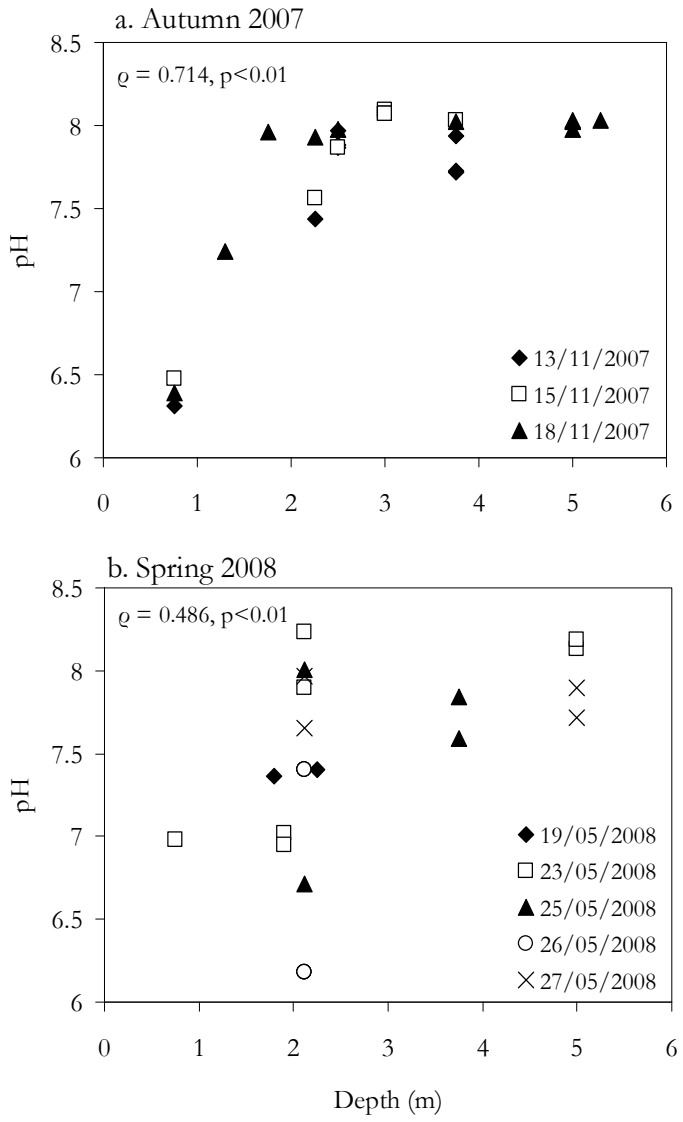

Figure 5.36. Relationship between pH and water depth (m) during a. Autumn 2007, and b. Spring 2008. Spearman's rho and associated probabilities are shown on the plots.

In both autumn and spring, pH was significantly positively correlated with water depth (Figure 5.37), and the majority of trace gases also showed significant correlations with this parameter. This suggests water depth is an important factor in determining both pH and trace gas concentrations at this site. There are a number of possible reasons for this:

1. In terms of pH, it may simply be a consequence of the seabed topography, due to increasing depth with distance along the pH gradient (See Figure 5.8).
2. Leading on from this, in shallow regions of the site, there was a greater density of CO_2 vents, driving the pH lower in these areas. In addition, as the water gets deeper along the transect, a dilution effect on CO_2 concentrations is likely.

3. In shallow regions of the site with the lowest pH, the influence of trace gas production by benthic macroalgae and seagrass may be stronger. As water depth increases, a dilution effect on trace gas concentrations is likely. Unfortunately, the distribution of macroalgae and seagrass was not quantified during this study.

5.8.3.2. Correlations with Chlorophyll *a* and Phaeopigments

In both autumn and spring, concentrations of all halocarbons and DMS were negatively correlated with chlorophyll *a*, with a number of those relationships identified as being significant ($CHBr_3$, CH_2Br_2, 2-C_3H_7I – autumn, 2-C_3H_7I, CH_2BrI, $CHBr_3$ – spring). In contrast, the majority of halocarbons were significantly positively correlated with phaeopigments concentrations (a biomarker of grazing and senescence (Litaker et al., 1988). Therefore in both seasons, as chlorophyll *a* concentrations increase, halocarbons tend to decrease, and *vice versa* for phaeopigments. With the available information, it is difficult to speculate at the causes of these relationships.

Unlike pH and concentrations of some of the trace gases, chlorophyll *a* was not correlated with water depth or pH, suggesting that the observed relationships are not related to a dilution effect.

Similarly to halocarbon concentrations, phaeopigments were negatively correlated with water depth. As halocarbons and phaeopigments also showed some coupling, it is possible that their production is related. However, as phaeopigments did not show any relation to pH, their controlling processes may not be directly linked.

5.8.4. Conclusions

The information derived from Spearman's Rank correlation analyses suggests that the influence of a benthic trace gas signal may overwhelm any pelagic trace gas production, particularly in shallow, low pH regions of the site. Furthermore, correlations with other measurements suggest that any change to the pelagic trace gas signal may not be representative of an impact of OA. Water depth appears to have a stronger influence on the concentrations of trace gases, and other related parameters such as chlorophyll *a* and phaeopigment concentrations than pH.

5.9 Benthic vs. Pelagic Trace Gas Production: Incubation Experiments

5.9.1. Introduction

Due to the shallow nature of the field site (< 6m) and the thick growth of benthic macroalgae and seagrass on the seabed, it was likely that some proportion of the trace gases that were detected in the water column were from a benthic rather than pelagic source. Macroalgae are known to be strong producers of halocarbons, strongly contributing to the flux of such compounds from coastal regions (Laturnus, 1996; Laturnus et al., 2000; Nightingale et al., 1995). Therefore in order to accurately assess the response of the pelagic community to the high CO_2 conditions, it was important to devise a way in which the pelagic trace gas signal could be isolated from the potentially strong benthic signal.

5.9.2. Experimental Setup

A benthic "tent" and pelagic bag were used to perform 24 hour *in situ* incubations. Over the 24 hours, the tent and bag would allow the accumulation of trace gases produced by the benthic macroalgae and pelagic community, respectively, with samples taken at T_0 and T_{Final} for analysis of trace gas concentrations and a number of additional parameters.

The benthic tent was constructed using a large Duran glass funnel, and was inverted and placed on the seabed on top of annular sandbag (Fig. 5.38 A). The sandbag was constructed from cloth filled with sand and used to stabilise and protect the glass funnel. A length of ¼" nylon tubing was inserted into the stem of the funnel, and a seal was created around the tubing to make it airtight. A luer valve was attached to the nylon tubing so samples could be withdrawn from the tent using a glass syringe. The benthic tent was moored to the seabed using a system of three mooring weights – string bags filled with large stones, all attached to the stem of the funnel using a reinforced loop of string. Once in place the benthic tent was extremely stable. Samples were taken from the benthic tent by duck diving and filling 100ml glass syringes with seawater through the nylon tubing (See Figure 5.38 B).

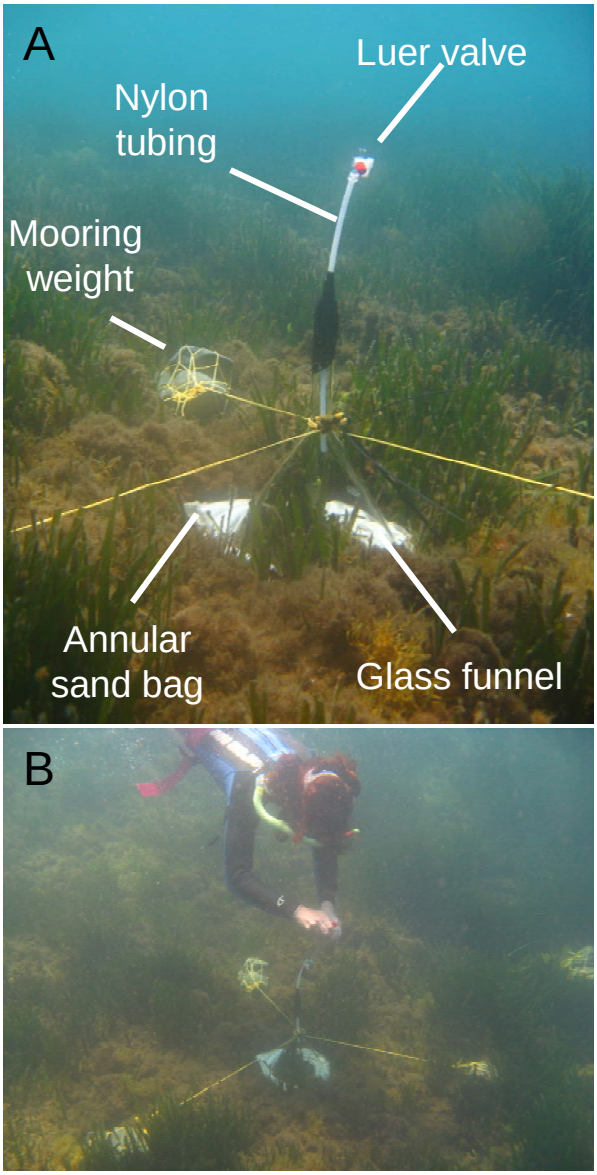

Figure 5.37. A. The benthic tent moored to the seabed, B. Sampling from the benthic tent: duck-diving with a glass syringe.

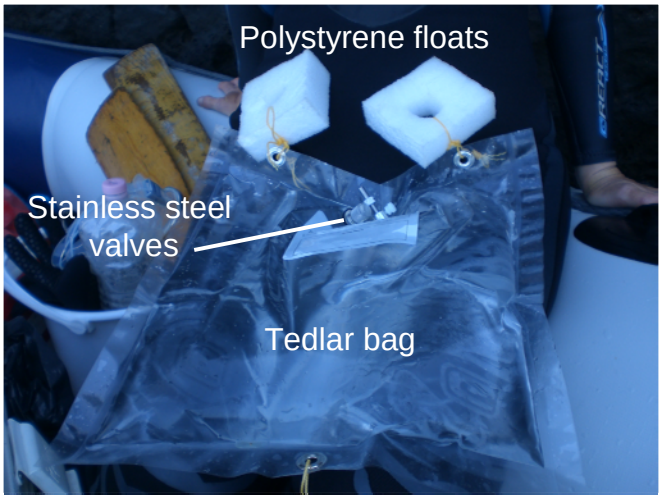

Figure 5.38. The Tedlar bag before deployment.

The pelagic community was incubated in 5 litre Tedlar bags (SKC Ltd.), anchored to the moorings of the benthic tent, at mid-depth in the water column (Fig. 5.39). The Tedlar bags had two in-built stainless steel valves and were filled with surface seawater collected in a Niskin bottle using Tygon tubing. Air was excluded from the bags so that no headspace existed. Two small polystyrene floats were attached to the top of the bag to ensure it maintained its position in the water column. Samples were taken from the bags by inserting a length of 1/8" nylon tubing into one of the valves on the bags and carefully withdrawing seawater samples using 100ml glass syringes. Seawater samples were taken back to the laboratory and photosynthetic efficiency was measured using FIRe. DMS samples were analysed within 6 hours of sample collection. Halocarbon samples were trapped and stored on Markes sorbent tubes at -20°C and analysed on return to the UK. Profiles of seawater temperature and pH were taken at each site immediately prior to T_0 and T_{Final}.

5.9.3. Incubation Sites

The location of the experiments was selected according to the information on pH that had previously been collected at the site, both during the Autumn and Spring field campaigns. Locations were also selected on depth, as it was necessary for duck-dive sampling to be possible.

For Experiment 1, Site 3 was chosen (See Figure 5.40). Although it was not on Transect A and therefore had not been monitored during this study as regularly, it offered a flat, 2.2 m deep location, and was considered to have a mean subtidal pH of 7.6 (Hall-Spencer et al., 2008), a value that may be reached in surface oceans by 2100 (Caldeira and Wickett 2003; Raven *et al.* 2005).

Experiment 2 was performed at 19m on Transect A (Fig. 5.40), a sampling station that had received frequent monitoring. The mean pH of ~7.7 was also considered to be representative of potential future acidification of the surface oceans (See Table 5.3). The benthic macroflora at this site was dominated by the seagrass *Posidonia oceanica*.

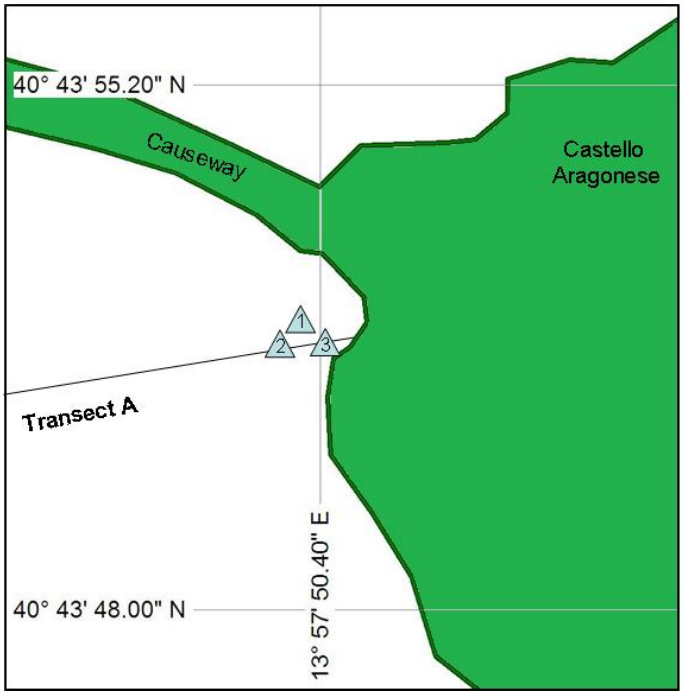

Figure 5.39. Location of Tedlar/Tent incubation experiments.
1. Site 3: 19-20 May 2008, 2. 19m Transect A: 24 – 25 May 2008, 3. 3m Transect A: 26 – 27 May 2008.

Finally, Experiment 3 was performed at 3 m on Transect A, on the shallow plateau, in a region that experienced very low pH levels. Unidentified brown macroalgae dominated the benthic flora. Although 4 m had been a more regular sampling station throughout the field campaigns, this location was chosen on the basis that it provided the most secure position for the incubations. Mean pH readings from both 3m and 4m taken in autumn and spring ranged from 5.89 to 6.47, as shown in Table 5.11. Such pH levels are unrealistic in terms of anthropogenic OA, but may provide interesting information on the production of trace gases under extreme conditions.

Table 5.11. Mean (± Standard deviation) of all pH readings made at 3m and 4m, Transect A during the autumn 2007 and spring 2008 field campaigns.

Season	Mean (± SD)	n
Autumn 2007	6.47 (± 0.11)	22
Spring 2008	5.89 (± 0.48)	28

5.9.4. Results

5.9.4.1. Experiment 1: 19 – 20 May 2008

5.9.4.1.1. Seawater pH and temperature

Plots of pH and temperature at T_0 and T_{Final} are shown in Figure 5.41. At T_0, pH measurements displayed strong water column structure, with a pH of 7.4 at the surface, dropping dramatically and rapidly between 0.5m and 0.75m to 6.35. Low pH values of this order were then maintained down through the remaining depths, of 6.23 at 2.25 m. Seawater temperature also showed some stratification, with a warmer upper layer down to 0.75 m (19.91 – 19.97°C). At 0.75 m temperature dropped to 19.84°C, with a further drop to 19.75°C at the bottom.

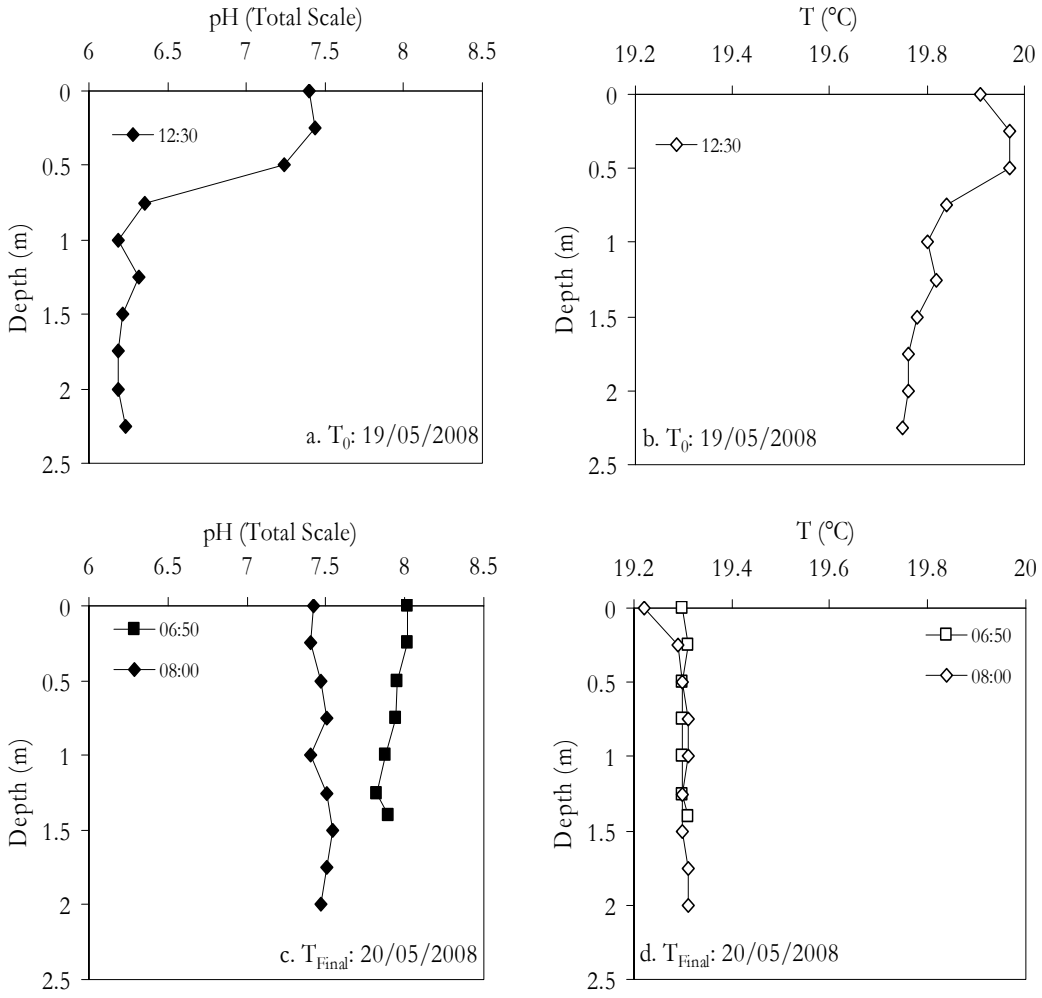

Figure 5.40. Depth profiles of pH (Total scale) (a and c) and seawater temperature (°C) (b and d) at T_0 and T_{Final} at Site 3 over the course of Experiment 1.

At T_{Final} 19 hours later, the pH at the incubation site was quite different to the previous day. The water column appeared to be better mixed than at T_0. Readings were taken twice, once immediately before taking the T_{Final} water samples, and once immediately afterwards, with a gap of 70 minutes. Within this time, a large change in pH was observed. The first profile gave measurements that could be likened to background seawater pH levels at the surface of 8.02, with only a small change through the water column to 7.9 at the bottom. 70 minutes later, the whole water column was characterised by pH levels of <7.5, highlighting the highly variable and rapidly changing pH conditions encountered at this site. Seawater temperatures also showed less structure than those for T_0 along with much cooler temperatures of ~19.3°C, although this difference in temperature is not surprising as T_{Final} measurements were made earlier in the day than those for T_0.

5.9.4.1.2. Trace gas concentrations

a. Iodocarbons

At T_0, concentrations of iodocarbons (Figure 5.42 a) were higher in the benthic tent, with a total iodocarbon pool of 85 pM compared to 60 pM in the pelagic incubation bag. In both the pelagic and benthic incubations CH_2I_2 was the dominant iodocarbon (62 percent of total in benthic and 63 percent in pelagic), followed by CH_2ClI (28 percent in benthic, 22 percent in pelagic). 2-C_3H_7I and 1-C_3H_7I made up the remainder, with a slightly greater contribution from 2-C_3H_7I (5 percent for both benthic and pelagic).

After 19 hours of incubation, both the benthic and pelagic incubation showed a reduction in total iodocarbon concentrations, a loss which was greater in the benthic tent (75 percent loss in benthic, 43 percent in pelagic). As well as a reduction in concentrations, the contribution of each compound to the iodocarbon pool showed some changes. CH_2I_2 ceased to be the dominant compound, and was surpassed by CH_2ClI, with 49 percent and 47 percent of the total pool for the benthic and pelagic incubations, respectively. 2-C_3H_7I continued to dominate over 1-C_3H_7I.

All compounds showed loss over the course of the incubation with the exception of pelagic CH_2ClI, which increased by 2.8 pM, evidence of some net production of this compound.

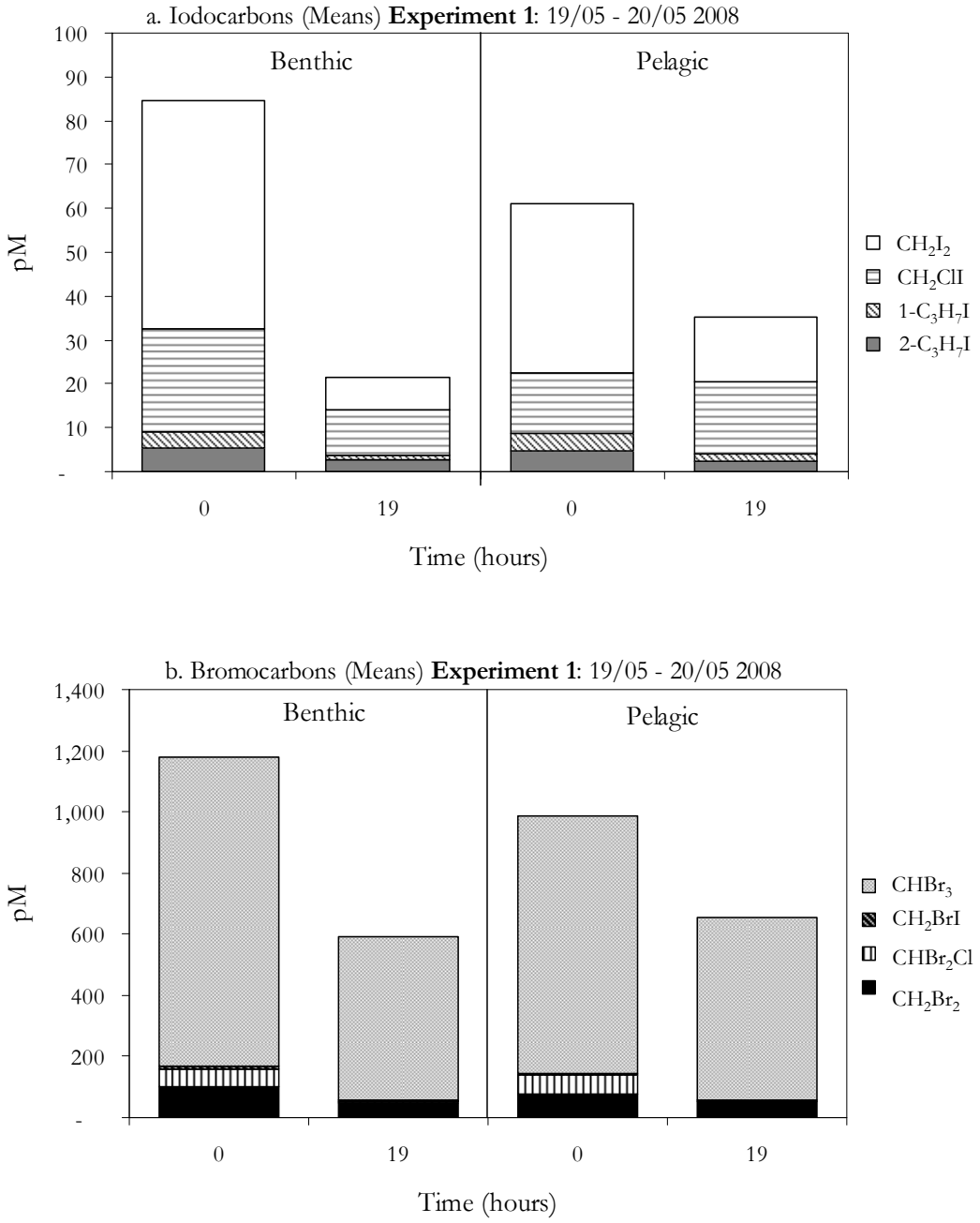

Figure 5.41. Mean concentrations (pM) of a. Iodocarbons and b. Bromocarbons in the benthic tent and the pelagic tedlar bag at T_0 and T_{Final} (19 hours) during Experiment 1.

b. Bromocarbons

Similarly to the iodocarbons, the concentrations of the bromocarbons at T_0 (Figure 5.42 b) were higher in the benthic tent, with a total bromocarbon pool of 1178 pM, compared to 984 pM in the pelagic. In both incubations, the bromocarbon pool was dominated by $CHBr_3$, which comprised over 85 percent of the total.

Concentrations of CH_2Br_2 were around 10-fold lower than $CHBr_3$, at 80 – 100 pM, whilst $CHBr_2Cl$ and CH_2BrI made up the remainder.

At T_{Final} after 19 hours of incubation, both the benthic and pelagic incubations showed a reduction in total bromocarbon concentrations, falling by ~50 percent in the benthic tent, and 33 percent in the pelagic bag. The relative proportions of $CHBr_3$ and CH_2Br_2 remained similar to those at T_0 (~90 percent and 8 percent, respectively). There was almost total loss of $CHBr_2Cl$ and CH_2BrI, with contributions of <1 percent to the total pool for each by T_{Final}.

c. DMS

DMS concentrations (Figure 5.43) at T_0 were higher in the benthic tent, with 6.9 nmol l^{-1} compared to 5.2 nmol l^{-1} in the pelagic incubation. After 19 hours, concentrations had fallen by around 30 percent in both incubations, indicating a dominance of loss processes.

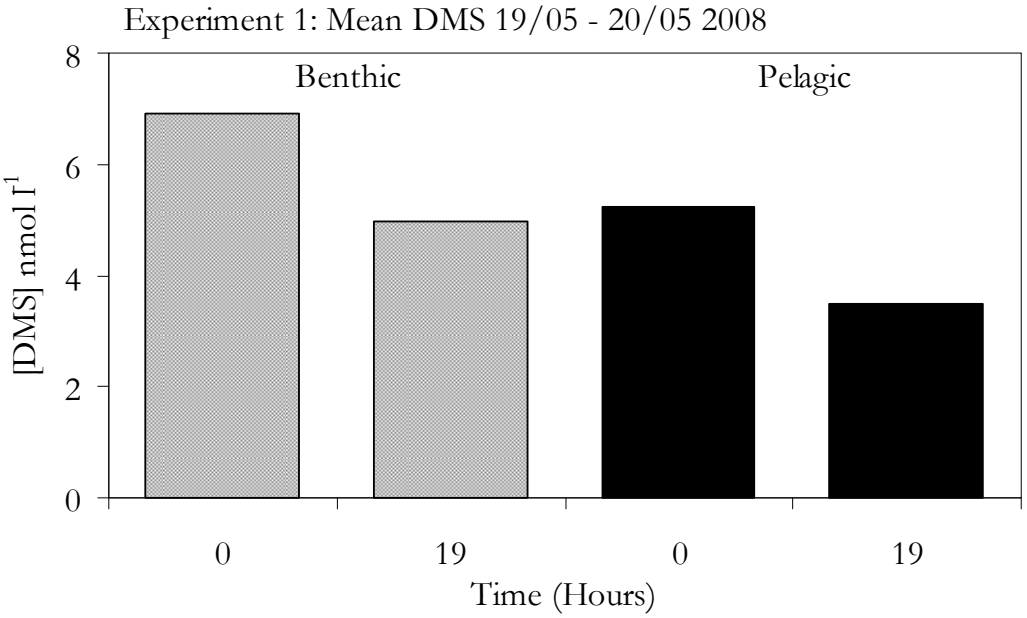

Figure 5.42. Mean concentrations (nmol l^{-1}) of DMS in the benthic tent and pelagic tedlar bag at T_0 and T_{Final} (19 hours) during Experiment 1.

5.9.4.2. Experiment 2: 24 – 25 May 2008

5.9.4.2.1. Seawater pH and temperature

At T_0 the water column displayed relative homogeneity in terms of pH, with 7.8 at the surface dropping to 7.5 at around 1.2m depth. The temperature profile at this

time point displayed similar characteristics, with a 0.2°C drop in temperature also at 1.2m. By T_{Final} 24 hours later, the pH and temperature characteristics of the site had changed dramatically. The water column displayed much greater structure, with pH levels near to background in the upper 1m (8.0 – 8.1), a rapid drop in pH between 1m and 1.5m, and very low pH levels of around 6.4 – 6.7 in the bottom 0.5m of water. The temperature of the water did not show such strong structure but there was evidence that the bottom 0.5m of water was cooler than the overlying water. The 08:34 cast at T_{Final} (Figure 5.44 d – triangles) displayed temperatures that were up to 0.7°C higher than the same time on the previous day.

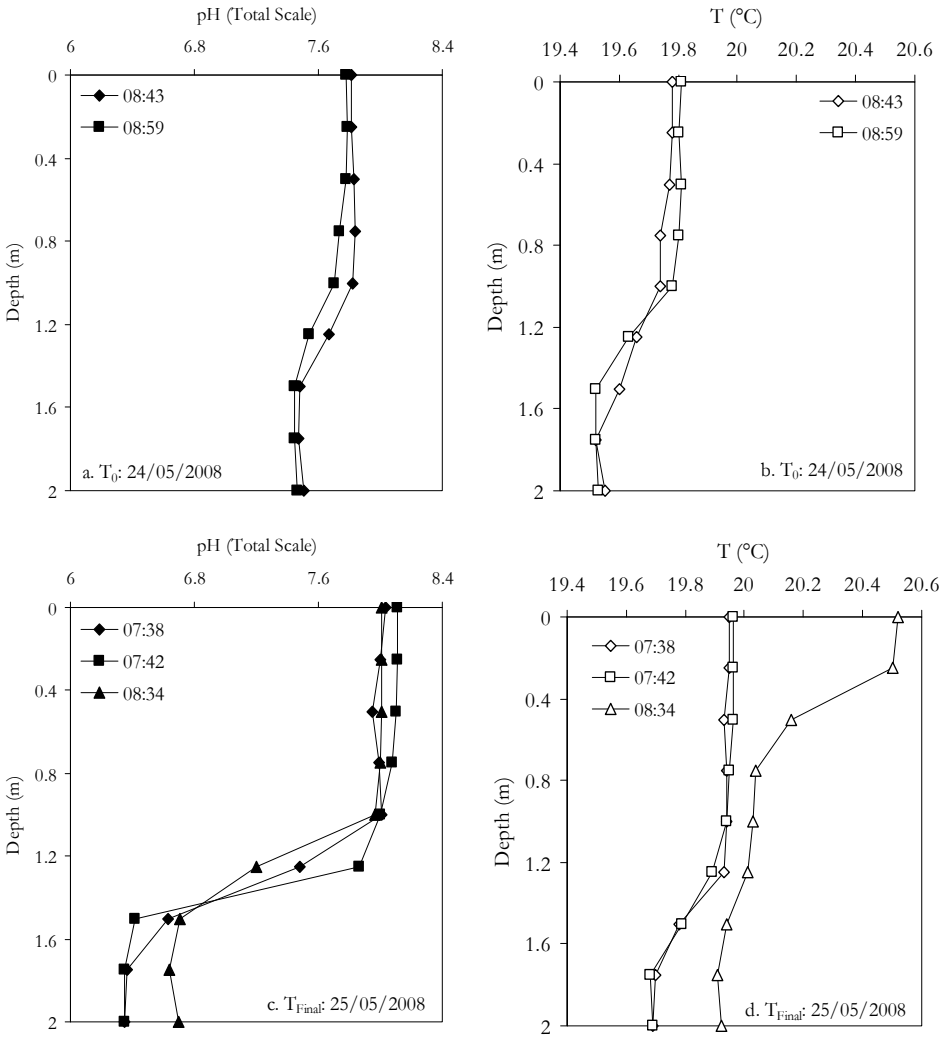

Figure 5.43. Depth profiles of pH (Total scale) (a and c) and seawater temperature (°C) (b and d) at T_0 and T_{Final} at 19m, Transect A, over the course of Experiment 2.

5.9.4.2.2. Trace gas concentrations

a. Iodocarbons

At T_0, total iodocarbon concentrations (Figure 5.45 a) were 80 pM higher in the benthic tent than in the pelagic bag. However, the majority of this difference was accounted for by the presence of high levels of CH_2I_2 in the benthic tent (72 pM) and a total absence of this compound in the pelagic bag.

After 24 hours of incubation, total iodocarbon concentrations in the benthic tent had fallen dramatically, the result of an 88 percent reduction in CH_2I_2 concentrations, as well as smaller decreases in the concentrations of all other iodocarbons. By contrast, the total iodocarbon pool in the pelagic tedlar bag increased by 25 percent, from 16 pM at T_0 to 22pM at T_{Final}. Concentrations of all compounds, except CH_2ClI, increased during the incubation. Most notably, concentrations of CH_2I_2 increased from 0 to 5 pM, suggesting net production of this compound in the pelagic incubation.

c. Bromocarbons

Concentrations of the bromocarbons were higher in the benthic tent over the course of the incubation, mainly accounted for by higher concentrations of $CHBr_3$. $CHBr_3$ dominated the bromocarbons pool in both benthic and pelagic incubations, contributing 84 – 85 percent to the benthic, and 86 - 87 percent to the pelagic (Figure 5.45 b). As also seen in Experiment 1, CH_2Br_2 concentrations were approximately 10-fold lower than $CHBr_3$, and $CHBr_2Cl$ contributed 5 – 6 percent to the pool. CH_2BrI concentrations were elevated in the benthic tent relative to the pelagic bag at T_0 (2.1 pM compared to 0.8 pM), suggesting a benthic source of this compound. By $T_{Final,}$ little change in bromocarbons was observed in either incubation, suggesting production and loss processes were fairly equal, although the small quantity of CH_2BrI present at T_0 had fallen to below detection limit.

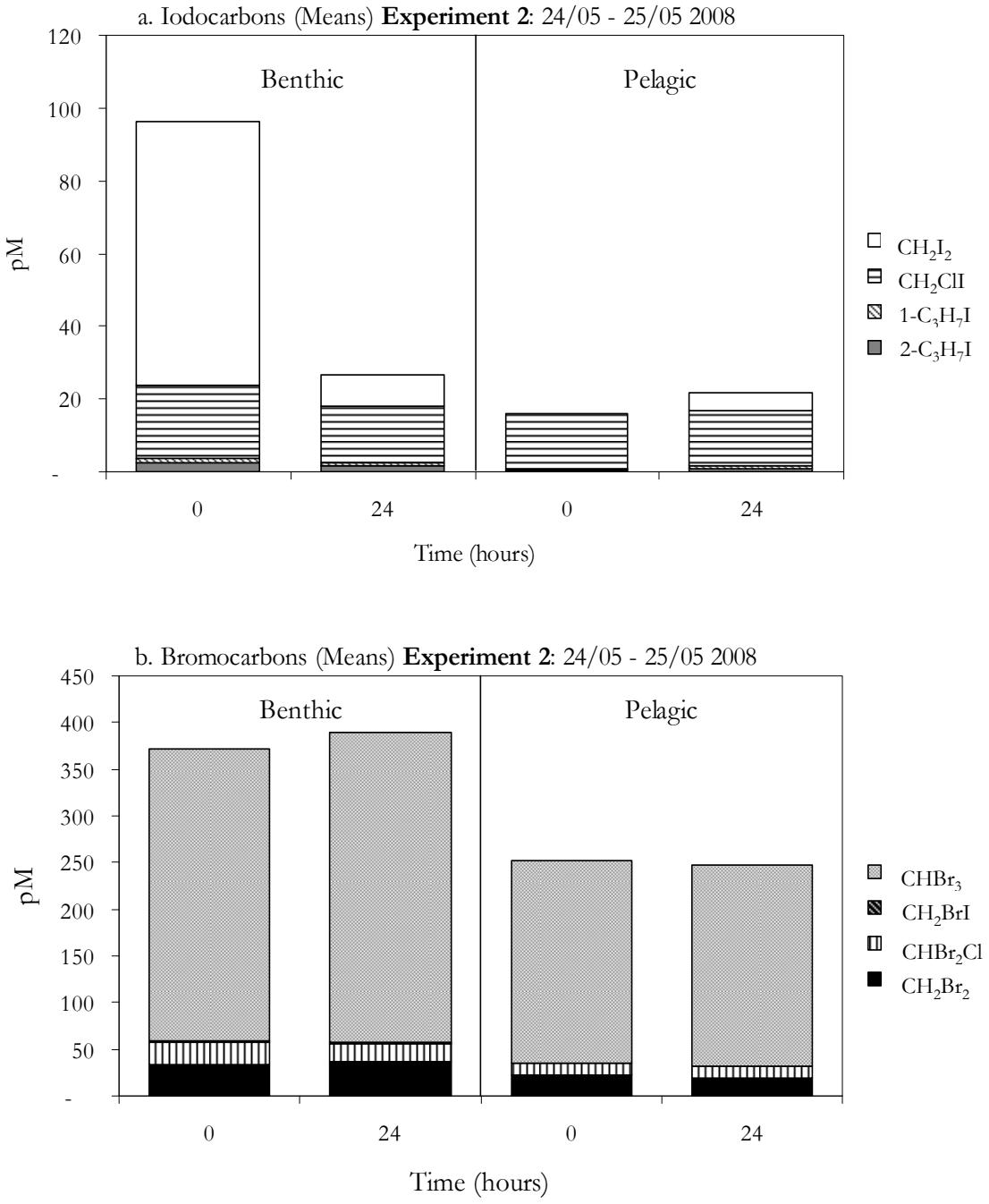

Figure 5.44. Mean concentrations (pM) of a. Iodocarbons and b. Bromocarbons in the benthic tent and the pelagic tedlar bag at T_0 and T_{Fnal} (24 hours) during Experiment 2.

c. DMS

Similarly to Experiment 1, concentrations of DMS (Figure 5.46) at T_0 were elevated in the benthic incubation relative to the pelagic, with concentrations of 8.9 nmol l^{-1} compared to 6.8 nmol l^{-1}. After 24 hours of incubation, opposite trends were

observed; a 1.7 nmol l^{-1} fall in concentrations occurred in the benthic tent, whilst concentrations in the pelagic bag increased by 3.7 nmol l^{-1} indicating the possible presence of a pelagic source of DMS.

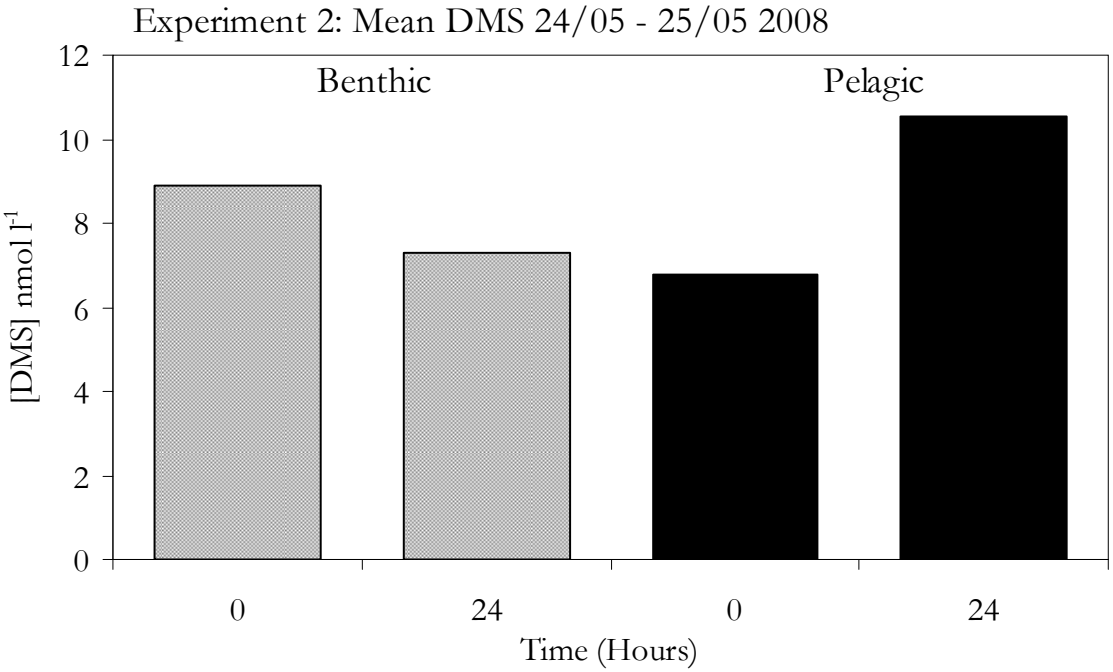

Figure 5.45. Mean concentrations (nmol l^{-1}) of DMS in the benthic tent and pelagic tedlar bag at T_0 and T_{Final} (24 hours) during Experiment 2.

5.9.4.3. Experiment 3: 26 – 27 May 2008

5.9.4.3.1. Seawater pH and Temperature

The location of Experiment 3 was very shallow (<1m), so as a result of the shallow depth and the turbulence created by the waves deflecting off the cliffs, little heterogeneity was detected in the water column. At T_0 the pH was low (~6.14) and the temperature was around 20°C (Figure 5.47). At T_{Final} the water column was still well mixed, but the pH had dropped by 0.3 units and the seawater temperature had increased by over 0.5°C.

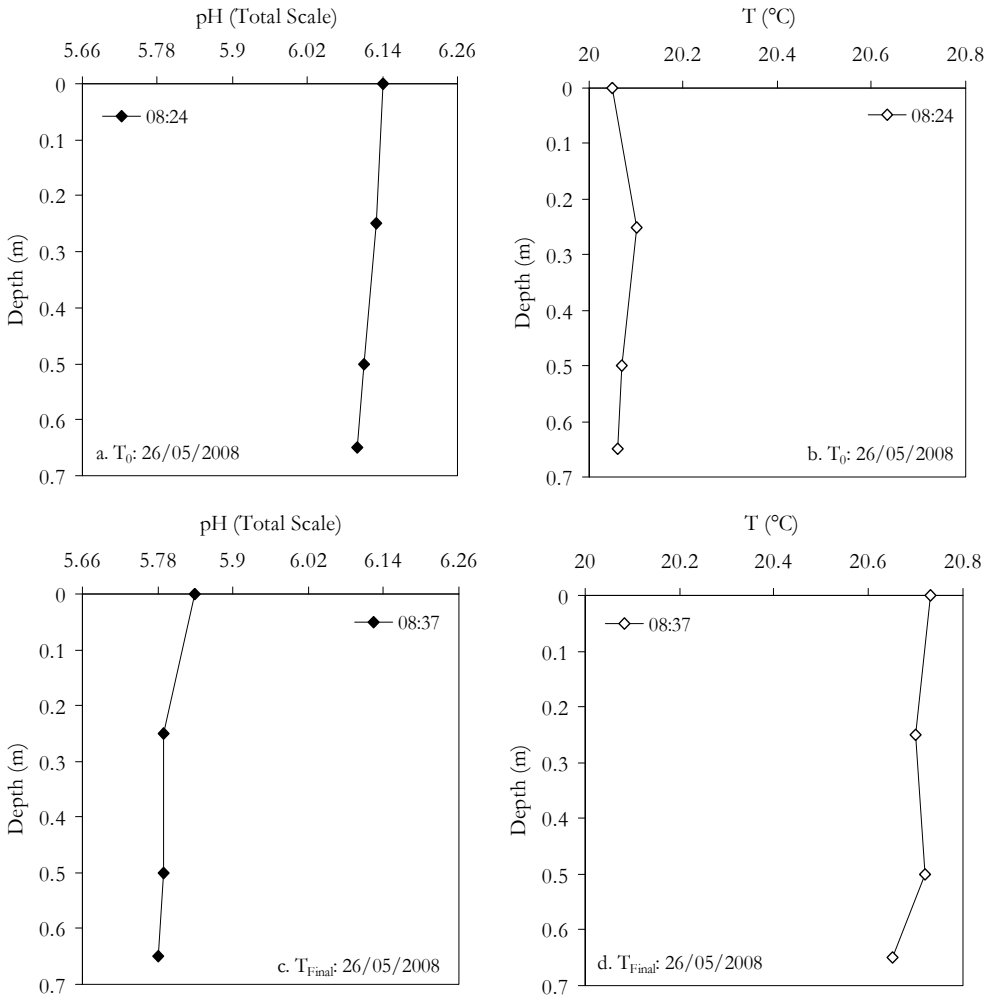

Figure 5.46. Depth profiles of pH (Total scale) (a and c) and seawater temperature (°C) (b and d) at T_0 and T_{Final} at 3m, Transect A, over the course of Experiment 3.

5.9.4.3.2. Trace gas concentrations

a. Iodocarbons

At T_0, total iodocarbon concentrations (Figure 5.48) in the benthic tent were double those in the pelagic tedlar bag (41 pM compared to 20 pM). However, almost all of this difference was accounted for by the presence of 19 pM of CH_2I_2 in the benthic, compared to <1 pM in the pelagic – a similar finding to that in Experiment 2. Concentrations of all other iodocarbons were very similar at T_0 in the two incubations.

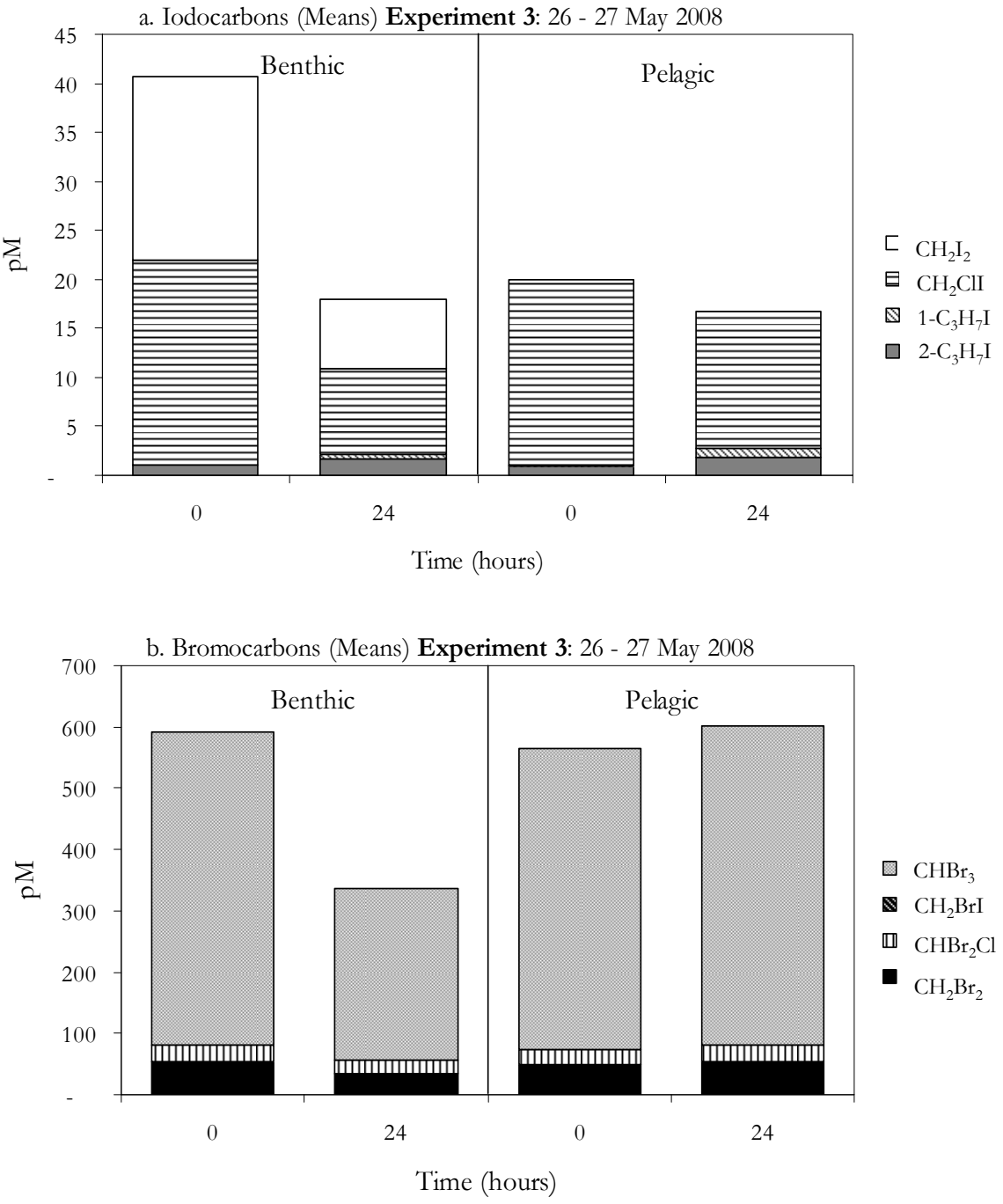

Figure 5.47. Mean concentrations (pM) of a. Iodocarbons and b. Bromocarbons in the benthic tent and the pelagic tedlar bag at T_0 and T_{Final} (24 hours) during Experiment 3.

By T_{Final} 24 hours later, the concentrations of CH_2I_2 in the benthic tent had fallen sharply by 11 pM, accompanied by a 12 pM drop in CH_2ClI. However, concentrations of 2-C_3H_7I and 1-C_3H_7I both increased by 0.7 pM and 0.5 pM, respectively, suggesting some net production of these compounds. Small increases of

0.9 pM and 0.8 pM in concentrations of 2-C_3H_7I and 1-C_3H_7I were also observed in the tedlar bags. However, concentrations of CH_2ClI dropped slightly, and there was no indication of any production of CH_2I_2.

b. Bromocarbons

The starting concentrations of bromocarbons at T_0 were similar in both the benthic and pelagic incubations, with totals of 593 pM and 564 pM, respectively (Figure 5.48). The small difference was attributable to higher levels of $CHBr_3$ and CH_2Br_2 in the benthic tent. Similarly to the other experiments, concentrations of CH_2Br_2 were around 10-fold lower than $CHBr_3$, and $CHBr_2Cl$ concentrations were ~50 percent of CH_2Br_2. CH_2BrI was present at low concentrations of <2 pM in both the benthic and pelagic at T_0.

At T_{Final}, slight increases in $CHBr_3$ (+29 pM), CH_2Br_2 (+5 pM) and $CHBr_2Cl$ (+4 pM) were observed in the pelagic incubation. Concentrations of CH_2BrI remained unchanged. By contrast, total bromocarbon concentrations in the benthic tent fell to 337 pM, a fall of 43 percent. Most of this loss was accounted for by ~40 percent decreases in both $CHBr_3$ and CH_2Br_2. $CHBr_2Cl$ concentrations also fell slightly, whilst CH_2BrI displayed a small increase. This data suggests that removal processes of bromocarbons dominated in the benthic tent at this site.

c. DMS

As seen during Experiments 1 and 2, starting concentrations of DMS (Figure 5.49) were slightly higher in the benthic tent, with 15.9 nmol l^{-1} compared to 15 nmol l^{-1}. By T_{Final}, DMS concentrations in both incubations had fallen sharply, by 58 percent and 36 percent in the benthic and pelagic respectively, suggesting strong removal processes were operating.

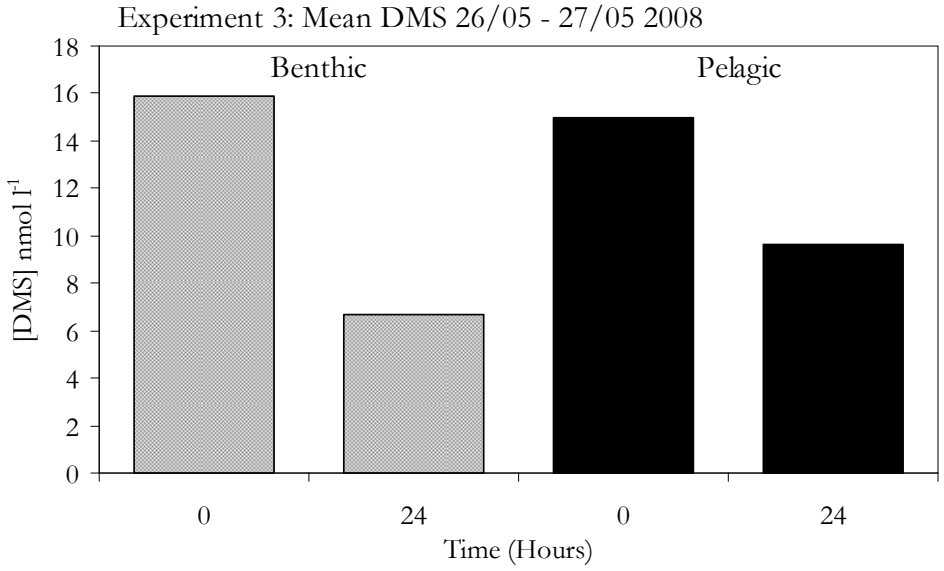

Figure 5.48. Mean concentrations (nmol l^{-1}) of DMS in the benthic tent and pelagic tedlar bag at T_0 and T_{Final} (24 hours) during Experiment 3.

5.9.5. Summary and Conclusions

Benthic and pelagic incubations were performed at three locations during May 2008. The sites were selected based on:

i) Mean pH characteristics

The incubations were carried out at sites that experienced a range of pH levels from 5.8 to 8.0, therefore potentially revealing the response of the pelagic and benthic organisms to a variety of pH conditions. Experiment 1 was carried out at Site 3, with mean pH readings for T_0 and T_{Final} of 6.6 and 7.7, respectively. Experiment 2 was at the routinely monitored 19 m station, with mean pH at T_0 of 7.7 and T_{Final} of 7.5. Finally, Experiment 3 was located at 3 m on Transect A, with mean pH at T_0 of 6.1, and T_{Final} of 5.8.

ii) The benthic macrofauna

Although this site is considered to be predominantly colonised by the seagrass *P. oceanica* (Hall-Spencer *et al.* 2008), brown macroalgae are found in the region closest to the cliff and in the region of most intense CO_2 venting. The benthic incubations for Experiments 1 and 2 were located on seagrass, while Experiment 3 was positioned over (unidentified) brown macroalgae. Therefore trace gas production by different benthic communities could be assessed.

iii) Ease of sampling

The selected sites could not be in water greater than ~2.5 – 3 m of water as the samples from the benthic tent incubations were taken by duck-diving. This meant that it was not possible to perform a control experiment at a site with background pH as such conditions are only found in deeper water.

Table 5.12 gives a summary of the percentage changes seen in pelagic (P) and benthic (B) incubations during each of the experiments.

5.9.5.1. Iodocarbons

For all three incubation experiments, iodocarbons concentrations were higher in benthic tent at T_0. For Experiment 1, concentrations of all iodocarbons were higher in the benthic tent. For Experiments 2 and 3, this difference was mainly accounted for by high CH_2I_2 concentrations in the benthic tent compared to the pelagic incubation.

Experiments 1 and 2 were performed in a seagrass meadow, and the benthic tents were therefore located over similar benthic communities. Both T_0 and T_{Final} iodocarbon concentrations were similar for these experiments, and this suggests that the iodocarbon pool observed during these incubations may represent the signature of iodocarbons produced by seagrass and the organisms living on and around them. Benthic iodocarbon concentrations during Experiment 3 were lower than in the previous two experiments. This is possibly a manifestation of the different benthic flora seen at this site, suggesting that brown macroalgae are not such strong producers of iodocarbons. In addition, the extremely low pH conditions that would be experienced by the macroalgae may result in physiological stress that may result in the impediment of the production mechanisms of these compounds. Experiment 3 also saw the lowest pelagic concentrations of iodocarbons. Low chlorophyll *a* concentrations were recorded here on a number of days during the campaign (0.19 – 0.3 mg m^{-3}, see figure 5.20). In addition, the dialysis experiments revealed a large drop in chlorophyll *a* concentrations in incubations of background seawater at 5 m on Transect A (Figure 5.22). Similarly to the benthic community, the extremely low pH renders survival of plankton in this region of the site difficult, and may indirectly result in lowered pelagic trace gas production.

Table 5.12. Summary of the percentage changes seen in pelagic (P) and benthic (B) incubations at Site 3, and 19 m and 3 m on Transect A.

					% Change															
	Mean pH	Mean pH	$[CH_2I_2]$		$[CH_2ClI]$		$[2C_3H_7I]$		$[1C_3H_7I]$		$[CHBr_3]$		$[CH_2Br_2]$		$[CHBr_2Cl]$		$[CH_2BrI]$		[DMS]	
	T_0	**T_{Final}**	**B**	**P**	**B**	**P**	**B**	**P**	**B**	**P**	**B**	**P**	**B**	**P**	**B**	**P**	**B**	**P**	**B**	**P**
1. Site 3	6.6	7.7	-86	-62	-56	-17	-67	+63	-53	-48	-47	-29	-71	-52	-95	-92	-52	-34	-28	-33
2. 19m	7.7	7.5	-88	+100	-23	-2	-32	+72	-35	+50	+5	-1	+5	-9	-13	+1	-62	-100	-18	+36
3. 3m	6.1	5.8	-63	-100	-58	-26	+40	+90	+100	+48	-39	+6	-39	+10	-11	+13	+20	-	-58	-36

Iodocarbon concentrations in the pelagic incubations were highest during Experiment 1, and unlike the benthic incubations, concentrations did not show any similarity to Experiment 2. This suggests that the benthic signal may not be greatly influential on pelagic trace gas concentrations. Furthermore, at T_{Final} all three experiments saw a greater loss of iodocarbons in the benthic tent than the pelagic bag, mainly attributable to a loss of CH_2I_2, and again highlighting the separate behaviour of benthic and pelagic trace gases. This loss may have occurred *via* a number of processes: the benthic tent was not a completely sealed system so some exchange with outside water was very likely to have occurred. In addition, loss may have occurred through the biological uptake of iodocarbons, a process that has not previously been quantified. Biological uptake of CH_3Br has been measured (Goodwin *et al.* 1997a; King and Saltzman 1997; Goodwin *et al.* 1998) suggesting bacteria may utilise other halocarbons as a carbon source.

5.9.5.2. Bromocarbons

At T_0, concentrations of bromocarbons were higher in all benthic incubations than in the pelagic, suggesting that there was a benthic source of these compounds at this site. However, the starting concentration varied, and did not seem to be related to the dominant benthic flora. In addition, as chlorophyll *a* concentrations at this site were very low compared to the Gulf of Naples as a whole (See 5.2.2), the benthic community may appear to be a stronger source simply due to higher biomass.

Although Experiments 1 and 2 were both located on seagrass, the starting concentrations were quite different (1178 pM for Experiment 1 and 373 pM for Experiment 2). However, the percentage contribution of bromocarbons to the overall pool was very similar for all experiments, particularly in terms of the CH_2Br_2: $CHBr_3$ ratio. Table 5.13 below shows benthic and pelagic CH_2Br_2: $CHBr_3$ ratios at T_0 and T_{Final} for each of the experiments. Ratios ranged from 0.09 – 0.12 in the benthic incubations, and 0.09 to 0.10 in the pelagic. Ratios of this order are usually encountered in coastal areas that experience strong sources of $CHBr_3$ (Moore and Tokarczyk 1993; Krysell and Nightingale 1994; Carpenter *et al.* 2003). The slightly higher ratios observed in the benthic incubations indicate a slightly stronger source of CH_2Br_2.

Table 5.13. Ratios of CH_2Br_2 to $CHBr_3$ at T_0 and T_{Final} in the benthic and pelagic incubations for Experiments 1, 2 and 3.

	Benthic		**Pelagic**	
	T_0	T_{Final}	T_0	TF_{inal}
Expt 1	0.10	0.09	0.09	0.09
Expt 2	0.11	0.11	0.10	0.09
Expt 3	0.11	0.12	0.10	0.10

5.9.5.3. DMS

DMS concentrations during the experiments ranged from 5.0 – 15.9 nM l^{-1} in the benthic incubations, and 3.5 to 15.0 nM l^{-1} in the pelagic, suggesting the benthic community represents a slightly stronger source of this compound. In all three experiments this was reinforced by higher concentrations in the benthic tents at T_0. Experiments 1 and 3 saw a fall concentrations in both the benthic and pelagic incubations over the course of the experiments. By contrast, there was an increase in concentrations from 6.8 to 10.6 nM l^{-1} in the pelagic incubation of Experiment 2, while benthic concentrations fell by 1.6 nM l^{-1}. This is an indication that the pelagic community at this site represented an active source of DMS, whilst DMS removal processes dominated in all other incubations.

Table 5.14 displays a summary of DMS concentrations at T_0 and T_{Final} for the three experiments. Concentrations during Experiments 1 and 2 were of a similar order, perhaps a reflection of the similar benthic community, as both were performed in an area of seagrass meadow. Starting concentrations were higher during Experiment 3, an indication that brown macroalgae that dominated the benthic flora at this site may be stronger producers of DMS. Additionally, it is possible that the increased DMS production was a result of the extremely low pH conditions inflicting stress on the macroalgae. Stress caused by a range of parameters, including desiccation, freezing, ultraviolet radiation and heavy metals have been shown to result in an increase of Reactive Oxygen Species (ROS) in macroalgae. This is due to inhibition of photosynthesis and excess energy, leading to a continual build up of ROS (Dring 2006). Seaweed species that have the ability to withstand such stresses are able to eliminate ROS with antioxidant compounds (Dring 2006). Additionally, it has been demonstrated that phytoplankton may utilise DMSP in an anti-oxidant role under stress conditions (Sunda *et al.* 2002). Although the effects of low pH on ROS

production and DMSP has not been reported, it is possible that both macroalgae and phytoplankton exposed to low seawater pH may produce additional DMSP, and hence DMS, in response to the stress induced by the abnormal conditions.

Table 5.14. Summary of DMS concentrations (nmol l^{-1}) at T_0 and T_{Final} for the benthic /pelagic incubations.

	Benthic [DMS] nmol l^{-1}		**Pelagic [DMS] nmol l^{-1}**	
	T_0	**T_{Final}**	**T_0**	**T_{Final}**
Experiment 1	6.9	5.0	5.2	3.5
Experiment 2	8.9	7.3	6.8	10.6
Experiment 3	15.9	6.7	15.0	9.6

5.9.5.4. Conclusions

Seawater pH and temperature displayed a large degree of variability over the course of the experiments. As these parameters were only measured at T_0 and T_{Final}, the overall variability over the course of the incubations is unknown. Although the sites were partly selected on the basis of mean pH characteristics, it is likely that the incubation sites experienced a large range of and rapidly changing seawater pH. This variability in pH would not have impacted on the pelagic incubations, as once filled with water, no exchange with outside water occurred. The benthic incubations were not completely sealed, so some exchange with the surrounding water will have occurred, allowing the benthic community enclosed within to potentially experience rapidly shifting seawater pH. Therefore, information derived from these incubations is more useful for providing information on the differences between pelagic and benthic trace gas production, rather than revealing any impacts of seawater pH on pelagic biogenic trace gas production.

This chapter has involved a thorough assessment of a volcanically-acidified shallow marine site at Ischia, Italy, to infer its suitability as a natural analogue of future OA and pelagic trace gas production. A discussion of the major findings, followed by a number of conclusions is given in Chapter 6, Section 6.2.3.

CHAPTER 6
Summary, Discussions and Conclusions

6.1 Summary of Research

6.1.1 Research context

Ever increasing atmospheric CO_2 concentrations as a result of human activities lead to the oceanic uptake of excess CO_2, and an alteration of seawater carbonate chemistry, manifested as increasing $[H^+]$, falling $[CO_3^{2-}]$ and a drop in pH. This process of OA is expected to negatively impact marine biota, with implications for both ecological processes and biogeochemical cycles. Through both experimental and *in situ* studies, in this thesis I have attempted to assess the potential impacts OA may have on the production of climatically- and atmospherically-important marine biogenic trace gases, including DMS and halocarbons. This chapter includes summaries of the major findings of this thesis, comparisons with previous studies, attempts to predict the atmospheric implications of changes to future trace gas production and recommendations of a number of areas that require further research.

6.2 Impacts of OA on marine biogenic trace gases

6.2.1 Synthesis of DMS OA studies

The work described in Chapter 3 represents the third mesocosm experiment to assess the impacts of OA on DMS and DMSP production during blooms of phytoplankton. Previous to this, Avgoustidi in 2003, and Vogt *et al*. and Wingenter *et al*. in 2005 determined concentrations of these compounds under high future CO_2 concentrations and present day CO_2 during similar mesocosm experiments. Table 6.1 gives a summary of the three OA mesocosm experiments. The concept and design of each of the experiments was very similar, each being initiated by the addition of nutrients, with the resultant phytoplankton blooms lasting 20 – 23 days. In order to encourage diatom blooms, the 2003 experiment received addition of silicate, as well as nitrate and phosphate, on day 0 and again on day 7, whereas the 2005 and 2006 experiments received only nitrate and phosphate on day 0.

Study	Experiment	Time (Days)	Nutrient addition (Initial concs)	Chl *a* max. mg m^{-3}		Mean DMS max. nM l^{-1}		Mean DMSPp max. nM l^{-1}	
				High CO_2	Present CO_2	High CO_2	Present CO_2	High CO_2	Present CO_2
Avgoustidi 2006	PeECE II April/May 2003	20	Day 0 and 7 0.5 µmol l^{-1} PO_4 9 µmol l^{-1} NO_3 12 µmol l^{-1} $Si(OH)_4$	4.0 Day 14	4.6 Day 12	21.5	32.3	143.8	258.7
Vogt *et al.* 2008	PeECE III May/June 2005	22	Day 0 0.7 µmol l^{-1} PO_4 15 µmol l^{-1} NO_3	13.5 Day 10	11.0 Day 10	27.4	29.5	366.0	370.0
Wingenter *et al.* 2007	PeECE III May/June 2005	22	As above	As above	As above	28.5	28.0	N/A	N/A
This study	NERC microbial metagenomics experiment May 2006	23	Day 0 0.8 µmol l^{-1} PO_4 15 µmol l^{-1} NO_3	6.0 Day 12	10.3 Day 12	11.8	34.7	262.2	414.3

Table 6.1. Summary of the ocean acidification mesocosm experiments performed at the Bergen Large-scale Facility, Raunefjord, Norway in 2003, 2005 and 2006. Includes duration of experiment (days), initial nutrient concentrations (µmol l^{-1}), maximum chl *a* concentrations (mg m^{-3}), and mean maximum DMS and DMSPp concentrations (nM) under high pCO_2 (~700 – 750 ppmv) and present day pCO_2 (~380 ppmv

Chlorophyll *a* characteristics varied between experiments; relatively low concentrations were experienced during 2003 with a maximum of 4.6 mg m^{-3}, whilst a maximum of 13.5 mg m^{-3} was recorded in 2005. There were no significant differences in chlorophyll *a* between treatments in either experiment. By contrast, chlorophyll *a* concentrations during this study were significantly lower under high CO_2 during the bloom phase, with maximum concentrations of 6 mg m^{-3} and 10.3 mg m^{-3} under high CO_2 and present day CO_2, respectively. The response of the communities to the perturbation varied between experiments. No significant differences in community structure were identified during the 2003 and 2005 experiments. In this study, most components of the nano- and picoplankton were significantly lower under high CO_2 (coccolithophores, large picoeukaryotes, Cryptophytes and *Synechococcus*). The abundance of coccolithophores, in particular *E. huxleyi*, showed some variation between experiments. In the 2005 experiment a strong coccolithophore bloom occurred, with maximum abundances of 56 x 10^6 cells ml^{-1}, whilst in 2003 *E. huxleyi* was less prolific (Max. 5.5 x 10^6 cells ml^{-1}). For this study, *E. huxleyi* was even less abundant, with maximum numbers of only 3 x 10^3 cells ml^{-1}.

These differences in biological characteristics and community structure, as well as the resilience or sensitivity of various components of the community to the CO_2 perturbation may have produced the variations in response of DMS and DMSP concentrations between the three experiments. This study showed similarity with the 2003 experiment, with lower DMS and DMSP under high CO_2. The 2005 experiment saw different temporal development of DMS, with greater production under high CO_2, although the differences were not significant. Vogt *et al*. (2008) concluded that as there were no significant differences in species composition or succession between treatments, the small observed differences in DMS concentrations are most likely due to differences in bacterial or viral activity. Avgoustidi (2007) came to similar conclusions again due to lack of changes in community, with the impact on secondary factors, such as grazing, viral infection and bacterial uptake considered to be likely to explain the lowered DMS concentrations under high CO_2. During this study, it appeared that the impact of high CO_2 was greatest on the conversion of DMSP to DMS, rather than the initial production of DMSP, again implicating an effect on similar secondary factors. In addition, unlike the other studies, the significant decreases in DMS could be directly attributable to significant changes in ecosystem composition. For all of the studies, a direct impact on DMS concentrations may be the

result of bacterial consumption of DMS, a process that may have been either enhanced (2003 and 2006) or diminished (2005) under high CO_2.

Despite some conflicting results, assimilation of the data from the three mesocosm experiments suggests that an impact of OA on DMS/DMSP production is likely. Avgoustidi (2007) performed *in vitro* experiments on natural seawater assemblages and monospecific cultures of *E. huxleyi*, the results of which back up the conclusions of the 2003 study (and thus also this study). Therefore, this suggests that there may be a decrease in DMS/DMSP in a future high CO_2 world. Differences between the experiments, particularly in terms of community composition and weather conditions, make it difficult to draw direct comparisons and solid conclusions. In an attempt to further elucidate the impacts of OA on DMS production, additional investigation is required, perhaps in the form of larger-scale mesocosm experiments, or incubation of natural assemblages from various oceanic regions.

6.2.2 Comparison between mesocosm and L4 incubations

The strong response of DMS and iodocarbons to high CO_2 seen during the mesocosm study (Chapter 3) initiated a plan to attempt to further these findings on a smaller and more controlled scale. Thus, two laboratory incubation experiments of natural seawater assemblages were performed (Chapter 4), with 4 replicate incubations vessels for each CO_2 treatment. Concentrations of halocarbons, as well as DMSP, and a range of biological parameters were assessed in order to compare the response to that seen during the mesocosm.

Table 6.2 is a summary of data from the mesocosm experiment, and L4 Experiments 1 and 2. Mean chlorophyll *a* concentrations during the mesocosm experiment were considerably lower than those experienced during the L4 incubations, not exceeding 10.3 mg m^{-3}, whilst concentrations reached 62.7 mg m^{-3} in Experiment 1 and 82.5 mg m^{-3} in Experiment 2. The phytoplankton community of Experiment 1 was heavily dominated by heterotrophic dinoflagellates, comprising 79 percent and 69 percent of total biomass under high CO_2 and present day CO_2, respectively. Flagellates were the second most abundant in terms of biomass, although this group made up only 7 percent of the total biomass. Experiment 2 was dominated by flagellates, with 73 percent and 87 percent of total biomass under the two respective treatments.

Table 6.2. Comparison table of the results from the mesocosm experiment, L4 Experiment 1 and L4 Experiment 2. [1] = mg m^{-3}, [2] = cells ml^{-1}, [3] = μg^{-1}, [4] = pM, [5] = pM mg^{-1} , * = differences between treatments considered significant at a threshold of $p<0.05$. In brackets, % contribution to total biomass.

	MESOCOSM EXPT.			L4 EXPT.1			L4 EXPT.2		
	High CO_2 Mean	Present CO_2 Mean	% CHANGE	High CO_2 Mean	Present CO_2 Mean	% CHANGE	High CO_2 Mean	Present CO_2 Mean	% CHANGE
Chl *a* [1]	2.5	3.4	-28*	21.5	20.5	+4.8	15.7	10.7	+31.6*
Picoeukaryotes [2]	24750	26585	-7	46675	31480	+32.6*	-	-	
Nanophytoplankton[2]	1160	1507	-25	8897	8243	+7.4	12924	13828	-6.5*
Synechococcus[2]	3907	8540	-55*	11668	14334	-18.6	29599	26921	+9.1
Flagellates[3]	107.7 **(71%)**	148.2 **(69%)**	-27	8.0 **(7%)**	8.9 **(7%)**	+2	40.8 **(73%)**	48.8 **(87%)**	-16
Ciliates[3]	30.6 **(20%)**	51.6 **(23%)**	-41	4.7 **(4%)**	4.4 **(4%)**	+18	3.0 **(5%)**	2.5 **(5%)**	+16
Autotrophic dinoflagellates [3]	7.8 **(5%)**	15.8 **(7%)**	-51	4.5 **(4%)**	3.6 **(3%)**	+29	5.3 **(10%)**	2.9 **(5%)**	+46
Heterotrophic dinoflagellates [3]	4.2 **(3%)**	3.8 **(2%)**	+8	84.9 **(79%)**	85.1 **(69%)**	+12	2.2 **(4%)**	2.6 **(5%)**	-14
Diatoms [3]	0.5 **(0.3%)**	2.4 **(1%)**	-81	5.4 **(5%)**	2.9 **(3%)**	+53	4.8 **(9%)**	1.0 **(2%)**	+79
CH_3I [4]	5.4	9.7	-44*	3.7	4.2	-12.8*	13.5	15.5	-13.3
C_2H_5I [4]	0.5	0.8	-35	0.57	0.62	-8.6	0.9	1.1	-20.5
CH_2I_2 [4]	127.8	175.9	-27	-	-	-2.7	39.4	36.0	+8.8
CH_2ClI [4]	136.9	179.0	-24	80.7	94.5	-15	46.8	45.0	+3.8
2-C_3H_7I [4]	-	-	-	0.37	0.37	-0.8	0.6	0.5	+7.8
$CHBr_3$ [4]	39.8	34.7	+13	2.6	3.7	-31	7.2	7.1	+0.8
CH_2Br_2 [4]	2.4	2.2	+8	11.2	7.1	+37*	6.5	6.3	+4.0
$CHBr_2Cl$ [4]	0.60	0.48	+22*	-	-	-	-	-	
CH_2BrCl [4]	-	-	-	3.8	4.3	-10.5	0.66	0.73	-10.1
CH_3I: chl *a* [5]	3.8	4.7	-39.6	0.2	0.3	-19.7	2.5	5.0	-50.5*
C_2H_5I: chl *a* [5]	0.30	0.34	-46.5	0.035	0.042	-16.7	0.1	0.2	-45.8*
CH_2I_2: chl *a* [5]	34.7	31.9	-23.8	-	-	-13.3	8.3	13.5	-38.7*
CH_2ClI chl-a [5]	48.2	57.5	-39.5	5.2	6.8	-23.7	12.0	16.0	-24.8
2-C_3H_7I: chl *a* [5]	-	-	-	0.024	0.027	-11.1	0.12	0.18	-33.3
$CHBr_3$: chl *a* [5]	42.7	34.3	+35.3	0.16	0.24	-34.5	1.5	2.5	-39.9*
CH_2Br_2: chl *a* [5]	2.3	2.5	-6.3	0.72	0.45	+60.5*	1.4	2.8	-49.7
$CHBr_2Cl$: chl *a* [5]	0.6	0.5	+28.1	-	-	-	-	-	-
CH_2BrCl: chl *a* [5]	-	-	-	0.25	0.31	-19.4	0.13	0.23	-43.5*

The communities of the mesocosms were also dominated by flagellates (71 percent and 69 percent of total biomass), with an additional fifth of the populations made up of ciliates. Ciliates were less important in the L4 incubations. A general trend seen in the biological data from the mesocosm was a reduction under high CO_2 of chlorophyll *a*, phytoplankton numbers and biomass, with only the heterotrophic

dinoflagellates showing an increase in biomass under high CO_2. In contrast, in Experiment 1 there was an increase in the majority of biological parameters under high CO_2, with reductions in only *Synechococcus* numbers. In Experiment 2 there was more variation in the response of the phytoplankton community to high CO_2, with decreases in nanophytoplankton numbers, and flagellate and heterotrophic dinoflagellates biomass. In carrying out these experiments, the response of three distinct plankton communities to future high CO_2 conditions has been achieved. The response of the communities in terms of trace gases was variable. A consistent decrease in CH_3I and C_2H_5I under high CO_2 was seen in all three experiments; for CH_3I a 13 percent decrease during both L4 experiments, and a large and significant 43 percent decrease during the mesocosm study, and for C_2H_5I, a 35 percent reduction during the mesocosm, and 9 percent and 21 percent declines during Experiment 1 and Experiment 2, respectively. In both Experiment 1 and the mesocosm experiment there were decreases in mean concentrations of all other iodocarbons. By contrast, in Experiment 2 there were increases in the mean concentrations of CH_2I_2, CH_2ClI and 2-C_3H_7I under high CO_2. When normalised to chlorophyll *a*, concentrations of all iodocarbons for all experiments were lower under high CO_2, an indication of reduced iodocarbon production per unit of chlorophyll *a* under the perturbed conditions.

The impacts of high CO_2 on concentrations of bromocarbons were less consistent. Whilst the mean concentrations of all bromocarbons showed some increase under high CO_2 during the mesocosm experiment, $CHBr_3$ decreased by 31 percent in Experiment 1 and increased by 0.8 percent in Experiment 2. CH_2BrCl showed a consistent ~10 percent decrease under high CO_2 in both L4 incubation experiments. A common feature across the three experiments was an increase in concentrations of CH_2Br_2 under high CO_2. Again, the response of the bromocarbon: chlorophyll *a* ratio was less clear-cut. Whilst in the mesocosm a large percentage increase in $CHBr_3$: chlorophyll *a* of 35 percent occurred, in Experiments 1 and 2 considerable decreases of 35 percent and 40 percent took place, respectively. A reduction in CH_2Br_2: chlorophyll *a* was observed during the mesocosm experiment and Experiment 2, whilst in Experiment 1 there was a large 61 percent increase. More consistent in nature was a decrease in CH_2BrCl: chlorophyll *a* during both L4 incubation experiments.

The response of halocarbon concentrations to high CO_2 during Experiment 2 was much more variable than for Experiment 1. Similarly to the mesocosm experiment and Experiment 1, mean concentrations of CH_3I and C_2H_5I were lower

under high CO_2. However, all of the other iodocarbons actually increased under high CO_2 during Experiment 2, as did $CHBr_3$ and CH_2Br_2. CH_2BrCl decreased, a response consistent with Experiment 1. None of the differences in trace gas concentrations between treatments were found to be statistically significant, suggesting a degree of resilience of the community to the high CO_2 conditions. However, the various components of the community showed a range of responses. There was a significant decrease in numbers of nanophytoplankton. By contrast, chlorophyll *a* concentrations showed a significant increase under high CO_2, accompanied by an increase in *Synechococcus* numbers. This large increase in chlorophyll *a*, along with only modest changes in trace gas concentrations, resulted in dramatic, and in the majority of cases, significant decreases in halocarbon: chlorophyll *a* ratios. This suggests that trace gas production by the community as a whole is less favourable under high CO_2 and lowered seawater pH conditions, a finding in common with both the mesocosm experiment and Experiment 1.

6.2.2.1 Conclusions

A decrease in net iodocarbon production under high CO_2 was observed during all 3 experiments. The production of halocarbons in seawater is not fully understood, but is considered to be is the result of a number of complex processes, involving DOM, the availability of halogen ions, bacterial and phytoplankton activity and photochemical reactions in surface seawater. Despite the consistent response of the iodocarbons to high CO_2, the response of the phytoplankton communities was more variable. So the decrease in iodocarbons cannot be directly attributed to a general decrease in phytoplankton productivity. Therefore it is necessary to consider the impacts of high CO_2 on other production mechanisms:

Iodocarbons can be produced photochemically in surface seawater. In the case of monohalogenated compounds (CH_3I, C_2H_5I etc.), this process involves the initial production of methyl radicals from photolysis of seawater DOM, followed by the reaction between these radicals and I^- radicals (Moore and Zafiriou 1994). Polyhalogenated compounds such as CH_2I_2 can also be produced photochemically, through haloform reactions between HOI or I_2 and DOM (Martino *et al.* 2009). Light can be considered to play a direct role in the process, with biology playing an indirect role through the production of organic precursors in the form of DOM (Richter and Wallace 2004). Therefore an impact of high CO_2 on the seawater concentrations of

DOM may result in a decrease in iodocarbon production through a reduction in the precursors necessary for their formation. DOM is mainly derived from phytoplankton, and is, for example, released from senescing algal cells into the surrounding water. Upon its release, it is rapidly utilised by free-living bacteria (Azam *et al.* 1983). The response of bacterial communities to high CO_2 conditions has not been investigated during this study, but it is possible that if there was: i. a general increase in bacterial biomass, and concomitant increase in DOM consumption, or ii. a bacterial community shift to species with a greater affinity for DOM, the resultant decrease in availability of the precursor may explain the reduced concentrations of iodocarbons seen during this work.

Marine bacteria can also stimulate DOM production, and hence potentially halocarbon formation, through the breakdown of organic matter. Hughes *et al.* (2008) observed the production of CH_3I, C_2H_5I, 2-C_3H_7I and 1-C_3H_7I from marine biogenic aggregates and diatom mucilages, and stated that enhanced microbial activity associated with such aggregates could supply the DOM precursors for iodocarbon production. As well as exerting a strong control on the availability of iodocarbon precursors, free-living marine bacteria have also been implicated in the direct production of these compounds. The production of CH_3I by *Rhizobium* sp. strain MRCD19 has been observed (Amachi *et al.* 2001) and a mechanism was proposed involving S-adenosyl-L-methionine serving as the methyl donor for methylation of seawater I^-. Therefore it is possible that an as-yet unidentified impact of OA on the microbial loop may indirectly impact on the production of iodocarbons.

The response of the bromocarbons during this work was less consistent, with no clear trend in response to high CO_2. This suggests that processes leading to net production of bromocarbons, including direct production of $CHBr_3$ by phytoplankton during growth and senescence (Quack and Wallace 2004; Quack *et al.* 2007b), and reductive halogenation of $CHBr_3$ to produce CH_2Br_2 and $CHBr_2Cl$ (Goodwin *et al.* 1997a; Quack and Wallace 2004), are more resilient to the changes in seawater pH of the magnitude and timing considered here.

6.2.3. Ischia: A Potential Natural Analogue for Future Ocean Acidification?

In the assessing the suitability of the volcanically-acidified site at Ischia in terms of the impacts of OA on pelagic trace gas production, the most important finding was the highly variable nature of seawater pH, on both temporal and spatial scales. This characteristic rendered this site un-ideal for such studies, as the rapid changes are likely to result in short-term impacts on the pelagic communities, rather than allowing any degree of adaptation to the conditions. Any observed responses are likely to be due to stress, or a toxic shock effect.

Mean surface chlorophyll *a* concentrations for period 1984 – 2000 for the Gulf of Naples were reported to be ~1 mg m^{-3} for November and ~ 6 mg m^{-3} for May (Ribera d'Alcalà 2007). Values for chlorophyll *a* measured at the study site were lower than this, particularly during May when all measurements were <0.5 mg m^{-3}. This suggests that phytoplankton productivity is far lower at the site in the vicinity of the CO_2 vents than in the Gulf of Naples as a whole. Thus the extreme pH conditions may make the area unfavourable for abundant phytoplankton growth. Further support for a pH impact on phytoplankton populations came from the results of the dialysis experiments. Samples that were transplanted to and incubated in low pH waters (< pH 6.7) saw >60 percent decreases in chlorophyll *a* concentrations after 24 hours. Extreme pH conditions may impact on the health of phytoplankton in a number of ways. With low external pH, an ion balance effect may be experienced, whereby cells have to expend energy in order to maintain an internal pH suitable for cell function (Raven 1980). In addition, as the reaction rate of enzymes is pH-dependent, any departure from optimum pH conditions may impair cellular function (Hinga 2002). A less direct impact may result from pH-induced changes to seawater chemical speciation, and alteration of the equilibrium between sorbed and dissolved phases of metals. This could lead to changes to availability of trace metals and increased toxicity of elements such as Cu (Granéli and Haraldsson 1993). Thus, extreme low seawater pH may negatively impact on phytoplankton cells by multiple mechanisms. Such extreme impacts on the phytoplankton may result in impacts on trace gas production, but far outside the context of anthropogenic OA research.

This site has been shown to be a poor natural analogue for OA in terms of the pelagic community and biogenic trace gas production. In order to continue to further our understanding of the impacts of OA, other such sites need to be identified, although perhaps with less extreme pH levels, and less exchange with outside waters. Alternatively, upwelling regions that experience seasonal or even constant upwelling

of high pCO_2/ low pH seawater e.g. west coast of North America (Feely *et al.* 2008) may prove to be useful alternatives to volcanically-acidified areas.

6.3 Marine biogenic trace gas production in the future oceans

6.3.1 Predictions of future ocean acidification

In the early 1990s, the realisation that the uptake of anthropogenic CO_2 emissions by the oceans could impact on ocean carbonate chemistry started to receive attention in the scientific literature, and included reports of measurable changes in ocean chemistry over the previous 200 years (Quay *et al.* 1992; Chen 1993; Siegenthaler and Sarmiento 1993; Cole *et al.* 1995), In 1996, Haugan and Drange discussed the implications of these changes in terms of seawater pH. At this stage, it was recognised that a decrease in pH of 0.1 units had already occurred, and an additional 0.2 – 0.3 unit drop in pH may be expected by the end of the century (Haugan and Drange 1996). However, the potential impacts of these changes on marine biota were little known and poorly researched.

Through the late 1990s and into the early 21st century, the potential consequences of anthropogenic OA began to receive wider interest, and a number of important studies were published that used various model simulations in an attempt to predict the spatial and temporal nature of the changes to oceanic carbonate chemistry that were likely to occur (Caldeira and Wickett 2003; 2005; Orr *et al.* 2005; Blackford and Gilbert 2007; Cao and Caldeira 2008). Using an ocean general circulation model with CO_2 observations for 1975-2000, the IS92a emissions scenario up to 2100, and a logistic function for emissions for 2100 - 2300, Caldeira and Wickett (2003) found a maximum pH reduction of 0.77 units, and it was noted that in the last 300 million years of Earth's history there was no evidence that ocean pH had been greater than 0.6 units lower than today. Importantly, it was found that when CO_2 change occurred over short time scales (< ~10^4 years), ocean pH was relatively sensitive to the CO_2 addition. In contrast, if the changes occurred over a longer time period (>~10^5 years) ocean chemistry was naturally buffered and showed lowered sensitivity to pH changes.

Further modelling studies (Caldeira and Wickett 2005; Orr *et al.* 2005) came to similar conclusions to those first proposed by Haugan and Drange (1996), with an

expected drop in pH of 0.3 – 0.5 units by the Year 2100. Orr *et al.* (2005) also showed that some polar and subpolar surface waters would become aragonite undersaturated when atmospheric CO_2 levels reach 2 x pre-industrial levels: such changes may occur within the next 50 years. Blackford and Gilbert (2007) looked specifically at the North Sea and concluded that acidification of this ecologically- and commercially-important region would exceed 0.1 pH units over the next 50 years, and 0.5 units when CO_2 concentrations reached 1000 ppmv. A recent modelling study by Cao and Caldeira (2008) concluded that even if atmospheric CO_2 is stabilised at 450 ppmv, major impacts will still be felt, and by the time CO_2 concentrations reach 750 ppmv, the entire global ocean may see a decrease in pH of >0.2 units. In 2008, evidence of anthropogenic OA was reported in the upwelling region off the west coast of North America (Feely *et al.* 2008) – an indicator that man's fossil fuel legacy is now clearly measurable in the oceans.

6.3.2 Ocean acidification and climatic change

It is now widely accepted by the scientific community, world governments and general public that human activities are contributing to global climatic changes. The rapid increase in atmospheric CO_2 from 280 – 380 ppm between 1780 and 2005, accompanied by increases in CH_4 and N_2O, means that atmospheric concentrations of these potent greenhouse gases now significantly exceed pre-industrial values derived from ice-core data that stretch back hundreds of thousands of years (Siegenthaler *et al.* 2005; Spahni *et al.* 2005; I.P.C.C. 2007). Evidence from observations of increasing global average temperatures means that the warming of the climate system is indisputable, with 11 of the 12 years from 1995 – 2006 ranking amongst the warmest 12 since records began (I.P.C.C. 2007). The oceans are far from immune to such climatic changes. Observations since 1961 show that the oceans have absorbed more than 80 percent of the additional heat in the Earth system (I.P.C.C. 2007).

The influence of this warming on changes to ocean carbonate chemistry has been investigated. As shown in Figure 1.4 (Chapter 1, section 1.3.2), the solubility of CO_2 decreases with increasing temperature. Therefore, in a warming ocean one may expect the solubility of CO_2 to decrease, and perhaps alleviate some of the impacts of oceanic uptake of atmospheric CO_2 and the ensuing OA. However, recent modelling studies have shown that this may not be the case, and ocean pH is in fact insensitive to climate change feedbacks such as rising SST, and changes to ocean circulation and

biological processes (Cao *et al.* 2007; McNeil and Matear 2007). Therefore future projections of OA do not need to consider climate change effects, only atmospheric CO_2 levels.

The climatic impacts on the oceans are expected to affect phytoplankton communities. Although the exact mechanisms involved are still elusive, changes to ocean mixing and stratification are likely to be central to the impacts (Hays *et al.* 2005). Such hydrodynamic shifts can lead to effects on light levels, SST and nutrient cycling, all of which influence phytoplankton growth. Changes have already been observed in the global oceans. For example, a regime shift in the North Sea in the mid-1980s occurred due to a switch in the behaviour of the North Atlantic Oscillation (NAO). The result was an increase in SST, an inflow of warm salty water from the Atlantic and a shift from a cold-water species-dominated ecosystem to one dominated by warm-water species (Beaugrand 2004; McQuatters-Gollop *et al.* 2007). Other studies have reported increases in photosynthesis and productivity as a result of increasing temperatures (Bopp *et al.* 2001; Hare *et al.* 2007). The implications that climate –induced community shifts and changes in productivity may have for trace gas production are not fully understood, but such impacts may act synergistically with OA.

6.3.3 OA impacts on marine biogenic trace gases

6.3.3.1 DMS

The results of the mesocosm study in Chapter 3 revealed decreases in mean concentrations of DMS and DMSPt (60 percent and 24 percent, respectively) during phytoplankton blooms that were exposed to high CO_2 and low seawater pH at levels predicted for the Year 2100. Although not applicable to the entire global ocean, mesocosm studies are arguably representative of highly productive regions such as high latitude waters, coastal waters and upwellings, with such areas expected to be rapidly, and in some cases dramatically, impacted by OA (Orr *et al.* 2005; Doney *et al.* 2007; I.P.C.C. 2007; Feely *et al.* 2008). Therefore, in the context of the climate-regulating properties of DMS and its atmospheric oxidation products, it is pertinent to make attempts to assess the impact that such a decrease in seawater concentrations of DMS may have.

DMS and climate regulation

By influencing both the reflection and absorption of solar radiation through a variety of complex radiative and microphysical processes, atmospheric aerosols are able to directly exert a strong influence on the Earth's radiative budget (Andreae and Crutzen 1997; Ramanathan *et al.* 2001). Aerosols also indirectly influence climate through involvement with CCN and cloud formation, further impacting on the reflection of solar radiation (Andreae and Crutzen 1997). Aerosols originate from both natural and anthropogenic sources. Anthropogenic sources include sulphate and carbonaceous materials produced during fossil fuel combustion and biomass burning. Such pollutants generally show localised distribution, more concentrated in the industrialised Northern Hemisphere (Ramanathan *et al.* 2001). Natural aerosols originate from both terrestrial and marine environments, most notably non-methane hydrocarbons such as terpenes that are emitted from forests, and of relevance to this work, DMS from the oceans. It has been estimated that marine DMS contributes to around 20 – 80 percent of the SO_4^{2-} in air over the Northern Hemisphere, and >80 percent over most of the Southern Hemisphere (Chin and Jacob 1996).

When DMS is emitted to the atmosphere, it undergoes oxidation in the MBL to produce, most commonly, SO_2. This compound represents the source of SO_4^{2-} aerosols in unpolluted marine regions (Shaw 1983; Lovelock 1986; Charlson *et al.* 1987). DMS oxidation leads to the production of new CCN by both supplying the starting material for formation of new particles, and by encouraging growth of smaller particles into CCN (Andreae and Crutzen 1997). Therefore, the extent of climate-regulation by the oxidation products of DMS is dependent on a number of processes, but ultimately relies on there being an overall increase in the number concentration of CCN (particles ~0.05 μm-diameter) (Charlson *et al.* 1987; Andreae and Crutzen 1997).

The CLAW hypothesis (Charlson *et al.* 1987) states that changes to oceanic DMS emissions would cause corresponding changes to atmospheric [SO_4^{2-}] and hence to the number of particles that grow to CCN size. Therefore a decrease in DMS production in the oceans as a result of OA may ultimately lead to a reduction in CCN and marine stratus cloud albedo, and therefore produce a positive feedback on climate that would increase the warming that will occur as a result of anthropogenic GHGs.

The flux (F) of DMS to atmosphere can be described as follows:

$$F = A.k.\Delta c$$

where A is the total ocean surface area, k is the transfer velocity and Δc is the concentration gradient across the air-sea interface. Due to the highly saturated nature of the ocean relative to the atmosphere, Δc can be considered to be identical to [DMS] in the surface oceans. Therefore, taking the results of this study singularly, and assuming no changes to other parameters, a 60 percent decrease in seawater [DMS] as a result of OA would be equivalent to a 60 percent decrease in Δc. This would lead to a proportional decrease in flux of DMS to the atmosphere. Despite difficulties in quantifying the magnitude of the impact of such changes to the DMS flux, it is likely that if such a change were seen over extensive ocean areas, the climate response would be large. Using a coupled ocean-atmosphere general circulation model, Gunson *et al.* (2006) saw a 1.6°C increase in surface air temperature in response to a halving of ocean DMS emissions.

However, despite such results, and for a variety of reasons discussed below, it is very difficult to make quantitative predictions about the implications for radiative forcing and climatic impacts in terms of the decrease in DMS seen during this study:

1. *Impacts/effects vary regionally*

The effect of CCN number on albedo is more prominent at low particle numbers, resulting in a greater climatic effect in oceanic areas away from the influence of terrestrial air heavily laden with aerosols (Watson and Liss 1998). As a demonstration of this, it has been calculated that if equal quantities of S were to enter the atmosphere in the two hemispheres, the impact on albedo would be 25 times more pronounced in the Southern than in the Northern Hemisphere (Twomey 1991). A number of modelling studies on the effects of climate change on DMS production and aerosol formation have revealed large spatial heterogeneities in both DMS concentrations and flux, and the climatic impacts (Gabric *et al.* 1998; Bopp *et al.* 2003; Gabric *et al.* 2005; Gunson *et al.* 2006). For example, Bopp *et al.* (2003) reported a mean decrease in global seawater DMS concentrations of ~1 percent in response to doubled atmospheric CO_2 concentrations, but the regional impacts were much more pronounced. The western Equatorial Pacific and the eastern Equatorial Atlantic saw a decrease of up to 50 percent, whilst the eastern Equatorial Pacific saw an increase of up to 50 percent. In addition the subtropical/subantarctic convergence zone

experienced a 20 percent enrichment, with smaller increases seen in the north Atlantic and Pacific. The global DMS flux showed similar regional variation, and resulted in heterogeneity in the climatic effects. Whilst the impact on radiative forcing was -1 W m^{-2} in the Southern ocean, it was calculated to be +0.5 W m^{-2} in the tropics.

2. *Difficult to quantify how many CCNs in atmosphere derived from marine DMS*

Atmospheric aerosols come from a range of sources. Thus, it is difficult to distinguish the impact of DMS-derived aerosols on climate from that from other aerosols. It is also unknown how much marine stratus cloud currently in the atmosphere is affected by them. Watson and Liss (1998) made attempts to calculate the current influence that DMS has on global albedo. By assuming that around half of CCN in typical Southern Hemisphere marine air is due to DMS, they calculated that a doubling of [CCN] would lead to a 6 – 46 percent increase in marine stratus cloud albedo. If one third of the globe is assumed to be covered by marine stratus clouds, this would result in a ~2 percent increase in global albedo, and a 3.8 k cooling of climate. However, the large margin of error highlights the difficulties involved in quantifying the influence of marine DMS on aerosols and climate.

3. *Different phytoplankton species differ in their ability to produce DMS/DMSP*

Haptophytes, in particular the coccolithophorids, are considered to be the most prolific planktonic producers of DMSP/DMS, followed by *Phaeocystis*, with lesser production by dinoflagellates and diatoms (Malin *et al.* 1992; Malin *et al.* 1994; Liss *et al.* 1997). The response of phytoplankton communities to changing climate is still not fully understood (Hays *et al.* 2005), and even less is known about how planktonic communities may react to OA. Ecosystem shifts in response to global changes are likely to impact on DMS production through changing species dominance. The differing ability of phytoplankton species to produce these compounds further complicates our capacity to make quantitative predictions about the impact of OA on DMS production and climate.

4. *Atmospheric effects of oxidised S non-linear*

In terms of climate impacts, it is not the bulk quantity of DMS oxidation that is important, but the ability of the oxidation products to enhance the CCN number

concentration (Charlson *et al.* 1987; Andreae and Crutzen 1997). However, the formation of CCN from the oxidation products of DMS (SO_2 and H_2SO_4) and the resulting climate sensitivity is complex and non-linear, and cannot be constrained using a simple, globally-applicable model (Korhonen *et al.* 2008; Carslaw *et al.* 2009).

5. *Impact of other climate change effects on DMS-CCN-climate feedback not fully understood*

The flux of DMS to the atmosphere is controlled by surface seawater [DMS] and the magnitude of the transfer velocity, both of which are influenced by climate variables. Seawater DMS concentrations are controlled by marine biological activity, which is dependent on solar irradiance, sea temperature and ocean dynamics, whilst the transfer velocity is controlled by temperature and wind velocity. Therefore, it is extremely unlikely that OA will be the only process that impacts on DMS production in the future oceans, and a range of other climatic changes will also have an effect. Increased solar irradiance and sea surface temperature will ultimately result in lowered marine productivity in some regions, due to enhanced stratification and reduced upwelling of nutrient-rich water. Using an atmosphere-ocean general circulation model coupled to a marine biogeochemical scheme, Bopp *et al.* (2003) observed such an effect in the western Equatorial Pacific in response to doubled atmospheric CO_2, with a resultant lowering of DMSPp and DMS concentrations. By contrast, a modelling study by Gunson *et al.* (2006) reported a promotion of phytoplankton growth and increased DMS production in response to increased temperatures and light. Clearly, the response of the DMS system to changing global temperatures is variable and difficult to predict or generalise. Changes to wind velocity are also likely to have an impact. Again during the modelling study performed by Bopp *et al.* (2003) a 19 percent increase in DMS flux was observed from 30°S - 50°S, a quarter of which could be attributed to an increase in wind speed. In brief, other climatic changes that may influence DMS production include: i. The contraction of Arctic sea ice due to increasing global temperatures. This would expose more seawater to the sun, and result in an increase in phytoplankton productivity and DMS production (Gabric *et al.* 2005), ii. Changes to atmospheric dust input to the oceans due to changing wind/land-use patterns. The iron fertilisation effect would enhance productivity, and increase DMS production (Jickells *et al.* 2005), iii. Changes to atmospheric convection patterns as a result of climatic shifts, which may effect the

transport of DMS to the troposphere and the subsequent CCN production (Shaw *et al.* 1998).

Taking the above into account, it is clear that the response of the DMS-CCN-climate system to global environmental changes is challenging to quantify, and despite more than 20 years of research since the CLAW hypothesis was first described, the sign of the feedback mechanisms that may be involved are still uncertain. This study, in combination with the work of Avgoustidi (2007), provides strong evidence that future OA may negatively impact oceanic DMS emissions. At this stage, the extent of the impact and any accompanying climate feedbacks are not certain.

6.3.3.2 Iodocarbons

The oceans are naturally enriched in iodine, a result of volcanism earlier in the Earth's history, and most iodine (>96 percent) is present in seawater in the thermodynamically-stable form of iodate (Fuge and Johnson 1986; Johnson 2003). Iodate is reduced to iodide in surface ocean waters by the activity of bacteria and phytoplankton (Johnson 2003). The iodide is subsequently taken up by seaweed and phytoplankton and can be released as volatile iodocarbons (CH_3I, CH_2I_2 etc.). These gases undergo sea-air exchange, and through photochemical reactions, iodine and its associated oxidised radicals (IO, OIO) are released to, or formed in, the atmosphere. This work revealed decreased seawater concentrations of all measured iodocarbons (normalised to chl *a*) during three separate experiments (mesocosm, and L4 incubations x 2), suggesting that OA can impact the net production of these gases. Once released to the atmosphere, these compounds play a number of important roles which may be affected by a decrease in their sea – to – air flux, as discussed below:

Oxidative capacity of the atmosphere

Ozone (O_3) is a highly oxidising atmospheric gas that performs a number of important roles. In the stratosphere (~25km above the surface of the Earth) it absorbs solar ultraviolet-B (UV-B) radiation, thus protecting the Earth's living organisms from its harmful effects (Solomon 1999). By contrast, ozone in the troposphere (surface – 10km) is not beneficial to life, adversely affecting plant, animal and human health, and acting as a potent greenhouse gas (Ramaswamy *et al.* 2001; Buse *et al.* 2003; West *et al.* 2006). Therefore a clear understanding of the processes

that control O_3 levels in the lower atmosphere is vital for predictions of the future environment to be made.

The production and use of man-made chlorofluorocarbons (CFCs) has resulted in depletions to stratospheric ozone (Farman *et al.* 1985; Farmer *et al.* 1987) allowing increased levels of UV-B to reach the Earth's surface. Not only harmful to plant and animal life, an increase in the penetration of UV-B results in an enhancement in the chemical activity of the troposphere, with implications for a number of processes (Tang *et al.* 1998).

In polluted air, such as the Northern Hemisphere, an increase in UV-B leads to an increase in tropospheric O_3 through the photo-oxidation of pollutants such as CH_4, NO_x and VOCs (Crutzen 1974; Tang *et al.* 1998). This "photochemical smog" has blighted industrialised cities for decades and is responsible for a range of severe respiratory diseases and premature deaths (Buse *et al.* 2003). However, this process leads to an increase in hydroxyl (OH) radicals which may be partly beneficial. OH radicals exert an important control on the oxidative capacity of the atmosphere and are effective atmospheric cleansers, promoting the removal of GHGs and other pollutants, such as CO, CH_4, NMHCs, SO_2, NO_x and CFCs (Tang *et al.* 1998). In clean, remote air, an increase in UV-B simply results in a decrease in tropospheric O_3 through photolysis in the presence of water vapour. This leads to an increase in OH radicals and an enhancement of the atmosphere's oxidative capacity (Tang *et al.* 1998).

Upon entering the atmosphere, marine volatile iodocarbons undergo rapid photolysis to produce free radicals (I, IO, Br, BrO) which act as effective catalytic ozone depleting species (Chameides and Davis 1980; Solomon *et al.* 1994; Davis *et al.* 1996). Due to weak I bonds, iodocarbons are very photochemically active, with an atmospheric lifetime of a few minutes to weeks (Solomon *et al.* 1994). This generally limits their ozone depleting capacity to the troposphere, where a significant impact on ozone levels is possible under certain conditions (Davis *et al.* 1996). Additionally, in regions that experience strong atmospheric convection, such as the Tropics, iodocarbons can be rapidly transported to the upper troposphere and lower stratosphere, and can contribute to ozone depletion at these levels (Solomon *et al.* 1994).

The regulation of the oxidative capacity of the atmosphere is clearly complex, and controlled by a number of processes, some of which have undergone significant anthropogenic perturbations. The impact of a decrease in marine emissions of volatile iodocarbons to the troposphere will have is therefore difficult to quantify, but may result in a decrease in tropospheric ozone destruction. This would reduce the atmosphere's capacity to remove this potent greenhouse gas and air pollutant, enhancing global warming and contributing to negative impacts on human health and mortality.

New particle formation in the MBL

The formation of new particles in the MBL from volatile iodocarbon precursors originating from marine macroalgae and kelp beds has been demonstrated by both observational and experimental studies (Makela *et al.* 2002; O'Dowd *et al.* 2002; McFiggans *et al.* 2004), suggesting that in coastal regions biogenic iodocarbons may exert a significant impact on local, and more speculatively, global radiative forcing.

Studies have shown that the oxidation of DMS in the MBL is also connected to this process (O'Dowd *et al.* 2002). DMS oxidation represents the first step in production of new particles, resulting in the production of small (~1nm) thermodynamically stable clusters. In order to achieve an increase in particle number concentration, these stable clusters must rapidly grow (~3 - 4 nm) to avoid colliding with larger pre-existing particles and being captured (Kulmala *et al.* 2007). The role in this second process of condensable iodine vapours (CIVs) produced by the photolysis of CH_2I_2 in the presence of ozone has been confirmed by observational and modelling studies (O'Dowd *et al.* 2002; Pechtl *et al.* 2005). The influence of Br and Cl oxides on DMS chemistry has also received some attention (Vogt *et al.* 1999; Glasow *et al.* 2002). In a modelling study, von Glasow *et al.* (2002) found that when atmospheric halogen chemistry was included, DMS oxidization in the MBL increased by ~63 percent. Therefore the potential climate impact of both DMS- and halocarbon-derived new particles and CCN are closely related. Future modelling studies on the impacts of OA on marine biogeochemistry and climate feedbacks need to consider the synergistic impacts of changes in the net production of these gases. A combined decrease in both DMS and iodocarbons, as seen during this study, would result in a decrease in both

steps involved in new particle formation in the MBL and lead to an overall positive feedback to global warming.

The work that O'Dowd *et al.* (2002) reported was based on studies of new particle bursts at Mace Head, Eire, over dense beds of kelp. Therefore it is most applicable to some coastal regions, and it becomes problematic to directly extrapolate such observations to the open oceans, resulting in uncertainty in the significance of any climatic impact. The situation in the open ocean is less clear, as particle burst events are less frequent and lower in intensity than their coastal analogues (O'Dowd and Leeuw 2007). Consequently, O'Dowd *et al.* (2002) expanded their observational and experimental work by simulating the process using a marine aerosol model. Further modelling work by Pechtl *et al.* (2005) confirmed the importance of iodine oxides in both primary particle formation and secondary growth of particles in the clean marine atmosphere. These simulations suggest that concentrations of iodocarbons over the open ocean may be high enough to influence marine particle production. Thus pelagic open ocean production of iodocarbons may exert a significant influence on climate through production of new particles and CCN. In order to fully understand and quantify the role of phytoplankton, and achieve an understanding of the latent global climatic impacts, further knowledge of production/consumption of halocarbons and DMS by phytoplankton and bacteria in surface seawater is required.

As discussed above, changes in the source of marine iodocarbon species to the atmosphere may significantly influence CCN concentration (O'Dowd *et al.* 2002), with implications for global radiative forcing and climate. During the mesocosm experiment (Chapter 3), the time integrated mean concentration of CH_3I was 49 percent lower in the high CO_2 mesocosms for a pH drop of ~0.4 units, and 38 percent and 35 percent for C_2H_5I and CH_2I_2, respectively. The current flux of I atoms from the oceans to the atmosphere, using a globally-averaged marine surface-mixed-layer height of 300 cm, is 1.4 x 10^3 atoms cm^{-3} s^{-1} (O'Dowd *et al.* 2002). With a mean 42 per cent reduction in iodocarbons in the future high CO_2 world (mean decrease in iodocarbon concentrations seen during mesocosm experiment) and assuming changes to no other parameters (e.g. sea surface temperature, mixed-layer depth, wind speed), this would decrease to 8.3 x 10^2 atoms cm^{-3} s^{-1}. Such a decrease in net input of particles into the aerosol population would result in a comparable percentage decrease in CCN (O'Dowd *et al.* 2002). As ~10 percent of new particles survive to CCN sizes (O'Dowd *et al.* 2002), this would correspond to a ~4.2 percent decrease in

available CCN in the clean marine atmosphere. It is difficult to quantify the impact a decrease of this kind would have on radiative forcing. The discussion on the problems of attempting to quantify the impact of DMS-derived aerosols (Section 6.3.3.1) can also be applied to I-derived aerosols. Additionally, understanding is lacking in a number of areas, ranging from the initial production and consumption of halocarbons by phytoplankton and bacteria in seawater, to the influence of I-derived particles on the present day climate. Further research is required to enable quantification of the climatic impacts of a decrease in the production of marine biogenic iodocarbons as a result of OA.

6.3.3.3. Bromocarbons

The impact of OA on bromocarbons appears to be less clear than for DMS and the iodocarbons, with a variable response to high CO_2 throughout this study. As some strong responses were observed (e.g. Mesocosm: $CHBr_2Cl$ +22 percent, L4 Expt 1: CH_2Br_2 +27 percent, L4 Expt 1 and 2: CH_2BrCl -10 percent) this suggests further investigation is required to gain a clearer picture. At this stage it is difficult to say whether an increase or decrease in marine bromocarbon net production in the future low pH oceans is likely.

6.4 Recommendations for further research

This work represents the beginning of our understanding of the impacts of OA on a range of halocarbon compounds. It also provides further information on the impacts of OA on net DMS and DMSP production. In order to take this work forward and gain a better mechanistic understanding of the impact of OA on marine biogenic trace gas production, there are a number of areas that warrant further research:

1. *Natural analogue sites.*

Regions that experience naturally-lowered seawater pH may lend themselves as ideal for studying the long term impacts of OA on a range of marine organisms and processes. Volcanically-acidified sites have received some attention, as the high CO_2 conditions have persisted for relatively long time periods (hundreds to thousands of years), allowing long-term adaptation of the biota to the perturbed conditions (Hall-Spencer *et al.* 2008). The site at Ischia has served as a good natural analogue in term

of OA impacts on the benthic communities that inhabit the area, as the organisms that have been studied are generally sessile (barnacles, calcareous algae) or slow-moving (sea urchins, limpets) so experience prolonged periods exposed to high CO_2 conditions (Hall-Spencer *et al.* 2008). During this study, it was concluded that this site did not offer itself as ideal for studying the impacts of OA on the pelagic community. This was primarily due to the rapid fluctuations in pH, but also as the pelagic community was likely to experience a fast turnover rate at the site, and therefore experience a toxic shock rather than adaptation to the high CO_2 conditions. Therefore other natural analogue sites need to be identified, ideally in more open ocean situations. Oceanic upwelling regions that experience prolonged periods of under saturation and low seawater pH may have some potential in this kind of research (Feely *et al.* 2008).

2. *Mesocosm experiments*.

Mesocosm experiments are currently the best tool available for assessing the impacts of OA on pelagic ecosystems and their associated processes, in relatively large volumes of water (compared to laboratory studies) and under quasi-natural meteorological and oceanic conditions (Riebesell *et al.* 2008). The results of mesocosm studies are most relevant in terms of highly productive regions (high latitude waters, coastal waters, bloom events, upwelling regions). Such regions are not only expected to experience the greatest changes as a result of anthropogenic OA and other global climatic changes (Orr *et al.* 2005; Doney *et al.* 2007; I.P.C.C. 2007; Feely *et al.* 2008), but also represent important source regions of a number of climatically-important trace gases (Class and Ballschmiter 1988; Carpenter and Liss 2000; Quack *et al.* 2004; Quack and Wallace 2004; Chuck *et al.* 2005; Quack *et al.* 2007a). For these reasons, the continued use of mesocosm experiments is vital for furthering our understanding of the impacts of OA on the pelagic community.

So far OA mesocosm experiments have been performed on relatively small-scales. For example, the enclosures at the mesocosm facility in Espegrend, Norway, could incubate a volume of approximately 11 m^3, a small volume in terms of comparison to the open ocean. Therefore efforts have been made to develop the mesocosm technology to enable larger volumes to be perturbed. To initiate this new era of OA research, an offshore mesocosm experiment, using free-floating 65 m^3 enclosures, was performed in the Baltic in July 2007 (Riebesell *et al.* 2008). Such

technology should now be employed in key OA regions, such as the high latitude polar seas and high productivity temperate regions, to assess the response of such ecosystems to future changes in seawater chemistry.

3. *Ocean acidification-sensitive regions.*

As discussed above, a number of regions of the oceans have been identified as being particularly sensitive to future OA. High latitude polar seas are particularly vulnerable due to low seawater temperatures favourable to dissolution of atmospheric CO_2,. Such regions may experience undersaturation with respect to aragonite as soon as 2050 (Orr *et al.* 2005). Similarly, upwelling regions are naturally-acidified by the influx of CO_2-rich water from depth, and anthropogenic CO_2 is now increasing the extent of such acidification (Feely *et al.* 2008). However, the highly variable temporal and spatial nature of upwelling systems may make such sites less ideal for OA studies.

Temperate coastal regions are expected to be substantially impacted by OA, particularly as the acidification is likely to be enhanced by deposition of sulphur and nitrogen from human activities (Doney *et al.* 2007). Such regions also generally experience high phytoplankton productivity, and act as important source regions of a range of climatically-active halocarbons (Class and Ballschmiter 1988; Carpenter and Liss 2000; Quack *et al.* 2004; Quack and Wallace 2004; Chuck *et al.* 2005; Quack *et al.* 2007a). Therefore, future research efforts should be focused in such regions, and involve: 1. Long-term *in situ* monitoring strategies to detect possible changes, and make distinctions between natural variability and anthropogenic impacts, 2. Bioassay experimental work, such as on-deck incubations of water from a range of oceanic locations, to assess the response of complex *in situ* ecosystems to elevated CO_2.

4. *Furthering a mechanistic understanding.*

A clear response of net iodocarbon and DMS production to OA has been observed during this work. Although there is some understanding of the processes involved for DMS, there is still information lacking on the biological mechanisms that result in net production of halocarbons, and on their cycling in seawater. Photochemistry (Moore and Zafiriou 1994; Richter and Wallace 2004; Jones and Carpenter 2005; Martino *et al.* 2005; Jones and Carpenter 2007), nucleophilic

substitution and hydrolysis of halocarbons in seawater have received some investigation (Elliott and Rowland 1993; Jeffers and Wolfe 1996). In addition, the use of stable isotope tracer techniques (e.g. measurement of formation of $H^{14}CO_3^{2-}$ from $^{14}CHBr_3$) has enabled some insight to be gained into biological loss rates of brominated methanes in both fresh and seawater (Goodwin *et al.* 1997a; King and Saltzman 1997; Goodwin *et al.* 1998; Tokarczyk *et al.* 2001), and bacteria are highly implicated in these processes. Furthermore, bacteria are likely to be involved in the cycling of iodinated methanes in seawater (Amachi *et al.* 2001). As the iodocarbons displayed a response to OA in some of the work described here, it is important to further our understanding of the cycling of these compounds in seawater. Similarly to previous work on bromomethanes, ^{14}C- or ^{13}C-labelled iodocarbons could be employed to derive loss rates of such compounds. The ^{14}C-tracer technique would involve addition of e.g. $^{14}CH_3I$ to incubations of seawater. Over a period of 12 – 24 hours samples would be analysed at regular intervals, and the $H^{14}CO_3^{2-}$ produced by the biological oxidation of $^{14}CH_3I$ would be measured by scintillation counting. Similarly, $^{13}CH_3I$ may be added to incubations, and the change in abundance of isotopes monitored using stable-isotope dilution - mass spectrometry techniques (King and Saltzman 1997). Initially the work could focus on whole phytoplankton communities, and perhaps assess seasonal changes in loss rates in terms of changes in phytoplankton speciation. Looking in more detail, the bacterial community may be isolated by filtration, giving an assessment of its contribution to the process. Molecular techniques could be employed to gain detailed information on the bacterial strains involved. This kind of experimental work could be extended to OA perturbation experiments, such as mesocosm experiments, or smaller-scale bioassay incubations, to assess the impacts of the perturbed conditions on the biological loss processes in seawater.

5. *Modelling studies*.

The ability to scale up from perturbation experiments and field observations to regional and global scales using model simulations is critical to OA research, enabling researchers to assess the temporal and spatial changes that may occur over the coming decades. As DMS and halocarbons are considered to exert a considerable influence on climatic processes, the inclusion of OA impacts on these compounds in global ocean- atmosphere modelling studies is vital to furthering our understanding of how the Earth system as a whole may respond to future climate change and OA.

6.5 Conclusions

This thesis has made an assessment of the potential impact of future OA on the production of a range of climatically- and atmospherically-important trace gases. Strong and consistent responses to high pCO_2 and low seawater pH were observed for DMS and a number of iodocarbons, suggesting that the future oceans may see a reduction in the net production and sea – to – air flux of these compounds. Such changes, if on a world-wide scale, could have implications for a number of global homeostatic processes, including the regulation of tropospheric oxidative capacity, radiative forcing and air quality, and the production of new particles and CCN in the MBL with potential climatic impacts.

If the incessant release of man-made CO_2 into the atmosphere is not dramatically reduced and stabilised within the next 50 years, not only should we expect severe climatic perturbations, we face a future ocean with a lower surface pH than anything experienced in the last 300 million years of Earth's history (Caldeira and Wickett 2003). Research into the effect this will have on marine organisms, ecosystems and biogeochemical processes, to which this thesis is a contribution, is still in its infancy. Further work is now required to fully understand how this legacy of human activity may impact on the marine trace gas-regulated homeostasis of Earth.

References

Abrahamsson, K., S. Bertilsson, M. Chierici, A. Fransson, P. W. Froneman, A. Lorén, and E. A. Pakhomov (2004a). Variations of biochemical parameters along a transect in the Southern Ocean, with special emphasis on volatile halogenated organic compounds, *Deep Sea Research Part II: Topical Studies in Oceanography*, **51**, 2745-2756.

Abrahamsson, K., A. Ekdahl, J. Collen, and M. Pedersen (1995). Marine algae - A source of trichloroethylene and perchloroethylene, *Limnology and Oceanography*, **40**, 1321-1326.

Abrahamsson, K., A. Lorén, A. Wulff, and S.-Å. Wängberg (2004b). Air-sea exchange of halocarbons: the influence of diurnal and regional variations and distribution of pigments, *Deep Sea Research Part II: Topical Studies in Oceanography*, **51**, 2789-2805.

Aiken, J., N. Rees, S. Hooker, P. Holligan, A. Bale, D. Robins, G. Moore, R. Harris, and D. Pilgrim (2000). The Atlantic Meridional Transect: overview and synthesis of data, *Progress In Oceanography*, **45**, 257-312.

Allgaier, M., U. Riebesell, M. Vogt, R. Thyrhaug, and H. P. Grossart (2008). Coupling of heterotrophic bacteria to phytoplankton bloom development at different pCO_2 levels: a mesocosm study, *Biogeosciences*, **5,** 1007-1022.

Amachi, S., Y. Kamagata, T. Kanagawa, and Y. Muramatsu (2001). Bacteria mediate methylation of iodine in marine and terrestrial environments, *Applied and Environmental Microbiology*, **67**, 2718-2722.

Anderson, R. A. (2005). Algal Culturing Techniques, Elsevier, pp.

Andersson, A., F. T. Mackenzie, and L. M. Ver (2003). Solution of shallow-water carbonates: An insignificant buffer against rising atmospheric CO_2, *Geology*, **31**, 513-516.

Andreae, M. O. (1986). The ocean as a source of atmospheric sulfur compounds, in The role of air-sea exchange in geochemical cycling, edited by P. Buat-Menard, pp. 331-362, D. Reidel Publishing Company, Dordrecht, Holland.

Andreae, M. O. (1990). Ocean-atmosphere interactions in the global biogeochemical sulfur cycle, *Marine Chemistry*, **30**, 1-29.

Andreae, M. O., and P. J. Crutzen (1997). Atmospheric Aerosols: Biogeochemical Sources and Role in Atmospheric Chemistry, *Science*, **276**, 1052-1058.

Archer, D. (2005). Fate of fossil fuel CO_2 in geologic time, *Journal of Geophysical Research*, 110, C09S05, **6**, doi:10.1029/2004JC002625.

Archer, D., H. Kheshgi, and E. Maier-Reimer (1998). Dynamics of fossil fuel CO_2 neutralization by marine $CaCO_3$, *Global Biogeochemical Cycles*, **12**, 259-276.

Archer, S. D., L. E. Goldson, M. I. Liddicoat, D. G. Cummings, and P. D. Nightingale (2007). Marked seasonality in the concentrations and sea-to-air flux of volatile

iodocarbon compounds in the western English Channel, *Journal of Geophysical Research*, **112**, doi:10.1029/2006JC003963.

Archer, S. D., G. C. Smith, P. D. Nightingale, C. E. Widdecombe, G. A. Tarran, A. P. Rees, and P. H. Burkhill (2002). Dynamics of particulate dimethylsulphoniopropionate during a Langrangian experiment in the northern North Sea, *Deep-Sea Research II*, **49**, 2979-2999.

Augustin, L., C. Barbante, P. R. F. Barnes, J. M. Barnola, M. Bigler, E. Castellano, O. Cattani, J. Chappellaz, D. Dahl-Jensen, B. Delmonte, G. Dreyfus, G. Durand, S. Falourd, H. Fischer, J. Flückiger, M. E. Hansson, P. Huybrechts, G. Jugie, S. J. Johnsen, J. Jouzel, P. Kaufmann, J. Kipfstuhl, F. Lambert, V. Y. Lipenkov, G. C. Littot, A. Longinelli, R. Lorrain, V. Maggi, V. Masson-Delmotte, H. Miller, R. Mulvaney, J. Oerlemans, H. Oerter, G. Orombelli, F. Parrenin, D. A. Peel, J.-R. Petit, D. Raynaud, C. Ritz, U. Ruth, J. Schwander, U. Siegenthaler, R. Souchez, B. Stauffer, J. P. Steffensen, B. Stenni, T. F. Stocker, I. E. Tabacco, R. Udisti, R. S. W. v. d. Wal, M. v. d. Broeke, J. Weiss, F. Wilhelms, J.-G. Winther, E. W. Wolff, and M. Zucchelli (2004). Eight glacial cycles from an Antarctic ice core, *Nature*, **429**, 623-628.

Avgoustidi, V. (2007). Dimethyl sulphide production in a high CO_2 world, PhD thesis, University of East Anglia, Norwich.

Ayers, G. P., J. P. Ivey, and R. W. Gillett (1991). Coherence between seasonal cycles of dimethyl sulphide, methanesulphonate and sulphate in marine air, *Nature*, **349**, 404-406.

Azam, F., T. Fenchel, J. G. Field, J. S. Gray, L. A. Meyerreil, and F. Thingstad (1983). The Ecological Role of Water-Column Microbes in the Sea, *Marine Ecology Progress Series*, **10**, 257-263.

Badger, M. R., and G. D. Price (2003). CO_2 concentrating mechanisms in cyanobacteria: molecular components, their diversity and evolution, *Journal of Experimental Botany*, **54**, 609-622.

Baker, J. M., C. E. Reeves, P. D. Nightingale, S. A. Penkett, S. W. Gibb, and A. D. Hatton (1999). Biological production of methyl bromide in the coastal waters of the North Sea and open ocean of the northeast Atlantic, *Marine Chemistry*, **64**, 267-285.

Balch, W. M., P. M. Holligan, S. G. Ackleson, and K. J. Voss (1991). Biological and optical properties of mesoscale coccolithophore blooms in the Gulf of Maine, *Limnology and Oceanography*, **36**, 629-643.

Ballschmiter, K. (2003). Pattern and sources of naturally produced organohalogens in the marine environment: biogenic formation of organohalogens, *Chemosphere*, **52**, 313-324.

Banse, K. (1982). Experimental marine ecosystem enclosures in a historical perspective, in Marine Mesocosms, edited by G. D. Grice and M. R. Reeve, pp. 11-24, Springer, Berlin Heidelberg.

Barker, S., and H. Elderfield (2002). Foraminiferal calcification response to glacial-interglacial changes in atmospheric CO_2, *Science*, **297**, 833-836.

Barker, S., J. A. Higgins, and H. Elderfield (2003). The future of the carbon cycle: review, calcification response, ballast and feedback on atmospheric CO_2, *Philosophical Transactions of the Royal Society London A*, **361**, 1977-1999.

Barlow, R. G., R. F. C. Mantoura, D. G. Cummings, D. W. Pond, and R. P. Harris (1998). Evolution of phytoplankton pigments in mesocosm experiments, *Estuarine Coastal and Shelf Science*, **46**, 15-22.

Barry, J. P., K. R. Buck, C. Lovera, L. Kuhnz, and P. J. Whaling (2005). Utility of deep sea CO_2 release experiments in understanding the biology of a high-CO_2 ocean: Effects of hypercapnia on deep sea meiofauna, *Journal of Geophysical Research*, **110**.

Bates, T. S., J. D. Cline, R. H. Gammon, and S. R. Kelly-Hanson (1987). Regional and seasonal variations in the flux of oceanic dimethylsulfide to the atmosphere, *Journal of Geophysical Research*, **92**, 2930-2938.

Bates, T. S., B. K. Lamb, A. Guenther, J. Dignon, and R. E. Stoiber (1992). Sulfur emissions to the atmosphere from natural sources, *Journal of Atmospheric Chemistry*, **14**, 315-337.

Bathgate, R. H., and E. A. Moelwyn-Hughes (1959). The kinetics of certain ionic exchange reactions of the four methyl halides in aqueous solution, *Journal of the Chemistry Society*, 2642-2648.

Beaugrand, G. (2004). The North Sea regime shift: Evidence, causes, mechanisms and consequences, *Progress In Oceanography*, **60**, 245-262.

Berge, J. A., B. Bjerkeng, O. Pettersen, M. T. Schaanning, and S. Oxnevad (2006). Effects of increased sea water concentrations of CO_2 on growth of the bivalve *Mytilus edulis* L., *Chemosphere*, **62**, 681-687.

Blackford, J. C., and F. J. Gilbert (2007). pH variability and CO_2 induced acidification in the North Sea, *Journal of Marine Systems*, **64**, 229-241.

Blomquist, B. W., C. W. Fairall, B. J. Huebert, D. J. Kieber, and G. R. Westby (2006). DMS sea-air transfer velocity: Direct measurements by eddy covariance and parameterization based on the NOAA/COARE gas transfer model, *Geophysical Research Letters*, **33**.

Bopp, L., O. Aumont, S. Belviso, and P. Monfray (2003). Potential impact of climate change on marine dimethyl sulphide emissions, *Tellus* B, **55**, 11-22.

Bopp, L., P. Monfray, O. Aumont, J.-L. Dufresne, H. L. Treut, G. Madec, L. Terray, and J. C. Orr (2001). Potential impact of climate change on marine export production, *Global Biogeochemical Cycles*, **15**, 81-99.

Brimblecombe, P., and D. Shooter (1986). Photo-oxidation of dimethylsulphide in aqueous solution, *Marine Chemisty*, **19**, 343-353.

Brown, C. W., and J. A. Yoder (1994). Coccolithophorid blooms in the global ocean, *Journal of Geophysical Research*, **99**, 7467-7482.

Budde, W. L. (2001). Analytical Mass Spectrometry: Strategies for Environmental and Related Applications, Oxford University Press, Oxford.

Burkhardt, S., G. Amoroso, U. Riebesell, and D. Sultemeyer (2001). CO_2 and HCO_3 uptake in marine diatoms acclimated to differnt CO_2 concentrations, *Limnology and Oceanography*, **46**, 1378-1391.

Burkhill, P. H., S. D. Archer, C. Robinson, P. D. Nightingale, S. B. Groom, G. A. Tarran, and M. V. Zubkov (2002). Dimethyl sulphide biogeochemistry within a coccolithophore bloom (DISCO) : an overview, *Deep-Sea Research II*, **49**, 2863-2885.

Buse, A., G. Mill, H. Harmens, P. Buker, F. Hayes, P. Williams, L. Emberson, S. Cinderby, M. Ashmore, and H. M. D. Temmerman (2003). Air Pollution and Vegetation, Bangor, UK.

Butler, A., and J. V. Walker (2002). Marine haloperoxidases, *Chemical Reviews*, **93**, 1937-1944.

Butler, J. H., D. B. King, J. M. Lobert, S. A. Montzka, S. A. Yvon-Lewis, B. D. Hall, N. J. Warwick, D. J. Mondeel, M. Aydin, and j. W. Elkins (2007). Oceanic distributions and emissions of short-lived halocarbons, *Global Biogeochemical Cycles*, **21**, doi:10.1029/2006GB002732.

Caldeira, K., and R. Berner (1999). Seawater pH and atmospheric carbon dioxide, *Science*, **286**, 2043.

Caldeira, K., and M. E. Wickett (2003). Anthropogenic carbon and ocean pH, *Nature*, **425**, 365-365.

Caldeira, K., and M. E. Wickett (2005). Ocean model predictions of chemistry changes from carbon dioxide emissions to the atmosphere and ocean, *Journal of Geophysical Research*, **110**, doi: 10.1029/2004JC002671.

Campos, M. L. A. M., R. Sanders, and T. Jickells (1999). The dissolved iodate and iodide distribution in the South Atlantic from the Weddell Sea to Brazil, *Marine Chemistry*, **65**, 167-175.

Cao, L., and K. Caldeira (2008). Atmospheric CO_2 stabilization and ocean acidification, *Geophysical Research Letters*, **35**, doi: 10.1029/2008GL035072.

Cao, L., K. Caldeira, and A. K. Jain (2007). Effects of carbon dioxide and climate change on ocean acidification and carbonate mineral saturation, *Geophysical Research Letters*, **34**, doi:10.1029/2006GL028605.

Carpenter, L. J., K. Hebestreit, U. Platt, and P. S. Liss (2001). Coastal zone production of IO precursors: a 2-dimensional study, *Atmospheric Chemistry and Physics*, **1**, 9-18.

Carpenter, L. J., C. E. Jones, R. M. Dunk, K. E. Hornsby, and J. Woeltjen (2009). Air-sea fluxes of biogenic bromine from the tropical and North Atlantic Ocean, *Atmospheric Chemistry and Physics*, **9**, 1805-1816.

Carpenter, L. J., and P. S. Liss (2000). On temperate sources of bromoform and other reactive organic bromine gases, *Journal of Geophysical Research*, **105**, 20539-20547.

Carpenter, L. J., P. S. Liss, and S. A. Penkett (2003). Marine organohalogens in the atmosphere over the Atlantic and Southern Oceans, *Journal of Geophysical Research*, **108**, doi:10.1029/2002JD002769.

Carpenter, L. J., W. T. Sturges, S. A. Penkett, P. S. Liss, B. Alicke, K. Hebestreit, and U. Platt (1999). Short-lived alkyl iodides and bromides at Mace Head, Ireland: Links to biogenic sources and halogen oxide production, *Journal of Geophysical Research*, 104.

Carpenter, L. J., D. J. Wevill, C. J. Palmer, and J. Michels (2007). Depth profiles of volatile iodine and bromine-containing halocarbons in coastal Antarctic waters, *Marine Chemistry*, 103, 227-236.

Carslaw, K. S., O. Boucher, D. V. Spracklen, G. W. Mann, J. G. L. Rae, S. Woodward, and M. Kulmala (2009). Atmospheric aerosols in the earth system: a review of interactions and feedbacks, *Atmospheric Chemistry and Physics Discussions*, 9, 11087-11183.

Challenger, F., and M. I. Simpson (1948). Studies on biological methylation. Part 12. A precursor of the dimethyl sulphide evolved by Polysiphonia fastigiata. Dimethyl-2-carboxyethylsulphonium hydroxide and its salts., *Journal of the Chemistry Society*, 3, 1591-1597.

Chameides, W. L., and D. D. Davis (1980). Iodine: Its Possible Role in Tropospheric Photochemistry, *Journal of Geophysical Research-Atmospheres*, 85, 7383-7398.

Charlson, R. J., J. E. Lovelock, M. O. Andreae, and S. G. Warren (1987). Oceanic phytoplankton, atmospheric sulphur, cloud albedo and climate, *Nature*, 326, 655-661.

Chen, C.-T. A. (1993). The oceanic anthropogenic CO_2 Sink, *Chemosphere*, 27, 1041-1064.

Chin, M., and D. J. Jacob (1996). Anthropogenic and natural contributions to tropospheric sulfate: A global model analysis, *Journal of Geophysical Research*, 101, 18691–18699.

Chuck, A. L., S. M. Turner, and P. S. Liss (2005). Oceanic distributions and air-sea fluxes of biogenic halocarbons in the open ocean, *Journal of Geophysical Research*, 110, doi:10.1029/2004JC002741.

Cicerone, R., J. Orr, P. B. P. Haugan, L. Merlivat, T. Ohsumi, S. Pantoja, H.-O. Poertner, M. Hood, and E. Urban (2004). The ocean in a high-CO_2 world, The SCOR/IOC Symposium Planning Committee.

Class, T., and K. Ballschmiter (1988). Chemistry of Organic Traces in Air. VIII. Sources and Distribution of Bromo- and Bromochloromethanes in Marine Air and Surfacewater of the Atlantic Ocean, *Journal of Atmospheric Chemistry*, 6, 35-46.

Cole, K., G. Stegen, and R. Bacastow (1995). Predicting future variability of dissolved inorganic carbon in the ocean, *Energy Conversion and Management*, 36, 457-460.

Collins, S., and G. Bell (2004). Phenotypic consequences of 1000 generations of selection at elevated CO_2 in a green alga, *Nature*, 431, 566-569.

Connell, T. L., S. B. Joye, L. G. Miller, and R. S. Oremland (1997). Bacterial Oxidation of Methyl Bromide in Mono Lake, California, *Environmental Science & Technology*, **31**, 1489-1495.

Crutzen, P. J. (1974). Photochemical reactions initiated by and influencing ozone in unpolluted tropospheric air, *Tellus*, **26** (1-2), 47-57.

Dason, J. S., and B. Colman (2004). Inhibition of growth in two dinoflagellates by rapid changes in external pH, *Candian Journal Of Botany*, **82**, 515-520.

Davis, D., J. Crawford, S. Liu, S. McKeen, A. Bandy, D. Thornton, F. Rowland, and D. Blake (1996). Potential impact of iodine on tropospheric levels of ozone and other critical oxidants, *Journal of Geophysical Research*, **101**, 2135-2147.

De Hoffmann, E., and V. Stroobant (2007). Mass spectrometry : principles and applications, Chichester [etc.]: John Wiley.

Delille, B., J. Harlay, I. Zondervan, S. Jacquet, L. Chou, R. Wollast, R. G. J. Bellerby, M. Frankignoulle, A. V. Borges, U. Riebesell, and J.-P. Gattuso (2005). Response of primary production and calcification to changes of pCO_2 during experimental blooms of the coccolithophorid Emiliana huxleyi, *Global Biogeochemical Cycles*, **19**, GB2023, doi:10.1029/2004GB002318.

Dickson, A. G., and F. J. Millero (1987). A comparison of the equilibrium constants for the dissociation of carbonic acid in seawater media, *Deep Sea Research Part A*. Oceanographic Research Papers, **34**, 1733-1743.

DOE (1994). Handbook of the methods for analysis of various parameters of the carbon dioxide system in seawater, ORNL/CDIAC-74.

Doney, S. C., N. Mahowald, I. Limar, R. A. Feely, F. T. Mackenzie, J.-F. Lamarque , and P. J. Rasch (2007). Impact of anthropogenic atmospheric nitrogen and sulfur deposition on ocean acidification and the inorganic carbon system, *Proceedings of the National Academy of Sciences*, **104**, 14580–14585.

Drake, B. G., M. A. Gonzalez-Meler, and S. P. Long (1997). More Efficient Plants: A Consequence of Rising Atmospheric CO_2? Annual Review of Plant Physiology and Plant *Molecular Biology*, **48**, 609-639.

Dring, M. J. (2006). Stress resisitance and disease resistance in seaweeds: The role of Reactive Oxygen Species, *Advances in Botanical Research*, **43**, 176-201.

Ekdahl, A., M. Pedersen, and K. Abrahamsson (1998). A study of the diurnal variation of biogenic volatile halocarbons, *Marine Chemistry*, **63**, 1-8.

Elliott, S., and F. S. Rowland (1993). Nucleophilic substitution rates and solubilities for methyl halides in seawater, *Geophysical Research Letters*, **20**, 1043-1046.

Engel, A. (2002). Direct relationship between CO_2 uptake and transparent exopolymer particles production in natural phytoplankton, *Journal Plankton Research*, **24**, 49-53.

Engel, A., B. Delille, S. Jacquet, U. Riebesell, E. Rochelle-Newall, A. Terbruggen, and I. Zondervan (2004). Transparent exopolymer particles and dissolved organic carbon production by Emiliana huxleyi exposed to different CO_2 concentrations: a mesocosm experiment, *Aquatic Microbial Ecology*, **34**, 93-104.

Engel, A., K. G. Schulz, U. Riebesell, R. Bellerby, B. Delille, and M. Schartau (2008). Effects of CO_2 on particle size distribution and phytoplankton abundance during a mesocosm bloom experiment (PeECE II), *Biogeosciences*, **5**, 509-521.

Engel, A., I. Zondervan, K. Aerts, L. Beaufort, A. Benthien, L. Chou, B. Delille, J.-P. Gattuso, J. Harlay, C. Heeman, L. Hoffman, S. Jacquet, J. Nejstgaard, M.-D. Pizay, E. Rochelle-Newall, U. Schneider, A. Terbrueggen, and U. Riebesell (2005). Testing the direct effect of CO_2 concentrations on a bloom of the coccolithophorid Emiliania huxleyi in mesocosm experiments, *Limnology and Oceanography*, **50**, 493-507.

Erikson, D. J., S. J. Ghan, and J. E. Penner (1990). Global ocean-to-atmosphere dimethyl sulfide flux, *Journal of Geophysical Research*, **95**, 7543-7552.

Farman, J. C., B. G. Gardiner, and J. D. Shanklin (1985). Large losses of total ozone in Antarctica reveal seasonal ClOx/NOx interaction, *Nature*, **315**, 207-210.

Farmer, C. B., G. C. Toon, P. W. Schaper, J. F. Blavier, and L. L. Lowes (1987). Stratospheric trace gases in the spring 1986 Antarctic atmosphere, *Nature*, **329**, 126-130.

Feely, R. A., C. L. Sabine, J. M. Hernandez-Ayon, D. Ianson, and B. Hales (2008). Evidence for upwelling of corrosive "acidified" water onto the continental shelf, *Science*, **320**, 1490-1492.

Feely, R. A., C. L. Sabine, K. Lee, W. Berelson, J. Kleypas, V. J. Fabry, and F. J. Millero (2004). Impact of anthropogenic CO_2 on the $CaCO_3$ system in the oceans, *Science*, **305**, 362-336.

Fei-Xue Fu, M. E. Warner, Y. Zhang, Y. Feng, and D. A. Hutchins (2007). Effects of increased temperature and CO_2 on photosynthesis, growth, and elemental ratios in marine Synechococcus and Prochlorococcus (Cyanobacteria), *Journal of Phycology*, **43**, 485-496.

Ferguson, R. L., E. N. Buckley, and A. V. Palumbo (1984). Response of marine bacterioplankton to differential filtration and confinement, *Applied and Environmental Microbiology*, **47**, 49-55.

Fogg, G. E., and O. Calvario-Martinez (1989). Effects of bottle size in determinations of primary productivity by phytoplankton, *Hydrobiologia*, **173**, 88-94.

Fuge, R., and C. C. Johnson (1986). The geochemistry of iodine - a review, *Environmental Geochemistry and Health*, **8**, 31-54.

Gabric, A. J., Q. U. Bo, M. Patricia, and H. Anthony C (2005). The simulated response of dimethylsulfide production in the Arctic Ocean to global warming, *Tellus B*, **57**, 391-403.

Gabric, A. J., P. H. Whetton, R. Boers, and G. P. Ayers (1998). The impact of simulated climate change on the air-sea flux of dimethylsulphide in the subantarctic Southern Ocean, *Tellus B*, **50**, 388-399.

Gattuso, J.-P., and R. W. Buddemeier (2000). Calcification and CO_2, *Nature*, **407**, 311-313.

Giese, B., F. Laturnus, F. C. Adams, and C. Wiencke (1999). Release of Volatile Iodinated C1-C4 Hydrocarbons by Marine Macroalgae from Various Climate Zones, *Environmental Science & Technology*, **33**, 2432-2439.

Glasow, R. v., and R. Sander (2002). Modelling halogen chemistry in the marine boundary layer 1. Cloud-free MBL, *Journal of Geophysical Research*, **107**, doi: 10.1029/2001JD000942.

Glasow, R. v., R. Sander, A. Bott, and P. J. Crutzen (2002). Modelling halogen chemistry in the marine boudary layer 2. Interactions with sulfur and the cloud-covered MBL, *Journal of Geophysical Research*, **107**, doi:10/1029JD000943.

Goodwin, K. D., M. E. Lidstrom, and R. S. Oremland (1997a). Marine Bacterial Degradation of Brominated Methanes, *Environmental Science & Technology*, **31**, 3188-3192.

Goodwin, K. D., J. K. Schaefer, and R. S. Oremland (1998). Bacterial oxididation of dibromomethane and methyl bromide in natural waters and enrichment cultures, *Applied and Environmental Microbiology*, 64**,** 4629-4636.

Goodwin, K. D., J. N. Wheeler, and M. E. Lidstrom (1997b). Production of bromoform and dibromomethane by Giant Kelp: Factors affecting release and comparison to anthropogenic bromine sources., *Limnology and Oceanography*, **42**, 1725-1734.

Graham, L. E., and L. W. Wilcox (2000). Algae, Prentice-Hall International Ltd., pp.

Granéli, E., and C. Haraldsson (1993). Can Increased Leaching of Trace Metals from Acidified Areas Influence Phytoplankton Growth in Coastal Waters?, *Ambio*, **22**, 308-311

Gribble, G. W. (2003). The diversity of naturally produced organohalogens, *Chemosphere*, **52**, 289-297.

Gschwend, P. M., J. K. Macfarlane, and K. A. Newman (1985). Volatile Halogenated Organic Compounds Released to Seawater from Temperate Marine Macroalgae, *Science*, **227**, 1033-1035.

Gunson, J. R., S. A. Spall, T. R. Anderson, A. Jones, I. J. Totterdell, and M. j. Woodage (2006). Climate sensitivity to ocean dimethylsulphide emissions, *Geophysical Research Letters*, **33**, doi:10.1029/2005GL024982.

Hall-Spencer, J. M., R. Rodolfo-Metalpa, S. Martin, E. Ransome, M. Fine, S. M. Turner, S. J. Rowley, D. Tedesco, and M.-C. Buia (2008). Volcanic carbon dioxide vents show ecosystem effects of ocean acidification, *Nature*, **454**, 96-99.

Hansson, I. (1973). A new set of pH-scales and standard buffers for seawater, *Deep Sea Research A*, **20**, 479-491.

Happell, J. D., and D. W. R. Wallace (1996). Methyl iodide in the Greenland/Norwegian Seas and the tropical Atlantic Ocean: Evidence for photochemical production, *Geophysical Research Letters*, **23**, 2105-2108.

Hare, C. E., K. Leblanc, G. R. DiTullio, R. M. Kudela, Y. Zhang, P. A. Lee, S. Riseman, and D. A. Hutchins (2007). Consequences of increased temperature and CO_2 for phytoplankton community structure in the Bering Sea, *Marine Ecology Progress Series*, **352**, 9-16.

Hassidim, M., N. Keren, I. Ohad, L. Reinhold, and A. Kaplan (1997). Acclimation of Synechococcus (Strain WH7802) to ambient CO_2 concentrations and to elevated light intensity. , *Journal of Phycology*, **33**, 811-817.

Hatton, A. D. (2002). Influence of photochemistry on the marine biogeochemical cycle of dimethylsulphide in the northern North Sea, *Deep-Sea Research Part Ii-Topical Studies in Oceanography*, **49**, 3039-3052.

Haugan, P. M., and H. Drange (1996). Effects of CO_2 on the ocean environment, *Energy Conversion and Management*, **37**, 1019-1022.

Hays, G. C., A. J. Richardson, and C. Robinson (2005). Climate change and marine plankton, *Trends in Ecology and Evolution*, **20**, 337-344.

Hegg, D. A., R. J. Ferek, P. V. Hobbs, and L. F. Radke (1991). Dimethyl sulphide and cloud condesation nucleus correlations in the northeast Pacific Ocean, *Journal of Geophysical Research*, **96**, 13189-13191.

Hein, M., and K. Sand-Jensen (1997). CO_2 increases oceanic primary production, *Nature*, **388**, 526-527.

Hinga, K. R. (2002). Effects of pH on coastal marine phytoplankton, *Marine Ecology Progress Series*, **238**, 281-300.

Hoegh-Guldberg, O. (2005). Low coral cover in a high-CO_2 world, *Journal of Geophysical Research*, **110**, doi:10.1029/2004JC002528.

Holligan, P. M., M. Viollier, D. S. Harbour, P. Camus, and M. Champagne-Philippe (1983). Satellite and ship studies of coccolithophore production along a continental shelf edge, *Nature*, **304**, 339-342.

Holmen, K. (2000). The Global Carbon Cycle, in Earth System Science. From Biogeochmeical Cycles to Global Change., edited by M. C. Jacobsen et al., pp. 282-321, Academic Press, London.

Hopkins, F., S. Turner, P. Nightingale, M. Steinke, and P. Liss (2010). Ocean acidification and marine biogenic trace gas production, *Proceedings of the National Academy of Sciences*, **107**, 760-765.

Houghton, J. T. (1992). Climate Change 1992: The Supplementary Report to the IPCC Scientifici Assessment.

Huebert, B. J., B. W. Blomquist, J. E. Hare, C. W. Fairall, J. E. Johnson, and T. S. Bates (2004). Measurement of the sea-air DMS flux and transfer velocity using eddy correlation, *Geophysical Research Letters*, **31**, L32113, doi:10.1029/2004GL021567.

Hughes, C. (2004). Biogenic iodocarbon production in the sea, University of East Anglia, Norwich.

Hughes, C., G. Malin, P. D. Nightingale, and P. S. Liss (2006). The effect of light stress on the release of volatile iodocarbons by three species of marine microalgae *Limnology and Oceanography* Notes, **51**, 2849-2854.

Hughes, C., G. Malin, C. Turley, B. Keely, P. Nightingale, and P. Liss (2008). The production of volatile iodocarbons by biogenic marine aggregates, *Limnology and Oceanography*, **53**, 867-872.

I.P.C.C. (2007). Climate Change 2007: The Physical Science Basis. Contribution of Working Group I to the Fourth Assessment Report of the Intergovernmental Panel on Climate Change, Cambridge University Press, Cambridge, United Kingdom and New York, USA, pp.

Iglesias-Rodriguez, M. D., P. R. Halloran, R. E. M. Rickaby, I. R. Hall, E. Colmenero-Hidalgo, J. R. Gittins, D. R. H. Green, T. Tyrrell, S. J. Gibbs, P. von Dassow, E. Rehm, E. V. Armbrust, and K. P. Boessenkool (2008). Phytoplankton calcification in a high-CO_2 world, *Science*, **320**, 336-340.

IPCC (1994). Radiative Forcing of Climate Change and An Evaluation of the IPCC IS92 Emission Scenarios Cambridge, UK.

Ishimatsu, A., M. Hayashi, and K.-S. Lee (2005). Physiological effects on fishes in a high-CO_2 world, *Journal of Geophysical Research*, **110**, doi:10.1029/2004JC002564.

Ishimatsu, A., T. Kikkawa, M. Hayashi, K.-S. Lee, and J. Kita (2004). Effects of CO_2 on marine fish: larvae and adults, *Journal of Oceanography*, **60**, 731-741.

Jeffers, P. M., and N. L. Wolfe (1996). On the degradation of methyl bromide in sea water, *Geophysical Research Letters*, **23**, 1773-1776.

Jeffrey, S. W. (1980). Algal Pigment Systems, in Primary Productivity in the Sea, edited by P. Falkowski, pp. 33 - 58, Plenum, New York.

Jickells, T. D., Z. S. An, K. K. Andersen, A. R. Baker, G. Bergametti, N. Brooks, J. J. Cao, P. W. Boyd, R. A. Duce, K. A. Hunter, H. Kawahata, N. Kubilay, J. laRoche, P. S. Liss, N. Mahowald, J. M. Prospero, A. J. Ridgwell, I. Tegen, and R. Torres (2005). Global iron connections between desert dust, ocean biogeochemistry, and climate, *Science*, **308**, 67-71.

Johnson, C. C. (1980). The geochemistry of iodine and a preliminary investigation into its potential use as a pathfinder element in geochemical exploration, University College of Wales, Aberystwyth, Wales.

Johnson, C. C. (2003). The geochemistry of iodine and its application to environmental strategies for reducing the risks from iodine deficiency disorders (IDD), British Geological Survey Commissioned Report CR/03/057N.

Johnston, A. M. (1996). The effect of environmental variables on ^{13}C discrimination by two marine phytoplankton, *Marine Ecology Progress Series*, **132**, 257-263.

Joint, I., and A. Pomroy (1993). Phytoplankton biomass and production in the southern North Sea, *Marine Ecology Progress Series*, **99**, 169-182.

Jones, C. E., and L. J. Carpenter (2005). Solar photolysis of CH_2I_2, CH_2ICl, and CH_2IBr in water, saltwater and seawater, *Environmental Science and Technology*, **39**, 6130-6137.

Jones, C. E., and L. J. Carpenter (2007). Chemical destruction of CH_3I, C_2H_5I, 1-C_3H_7I and 2-C_3H_7I in saltwater, *Geophysical Research Letters*, **34**, doi:10.1029/2007GL029775.

Kettle, A. J., M. O. Andreae, D. Amouroux, T. W. Andreae, T. S. Bates, H. Berresheim, H. Bingemer, R. Boniforti, M. A. J. Curran, G. R. DiTullio, G. Helas, G. B. Jones, M. D. Keller, R. P. Kiene, C. Leck, M. Levasseur, G. Malin, M. Maspero, P. Matrai, A. R. McTaggart, N. Mihalopoulos, B. C. Nguyen, A. Novo, J. P. Putaud, S. Rapsomanikis, G. Roberts, G. Schebeske, S. Sharma, R. Simo, R. Staubes, S. Turner, and G. Uher (1999). A global database of sea surface dimethylsulfide (DMS) measurements and a procedure to predict sea surface DMS as a function of latitude, longitude, and month, *Global Biogeochemical Cycles*, **13**, 399-444.

Kettle, J., and M. Andreae (2000). Flux of dimethylsulfide from the oceans: A comparison of updated data sets and flux models, *Journal of Geophysical Research*, **105**, 793-808.

Kieber, D. J., J. F. Jiao, R. P. Kiene, and T. S. Bates (1996). Impact of dimethylsulfide photochemistry on methyl sulfur cycling in the equatorial Pacific Ocean, *Journal of Geophysical Research-Oceans*, **101**, 3715-3722.

Kiene, R. P., and T. S. Bates (1990). Biological removal of dimethyl sulphide from seawater, *Nature*, **345**, 702-705.

Kiene, R. P., L. J. Linn, and J. A. Bruton (2000). New and important roles for DMSP in marine microbial communuties, *Journal of Sea Research*, **43**, 209-224.

Kim, J. M., K. Lee, K. Shin, J. H. Kang, H. W. Lee, M. Kim, P. G. Jang, and M. C. Jang (2006). The effect of seawater CO2 concentration on growth of a natural phytoplankton assemblage in a controlled mesocosm experiment, *Limnology and Oceanography*, **51**, 1629-1636.

King, D. B., and E. S. Saltzman (1997). Removal of methyl bromide in coastal seawater: chemical and biological rates, *Journal of Geophysical Research*, **102**, 18715-18721.

Kladi, M., C. Vagias, and V. Roussis (2004). Volatile halogenated metabolites from marine red algae, *Phytochemistry Reviews*, 3**,** 337-366.

Kleypas, J. A., R. W. Buddemeier, D. Archer, J.-P. Gattuso, C. Langdon, and B. N. Opdyke (1999). Geochemical consequences of increased atmospheric carbon dioxide on coral reefs, *Science*, **284**, 118-120.

Kleypas, J. A., R. A. Feely, V. J. Fabry, C. Langdon, C. L. Sabine, and L. L. Robbins (2006). Impacts of ocean acidification on coral reefs and other marine calcifiers: A guide for future research, report of a workshop held 18-20 April 2005, 88 pp, Sponsored by NSF, NOAA and the US Geological Survey, St. Petersburg, FL.

Klick, S. (1992). Seasonal variations of biogenic and anthropogenic halocarbons in seawater from a coastal site, *Limnology and Oceanography*, **37**, 1579-1585.

Klick, S., and K. Abrahamsson (1992). Biogenic volatile iodated hydrocarbons in the ocean, *Journal of Geophysical Research*, **97**, 12683-12687.

Korhonen, H., K. S. Carslaw, D. V. Spracklen, G. W. Mann, and M. T. Woodhouse (2008). Influence of oceanic dimethyl sulfide emissions on cloud condensation nuclei concentrations and seasonality over the remote Southern Hemisphere oceans: A global model study, *Journal of Geophysical Research-Atmospheres*, **113**, D15204, doi:10.1029/2007jd009718

Krysell, M. (1991). Bromoform in the Nansen Basin in the Arctic Ocean, *Marine Chemistry*, 33, 187-197.

Krysell, M., and P. D. Nightingale (1994). Low molecular weight halocarbons in the Humber and Rhine estuaries determined using a new purge-and-trap gas chromatographic method, *Continental Shelf Research*, 14, 1311-1329.

Kuiper, J., and J. C. Gamble (1988). Between test-tubes and the North Sea, in Pollution of the North Sea, edited by W. Salomons et al., pp. 638-654, Springer Verlag, Berlin.

Kulmala, M., I. Riipinen, M. Sipila, H. E. Manninen, T. Petaja, H. Junninen, M. D. Maso, G. Mordas, A. Mirme, M. Vana, A. Hirsikko, L. Laakso, R. M. Harrison, I. Hanson, C. Leung, K. E. J. Lehtinen, and V.-M. Kerminen (2007). Toward Direct Measurement of Atmospheric Nucleation, *Science*, 318, 89-92.

Kurihara, H., C. Shimode, and Y. Shirayama (2005). Sub-lethal effects of elevated concentrations of CO_2 on planktonic copepods and sea urchins, *Journal of Oceanography*, 60, 743-750.

Kwint, R. L. J., and K. J. M. Kramer (1995). DMS production by plankton communities, *Marine Ecology Progress Series*, 121, 227-237.

Lalli, C. M., and T. R. Parsons (1997). Biological Oceanography An Introduction, Butterworth-Heinemann.

Langdon, C., and M. J. Atkinson (2005). Effect of elevated pCO_2 on photosynthesis and calcification of corals and interactions with seasonal change in temperature/irradiance and nutrient enrichment, *Journal of Geophysical Research*, **110**, doi:10.1029/2004JC002576.

Larsen, S. H. (2005). Solar variability, dimethyl sulphide, clouds and climate, *Global Biogeochemical Cycles*, **19**. doi:10.1029/2004GB002333.

Laturnus, F. (1995). Release of volatile halogenated organic compounds by unialgal cultures of polar macroalgae, *Chemosphere*, **31**, 3387-3395.

Laturnus, F. (1996). Volatile halocarbons released from Arctic macroalgae, *Marine Chemistry*, 55, 359-366.

Laugenbuch, M., and H. O. Portner (2004). High sensitivity to chronically elevated CO_2 levels in a eurybathic marine sipunculid, *Aquatic Toxicology*, 70, 55-61.

Leonardos, N., and R. J. Geider (2005). Elevated atmospheric carbon dioxide increases organic carbon fixation by Emiliania huxleyi (Haptophyta), under nutrient-limited high-light conditions, *Journal of Phycology*, 41, 1196-1203.

Levasseur, M., S. Michaud, J. Egge, G. Cantin, J. C. Nejstgaard, R. Sanders, E. Fernandez, P. T. Solberg, B. Heimdal, and M. Gosselin (1996). Production of DMSP and DMS during a mesocosm study of an Emiliania huxleyi bloom: influence of bacteria and Calanus finmarchicus grazing *Marine Biology*, 126, 609-618.

Levitan, O., G. Rosenberg, E. Setlikova, J. Grigel, J. Klepetar, O. Prasil, and J. Berman-Frank (2007). Elevated CO_2 enhances nitrogen fixation and growth in the marine cyanobacterium Trichodesmium, *Global Change Biology*, 13, 531-538.

Lewis, E., and D. W. R. Wallace (1998). Program Developed for CO2 System Calculations, Carbon Dioxide Information Analysis Center, Oak Ridge National Laboratory, U.S. Department of Energy, Oak Ridge, Tennessee.

Libes, S. M. (1992). An Introduction To Marine Biogeochemistry, pp.

Liss, P. S. (1983). Gas Transfer: Experiments and Geochemical Implications, in Air-Sea Exchange of gases and Particles, edited by P. S. Liss and W. G. N. Slinn, pp. 241-298, D. Reidel Publishing Company, Dordrecht, Holland.

Liss, P. S., A. D. Hatton, G. Malin, P. D. Nightingale, and S. Turner (1997). Marine sulphur emissions, *Philosophical Transactions of the Royal Society London* B, 352, 159-169.

Liss, P. S., and L. M. Merlivat (1986). Air-sea gas exchange rates: Introduction and synthesis, in The role of air-sea exchange in geochemical cycling, edited by P. Buat-Menard, pp. 113-127, D. Reidel Publishing Company, Dordrecht.

Liss, P. S., and P. G. Slater (1974). Flux of Gases across the Air-Sea Interface, *Nature*, **247**, 181-184.

Longhurst, A. R., and W. G. Harrison (1989). The biological pump: Profiles of plankton production and consumption in the upper ocean, *Progress In Oceanography*, **22**, 47-123.

Lovelock, J. E. (1975). Natural halocarbons in the air and in the sea, *Nature*, **256**, 193-194.

Lovelock, J. E. (1986). Geophysiology - a New Look at Earth-Science (Reprinted from Geophysiology in Amazonia - Vegetation and Climate Interactions), *Bulletin of the American Meteorological Society*, **67**, 392-397.

Lovelock, J. E., R. J. Maggs, and R. A. Rasmussen (1972). Atmospheric dimethyl sulphide and the natural sulphur cycle, *Nature*, **237**, 452-453.

Lovelock, J. E., R. J. Maggs, and R. J. Wade (1973). Halogenated hydrocarbons in and over the Atlantic, *Nature*, **241**, 194 - 196.

Makela, J. M., T. Hoffman, C. Holzke, M. Vakeva, T. Suni, T. Matilla, P. P. Aalto, U. Tapper, E. I. Kauppinen, and C. D. O'Dowd (2002). Biogenic iodine emissions and identification of end-products in coastal ultrafine particles during nucleation bursts, *Journal of Geophysical Research*, **107**, 8110, doi:8110/1029JD000580.

Malin, G., P. S. Liss, and S. M. Turner (1994). Dimethyl Sulfide: production and atmospheric consequences, in The Haptophyte Algae, edited by J. C. Green and B. S. C. Leadbeater, pp. 303-320, Clarendon Press, Oxford.

Malin, G., S. Turner, P. Liss, P. Holligan, and D. Harbour (1993). Dimethylsulphide and dimethylsulphoniopropionate in the Northeast Atlantic during the summer coccolithophore bloom, *Deep-Sea Research* I, **40**, 1487-1508.

Malin, G., S. M. Turner, and P. S. Liss (1992). Sulfur: The plankton/climate connection, *Journal of Phycology*, **28**, 590-597.

Malin, G., W. H. Wilson, G. Bratbak, P. S. Liss, and N. H. Mann (1998). Elevated production of dimethyl sulphide resulting from viral infection of cultures of *Phaeocystis pouchetii*, Limnology and Oceanography, **43**, 1389-1393.

Manley, S. L. (2002). Phytogenesis of halomethanes: a product of selection or a metabolic accident?, *Biogeochemistry*, **60**, 163-180.

Manley, S. L., and P. B. Barbero (2001). Physiological constraints on bromoform ($CHBr_3$) production, *Limnology and Oceanography*, 46**,** 1392-1399.

Manley, S. L., and J. L. d. l. Cuesta (1997). Methyl iodide production from marine phytoplankton cultures, *Limnology and Oceanography*, **42**, 142-147.

Manley, S. L., and M. N. Dastoor (1987). Methyl halide (CH_3X) production from the giant kelp, Macrocystis, and estimates of global CH_3X production by kelp, *Limnology and Oceanography*, **32**, 709-715.

Manley, S. L., and M. N. Dastoor (1988). Methyl iodide (CH_3I) production by kelp and associated microbes, *Marine Biology*, **98**, 477-482.

Martin, J. H., K. H. Coale, K. S. Johnson, S. E. Fitzwater, R. M. Gordon, S. J. Tanner, C. N. Hunter, V. A. Elrod, J. L. Nowicki, T. L. Coley, R. T. Barber, S. Lindley, A. J. Watson, K. Van Scoy, C. S. Law, M. I. Liddicoat, R. Ling, T. Stanton, J. Stockel, C. Collins, A. Anderson, R. Bidigare, M. Ondrusek, M. Latasa, F. J. Millero, K. Lee, W. Yao, J. Z. Zhang, G. Friederich, C. Sakamoto, F. Chavez, K. Buck, Z. Kolber, R. Greene, P. Falkowski, S. W. Chisholm, F. Hoge, R. Swift, J. Yungel, S. Turner, P. Nightingale, A. Hatton, P. Liss, and N. W. Tindale (1994). Testing the iron hypothesis in ecosystems of the equatorial Pacific Ocean, *Nature*, **371**, 123-129.

Martino, M., P. S. Liss, and J. M. C. Plane (2005). The photolysis of dihalomathanes in surface seawater, *Environmental Science and Technology*, **39**, 7097-7101.

Martino, M., G. P. Mills, J. Woeltjen, and P. S. Liss (2009). A new source of volatile organoiodine compounds in surface seawater, *Geophysical Research Letters*, **36**, 5, L01609, doi: 10.1029/2008gl036334

Matrai, P. A., W. M. Balch, D. J. Cooper, and E. S. Saltzman (1993). Ocean color and atmospheric dimethyl sulphide: on their mesoscale variability., *Journal of Geophysical Research*, 98, 23469 - 23476.

McFiggans, G., H. Coe, R. Burgess, J. Allan, M. Cubison, M. R. Alfarra, R. Saunders, A. Saiz-Lopez, J. M. C. Plane, D. Wevill, L. Carpenter, A. R. Rickard, and P. S. Monks (2004). Direct evidence for coastal iodine particles from Laminaria macroalgae - linkage to emissions of molecular iodine, *Atmospheric Chemistry and Physics Discussions*, 4, 701-713.

McMaster, M. C., and C. McMaster (1998). GC/MS : a practical user's guide, Wiley, New York.

McNeil, B. I., and R. J. Matear (2007). Climate change feedbacks on future oceanic acidification, *Tellus*, 59B, 191-198.

McQuatters-Gollop, A., E. R. Dionysios, M. Edwards, Y. Pradhan, L. D. Mee, S. J. Lavender, and M. J. Attrill (2007). A long-term chlorophyll dataset reveals regime shift in North Sea phytoplankton biomass unconnected to nutrient levels. *Limnology and Oceanography*, 52, 635-648.

Mehrbach, C., C. H. Culberson, J. E. Hawley, and R. M. Pytkowicz (1973). Measurement of the apparent dissociation constants of carbonic acid in seawater at atmospheric pressure, *Limnology and Oceanography*, 18, 897-907.

Menden-Deuer, S., and E. J. Lessard (2000). Carbon to volume relationships for dinoflagellates, diatoms, and other protist plankton, *Limnology and Oceanography*, 45, 569-579.

Michaelidis, B., C. Ouounis, A. Paleras, and H. O. Portner (2005). Effects of long-term moderate hypercapnia on acid-base balance and growth rate in marine mussels Mytilus galloprovincialis, *Marine Ecology Progress Series*, 293, 109-118.

Millero, F. J. (2006). Chemical Oceanography, Taylor and Francis Group, New York,

Millero, F. J., and M. L. Sohn (1992). Chemical Oceanography, CRC Press, Inc., Florida, pp.

Milliman, J. D. (1974). Recent Sedimentary Carbonates. Part 1 Marine Carbonates, Springer-Verlag, Berlin.

Miyake, Y., and S. Tsunogai (1963). Evaporation of iodine from the ocean., *Journal of Geophysical Research*, 68, 3989.

Moelwyn-Hughes, E. A. (1938). The hydrolysis of the methyl halides, *Proceedings of the Royal Society A*, 164, 295-306.
Mojica Prieto, F. J., and F. J. Millero (2002). The values of pK1 + pK2 for the dissociation of carbonic acid in seawater, *Geochimica et Cosmochimica Acta*, 66, 2529-2540.

Moore, R. M. (2003). Marine Sources of Volatile Organohalogens, *The Handbook of Environmental Chemistry*, 3, 85 - 101.

Moore, R. M., and W. Groszko (1999). Methyl iodide distribution in the ocean and fluxes to the atmosphere, *Journal of Geophysical Research*, 104, 11163-11171.

Moore, R. M., and R. Tokarczyk (1993). Volatile biogenic halocarbons in the northwest Atlantic, *Global Biogeochemical Cycles*, 7, 195-210.

Moore, R. M., M. Webb, and R. Tokarczyk (1996). Bromoperoxidase and iodoperoxidase enzymes and production of halogenated methanes in marine diatom cultures, *Journal of Geophysical Research*, 101, 20899-20908.

Moore, R. M., and O. C. Zafiriou (1994). Photochemical production of methyl iodide in seawater, *Journal of Geophysical Research*, 99, 16415-16420.

Morris, A. S. (2001). Measurement and instrumentation principles, Butterworth-Heinemann, Oxford [England]; Boston.

Murphy, C. D., R. M. Moore, and R. L. White (2000). An isotopic labelling method for determining production of volatile organohalogens by marine microalgae, *Limnology and Oceanography*, 45, 1868-1871.

Nguyen, B. C., N. Mihalopoulos, and S. Belviso (1990). Seasonal variation of atmospheric dimethyl sulphide at Amsterdam Island in the Southern Indian Ocean, *Journal of Atmospheric Chemistry*, 11, 123-141.

Nightingale, P. D. (1991). Low molecular weight halocarbons in seawater, PhD thesis, University of East Anglia, Norwich, UK.

Nightingale, P. D., and P. S. Liss (2003). Gases in seawater, in A Treastise On Geochemistry, edited by K. K. Turekian and H. D. Holland.

Nightingale, P. D., G. Malin, and P. S. Liss (1995). Production of chloroform and other low-molecular weight halocarbons by some species of macroalgae, *Limnology and Oceanography*, 40, 680-689.

O'Dowd, C., and G. d. Leeuw (2007). Marine aerosol production: a review of the current knowledge, *Philosophical Transactions of the Royal Society London A*, 365, 1753-1774.

O'Dowd, C. D., J. L. Jimenez, R. Bahreini, R. C. Flagan, J. H. Seinfeld, K. Ha¨meri, L. Pirjola, M. Kulmala, S. G. Jennings, and T. Hoffmann (2002). Marine aerosol formation from biogenic iodine emissions, *Nature*, **417**, 632-636.

Orr, J. C., K. Caldeira, V. Fabry, J.-P. Gattuso, P. Haugan, P. Lehodey, S. Pantoja, H.-O. Pörtner, U.Riebesell, T. Trull, M. Hood, E. Urban, and W. Broadgate (2009). Research Priorities for Ocean Acidification, report from the Second Symposium on the Ocean in a High-CO_2 World, Monaco, SCOR, UNESCO-IOC, IAEA, and IGBP.

Orr, J. C., V. J. Fabry, O. Aumont, L. Bopp, S. C. Doney, R. A. Feely, A. Gnanadesikan, N. Gruber, A. Ishida, F. Joos, R. M. Key, K. Lindsay, E. Maier-Reimer, R. Matear, P. Monfray, A. Mouchet, R. G. Najjar, G.-K. Plattner, K. B. Rodgers, C. L. Sabine, J. L. Sarmiento, R. Schlitzer, R. D. Slater, I. J. Totterdell, M.-F. Weirig, Y. Yamanaka, and A. Yool (2005). Anthropogenic ocean acidification over the twenty-first century and its impact on calcifying organisms, *Nature*, **437**, 681-686.

Partensky, F., J. Blanchot, and D. Vaulot (1999). Differential distribution and ecology of Prochlorococcus and Synechococcus in oceanic waters: a review, Bulletin of the Institute of Oceanography Monaco Special, **19**, 457-475.

Passow, U., and U. Riebesell (2005). Mesocosm perturbation experiments and the sensitivity of marine biological systems to global change, SOLAS - Discussion Sessions.

Paulino, A. I., J. K. Egge, and A. Larsen (2008). Effects of increased atmospheric CO2 on small and intermediate sized osmotrophs during a nutrient induced phytoplankton bloom, *Biogeosciences*, **5**, 739-748.

Pearson, P. N., and M. R. Palmer (2000). Atmospheric carbon dioxide concentrations over the past 60 million years, *Nature*, **406**, 695-699.

Pechtl, S., E. R. Lovejoy, J. B. Burkholder, and R. v. Glasow (2005). Modelling the possible role of iodine oxides in atmospheric new particle formation, *Atmospheric Chemistry and Physics Discussions*, 5**,** 9907-9952.

Petit, J. R., J. Jouzel, D. Raynaud, N. I. Barkov, J.-M. Barnola, I. Basile, M. Bender, J. Chappellaz, M. Davis, G. Delaygue, M. Delmotte, V. M. Kotlyakov, M. Legrand, V. Y. Lipenkov, C. Lorius, L. PEpin, C. Ritz, E. Saltzman, and M. Stievenard (1999). Climate

and atmospheric history of the past 420,000 years from the Vostok ice core, Antarctica, *Nature*, **399**, 429-436.

Portner, H. O., M. Langenbuch, and B. Michaelidis (2005). Synergistic effects of temperature extremes, hypoxia, and increases in CO_2 on marine animals: From Earth history to global change, *Journal of Geophysical Research*, **110**, doi:10.1029/2000JC002561.

Price, N. M., B. A. Ahner, and F. M. M. Morel (1994). The Equatorial Pacific Ocean: Grazer-Controlled Phytoplankton Populations in an Iron-Limited Ecosystem, *Limnology and Oceanography*, **39**, 520-534.

Quack, B., E. Atlas, G. Petrick, V. Stroud, S. Schauffler, and D. W. R. Wallace (2004). Oceanic bromoform sources for the tropical atmosphere, *Geophysical Research Letters*, **31**, doi:10.1029/2004GL020597

Quack, B., E. Atlas, G. Petrick, and D. W. R. Wallace (2007a). Bromoform and dibromomethane above the Mauritanian upwelling: Atmospheric distributions and oceanic emissions, *Journal of Geophysical Research*, **112**, doi:10.1029/2006JD007614.

Quack, B., I. Peeken, G. Petrick, and K. Nachtigall (2007b). Oceanic distribution and sources of bromoform and dibromomethane in the Mauritanian upwelling, *Journal of Geophysical Research*, **112**, doi:10.1029/2006JC003803.

Quack, B., and D. W. R. Wallace (2004). Air-sea flux of bromoform: Controls, rates, and implications, *Global Biogeochemical Cycles*, **17**, 1023, doi:1010.1029/2002GB001890.

Quay, P. D., B. Tilbrook, and C. S. Wong (1992). Oceanic Uptake of Fossil Fuel CO2: Carbon-13 Evidence, *Science*, **256**, 74-79.

Ramanathan, V., P. J. Crutzen, J. T. Kiehl, and D. Rosenfeld (2001). Aerosols, Climate, and the Hydrological Cycle, *Science*, **294**, 2119-2124.

Ramaswamy, V., O. Boucher, J. Haigh, D. Hauglustaine, J. Haywood, N. Myhre G., T. Shi, and S. Solomon (2001). Radiative Forcing of Climate Change,, in Climate Change 2001, The scientific basis: Contribution of working group I to the Third assessment report of the Intergovernmental Panel on Climate,, edited by J. T. Houghton et al., Cambirdge, UK and New York.

Raven, J., K. Caldeira, H. Elderfield, O. Hoegh-Guldberg, P. Liss, U. Riebesell, J. Shepherd, C. Turley, and A. Watson (2005). Ocean acidification due to increasing atmospheric carbon dioxide, The Royal Society, Policy Document 12/05, London.

Raven, J. A. (1980). Nutrient transport in microalgae, *Advanced Microbial Physiology*, **21**, 47-226.

Read, K. A., A. S. Mahajan, L. J. Carpenter, M. J. Evans, B. V. E. Faria, D. E. Heard, J. R. Hopkins, J. D. Lee, S. J. Moller, A. C. Lewis, L. Mendes, J. B. McQuaid, H. Oetjen, A. Saiz-Lopez, M. J. Pilling, and J. M. C. Plane (2008). Extensive halogen-mediated ozone destruction over the tropical Atlantic Ocean, *Nature*, **453**, 1232-1235.

Redfield, A. C., B. M. Ketchum, and F. A. Richards (1963). The influence of organisms on the composition of seawater, in The Sea, edited by M. N. Hill, pp. 26-77, John Wiley & Sons, New York.

Reifenhauser, W., and K. G. Heumann (1992). Bromo- and bromochloromethanes in the Antarctic atmosphere and the South Polar Sea, *Chemosphere*, **24**, 1293-1300.

Reinfelder, J. R., A. M. L. Kraepiel, and F. M. M. Morel (2000). Unicellular C4 photosynthesis in a marine diatom, *Nature*, **407**, 996-999.

Revelle, R., and H. E. Suess (1957). Carbon dioxide exchange between atmosphere and ocean and the question of an increase of atmospheric CO_2 during the past decades, *Tellus*, 9**,** 18-27.

Ribera d'Alcalà, M., F. Conversano, F. Corato, P. Licandro, O. Mangoni, D. Marino, M.G. Mazzocchi, M. Modigh, M. Montresor, M. Nardella, V. Saggiomo, D. Sarno and A. Zingone (2007). Seasonal patterns in plankton communities in a pluriannual time series at a coastal Mediterranean site (Gulf of Naples): an attempt to discern recurrences and trends, *Scientia Marina*, **68**, 65-83.

Richter, U., and D. W. R. Wallace (2004). Production of methyl iodide in the tropical Atlantic Ocean, *Geophysical Research Letters*, **31**, doi:10.1029/2004GL020779.

Ridgwell, A., I. Zondervan, J. C. Hargreaves, J. Bijma, and T. M. Lenton (2007). Assessing the potential long-term increase of oceanic fossil fuel CO_2 uptake due to CO_2-calcification feedback, *Biogeosciences*, **4**, 481-492.

Riebesell, U. (2000). Carbon fix for a diatom, *Nature*, **407**, 959-960.

Riebesell, U. (2004). Effects of CO_2 enrichment on marine phytoplankton, *Journal of Oceanography*, **60**, 719-729.

Riebesell, U., R. G. J. Bellerby, H.-P. Grossart, and F. Thingstad (2008). Mescosm CO_2 perturbation studies: from organism to community level, *Biogeosciences*, **5**, 1157-1164.

Riebesell, U., A. T. Revill, D. G. Holdsworth, and J. K. Volkman (2000a). The effects of varying CO_2 concentration on lipid composition and carbon isotope fractionation in *Emiliana huxleyi, Geochimica et Cosmochimica Acta*, **64**, 4179-4192.

Riebesell, U., I. Zondervan, B. Rost, P. D. Tortell, R. E. Zeebe, and F. M. M. Morel (2000b). Reduced calcification of marine plankton in response to increased atmospheric CO_2, *Nature*, **407**, 364-367.

Roberts, K., E. Granum, R. C. Leegood, and J. A. Raven (2007). Carbon acquisition by diatoms *Photosynthesis Reseach*, **93**, 79-88.

Rochelle-Newall, E., B. Delille, M. Frankignoulle, J.-P. Gattuso, S. p. Jacquet, U. Riebesell, A. Terbruggen, and I. Zondervan (2004). Chromophoric dissolved organic matter in experimental mesocosms maintained under different pCO_2 levels, *Marine Ecology Progress Series*, **272**, 25-31.

Rodriguez, F., E. Fernandez, R. N. Head, D. S. Harbour, G. Bratbak, M. Heldal, and R. P. Harris (2000). Temporal variability of viruses, bacteria, phytoplankton and zooplankton in the western English Channel off Plymouth, *Journal of the Marine Biological Association* of the UK, **80**, 575-586.

Rost, B., and U. Riebesell (2004). Coccolithophores and the biological pump: responses to environmental changes, in Coccolithophores - From Molecular Processes to Global Impact, edited by H. R. Thierstein and J. R. Young, pp. 99-126, Springer, Berlin.

Sabine, C. L., R. A. Feely, N. Gruber, R. M. Key, K. Lee, J. L. Bullister, R. Wanninkhof, C. S. Wong, D. W. R. Wallace, B. Tilbrook, F. J. Millero, T.-H. Peng, A. Kozyr, T. Ono, and A. F. Rios (2004). The oceanic sink for anthropogenic CO_2, *Science*, **305**, 367-371.

Saemundsdottir, S., and P. A. Matrai (1998). Biological production of methyl bromide by cultures of marine phytoplankton, *Limnology and Oceanography*, **43**, 81-87.

Sanders, R., and D. A. Purdie (1998). Bacterial response to blooms dominated by diatoms and Emiliania huxleyi in nutrient-enriched mesocosms, *Estuarine Coastal and Shelf Science*, **46**, 35-48.

Scarratt, M. G., and R. M. Moore (1996). Production of methyl chloride and methyl bromide in laboratory cultures of marine phytoplankton, *Marine Chemistry*, **54**, 263-272.

Scarratt, M. G., and R. M. Moore (1998). Production of methyl bromide and methyl chloride in laboratory cultures of marine phytoplankton II, *Marine Chemistry*, **59**, 311-320.

Schippers, P., M. Lurling, and M. Scheffer (2004). Increase of atmospheric CO_2 promotes phytoplankton productivity, *Ecology Letters*, **7**, 446-451.

Shaw, G. E. (1983). Bio-Controlled Thermostasis Involving the Sulfur Cycle, *Climatic Change*, **5**, 297-303.

Shaw, G. E., R. L. Benner, W. Cantrell, and A. D. Clarke (1998). The regulation of climate: A sulfate particle feedback loop involving deep convection - An editorial essay, *Climatic Change*, **39,** 23-33.

Shenoy, D. M., and J. S. Patil (2003). Temporal variations in dimethylsulphoniopropionate and dimethyl sulphide in the Zuari estuary, Goa (India), *Marine Environmental Research*, **56**, 387-402.

Shirayama, Y., and H. Thornton (2005). Effect of increased atmospheric PCO_2 on shallow water marine benthos, *Journal of Geophysical Research*, **110**, doi:10.1029/2004JC002618.

Siegenthaler, U., and J. L. Sarmiento (1993). Atmospheric carbon dixide and the ocean, *Nature*, **365**, 119-125.

Siegenthaler, U., T. F. Stocker, E. Monnin, D. Luthi, J. Schwander, B. Stauffer, D. Raynaud, J.-M. Barnola, H. Fischer, V. Masson-Delmotte, and J. Jouzel (2005). Stable

Carbon Cycle-Climate Relationship During the Late Pleistocene, *Science*, **310**, 1313-1317.

Simo, R. (2001). Production of atmospheric sulfur by oceanic plankton: biogeochemical, ecological and evolutionary links, *Trends in Ecology and Evolution*, **16**, 287-294.

Simo, R., and J. O. Grimalt (1998). Spring-summer emission of dimethyl sulphide from the north-western Mediterranean Sea, *Estuarine, Coastal and Shelf Science*, **47**, 671-677.

Simo, R., J. O. Grimalt, and J. Albaiges (1997). Dissolved dimethylsulphide, dimethylsulphoniopropionate and dimethylsulphoxidein western Mediterranean waters, *Deep-Sea Research II*, **44**, 929-950.

Skirrow, G. (1975). The dissolved gases - carbon dioxide, in Chemical Oceanography, edited by J. P. Riley and G. Skirrow, Plenum, New York.

Smith, D. C., M. Simon, A. L. Alldredge, and F. Azam (1992). Intense hydrolytic enzyme activity on marine aggregates and implications for rapid particle dissolution, *Nature*, **359**, 139-142.

Smythe-Wright, D., S. M. Boswell, P. Breithaupt, R. D. Davidson, C. H. Dimmer, and L. B. E. Diaz (2006). Methyl iodide production in the ocean: Implications for climate change, *Global Biogeochemical Cycles*, **20**, doi:10.1029/2005GB002642.

Smythe-Wright, D., S. M. Boswell, C. H. Lucas, A. L. New, and M. S. Varney (2005). Halocarbon and dimethyl sulphide studies around the Mascarene Plateau, *Philosophical Transactions of the Royal Society London A*, **363**, 169-185.

Solomon, S. (1999). Stratospheric ozone depletion: A review of concepts and history, *Reviews of Geophysics*, **37**, 275-316.

Solomon, S., R. R. Garcia, and A. R. Ravishankara (1994). On the role of iodine in ozone depletion, *Journal of Geophysical Research*, **99**, 20491-20499.

Spahni, R., J. Chappellaz, T. F. Stocker, L. Loulergue, G. Hausammann, K. Kawamura, J. Fluckiger, J. Schwander, D. Raynaud, V. Masson-Delmotte, and J. Jouzel (2005). Atmospheric Methane and Nitrous Oxide of the Late Pleistocene from Antarctic Ice Cores, *Science*, **310**, 1317-1321.

Stabile, T. A., A. Zollo, M. Vassallo, and G. Iannaccone (2007). Underwater acoustic channel properties in the Gulf of Naples and their effects on digital data transmission, *Annals of Geophysics*, **50** (3), 411-426.

Stefels, J. (2000). Physiological aspects of the production and conversion of DMSP in marine algae and higher plants, *Journal of Sea Research*, **43**, 183-197.

Stefels, J., W. W. C. Gieskes, and L. Dijkhuizen (1996). Intriguing functionality of the production and conversion of DMSP in Phaeocystis sp., in Biological and environmental chemistry of DMSP and related sulfonium compounds, edited by P. T. V. R. P. Kiene, M. D. Keller & G. O. Kirst, Plenum, New York.

Stefels, J., M. Steinke, S. Turner, G. Malin, and S. Belviso (2007). Environmental constraints on the production and removal of the climatically active gas dimethylsulphide (DMS) and implications for ecosystem modelling, *Biogeochemistry*, **83**, 245-275.

Steinke, M., C. Daniel, and G. O. K. . (1996). DMSP lyase in marine macro- and microalgae., in Biological and environmental chemistry of DMSP and related sulfonium compounds, edited by P. T. V. R. P. Kiene, M. D. Keller & G. O. Kirst, Plenum, New York.

Steinke, M., C. Evans, G. A. Lee, and G. Malin (2007). Substrate kinetics of DMSP-lyases in axenic cultures and mesocosm populations of *Emiliania huxleyi*, *Aquatic Sciences*, **69**, 352-359.

Stewart, A. J., and R. G. Wetzel (1986). Cryptophytes and other microflagellates as couplers in planktonic community dynamics, *Archiv fur Hydrobiology*, **106**, 1-19.

Sturrock, G. A., C. E. Reeves, G. P. Mills, S. A. Penkett, C. R. Parr, A. McMinn, G. Corno, N. W. Tindale, and P. J. Fraser (2003). Saturation levels of methyl bromide in the coastal waters off Tasmania, *Global Biogeochemical Cycles*, **17**, 1101.

Sunda, W., D. J. Kieber, R. P. Kiene, and S. Huntsman (2002). An antioxidant function for DMSP and DMS in marine algae, *Nature*, **418**, 317-320.

Sundstrom, J., J. Collen, K. Abrahamsson, and M. Pedersen (1996). Halocarbon production and in vivo brominating activity of *Eucheuma denticulatum*, *Phytochemistry*, **42**, 1527-1530.

Tait, V. K., and R. M. Moore (1995). Methyl chloride (CH_3Cl) production in phytoplankton cultures, *Limnology and Oceanography*, **40**, 189-195.

Tang, X., S. Madronich, T. Wallington, and D. Calamari (1998). Changes in tropospheric composition and air quality, *Journal of Photochemistry and Photobiology B: Biology*, **46**, 83-95.

Thomas, H., A. E. F. Prowe, S. v. Heuven, Y. Bozec, H. J. W. d. Baar, L.-S. Schiettecatte, K. Suykens, M. Koné, A. V. Borges, I. D. Lima, and S. C. Doney (2007). Rapid decline of the CO_2 buffering capacity in the North Sea and implications for the North Atlantic Ocean *Global Biogeochemical Cycles*, **21**, doi:10.1029/2006GB002825.

Tokarczyk, R., K. D. Goodwin, and E. S. Saltzman (2001). Methyl bromide loss rate constants in the North Pacific Ocean, *Geophysical Research Letters*, **28**, 4429-4432.

Tokarczyk, R., and R. M. Moore (1994). Production of volatile organohalogens by phytoplankton cultures, *Geophysical Research Letters*, **21**, 285-288.

Toole, D. A., D. J. Kieber, R. P. Kiene, D. A. Siegel, and N. B. Nelson (2003). Photolysis and the Dimethylsulfide (DMS) Summer Paradox in the Sargasso Sea, *Limnology and Oceanography*, **48**, 1088-1100.

Turner, S. M., G. Malin, L. E. Badanger, and C. Leck (1990). Interlaboratory Calibration and Sample Analysis of Dimethyl Sulphide in Water, *Marine Chemistry*, **29**, 47-62.

Turner, S. M., G. Malin, P. S. Liss, D. S. Harbour, and P. M. Holligan (1988). The Seasonal Variation of Dimethyl Sulfide and Dimethylsulfoniopropionate Concentrations in Nearshore Waters, *Limnology and Oceanography*, **33**, 364-375.

Turner, S. M., G. Malin, P. D. Nightingale, and P. S. Liss (1996). Seasonal variation of dimethyl sulphide in the North Sea and an assessment of fluxes to the atmosphere, *Marine Chemistry*, **57**, 245-262.

Twomey, S. (1991). Aerosols, clouds and radiation, *Atmospheric Environment*, **25A**, 2435-2442.

Urhahn, T., and K. Ballschmiter (1998). Chemistry of the biosynthesis of halogenated methanes: C1-organohalogens as pre-industrial chemical stressors in the environment?, *Chemosphere*, **37**, 1017-1032.

Utermohl, H. (1958). Zur Vervollkommnung der quantitativen Phytoplankton Methodik. , *Mitt Int Verein Theor Angew Limnol*, **9**, 1-38.

Vairavamurthy, A., M. O. Andreae, and R. L. Iverson (1985). Biosynthesis of dimethylsulphide and dimethyl propiothetin by Hymenomonas caterae in relation to sulfur sourse and salinity variations, *Limnology and Oceanography*, **30**, 59-70.

Vallino, J. J. (2000). Improving marine ecosystem models: Use of data assimilation and mesocosm experiments, *Journal of Marine Research*, **58**, 117-164.

Venrick, E. L., J. R. Beers, and J. F. Heinbokel (1977). Possible consequences of containing microplankton for physiological rate measurements, *Journal of Experimental Marine Biology and Ecology*, **26**, 55-76.

Vila-Costa, M., R. Simo, H. Harada, J. M. Gasol, D. Slezak, and R. P. Kiene (2006). Dimethylsulfoniopropionate Uptake by Marine Phytoplankton, *Science*, **314**, 652-654.

Vogt, M., M. Steinke, S. Turner, A. Paulino, M. Meyerhöfer, U. Riebesell, C. LeQuéré, and P. Liss (2008). Dynamics of dimethylsulphoniopropionate and dimethylsulphide under different CO_2 concentrations during a mesocosm experiment, *Biogeosciences*, **5**, 407-419.

Vogt, R., R. Sander, R. v. Glasow, and P. J. Crutzen (1999). Iodine Chemistry and its Role in Halogen Activation and Ozone Loss in the Marine Boundary Layer: A Model Study, *Journal of Atmospheric Chemistry*, **32**, 375-395.

Wang, L., R. M. Moore, and J. J. Cullen (2009). Methyl iodide in the NW Atlantic: Spatial and seasonal variation, *Journal of Geophysical Research-Oceans*, **114**, C07007, 13, doi:10.1029/2007JC004626.

Wanninkhof, R., and K. Thoning (1993). Measurement of fugacity of CO_2 in surface water using continuous and discrete sampling methods, *Marine Chemistry*, **44**, 189-204.

Waterbury, J. B., S. W. Watson, R. R. L. Guillard, and L. E. Brand (1979). Widespread occurrence of a unicellular, marine, planktonic, cyanobacterium, *Nature*, **277**, 293-294.

Watson, A. J., and P. S. Liss (1998). Marine biological controls on climate via the carbon and sulphur geochemical cycles, *Philosophical Transactions of the Royal Society London* B, **353**, 41-51.

Watson, J. T., and O. D. Sparkman (2008). Introduction to mass spectrometry : instrumentation, applications and strategies for data interpretation, John Wiley & Sons, Chichester, England; Hoboken, NJ, pp.

Watts, M. C., and G. R. Biggs (2001). Modelling and monitoring of mesocosm experiments: two case studies, *Journal of Plankton Research*, **23**, 1081-1093.

West, J. J., A. M. Fiore, L. W. Horowitz, and D. L. Mauzerall (2006). Global health benefits of mitigating ozone pollution with methane emission controls, *Proceedings of the National Academy of Sciences of the United States of America*, **103**, 3988-3993.

Williams, P. J. l. B., and J. K. Egge (1998). The management and behaviour of the mesocosms, *Estuarine, Coastal and Shelf Science*, **46** (Supplement A), 3-14.

Wilson, W. H., S. Turner, and N. H. Mann (1998). Population dynamics of phytoplankton and viruses in a phosphate-limited mesocosm and their effect on DMSP and DMS production, *Estuarine Coastal and Shelf Science*, **46**, 49-59.

Winchester, M. R., and J. K. Miller (2000). Drift-corrected calibration in glow discharge optical emission spectrometry, *Journal of Analytical Atomic Spectrometry*, **15**, 169-175.

Wingenter, O. W., K. B. Haase, M. Zeigler, D. R. Blake, F. Rowland, S. S., B. C., A. Paulino, R. Thyrhaug, A. Larsen, K. G. Schulz, M. Meyerhofer, and U. Riebesell (2007). Unexpected consequences of increasing CO_2 and ocean acidity on marine production of DMS and CH_2ClI: Potential climate impacts, *Geophysical Research Letters*, **34**, doi.org/10.1029/2006GL028139.

Wofsy, S., M. B. McElroy, and Y. L. Yung (1975). The chemistry of atmospheric bromine (catalyst for ozone destruction), *Geophysical Research Letters*, **2**, 215-218.

Wolf-Gladrow, D. A., U. Riebesell, S. Burkhardt, and J. Bijma (1999). Direct effects of CO_2 concentration on growth and isotopic composition of marine plankton, *Tellus*, **51** B, 461-476.

Wolfe, G. V., M. Steinke, and G. O. Kirst (1997). Grazing-activated chemical defence in a unicellular marine alga, *Nature*, **387**, 894-897.

Wuosmaa, A. M., and L. P. Hager (1990). Methyl chloride transferase: a carbocation route for biosynthesis of halometabolites, *Science*, **249**, 160-162.

Yamamoto, H., Y. Yokouchi, A. Otsuki, and H. Itoh (2001). Depth profiles of volatile halogenated hydrocarbons in seawater in the Bay of Bengal, *Chemosphere*, **45**, 371-377.

Yang, X., R. A. Cox, N. J. Warwick, J. A. Pyle, G. D. Carver, F. M. O'Connor, and N. H. Savage (2005). Tropospheric bromine chemistry and its impacts on ozone: A model study, *Journal of Geophysical Research*, **110**, D23311, doi:10.1029/2005JD006244.

Yvon-Lewis, S. A., K. H. Butler, E. S. Saltzman, P. Matrai, D. B. King, R. Tokarczyk, R. M. Moore, and J.-Z. Zhang (2002). Methyl bromide cycling in a warm-core eddy of the North Atlantic Ocean, *Global Biogeochemical Cycles*, **16**, 1141.

Zafiriou, O. C. (1975). Reaction of methyl halides with seawater and marine aerosols, *Journal of Marine Research*, **33**, 75-81.

Zeebe, R. E., and D. Wolf-Gladrow (2001). CO_2 in seawater: Equilibrium, Kinetics, Isotopes, Elsevier Science B.V., Amsterdam, The Netherlands, pp.

Zondervan, I., R. E. Zeebe, B. Rost, and U. Riebesell (2001). Decreasing marine biogenic calcification: A negative feedback on rising atmospheric pCO_2, *Global Biogeochemical Cycles*, **15**, 507-516.

Zubkov, M. V., B. M. Fuchs, G. A. Tarran, P. H. Burkill, and R. Amann (2002). Mesoscale distribution of dominant bacterioplankton groups in the northern North Sea in early summer, *Aquatic Microbial Ecology*, **29**, 135-144.

Appendices

Ocean Acidification and
Marine Biogenic Trace Gas Production

Frances Elizabeth Hopkins
March 2010

Contents

Appendix **Page**

Appendix 1. Summary of the statistical analyses on trace gases and chlorophyll *a* data for the whole mesocosm experiment (DMS/DMSP 6 – 22 May) (Halocarbons 8 – 23 May). M3 and M4 only included in analyses after 15 May. Shaded in grey = differences considered significant at a threshold of $p<0.05$, $^{+}$ = T-test performed assuming equal variances, $^{\$}$ = T-test performed NOT assuming equal variances considered significant at a threshold of $p<0.05$.

Parameter	**Mean**		**SD**		**Normality** (Anderson-Darling) p>0.05 = normal distribution		**Data Transformation**	**Test of Equal Variances** (Levene's statistic) p>0.05 = equal variances	**2-Sample T-test** p<0.05 = significant difference between means	**Mann-Whitney nonparametric test W** p<0.05 = significant difference between means
	High CO_2	**Present day CO_2**	**High CO_2**	**Present day CO_2**	**High CO_2**	**Present day CO_2**				
DMS	5.7	14.1	5.0	14.6	0.700 p=0.062	0.752 p=0.050	Log	3.61 p=0.062	2.88, DF=70, p=0.05^{+}	
DMSPp	139.0	175.6	74.5	117.7	0.956 p=0.014	1.180 p<0.005	None	3.87 p=0.053		1225 p=0.3189
DMSPt	190.3	248.3	66.2	108.4	0.318 p=0.522	0.505 p=0.190	Square root	3.14 p=0.081	2.60, DF=70, p=0.011^{+}	
CH_3I	5.4	9.7	3.3	6.5	0.697 p=0.062	0.801 p=0.033	Log	1.19, p=0.280		691 p=0.0108
C_2H_5I	0.49	0.76	0.42	0.57	0.252 p=0.713	0.376 p=0.389	Square root	2.79 p=0.100	1.74, DF=56, p=0.087^{+}	
CH_2I_2	127.8	175.9	169.5	231.6	3.050 p<0.005	2.914 p<0.005	None	0.82 p=0.370		786 p=0.2833

CH_2ClI	136.9	179.0	172.6	206.9	2.678 p<0.005	2.248 p<0.005	None	1.64 p=0.206		828 p=0.6746
$CHBr_3$	39.8	35.3	20.1	17.2	1.180 p<0.005	1.592 p<0.005	None	0.32 p=0.576		967 p=0.0843
CH_2Br_2	2.42	1.3	2.39	0.9	0.443 p=0.268	0.543 p=0.149	None	1.37 p=0.247	-0.08,DF=56, p=0.936[+]	
$CHBr_2Cl$	0.60	0.48	0.2	0.1	0.634 p=0.089	0.577 p=0.122	None	2.02 p=0.162	-3.28, DF=55, p=0.002[+]	
Chl-a	2.48	3.44	2.0	3.4	1.075 p=0.007	2.217 p<0.005	Log	0.40 p=0.527		1106.5 p=0.4182
CH_3I: chl-a	3.83	4.74	6.5	7.1	0.729 p=0.050	0.503 p=0.187	Log	0.43 p=0.513	1.51, DF = 50, p=0.137[+]	
C_2H_5I: chl-a	0.31	0.34	0.6	0.5	0.509 p=0.180	0.231 p=0.781	Log	0.02 p=0.876	0.87, DF = 49, p=0.389[+]	
CH_2I_2: chl-a	34.7	31.9	41.3	35.9	0.525 p=0.165	0.528 p=0.162	Square Root	0.27 p=0.608	-0.04, DF = 54, p=0.970[+]	
CH_2ClI: chl-a	48.2	57.5	56.3	66.9	0.709 p=0.056	0.591 p=0.113	Log	1.45 p=0.234	-0.05, DF = 50, p=0.964[+]	
$CHBr_3$: chl-a	42.7	34.3	79.4	68.5	0.742 p=0.047	1.402 p<0.005	Log	0.02 p=0.878		757.0 p=0.2167
CH_2Br_2: chl-a	2.3	2.5	4.8	4.4	1.125 p<0.005	0.660 p=0.075	Log	1.45 p=0.234		691.0 p=0.9781
$CHBr_2Cl$: chl-a	0.6	0.5	1.1	1.0	1.671 p<0.005	0.692 p=0.062	Log	1.68 p=0.202		707.0 p=0.2871

Appendix 2. Summary of the statistical analyses performed on trace gas and chlorophyll *a* data for Mesocosms 1 to 6 for Phase 2 of the experiment (Bloom 10-17 May). Shaded in grey = differences considered significant at a threshold of $p<0.05$, $^{+}$ = T-test performed assuming equal variances, $^{\$}$ = T-test performed NOT assuming equal variances considered significant at a threshold of $p<0.05$.

Parameter	**Mean**		**SD**		**Normality** (Anderson-Darling) p>0.05 = normal distribution		**Data Transformation**	**Test of Equal Variances** (Levene's statistic) p>0.05 = equal variances	**2-Sample T-test** p<0.05 = significant difference between means	**Mann-Whitney nonparametric test W** p<0.05 = significant difference between means
	High CO_2	**Present day CO_2**	**High CO_2**	**Present day CO_2**	**High CO_2**	**Present day CO_2**				
DMS	6.1	14.1	3.96	7.46	0.471 p=0.217	0.329 p=0.487	None	9.84 p=0.003	4.75, DF=24, p<0.001$^{\$}$	
DMSPp	177.9	243.3	64.0	113.8	0.259 p=0.675	0.422 p=0.289	None	5.09 p=0.030	2.18, DF=28, p=0.038$^{\$}$	
DMSPt	225.0	303.8	51.3	106.7	0.272 p=0.629	0.353 p=0.427	None	13.35 p=0.001	2.90, DF=25, p=0.008$^{\$}$	
CH_3I	6.88	11.88	3.28	6.80	0.201 p=0.859	0.431 p=0.271	None	8.11 p=0.008	2.75, DF=22, p=0.012$^{\$}$	
C_2H_5I	0.64	0.92	0.44	0.58	0.179 p=0.903	0.716 p=0.050	Square root	1.14 p=0.294	1.36, DF=33, p=0.182	
CH_2I_2	203.8	285.1	176.5	243.9	0.663 p=0.069	0.504 p=0.176	None	2.28 p=0.140	1.13, DF=33, p=0.265^{+}	

CH_2ClI	174.8	189.6	198.2	220.1	1.429 p<0.005	1.416 p<0.005	None	0.20 p=0.661		307.5 p=0.5974
$CHBr_3$	42.33	38.85	11.99	11.77	1.864 p<0.005	1.229 p<0.005	None	0.00 p=0.973		381 p=0.0622
CH_2Br_2	1.703	1.804	0.86	0.47	0.556 p=0.129	0.259 p=0.671	None	5.24 p=0.029	0.44, DF=26, p=0.667$^{\$}$	
$CHBr_2Cl$	0.52	0.43	0.10	0.09	0.390 p=0.345	0.540 p=0.141	None	0.50 p=0.484	-2.82, DF=33, p=0.008^{+}	
Chl-a	3.12	5.22	1.78	3.38	0.452 p=0.245	0.664 p=0.070	None	7.07 p=0.011	2.45, DF = 28, p=0.021$^{\$}$	

Appendix 3. Summary of the statistical analyses performed on flow cytometry phytoplankton count data for Mesocosms 1 to 6 for Phase 2 of the experiment (Bloom 10-17 May). Shaded in grey = differences considered significant at a threshold of p<0.05, $^{+}$ = T-test performed assuming equal variances, $^{\$}$ = T-test performed NOT assuming equal variances considered significant at a threshold of p<0.05.

	Mean (± SD)	**Data transformation**	**Normality Anderson-Darling (Normal p>0.05)**	**Test of Equal Variances Levene's statistic (Equal p>0.05)**	**Test of Significance (Significantly different p<0.05)**
Coccolithophores	**High CO_2:** 728.9 ± 556 **Present CO_2:** 1252 ± 802	Square root	**High CO_2:** 0.458, p= 0.250 **Present CO_2:** 0.565, p= 0.134	4.88 p = 0.03	2-sample T-test T = 3.17 DF = 68 p = 0.002$^{\$}$
Small Picoeukaryotes	**High CO_2:** 22503 ± 15303 **Present CO_2:** 20739 ± 15491	Log	**High CO_2:** 0.567, p = 0.132 **Present CO_2:** 0.849, p= 0.026	0.05 p = 0.822	Mann-Whitney W = 1431 p = 0.822

	Mean (± SD)	Data transformation	Normality Anderson-Darling (Normal p>0.05)	Test of Equal Variances Levene's statistic (Equal p>0.05)	Test of Significance (Significantly different p<0.05)
Large Picoeukaryotes	**High CO_2:** 3067 ± 2089 **Present CO_2:** 7683 ± 9098	Log	**High CO_2:** 0.906, p = 0.019 **Present CO_2:** 0.641, p = 0.087	9.30 p = 0.003	2-sample T-test T = -2.33 DF = 59 P = 0.023[$]
Large Picoeukaryotes Phase 2 Bloom 10 – 17 May	**High CO_2:** 3905 ± 2128 **Present CO_2:** 12157 ± 9924	Square root	**High CO_2:** 0.654, p = 0.075 **Present CO_2:** 0.496, p = 0.189	8.16 p = 0.007	2-sample T-test T = 4.05 DF = 25 p < 0.001[$]
Nanophytoplankton	**High CO_2:** 1212 ± 1006 **Present CO_2:** 1617 ± 1318	Log	**High CO_2:** 0.389, p = 0.367 **Present CO_2:** 1.176, p < 0.005	1.07 p = 0.305	Mann-Whitney W = 1175 p = 0.1188
Cryptophytes	**High CO_2:** 109.1 ± 108 **Present CO_2:** 194.6 ± 194	Log	**High CO_2:** 0.634, p = 0.091 **Present CO_2:** 0.495, p = 0.202	0.19 p = 0.668	2-sample T-Test T = 2.93 DF = 72 p = 0.005[+]
Synechococcus	**High CO_2:** 4135 ± 2286 **Present CO_2:** 9126 ± 6245	Log	**High CO_2:** 1.014, p = 0.01 **Present CO_2:** 0.513, p = 0.182	18.40 p < 0.001	Mood's Median X^2 = 9.14 DF = 1 p = 0.03

Appendix 4. Biomass (mg C m^{-3}) for phytoplankton taxonomic groups in a. Mesocosm 1 and b. Mesocosm 6.

a. Mesocosm 1

Date in May 2006	Flagellates mg C m^{-3}	Diatoms mg C m^{-3}	Autotrophic Dinoflagellates mg C m^{-3}	Heterotrophic dinoflagellates mg C m^{-3}	Ciliates mg C m^{-3}	**Total**
9	38.52	3.22	0.68	6.50	46.05	**94.96**
11	83.02	0.17	3.23	0.92	63.89	**151.23**
12	86.60	0.26	1.90	4.60	2.86	**96.22**
13	158.79	0.00	19.59	0.60	1.54	**180.52**
14	163.10	0.01	4.49	3.48	43.12	**214.21**
15	194.16	0.03	7.28	2.71	60.30	**264.48**
18	67.47	0.00	7.58	7.15	23.84	**106.05**
21	69.56	0.03	17.70	7.22	3.39	**97.90**
Total	**861.23**	**3.73**	**62.44**	**33.18**	**245.00**	**1205.58**
% of total biomass	**71.44**	**0.31**	**5.18**	**2.75**	**20.32**	

b. Mesocosm 6

Date in May 2006	Flagellates mg C m^{-3}	Diatoms mg C m^{-3}	Autotrophic Dinoflagellates mg C m^{-3}	Heterotrophic dinoflagellates mg C m^{-3}	Ciliates mg C m^{-3}	**Total**
9	44.58	18.09	0.92	1.64	268.63	**333.86**
11	119.70	0.80	0.78	2.60	15.45	**139.33**
12	143.77	0.15	1.66	1.96	17.06	**164.61**
13	187.40	0.27	42.24	2.49	10.82	**243.22**
14	170.69	0.02	11.54	2.68	10.52	**195.46**
15	282.61	0.19	28.04	2.08	10.27	**323.19**
18	157.47	0.00	24.88	5.30	24.28	**211.92**
21	79.31	0.03	16.28	11.83	55.84	**163.29**
Total	**1185.52**	**19.55**	**126.34**	**30.59**	**412.88**	**1774.88**
% of total biomass	**66.79**	**1.10**	**7.12**	**1.72**	**23.26**	

Appendix 5. Biomass (mg C m^{-3}) for flagellate groups 1 – 8* in a. Mesocosm 1 and b. Mesocosm 6.

a. MESOCOSM 1 Date in May 2006	1	2	3	4	5	6	7	8	**TOTAL**
9	0.23	4.33	5.42	0.00	6.66	7.90	10.40	1.94	**36.87**
11	1.04	9.62	23.54	4.22	13.32	11.85	14.55	4.85	**83.01**
12	1.77	17.57	24.85	4.22	17.32	11.85	4.16	4.85	**86.59**
13	3.38	9.86	16.19	21.12	17.76	43.89	14.55	32.04	**158.79**
14	3.07	25.78	8.97	1.41	50.62	32.92	22.87	17.48	**163.10**
15	2.08	16.60	22.98	0.94	45.29	27.65	12.47	64.08	**192.09**
18	1.66	4.94	1.49	0.00	5.33	44.77	4.16	4.85	**67.21**
21	11.72	3.27	11.77	5.63	2.66	21.07	12.47	0.97	**69.56**
Total	**24.96**	**91.95**	**115.22**	**37.54**	**158.96**	**201.89**	**95.64**	**131.07**	**857.23**
% of total biomass	**2.91**	**10.73**	**13.44**	**4.38**	**18.54**	**23.55**	**11.16**	**15.29**	

b. MESOCOSM 6 Date in May 2006	1	2	3	4	5	6	7	8	**TOTAL**
9	0.48	9.27	6.73	0.47	10.66	13.17	2.08	0.97	**43.82**
11	2.51	25.33	28.21	6.10	13.32	13.17	29.11	1.94	**119.69**
12	2.23	27.37	22.42	6.57	37.30	17.12	24.95	5.83	**143.77**
13	6.82	10.06	30.08	13.14	63.94	26.33	16.63	20.39	**187.40**
14	1.94	26.48	14.95	2.35	54.62	25.02	24.95	20.39	**170.69**
15	5.18	26.66	20.55	7.04	118.56	39.50	47.82	16.50	**281.81**
18	2.59	4.59	5.23	0.47	49.29	67.15	14.55	13.59	**157.47**
21	1.35	2.47	2.99	0.00	6.66	36.87	27.03	1.94	**79.31**
Total	**23.10**	**132.24**	**131.16**	**36.14**	**354.34**	**238.31**	**187.11**	**81.55**	**1183.96**
% of total biomass	**1.95**	**11.17**	**11.08**	**3.05**	**29.93**	**20.13**	**15.80**	**9.51**	

*1 = undetermined flagellates 2 µm, 2 = Prymnesiophytes 3-4 µm, 3 = Prymnesiophytes 5 µm, 4 = Prasinophytes 8µm, 5 = undetermined flagellates 10 µm, 6 = Cryptophytes, 7 = Euglenophytes, 8 = undetermined flagellates 12 µm

Appendix 6. Spearman's Rank Correlation Coefficients (ρ) and associated significance level for mean CH_3I, C_2H_5I, CH_2I_2, CH_2ClI, chlorophyll *a* and phytoplankton community components under high CO_2 (M1, M2, M3) and present-day CO_2 (M4, M5, M6). M3 and M4 only are included in the analysis after 15 May. * = 95% confidence level (p<=0.05), ** = 98% confidence level (p<=0.02), *** = 99% confidence level (p<=0.01), NS = not significant.

	CH_3I	**C_2H_5I**	**CH_2I_2**	**CH_2ClI**
CH_3I High CO_2	-	-	-	-
CH_3I Present CO_2	-	-	-	-
C_2H_5I High CO_2	0.821***	-	-	-
C_2H_5I Present CO_2	0.914***	-	-	-
CH_2I_2 High CO_2	0.650**	0.632**	-	-
CH_2I_2 Present CO_2	0.686***	0.618**	-	-
CH_2ClI High CO_2	0.529*	0.514*	NS	-
CH_2ClI Present CO_2	0.804***	0.900***	NS	-
Chlorophyll-a High CO_2	0.654**	0.522*	NS	NS
Chlorophyll-a Present CO_2	0.775***	0.555*	0.709***	NS
Coccolithophores High CO_2	NS	NS	0.532*	NS
Coccolithophores Present CO_2	NS	NS	NS	NS
Small picoeukaryotes High CO_2	NS	NS	NS	-0.629**
Small picoeukaryotes Present CO_2	0.521*	NS	0.557*	NS
Large picoeukaryotes High CO_2	NS	NS	NS	NS
Large picoeukaryotes Present CO_2	NS	NS	0.807***	NS
Nanophytoplankton High CO_2	0.543*	NS	0.618**	NS
Nanophytoplankton Present CO_2	NS	NS	0.632**	NS
Cryptophytes High CO_2	NS	0.532*	0.632**	NS
Cryptophytes Present CO_2	NS	NS	NS	NS
Synechococcus High CO_2	0.532*	0.614**	0.889***	NS
Synechococcus Present CO_2	0.596*	0.525*	NS	NS

Appendix 7. Spearman's Rank Correlation Coefficients (ρ) and associated significance level for mean $CHBr_3$, CH_2Br_2, $CHBr_2Cl$, chlorophyll-a and phytoplankton community components under high CO_2 (M1, M2, M3) and present-day CO_2 (M4, M5, M6). M3 and M4 only are included in the analysis after 15 May. * = 95% confidence level (p<=0.05), ** = 98% confidence level (p<=0.02), *** = 99% confidence level (p<=0.01), NS = not significant.

		$CHBr_3$	**CH_2Br_2**	**$CHBr_2Cl$**
CH_2Br_2	High CO_2	-0.301	-	-
CH_2Br_2	Present CO_2	-0.407	-	-
$CHBr_2Cl$	High CO_2	-0.275	0.802***	-
$CHBr_2Cl$	Present CO_2	0.200	0.653	-
Chlorophyll *a*	High CO_2	0.165	0.209	0.064
Chlorophyll *a*	Present CO_2	0.662**	0.108	0.099
Coccolithophores	High CO_2	0.512	-0.811***	-0.807***
Coccolithophores	Present CO_2	0.710**	-0.618*	-0.380
Small picoeukaryotes	High CO_2	0.341	-0.398	-0.653**
Small picoeukaryotes	Present CO_2	0.640*	-0.385	-0.169
Large picoeukaryotes	High CO_2	0.327	0.191	-0.134
Large picoeukaryotes	Present CO_2	0.921***	-0.5528	0.081
Nanophytoplankton	High CO_2	0.600*	-0.358	-0.587*
Nanophytoplankton	Present CO_2	0.842***	-0.662**	-0.226
Cryptophytes	High CO_2	0.640*	-0.415	-0.600*
Cryptophytes	Present CO_2	0.596*	-0.314	0.015
Synechococcus	High CO_2	0.771***	-0.552*	-0.451
Synechococcus	Present CO_2	0.218	0.191	0.064

Appendix 8. Spearman's Rank Correlation Coefficients (ρ) and associated significance level for mean DMS, DMSPt, chlorophyll *a* and phytoplankton community components under high CO_2 (M1, M2, M3) and present-day CO_2 (M4, M5, M6). M3 and M4 only are included in the analysis after 15 May. * = 95% confidence level (p<=0.05), ** = 98% confidence level (p<=0.02), *** = 99% confidence level (p<=0.01), NS = not significant.

		DMS	**DMSP*t***	**Chlorophyll a**
DMS	High CO_2	-	-	-
DMS	Present CO_2	-	-	-
DMSPt	High CO_2	0.624**	-	-
DMSPt	Present CO_2	NS	-	-
Chlorophyll *a*	High CO_2	0.521*	0.853***	-
Chlorophyll *a*	Present CO_2	NS	0.750***	-
Coccolithophores	High CO_2	NS	NS	NS
Coccolithophores	Present CO_2	NS	NS	0.753***
Small picoeukaryotes	High CO_2	-0.635**	NS	NS
Small picoeukaryotes	Present CO_2	NS	0.700***	0.847***
Large picoeukaryotes	High CO_2	NS	0.535*	0.574*
Large picoeukaryotes	Present CO_2	NS	0.526*	0.679**
Nanophytoplankton	High CO_2	-0.550*	NS	NS
Nanophytoplankton	Present CO_2	NS	NS	0.562*
Cryptophytes	High CO_2	NS	NS	0.876***
Cryptophytes	Present CO_2	NS	0.862***	NS
Synechococcus	High CO_2	NS	NS	NS
Synechococcus	Present CO_2	0.712***	0.729***	0.779***

Appendix 9. Spearman's Rank Correlation Coefficients (ρ) and associated significance level for mean iodocarbon concentrations and a. Total phytoplankton biomass (this page), and b. Flagellate biomass (next page) under high CO_2 (M1) and present-day CO_2 (M6). * = 95% confidence level (p<=0.05), ** = 98% confidence level (p<=0.02), *** = 99% confidence level (p<=0.01), NS = not significant.

a. TOTAL BIOMASS

Mesocosm 1: 9,11-15,18,21 May	CH_3I	C_2H_5I	CH_2I_2	CH_2ClI
C_2H_5I	0.762*			
CH_2I_2	NS	0.762*		
CH_2ClI	NS	0.857**	NS	
Flagellates	0.881***	0.762*	0.881***	NS
Diatoms	NS	NS	NS	NS
Autotrophic dinoflagellates	NS	NS	NS	NS
Heterotrophic dinoflagellates	NS	NS	NS	NS
Ciliates	NS	NS	NS	NS
Mesocosm 6: 9,11-15,18,21 May	CH_3I	C_2H_5I	CH_2I_2	CH_2ClI
C_2H_5I	0.929***			
CH_2I_2	NS	0.810		
CH_2ClI	NS	NS	NS	
Flagellates	0.881***	0.976***	0.833**	NS
Diatoms	NS	NS	NS	NS
Autotrophic dinoflagellates	0.738*	0.833**	NS	NS
Heterotrophic dinoflagellates	NS	NS	NS	NS
Ciliates	NS	NS	NS	NS

b. FLAGELLATE BIOMASS

Mesocosm 1: 9,11-15,18,21 May	CH_3I	C_2H_5I	CH_2I_2	CH_2ClI
Undetermined flagellates 2µm	NS	NS	NS	NS
Prymnesiophytes 3 - 4 µm	NS	NS	NS	NS
Prymnesiophytes 5 µm	NS	NS	NS	NS
Prasinophytes 5 µm	NS	NS	NS	NS
Undetermined flagellate 10 µm	NS	NS	NS	NS
Cryptophytes	NS	NS	NS	NS
Euglenophytes	NS	NS	NS	NS
Undetermined flagellate 12 µm	NS	0.833**	0.905***	NS

Mesocosm 6: 9,11-15,18,21 May	CH_3I	C_2H_5I	CH_2I_2	CH_2ClI
Undetermined flagellates 2µm	NS	NS	NS	NS
Prymnesiophytes 3 - 4 µm	NS	NS	NS	-0.786*
Prymnesiophytes 5 µm	NS	NS	NS	-0.786*
Prasinophytes 5 µm	NS	NS	NS	NS
Undetermined flagellate 10 µm	0.786*	0.905***	0.762*	NS
Cryptophytes	NS	NS	NS	NS
Euglenophytes	NS	NS	NS	NS
Undetermined flagellate 12 µm	NS	0.810*	0.738*	NS

Appendix 10. Spearman's Rank Correlation Coefficients (ρ) and associated significance level for mean bromocarbon concentrations and a. Total phytoplankton biomass (this page), and b. Flagellate biomass (next page) under high CO_2 (M1) and present-day CO_2 (M6). * = 95% confidence level (p<=0.05), ** = 98% confidence level (p<=0.02), *** = 99% confidence level (p<=0.01), NS = not significant

a. TOTAL BIOMASS

Mesocosm 1: 9,11-15,18,21 May	$CHBr_3$	CH_2Br_2	$CHBr_2Cl$
CH_2Br_2	NS		
$CHBr_2Cl$	NS	NS	
Flagellates	NS	NS	NS
Diatoms	NS	NS	NS
Autotrophic dinoflagellates	NS	NS	NS
Heterotrophic dinoflagellates	NS	NS	NS
Ciliates	NS	NS	NS
Mesocosm 6: 9,11-15,18,21 May	$CHBr_3$	CH_2Br_2	$CHBr_2Cl$
CH_2Br_2	NS		
$CHBr_2Cl$	NS	NS	
Flagellates	NS	NS	NS
Diatoms	NS	NS	NS
Autotrophic dinoflagellates	NS	NS	NS
Heterotrophic dinoflagellates	NS	NS	NS
Ciliates	NS	NS	NS

b. FLAGELLATES

Mesocosm 1: 9,11-15,18,21 May	$CHBr_3$	CH_2Br_2	$CHBr_2Cl$
Undetermined flagellates 2µm	-0.762*	NS	NS
Prymnesiophytes 3 - 4 µm	NS	NS	NS
Prymnesiophytes 5 µm	NS	NS	NS
Prasinophytes 5 µm	NS	NS	-0.874**
Undetermined flagellates 10 µm	0.762*	NS	NS
Cryptophytes	NS	NS	NS
Euglenophytes	NS	NS	NS
Undetermined flagellates 12 µm	NS	NS	NS
Mesocosm 6: 9,11-15,18,21 May	$CHBr_3$	CH_2Br_2	$CHBr_2Cl$
Undetermined flagellates 2µm	NS	NS	NS
Prymnesiophytes 3 - 4 µm	NS	NS	NS
Prymnesiophytes 5 µm	NS	NS	NS
Prasinophytes 5 µm	NS	-0.833**	NS
Undetermined flagellates 10 µm	NS	NS -0.143	NS
Cryptophytes	NS	0.857**	NS
Euglenophytes	-0.833**	NS	NS
Undetermined flagellates 12 µm	NS	NS	NS

Appendix 11. Reproducibility between triplicate mesocosms calculated as Coefficient of Variations (CoV = (stdev/mean) x 100), High CO_2 = M1, M2, M3, Present day CO_2 = M4, M5, M6.

	High CO_2: Coefficient of Variation (%)	**Present day CO_2: Coefficient of Variation (%)**
CH_3I	18	12
C_2H_5I	33	32
CH_2I_2	15	23
CH_2ClI	7	7
$CHBr_3$	11	10
CH_2Br_2	37	14
$CHBr_2Cl$	8	11
DMS	17	15
DMSPt	22	28
Chlorophyll *a*	38	28

Appendix 12. Analytical error calculated as Coefficient of Variation between triplicate samples taken from M1 (High CO_2) and M6 (Present day CO_2) on alternate days during the mesocosm experiment.

	High CO_2 Analytical Error (% CoV M1)	Mean analytical error (% CoV)	Present day CO_2 Analytical Error (% CoV M6)	Mean analytical error (% CoV)
CH_3I	6 - 42	17.7	1 - 41	10.4
C_2H_5I	4 - 32	18.5	5 - 31	9.9
CH_2I_2	2 - 67	19.1	5 - 17	11.2
CH_2ClI	2 - 30	11.3	5 - 10	6.9
$CHBr_3$	2 - 13	7.9	2 - 10	5.1
CH_2Br_2	6 - 26	16.4	3 - 14	7.6
$CHBr_2Cl$	4 - 20	8.2	2 - 14	8.0
DMS	2 - 11	6.7	2 - 15	6.5
DMSPt	7 - 27	17.8	4 - 37	21.7

Appendix 13. Summary of the statistical analyses for pH, chlorophyll-a, phytoplankton community, and trace gases for L4 incubation Experiment 1. Shaded in grey = differences considered significant at a threshold of $p<0.05$, $^{+}$ = T-test performed assuming equal variances, $^{\$}$ = T-test performed NOT assuming equal variances considered significant at a threshold of $p<0.05$
* mg m^{-3}, § = cell ml^{-1}, ¤ = pM.

Parameter	Mean		SD		Normality (Anderson-Darling) p>0.05 = normal distribution		Data Transformation	Test of Equal Variances (Levene's statistic) p>0.05 = equal variances	2-Sample T-test p<0.05 = significant difference between means	Mann-Whitney nonparametric test W p<0.05 = significant difference between means
	High CO_2	Present day CO_2	High CO_2	Present day CO_2	High CO_2	Present day CO_2				
pH	7.855	8.082	0.129	0.143	0.893, p = 0.021	1.061, p = 0.008	None	0.34, p = 0.562		W = 2582.5, p<0.001
Chlorophyll *a**	21.53	20.50	13.11	13.93	0.250, p = 0.730	0.278, p = 0.636	Log	0.31, p = 0.580	T = -0.68, DF = 94, p = 0.496^{+}	
Nano-Phytoplankton§	8897	8243	3566	4748	0.311, p = 0.541	0.553, p = 0.147	Log	4.01, p = 0.048	T = 1.50, DF = 89, p = 0.136$^{\$}$	
Pico-Eukaryotes§	46675	31480	29242	20773	0.491, p = 0.210	0.450, p = 0.265	Log	0.00, p = 0.988	T = 3.53, DF = 98, p = 0.001^{+}	
Pico-eukaryotes§ Day 10-16	58778	32367	33971	26952	0.507, p = 0.185	2.517, p<0.005	None	2.43, p = 0.125		W = 1005.0, p = 0.0007
Synechococcus§	11668	14334	13340	21958	0.422, p = 0.310	0.221, p = 0.822	Log	0.03, p = 0.869	T = -0.37, DF = 98, p = 0.711^{+}	
CH_3I ¤	3.654	4.192	0.718	0.972	0.343, p = 0.477	0.242, p = 0.757	None	3.66, p = 0.059	T = -3.06, DF = 92, p = 0.003^{+}	
C_2H_5I¤	0.5656	0.6192	0.3453	0.3784	3.699, p<0.005	2.877, p<0.005	None	0.35, p = 0.557		W = 2187, p = 0.4842

CH_2I_2/2-IP(D)	0.2047	0.2103	0.065	0.060	0.345, p = 0.472	0.217, p = 0.833	Log	0.02, p = 0.887	T = -0.53, DF = 92, p = 0.595[+]	
CH_2ClI¤	80.73	94.45	25.66	16.77	0.378, p = 0.393	0.345, p = 0.471	Log	0.53, p = 0.469	T = -1.84, DF = 92, p = 0.069[+]	
2-C_3H_7I¤	0.3677	0.3708	0.0748	0.0817	0.203, p = 0.869	0.624, p = 0.098	None	2.00, p = 0.161	T = -0.19, DF = 92, p = 0.848[+]	
2-C_3H_7I ¤ Days 3 - 10	0.3339	0.3783	0.0628	0.0804	0.551, p = 0.142	0.476, p = 0.221	None	1.65, p = 0.205	T = -2.30, DF = 54, p = 0.025[+]	
$CHBr_3$¤	2.583	3.732	2.429	5.781	2.183, p<0.005	6.167, p<0.005	None	1.97, p = 0.164		W = 1910, p = 0.3345
CH_2Br_2¤	11.231	7.082	3.153	2.537	1.337, p<0.005	1.404, p<0.005	None	3.09, p = 0.082		W = 3035, p<0.001
CH_2BrCl¤	3.829	4.280	1.278	1.803	0.371, p = 0.409	0.382, p = 0.366	None	4.64, p = 0.034	T = -1.39, DF = 80, p = 0.167[$]	

Appendix 14. Summary of the statistical analyses for phytoplankton biomass data for L4 incubation Experiment 1. Differences between treatments on day 3, day 16, and as a total of both days. Shaded in grey = differences considered significant at a threshold of $p<0.05$, $^{+}$ = T-test performed assuming equal variances, $^{\$}$ = T-test performed NOT assuming equal variances considered significant at a threshold of $p<0.05$. ¥ = µg l^{-1} Auto. Dinos. = Autotrophic dinoflagellates, Hetero. Dinos. = Heterotrophic dinoflagellates.

Parameter	**Mean**		**SD**		**Normality** (Anderson-Darling) p>0.05 = normal distribution	**Data Transformation**	**Test of Equal Variances** (Levene's statistic) p>0.05 = equal variances	**2-Sample T-test** p<0.05 = significant difference between means
	High CO_2	**Present day CO_2**	**High CO_2**	**Present day CO_2**				
Diatoms¥ All data	5.36	2.87	2.44	3.08	0.505 p = 0.170	None	0.15 p = 0.708	T = -1.74, DF = 13, p = 0.105^{+}
Diatoms¥ Day 3	6.89	0.63	2.40	0.45	0.400 p = 0.260	None	71.94, p<0.001	T = -5.09, DF = 5, p = 0.015$^{\$}$
Diatoms¥ Day 16	3.83	4.56	1.37	3.17	0.513 p = 0.132	None	0.43 p = 0.537	T = 0.42, DF = 6, p = 0.687^{+}
Auto. Dinos.¥ All data	4.48	3.63	3.17	1.20	0.662 p = 0.067	None	2.30 p = 0.153	T = -0.67, DF = 13, p = 0.513^{+}
Auto. Dinos.¥ Day 3	5.53	3.45	3.38	1.49	0.268 p = 0.559	Log	0.09 p = 0.773	T = -1.08, DF = 5, p = 0.330^{+}
Auto. Dinos.¥ Day 16	3.44	3.76	3.03	1.16	0.286 p = 0.527	None	2.28 p = 0.182	T = 0.20, DF = 6, p = 0.849^{+}
Flagellates¥ All data	7.97	8.90	3.04	2.22	0.127 p = 0.980	None	1.65 p = 0.221	T = 0.67, DF = 13, p = 0.517^{+}
Flagellates¥ Day 3	10.45	9.34	1.77	0.42	0.251 p = 0.615	None	3.91 p = 0.105	T = -1.05, DF = 5, p = 0.343^{+}

Flagellates¥ Day 16	5.48	8.56	1.40	3.6	0.380 p = 0.311	None	0.97 p = 0.362	T = 1.83, DF = 6, p = 0.116+
Hetero. Dinos.¥ All data	84.90	85.10	33.50	54.40	0.462 p = 0.222	None	0.40 p = 0.537	T = 0.01, DF = 13, p = 0.993+
Hetero. Dinos.¥ Day 3	98.20	46.12	28.90	16.93	0.178 p = 0.871	None	0.37 p = 0.572	T = -2.75, DF = 5, p = 0.040+
Hetero. Dinos.¥ Day 16	71.50	114.30	36.20	55.50	0.423 p = 0.237	None	1.24 p = 0.307	T = 1.29, DF = 6, p = 0.245+
Ciliates¥ All data	4.68	4.41	4.34	5.23	0.715 p = 0.050	Square Root	0.05 p = 0.825	T = -0.11, DF = 13, p = 0.916+
Ciliates¥ Day 3	1.07	0.59	0.65	0.29	0.648 p = 0.052	None	0.33 p = 0.593	T = -1.18, DF = 5, p = 0.290+
Ciliates¥ Day 16	8.29	7.28	2.97	5.40	0.381 p = 0.307	None	1.04 p = 0.347	T = -0.33, DF = 6, p = 0.755+
Total biomass¥ All data	107.4	91.8	34.5	63.9	0.206 p = 0.843	None	1.65 p = 0.220	T = -0.61, DF = 13, p = 0.554+
Total biomass¥ Day 3	122.2	45.1	27.7	32.9	0.132 p = 0.964	None	0.11 p = 0.754	T = -3.58, DF = 6, p = 0.012+
Total biomass¥ Day 16	92.6	138.4	37.9	51.5	0.364 p = 0.341	None	1.11 p = 0.333	T = 1.44, DF = 6, p = 0.201+

Appendix 15. Summary of the statistical analyses for trace gas: chlorophyll *a* ratios for L4 incubation Experiment 1. Shaded in grey = differences considered significant at a threshold of $p<0.05$, $^{+}$ = T-test performed assuming equal variances, $ = T-test performed NOT assuming equal variances considered significant at a threshold of $p<0.05$.

Parameter	**Mean**		**SD**		**Normality** (Anderson-Darling) $p>0.05$ = normal distribution		**Data Transformation**	**Test of Equal Variances** (Levene's statistic) $p>0.05$ = equal variances	**2-Sample T-test** $p<0.05$ = significant difference between means
	High CO_2	**Present day CO_2**	**High CO_2**	**Present day CO_2**	**High CO_2**	**Present day CO_2**			
CH_3I: Chl *a*	0.237	0.295	0.152	0.192	0.347 p=0.465	0.424 p=0.306	Log	0.45 p=0.504	T = 1.55, DF = 92, p = 0.124
C_2H_5I: Chl *a*	0.035	0.042	0.028	0.039	0.306 p=0.553	0.263 p=0.685	Log	0.56 p=0.456	T = 0.88, DF = 92, p = 0.381
CH_2I_2/2-IP(D): Chl *a*	0.013	0.015	0.008	0.010	0.496 p=0.203	0.305 p=0.554	Log	0.18 p=0.674	T = 0.81, DF = 92, p = 0.418
CH_2ClI: Chl *a*	5.164	6.768	3.511	5.174	0.221 p=0.823	0.475 p=0.229	Log	1.01 p=0.318	T = 1.48, DF = 92, p = 0.142
2-C_3H_7I: Chl *a*	0.024	0.027	0.015	0.019	0.320 p=0.522	0.180 p=0.912	Log	0.02 p=0.886	T = 0.54, DF = 92, p = 0.590
$CHBr_3$: Chl *a*	0.156	0.238	0.163	0.375	0.505 p=0.193	0.148 p=0.962	Log	0.82 p=0.368	T = 1.16, DF = 85, p = 0.247
CH_2Br_2: Chl *a*	0.716	0.466	0.453	0.310	0.488 p=0.213	0.296 p=0.579	Log	0.19 p=0.663	T = -3.00, DF = 92, p = 0.003
CH_2BrCl: Chl *a*	0.250	0.310	0.179	0.251	0.169 p=0.930	0.463 p=0.246	Log	1.19 p=0.278	T = 0.95, DF = 92, p = 0.344

Appendix 16. Spearman's Rank Correlation Coefficients (ρ) and associated significance level for mean iodocarbons, bromocarbons, chlorophyll *a* and phytoplankton community components under high CO_2 (V1 V2, V3, V4) and present-day CO_2 (V5, V6, V7, V8) during Experiment 1. N = 48, critical value at 0.05 significance level = 0.286, shaded in grey = significant.

	CH_3I	**C_2H_5I**	**CH_2I_2**	**CH_2ClI**	**2-C_3H_7I**
C_2H_5I High CO_2	-0.160	-	-	-	-
C_2H_5I Present CO_2	0.180	-	-	-	-
CH_2I_2 High CO_2	0.400	-0.360	-	-	-
CH_2I_2 Present CO_2	0.098	-0.317	-	-	-
CH_2ClI High CO_2	0.544	-0.411	0.641	-	-
CH_2ClI Present CO_2	0.416	-0.165	0.559	-	-
2-C_3H_7I High CO_2	-0.339	0.364	-0.315	-0.211	-
2-C_3H_7I Present CO_2	0.279	0.386	0.141	0.361	-
$CHBr_3$ High CO_2	-0.089	0.450	-0.104	-0.064	0.098
$CHBr_3$ Present CO_2	0.050	0.344	-0.181	0.021	0.116
CH_2Br_2 High CO_2	0.287	-0.073	0.122	0.139	-0.146
CH_2Br_2 Present CO_2	0.606	-0.239	0.150	0.363	0.190
CH_2BrCl High CO_2	0.043	0.554	-0.487	-0.398	0.356
CH_2BrCl Present CO_2	0.042	0.391	-0.351	-0.457	0.118
Chlorophyll *a* High CO_2	0.121	0.058	0.367	0.139	-0.159
Chlorophyll *a* Present CO_2	0.220	0.028	0.303	0.149	0.106
Nanophytoplankton High CO_2	-0.374	0.663	-0.483	-0.533	0.290
Nanophytoplankton Present CO_2	0.239	0.204	-0.284	-0.239	0.002
Picoeukaryotes High CO_2	-0.504	0.664	-0.475	-0.538	0.306
Picoeukaryotes Present CO_2	-0.143	0.478	0.040	0.029	0.036
Synechococcus High CO_2	-0.043	0.595	-0.294	-0.189	0.115
Synechococcus Present CO_2	-0.298	0.408	-0.093	-0.273	-0.071

Appendix 17. Spearman's Rank Correlation Coefficients (ρ) and associated significance level for mean bromocarbons, chlorophyll *a* and phytoplankton community components under high CO_2 (V1 V2, V3, V4) and present-day CO_2 (V5, V6, V7, V8) During Experiment 1. N = 48, critical value at 0.05 significance level = 0.286, shade in grey = significant

		$CHBr_3$	**CH_2Br_2**	**CH_2BrCl**
CH_2Br_2	High CO_2	-0.067		
CH_2Br_2	Present CO_2	0.146		
CH_2BrCl	High CO_2	0.305	-0.030	
CH_2BrCl	Present CO_2	0.362	0.031	
CH_3I	High CO_2	-0.089	0.2878	0.043
CH_3I	Present CO_2	0.050	0.606	0.042
C_2H_5I	High CO_2	0.450	-0.073	0.554
C_2H_5I	Present CO_2	0.344	-0.239	0.391
CH_2I_2	High CO_2	-0.104	0.122	-0.487
CH_2I_2	Present CO_2	-0.181	0.150	-0.351
CH_2ClI	High CO_2	-0.064	0.139	-0.398
CH_2ClI	Present CO_2	0.021	0.363	-0.457
2-C_3H_7I	High CO_2	0.098	-0.146	0.356
2-C_3H_7I	Present CO_2	0.116	0.190	0.118
Chlorophyll *a*	High CO_2	0.119	0.142	-0.020
Chlorophyll *a*	Present CO_2	0.012	0.249	-0.021
Nanophytoplankton	High CO_2	0.441	-0.087	0.484
Nanophytoplankton	Present CO_2	0.012	0.142	0.271
Picoeukaryotes	High CO_2	0.461	-0.159	0.393
Picoeukaryotes	Present CO_2	0.442	-0.258	0.101
Synechococcus	High CO_2	0.381	-0.173	0.455
Synechococcus	Present CO_2	0.298	-0.248	0.197

Appendix 18. Spearman's Rank Correlation Coefficients (ρ) and associated significance level for chlorophyll-a and phytoplankton community components under high CO_2 (V1 V2, V3, V4) and present-day CO_2 (V5, V6, V7, V8) during Experiment 1. N = 48, critical value at 0.05 significance level = 0.286, shaded in grey = significant.

	Nanophytoplankton	**Picoeukaryotes**	**Synechococcus**
Chlorophyll *a* High CO_2	0.221	0.233	0.077
Chlorophyll *a* Present CO_2	0.472	0.319	0.239

Appendix 19. Spearman's Rank Correlations – Individual Incubation Vessels (V1 – V4 High CO_2, V5 – V8 Present day CO_2) Experiment 1. N = 12, Shaded in grey = significant, * = 95% confidence level (Crit. Value = 0.591, p<=0.05), ** = 98% confidence level (Crit. Value = 0.712, p<=0.02), *** = 99% confidence level (Crit. Value = 0.777, p<=0.01). § Nano. = Nanophytoplankton, Pico. = Picoeukaryotes, Synecho. = Synechococcus

Vessel 1: High CO_2

	Chl *a*	CH_3I	C_2H_5I	CH_2I_2	CH_2ClI	2-C_3H_7I	$CHBr_3$	CH_2Br_2	CH_2BrCl	Nano.§	Pico.§
CH_3I	0.189	-	-	-	-	-	-	-	-	-	-
C_2H_5I	-0.182	-0.364	-	-	-	-	-	-	-	-	-
CH_2I_2	0.266	0.601*	-0.196	-	-	-	-	-	-	-	-
CH_2ClI	-0.406	0.378	-0.287	0.462	-	-	-	-	-	-	-
2-C_3H_7I	-0.336	-0.713**	0.566	-0.483	-0.399	-	-	-	-	-	-
$CHBr_3$	-0.203	-0.133	0.371	0.049	0.091	0.070	-	-	-	-	-
CH_2Br_2	0.259	0.252	-0.112	0.231	0.378	-0.161	-0.021	-	-	-	-
CH_2BrCl	0.245	-0.147	0.280	-0.455	-0.608*	0.273	0.357	-0.210	-	-	-
Nano.§	-0.008	-0.059	0.580	-0.373	-0.563	0.310	0.182	-0.040	0.655*	-	-
Pico.§	0.048	-0.394	0.654*	-0.590	-0.611*	0.502	0.091	-0.064	0.745**	0.827***	-
Synecho.§	0.016	-0.553	0.670*	-0.650*	-0.603*	0.553	0.064	-0.200	0.682*	0.718**	0.955***

Vessel 2: High CO_2

	Chl *a*	CH_3I	C_2H_5I	CH_2I_2	CH_2ClI	2-C_3H_7I	$CHBr_3$	CH_2Br_2	CH_2BrCl	Nano.§	Pico.§
CH_3I	0.566	-	-	-	-	-	-	-	-	-	-
C_2H_5I	-0.266	-0.273	-	-	-	-	-	-	-	-	-
CH_2I_2	0.350	0.371	-0.434	-	-	-	-	-	-	-	-
CH_2ClI	0.336	0.420	-0.664*	0.804***	-	-	-	-	-	-	-
2-C_3H_7I	-0.406	-0.252	0.448	-0.175	-0.413	-	-	-	-	-	-
$CHBr_3$	-0.308	-0.315	0.399	-0.182	-0.441	-0.105	-	-	-	-	-
CH_2Br_2	0.385	0.699*	-0.049	-0.042	0.084	0.112	-0.399	-	-	-	-
CH_2BrCl	-0.427	-0.091	0.636	-0.671	-0.797	0.615	0.126	0.196	-	-	-
Nano.§	-0.193	-0.343	0.791***	-0.621*	-0.941***	0.431	0.494	-0.176	0.776	-	-
Pico.§	-0.117	-0.425	0.845***	-0.531	-0.869***	0.263	0.645*	-0.301	0.605	0.937***	-
Synecho.§	-0.276	-0.523	0.818***	-0.580	-0.901***	0.367	0.486	-0.360	0.662	0.927***	0.927***

Vessel 3: High CO_2

	Chl *a*	CH_3I	C_2H_5I	CH_2I_2	CH_2ClI	2-C_3H_7I	$CHBr_3$	CH_2Br_2	CH_2BrCl	Nano.§	Pico.§
CH_3I	0.301	-	-	-	-	-	-	-	-	-	-
C_2H_5I	0.018	0.007	-	-	-	-	-	-	-	-	-
CH_2I_2	0.322	0.399	-0.643*	-	-	-	-	-	-	-	-
CH_2ClI	0.235	0.154	-0.818***	0.839***	-	-	-	-	-	-	-
2-C_3H_7I	-0.312	-0.392	0.301	-0.301	-0.287	-	-	-	-	-	-
$CHBr_3$	0.375	-0.112	0.413	-0.154	-0.070	0.021	-	-	-	-	-
CH_2Br_2	-0.088	0.503	0.301	-0.231	-0.280	-0.350	0.014	-	-	-	-
CH_2BrCl	-0.165	-0.224	0.497	-0.748	-0.608	0.161	-0.007	0.510	-	-	-
Nano.§	0.476	-0.210	0.671*	-0.559	-0.524	0.168	0.685*	-0.091	0.301	-	-
Pico.§	0.459	-0.315	0.497	-0.245	-0.245	0.210	0.727**	-0.385	-0.119	0.853***	-
Synecho.§	0.725**	0.035	0.392	0.056	-0.056	-0.336	0.678*	-0.098	-0.019	0.692*	0.755**

Vessel 4: High CO_2

	Chl *a*	CH_3I	C_2H_5I	CH_2I_2	CH_2ClI	2-C_3H_7I	$CHBr_3$	CH_2Br_2	CH_2BrCl	Nano.§	Pico.§
CH_3I	0.000	-	-	-	-	-	-	-	-	-	-
C_2H_5I	0.594	-0.273	-	-	-	-	-	-	-	-	-
CH_2I_2	0.524	0.469	-0.189	-	-	-	-	-	-	-	-
CH_2ClI	0.238	0.517	-0.364	0.643*	-	-	-	-	-	-	-
2-C_3H_7I	0.392	-0.399	0.231	-0.014	0.210	-	-	-	-	-	-
$CHBr_3$	0.469	0.084	0.615*	-0.189	-0.091	0.483	-	-	-	-	-
CH_2Br_2	-0.035	0.769**	-0.266	0.189	0.517	-0.266	0.042	-	-	-	-
CH_2BrCl	0.280	-0.098	0.629*	-0.175	-0.455	0.259	0.650*	-0.175	-	-	-
Nano.§	0.587	-0.350	0.776**	-0.245	-0.210	0.629*	0.692*	-0.133	0.601*	-	-
Pico.§	0.266	-0.517	0.671*	-0.490	-0.727	0.273	0.455	-0.336	0.559	0.748	-
Synecho.§	0.287	-0.350	0.580	-0.378	-0.657	0.168	0.455	-0.273	0.420	0.678	0.923

Vessel 5: Present day CO_2

	Chl *a*	CH_3I	C_2H_5I	CH_2I_2	CH_2ClI	2-C_3H_7I	$CHBr_3$	CH_2Br_2	CH_2BrCl	Nano.§	Pico.§
CH_3I	0.371	-	-	-	-	-	-	-	-	-	-
C_2H_5I	0.441	-0.097	-	-	-	-	-	-	-	-	-
CH_2I_2	0.469	0.455	-0.502	-	-	-	-	-	-	-	-
CH_2ClI	0.049	0.420	-0.694*	0.671*	-	-	-	-	-	-	-
2-C_3H_7I	0.322	-0.182	0.073	0.294	0.224	-	-	-	-	-	-
$CHBr_3$	0.028	0.559*	0.008	0.014	0.049	-0.392	-	-	-	-	-
CH_2Br_2	-0.301	0.301	-0.825***	0.455	0.608	-0.084	0.350	-	-	-	-
CH_2BrCl	0.266	-0.028	0.346	-0.119	-0.378	-0.343	0.545	-0.175	-	-	-
Nano.§	0.552*	-0.273	0.311	-0.014	-0.350	-0.224	-0.161	-0.406	0.378	-	-
Pico.§	0.119	0.070	0.236	-0.084	-0.552*	-0.692*	0.371	-0.056	0.594*	0.154	-
Synecho.§	-0.266	-0.259	0.555	-0.734**	-0.811***	-0.545	0.357	-0.308	0.462	0.035	0.671*

Vessel 6: Present day CO_2

	Chl *a*	CH_3I	C_2H_5I	CH_2I_2	CH_2ClI	2-C_3H_7I	$CHBr_3$	CH_2Br_2	CH_2BrCl	Nano.§	Pico.§
CH_3I	0.081	-	-	-	-	-	-	-	-	-	-
C_2H_5I	0.147	0.021	-	-	-	-	-	-	-	-	-
CH_2I_2	0.879***	0.126	-0.154	-	-	-	-	-	-	-	-
CH_2ClI	0.627*	0.147	-0.462	0.811***	-	-	-	-	-	-	-
2-C_3H_7I	0.133	-0.210	0.091	-0.112	-0.063	-	-	-	-	-	-
$CHBr_3$	-0.014	0.336	0.329	-0.231	-0.070	0.203	-	-	-	-	-
CH_2Br_2	0.098	0.587	0.042	-0.042	0.049	0.070	0.594*	-	-	-	-
CH_2BrCl	-0.357	0.252	0.350	-0.580	-0.524	0.231	0.406	0.329	-	-	-
Nano.§	0.637*	0.056	0.650*	0.413	0.070	-0.063	0.189	-0.007	0.014	-	-
Pico.§	0.729**	-0.217	0.503	0.587	0.273	-0.133	-0.077	-0.203	-0.280	0.888***	-
Synecho.§	0.039	-0.007	0.867***	-0.161	-0.322	-0.182	0.175	-0.140	0.329	0.636*	0.531

Vessel 7: Present day CO_2

	Chl *a*	CH_3I	C_2H_5I	CH_2I_2	CH_2ClI	2-C_3H_7I	$CHBr_3$	CH_2Br_2	CH_2BrCl	Nano.§	Pico.§
CH_3I	0.559	-	-	-	-	-	-	-	-	-	-
C_2H_5I	0.049	0.276	-	-	-	-	-	-	-	-	-
CH_2I_2	-0.104	0.100	-0.435	-	-	-	-	-	-	-	-
CH_2ClI	-0.343	0.036	0.059	0.673*	-	-	-	-	-	-	-
2-C_3H_7I	-0.383	0.000	0.368	-0.045	0.109	-	-	-	-	-	-
$CHBr_3$	-0.136	0.114	0.617*	-0.187	-0.046	0.246	-	-	-	-	-
CH_2Br_2	0.056	0.145	0.084	-0.136	-0.336	-0.473	0.460	-	-	-	-
CH_2BrCl	0.120	-0.000	0.511	-0.718**	-0.673*	0.064	0.296	0.418	-	-	-
Nano.§	0.128	0.158	0.655*	-0.575	-0.232	0.384	0.546	-0.204	0.464	-	-
Pico.§	0.016	0.168	0.918***	-0.080	0.304	0.280	0.628*	-0.206	0.103	0.555	-
Synecho.§	0.551	0.410	0.436	0.252	0.334	-0.357	0.344	0.008	-0.283	0.173	0.627*

Vessel 8: Present day CO_2

	Chl *a*	CH_3I	C_2H_5I	CH_2I_2	CH_2ClI	2-C_3H_7I	$CHBr_3$	CH_2Br_2	CH_2BrCl	Nano.§	Pico.§
CH_3I	0.173	-	-	-	-	-	-	-	-	-	-
C_2H_5I	-0.069	0.336	-	-	-	-	-	-	-	-	-
CH_2I_2	0.061	-0.600*	-0.427	-	-	-	-	-	-	-	-
CH_2ClI	-0.147	-0.545	-0.191	0.245	-	-	-	-	-	-	-
2-C_3H_7I	0.598*	-0.018	0.318	0.191	-0.045	-	-	-	-	-	-
$CHBr_3$	0.191	0.300	0.218	-0.209	0.473	0.345	-	-	-	-	-
CH_2Br_2	0.642*	0.491	-0.382	-0.064	-0.182	0.082	0.273	-	-	-	-
CH_2BrCl	0.182	0.527	0.055	-0.164	-0.718**	0.300	0.055	0.382	-	-	-
Nano.§	0.503	0.534	0.045	-0.494	-0.587	0.120	-0.237	0.554	0.477	-	-
Pico.§	0.215	-0.114	0.679*	0.094	0.275	0.763**	0.480	-0.393	-0.110	-0.127	-
Synecho.§	0.758**	-0.193	-0.047	0.393	0.198	0.414	0.090	0.365	-0.222	0.273	0.336

Appendix 20. Summary of the statistical analyses for pH, chlorophyll *a*, phytoplankton community, and trace gases for L4 incubation Experiment 2. Shaded in grey = differences considered significant at a threshold of $p<0.05$, $^{+}$ = T-test performed assuming equal variances, $^{\$}$ = T-test performed NOT assuming equal variances considered significant at a threshold of $p<0.05$. * mg m^{-3}, § = cell ml^{-1}, ¤ = pM.

Parameter	**Mean**		**SD**		**Normality** (Anderson-Darling) p>0.05 = normal distribution		**Data Transformation**	**Test of Equal Variances** (Levene's statistic) p>0.05 = equal variances	**2-Sample T-test** p<0.05 = significant difference between means	**Mann-Whitney nonparametric test W** p<0.05 = significant difference between means
	High CO_2	**Present day CO_2**	**High CO_2**	**Present day CO_2**	**High CO_2**	**Present day CO_2**				
pH	8.045	8.220	0.158	0.163	1.242, p<0.005	1.723, p<0.005	None	0.17, p = 0.681		W = 3014, p<0.001
Chlorophyll-a*	15.66	10.71	16.10	12.80	0.412, p=0.329	0.997, p=0.012	Log	0.80, p = 0.372		W = 3095, p = 0.0178
Nano-phytoplankton§	12924	13828	6787	8565	0.233, p = 0.722	0.309, p = 0.546	Log	2.52, p = 0.115	T = -0.20, DF = 102, p = 0.841^{+}	
Synechococcus§	29599	26921	45916	54529	6.292, p<0.005	9.375, p<0.005	None	0.05, p = 0.8.17		W = 2877, p = 0.3409
CH_3I¤	13.46	15.53	7.16	7.58	1.866, p<0.005	0.707, p = 0.061	None	0.42, p = 0.520		W = 2518, p = 0.1619
C_2H_5I¤	0.849	1.068	0.925	1.342	8.511, p<0.005	10.442, p<0.005	None	0.45, p = 0.502		W = 2542, p = 0.229
CH_2I_2¤	39.41	35.96	13.47	13.07	2.359, p<0.005	4.593, p<0.005	None	0.82, p = 0.367		W = 2378, p = 0.1337
CH_2ClI¤	46.77	44.98	28.62	41.7	0.664, p = 0.078	0.711, p = 0.060	Log	0.58, p = 0.449	T = 0.16, DF = 102, p = 0.876^{+}	
2-C_3H_7I¤	0.5804	0.5354	0.2611	0.1729	0.687, p = 0.069	0.562, p = 0.139	Log	9.32, p = 0.003	T = 0.39, DF = 92, p = 0.696$^{\$}$	

$CHBr_3$¤	7.181	7.122	2.856	2.267	0.494, p =	0.254, p = 0.718	Log	1.52, p = 0.221	T = -0.23, DF = 102, p = 0.822+	
CH_2Br_2¤	6.541	6.279	3.542	2.853	0.820, p = 0.032	0.357, p = 0.442	None	0.71, p = 0.401		W = 2731, p = 0.9974
CH_2BrCl¤	0.6555	0.7290	0.1999	0.2803	0.491, p = 0.211	1.542, p<0.005	None	2.54, p = 0.114		W = 2565, p = 0.2849

Appendix 21. Summary of the statistical analyses for phytoplankton biomass data for L4 incubation Experiment 2. Differences between treatments on day 3, day 16, and as a total of both days. Shaded in grey = differences considered significant at a threshold of p<0.05, + = T-test performed assuming equal variances, $ = T-test performed NOT assuming equal variances considered significant at a threshold of p<0.05. ¥ = µg l^{-1} Auto. Dinos. = Autotrophic dinoflagellates, Hetero. Dinos. = Heterotrophic dinoflagellates.

Parameter	**Mean**		**SD**		**Normality** (Anderson-Darling) p>0.05 = normal distribution	**Data Transformation**	**Test of Equal Variances** (Levene's statistic) p>0.05 = equal variances	**2-Sample T-test** p<0.05 = significant difference between means	**Mann-Whitney nonparametric test W** p<0.05 = significant difference between means
	High CO_2	**Present day CO_2**	**High CO_2**	**Present day CO_2**					
Diatoms¥ All data	4.79	0.995	9.87	0.973	0.573 p = 0.116	Log	1.10 p = 0.312	T = -0.92, DF = 14, p = 0.373+	
Diatoms¥ Day 4	0.37	0.25	9.20	1.74	0.645 p = 0.058	Log	30.13 p = 0.002	T = -0.89, DF = 3, p = 0.438$	
Diatoms¥ Day 17	9.20	1.74	13.24	0.85	1.921 p<0.005	None	1.43 p = 0.277		W = 24.0, p = 0.1124
Auto. Dinos.¥ All data	5.34	2.86	9.52	2.40	0.559 p = 0.124	Log	0.03 p = 0.859	T = -0.44, DF = 14, p = 0.670+	

Auto. Dinos.¥ Day 4	1.51	1.04	0.58	0.45	0.611 p = 0.072	None	0.04 p = 0.846	T = -1.27, DF = 6, p = 0.251⁺	
Auto. Dinos.¥ Day 17	9.17	4.68	13.11	2.10	0.364 p = 0.341	Log	1.72 p = 0.238	T = -0.02, DF = 6, p = 0.985⁺	
Flagellates All data¥	40.8	48.8	51.2	55.4	0.713 p = 0.050	Log	0.25 p = 0.626	T = 0.70, DF = 14, p = 0.479⁺	
Flagellates Day 4¥	20.59	25.08	5.63	4.12	0.298 p = 0.824	None	0.19 p = 0.678	T = 1.29, DF = 6, p = 0.246⁺	
Flagellates Day 17¥	61.10	72.50	70.60	75.20	0.274 p = 0.557	Log	0.93 p = 0.373	T = 0.45, DF = 6, p = 0.667⁺	
Hetero. Dinos.¥ All data	2.21	2.56	1.03	1.60	0.278 p = 0.602	None	0.84 p = 0.376	T = 0.52, DF = 14, p = 0.609⁺	
Hetero. Dinos.¥ Day 4	2.72	2.67	0.73	1.11	0.342 p = 0.392	None	1.71 p = 0.239	T = -0.08.DF = 6, p = 0.939⁺	
Hetero. Dinos.¥ Day 17	1.69	2.45	1.12	2.17	0.453 p = 0.196	None	0.88 p = 0.384	T = 0.62, DF = 6, p = 0.557⁺	
Ciliates¥ All data	3.01	2.52	2.81	1.87	0.831 p = 0.025	None	0.07 p = 0.798		W = 71.0 p = 0.7929
Ciliates¥ Day 4	4.19	3.48	3.11	1.35	0.361 p = 0.349	None	1.45 p = 0.274	T = -0.42, DF = 6, p = 0.688⁺	
Ciliates¥ Day 17	1.83	1.57	2.23	1.98	0.787 p = 0.023	Log	0.04 p = 0.857		W = 20.0 p = 0.6650
Total biomass¥ All data	56.2	57.7	49.9	55.3	2.273 p<0.005	None	0.01 p = 0.914		W = 62.0 p = 0.5635
Total biomass¥ Day 4	29.30	32.51	2.47	2.81	0.322 p = 0.439	None	0.02 p = 0.891	T = 1.67, DF = 6, p = 0.145⁺	
Total biomass¥ Day 16	83.0	82.90	62.4	73.7	0.517 p = 0.129	None	0.13 p = 0.731	T = -0.01, DF = 6, p = 0.999⁺	

Appendix 22. Summary of the statistical analyses for trace gas: chlorophyll *a* ratios for L4 incubation Experiment 2. Shaded in grey = differences considered significant at a threshold of $p<0.05$, $^{+}$ = T-test performed assuming equal variances, $^{\$}$ = T-test performed NOT assuming equal variances considered significant at a threshold of $p<0.05$

Parameter	Mean		SD		Normality (Anderson-Darling) p>0.05 = normal distribution		Data Transformation	Test of Equal Variances (Levene's statistic) p>0.05 = equal variances	2-Sample T-test p<0.05 = significant difference between means	Mann-Whitney nonparametric test W p<0.05 = significant difference between means
	High CO_2	Present day CO_2	High CO_2	Present day CO_2	High CO_2	Present day CO_2				
CH_3I:Chl *a*	2.475	5.012	3.154	5.544	0.730 p=0.053	0.773 p=0.042	Log	1.13 p=0.290		2332 p=0.0098
C_2H_5I: Chl *a*	0.133	0.236	0.155	0.208	0.418 p=0.318	1.226 p<0.005	Log	0.01 p=0.909		2263 p=0.0024
CH_2I_2/2-IP(D): Chl *a*	8.29	13.53	11.00	13.74	0.187 p=0.899	0.691 p=0.066	Log	0.02 p=0.887	T = 2.21, DF = 90, p = 0.030	
CH_2ClI: Chl *a*	12.03	16.00	19.53	17.53	0.546 p=0.153	1.566 p<0.005	Log	0.13 p=0.724		2486 p=0.1134
2-C_3H_7I: Chl *a*	0.124	0.182	0.155	0.178	5.288 p<0.005	2.022 p<0.005	None	2.15 p=0.145		2472 p=0.0941
$CHBr_3$: Chl *a*	1.524	2.528	2.249	2.656	0.238 p=0.772	1.230 p<0.005	Log	0.85 p=0.359		2409 p=0.0372
CH_2Br_2: Chl *a*	1.428	2.484	2.128	2.751	0.380 p=0.392	1.799 p<0.005	Log	0.94 p=0.336		2451 p=0.0702
CH_2BrCl: Chl *a*	0.135	0.231	0.174	0.249	0.339 p=0.488	1.763 p<0.005	Log	1.18 p=0.280		2377 p=0.0219

Appendix 23. Spearman's Rank Correlation Coefficients (ρ) and associated significance level for mean iodocarbons, bromocarbons, chlorophyll *a* and phytoplankton community components under high CO_2 (V1 V2, V3, V4) and present-day CO_2 (V5, V6, V7, V8) during Experiment 2. N = 48, critical value at 0.05 significance level = 0.286, shaded in grey = significant.

		CH_3I	**C_2H_5I**	**CH_2I_2**	**CH_2ClI**	**2-C_3H_7I**
C_2H_5I	High CO_2	0.435	-	-	-	-
C_2H_5I	Present CO_2	0.561	-	-	-	-
CH_2I_2	High CO_2	0.084	0.213	-	-	-
CH_2I_2	Present CO_2	0.227	0.084	-	-	-
CH_2ClI	High CO_2	-0.014	0.243	0.518	-	-
CH_2ClI	Present CO_2	0.134	0.034	0.662	-	-
2-C_3H_7I	High CO_2	0.222	0.609	0.575	0.665	-
2-C_3H_7I	Present CO_2	0.512	0.521	0.462	0.489	-
$CHBr_3$	High CO_2	-0.192	0.176	0.645	0.576	0.478
$CHBr_3$	Present CO_2	0.041	0.098	0.702	0.747	0.444
CH_2Br_2	High CO_2	-0.212	0.063	0.661	0.604	0.514
CH_2Br_2	Present CO_2	-0.035	0.022	0.692	0.728	0.509
CH_2BrCl	High CO_2	-0.199	0.266	0.573	0.654	0.604
CH_2BrCl	Present CO_2	0.166	0.214	0.597	0.668	0.529
Chlorophyll *a*	High CO_2	0.099	-0.084	-0.402	-0.567	-0.418
Chlorophyll *a*	Present CO_2	-0.089	-0.006	-0.582	-0.417	-0.439
Nanophytoplankton	High CO_2	0.132	-0.005	-0.474	-0.600	-0.384
Nanophytoplankton	Present CO_2	-0.095	-0.101	-0.311	-0.206	-0.293
Synechococcus	High CO_2	-0.356	0.066	0.500	0.531	0.334
Synechococcus	Present CO_2	-0.250	-0.093	0.436	0.482	0.212

Appendix 24. Spearman's Rank Correlation Coefficients (ρ) and associated significance level for mean bromocarbons, chlorophyll *a* and phytoplankton community components under high CO_2 (V1 V2, V3, V4) and present-day CO_2 (V5, V6, V7, V8) during Experiment 2. N = 48, critical value at 0.05 significance level = 0.286, shaded in grey = significant.

		$CHBr_3$	**CH_2Br_2**	**CH_2BrCl**
CH_2Br_2	High CO_2	0.896	-	-
CH_2Br_2	Present CO_2	0.809	-	-
CH_2BrCl	High CO_2	0.767	0.833	-
CH_2BrCl	Present CO_2	0.659	0.759	-
CH_3I	High CO_2	-0.192	-0.212	-0.199
CH_3I	Present CO_2	0.041	-0.035	0.166
C_2H_5I	High CO_2	0.176	0.063	0.266
C_2H_5I	Present CO_2	0.098	0.022	0.214
CH_2I_2	High CO_2	0.645	0.661	0.573*
CH_2I_2	Present CO_2	0.702	0.692	0.597
CH_2ClI	High CO_2	0.576	0.604	0.654
CH_2ClI	Present CO_2	0.747	0.728	0.668
2-C_3H_7I	High CO_2	0.478	0.514	0.604
2-C_3H_7I	Present CO_2	0.444	0.509	0.529
Chlorophyll *a*	High CO_2	-0.374	-0.441	-0.432
Chlorophyll *a*	Present CO_2	-0.565	-0.737	-0.477
Nanophytoplankton	High CO_2	-0.507	-0.636	-0.536
Nanophytoplankton	Present CO_2	-0.326	-0.372	-0.136
Synechococcus	High CO_2	0.760	0.795	0.628
Synechococcus	Present CO_2	0.509	0.781	0.490

Appendix 25. Spearman's Rank Correlation Coefficients (ρ) and associated significance level for chlorophyll-a and phytoplankton community components under high CO_2 (V1 V2, V3, V4) and present-day CO_2 (V5, V6, V7, V8) during Experiment 2. N = 48, critical value at 0.05 significance level = 0.286, shaded in grey = significant.

		Nanophytoplankton	**Synechococcus**
Chlorophyll *a*	High CO_2	0.752	-0.502
Chlorophyll *a*	Present CO_2	0.615	-0.694

Appendix 26- Spearman's Rank Correlations – Individual Incubation Vessels (1 – 4 High CO_2, 5 – 8 Present day CO_2) Experiment 2. N = 12, Shaded in grey = significant, * = 95% confidence level (Crit. Value = 0.591, p<=0.05), ** = 98% confidence level (Crit. Value = 0.712, p<=0.02), *** = 99% confidence level (Crit. Value = 0.777, p<=0.01). § Nano. = Nanophytoplankton, Synecho. = Synechococcus.

Vessel 1: High CO_2

	Chl *a*	**CH_3I**	**C_2H_5I**	**CH_2I_2**	**CH_2ClI**	**2-C_3H_7I**	**$CHBr_3$**	**CH_2Br_2**	**CH_2BrCl**	**Nano.§**
CH_3I	0.429	-	-	-	-	-	-	-	-	-
C_2H_5I	-0.203	0.148	-	-	-	-	-	-	-	-
CH_2I_2	-0.510	-0.069	0.581	-	-	-	-	-	-	-
CH_2ClI	-0.407	-0.187	0.500	0.924***	-	-	-	-	-	-
2-C_3H_7I	-0.148	0.313	0.429	0.596*	0.473	-	-	-	-	-
$CHBr_3$	-0.511	-0.005	0.533	0.849***	0.868***	0.379	-	-	-	-
CH_2Br_2	-0.522	-0.055	0.423	0.914***	0.874***	0.522	0.923***	-	-	-
CH_2BrCl	-.527	-0.044	0.775**	0.824***	0.797***	0.467	0.885***	0.830***	-	-
Nano.§	0.676*	0.423	-0.352	-0.742**	-0.731**	-0.505	-0.742**	-0.764**	-0.698**	-
Synecho.§	-0.604*	-0.148	0.286	0.841***	0.868***	0.418	0.912***	0.929***	0.725	-0.824***

Vessel 2: High CO_2

	Chl *a*	**CH_3I**	**C_2H_5I**	**CH_2I_2**	**CH_2ClI**	**2-C_3H_7I**	**$CHBr_3$**	**CH_2Br_2**	**CH_2BrCl**	**Nano.§**
CH_3I	-0.124	-	-	-	-	-	-	-	-	-
C_2H_5I	-0.550	0.093	-	-	-	-	-	-	-	-
CH_2I_2	-0.612*	-0.161	0.427	-	-	-	-	-	-	-
CH_2ClI	-0.578	-0.286	0.330	0.704*	-	-	-	-	-	-
2-C_3H_7I	-0.696*	-0.170	0.566	0.749**	0.885***	-	-	-	-	-
$CHBr_3$	-0.470	-0.374	0.571	0.895***	0.566	0.676*	-	-	-	-
CH_2Br_2	-0.525	-0.341	0.495	0.912***	0.698*	0.797***	0.918***	-	-	-
CH_2BrCl	-0.641*	-0.319	0.604*	0.830***	0.654*	0.830***	0.819***	0.918***	-	-
Nano.§	0.713**	0.055	-0.374	-0.625*	-0.654*	-0.731**	-0.527	-0.618*	-0.753**	-
Synecho.§	-0.382	-0.681*	0.418	0.755**	0.769**	0.742**	0.736**	0.775**	0.797***	-0.440

Vessel 3: High CO_2

	Chl *a*	CH_3I	C_2H_5I	CH_2I_2	CH_2ClI	2-C_3H_7I	$CHBr_3$	CH_2Br_2	CH_2BrCl	Nano.§
CH_3I	-0.022	-	-	-	-	-	-	-	-	-
C_2H_5I	0.154	0.560	-	-	-	-	-	-	-	-
CH_2I_2	-0.385	0.582	0.225	-	-	-	-	-	-	-
CH_2ClI	-0.665*	0.308	0.033	0.516	-	-	-	-	-	-
2-C_3H_7I	-0.489	0.401	0.110	0.533	0.753**	-	-	-	-	-
$CHBr_3$	-0.363	-0.203	-0.203	0.440	0.297	0.418	-	-	-	-
CH_2Br_2	-0.615*	-0.082	-0.033	0.527	0.687*	0.676*	0.852***	-	-	-
CH_2BrCl	-0.412	-0.159	-0.011	0.302	0.643*	0.505	0.604*	0.824***	-	-
Nano.§	0.687*	-0.313	-0.253	-0.478	-0.742**	-0.599	-0.165	-0.500	-0.396	-
Synecho.§	-0.429	-0.302	0.143	0.352	0.386	0.357	0.753**	0.846***	0.665*	-0.291

Vessel 4: High CO_2

	Chl *a*	CH_3I	C_2H_5I	CH_2I_2	CH_2ClI	2-C_3H_7I	$CHBr_3$	CH_2Br_2	CH_2BrCl	Nano.§
CH_3I	0.099	-	-	-	-	-	-	-	-	-
C_2H_5I	-0.011	0.231	-	-	-	-	-	-	-	-
CH_2I_2	-0.484	-0.044	0.269	-	-	-	-	-	-	-
CH_2ClI	-0.264	-0.071	-0.159	0.319	-	-	-	-	-	-
2-C_3H_7I	-0.571	-0.148	0.280	0.533	0.786***	-	-	-	-	-
$CHBr_3$	-0.313	-0.242	0.357	0.610*	0.374	0.604*	-	-	-	-
CH_2Br_2	-0.593	-0.346	0.187	0.736**	0.593*	0.802***	0.819***	-	-	-
CH_2BrCl	-0.505	-0.352	0.275	0.555	0.560	0.736**	0.681*	0.885***	-	-
Nano.§	0.775**	0.176	-0.286	-0.813***	-0.352	-0.703*	-0.434	-0.681*	-0.555	-
Synecho.§	-0.374	-0.478	0.495	0.538	0.170	0.637*	0.703*	0.703*	0.582	-0.626*

Vessel 5: Present day CO_2

	Chl *a*	CH_3I	C_2H_5I	CH_2I_2	CH_2ClI	2-C_3H_7I	$CHBr_3$	CH_2Br_2	CH_2BrCl	Nano.§
CH_3I	0.231	-	-	-	-	-	-	-	-	-
C_2H_5I	0.412	0.604*	-	-	-	-	-	-	-	-
CH_2I_2	-0.478	0.220	-0.357	-	-	-	-	-	-	-
CH_2ClI	-0.379	0.055	-0.407	0.588	-	-	-	-	-	-
2-C_3H_7I	-0.478	0.363	0.341	0.302	0.495	-	-	-	-	-
$CHBr_3$	-0.330	0.011	-0.286	0.374	0.868***	0.544	-	-	-	-
CH_2Br_2	-0.742**	-0.033	-0.451	0.736**	0.852***	0.588	0.786***	-	-	-
CH_2BrCl	-0.286	0.253	-0.247	0.709*	0.731**	0.319	0.676*	0.670*	-	-
Nano.§	0.462	-0.181	-0.159	-0.110	0.088	-0.242	-0.077	-0.209	-0.005	-
Synecho.§	-0.907***	-0.093	-0.412	0.659*	0.637*	0.571	0.516	0.907***	0.500	-0.231

Vessel 6: Present day CO_2

	Chl *a*	CH_3I	C_2H_5I	CH_2I_2	CH_2ClI	2-C_3H_7I	$CHBr_3$	CH_2Br_2	CH_2BrCl	Nano.§
CH_3I	0.231	-	-	-	-	-	-	-	-	-
C_2H_5I	-0.368	0.445	-	-	-	-	-	-	-	-
CH_2I_2	-0.775**	-0.308	0.192	-	-	-	-	-	-	-
CH_2ClI	-0.418	-0.324	-0.049	0.418	-	-	-	-	-	-
2-C_3H_7I	-0.698*	-0.121	0.214	0.637*	0.555	-	-	-	-	-
$CHBr_3$	-0.764**	-0.462	0.253	0.725**	0.324	0.407	-	-	-	-
CH_2Br_2	-0.846***	-0.560	0.214	0.747**	0.615*	0.720**	0.802***	-	-	-
CH_2BrCl	-0.742**	-0.560	0.297	0.676*	0.560	0.566	0.775**	0.885***	-	-
Nano.§	0.473	0.418	-0.258	-0.467	-0.352	-0.418	-0.692*	-0.549	-0.725**	-
Synecho.§	-0.687*	-0.654*	0.044	0.615*	0.632*	0.582	0.665*	0.885***	0.819***	-0.456

Vessel 7: Present day CO_2

	Chl *a*	CH_3I	C_2H_5I	CH_2I_2	CH_2ClI	2-C_3H_7I	$CHBr_3$	CH_2Br_2	CH_2BrCl	Nano.§
CH_3I	-0.253	-	-	-	-	-	-	-	-	-
C_2H_5I	-0.033	0.764**	-	-	-	-	-	-	-	-
CH_2I_2	-0.615*	0.379	0.253	-	-	-	-	-	-	-
CH_2ClI	-0.747**	0.093	-0.038	0.736**	-	-	-	-	-	-
2-C_3H_7I	-0.692*	0.560	0.412	0.566	0.714**	-	-	-	-	-
$CHBr_3$	-0.615*	0.104	0.088	0.736**	0.912***	0.687*	-	-	-	-
CH_2Br_2	-0.714**	0.308	0.192	0.720**	0.907***	0.835***	0.863***	-	-	-
CH_2BrCl	-0.538	0.016	-0.033	0.495	0.813***	0.522	0.720**	0.791***	-	-
Nano.§	0.621*	-0.654*	-0.522	-0.742**	-0.478	-0.703*	-0.484	-0.516	-0.148	-
Synecho.§	-0.533	0.544	0.571	0.802***	0.538	0.604*	0.626*	0.621*	0.220	-0.835***

Vessel 8: Present day CO_2

	Chl *a*	CH_3I	C_2H_5I	CH_2I_2	CH_2ClI	2-C_3H_7I	$CHBr_3$	CH_2Br_2	CH_2BrCl	Nano.§
CH_3I	-0.632*	-	-	-	-	-	-	-	-	-
C_2H_5I	-0.209	0.665*	-	-	-	-	-	-	-	-
CH_2I_2	-0.659*	0.505	0.170	-	-	-	-	-	-	-
CH_2ClI	-0.253	0.462	0.104	0.731**	-	-	-	-	-	-
2-C_3H_7I	-0.473	0.753**	0.418	0.143	0.198	-	-	-	-	-
$CHBr_3$	-0.522	0.527	0.110	0.874***	0.841***	0.225	-	-	-	-
CH_2Br_2	-0.764**	0.407	-0.033	0.698*	0.615*	0.236	0.709*	-	-	-
CH_2BrCl	-0.516	0.313	-0.011	0.659*	0.643*	0.099	0.736**	0.841***	-	-
Nano.§	0.725**	-0.500	-0.253	-0.269	-0.165	-0.478	-0.176	-0.604	-0.258	-
Synecho.§	-0.390	-0.242	-0.363	0.352	0.110	-0.286	0.242	0.670*	0.599*	-0.302

Appendix 27. Summary of the statistical analyses for pH, chlorophyll *a* and phytoplankton data between individual vessels within the same treatment for L4 incubation Experiment 1. Underlined = differences considered significant at a threshold of $p<0.05$, $^{+}$ = T-test performed assuming equal variances, $^{\$}$ = T-test performed NOT assuming equal variances considered significant at a threshold of $p<0.05$**, *** mg m^{-3}, § = cell ml^{-1}.

Parameter	Mean	SD	Normality (Anderson-Darling) p>0.05 = normal distribution	Data Trans-formation	Test of Equal Variances (Levene's statistic) p>0.05 = equal variances	2-Sample T-test p<0.05 = significant difference between means	Mann-Whitney nonparametric test W p<0.05 = significant difference between means
pH High CO_2	**V1** 7.77 **V2** 7.86 **V3** 7.88 **V4** 7.90	**V1** 0.09 **V2** 0.14 **V3** 0.13 **V4** 0.12	**V1** 0.432, p = 0.267 **V2** 0.791, p = 0.031 **V3** 0.478, p = 0.203 **V4** 0.472, p = 0.210	None	0.92 p = 0.438	**V1 vs. V3** T= -2.64, DF=30, p = 0.013^{+} **V1 vs. V4** T= -3.44, DF=30, p = 0.002^{+} **V3 vs. V4** T= -0.57, DF=30, p = 0.572^{+}	**V1 vs. V2** W= 210.5, p = 0.0457 **V2 vs. V3** W= 254.0, p = 0.0720 **V2 vs. V4** W= 247.0, p = 0.5339
pH Present CO_2	**V5** 8.00 **V6** 8.07 **V7** 8.14 **V8** 8.12	**V5** 0.08 **V6** 0.11 **V7** 0.15 **V8** 0.18	**V5** 0.254, p = 0.684 **V6** 0.183, p = 0.894 **V7** 0.324, p = 0.494 **V8** 0.387, p = 0.347	None	4.46 p = 0.007	**V5 vs. V6** T= -1.97, DF=27, p = 0.059$^{\$}$ **V5 vs. V7** T= -3.16, DF=22, p = 0.005$^{\$}$ **V5 vs. V8** T= -2.40, DF=20, p = 0.026$^{\$}$ **V6 vs. V7** T= -1.46, DF=27, p = 0.156$^{\$}$ **V6 vs. V8** T= -0.97, DF=24, p = 0.342$^{\$}$ **V7 vs. V8** T= -0.29, DF=29, p = 0.771$^{\$}$	

Parameter	**Mean**	**SD**	**Normality** (Anderson-Darling) p>0.05 = normal distribution	**Data Trans-formation**	**Test of Equal Variances** (Levene's statistic) p>0.05 = equal variances	**2-Sample T-test** p<0.05 = significant difference between means	**Mann-Whitney nonparametric test W** p<0.05 = significant difference between means
Chlorophyll *a* * High CO_2	**V1** 22.49 **V2** 20.09 **V3** 18.02 **V4** 22.15	**V1** 8.06 **V2** 15.6 **V3** 13.3 **V4** 14.7	**V1** 0.290, p = 0.554 **V2** 0.606, p = 0.090 **V3** 0.574, p = 0.110 **V4** 0.620, p = 0.083	Square root	0.68 p = 0.571	**V1 vs. V2** T= 0.89, DF=24, p = 0.380+ **V1 vs. V3** T= 1.40, DF=24, p = 0.174 + **V1 vs. V4** T= 0.35, DF=24, p = 0.729+ **V2 vs. V3** T= 0.36, DF=24, p = 0.719+ **V2 vs. V4** T= -0.48, DF=24,p = 0.633+ **V3 vs. V4** T= -0.88, DF=24, p = 0.385+	
Chlorophyll *a Present CO_2**	**V5** 18.66 **V6** 16.40 **V7** 22.13 **V8** 21.78	**V5** 10.0 **V6** 14.0 **V7** 14.0 **V8** 16.8	**V5** 0.540, p = 0.132 **V6** 0.517, p = 0.153 **V7** 0.304, p = 0.522 **V8** 0.451, p = 0.230	Square root	0.57 p = 0.637	**V5 vs. V6** T= 0.82, DF=24, p = 0.422+ **V5 vs. V7** T= -0.62, DF=24, p = 0.539+ **V5 vs. V8** T= -0.36, DF=24, p = 0.723+ **V6 vs. V7** T= -1.26, DF=24, p = 0.218+ **V6 vs. V8** T= -1.00, DF=24, p = 0.329+ **V7 vs. V8** T= 0.19, DF=24, p = 0.854+	

Parameter	**Mean**	**SD**	**Normality** (Anderson-Darling) p>0.05 = normal distribution	**Data Trans-formation**	**Test of Equal Variances** (Levene's statistic) p>0.05 = equal variances	**2-Sample T-test** p<0.05 = significant difference between means	**Mann-Whitney nonparametric test W** p<0.05 = significant difference between means
Nano-phytoplankton§ High CO_2	**V1** 9767 **V2** 10043 **V3** 8055 **V4** 7878	**V1** 4672 **V2** 3366 **V3** 3028 **V4** 2896	**V1** 0.487, p = 0.181 **V2** 0.211, p = 0.814 **V3** 0.335, p = 0.452 **V4** 0.298, p = 0.534	None	1.41 p = 0.252	**V1 vs. V2** T= -0.17, DF=22, p = 0.870+ **V1 vs. V3** T= 1.10, DF=23, p = 0.284 + **V1 vs. V4** T= 1.23, DF=23, p = 0.232+ **V2 vs. V3** T= 1.55, DF=23, p = 0.134+ **V2 vs. V4** T= 1.73, DF=23, p = 0.097+ **V3 vs. V4** T= 0.15, DF=24, p = 0.880+	
Nano-phytoplankton§ Present CO_2	**V5** 8158 **V6** 6224 **V7** 8074 **V8** 10691	**V5** 7191 **V6** 2660 **V7** 2792 **V8** 4134	**V5** 0.395, p = 0.321 **V6** 0.460, p = 0.218 **V7** 1.010, p = 0.007 **V8** 1.202, p <0.005	Log	1.47 p = 0.234	**V5 vs. V6** T= 0.35, DF=24, p = 0.733+	**V5 vs. V7** W= 147.0, p = 0.242 **V5 vs. V8** W= 139.0, p = 0.109 **V6 vs. V7** W= 136.0, p = 0.077 **V6 vs. V8** W= 123.0, p = 0.013 **V7 vs. V8** W= 112.0, p = 0.030

Parameter	Mean	SD	**Normality** (Anderson-Darling) p>0.05 = normal distribution	**Data Trans-formation**	**Test of Equal Variances** (Levene's statistic) p>0.05 = equal variances	**2-Sample T-test** p<0.05 = significant difference between means	**Mann-Whitney nonparametric test W** p<0.05 = significant difference between means
Picoeukaryotes§ High CO_2	**V1** 58561 **V2** 48034 **V3** 32331 **V4** 48792	**V1** 41925 **V2** 24226 **V3** 17274 **V4** 25943	**V1** 0.585, p = 0.100 **V2** 0.339, p = 0.436 **V3** 0.273, p = 0.606 **V4** 0.345, p = 0.426	Log	0.49 p = 0.693	**V1 vs. V2** T= 0.41, DF=22, p = 0.688+ **V1 vs. V3** T= 2.18, DF=23, p = 0.040 + **V1 vs. V4** T= 0.42, DF=23, p = 0.675+ **V2 vs. V3** T= 2.12, DF=23, p = 0.045+ **V2 vs. V4** T= 0.03, DF=23, p = 0.977+ **V3 vs. V4** T= -2.04, DF=24, p = 0.053+	
Picoeukaryotes§ Present CO_2	**V5** 47232 **V6** 24476 **V7** 27689 **V8** 25793	**V5** 30529 **V6** 10284 **V7** 15004 **V8** 12758	**V5** 0.606, p = 0.091 **V6** 0.336, p = 0.449 **V7** 0.433, p = 0.252 **V8** 0.369, p = 0.368	Log	0.25 p = 0.860	**V5 vs. V6** T= 3.07, DF=24, p = 0.005+ **V5 vs. V7** T= 2.36, DF=23, p = 0.027+ **V5 vs. V8** T= 2.70, DF=23, p = 0.013+ **V6 vs. V7** T= -0.34, DF=23, p = 0.734+	

Parameter	**Mean**	**SD**	**Normality** (Anderson-Darling) p>0.05 = normal distribution	**Data Trans-formation**	**Test of Equal Variances** (Levene's statistic) p>0.05 = equal variances	**2-Sample T-test** p<0.05 = significant difference between means	**Mann-Whitney nonparametric test W** p<0.05 = significant difference between means
Synechococcus§ **High CO_2**	**V1** 2401 **V2** 15171 **V3** 9566 **V4** 19091	**V1** 1811 **V2** 15301 **V3** 9319 **V4** 16110	**V1** 0.586, p = 0.100 **V2** 0.300, p = 0.525 **V3** 0.256, p = 0.665 **V4** 0.575, p = 0.109	Log	0.22 p = 0.884	**V1 vs. V2** T= -3.56, DF=22, p = 0.002+ **V1 vs. V3** T= -3.06, DF=23, p = 0.006+ **V1 vs. V4** T= -4.04, DF=23, p = 0.001+ **V2 vs. V3** T= 0.72, DF=23, p = 0.478+	
Synechococcus§ **Present CO_2**	**V5** 32385 **V6** 10601 **V7** 5994 **V8** 7164	**V5** 35801 **V6** 8380 **V7** 7341 **V8** 9256	**V5** 0.228, p = 0.764 **V6** 0.809, p = 0.026 **V7** 0.267, p = 0.621 **V8** 0.249, p = 0.683	Log	0.83 p = 0.483	**V5 vs. V7** T= 2.72, DF=23, p = 0.012+ **V5 vs. V8** T= 2.52, DF=23, p = 0.019+ **V7 vs. V8** T= -0.17, DF=22, p = 0.870+	**V5 vs. V6** W= 202.0, p = 0.182 **V6 vs. V7** W= 206.0, p = 0.047 **V6 vs. V8** W= 202.0, p = 0.077

Appendix 28 - Summary of the statistical analyses for pH, chlorophyll *a* and phytoplankton data between individual vessels within the same treatment for L4 incubation Experiment 2. Underlined = differences considered significant at a threshold of $p<0.05$, $^{+}$ = T-test performed assuming equal variances, $^{\$}$ = T-test performed NOT assuming equal variances considered significant at a threshold of $p<0.05$**, *** mg m^{-3}, § = cell ml^{-1}.

Parameter	Mean	SD	Normality (Anderson-Darling) p>0.05 = normal distribution	Data Trans-formation	Test of Equal Variances (Levene's statistic) p>0.05 = equal variances	2-Sample T-test p<0.05 = significant difference between means	Mann-Whitney nonparametric test W p<0.05 = significant difference between means
pH High CO_2	**V1** 8.02 **V2** 8.12 **V3** 8.01 **V4** 8.04	**V1** 0.18 **V2** 0.19 **V3** 0.12 **V4** 0.12	**V1** 0.919, p = 0.015 **V2** 1.193, p < 0.005 **V3** 0.909, p = 0.015 **V4** 1.351, p < 0.005	None	1.28 p = 0.291		**V1 vs. V2** W= 211.0, p = 0.048 **V1 vs. V3** W= 286.0, p = 0.418 **V1 vs. V4** W= 277.0, p = 0.638 **V2 vs. V3** W= 318.0, p = 0.044 **V2 vs. V4** W= 314.0, p = 0.062 **V3 vs. V4** W= 223.0, p = 0.127
pH Present CO_2	**V5** 8.16 **V6** 8.25 **V7** 8.26 **V8** 8.21	**V5** 0.13 **V6** 0.18 **V7** 0.18 **V8** 0.15	**V5** 0.810, p = 0.028 **V6** 0.668, p = 0.066 **V7** 0.862, p = 0.021 **V8** 1.357, p < 0.005	None	0.35 p = 0.786		**V5 vs. V6** W= 213.0 , p = 0.057 **V5 vs. V7** W= 209.0, p = 0.040 **V5 vs. V8** W= 212.0, p = 0.052 **V6 vs. V7** W= 253.5, p = 0.706 **V6 vs. V8** W= 287.0, p = 0.396 **V7 vs. V8** W= 303.0, p = 0.147

Parameter	**Mean**	**SD**	**Normality** (Anderson-Darling) p>0.05 = normal distribution	**Data Trans-formation**	**Test of Equal Variances** (Levene's statistic) p>0.05 = equal variances	**2-Sample T-test** p<0.05 = significant difference between means	**Mann-Whitney nonparametric test W** p<0.05 = significant difference between means
Chlorophyll *a High CO_2**	**V1** 13.44 **V2** 22.75 **V3** 11.42 **V4** 15.05	**V1** 8.9 **V2** 20.4 **V3** 15.1 **V4** 17.3	**V1** 0.374, p = 0.362 **V2** 0.607, p = 0.090 **V3** 0.241, p = 0.719 **V4** 0.580, p = 0.106	Log	2.21 p = 0.100	**V1 vs. V2** T= -1.59, DF=24, p = 0.126+ **V1 vs. V3** T= 1.49, DF=24, p = 0.150 + **V1 vs. V4** T= 0.51, DF=24, p = 0.617+ **V2 vs. V3** T= 2.74, DF=24, p = 0.012+ **V2 vs. V4** T= 1.85, DF=24, p = 0.076+ **V3 vs. V4** T= -0.93, DF=24, p = 0.363+	
Chlorophyll *a Present CO_2**	**V5** 9.80 **V6** 14.07 **V7** 10.01 **V8** 8.97	**V5** 11.6 **V6** 15.9 **V7** 12.3 **V8** 11.9	**V5** 0.632, p = 0.077 **V6** 0.697, p = 0.052 **V7** 0.503, p = 0.167 **V8** 0.422, p = 0.273	Log	0.15 p = 0.927	**V5 vs. V6** T= -1.23, DF=24, p = 0.232+ **V5 vs. V7** T= -0.13, DF=24, p = 0.898+ **V5 vs. V8** T= 0.32, DF=24, p = 0.749+ **V6 vs. V7** T= 1.11, DF=24, p = 0.276+ **V6 vs. V8** T= 1.54, DF=24, p = 0.136+ **V7 vs. V8** T= 0.46, DF=24, p = 0.653+	

Parameter	Mean	SD	Normality (Anderson-Darling) p>0.05 = normal distribution	Data Trans-formation	Test of Equal Variances (Levene's statistic) p>0.05 = equal variances	2-Sample T-test p<0.05 = significant difference between means	Mann-Whitney nonparametric test W p<0.05 = significant difference between means
Nano-phytoplankton § **High CO_2**	**V1** 9630 **V2** 16847 **V3** 12777 **V4** 12443	**V1** 3934 **V2** 7172 **V3** 8051 **V4** 5946	**V1** 0.527, p = 0.144 **V2** 0.410, p = 0.294 **V3** 0.322, p = 0.485 **V4** 0.606, p = 0.090	Log	0.46 p = 0.712	**V1 vs. V2** T= -3.40, DF=24, p = 0.002+ **V1 vs. V3** T= -1.08, DF=24, p = 0.291+ **V1 vs. V4** T= -1.52, DF=24, p = 0.142+ **V2 vs. V3** T= 1.90, DF=24, p = 0.070+ **V2 vs. V4** T= 2.02, DF=24, p = 0.055+ **V3 vs. V4** T= -0.23, DF=24, p = 0.821+	
Nano-phytoplankton § **Present CO_2**	**V5** 11384 **V6** 23094 **V7** 9850 **V8** 11030	**V5** 4235 **V6** 9384 **V7** 6749 **V8** 6001	**V5** 0.244, p = 0.708 **V6** 0.255, p = 0.669 **V7** 0.324, p = 0.479 **V8** 0.338, p = 0.445	Log	1.06 p = 0.375	**V5 vs. V6** T= -4.85, DF=24, p < 0.001+ **V5 vs. V7** T= 1.36, DF=24, p = 0.185+ **V5 vs. V8** T= 0.53, DF=24, p = 0.604+ **V6 vs. V7** T= 4.89, DF=24, p < 0.001+ **V6 vs. V8** T= 4.61, DF=24, p < 0.001+ **V7 vs. V8** T= -0.82, DF=24, p = 0.418+	

Parameter	Mean	SD	**Normality** (Anderson-Darling) p>0.05 = normal distribution	**Data Trans-formation**	**Test of Equal Variances** (Levene's statistic) p>0.05 = equal variances	**2-Sample T-test** p<0.05 = significant difference between means	**Mann-Whitney nonparametric test W** p<0.05 = significant difference between means
Synechococcus § **High CO_2**	**V1** 56658 **V2** 10818 **V3** 34173 **V4** 16747	**V1** 73613 **V2** 11747 **V3** 42003 **V4** 16195	**V1** 0.429, p = 0.262 **V2** 0.479, p = 0.194 **V3** 0.509, p = 0.161 **V4** 0.630, p = 0.078	Log	0.95 p = 0.426	**V1 vs. V2** T= 1.63, DF=24, p = 0.115+ **V1 vs. V3** T= 0.36, DF=24, p = 0.720+ **V1 vs. V4** T= 0.90, DF=24, p = 0.376+ **V2 vs. V3** T= -1.36, DF=24, p = 0.186+ **V2 vs. V4** T= -0.89, DF=24, p = 0.381+ **V3 vs. V4** T= 0.56, DF=24, p = 0.582+	
Synechococcus §**Present CO_2**	**V5** 68156 **V6** 6661 **V7** 5318 **V8** 27547	**V5** 93116 **V6** 7558 **V7** 5608 **V8** 32939	**V5** 0.476, p = 0.197 **V6** 0.473, p = 0.201 **V7** 0.339, p = 0.443 **V8** 0.795, p = 0.029	Log	3.73 p = 0.017	**V5 vs. V6** T= 2.28, DF=19, p = 0.035$ **V5 vs. V7** T= 2.47, DF=17, p = 0.024$ **V6 vs. V7** T= 0.13, DF=23, p = 0.897$	**V5 vs. V8** W= 187.0, p = 0.573 **V6 vs. V8** W= 150.0, p = 0.199 **V7 vs. V8** W= 154.0, p = 0.282

Appendix 29. Spearman's Rank Correlation Coefficients (ρ) and associated significance level for correlations between halocarbon concentrations and various other parameters. Data from Autumn 2007. n = 25, * = 95% confidence level (Critical value = 0.409, p<=0.05), ** = 98% confidence level (Critical value = 0.485, p<=0.02), *** = 99% confidence level (Critical value = 0.537, p<=0.01).

	[CH_3I] pM	**[C_2H_5I] pM**	**[2-C_3H_7I] pM**	**[1-C_3H_7I] pM**	**[CH_2ClI] pM**	**[CH_2I_2] pM**	**[$CHBr_3$] pM**	**[CH_2Br_2] pM**
Temp. °C	-0.122	-0.239	0.121	-0.429*	0.597***	0.477*	0.812***	0.818***
Salinity	-0.517**	0.022	0.140	-0.127	0.425*	-0.008	0.789***	0.716***
Depth m (sample)	-0.139	-0.237	-0.192	0.332	-0.238	-0.187	0.164	0.157
Depth m (water)	-0.205	-0.096	-0.496**	0.502**	-0.438*	-0.594***	-0.124	-0.136
pH	-0.274	-0.221	-0.715***	0.217	-0.215	-0.643***	-0.133	-0.180
Chlorophyll *a* mg m^{-3}	0.172	-0.115	-0.417*	-0.145	-0.087	-0.399	-0.612***	-0.616***
Phaeopigments mg m^{-3}	0.306	0.006	0.539***	-0.268	0.362	0.842***	0.538***	0.608***
Wind direction Degrees	-0.137	0.267	-0.089	0.488**	-0.534***	-0.688***	-0.695	-0.748
Wind speed km/h	-0.224	0.061	-0.112	0.540***	-0.462*	-0.416*	-0.005	-0.032

Appendix 30. Spearman's Rank Correlation Coefficients (ρ) and associated significance level for correlations between various parameters. Data from Autumn 2007. n = 25, * = 95% confidence level (Critical value = 0.409, p<=0.05), ** = 98% confidence level (Critical value = 0.485, p<=0.02), *** = 99% confidence level (Critical value = 0.537, p<=0.01).

	pH	**Chlorophyll *a* (mg m^{-3})**	**Phaeopigments (mg m^{-3})**
Temperature (°C)	-0.028	-0.294	0.578***
Salinity	-0.028	-0.655***	0.248
Depth m (sample)	0.240	-0.009	-0.168
Depth m (water)	0.714***	0.121	-0.511**
Wind direction (Degrees)	0.079	0.159	-0.658***
Wind speed (km/h)	0.301	-0.133	-0.275
Chlorophyll *a* (mg m^{-3})	0.428*	-	-0.568***
Phaeopigments (mg m^{-3})	-0.630***	-0.568***	-

Appendix 31. Spearman's Rank Correlation Coefficients (ρ) and associated significance level for correlations between halocarbon concentrations and various other parameters. Data from Spring 2008. n = 31, * = 95% confidence level (Critical value = 0.364, p<=0.05), ** = 98% confidence level (Critical value = 0.432, p<=0.02), *** = 99% confidence level (Critical value = 0.478, p<=0.01).

	[2-C_3H_7I] pM	[1-C_3H_7I] pM	[CH_2ClI] pM	[CH_2I_2] pM	[CH_2Br_2] pM	[$CHBr_2Cl$] pM	[CH_2BrI] pM	[$CHBr_3$] pM
Temp. °C	0.180	0.089	0.038	-0.082	-0.298	-0.182	-0.123	-0.349
Salinity	0.469**	-0.023	0.002	0.230	-0.218	0.021	0.481***	-0.149
Depth m (sample)	-0.084	0.074	-0.172	0.299	-0.136	-0.112	-0.203	-0.165
Depth m (water)	-0.364*	-0.150	-0.295	0.189	-0.682***	-0.711***	-0.531***	-0.657***
pH	0.089	-0.653*	-0.013	0.135	-0.712***	-0.634***	0.683	-0.607***
Chlorophyll *a* mg m^{-3}	-0.238	-0.105	0.358	-0.188	0.143	0.001	-0.228	0.119
Phaeopigments mg m^{-3}	0.374*	-0.047	0.218	-0.176	0.691***	0.617***	0.500***	0.610***
Wind direction Degrees	-0.627***	0.052	0.099	-0.482***	-0.061	-0.293	-0.864***	-0.247
Wind speed km/h	0.800***	-0.137	-0.434**	0.645***	-0.492***	-0.275	0.460***	-0.353
Tidal Height m	-0.458**	-0.238	0.254	-0.470**	0.032	-0.221	-0.441**	0.006

Appendix 32. Spearman's Rank Correlation Coefficients (ρ) and associated significance level for correlations between various parameters. Data from Spring 2008. n = 25, * = 95% confidence level (Critical value = 0.409, p<=0.05), ** = 98% confidence level (Critical value = 0.485, p<=0.02), *** = 99% confidence level (Critical value = 0.537, p<=0.01).

	pH	Chlorophyll *a* (mg m^{-3})	Phaeopigments (mg m^{-3})
Temperature (°C)	-0.002	0.418*	-0.396*
Salinity	0.304	-0.381*	-0.357
Depth m (sample)	-0.027	-0.350	-0.168
Depth m (water)	0.486***	-0.223	-0.578***
Tidal height m	0.189	0.036	0.337
Wind direction (Degrees)	-0.304	0.407*	0.513***
Wind speed (km/h)	0.593***	-0.657***	-0.886***
Chlorophyll *a* (mg m^{-3})	-0.035	-	-
Phaeopigments (mg m^{-3})	-0.192	0.164	-

Appendix 33. Spearman's Rank Correlation Coefficients (ρ) and associated significance level for correlations between DMS concentrations, pH, chlorophyll-a, phaeopigments and various other parameters. Data from Spring 2008. n = 30, * = 95% confidence level (Critical value = 0.364, p<=0.05), ** = 98% confidence level (Critical value = 0.432, p<=0.02), *** = 99% confidence level (Critical value = 0.478, p<=0.01).

	DMS nM/l^{-1}	**pH**	**Chlorophyll *a* (mg m^{-3})**	**Phaeopigments (mg m^{-3})**
Temp. °C	0.248	0.222	0.046	-0.460 **
Salinity	-0.367 *	0.323	-0.076	0.072
Depth m (sample)	0.602 ***	0.208	-0.240	-0.082
Depth m (water)	0.534 ***	0.549 ***	-0.217	-0.532 ***
pH	-0.040	-	0.043	-0.220
Chlorophyll *a* mg m^{-3}	-0.103	0.043	-	0.400 *
Phaeopigments mg m^{-3}	-0.467 **	-0.220	0.400 *	-
Wind direction Degrees	-0.201	-0.210	0.075	0.075
Wind speed km/h	0.403	0.138	-0.197	-0.197
Tidal Height m	-0.413 *	-0.204	0.354	0.354